THE TWENTY FOURTH ANNUAL CONFERENCE ON MASS SPECTROMETRY AND ALLIED TOPICS

MAY 9-13, 1976

SAN DIEGO, CALIFORNIA

THE TWENTY-FOURTH ANNUAL CONFERENCE ON MASS SPECTROMETRY AND ALLIED TOPICS

MAY 9-14, 1976

SAN DIEGO, CALIFORNIA

TABLE OF CONTENTS

		Page No.
1.	Introduction	1
2.	Acknowledgements	2
3.	Proceedings of the Twenty-Fourth Annual Conference	4
4.	Author Index	747
5.	ASMS Committees and ASTM E-14 Subcommittees	754
6.	Committee and Subcommittee Reports	755
7.	ASTM Publications	772
8.	Mass Spectrometry Organizations	774

INTRODUCTION

In this volume are collected abstracts and extended versions of the papers presented at the Twenty-Fourth Annual Conference on Mass Spectrometry and Allied Topics, held in San Diego, California, May 9-13, 1976. It is intended that this volume be distributed only to members of ASMS, and registrants of the Conference, and therefore it should not be considered as a publication.

It is suggested that any future reference to individual reports be cited in the form: author(s), presented at the Twenty-Fourth Annual Conference on Mass Spectrometry and Allied Topics, 1976.

The final collection, editing, and assembly of the papers for this volume were carried out at Rice University, and it is a pleasure to recognize the meticulous and dedicated efforts of Brenda and Larry Robey in the actual preparation of the publication copy and the cover design.

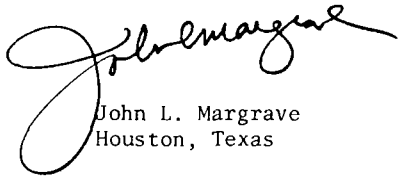

John L. Margrave
Houston, Texas

American Society of Mass Spectrometry

President: H. J. Svec, Department of Chemistry, Iowa State University, Ames, Iowa 50010

Vice President(Program): J. H. Futrell, Department of Chemistry, University of Utah, Salt Lake City, Utah 84112

Vice President(Arrangements): Wilson M. Brubaker, Hewlett-Packard, 1954 Highland Oaks, Arcadia, California 91006

Secretary: J. A. McCloskey, Department of Biopharmaceutical Sciences, University of Utah, Salt Lake City, Utah 84112

Treasurer: M. T. Laug, Argonne National Laboratory, Box 2528, Idaho Falls, Idaho 83401

Past President: F. H. Field, Department of Chemistry, Rockerfeller University, New York, New York 10021

Directors-at-Large:

P. Kebarle, Department of Chemistry, University of Alberta, Edmonton 7, Alberta, Canada

J. L. Margrave, Office of Advanced Studies and Research, Rice University, Houston, Texas 77001

The American Society for Mass Spectrometry is grateful for support of the 1976 Conference from the following sponsors and corporate members.

Company	Representatives
AEI SCIENTIFIC APPARATUS, INC. 500 Executive Boulevard Elmsford, New York 10523	Mr. Clive Segal
ANALOG TECHNOLOGY CORPORATION 3410 East Foothill Boulevard Pasadena, California 91107	Dr. Charles Judson
CAMECA INSTRUMENTS, INC. Brownhouse Road Stamford, Connecticut 06902	Mr. Autier
CVC PRODUCTS, INC. 575 Lee Road Rochester, New York 14603	Mr. S. Rothstein
CYPHERNETICS CORPORATION 175 Jackson Plaza Ann Arbor, Michigan 48106	Dr. Chamberland
E. I. DUPONT DE NEMOURS & CO., INC. 1500 South Shamrock Avenue Monrovia, California 91096	Dr. E. M. Chait
EXTRANUCLEAR LABORATORIES, INC. P. O. Box 11512 Pittsburgh, Pennsylvania 15238	Mr. Michael C. McKeown
FINNIGAN CORPORATION 845 West Maude Avenue Sunnyvale, California 94304	Dr. Robert E. Finnigan
HEWLETT-PACKARD * Scientific Instruments Division 1601 California Avenue Palo Alto, California 94304	Dr. Harmon Brown
INCOS CORPORATION 1332 Sixth Street Berkeley, California 94710	Dr. D. E. Hagge
ION INSTRUMENTS, INC. 1875 North 105th Street East Avenue Tulsa, Oklahoma 74116	Mr. B. A. Hopper
JEOL (U.S.A.), INC. 235 Birchwood Avenue Cranford, New Jersey 07016	Mr. R. S. Martin

THE KEARNS GROUP AND VG INSTRUMENTS 58 Buckingham Drive Stamford, Connecticut 06902	Mr. G. L. Kearns
LKB INSTRUMENTS DIVISION 12221 Parklawn Drive Rockville, Maryland 20852	Mr. Fred F. Schaub
MERCK, SHARP, AND DOHME R 33-65 Rahway, New Jersey 07605	Mr. Donn M. Gordon
3M COMPANY 3M Center St. Paul, Minnesota 55101	Mr. Gene Sparrow
MONSANTO RESEARCH CORPORATION P. O. Box 32 Miamisburg, Ohio 45342	Mr. V. L. Avona
NUCLIDE CORPORATION 642 East College Avenue State College, Pennsylvania 16801	Dr. L. F. Herzog
J. C. PERNICKA AND ASSOCIATES * P. O. Box 5222 San Mateo, California 94402	Mr. J. C. Pernicka
STOHLER ISOTOPE CHEMICALS, INC. 49 Jones Road Waltham, Massachusetts 02154	Mr. Jack Turgel
SYSTEM INDUSTRIES 535 Del Rey Avenue Sunnyvale, California 94086	Dr. Neville L. Crook
UTHE TECHNOLOGY INTERNATIONAL * 325 North Mathilda Avenue Sunnyvale, California 94086	Mr. R. E. Carr
VACUMETRICS/CALIFORNIA 2261 Palma Drive, Suite 1 Ventura California 93003	Mr. R. Doucet
VARIAN MAT/U.S. OPERATIONS 25 Route 22 Springfield, New Jersey 07081	Dr. W. A. Wolstenholme

*Corporate Member

PROCEEDINGS OF THE TWENTY-FOURTH ANNUAL CONFERENCE

Paper No.		Page No.
PL-1*	Computer Applications In Mass Spectrometry. A Review. K. Biemann	30
PL-2*	Penning Ionization Electron Spectroscopy. V. Cermak	31
PL-3*	Ion-Neutralization Phenomena At Solid Surfaces. H. D. Hagstrum	37
A-1	High Resolution Photoelectron Spectroscopy. F. A. Grimm	42
A-2	The Effects Of Molecular Rotation And Vibrational Hot Bands On Photoionization Thresholds. K. E. McCulloh	43
A-3	Photoelectron Spectra Of Transients. T. Koenig, T. Balle, W. Snell	44
A-4	Electron Monochromator Studies Of Organic Ions. F. P. Lossing	45
A-5	Electron Impact Threshold Measurements On High Temperature Beam Species. D. L. Hildenbrand	46
A-6	High-Temperature Photoionization And Photoelectron Measurements. J. Berkowitz	47
A-7	Kinetic Aspects of Threshold Determination. A. L. Wahrhaftig	62
A-8	Application Of IKES To Ion Enthalpy Determination. J. H. Beynon, R. K. Boyd	67
A-9	Auger Electron Spectrometry Involving Valence Levels. M. O. Krause	68
A-10	High Energy Ion/Molecule Reactions. R. G. Cooks, J. H. Beynon, T. Keough, T. Ast, L. Hendricks, J. F. Litton, D. L. Kemp, C. S. Hsu, M. Medved, T. L. Kruger, V. Franchetti, R. Kondrat	73
A-11	Laser Photodetachment. W. C. Lineberger	82
A-12	Electron Affinities Of Polyatomic Species. J. I. Brauman	83

* Plenary Lecture

Paper No.		Page No.
A-13	Determination Of Ion Thermochemical Properties By Ion Cyclotron Resonance Spectroscopy. J. L. Beauchamp	84
A-14	Thermochemical Results From Pulsed ICR Equilibrium Studies. R. T. McIver, Jr., J. S. Miller	85
A-15	Flowing Afterglow Measurements Bearing On The Thermochemistry of Gaseous Ions. D. K. Bohme, G. I. Mackay	86
A-16	Ion Thermochemistry By Pulsed High Ion Source Pressure Mass Spectrometry. K. Hiraoka, P. Kebarle	93
A-17	The Thermochemistry Of Carbonium Ions By MS Equilibrium Measurements. F. H. Field	94
A-18	Ion Thermochemistry In Ionospheric Problems. E. E. Ferguson	95
A-19	Systematics of Organic Ion Decompositions. M. M. Bursey, W. R. Kenan, Jr.	96
A-20	Use Of Gaseous Ion Thermochemistry In Physical Organic Chemistry. R. W. Taft	98
B-1	GC-MS Development In Forensic Science. B. S. Finkle	102
B-2	Differentiation Of Window Glasses By Spark Source Mass Spectrometry. M. A. Haney	103
B-3	Chemical Ionization Mass Spectrometry In Pharmacology Studies. R. L. Wolen, C. M. Gruber, Jr.	104
B-4	Advantages Of Chemical Ionization in Forensic Toxicology. R. F. Skinner, E. J. Heron	105
B-5	GC-MS Of Simulated Gasoline Residues Suspected Arson Cases. M. H. Mach	109
C-1	CAMS-11, The Navy's Approach To Atmosphere Monitoring. J. R. Wyatt, J. J. DeCorpo, F. E. Saalfeld	111

Paper No.		Page No.
C-2	Quantitative Analysis Of Trace Environmental Samples Using Computer Controlled High Resolution Scanning Multiple Ion Detection (SMID). D. Schuetzle, D. E. Hagge	115
C-3	Analysis Of Trace Levels Of Organic Vapors In Ambient Air By Glass Capillary Gas-Liquid Chromatography-Mass Spectrometry-Computer. E. D. Pellizzari, J. E. Bunch, R. E. Berkley, J. Bursey	120
C-4	Sampling And Analysis Of Submarine Atmospheres. J. J. DeCorpo, F. E. Saalfeld, J. R. Wyatt, F. W. Williams, H. G. Eaton, D. E. Smith	124
C-5	Mass Spectra Of Carcinogenic Particulate Organic Matter (POM) Found In The Environment. R. C. Lao, R. S. Thomas	125
C-6	Application Of Direct Thermal Desorption GC-MS To The Analysis Of Volatiles In Commercial Polymers. W. V. Ligon, Jr.	126
C-7	Analysis Of Brazilian Natural Waters For Organic Pollutants By GC/MS/Computer. C. H. Williams, Jr.	127
C-8	Use Of High Sensitivity GC-MS For Identifying Organic Water Pollutants At The Sup-PPB Level. R. M. Milberg, J. C. Cook, Jr.	130
C-9	GC/MS Identification Of Synthetic Organic Pollutants In Industrial Effluents And Receiving Waters. G. Jungclaus, L. M. Games, M. L. Lee, R. A. Hites	131
D-1	Computerized Mass Spectrometer Data System at LLL*. R. D. Friesen, R. J. Dupzyk	134
D-2	Sensitivity, Dynamic Range And Mass Accuracy Optimization In A Mass Spectrometer Data System. D. E. Hagge, P. G. Blaney B. M. Grinberg	137
D-3	DA/CS-VII-A New Data Analysis And Control System For 12-90-HT Mass Spectrometers And Others Used For Thermodynamic Studies. G. L. Brezler	138
D-4	Solutions To Some Problems In Computerized Data Analysis Of Multicomponent Mass Spectra. M. E. Scolnick	141

Paper No.		Page No.
D-5	Extraction Of Mass Spectra Free Of Background And Neighboring Component Contributions From GC/MS Data. T. C. Rindfleisch, R. G. Dromey, M. J. Stefik, A. M. Duffield	145
D-6	A Method For The Automatic Detection Of Isotopic Clusters In Repetitive GC-MS Scans. J. A. Steinborn, D. J. Jenden	146
D-7	Codification Of Mass Spectra By Functional Group Classification. D. H. Robertson, R. A. Graham, C. Merritt, Jr.	147
D-8	Low Resolution Mass Spectra Search By Mini Computer. W. G. Urban, J. A. Thompson, P. V. Fennessey	150
D-9	Forward And Reverse Library Search Methods Applied To Mass Reconstructed GC MS Data. P. Powers, A. J. Hopkinson, J. D. Robinson, M. J. Wallington	155
D-10	A Chemical Analysis Information System. J. J. Downs, J. L. Spigarelli, M. J. Serrone, J. B. High	160
D-11	An Improved Self-Training Interpretive And Retrieval System. H. E. Dayringer, F. W. McLafferty, R. Venkataraghavan	161
D-12	The Use Of Mass Spectrometric Data In Computer Assisted Structure Elucidation. R. E. Carhart, D. H. Smith	162
E-1	Structural Investigation Of Narasin And Related Ionophores. D. Berg, J. L. Occolowitz	163
E-2	Stereospecificity Of Eliminations From Arylcyclohexyl Derivatives Under Electron Impact. J. Sharvit, M. Weissdorf, A. Mandelbaum	164
E-3	Sterically Crowded Trialkylsilyl Derivatives In The Analysis And Characterization Of Steroids. M. A. Quilliam, J. B. Westmore	165
E-4	The Temperature Dependence Of An Electron Impact Induced Stereoselective Rearrangement Reaction. M. M. Green, T. J. Mangner, F. J. Brown, S. P. Turner	166
E-5	Mass Spectrometric Study Of Antipyrine And Its Metabolites. J-P. Thenot, M. Stafford, K. D. Haegele	174

Paper No.		Page No.
E-6	The Study Of The Isomerisation Behavior Of Organic Ions By Collisional Activation Spectrometry. K. Levsen	175
E-7	An Analysis Of The Electron Impact Mass Spectrum Of Diphenylketenediphenyl Ketal. W. V. Ligon, Jr., C. B. Quinn, T. Takekoshi	177
E-8	Isobutane CIMS Of Urethane Protecting Groups. G. Barany, A. L. C. Smit, D. V. Bowen, R. B. Merrifield, F. H. Field	178
E-9	Use Of Gas Chromatography/Mass Spectrometry With Chemical Ionization To Determine Double Bond Position In Complex Olefin Mixtures. G. W. Mappes, O. E. Kinast, M. W. Dietrich	181
E-10	Reactions Of Methyl Cations With Acetone Neutrals. R. D. Smith, T. A. Elwood, D. A. Herold, J. H. Futrell	184
E-11	Organic Reactions Of Anions In A Flowing Afterglow. R. H. Shapiro, C. H. DePuy, V. M. Bierbaum, J. H. Stewart	186
E-12	Ion Molecule Reactions Of The 1,3-Butadiene Ion--Possible Ionic Cyclo Additions. M. L. Gross, P-H Lin, D. H. Russell	189
F-1	Analysis Of A Three-Component Deuterium-Labeled Mixture By Multiple Ion-Monitoring Mass Spectrometry. W. K. Rohwedder, W. F. Kwolek, D. J. Wolf, W. L. Everhart	190
F-2	Quantification Of Prostaglandins In Human Seminal Fluid By Single Ion Monitoring. D. L. Perry, D. M. Desiderio	191
F-3	Chemical Ionization Mass Spectrometry Of Urinary Compounds For Clinical Diagnosis. D. Issachar, J. Yinon	193
F-4	Analysis Of Polyamines In Urine By Stable Isotope Mass Fragmentography. E. T. Everhart, W. E. Pereira, T. C. Rindfleisch, A. M. Duffield	200
F-5	Biogenic Amine Derivatives For Use In Negative Chemical Ionization Analysis. E. A. Bergner, R. C. Dougherty	201

Paper No.		Page No.
F-6	Simultaneous Kinetic Studies And Quantitation Of Catecholamines In Selected Areas Of Rat Brain. C. R. Freed, R. C. Murphy	203
F-7	Deuterium Labelled Internal Standards For Polyamine Analysis. R. G. Smith, G. D. Daves Jr.	206
F-8	Aldehyde Condensation Products As Derivatives For The Analysis Of Biogenic Amines. B. S. Middleditch	209
F-9	GC-MS Studies Of Thiocarbamic Acid Derivatives Of Some Biologically Important Secondary Amines. N. Narasimhachari, P. Vouros, D. E. Green	210
F-10	Simultaneous Analysis Of Chlorpromazine And Its Major Metabolites By Stable Isotope Ratio Measurements Using Improved Voltage Sweep Instrumentation. L. D. Gruenke, J. C. Craig.	211
G-1	Characteristics Of A Double Blade Field Ionization Source. W. Aberth, A. M. Falick, J. T. Wilder, A. L. Burlingame	214
G-2	A Field Ionization/Field Desorption (FI/FD) Source For AEI-MS9 And MS50 Mass Spectrometers. G. K. Eigendorf, C. A. McDowell	217
G-3	Comparative Efficiencies Of Various Types Of Field Ionization Sources. H. L. Brown, R. H. Cross, M. Anbar	220
G-4	Structural Determination By Combined Field Ionization-Collision Induced Dissociation. J. H. McReynolds, M. Anbar, W. Aberth	223
H-1	GC/MS Analysis Of Low Level Contaminants In Tap Water By Direct Water Injection. R. G. Beimer, E. M. Chait, B. N. Colby	225
H-2	Elemental Composition Chromatography (ECC): The Characterization Of Complex Mixtures Of Organic Substances In Aqueous Effluents. A. L. Burlingame, B. J. Kimble, E. Scott, F. C. Walls	226
H-3	Studies Of Volatile Metal Compounds With Chemical Ionization Mass Spectrometry. S. R. Prescott, P. C. Jurs, T. H. Risby	227

Paper No.		Page No.
H-4	Nature Of Ions Observed In Plasma Chromatography. F. W. Karasek	228
H-5	Levels Of Tetrachlorodibenzo-p-Dioxin In Environmental And Biological Samples As Determined By Gas Chromatography-High Resolution Mass Spectrometry. M. L. Taylor, R. L. C. Wu, C. D. Miller, T. O. Tiernan	231
J-1	The Application Of New Techniques In GC/MS To The Analysis Of Drugs And Complex Mixtures. P. Dobberstein, A. Zune, W. A. Wolstenholme	234
J-2	Quantitative Determination Of Phenacetin And Its Metabolite Acetaminophen By GC-MS. W. A. Garland, K.-C. Hsiao*, E. J. Pantuck*, A. H. Conney	239
J-3	A Single-Ion-Monitoring GC-MS Assay For Methylphenidate In Biological Media. J. Gal, B. J. Hodshon, B. L. Flamm, A. K. Cho, C. Pintauro	242
J-4	Quantification Of Caffeine, Theophylline, Theobromine And 1,7-Dimethylxanthine By Chemical Ionization Using N^+ and N_2^+. M. G. Horning, J. Nowlin	243
J-5	Determination Of Phosphonoacetic Acid In Serum By Chemical Ionization-Mass Fragmentography. J. Roboz, R. Suzuki, S. Sivakoff, G. Bekesi	244
J-6	Quantitative Analysis Of Phenobarbital , Diphenylhydantoin And Clonazepam Using Atmospheric Pressure Ionization Mass Spectrometry. D. I. Carroll, I. Dzidic, R. N. Stillwell, E. C. Horning	245
J-7	Identification Of Drugs Using A GC/MS-System Equipped With EI/CI And EI/FI/FD Ion Sources. A. Zune, K. H. Maurer, U. Rapp, W. A. Wolstenholme	246
J-8	Clinical Diagnosis By Molecular Profiles Of Metabolites In Urine. M. Anbar, R. Dyer, M. E. Scolnick	247
J-9	Accuracy Of Organic Analysis By Isotope Dilution-Mass Spectrometry (ID-MS). T. Sun, A. Cohen, H. S. Hertz, R. Schaffer	250
J-10	Sterochemistry Of Amphetamine Metabolism: A Study By Stable Isotope GC/MS. J. Wright, J. Gal, A. K. Cho	252

Paper No.		Page No.
J-11	Identification Of New Meperidine Metabolites By Gas Chromatography-Mass Spectrometry. J. T. Stewart, M. G. Horning, W. G. Stillwell, K. Haegele	253
J-12	GC-MS Identification Of p,p'-Dihydroxydiphenylhydantoin As A Minor Metabolite or Dilantin In The Rat And Human. R. M. Thompson, J. Beghin, W. K. Fife, N. Gerber	255
K-1	Mass Spectrometer Sensitivity Data For Selected Compounds. B. A. Petersen, P. Vouros, D. J. Marshall	256
K-2	Mass And Microwave Spectral Studies Of The Mechanism Of Ozonolysis. R. P. Lattimer, C. W. Gillies, R. L. Kuczkowski	259
K-3	Acylated Fatty Acids In Commercial Fats From Natural Sources. R. S. Ampulski	262
K-4	Field Ionization Kinetics Studies Of Stereoisomers. J. S. Holler, D. G. Patterson, R. B. Scott, M. E. Munk, P. Brown	265
K-5	Rearrangement And Decay Of 1-Hexene Ions: Field Ionization Kinetic (FIK) Measurements. A. M. Falick, T. Gaumann	267
K-6	Mixture Analysis By Collisional Activation Spectrometry. K. Levsen	270
K-7	Interpretation Of The Field Desorption Mass Spectra Of Diionic Salts. C. N. McEwen, S. F. Layton	271
K-8	Field Desorption Mass Spectrometry Of Organic, Inorganic And Organometallic Salts. D. E. Games, J. L. Gower, L. A. P. Kane-Maguire	274
K-9	Field Desorption Mass Spectrometry Of Cationic And Anionic Dyes. C. N. McEwen, S. F. Layton	277
K-10	Some Quantitative Aspects Of Field Desorption Mass Spectrometry. D. F. Barofsky, R. Held, E. Barofsky	279
K-11	Qualitative And Quantitative Field Desorption Mass Spectrometry Of Mixtures. H-R. Schulten, H. D. Beckey	282

Paper No.		Page No.
K-12	Emission-Controlled Field Desorption Mass Spectrometry Of Large Organic Salts. H. R. Schulten, H. D. Beckey	286
L-1	A Device For The Direct Measurement Of Atomic Weights. W. H. Johnson	288
L-2	Accurate Mass Measurement With The AEI MS5074 Mass Spectrometer. S. Evans, D.Hazelby, K. R. Compson, A. E. Holme	289
L-3	Precision Of Relative Abundance Measurements As A Function Of Mass Difference. W. R. Sherman, W. J. Fies, E. J. Heron	293
L-4	Mass Measurement Accuracy In The Trapped ICR Mass Spectrometer. E. B. Ledford, Jr., R. T. McIver, Jr.	297
M-1	A Simple Approach To Quantitative SIMS. G. R. Sparrow	298
M-2	Some Practical Applications Of SIMS. G. R. Sparrow, J. A. Leys	306
M-3	SIMS Analysis Of Cu_2S/CdS Solar Cell Samples F. G. Satkiewicz, H. K. Charles, Jr.	307
M-4	A SIMS Investigation Of Heteroepitaxial Silicon On Sapphire. W. L. Harrington, C. W. Magee, G. W. Cullen, J. F. Corboy	310
M-5	Study Of Negative Secondary Ion Spectra Produced By CS^+ Primary Beam On Metal Targets. M. Baril, P. Vallerand	314
M-6	Study Of An Iodine Discharge In A Duoplasmatron. W. W. Harrison, H. Liebl	317
M-7	The Measurement Of Isotopic Ratios With Sputtering Ion Source Mass Spectrometers. J. R. Hinthorne, R. L. Conrad, R. D. Fralick, C. A. Andersen	318
M-8	Ion Imaging And Ion Counting: Complementary Techniques For Diffusion Studies. G. Sweeney	319
M-9	The Role Of Sampling In Ion Probe Analysis. G. J. Scilla, G. H. Morrison	320

Paper No.		Page No.
M-10	A New Laser-Arc Milliprobe Mass Spectrometer. R. J. Conzemius, H. J. Svec	323
M-11	System For Quantitation Of Ion Micrographic Images. J. D. Fassett, J. R. Roth, G. H. Morrison	327
N-1	Low Pressure Chemical Ionization Of Some Complex Biological Molecules. E. B. Ledford, Jr., R. T. McIver, Jr.	329
N-2	^{252}Cf-Plasma Desorption Mass Spectrometry-Nuclear Particles To Probe Biomolecules. R. D. Macfarlane, D. F. Torgerson	330
N-3	Atmospheric Pressure Ionization (API) Mass Spectrometry. E. C. Horning, D. I. Carroll, I. Dzidic, K. D. Haegele, R. N. Stillwell	333
N-4	Techniques And Applications Of Precise Isotope Ratio Measurements. J. M. Hayes, D. E. Matthews, D. W. Peterson, Z. Sofer, E. Vogler	334
O-1	Studies Of Rydberg-State Reactions. C. E. Klots	335
O-2	Variable Fragmentation Mass Spectrometry Using Chemiionization. J. B. Laudenslager, L. P. Theard	327
O-3	Experimental Breakdown Curves Of Propane And Deuterated Propane Molecular Ions. R. Stockbauer, M. G. Inghram	340
O-4	Kinetic Energy Release Distributions For The Dissociation Of Internal Energy Selected CH_3I^+ and CD_3I^+ Ions. D. M. Mintz, T. Baer, W. R. Kenan, Jr.	341
O-5	Photoionization Mass Spectrometry Of Ozone. M. J. Weiss , J. Berkowitz, E. H. Appelman	342
O-6	Measurement Of Angular Distribution And Energy Of Ionic Fragments From Photodissociation Of Molecular Ions. R. Orth, R. C. Dunbar, M. Riggin	343
O-7	Laser Photodissociation Spectrum Of Hexatriene Cation. R. C. Dunbar	344
O-8	Photodissociation Of Ion Beams In A Tandem Mass Spectrometer Using A Tunable Dye Laser. T. F. Thomas, J. F. Paulson	345

Paper No.		Page No.
O-9	Photoionization Of Halocarbons. F. P. Tully, E. J. Darland, G. W. Ray, P. L. Kronebusch, C. G. Enke, G. E. Leroi	349
O-10	Photo-Assisted Ionization. A. B. Denison, J. M. Phillips, J. M. Knox, J. H. Weber	352
O-11	A Time-Resolved Study Of The Fragmentation Of 1,5-Hexadiyne. P.P. Dymerski, A. G. Harrison	354
P-1	Preparative Mass Spectrometry. V. Franchetti, R. G. Cooks,	355
P-2	Mass Spectrometric Determination Of Water Using Cryogenic Concentration And Acetylene Conversion. G. L. Carlson, W. M. Hickman	358
P-3	Scope And Limitations Of Mass Spectrometric Determination Of Carbon 14. R. Schnitzer, M. Anbar	361
Q-1	Polyatomic Phase Space Theory: Applications To Bimolecular And Unimolecular Reactions. W. J. Chesnavich, M. T. Bowers	363
Q-2	A Theoretical Approach To Ion Polar Neutral Momentum Transfer Collision Frequencies. D. P. Ridge, R. A. Barker	364
Q-3	Vibrational Energy Dependence Of Ion-Molecule Reaction Cross Sections. A. D. Williamson	365
Q-4	Crossed-Beam Study Of The Reaction $ArH^+(H_2,Ar)H_3^+$. M. L. Vestal, C. R. Blakley, J. H. Futrell	366
O-5	Ion-Moleucle Reactions Between Kr^+ And H_2, and IID. J. Ige, M. J. Henchman	369
O-6	Luminescence From He^+/Cl_2 Collisions In The Energy Range 2-170 eV. K. E. Siegenthaler, B. M. Hughes, E. G. Jones, T. O. Tiernan	370
Q-7	Lifetimes Of Intermediate Complexes In Ion-Molecule Reactions. G. G. Meisels, F. Botz[a] and E. F. Heckel[b]	373

Paper No.		Page No.
Q-8	Unimolecular Decomposition Of Protonated Methanol Ions From Metastable Peaks In Chemical Ionization Mass Spectrometry. W. T. Huntress, Jr., M. T. Bowers, K. R. Jennings	376
Q-9	Thermal Energy Reactions Of $^{12}C^{+}(^{2}P)$ And $^{13}C^{+}(^{2}P)$ Ions With Hydrocarbon Molecules. R. D. Smith, J. H. Futrell	377
Q-10	Vibrational Energy Transfer In Excited Ionic Species: Rates And Mechanism Of Dimerization Of Protonated Nitrogen Bases. M. T. Bowers, W. R. Davidson, T. Su, L. Bass, P. Neilson, D. H. Aue	379
Q-11	Reaction Of Ground State C^{+} Ions. V. G. Anicich, W. T. Huntress, J. H. Futrell	380
Q-12	The Temperature Dependence Of A Third Order Rate Constant As A Function Of The Complexity Of The Third Body. L. Su, L. I. Bone	383
R-1	Quantitative Field Desorption Mass Spectrometry (FDMS) Using Computer Controlled Selected Ion Monitoring. G. W. Wood, R. C. Charlton, D. E. Hagge	385
R-2	Field Desorption And Chemical Ionization Analysis Using Double Beam Mass Spectrometers. H. R. Morris, K. R. Compson, R. A. McDowell, D. Hazelby	387
R-3	Application Of Quantitative Field Desorption Mass Spectrometry (FDMS) To Determination Of Human Fetal Lung Maturity. R. C. Charlton, K.-L. Kan, P.-Y. Lau, L. Linnell, G. N. S. Rao, G. W. Wood	390
R-4	Field Desorption Sensitivity Measurements. J. C. Cook, Jr., K. L. Olson, K. L. Rinehart, Jr.	393
R-5	GC-CI-MS Multiple Ion Monitoring Quantitative Analysis Of 1- -acetyl Methadol (LAAM) In Biological Samples. T. A. Jennison, B. S. Finkle	394
R-6	Phosphazenes: High Molecular Weight Reference Compounds. K. L. Olson, J. C. Cook, Jr., K. L. Rinehart, Jr.	395
R-7	High Resolution Field Desorption Mass Spectrometry Of Oligonucleotides. H-R Schulten, H. M. Schiebel	396

Paper No.		Page No.
R-8	Mass Spectral Analysis Of The Carbohydrate Portion Of CEA. W. C. Schnute, Jr., J. E. Coligan, D. G. Pritchard, C. W. Todd	399
R-9	Structure Elucidation Of Alkylated Nucleosides. C. Fenselau	402
R-10	Human Vaginal Secretions: Identity And Cyclical Changes In Small Orgainc Constituents By GC-MS. G. Preti, G. R. Huggins, R. L. Doty	403
R-11	Mixture Analysis By Mass Selection And Collision Induced Dissociation. T. L. Kruger, J. F. Litton, R. G. Cooks	404
R-12	Comparison Of Techniques Of Collecting Breath CO_2 For Isotopic Analysis. D. A. Schoeller, P. D. Klein	407
S-1	Design Considerations Of GC/MS System Incorporating Glass Capillary Columns. G. W. Eaves, J. R. Reeher	409
S-2	A New Integrated Real-Time Glass Capillary GC/MS: Performance Specifications And Biomedical And Environmental Applications. T. Taylor, A. L. Burlingame, Y. Katoh, T. Noda	410
S-3	Thermogravimetric (TG)- Gas Chromatographic (GC)- Mass Spectrometric (MS) Instrumentation For Material Evaluation. D. L. Geiger, G. A. Kleineberg	411
S-4	An In-Situ Sampling System For Thermo-Head-Space-Analysis Of Non-Volatile Materials Using A GC/MS/Data System. J. Shen	412
S-5	An Efficient Interface For Combined Liquid Chromatography/ Mass Spectrometry Analysis. W. H. McFadden, H. L. Schwartz	413
S-6	LC/MS/COM Using An Unchanged Commercially Available Quadrupole Mass Spectrometer. J. D. Henion	414
S-7	A Very Rapid Heating CIMS Probe For The Evaporation Of Fragile Moleucles. R. C. Pierce, L. Friedman	416
S-8	Design And Performance Of An Advanced Dual-Purpose EI/CI Ion Source For A Quadrupole GC/MS. J. R. Reeher, R. D. Smith, M. S. Story	417

Paper No.		Page No.
S-9	Analysis Of Mixtures By Collisional Activation (CA-DADI) Of Ions By Chemical Ionization. S. Meier, U. Rapp, W. A. Wolstenholme	418
S-10	Atmospheric Pressure Chemical Ionization Studies Using A Hypersensitive Trace Gas Analyser. N. M. Reid, J. B. French, C. C. Poon, J. A. Burkley	422
S-11	Applications Of Atmospheric Pressure Ionization To Species Of Atmospheric Interest. M. W. Siegel	425
S-12	A Negative Ion Source For Detection Of Trace (PPT) Electrophilics In Air. R. K. Gould, W. J. Miller	426
T-1	Formation Of Dissociation Of Hydrogen Negative Ions H_2^-, H_3^-, And H^{2-}. R. Schnitzer, M. Anbar	427
T-2	Structures, Exothermicities, Rates And Temperature Coefficients, In H^- Transfer Reactions. M. Meot-Ner, F. H. Field	431
T-3	Orbital Ionization Energies And Molecular Properties. Proton Affinities And Photoelectron Spectra Of Nitriles. R. H. Staley, J. E. Kleckner, J. L. Beauchamp	432
T-4	Proton Affinities Of Monosubstituted Benzenes. Y. K. Lau, P. Kebarle	433
T-5	Hydrated Carbenium Ions, Protonated Alcohols ROH_2^+ And Acid Catalyzed Dehydration Of Alcohols As Studied In A Pulsed High Pressure Ion Source. K. Hiraoka, P. Kebarle	434
T-6	Charge Transfer Reactions In Alkane And Cycloalkane Systems Estimated Ionization Potentials. S. G. Lias, P. Ausloos, Z. Horvath	435
T-7	Ion-Molecule Reactions Involving Halomethyl Ions; Heats Of Formation Of Halomethyl Ions. S. G. Lias, P. Ausloos	437
T-8	Stabilities Of Unsaturated Carbocations. W. R. Davidson, D. H. Aue, M. T. Bowers	439
T-9	Association Of H_2O To $H^+(H_2O)_n$ Between 80 And 120K For $I < n < 60$. R. Thomas, R. R. Burke	442

Paper No.		Page No.
T-10	Conservation Of Spin Angular Momentum In Proton-Transfer Reactions Involving $C^{-4}(S)$. K. Tanaka, L. D. Betowski, G. I. Mackay, D. K. Bohme	443
T-11	A High Pressure Mass Spectrometric Study Of Ion-Molecule Reactions In C_2H_5F And C_2H_5Cl. H. S. Tan, M. J. K. Pabst, J. L. Franklin	445
T-12	Binding Energies Of $(\eta^5\text{-}C_5H_5)Ni^+$ To n-Donor Ligands In The Gas Phase By Ion Cyclotron Resonance Spectroscopy. R. R. Corderman, J. L. Beauchamp	446
T-13	Gas Phase Ion Chemistry Of Chloromethanes And Chlorosilanes. R. D. Kinser, A. H. Moskowitz, M. de Angelis, D. P. Ridge	447
T-14	Photochemistry Of Weakly Bound Li^+ Complexes In The Gas Phase. A Novel Probe Of Charge Distribution And Acid-Base Properties Of Excited Electronic States. B. S. Freiser, R. H. Staley, J. L. Beauchamp	449
T-15	Ion-Molecule Reactions In Systems Of Metal Carbonyls With Alkyl Halides And Alcohols - An ICR Study. J. Allison, D. P. Ridge	450
U-1	Gas Chromatography-Mass Spectrometry Of Boronate Esters Of Sphingosines And Related Compounds. S. J. Gaskell, C. J. W. Brooks	452
U-2	GC-MS Of Methylated Steroids. A. L. C. Smit, A. P. de Jong, P. A. Leclercq	455
U-3	Mass Spectrometric Studies Of A New Mechanism Of Drug Biotransformation In Rats. I. Matsumoto, T. Kuhara, Y. Inoue, S. Haraguchi	457
U-4	Studies Of Novel Dipeptide Derivatives With GC/MS. H. Frank, K. D. Haegele, D. M. Desiderio	459
U-5	Quantitative Analysis Of Biological Samples Using HPLC-MS Techniques. P. L. Gutshall, P. J. Bryant, J. L. Valentine, O. H. M. Gan, H. C. Niu.	461
U-6	Polypeptide Sequencing Using Liquid Chromatography/Mass Spectrometry. B. G. Dawkins, F. W. McLafferty, R. Venkataraghavan	462
U-7	Mass Spectrometric Analysis Of Anticonvulsant And Related Drugs After Separation By High Pressure Liquid Chromatography. S-N Lin, E. C. Horning, M. G. Horning	463

Paper No.		Page No.
U-8	Identification Of Liquid Chromatography Effluents By Mass Spectrometry. R. P. Lattimer, K. R. Welch, J. B. Pausch	464
V-1	Spectral Analysis Of Coal-Derived Fuels: An Overview. A. G. Sharkey, Jr.	466
V-2	Field Ionization-Field Desorption Determination Of Molecular Weight Profiles Of Coal Liquef tion Products. M. Anbar, E. Kempster, M. Scolnick, G. St. John	467
V-3	Biomarker Hydrocarbon Identifications In The Pyrolysis Oil Of Hiawatha Coal Using GC-MS-C. J. C. Bendoraitis, B. Tissot, F. Bienner	470
V-4	Group-Type Analysis Of The Aromatic Fraction Of Products From The Catalytic Liquefaction Of Coal. H. T. Best, A. B. Marcus	475
V-5	Mass Spectral Characterization Of Heavy Coal Liquefaction Products. T. Aczel, H. E. Lumpkin	478
V-6	Mass Spectrometric Analysis Of Coal Liquids And Their Hydrogenation-Hydrogenolysis Products. S. E. Scheppele, G. J. Greenwood, P. L. Grizzle T. D. Marriott, N. B. Perreira	482
V-7	Compositional Analyses Of Synthoil From West Virginia Coal. P. W. Woodward, G. P. Sturm, Jr., J. W. Vogh, S. A. Holmes, J. E. Dooley	487
V-8	Spectral Characterization Of Shale Oils Produced By In Situ Retorting. J. H. Weber	490
W-1	Energetics Of Negative Ions From The Group VA Pentahalides. R. E. Pabst, J. L. Margrave, J. L. Franklin	491
W-2	Endoergic Collision Of I^- On Cyanogen And Nitrosyl Chloride. K. M. A. Refaey	492
W-3	Electron Attachment In CBz-Amino Acid Methyl Esters. C. L. Brown, A. F. T. Chen	493
W-4	Negative Ion Mass Spectrometry Of Some Fatty Acid Derivatives. C. L. Brown, C. L. Chan	494
W-5	Apparent Activation Energies In Gas-Phase Reactions Of Anions With Halogenated Methanes At $297 \pm 2^{o}K$. K. Tanaka, G. I. Mackay, J. D. Payzant, D. K. Bohme	495

Paper No.		Page No.
W-6	Negative Ion Chemical Ionization Spectra Of Some Aromatic Compounds. R. K. Mitchum, A. G. Harrison, A. J. Ferrer-Correia, K. R. Jennings	496
X-1	The Effect Of Sample Purity On Mass Spectrometric Isotope Ratio Measurements. J. W. Gramlich	498
X-2	Chemical Techniques For The Reduction Of The Chromium Analytical Blank For Isotope Dilution Analysis. L. P. Dunstan, E. L. Garner	500
X-3	Isotope Dilution Analysis Of Synthetic Water Standards Using Electronic Detection SSMS. P. J. Paulsen, J. R. Moody	501
X-4	Modification Of An A.E.I. MS7 Spark Source Mass Spectrograph For Increased Plate Resolution. M. L. Jacobs, S. L. Sweeney, E. G. Kerfoot	504
Y-1	Analytical Applications Of A Drift Tube CI Source. P. Price, H. S. Swofford, Jr., S. E. Buttrill, Jr.	505
Y-2	Reagent Gases For Negative Ion Chemical Ionization Mass Spectrometry. D. F. Hunt, T. Harvey, T. Knudsen	509
Y-3	Ammonia Chemical Ionization Of Some Free Amino Acids And Underivatized Peptides. J. S. Gaffney, R. C. Pierce, L. Friedman	510
Y-4	Reactions Of Lysine Under Chemical Ionization Conditions. R. J. Weinkam, J. D'Angona	511
Y-5	An Ion Cyclotron Resonance Investigation Of Chemical Ionization Reactions Of Ketones. D. P. Ridge, R. H. Dianich	513
Y-6	Determination Of The Site Of Protonation In The Water Chemical Ionization Of Aromatic Compounds. D. P. Martinsen, S. E. Buttrill, Jr.	516
Y-7	Structural Effects On Water Cluster Ion Formation In The Water CI Spectra Of Simple Aromatic Compounds. D. P. Martinsen, S.E. Buttrill, Jr.	517
Y-8	Ion Molecule Reactions Of Copper Acetylacetonate (ACAC). J. G. Dillard, G. H. Weddle, T. C. Rhyne	520

Paper No.		Page No.
Y-9	Application Of CI Fragmentation To Structural Elucidation. T. Chang	521
Y-10	Forensic Identification Of Drug Mixtures By Chemical Ionization Mass Spectrometry. S. Zitrin, J. Yinon	522
Y-11	Resonance Electron Capture Negative Ion Chemical Ionization Mass Spectrometry. D. F. Hunt, F. Crow, J. Lambrecht	527
Y-12	Mechanism Of The Ion-Molecule Reactions And Proton Affinity Of Phosphirane And Phosphirane-d_5. Z. C. Profous, K. P. Wanczek, H. Hartmann	528
Y-13	Ion-Molecule Reactions In Thiols And Thioethers. J. E. Kronberg, J. A. Stone	531
Y-14	The Ion Chemistry In Organic RF Discharges: Ethylene. M. J. Vasile, G. Smolinsky	533
Y-15	Use Of Molecular Sieve Pellets As A Source Of CI Reagent Gas Or Additive Within The Solid Sample Probe. S. E. Buttrill, Jr., R. Olson	534
Z-1	Mass Analyzer For Trace Gas Analysis. C. M. Judson, G. Wood, P. Yeager	537
Z-2	Ion Optics Using Resistive Lenses. M. W. Siegel	540
Z-3	Modification Of A Mattauch-Herzog Mass Spectrometer For Medium Resolution Ion Kinetic Energy Spectrometry. R. Ryba, G. J. Mains	543
Z-4	Voltage Scanning Of A Double Focussing Mass Spectrometer Under Computer Control. K. B. Denson, S. P. Taylor, J. M. Hayes	548
Z-5	Computerized Routine Mass Fragmentography Of Some Transmitter Metabolites. C. G. Fri	551
Z-6	Mass Spectrometry Of Nonvolatile Materials And Solutions By The Particulate Impact Technique. F. T. Greene	552
Z-7	Direct Air-Sampling Inlet For Surface Ionization Mass Spectrometry Of Airborne Particles. J. J. Stoffels	553

Paper No.		Page No.
Z-8	Extending The Detection Limits Of Mass Spectrometers By Erasing Background And Memory Peaks By Sample Beam Modulation. L. F. Herzog, T. J. Eskew	554
Z-9	Velocity Distribution Effects Observed Using Modulated Molecular Beam Inlets. M. J. Vasile, F. A. Stevie	559
Z-10	Estimation Of Ionization Potentials Of Heavy Elements Using A Pulse-Counting Mass Spectrometer. R. S. Newbury	560
Z-11	High Temperature Gas-Solid Interaction Studies. G. D. Blue, S-Y Tang, E. J. Rolinski	561
Z-12	Stability Of Complex Gaseous Cerium And Cerium-Ruthenium Carbides. K. Gingerich, D. L. Cocke, J. E. Kingcade	562
AA-1	Computer Simulation Of The Quadrupole Mass Filter. J. E. Campana, T. H. Risby, P. C. Jurs	563
AA-2	Theory Of Mass-Discrimination Effects In Ion Extraction From A Continuum Plasma. J-S Chang, J. G. Laframboise, K. Kodera	564
AA-3	Measurement Of The Secondary Electron Distributions From Polyatomic Ion Impacts In The Energy Rance $\leq$ 100 KV: Theory And Practice. R. J. Beuhler, L. Friedman	567
AA-4	Preliminary Results With An Electro-Optical Ion Detector (EOID) On A Focal Plane Mass Spectrometer. C. E. Giffin, D. D. Norris, H. G. Boettger	568
AA-5	Instrumentation For The Simultaneous Recording Of Positive And Negative Ion Chemical Ionization Mass Spectra*. D. F. Hunt, G. C. Stafford, F. Crow, J. W. Russell	571
AA-6	Collisional Activation (CA) Spectra Of Gaseous Organic Ions. C. Koppel, T. Wachs, F. M. Bockhoff, B. Van De Graaf, P. P. Dymerski, F. W. McLafferty	572
PSA-1	Statistical Analysis Of Elimination Curves Obtained From The Microdistillation Of Mixtures. R. D. Grigsby, E. J. Norman, J. S. Richardson	573
PSA-2	Mass Spectrometric Identification Of The Non-Saponifiable Lipids Of Eimeria Tenella Oocysts. W. J. A. VandenHeuvel, C. C. Wang, R. M. Weppelman	574

Paper No.		Page No.
PSA-3	Chemical Ionization Mass Spectrometry Of Amino Acid-Fluorescamine Derivatives. J. J. Shieh, K. Leung, D. M. Desiderio	575
PSA-4	The GLC/CI/MS Determination Of Lithocholic Acid And Its Potential Metabolites. G. M. Muschik, L. H. Wright, J. A. Schroer, W. L. Zielinski, Jr.	576
PSA-5	Identification Of Acidic Metabolites Of Corticosteroid By Mass Spectrometry. H. J. Lee, J. Roboz, C. Monder	578
PSA-6	Aromatic Hydroxylation Of A Deuterated Ellipticine In Rats: Lack Of An NIH Shift. R. J. Bruni, V. N. Reinhold, A. D. Little	581
PSA-7	Evaluation Of Isotopic Variants Of 3-Methoxy-4-Hydroxy-Mandelic Acid (VMA) For Selected Ion Recording. S. P. Markey, M. Claeys, K. Powers, M. Ebert	584
PSA-8	Mass Spectrometric Characterization Of 2-Azahypoxanthine: An *in vivo* Diazotization Product Of Biogenic 4-Aminoimidazole-5-Carboxamide. B. M. Johnson, G. M. Lower, Jr., S. P. Lanphear	585
PSA-9	Determination Of Drug Concentration In Serial Body Fluid Samples From Drug Intoxicated Patients By Mass Spectrometry. D. C. K. Lin, R. L. Foltz, S. M. Cattaneo	588
PSA-10	Quantitation Of Amino Acids In Physiological Fluids Using ^{13}C Mass Fragmentography. W. E. Pereira, P. J. Anderson, E. T. Everhart, T. C. Rindfleisch, A. M. Duffield	590
PSA-11	Mass Spectrometry Of 3-Methoxy Fatty Acid Methyl Esters Origin Of The Base Peak At M/e 75. J. A. Zirrolli, R. C. Murphy	591
PSA-12	Isotope Dilution Analysis Of Drugs And Metabolites Using Field Ionization Mass Spectrometry. M. Anbar, R. Dyer, G. Gonser, H. Heck, K. Maloney, J. McReynolds, R. Sperry	593
PSA-13	Applications Of CO_2 Carbon Isotope Ratio Mass Spectrometry In Clinical Chemistry. D. A. Schoeller, P. D. Klein, J. F. Schneider, N. W. Solomons, J. B. Watkins	594
PSA-14	Di-Alkaneboronates With Non-Identical Side Chains. Applications In Mass Spectrometry Of Carbohydrate Derivatives. J. Wiecko, W. R. Sherman	596

Paper No.		Page No.
PSA-15	SIM Determination Of Inositol In Single Cells Of The Central Nervous System. W. R. Sherman, M. H. Laird, R. Boshans, P. Packman	598
PSA-16	A Combined Radio Gas Chromatography/Mass Spectrometer (RGC/MS) Detects Intermediates In Mycophenolic Acid Biosynthesis. C. P. Nulton, J. D. Naworal, I. M. Campbell	601
PSA-17	Simultaneous Quantitation Of Glycine, γ-Amino Butyrate, Glutamate, And Aspartate In Neural Tissue Using CI-GC-MS-COM. F. Petty, J. G. Wood, N. Flynn, J. D. Wander	604
PSA-18	The Potential Of Ion Traps For Analysis. R. T. McIver, Jr., E. B. Ledford, Jr., R. L. Hunter	605
PSA-19	A GC-MS-COM System To Monitor Metabolic Switching Of Drug Pathways. K. R. Sommer, J. P. Thenot, K. Haegele, J. Nowlin, M. Stafford, M. G. Horning	606
PSA-20	Mass Spectral Analysis Of Glutethimide Metabolites. W. G. Stillwell, M. G. Horning, W. Riess, H. Keberle	607
PSA-21	Quantitation Of Cancer Chemotherapeutic Agents: Cyclophosphamide And Its Active Metabolites By GC-CIMS. I. Jardine, M. Colvin, C. Fenselau	608
PSBI-a	Chemical Ionization And Electron Impact Mass Spectra Of 5,6 Dihydro-2-Methy -1,4-Oxathiin 3-Carboxanilid And Its Metabolites. F. I. Onuska, A. G. Harrison	610
PSBI-c	Identification Of Trace Contaminants In Environmental Samples By Two New Techniques: 1. Selected Ion Summation Profile Analysis Of Computerized GC/MS Data 2. Dual-GC/MS/COM Operation For The Analysis Of Different Sample Types. D. W. Kuehl, G. D. Veith	612
PSBI-d	Identification And Estimation Of N-Nitrosodimethylamine In Ambient Air By Gas-Liquid Chromatography-Mass Spectrometry-Computer. E. D. Pellizzari, J. E. Bunch, R. E. Berkley, J. Bursey	613
PSBI-e	GC/MS Analysis Of Products From The Catalyzed Dechlorination Of DDT And Heptachlor. W. J. Cooper, W. H. Dennis, Jr.	616
PSBI-f	Sampling And Characterization Of Air For Organic Compounds. R. D. Kleopfer, W. W. Bunn, B. Haas, E. R. Deane	617

Paper No.		Page No.
PSBI-g	Low-And High-Resolution Gas-Chromatography/Mass Spectrometry (GC/MS) Method Of Analysis For The Presence Of 2,3,7,8-Tetrachlorodibenzo-P-Dioxin (TCDD) In Environmental Samples. R. L. Harless, E. O. Oswald	618
PSBI-h	Analysis Of Sulfuric Acid By Mass Spectrometry. T. M. Harvey, T. J. Prater, D. Schuetzle	621
** PSBI-i		
PSBII-a	Identification Of The Origin Of Oil Spills By Field Ionization Molecular Weight Profile Analysis. M. . Scolnick, A. C. Scott, M. Anbar	629
PSBII-b	Mass Spectrometric Analyses Performed On Samples Of Ethylene BIS Isothiocyanate Sulfide (EBIS). R. L. Harless, E. O. Oswald	633
PSBII-c	Potential Use Of GC/MS In Regulatory Confirmation Of Sulfonmaide Residues In Animal Tissue. J. Anderson, J. D. King	636
PSBII-d	Toxaphene Analysis By Computerized Gas Chromatography-Mass Spectrometry. W. L. Budde, J. W. Eichelberger	637
PSBII-e	Spark Source Mass Spectrometric Analysis Of Air Pollution Particulates. E. H. Daughtrey, Jr.	638
PSBII-f	GC-MS Analysis Of Tetrachlorodibenzodioxin. D. L. Smith, F. Hileman, J. Futrell	641
PSBII-g	Aflatoxin Detection Using High Resolution Selected Ion Monitoring. W. F. Haddon	644
PSBII-h	Direct Monitoring Of Air Pollutants By Field Ionization Mass Spectrometry. G. A. St. John, M. Anbar	645
PSBIII-a	An Improved System For Selected Ion Recording. W. F. Holmes, P. D. Norberg, R. W. Scheifler	646
PSBIII-b	Real Time GC/MS Data Acquisition And Processing. D. E. Hagge, J. R. Karnofsky, E. J. Gallegos	648
PSBIII-c	Programmable Selected Ion Monitoring In GC-MS. J. T. Watson, D. R. Pelster	649
PSBIII-d	An On-Line Computer Controlled System For Ion Microprobe Automation. M. C. Gregory, J. D. Stein, H. A. Storms	651

** Page 29

Paper No.		Page No.
PSBIII-e	Automated Isotopic Analysis Using A Programmable Calculator. T. L. Futrell	654
PSBIII-f	Ion-Counting Interface For LKB-9000 Mass Spectrometer. R. N. Stillwell, D. I. Carroll, S. S. Bates, J. R. Jenkins	655
PSBIII-g	Data Systems For A Chemical Ionization Mass Spectrometer. S. E. Buttrill, Jr., R. Olson	657
PSCI-a	Ion Kinetic Energy Spectra Of Alkyl-Substituted Thiophenes. R. Ryba, G. J. Mains	660
PSCI-b	Kinetic Study Of Heterogeneous Reactions By Linear Temperature Programming. M. A. Frisch	667
PSCI-c	Stress Mass Spectrometry Of Polymeric Materials. M. A. Grayson, R. L. Levy, D. L. Fanter, C. J. Wolf	668
PSCI-d	A Mechanistic Study Of The Electron Impact Reactions Of Substituted Bicyclophosphates And Bicyclophosphites. K. J. Voorhees, F. D. Hileman, T. A. Elwood, J. H. Futrell	671
PSCI-e	Applications Of Pyrolysis GC-MS To The Analysis Of Polymers And Other Compounds Adsorbed On Inorganic Substrates. H. M. Curtis, Jr., R. B. Twelves	674
PSCI-f	EI And CI Mass Spectra Of Alkyldiphenyl-Phosphine Oxides. B. L. Jelus, S. D. Goff, E. E. Schweizer	677
PSCI-g	Cycloreversion Reactions In The Mass Spectra Of Various Tetralins. M. L. Gross, F. R. DeRoos	678
PSCI-h	Hydrogen-bonding Effects In The Mass Spectra Of Phenylpyridylketoximes. T. L. Folk, L. G. Widemann	679
PSCI-i	Mass Spectrometric Analysis Of Polyoxymethylenes. R. Schubert	680
PSCII-a	Hydrogen-Deuterium Exchange In Water Vapor: The Mass Spectrometric Sensitivities And The Equilibrium Constant. J. W. Pyper, R. J. Dupzyk, R. D. Friesen, S. L. Bernasek, C. A. May, A. W. Echeverria, L. F. Tolman	681
PSCII-b	On The Measurement Of Trace Concentrations Of Carbon And Oxygen In Solids By SSMS. D. L. Dugger, D. W. Oblas	682

Paper No.		Page No.
PSCII-d	Mass Spectral Studies Of Ploymeric Sulfur Nitride. J. R. Wyatt, J. J. DeCorpo, R. D. Smith, F. E. Saalfeld	685
PSCII-e	An Evaluation Of A Thermal Ionization Mass Spectrometer Using A NBS System Calibration Procedure. V. E. Connolly, E. L. Callis, A. W. Summers	690
PSCII-f	Pyrolysis-GC-MS Techniques In Organic Geochemistry. J. G. Lawless, F. M. Church	691
PSCII-g	Mass Spectra Of Some Salts Of Carboxylic Acids With Group Ia Metals. E. White, V.	692
PSCII-h	Mass Spectra Obtained By The SRI Field Desorption Source. G. A. St. John, M. Anbar	695
PSCIII-a	Power Emission: A High Performance Detection System For Ion Cyclotron Resonance Spectroscopy. R. L. Hunter, E. B. Ledford, Jr., R. T. McIver, Jr.	698
PSCIII-b	A Novel Scanning-Storage System For Magnetic Mass Spectrometers. G. S. St. John, C. Biltz, M. Anbar	699
PSCIII-c	Conversion Of Hitachi RMU-6D to GC/MS With Solid State Electronics And Differential Pumping. R. A. Upham	700
PSCIII-d	Solid State Magnetic Scanning Unit For Mass Spectrometer. H. Bishop, J. Sharp, P. V. Fennessey	703
PSCIII-e	GC/MS Interfacing Simplified And Quantified. J. P. Lehman, R. A. Day	706
PSDI-a	Studies In GC/CIMS. F. Hatch, B. Munson	710
PSDI-b	A Qualitative And Quantitative Comparison Of EI Ionization And CI Using Various Reagent Gases. R. L. Foltz, D. C. K. Lin	711
PSDI-c	Alkali Ion Chemical Ionization Mass Spectrometry. R. V. Hodges, J. L. Beauchamp	719
PSDI-d	A Mechanistic Study Of The Ammonium Ion In Chemical Ionization Mass Spectrometry. D. Jerolamon, J. S. Smith, D. E. Smith, E. J. Brozowski	720

Paper No.		Page No.
PSDI-e	Quantitative Analysis Of Ethylene Glycol Impurities By G.C.-C.I. Using Ammonia As The Carrier And Reagent Gas. J. S. Smith, D. E. Smith, D. Jerolamon, E. J. Brozowski	721
PSDI-f	Industrial Applications Of Chemical Ionization With The Ammonium Ion. D. E. Smith, J. S. Smith, D. Jerolamon, E. J. Brozowski	722
PSDI-g	Gaseous Ionic Reactions And The Proton Affinity Of No_2. C. Polley, B. Munson	723
PSDI-h	SIQMS Secondary Ion Quadrupole Mass Spectrometer. C. W. Magee, W. L. Harrington, R. E. Honig	725
PSDII-a	Energetics Of Formation Of $R'CO_2H_2^+$ In The Mass Spectra Of $R'CO_2R$. A. G. Harrison, F. M. Benoit, F. P. Lossing	728
PSDII-b	Gas Phase Reactions Of Metal-Containing Ions In Mixtures Of $TiCl_4$ With Alkenes. J. Allison, D. P. Ridge	729
PSDII-c	The Effects Of Methyl Substitution On Negative Ion Stability. J. E. Bartmess, R. T. McIver, Jr.	731
PSDII-d	The Gas Phase Acidity Scale. J. E. Bartmess, R. T. McIver, Jr.	732
PSDII-e	Relative Stabilities Of Carbonium Ions, $(CH_3)_nF_{3-n}C^+$, And Siliconium Ions, $(CH_3)_nF_{3-n}Si^+$, (n=0-3) In The Gas Phase By Ion Cyclotron Resonance Spectroscopy. M. K. Murphy, J. L. Beauchamp	733
PSDII-f	Li^+ Binding Energies By Ion Cyclotron Resonance Spectroscopy. R. Woodin, J. L. Beauchamp	734
PSDII-g	Analysis Of Ion-Loss Mechanisms In A Magnetic Ion Trap. M. B. Ruggera, Jr., R. T. McIver, Jr.	735
PSDIII-b	Production Of H_2O^+ In The Ground Electronic State Using Energy-Resolved Electron Beams. P. L. Grizzle, S. E. Scheppele	736
PSDIII-c	Photodissociation Study Of Parent Ions Of Styrene, Cyclooctatetraene And Three C_9H_{10} Hydrocarbons. E. W. Fu, R. C. Dunbar	739
PSDIII-d	Crossed Beam Techniques For Studying Energy Transfer Process In Ion-Molecule Reactions. M. L. Vestal, C. R. Blakley, J. H. Futrell	746

Paper No.		Page No.
PSDIII-e	Negative Ions Production In Co_2, NO_2, SO_2 And TlCl By Electron Impact With A High Resolution Electron Beam. R. Abouaf, J. P. Ziesel, F. Fiquet-Fayard	742
PSDIII-f	Internal Energy Distribution In The Products Of Charge-Transfer Between He^+ And Rare Gases. E. G. Jones, B. M. Hughes, D. C. Fee, T. O. Tiernan	743
PSDIII-g	Experimental And Theoretical Characterization Of The $N_2O^-(X^2A')$ Potential Energy Surface. D. G. Hopper, A. C. Wahl, R. L. C. Wu, T. O. Tiernan	744
PSBI-i	Capillary GC/High Accuracy Mass Spectrometric Analysis Of Exhaust Emissions From Methanol Fueled Cars. T. J. Prater, T. M. Harvey, D. Schuetzle	625

Computer Applications in Mass Spectrometry. A Review. K. BIEMANN, M.I.T., Dept. of Chem., Cambridge, Mass. 02139.

The use of computers in mass spectrometry has become commonplace over the last decade. The techniques for data acquisition and data processing have undergone an evolutionary development aiming towards increased sophistication and speed on the one hand or simplification (to reduce cost) on the other. These developments and the present state of the field will be critically reviewed.

Penning Ionization Electron Spectroscopy

Vladimir Čermák
The J.Heyrovsky Institute of Physical Chemistry and Electrochemistry,
Czechoslovak Academy of Sciences-Prague

I shall try to present a short survey of the socalled Penning Ionization Electron Spectroscopy (PIES). This is a technique based on the measurement of the energy of electron's released in the ionization of atoms and molecules by means of thermal particles in longlived excited states. The various types of electron spectroscopy are all based on the fact that in the particular ionization process only one electron appears among the ionization products. This is the case in photoionization (1) and among other reactions, also in Penning and Associative ionization (2) and (3):

$$h\nu + AB = AB^{+} + e \qquad (1)$$

$$X^{x} + AB = AB^{+} + e + X \qquad (2)$$

$$X^{x} + AB = XAB^{+} + e \qquad (3)$$

In photoionization (1) the energy of the released electron, E_e, is given by the energy balance:

$$E_e = E(h\nu) - IP(AB) - E_{j,v}(AB^{+})$$

where E(hv) is the known energy of the photon, IP(AB) is the first or higher ionization potential and $E_{j,v}(AB^{+})$ is the rotational and vibrational energy of the AB^{+} ion.

If, however, the same particle, e.g. the argon atoms, are ionized by metastable helium in the 2^1S (20.6 eV) and 2^3S (19.8 eV) states new phenomena appear as shown on Fig. 1. When compared with photoionization peaks at 5.45 eV and 5.28 eV the peaks due to Penning ionization are evidently broadened. Their centers are shifted positively (towards greater electron energy) by about 35 meV. In the ionization of H_2S (Fig.2) into the ionic $^2B_1$ ground state both peaks are shifted negatively (towards smaller energy) Fig.2. The peak of ionization by He(2^1S) atoms is both very broad and asymmetrical, and it is shifted more than the He (2^3S) peak. In the ionization of H_2O peak maxima are shifted by -820 meV and -360 meV negatively and the peak widths are especially great (Fig.3) . Peak shifts and broadening become, however, successovely smaller when Ne or Ar metastables are used instead of helium metastable atoms.

To take account of these facts, the energy balance equation for released electrons must be corrected by a term ΔE which accounts for the positive or negative shifts with respect to the nominal energy E_o:

$$E_e = E(X^{x}) - IP(AB) - E_{j,v}(AB^{+}) \pm \Delta E$$

$$E_e = E_o - E_{j,v}(AB^{+}) \pm \Delta E$$

The peak shifts and broadening must necessarily be connected with the nature of the collision which, in this case, is not the interaction with the electromagnetic field but a collision of two heavy thermal particles.

Accordingly Penning ionization electron spectroscopy aims at new goals: the main object is to investigate those factors which specifically modify the distribution of energy of the released electrons.

In Penning ionization the system during collision behaves like a quasi-molecule characterized by a certain probability of autoionization, W, which depends, in atomic systems, on the particle separation, R[1,2]:

$$X^x + AB \longrightarrow X^x AB \xrightarrow{W(R)} AB^+ + e + X .$$

The motion of the two particles during the collision is dominated by the interaction potential which changes with distance according to the schematic curve shown on Fig.4. The ionization itself is the vertical downward transition from the input channel curve for reactants, $V^x(R)$, to the output channel curve for products, $V^+(R)$. If the ionization transition occurred at very large separation where the interaction of the particles is zero the energy of the released electrons would be E_o. At smaller separations the energy is $E_e < E_o$, i.e., ΔE becomes negative. Close to the classical turning point or in it the energy might be $E_e > E_o + E_{kin}$ if the ionic curve is attractive at this separation. In such a case associated ionization takes place and rotationally and vibrationally excited complex ions XAB^+ are obtained. If the ionic potential energy curve is more attractive than the $V^x(R)$ curve in a certain range of particle separations associative ionization readily occurs (Fig.5). It might be followed by disociation if the primarily formed associated ions are highly rotationally and vibrationally excited.

The examples of potential energy curves show that the electron energy distribution curves are determined by the shape of both input and output curves and by the transition probability per unit time or transition frequency W(R)[1,2]. This means that PIES becomes a method which enables one, in optimal cases, to determine interaction potentials in collisions of excited particles with atoms or molecules if the broadness and shape of electron energy distribution curves are correctly interpreted. In this sense PIES is among the few methods for the determination of interaction potentials. Other methods include the studies of collisional broadening of optical spectral lines or the studies of rainbow effects in elastic scattering.

The classical, semiclassical and quantum mechanical theory of Penning ionization has been worked out already but only for atomic systems at present[1,2]. It enables one to calculate the ionization cross sections, the ratio of cross sections for Penning and associative ionization and their velocity and angular dependence, the electron energy distribution curves and the transition frequency W(R). In favorable cases the theory helps to determine $V^x(R)$, $V^+(R)$ and W(R) from experimental data (or at least the depth of the minimum on the potential energy curves). Some examples of the experimental distribution curves are shown on Fig.6.

If polyatomic molecules are ionized the electron energy distribution curve becomes more difficult to explain. The interaction potentials of re-

actants and products become generally anisotropic. The potentials of reactants may depend on the orientation of the molecules with respect to the relative velocity vector and may have dipole and quadrupole components. Also the interactions of not only reactants but also of the deexcited atoms with ions formed in different electronic states may differ considerably. Some of these effects are summarized on Fig. 7.

At present it is difficult to give the right explanation of the effects just described. The necessary potential energy surfaces are not known and even the equations for the calculation of the dispersion and dipolar energies in the interaction with excited particles are not available. This is a practically untouched field. One can give only a tentative explanation. The different peak shifts and peak forms could arise if the ionization frequency into various final states depended on the orientation of the molecules. This is a plaisible assumption because the shape of the molecular orbitals themselves is very different according to their type and symmetries. As the interaction potentials are orientation dependent peaks differing in shape and shifts might easily result

One striking example of this dependence is shown on Fig.8. It concerns the ionization of compounds containing the CN-group[4]. In Fig.8 the peaks of ionization of sigma electrons from the lone pair localized on the N atoms (peaks No.2 and No.3) are considerably enhanced and are very sharp. The ionization evidently takes place at very large particle separations where the interaction is still very small but the ionization probability has already become not negligible. Very probably the extended shape of the sigma lone pair orbitals localized on the N atoms is responsible for it. Such an effect does not exist if electrons from lone pairs localized on O atoms in formaldehyde, methylalcohol, water or dimethylether are ionized.

The PIES of molecules by the interaction with excited particles has already produced a number of other interesting results. As shown on Fig. 9, a group of sharp peaks appears on the distribution curve of COS, mostly at energies lower than 1 eV, which do not form any vibrational sequence and do not belong to any known electronic state of the COS^+ ions[3]. Similar peaks appear on the distribution curve of NO, O_2 and N_2O[5]. These peaks were plausibly ascribed to autoionization of highly excited neutral O atoms formed from primary excited molecules COS by dissociation according to the general process:

$$X^x + ABO = ABO^{xx} + X$$
$$ABO^{xx} = AB + O^{xx}$$
$$O^{xx} = O^+ + e$$

The atomic autoionizing states must have a lifetime longer than the time of collision and do ionize as free atoms. In this case PIES enabled one to determine the levels of autoionizing states of reactive atoms like O, N, Cl and Br even if the starting material was not free atoms but stable molecules like O_2, NO, N_2O, N_2, Cl_2, HCl and Br_2[6]. If the appearance of these ions were studied mass spectrometrically it would be difficult to distinguish wheather the atomic ions originated from dissociation of directly

formed molecular ions or from primary highly excited molecules according to the processes shown.

PIES is also capable of yielding data concerning the mechanism of ionization. It was suggested that Penning ionization is an electron exchange process in which the electron released originates not from the target particle but from the metastable projectile[1,2] (Fig. 10) According to this explanation Penning ionization is a sort of Auger transition taking place during the collision. This explanation was found correct at least for the ionization of atoms. To prove it spin polarized helium metastable 2^3S atoms were used. In ionization an electron was released whose polarization was the same as the spin polarization of the helium triplet state

This mechanism of ionization does not necessarily apply to all particles, especially to polyatomic molecules. Consider, for instance, the ionization of NO_2. This molecule is a free radical and it is plausible to expect that its interaction with triplet helium will be quite strong and negative shifts will be found. Contrary to this, sharp and unshifted peaks were registered[3]. Evidently the ionization must take place at great particle separation where the interaction potential is still very small. To explain the ionization at such a large distance one may invoke the great electron affinity of NO_2(2.36 eV). It favours the formation of the ion pair $He^+ + NO_2^-$ by an electron shift. However, the collision complex $He^+ + NO_2^-$ is unstable against autoionization. If the probability of autoionization becomes appreciable already at $R > R_c$ (Fig.11) then the starting He^x-NO_2 system will be ionized to the extent in which its wave function acquires ionic character, i.e. very near and at the crossing point R_c. In the vertical downward transition electrons with nominal energy E_o^c will be released and zero shifts will be found as is actually the case.

REFERENCES

1. A.Niehaus, Ber.Bunsen Ges.,77 (1973) 632.
2. H.Hotop, Rad.Research, 59 (1974) 379.
3. V.Čermák, J.Electron Spectrosc., in press.
4. V.Čermák and A.J.Yencha, J.Electron Spectrosc., 8(1976) 109.
5. V.Čermák, J.Electron Spectrosc., 6(1975) 135.
6. V.Čermák, J.Electron Spectrosc., 3(1974) 329.
7. L.D.Schearer and L.A.Riseberg, Phys.Rev.Letters 26(1971) 599.
8. P.J.Keliher, R.E.Gleason and G.K.Walters, Phys.Rev.A 11(1975) 1279.

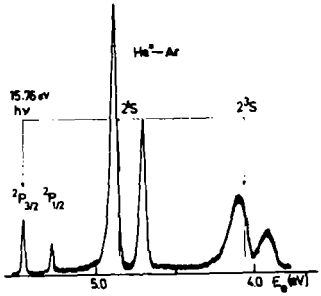

Fig.1

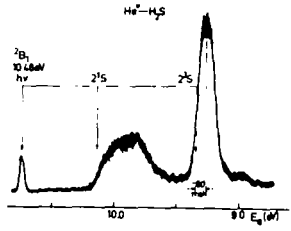

Fig.2

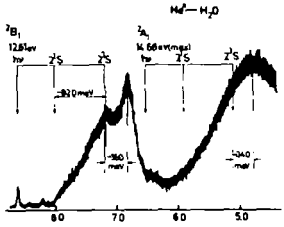

Fig.3

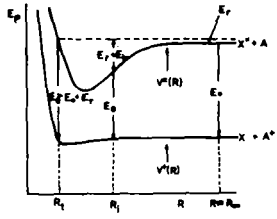

Fig.4

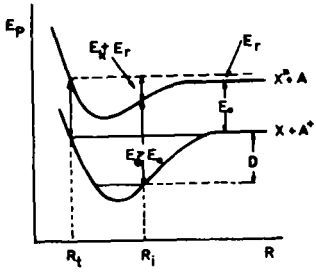

Fig.5

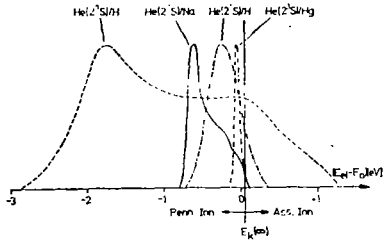

Fig.6

IONIZATION BY He(2¹S)
Shifts in meV

	$X^2\Pi$	$B^2\Sigma$	$C^2\Sigma$
N_2O	-85		-100
CO_2	-60	-90	-185
COS	-90	-45	-190

	$X^2\Pi$	$A^2\Sigma$
HCl	-145	-50

Fig.7

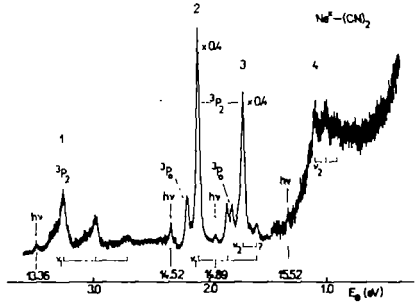

Fig.8

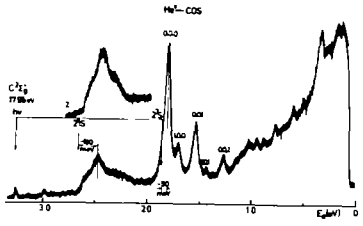

Fig.9

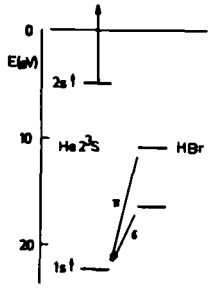

Fig.10

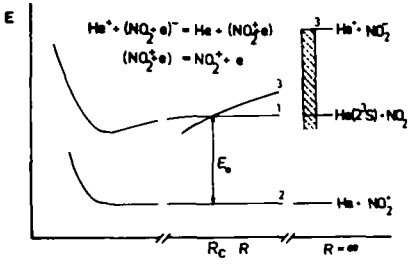

Fig.11

Fig.1 Ionization of Ar by photons (21.21 eV) and He (2^1S, 2^3S) atoms. Unshifted poditions of peak centers are indicated by arrows. The photoelectron peaks serve for scale calibration.

Fig.2 Ionization of H_2S by photons and helium metastables.

Fig.3 Ionization of H_2O by photons and helium metastables.

Fig.4 Schematic potential energy curves for the collision of X^x + A and X_+ A^+. E_r is the relative translational energy of the reactants X^x + A. In the text the notation E_{kin} is used.

Fig.5 Schematic potential energy curves explaining the occurence of associative ionization.

Fig.6 Experimental electron energy distribution curves for ionization of atoms[1,2].

Fig.7 Peak shifts in Penning ionization of some tri- and diatomic molecules into various final ionic states.

Fig.8 Ionization of $(CN)_2$ by neon metastables in the ^3P_o and $^3P_2$ states.

Fig.9 Ionization of COS into excited COS^+ states.

Fig.10 Schematic representation of the Auger transition in the Penning ionization of HBr.

Fig.11 Schematic representation of the Penning ionization of NO_2 by He(2^3S) atoms. Dashed region: ionization continuum of the $He^+ + NO_2^-$ pair. Curve 1: potential energy curve for reactants. Curve 2: potential energy curve for the $He^+ + NO_2^-$ pair.

ION-NEUTRALIZATION PHENOMENA AT SOLID SURFACES

Homer D. Hagstrum
Bell Laboratories
Murray Hill, New Jersey 07974

INTRODUCTION - My purpose in this lecture is to discuss one aspect of the field of particle-solid interactions, namely that comprising the interactions of particles carrying potential energy. When you excite or ionize an atom you store in it energy that can be reclaimed when the particle is deexcited or neutralized. If these phenomena occur at a solid surface the energy released can eject an electron from the solid in a process called potential ejection. This is one process which can occur at the low kinetic energy end of the spectrum of particle-solid interactions. Here the particle's kinetic energy is insufficient in itself to cause the processes to occur.

PROCESSES - We can conceive of three types of electronic transition process that can occur when an ion or excited atom approaches a solid surface. The first is radiative neutralization of an ion shown at the left in Fig. 1. This process is highly improbable because of its long lifetime, $\tau \sim 10^{-8}$ sec., compared to the resonance and the Auger processes which, having lifetimes $\tau \sim 10^{-14}$ sec., are of the order of 10^6 times faster. Two types of resonance tunneling process are shown at the middle and right of Fig. 1. In resonance neutralization an electron tunnels isoenergetically into an unfilled atomic level that lies opposite filled levels in the solid. Or, in a process called resonance ionization, an electron in the incoming atom can tunnel into unfilled states in the solid if its atomic level lies above the Fermi level of the solid.

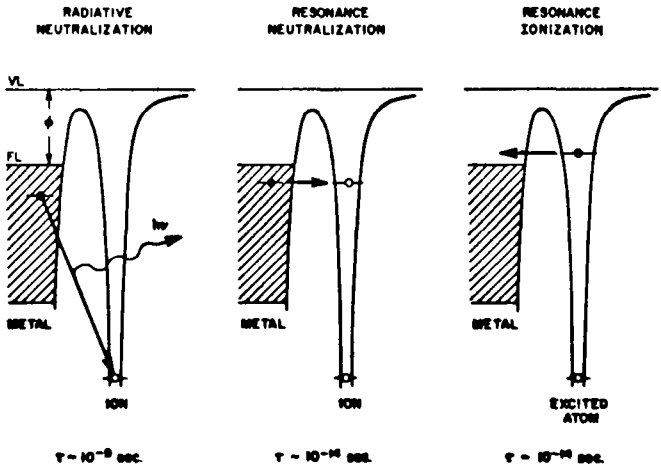

Fig. 1

In Fig. 2 are shown two Auger-type processes by means of which electrons are ejected from a solid by an ion or an excited atom. These are radiationless processes in which the down-transiting electron loses exactly the energy that the up-transiting electron gains. Some of these "up" electrons can leave the solid if properly directed relative to the surface. Their kinetic energy outside the solid is E as indicated in Fig. 2. ϕ in Figs. 1 and 2 is the work function of the metal.

The Auger processes of Fig. 2 have the same electron transition character as other Auger processes in solids or free atoms. In Fig. 3 the family of resonance and Auger processes of Figs. 1 and 2 are arranged in a "triangle" indicating their inter-relations. The charge and excitation state of the atomic particle X, the number of electrons in the metal e_M^-, and the free electron e^- are indicated for isoelectronic

systems in a form of "chemical" notation. It is possible to find systems where one can start at either upper corner and arrive at the bottom result by two paths. The kinetic energy of the free electron e^- will depend upon the process, however.

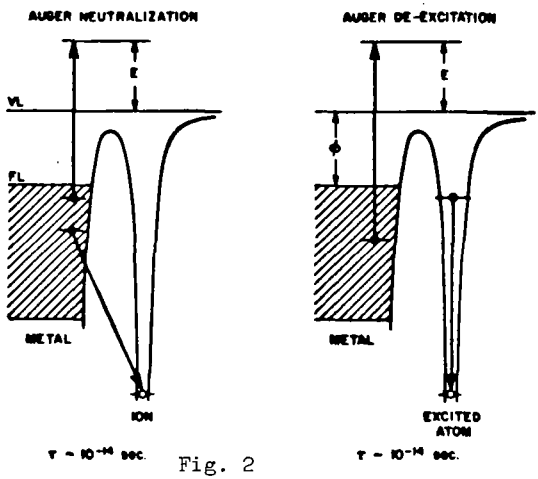

Fig. 2

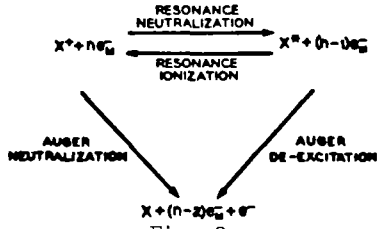

Fig. 3

APPARATUS - A number of types of apparatus have been developed for the study of ion-solid interactions.[1] The latest version is shown in Fig. 4.[2] Here at port 1 is the ion-neutralization apparatus consisting of a carefully focused ion beam produced by electron impact in a gas and the electron retardation spectrometer between electrodes S_1 and S_2. At port 2 sample processing by sputtering and evaporation can be done. At port 3 low-energy electron diffraction is applied to the surface as well as gas dosing and evaporation. At port 4 a resonance lamp and electron gun are provided for photoemission and Auger electron spectroscopy studies. The solid sample can be positioned at each port by rotating about axis A-A and the angle of incidence at the sample surface T varied by rotation about axis B-B. Ultrahigh vacuum conditions ($p \sim 10^{-10}$ Torr) prevail in the system and atomically clean surfaces or specifically "doped" surfaces can be produced. This apparatus is designed so that the specific surfaces produced can be studied and characterized by several surface tools and ion-solid interaction phenomena compared with photoemission from the same surface.

EXPERIMENTAL DATA - Representative data on electron ejection by the neutralization of singly-charged noble gas ions are shown in Figs. 5, 6, 7, 8. In Fig. 5 the total electron yield, γ_i, in number of electrons per

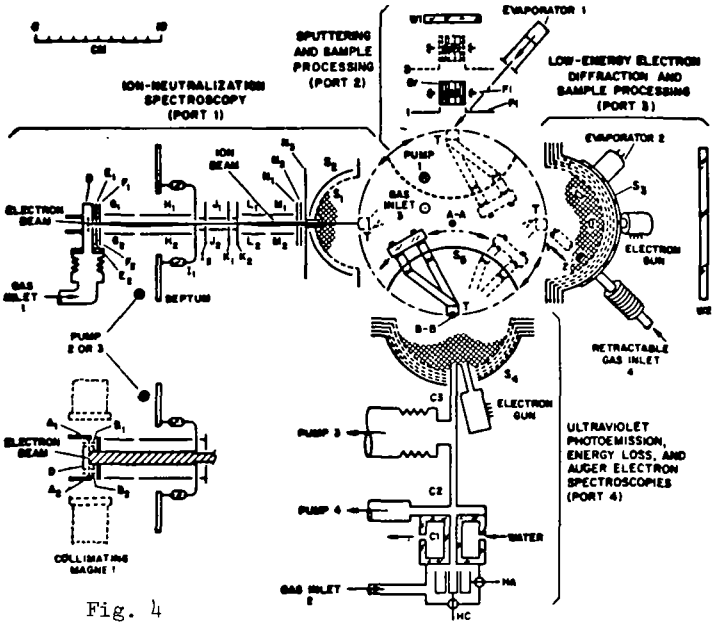

Fig. 4

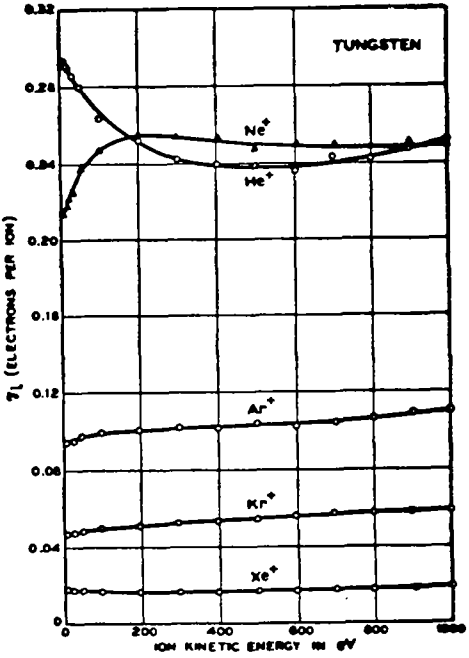

Fig. 5

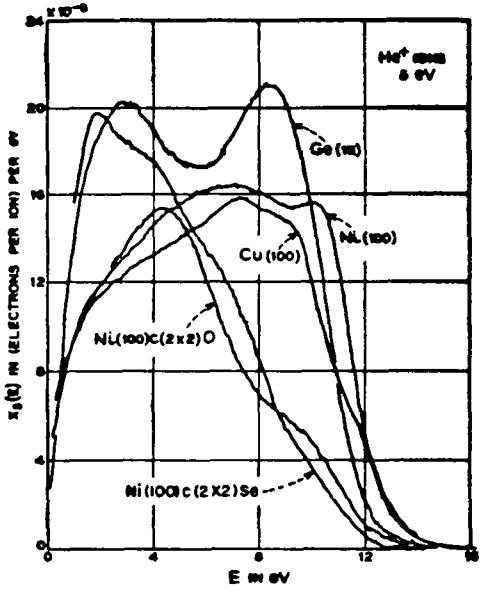

Fig. 6

incident ion is plotted as a function of ion kinetic energy from 10 to 1000 eV. Note that the yield is almost independent of kinetic energy indicating that the ejection process is caused by potential energy of the particle. This view is also buttressed by the decrease in γ_i with ionization energy, E_i, of the parent atom.

In Fig. 6 are shown kinetic energy distributions of electrons ejected by 5 eV He^+ ions from several atomically clean surfaces, Ni(100), Ge(111), and Cu(100), as well as from nickel surfaces, Ni(100)c(2×2)O and Ni(100)c(2×2)Se, with ordered overlayers of chalcogen atoms upon them. It is abundantly evident that the Auger neutralization process responsible for these ejected electrons is very surface sensitive and that the electron kinetic energy distributions contain spectroscopic information concerning the local density of electron states in the surface of the solid.

In Fig. 7 electron distributions from a Cu(110) surface for three different ions are shown. Note that the bump on the higher-energy side of the He^+ curve is reproduced in the Ne^+ and Ar^+ curves with the same placement relative to the $\zeta=0$ point for each curve. $\zeta=0$ is the position of top of the filled band in the solid. Energy broadening puts a "tail" of electrons above this point in each case. Finally, in Fig. 8 the variation of electron distribution with ion incident kinetic energy, K, is shown for He^+ incident on the surface Ni(100)c(2×2)Se. As K increases energy broadening increases with ion energy but the general structures remain.

THEORY - There are two types of energy diagram that are helpful in understanding any of the processes of Fig. 3. These are the potential energy diagram familiar from its use in the theory of diatomic molecules. The other is the electron energy diagram used extensively in solid-state physics. Figure 9 presents a potential energy diagram for the Auger neutralization process: $He^+ + ne_M^- \rightarrow He + e^- + (n-2)e_M^-$. Suppose the total energy of the system is E_t. Then the ion He^+ incident on the surface will have kinetic energy K(s) as shown. It will vary with ion-solid

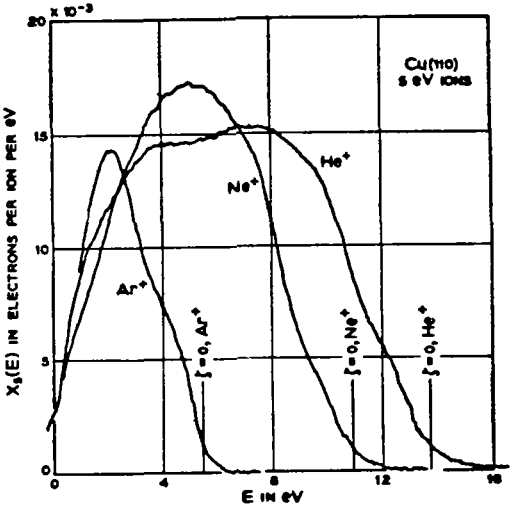

Fig. 7

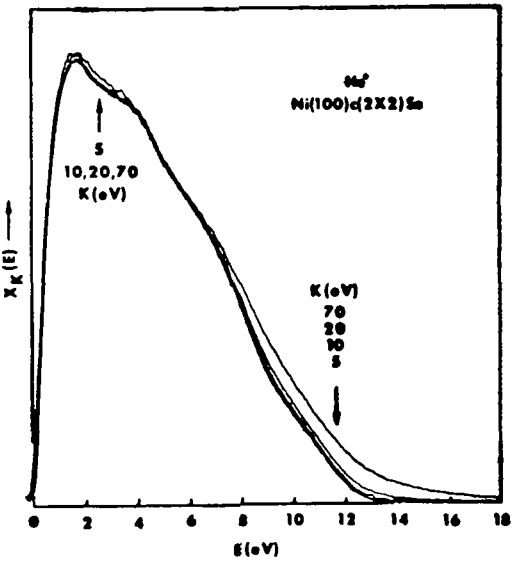

Fig. 8

separation s by virtue of the image force and eventual repulsive interactions between He^+ and the solid depicted by curve 1. The final state of the process involves the interaction of the neutralized He atom with the surface. This has a small van der Waals component in addition to a repulsive term closer to the surface. We must depict many final states because the two electrons drawn from the solid may come from any energy level in the filled band. Thus curves 2 and 3 are separated by twice the electron band width in the solid and curve 3 lies below curve 1 by the energy $E_i(s)-2\phi$, the effective ionization energy of He at the distance s from the surface less twice the work function of the solid. The kinetic energy of the free electron may have any value given by the vertical distance between curve 1 and any of the family of curves between curve 2 and curve 3. The maximum electron kinetic energy measured outside the solid, neglecting broadening, is $E_i(s)-2\phi$, the positions marked by $\zeta=0$ in Fig. 7. The Auger process occurs over a narrow band of separations s near the position where the quantities K(S) and $E_i(s)-2\phi$ are specified in Fig. 9.

The second type of energy diagram is the electron energy diagram of Fig. 10 where the pairs of transitions of the Auger process are shown, 1 and 2 or 1′ and 2′. The midpoint between the initial states at $\zeta=\zeta_1$, ζ_2 is the point labelled ζ lies halfway between the ground state of the atom and the energy E to which the up electron is translated. We see, however, that there is an infinite set of paired initial-state electrons which give an excited electron at E. These are the pairs symmetrical about ζ, i.e. $\zeta\pm\Delta$ for any Δ less than ζ or $\zeta_0-\zeta$, whichever is smaller. Thus the energy distribution (Figs. 6, 7, 8) of electrons excited above the vacuum level, E=0, is proportional to the self convolution $\int_{-\zeta}^{\zeta} U(\zeta-\Delta)U(\zeta+\Delta)d\Delta$, where, if transition probability is constant over the band, $U(\zeta)$ is an average local initial-state density in the region where the up and down electrons are selected. The matter is more complicated than this but the above discussion gives its gist.

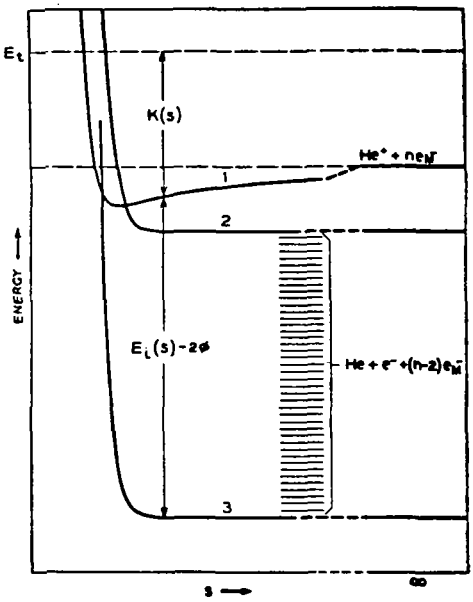

Fig. 9

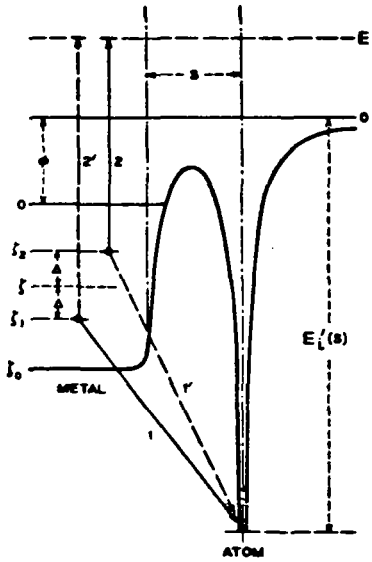

Fig. 10

SURFACE STUDIES - The study of ion-solid interactions is of interest in itself and its ideas find applications in several fields. It has led, however, to the development of an electron spectroscopy of surfaces which has its own peculiar set of characteristics such as transition probability, volume of sensitivity, etc.[2] The method of ion-neutralization spectroscopy (INS) involves the measurement of electron energy distributions at two ion energies, say 10 and 20 eV (Fig. 8), the extrapolation from these to a curve from which the natural broadenings have been removed, a change of variable from E to ζ and a sequential inversion of the resulting integral given above to obtain the $U(\zeta)$ function. As Fig. 4 indicates, it is possible to compare the experimental results by INS (port 1) with those obtained by ultraviolet photoemission spectroscopy (UPS) (port 4) which processes a different set of characteristics. The use of two electron spectroscopies in the study of surface electronic structure is considerably more informative than is the use of one alone.

REFERENCES

1. H. D. Hagstrum, J. Vac. Sci. Technol. 12, 7-16 (1975).
2. H. D. Hagstrum, Science 178, 275-282 (1972).

High Resolution Photoelectron Spectroscopy, F. A. GRIMM, University of Tennessee, Dept. of Chem., Knoxville, TN, 37916

A discussion of the uses of high resolution ($\leq$ mev fwhm measured on the $^2P_{3/2}$ line) photoelectron spectroscopy obtained with vacuum UV radiation will be presented. Included will be the present uses of high resolution photoelectron spectroscopy in the investigation of the phoionization process, the assignment of the photoelectron spectrum, and some suggested areas in which high resolution may be applied to current problems. The calculation of rotational band contours and a spectrometer designed for high resolution will be presented.

The Effects of Molecular Rotation and Vibrational Hot Bands on Photoionization Thresholds

K. E. McCulloh
National Bureau of Standards
Washington, DC 20234

ABSTRACT

The accurate determination of ionization and appearance potentials and ionic heats of formation from photoionization threshold data for molecules requires that corrections be made for initial internal energy. Initial vibrational energy is manifested by hot bands appearing below the 0°K threshold, while rotational energy broadens the jump at a molecular ionization threshold, in general asymmetrically, and causes a temperature shift and rotational tailing of a fragment photoion yield curve. Correction for these effects on the basis of data obtained as a function of gas temperature will be discussed. The problem of obtaining reliable error estimates for fragment ion appearance potentials will be considered. Applications to thermochemistry will be reviewed, including the ionization potentials of several small molecules, the dissociation energies of F_2 and HF, the heats of formation of CH_3^+ and CH_3, and the electron affinities of O and H.

Photoelectron Spectra of Transients.

T. KOENIG, T. BALLE and W. SNELL, Univ. of Oregon, Dept. of Chem., Eugene, Oregon 97403.

A simple modification of Perkin Elmer PS-18 Photoelectron Spectrometer, patterned after the flash vacuum pyrolysis method used by Lossing[1] and Hedaya[2] in mass spectrometry, allows the observation of the He(1) photoelectron spectra of transient species. Results with a series of aliphatic radicals are in excellent agreement with ionization potentials determined by mass spectrometry in most cases though the vertical ionization potential of 1-cyanoisopropyl (8.65 eV) was 0.5 eV lower than the previous determination. The Frank Condon factors for t-butyl suggest it is nearly tetrahedral. In addition to radicals, unstable xylenes have also been investigated.

1. F. P. Lossing and G. P. Semuluk, Can. J. Chem., 48, 955 (1970).
2. E. Hedaya, Accounts Chem. Res., 2, 367 (1969).

Electron Monochromator Studies of Organic Ions. FRED P. LOSSING, Div. of Chemistry, National Research Council, Ottawa, Canada KIA OR6.

A brief description will be given of the apparatus, techniques and assumptions employed in the author's monoenergetic electron impact studies. The principal aim of this work is to obtain improved heat of formation data for even-electron organic ions ("fragment ions") of known structure, starting with free radicals of known identity. With a few exceptions, current ∇H_f data for such ions refer to undifferentiated isomeric structures or are uncertain to several tenths of a volt, or most commonly, both. For this special purpose the experimental disadvantages of electron impact vis-a-vis photon impact, such as inferior energy resolution, uncertainty in the energy calibration and others, are compensated to a considerable extent by the inherently greater cross section, energy range, and flexibility of operation. Comparison of results shows that the electron impact thresholds for ionization, while less precise than the photoionization data, are in most cases as reliable as the radical ∇H_f data, i.e. errors of $\sim$0.1 ev. are to be expected.

Electron Impact Threshold Measurements on High Temperature Beam Species. D. L. HILDENBRAND, Stanford Research Institute, Menlo Park, Ca., 94025

A technique for the determination of ionization thresholds with an accuracy of about 0.10 eV, using the conventional Nier-type electron impact ion source, will be described, and the application of the method to the study of ionization processes involving high temperature effusion beam species will be discussed. Results will be critically compared with similar determinations made by other techniques such as photoelectron spectroscopy, photoionization mass spectrometry and optical spectroscopy. The inherent limitations of the technique, both instrumental and interpretive, will be outlined.

High-Temperature Photoionization and Photoelectron Measurements*

J. Berkowitz, Argonne National Laboratory, Argonne, IL 60439

For the purpose of this symposium, the ionization potential of a molecule will be taken to mean the adiabatic ionization potential, i. e., the energy separation between the vibrationless, rotationless state of a molecule and the corresponding state of the parent molecular ion. Higher ionization potentials, i. e., energies required for forming excited electronic states of the molecular ion will not be explicitly discussed, although they are obtained in photoelectron spectroscopic studies at the same time as the first ionization potential, and analysis of the data is similar.

We shall sub-divide this talk into

a) Determination of ionization potentials, by photoelectron spectroscopic and photoionization mass spectrometric methods.

b) Determination of appearance potentials of fragment ions, which are most directly done only by the mass spectrometric technique.

We shall further sub-divide a) into

i) Small molecules (1, 2, 3 atoms) and

ii) Large molecules (usually ≥ 4 atoms).

SMALL MOLECULES

Ideally, one would like to begin with a pure rotationless, vibrationless target species, direct light of variable wavelength on the system, and detect the onset of ionization to the vibrationless, rotationless state of the ion. In practice, this is difficult even for volatile systems. In the case of H_2 for example, it is possible to prepare a rotationless, vibrationless target (excluding zero point energy) but the photoionization process near threshold is dominated by autoionization and hence (partly due to a weak Franck-Condon factor) it is difficult to detect the onset of direct ionization. The most accurate ionization potential of H_2 is based upon an analysis of the Rydberg states that may lead to autoionization. For virtually all other systems, we cannot even prepare molecules in rotationless states, but must contend with a Boltzmann distribution. Hence, accurate ionization potentials based on photoionization techniques would require an analysis of the rotationally-averaged structure, which is usually not done. (Exceptions are recent studies on HF (Walker and Berkowitz) and O_2 (Samson and Gardner).

A major difference between normally-volatile and high-temperature molecules, however, is the vibrational population of the target. For most small volatile molecules the zeroth vibrational levels are the only significant ones (e. g., O_2, N_2, CO, NO, H_2O, CO_2) whereas for most small high-temperature molecules (diatomic thallium and indium and alkali halides, Se_2, Te_2, triatomic Hg, Cd, Zn dihalides, Sn, Pd dihalides) one must contend with a Boltzmann population of vibrational levels.

One of the goals of future studies with high-temperature systems is the production of species in their lowest vibrational states. This has

apparently been achieved with S_2 by vaporizing this material in a diluent of He, and vibrationally cooling the S_2 by collision before photoionization has occurred. Other possible techniques for future investigation include hydrodynamic expansion through a Laval jet, which cools internal degrees of freedom, or matrix isolation photoelectron spectroscopy.

Heretofore, most high-temperature studies have had to contend with a Boltzmann distribution of target material, both rotationally and vibrationally. In this circumstance, some de-Boltzmannizing procedure must be used. In early photoionization mass spectrometric work, this was achieved by assuming that each Boltzmann vibrational component had an equal transition probability, and that transition probability was a step function. One could then construct an idealized threshold function, and find the best fit to the experimental function. From this fit, the position of the 0-0 transition could be immediately extracted. Examples of this procedure (TII, NaI) are shown in Fig. 1. On this scale, the rotational uncertainty is well within the experimental uncertainty.

An equivalent, but less tedious analysis can be performed by plotting the ion intensity as a function of photon energy on a semi-log plot, as used by Watanabe for larger volatile molecules. One looks for the departure from straight-line behavior on an initial linear portion on the semi-log plot. Implicit in such an analysis is the assumption that the exponential Boltzmann function is a more rapidly varying function than Franck-Condon factors or deviations from step-function behavior. Autoionization is also ignored in this procedure.

Examples to which this approach has been applied include TlBr, CsX, S_2, Se_2, Te_2. See Fig. 2.

Note the abrupt departure in most instances. For the molecules shown, the values obtained are the most precise ionization potentials we have to date (generally ± 0.02 eV). The I. P. 's deduced are presumably the adiabatic ones, according to the assumptions made above.

Note that in the case of Te_2, evidence can be seen for an excited electronic state of neutral Te_2, which has since been verified by other (spectroscopic) techniques. The semi-log display makes this apparent; it would be lost in a linear plot. For these small, high-temperature species, photoelectron spectroscopy is not quite as accurate as PIMS for deducing adiabatic I. P. s, but it does provide the vertical I. P. 's directly. In principle, one could make a semi-log plot of the threshold region in PES, but usually the dynamic signal : background range is not as large as in PIMS. See Fig. 3. In special cases, if one knows r_e and w_e for both the neutral and ionic states but cannot resolve individual vibrational components in the photoelectron spectrum, it is possible to perform a Franck-Condon analysis to determine the shape of the band, and hence one can infer which portion of this band corresponds to the 0-0 transition. Another advantage of PIMS exists if the vapor consists of more than one species. It would be extremely difficult to accurately measure a minor species by photoelectron spectroscopy.

For small volatile molecules, the photoelectron spectroscopic technique may still be the preferred one, when high resolution is attainable. As

an example, we show PES and PIMS approaches to the adiabatic ionization potential of H_2O.

In a high-resolution PES study of the 1st vibrational band of the ground state of H_2O^+. Asbrink et al. compare the rotational structure of this band with the calculated rotational structure of a Rydberg state of H_2O, and from this analogy deduce the 0-0 transition to be 12.614 eV. Karlsson et al., in a similar more recent experiment with equivalent resolution, give 12.615 eV.

Some 10 years ago Brehm performed a photoionization mass spectrometric study of H_2O, plotting the data on semi-log coordinates. He deduced the departure from linearity at 12.614 eV.

If, however, we examine the threshold region under higher resolution, and plot it on a linear scale (unpublished work, Eland & Berkowitz) we note:

a) Autoionization is super-posed upon the direct ionization of the threshold region. If this were not so, it might be possible to relate the photoionization threshold region to an integral of the PES structure.

b) The 0-0 transition corresponds to a point rather high on the threshold curve (see arrow). If one were trying to deduce the adiabatic I. P. from this curve, without additional information, it would be a formidable task.

A surprising consequence of this comparison is the accurate I. P. that can apparently be deduced from a semi-log PIMS plot.

LARGE MOLECULES

As examples of this class, we shall focus on the various sulfur-molecular species. In Figs. 4 a-f we provide examples of semi-log plots for S_2, S_3, S_5, S_6, S_7 and S_8.

Note how the abruptness of departure from linearity is satisfactory for S_2, but becomes progressively less marked as one proceeds to the larger molecules. This increasing curvature prompted P. M. Guyon and me to concoct a model for ionization of large molecules. We used one version of the density of states expression to determine the number of vibrational states for a polyatomic molecule having energy (above zero) between ϵ and $\epsilon + d\epsilon$. Then, assuming a linear post-threshold cross section with excess photon energy, we calculated a variation of cross section with photon energy which was now no longer a pure exponential, but had a pre-exponential polynomial of degree s-1.

This model explained the curvature to some extent, and in the process predicted a substantially higher adiabatic ionization potential than the departure from linearity on semi-log coordinates. See Fig. 5a, b.

We recently had occasion to return to this problem by obtaining the 21.2-eV photoelectron spectra of S_6 and S_8. See Figs. 6 a, b.

The somewhat surprising result is that the more complicated many-oscillator model yields values for the adiabatic I. P.'s of S_6 and S_8 which are larger than the vertical I. P.'s obtained from photoelectron spectroscopy, which is unrealistic, whereas the simple "departure-from-linearity"

model yields a reasonable result. The most likely explanation for this surprising result is that the linear post-threshold cross section assumed in the complicated calculation is not appropriate, and that a more abrupt (step-like) function should be used. This, in turn, implies that the Franck-Condon factors favor the 0-0 transitions, which further implies that the geometry of the S_6^+ and S_8^+ ions are very similar to the corresponding neutrals. This is also implied by the poor fit of calculation and experiment in the pre-threshold region.

Now let us turn to appearance potentials of fragment ions. Up to this time, the most effective use of fragment ion appearance potentials in high-temperature studies has been to deduce bond energies of neutral diatomic molecules, including the diatomic thallium halides, ocesium, rubidium and sodium halides, and the homonuclear halcogens S_2, Se_2 and Te_2. For these systems, the heats of formation of the products (atoms and atomic ions) are well known, and one seeks to determine the heat of formation of the target diatomic molecule.

The method of analysis has sometimes been linear extrapolation, taking into account the internal thermal (vibrational and rotational) energy which is available for the dissociation process, or using the semi-logarithmic approach. Examples of the first method are S_2, Se_2 and Te_2. See Fig. 7.

The linear plot is particularly revealing when structure attributable to excited states can be observed (c.f. the $S^+(S_2)$ case) providing corroboration for the interpretation. The experiments on S_2, Se_2 and Te_2 have provided the most reliable measurements of these dissociation energies. (A more precise value of $D_o(S_2)$ has since been deduced from spectroscopic predissociation, but the interpretation was greatly aided by the earlier photoionization result).

For the thallium halides, the semi-log approach yields dissociation energies which are compared with the results of other experiments in Table 1. Again, these results are the most accurate currently available.

A prevailing assumption, in this study as well as corresponding studies with volatile samples, is that observable fragmentation occurs at the thermochemical threshold. In a very few cases, where the initial fragmentation is spin-forbidden, this assumption is not borne out, but it(perhaps surprisingly) leads to accurate results in the vasp majority of examples studies to date.

Heretofore I have differentiated the studies of high-temperature molecules and volatile ones in terms of Boltzmann populations. There are, of course, additional experimental problems. One must work with molecular beams, and this generally results in a lower number density, hence a poorer signal: background ratio. When using the semi-logarithmic plot, fewer decades of the linear portion can be obtained.

In photoelectron spectroscopic measurements, the heating elements must not introduce weak electric or magnetic fields which can alter the electron trajectories and hence affect the resolution or the electron energy scale. This problem has limited such measurements thus far to ~1000 °C.

Deposition of the beam material on sensitive surfaces can cause high-voltage breakdown and spurious ion counts, or (in the case of PES) alter resolution and the energy scale.

Finally, thermal electron emission from the oven or sample material itself must be guarded against in the very high temperature experiments.

In summary, adiabatic ion thresholds for high-temperature species can be obtained by the aforementioned PES and PIMS methods to ~.01 eV accuracy in favorable cases, whereas the accuracy obtainable with small volatile molecules may be an order of magnitude better.

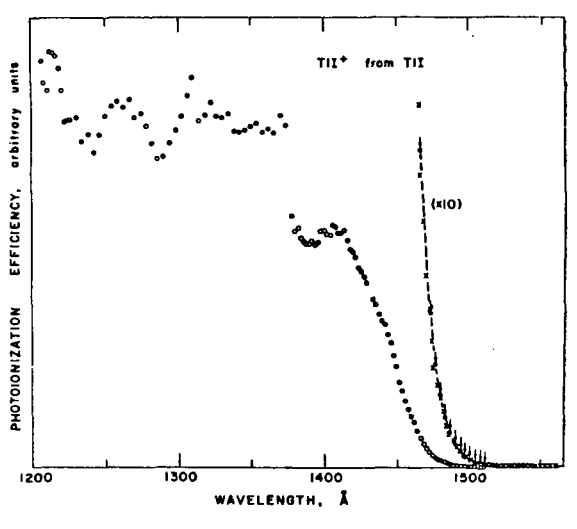

FIG. 1(a)

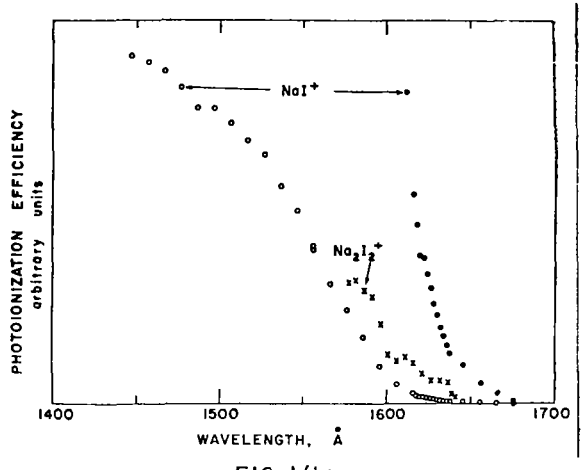

FIG. 1(b)

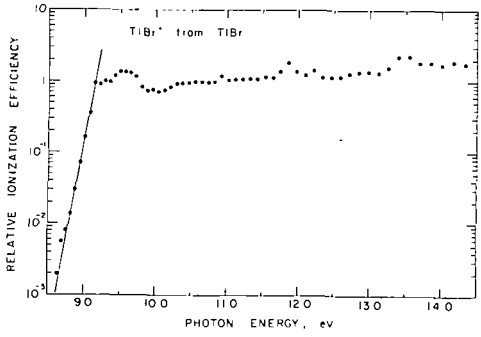

FIG. 2(a)

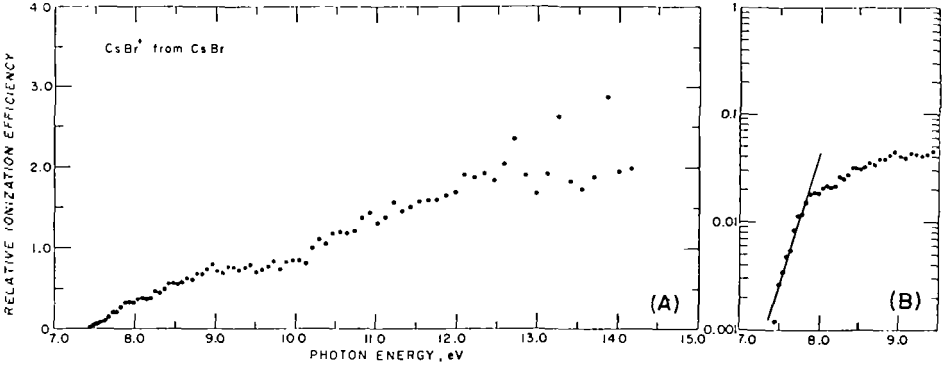

FIG. 2(b)

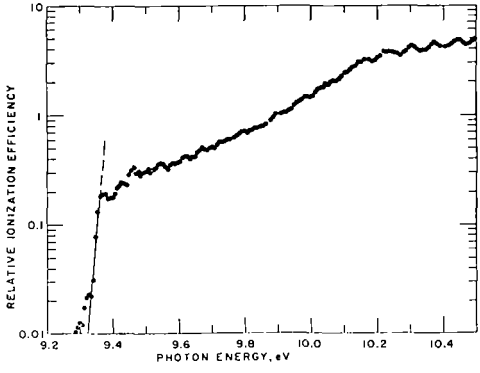

FIG. 2(c)

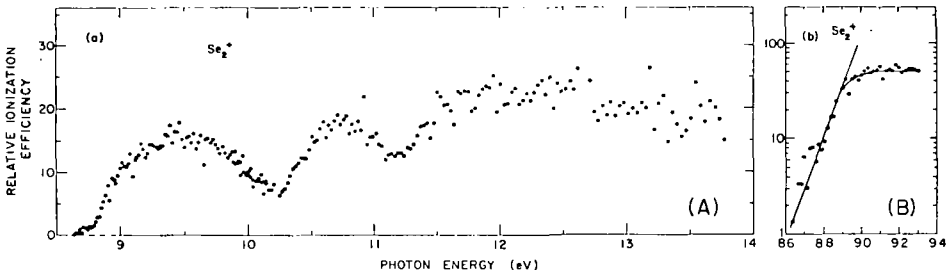

FIG. 2(d)

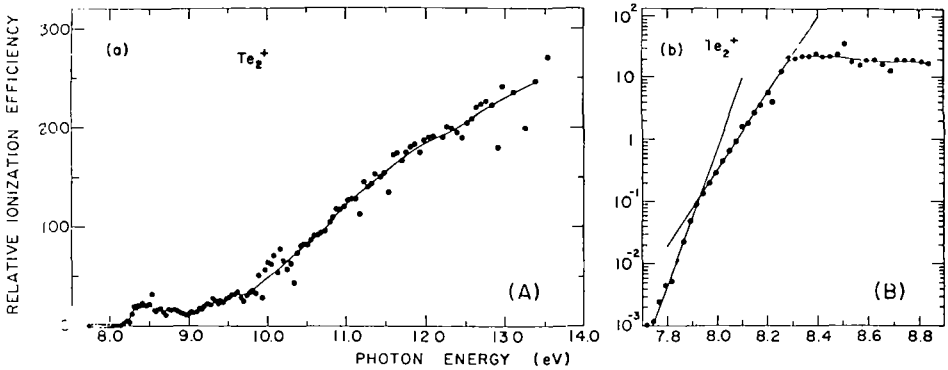

FIG. 2(e)

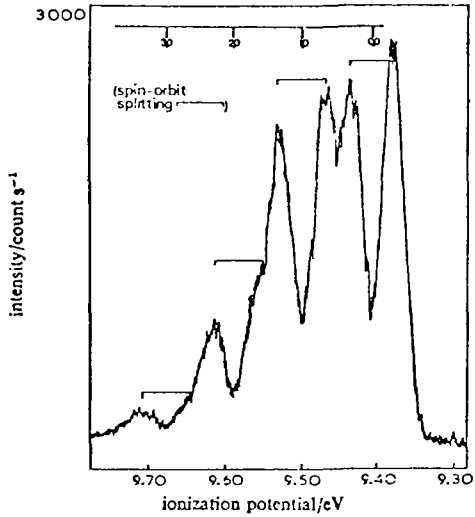

FIG. 3(a)

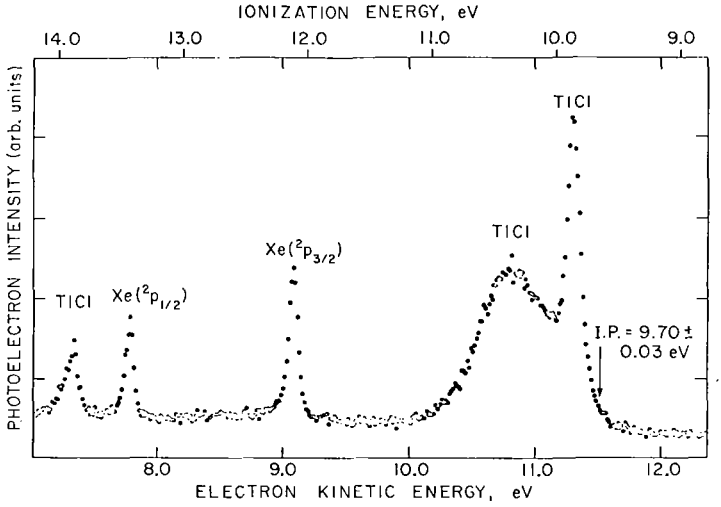

FIG. 3 (b)

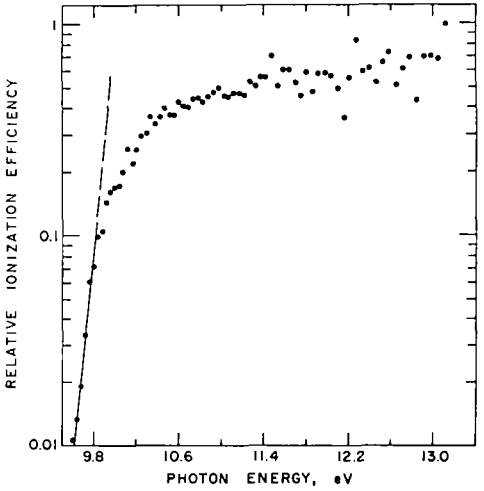

FIG. 4 (a)

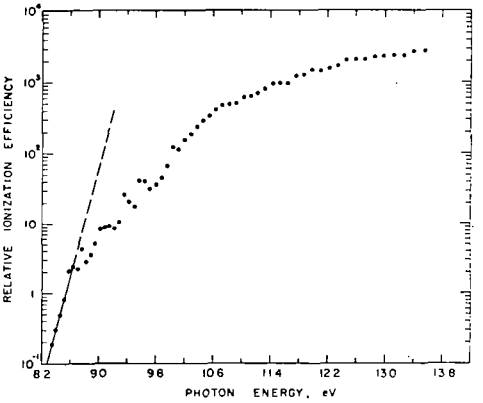

FIG. 4 (b)

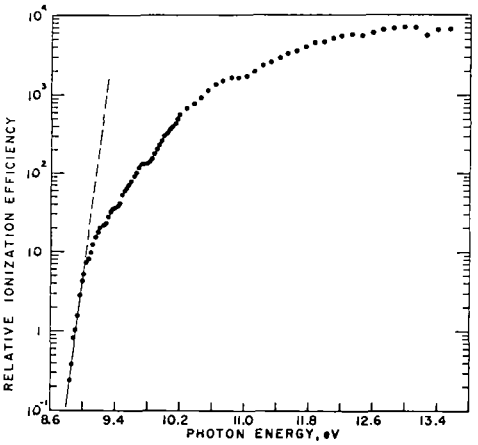

FIG. 4 (c)

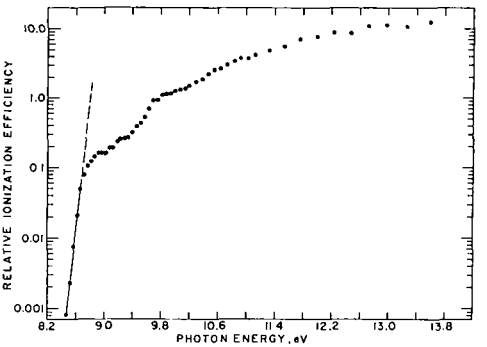

FIG. 4 (d)

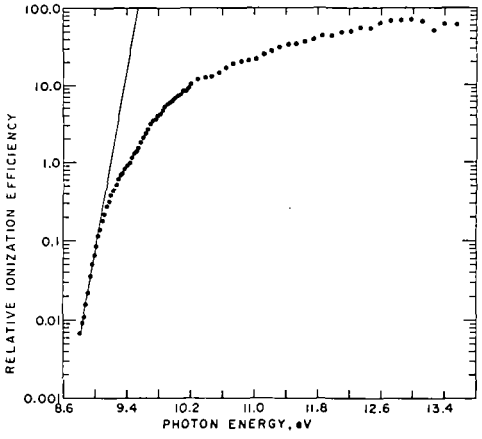

FIG. 4(e)

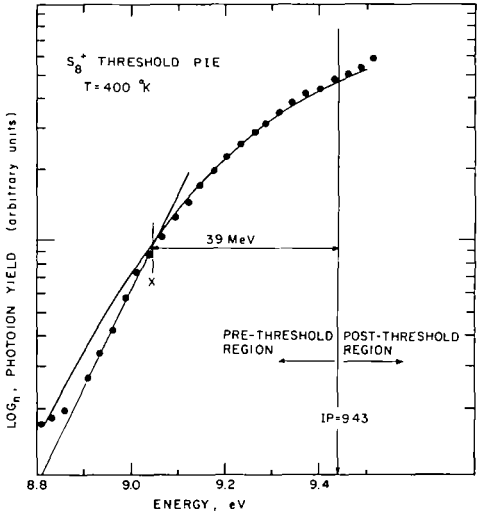

FIG. 5(a)

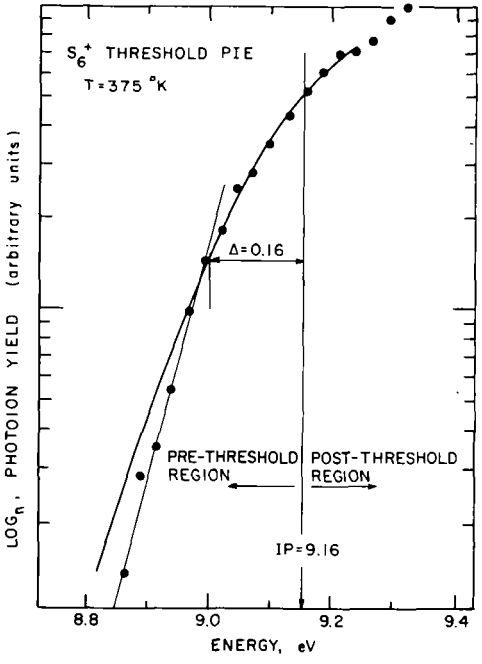

FIG. 5(b)

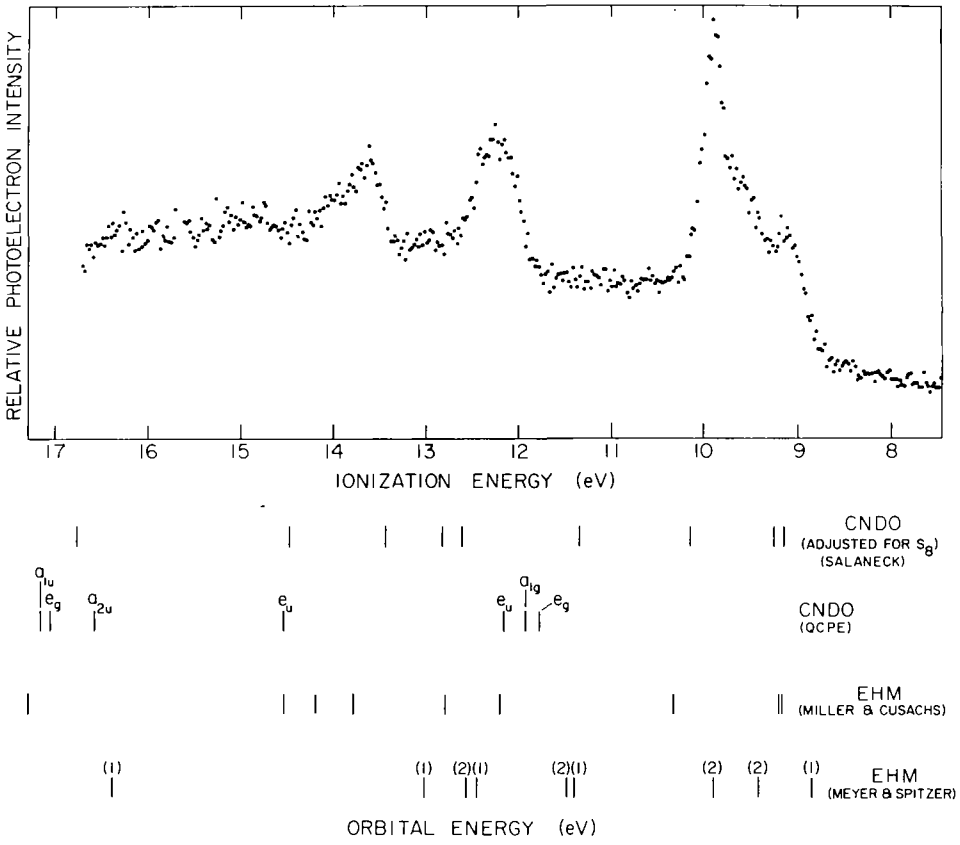
RELATIVE PHOTOELECTRON INTENSITY
17
16
15
14
13
12
11
10
9
8
IONIZATION ENERGY (eV)
CNDO
(ADJUSTED FOR S_8)
(SALANECK)
a_{1u}
e_g
a_{2u}
e_u
e_u
a_{1g}
e_g
CNDO
(QCPE)
EHM
(MILLER & CUSACHS)
(1)
(1)
(2)(1)
(2)(1)
(2)
(2)
(1)
EHM
(MEYER & SPITZER)
ORBITAL ENERGY (eV)

FIG. 6 (a)

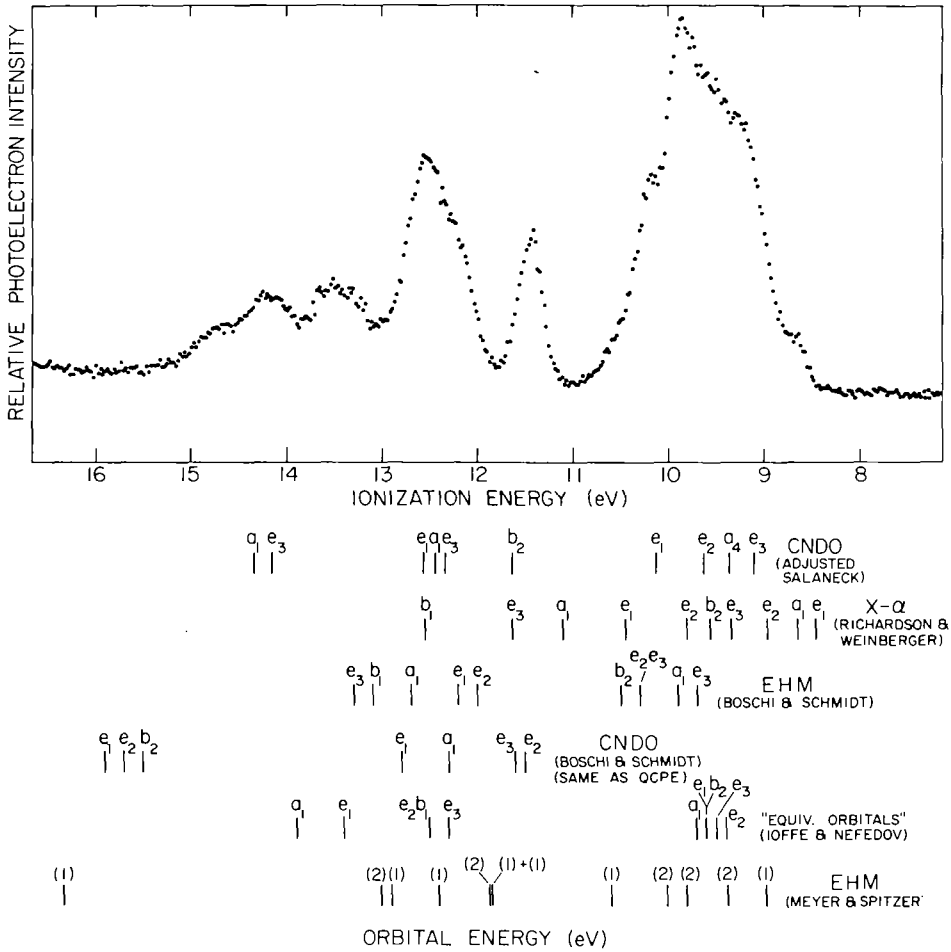
RELATIVE PHOTOELECTRON INTENSITY
16
15
14
13
12
11
10
9
8
IONIZATION ENERGY (eV)
CNDO
(ADJUSTED SALANECK)
X-α
(RICHARDSON & WEINBERGER)
EHM
(BOSCHI & SCHMIDT)
CNDO
(BOSCHI & SCHMIDT)
(SAME AS QCPE)
"EQUIV. ORBITALS"
(IOFFE & NEFEDOV)
EHM
(MEYER & SPITZER)
ORBITAL ENERGY (eV)

FIG. 6 (b)

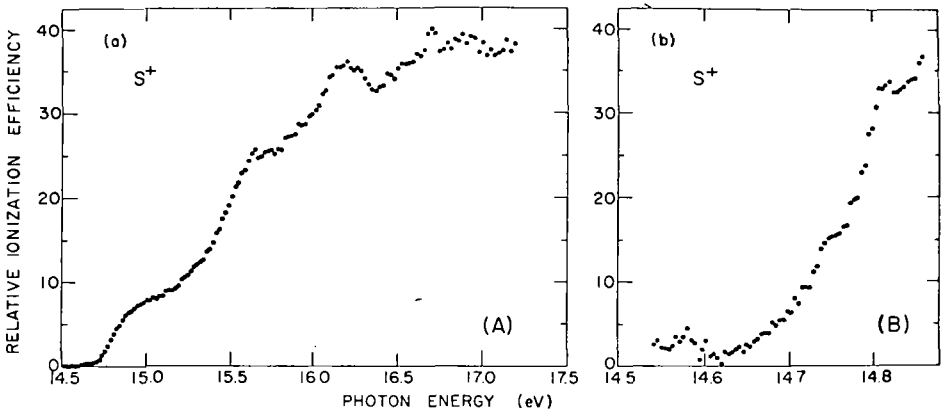

FIG. 7 (a)

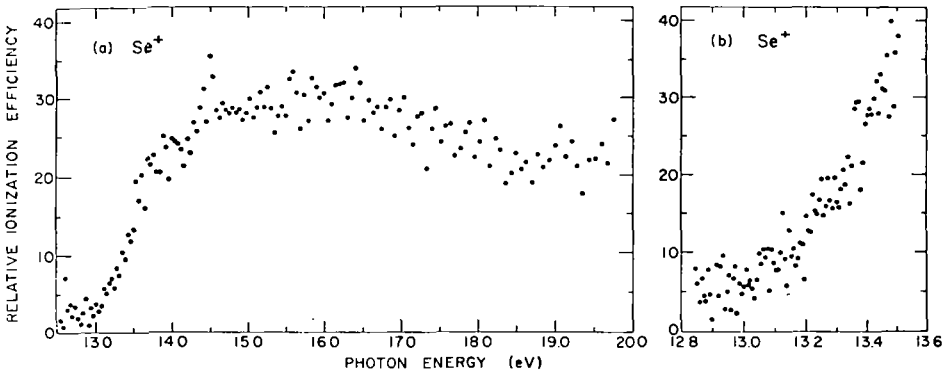

FIG. 7 (b)

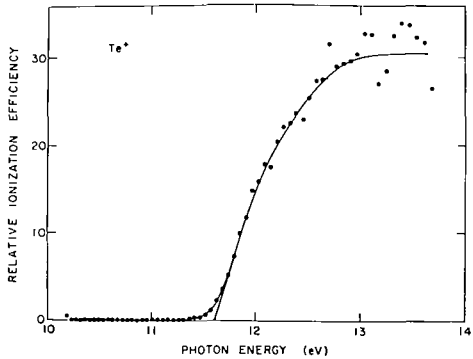

FIG. 7 (c)

FIGURE CAPTIONS

Fig. 1(a) Photoionization efficiency curve for formation of TlI^+. Threshold region. On the magnified scale, the closed circles are for the Boltzmann-type fit and the arrows mark the successive vibrational contributions.

Fig. 1(b) The photoionization efficiency curves of the parent ions NaI^+ (circles) and $Na_2I_2^+$ (crosses), threshold region.

Fig. 2(a) Ionization efficiency of $TlBr^+$ from TlBr.

Fig. 2 (b) Photoionization efficiency curve of $CsBr^+$ from CsBr. (A) Linear plot of data obtained with 1.0-mm entrance and 0.3-mm exit slitwidths. (B) Semilogarithmic plot of the threshold region.

Fig. 2(c) Semilog plot of the photoionization efficiency of S_2^+ obtained from an HgS source.

Fig. 2(d) Relative photoionization efficiency of Se_2^+ from Se_2. The hydrogen-lamp region plotted on a linear scale. (B) The threshold region, on a semilog scale.

Fig. 2(e) Relative photoionization efficiency of Te_2^+ from Te_2. (A) The hydrogen-lamp region. (B) The threshold region, plotted on a semilog scale.

Fig. 3(a) The band assigned as involving transitions to the $X^2\Pi_g$ state of S_2^+

Fig. 3(b) He(I) photoelectron spectrum of TlCl with Xe calibrating gas.

Fig. 4(a) Semilog plot of the photoionization efficiency of S_2^+ obtained from an HgS source.

Fig. 4(b) Semilog plot of the photoionization efficiency of S_5^+. HgS was the source of vapor.

Fig. 4(c) Semilog plot of the photoionization efficiency of S_6^+. Partially equilibrated orthorhombic sulfur was the source of vapor.

Fig. 4(d) Semilog plot of the photoionization efficiency of S_7^+ from sulfur vapor equilibrated with the aid of an Al_2O_3 catalyst.

Fig. 4(e) Semilog plot of the photoionization efficiency of S_8^+ from orthorhombic sulfur.

Fig. 5 Photoionization thresholds of the polyatomic molecules S_8^+ and S_6^+. Full line: PIE calculated for a linear idealized cross section at 0^oK. Dots: experimental points. Crosses: previously reported thresholds.

Fig. 6(a) 584 Å photoelectron spectrum of S_6, plotted together with orbital energies of S_6 obtained by various calculational schemes.

Fig. 6(b) 584Å photoelectron spectrum of S_8, plotted together with orbital energies of S_8 obtained by various calculational schemes. A band

attributed to S_7 can be seen at ~ 8.65 eV.

Fig. 7(a) Relative photoionization efficiency of S^+ from S_2. (A) The overall curve. (B) the threshold region, shown in magnified form.

Fig. 7(b) Relative photoionization efficiency of Se^+ from Se_2.

Fig. 7(c) Relative photoionization efficiency of Te^+ from Te_2.

TABLE I. Comparison of the Dissociation Energies (kcal/mole) of the Thallium Halides, as Measured by Various Investigators

Method	TlF	TlCl	TlBr	TlI
Spectroscopic	109.6	89.6	73.9< 83.8	<72.2
Thermochemical	105.3 ± 3	88.0	79.2	64.9
Equilibrium mass spectrometry	101 ± 3.5	-	-	--
Electron-impact mass spectrometry	-	90 ± 2.5	79 ± 4.5	69 ± 4.5
Flame photometry	110 ± 10	87.0 ± 2	77.6 ± 2	68.0 ± 3
Photoionization	105.5 ± 0.5	88.1 ± 0.5	78.9 ± 0.5	64.4 ± 0.5

KINETIC ASPECTS OF THRESHOLD DETERMINATION

Austin L. Wahrhaftig, Department of Chemistry
University of Utah, Salt Lake City, UT 84112

By 1941, the formation of stable diatomic ions and of fragment ions--of both low and high kinetic energy--had been described in terms of electron bombardment initially giving diatomic ions in well-defined electronic states.[1] No similar studies existed for polyatomic ions, although there were quite early studies of ionization efficiency curves relating ion production to electron voltage for simple polyatomic molecules. Early workers noted that at the low pressures of an ion source, each molecule was isolated; hence, the law of conservation of energy could be applied to the reaction (1) yielding equation (2):

$$R_1R_2 + e \rightarrow R_1^+ + R_2 + 2e \qquad (1)$$

$$KE(R_1R_2) + IE(R_1R_2) + KE(e) = D_0 + I_z(R_1) + KE(R_1^+) + KE(R_2) + KE(e_1) + KE(e_2) + IE(R_1^+) + IE(R_2) \qquad (2)$$

The total energy before impact consists of the three terms on the left: the kinetic energy of the molecule, the internal energy (electronic, vibrational, and rotational) in the molecule, and the kinetic energy of the electron. After impact, the total energy is given by the terms on the right: D_0, the energy difference between the ground states of the molecule R_1R_2, and the fragments R_1 and R_2; $I_z(R_1)$, the ionization potential of R_1; and the remaining terms, the translational kinetic energy, and the internal energy of the products. As the kinetic energy of the incident electron is lowered, the kinetic energies of the departing electrons also decrease, approaching zero at the lowest-energy incident electrons by which the ion R_1^+ is produced. This energy then defines the theoretical "appearance potential" of R_1^+ as stated in equation (3):

$$AP(R_1^+) = D_0 + I_z(R_1) + KE(R_1^+) + KE(R_2) - KE(R_1R_2) + IE(R_1^+) + IE(R_2) - IE(R_1R_2) \qquad (3)$$

The additional assumptions, that the internal and kinetic energy terms of the product ion and the neutral fragment also approach zero with decreasing incident-electron energy and that the kinetic and internal energies of the molecule at room temperature are negligible, give the simple relationship,

$$AP(R_1^+) = D_0 + I_z(R_1) \qquad (4)$$

The studies on diatomic molecules were consistent with equation (3) but not with equation (4). In his bond energy determinations, Stevenson assumed that in similar ion dissociation reactions the internal and kinetic energy terms would be similar so that these energy terms should essentially cancel in calculations involving the difference of two appearance potentials.[2]

While, obviously, there must be some mechanism by which the initial parent molecule ion dissociates to give each observed fragment ion and neutral fragment(s), there were no considerations of mechanism or kinetics and certainly no concept of a "chemistry" in the early discussions. In 1950, Langer[3] noted that the assumption of immediate dissociation following ionization, such as occurs with diatomic molecules, was inconsistent with the data for larger polyatomic molecules and that hydrogen migration followed by simple bond break adequately explained the limited data on several oxygen-containing compounds. However, he postulated no rational physical-chemical basis for rearrangements, and his final conclusion was only that more experimental evidence was required to understand rearrangement.

The first general discussion of the mass spectra of polyatomic molecules was given by Henry Eyring in 1950.[4] It was noted that the mass spectra of polyatomic molecules strongly indicated that the reactions were "quasi-equilibrium" in that dissociations were slow relative to the rate of energy transfer within the fragmenting molecular ion. This idea, implicit in much of the earlier work but only relative to simple bond cleavage, permitted a consistent discussion of rearrangement reactions, secondary reactions of fragment ions formed by parent ion dissociation, metastable ions, isotope effects, and temperature effects. The basic idea of QET is simply expressed by the equation, $k_i = k_i(E_i)$, i.e., the rate for each reaction involved in producing a mass spectrum depends only upon the internal energy of the reacting species. The first calculations based upon QET used appearance potential differences as activation energies. This is inconsistent with theory[5] which requires that an observed appearance potential for a fragment ion be interpreted not as the lowest electron (or photon) energy at which that ion might be produced, but as the energy at which there are produced enough reactant ions with energy to dissociate on the time scale of the mass spectrometer so as to permit fragment ion detection.

In a very important paper, William A. Chupka[6] noted that the effect of thermal energy in the initial parent ion is significant. He showed that photoionization data were in excellent agreement with the assumption that the initial thermal energy distribution over molecules prior to ionization was additive to the energy imparted by the ionizing photon. He also observed that the excess energy required to give an observable rate was essentially the same as the molecular thermal energy at the normal ion source temperatures. Thus, it was quite reasonable that this cancellation of effects, especially in work employing appearance potential differences, gave rise to results not only internally consistent but also consistent with data from other sources. While early workers primarily derived bond energies, later workers have set for themselves the more ambitious task of listing tables of heats of formation of ions. Here, one no longer uses only differences of appearance potentials and must examine the effect of the dissociation kinetics upon the relationship between the ion heat of formation, the activation energy for the dissociation reaction involved, and the appearance potential measured with a given apparatus in a specific manner.

The energy terms involved are defined as indicated in Figure 1, where the multidimensional nature of the potential surfaces for a molecular ion and its activated complex is emphasized. Quantities of interest are E_{th}, the internal (thermal) energy of P prior to ionization; I_z, the energy difference between the ground states of molecule and ion; and ΔH_0^0, the energy difference between ground states of the molecule and the two products. For a collection of reactant molecules or of products at thermal equilibrium, e.g., 298 K, the enthalpy of each, relative to its ground state, $H_{298}^0 - H_0^0$, can be measured or calculated and so ΔH_{298}^0, the standard enthalpy change in the overall reaction may be determined.

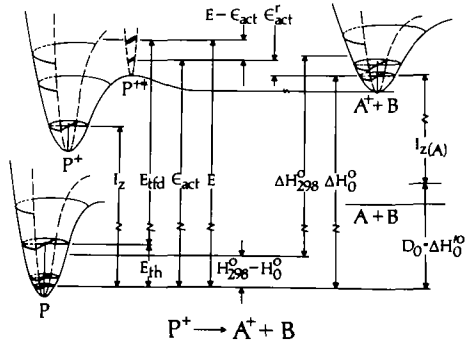

$P^+ \longrightarrow A^+ + B$

Figure 1

In any of the activated complex theories of reaction kinetics, it is assumed that there exists a reaction coordinate and an activated complex configuration. The energy of activation, ε_{act}, is taken as the energy difference between the molecular ground state and that of the activated complex. There may be a small reverse activation energy, ε^{r}_{act}, as shown. On interaction with an electron or photon, a molecule acquires an amount of transferred energy, E_{tfd}, which added to E_{th} gives the molecule a total energy E. Three energy quantities must be considered in relating an appearance potential determined by measurements of ion abundance versus E_{tfd} to ΔH^0_0 or its near equivalent ΔH^0_{298}: the occurrence of a significant ε^{r}_{act}; the minimum excess energy, $E - \varepsilon_{act}$, required to give an observable ion yield; and the effect of an energy distribution in E_{th} on E_{tfd}.

The existence of a long range ion induced dipole (or ion permanent dipole) forces between the separating fragments should reduce ε^{r}_{act} below that in a similar reaction between neutral species but not necessarily to zero. In the simple diatomic case, ε^{r}_{act} is converted into translational energy of the separating fragments, but this is not necessarily correct for polyatomic molecules. For an appropriate potential surface, a large ε^{r}_{act} might be converted solely into internal energy in the separating fragments. The basic quasi-equilibrium hypothesis makes no predictions as to the excess energy above ε_{act} required to give an observable ion yield. On the assumption that "normal" product ions decompose faster than metastable ions, the difference observed with some measuring techniques between the appearance potential for a normal product ion and the same ion from a metastable decomposition is called the "measurable" part of the kinetic shift. The excess energy over ε_{act} required for observation of the metastable ion is then the "unmeasurable part" of the kinetic shift. Since this latter quantity has no significance except in regard to a particular set of instrumental conditions and mode of date reduction, the separation is completely arbitrary. While some authors list reverse activation energy separately from the kinetic shift, this distinction has not been made by others who seem to combine all excess energy terms over the minimum absolute zero enthalpy change into a kinetic shift.

The question as to the size of the kinetic shift is inseparable from the question of the experimental method of appearance potential determination. Early workers felt that the proper way to obtain internally consistent values for appearance potentials was to adjust instrument sensitivity for the measurement of each fragment ion intensity versus electron energy curve so that all curves would have about the same height at some moderate voltage such as 30 or 50 volts. Thus, a much higher sensitivity was used for the determination of a metastable ion appearance potential than for the same fragment ion appearing as a "normal" ion in the mass spectrum. As was noted by Rosenstock, et al., in 1955,[7] one then would expect to observe a higher appearance potential for the fragment ion than for the same ion appearing as a metastable. If, however, one used the same instrument sensitivity for both measurements, one should observe essentially the same appearance potential for both.

The discussion so far properly applies only to the lowest activation energy path for decomposition. The more complex situation for other reactions will be considered only briefly in the presentation of this paper.

Vestal has noted[8] that interpretations of experimental data have varied from complete neglect of the possibility of a kinetic shift to gross overestimates of its magnitude. He calculated that for small ions and low $(\varepsilon_{act} - I_z)$ the kinetic shift is small but that in other cases the kinetic shift can be greater than an ev.

The kinetic shift can be studied by examining the variation of the product ion appearance potential with variation in time scale for its production. Gordon and Reid[9] utilized an ion trapping technique to retain ions in the source of a conventional magnetic mass spectrometer for times up to 1200 μs. Using a standard electron impact ion source and determining appearance potentials by a semi-logarithmic plot method, they found, in agreement with theory, no kinetic shift for ethylene giving acetylene ion. However, they reported large shifts in other cases; 0.7 v for $C_6H_5CN \rightarrow C_6H_4^+$, 1.5 v for $C_6H_6 \rightarrow C_6H_5^+$, and 1.3 v for $C_7H_8 \rightarrow C_7H_7^+$. Appearance potentials from long ion residence times yielded values for ionic heats of formation in agreement with thermochemical values, indicating zero reverse activation energy for all three of these reactions (within experimental precision of 0.2 ev). Their results were generally in agreement with previous workers who reported large differences in appearance potentials between normal product ion and metastable ion in the above reactions.

Gross[10] used an ion cyclotron resonance mass spectrometer with ion residence times of the order of 10 ms compared to the <10 μs of most other mass spectrometers. A semi-logarithmic method was used to determine appearance potentials and the results were in agreement with short residence time measurements on the fragmentation of small polyatomic ions, but were significantly lower for larger ion fragmentations. In contradiction Bentley, Johnstone, and McMaster,[11] using their IE/EDD technique to determine appearance potentials, found NO difference between normal fragment ion and metastable ion appearance potential (<0.2 ev). The explanation, I believe, is that the semi-logarithmic method as usually applied involves an arbitrary normalization while the method of Bentley et al., essentially involves the determination of ion appearance potentials at high and constant sensitivity for all measurements. Similarly, "kinetic shifts" reported in many other publications in general can be related to differences in the acquisition of ionization efficiency data and in its analysis to give an appearance potential.

The kinetic shift may also be investigated by studying the translational kinetic energy of product ions. Franklin and co-workers[12] have examined the translational energy of fragment ions. The assumption that the average translational energy of products is given directly by the average energy in the activated complex reaction coordinate gave reasonable agreement with experiment for fourteen reactions studied. This agreement implies a zero or negligible reverse activation energy for these reactions, not only those resulting from a simple bond break but also those requiring a hydrogen transfer to yield H_2O or CH_4 as the neutral fragment.

Klots[13] has developed an alternative formulation of QET. He has discussed the translational energy expected in ion dissociation reactions and also how thermal and kinetic information can be obtained from data on metastable transitions by use of his model. As is the case with the usual QET, the lack of sufficiently precise data makes a rigorous comparison with experiment impossible.

Beynon[14] and co-workers note that the shape of a metastable peak obtained in a double-focusing mass spectrometer contains information not only about average translational energy of the fragment ion but also about the distribution of metastable fragment ion translational energy. Since Dr. Beynon is the next speaker, I shall leave this topic to him.

As the size of molecule studied increases, the expected kinetic shift for a fragmentation increases, but so does the thermal energy of the molecule before ionization and hence also the internal energy of the ion after

the transfer of some specific amount of energy by an incident photon or electron. Thus, a complete correction for chemical shift, without a simultaneous correction for molecular thermal energy, would be an over-correction and lead to too low a value for ΔH for the ionization-dissociation reaction.

I wish to acknowledge the great help of Mrs. Lenore Frank in the preparation of this paper.

REFERENCES

1. Homer D. Hagstrum and John T. Tate, Physical Review 59, 354-370 (1941).

2. D. P. Stevenson, J. Chem. Phys. 10, 291-294 (1942).

3. Alois Langer, J. Phys. and Colloid Chem. 54, 618-629 (1950).

4. H. M. Rosenstock, M. B. Wallenstein, A. L. Wahrhaftig and H. Eyring, Proc. Natl. Acad. Sci. U.S. 38, 677-698 (1952).

5. L. Friedman, F. A. Long, and M. Wolfsberg, J. Chem. Phys. 26, 714-715 (1957).

6. William A. Chupka, J. Chem. Phys. 30, 191-211 (1959).

7. H. M. Rosenstock. A. L. Wahrhaftig, and H. Eyring, J. Chem. Phys. 23, 2200 (1955).

8. Marvin L. Vestal, Fundamental Processes of Radiation Chemistry, P. Ausloos (ed.), Ieterscience Publishers, pp. 59-118 (1968).

9. S. M. Gordon and N. W. Reid, Int. J. Mass Spectrom. Ion Phys. 18, 379-391 (1975).

10. Michael L. Gross, Org. Mass Spectrom. 6, 827-831 (1972).

11. T. William Bentley, Robert A. W. Johnstone, and Blair N. McMaster, J. C. S. Chem. Comm., 510-511 (1973).

12. Ellen L. Spotz, William A. Seitz, and J. L. Franklin, J. Chem. Phys. 51, 5142-5148 (1969).

13. Cornelius E. Klots, Z. Naturforsch. 27a, 533-561 (1972); J. Chem. Phys. 58, 5364-5367 (1973).

14. J. H. Beynon, J. A. Hopkinson and G. R. Lester, Int. J. Mass Spectrom. Ion Phys. 1, 343-351 (1968).

Application of IKES to ion enthalpy determination.

J. H. BEYNON and R. K. BOYD,
University College of Swansea, Chemistry Department,
Swansea SA2 8PP, U.K.

To obtain a complete picture of the thermochemistry of a fragment ion formed in a mass spectrometer, both the appearance potential and reverse activation energy are necessary. The technique of ion kinetic energy spectrometry (IKES), which permits high-sensitivity studies of fragmentation products of metastable ions, yields values of both these energetic quantities. Choice of metastable ions, rather than ions, fragmenting in the source, results in higher sensitivity in appearance potential measurements, due to the shapes of curves of fragment ion current *vs*. bombarding electron energy. Measurement of the detailed shape of the IKE peak yields complete information concerning the profile of translational energy release during fragmentation. The necessary assumptions concerning partitioning of transition state energy between internal and translational modes during fragmentation, and their effect on estimates of product ion enthalpies, will be discussed.

Auger Electron Spectrometry Involving Valence Levels*

M. O. Krause

Transuranium Research Laboratory
Oak Ridge National Laboratory
Oak Ridge, Tennessee 37830

While determinations of single ionization energies of molecules have reached a point at which various threshold effects need to be taken into account [1], determinations of double ionization energies of molecules are still at an early stage of development. The first determinations have come from mass spectrometric studies in which the appearance potentials of stable doubly charged molecular ions, M^{2+}, were measured or in which the observation of a certain fragment ion or the coincidence of two fragments, could be correlated with an initially doubly ionized molecular ion. However, as stable M^{2+} ions are rare and pathways leading to a given fragment ion often uncertain, few M^{2+} states are accessible by this technique. More recent determinations are due to (a) double charge transfer spectroscopy [2], in which the translational energy of H^- from $H^+ + M \rightarrow H^- + M^{2+}$ is measured; and (b) Auger electron spectrometry [3,4,5] in which the energies of those Auger events that involve the valence levels of a molecule are measured.

In this paper, I shall discuss the potential of Auger spectrometry to delineate the various M^{2+} states. More familiar to the mass spectrometrist than the Auger effect is the autoionization process. However, autoionization involving two electrons is an Auger process and an Auger process is an autoionization event, even though the term Auger process is generally reserved for events involving at least one core electron. The initial inner-shell vacancy can be created by electron, photon, or particle excitation [6], and in competition with radiative processes can decay by an Auger process in which one of the valence electrons fills the core vacancy and another carries away the excess energy of the process. We have

$$E(\text{Auger}) = E(\text{initial state}) - E(\text{final state}) \qquad (1)$$

where the initial state is a single core vacancy and the final state is a double vacancy in the valence levels. Since the energy of the initial state is usually known, a measurement of the Auger energies yields the double ionization energies of the molecule. This is the energy that has been deposited in the molecule before its potential fragmentation; and the locus of this energy deposition can be identified in simple cases.

According to the selection rules the total angular momentum J and the symmetry are conserved, $u \rightarrow u$ and $g \rightarrow g$ for homonuclear molecules, and $\Delta S = 0$, $\Delta\Lambda = 0, \pm 1$ for Hund's coupling.

The width (FWHM) of an Auger line is given by

$$\Gamma(\text{Auger}) = \Gamma(\text{initial state}) + \Gamma(\text{final state}) \qquad (2)$$

*Part of this study was done under a Humboldt Award at the University of Freiburg/Germany, and part was sponsored by the U. S. Energy Research and Development Administration under contract with Union Carbide Corporation.

provided the widths of the initial and final states are governed solely by the decay rates and hence are Lorentzian. In atoms, Γ(Auger) $\approx$ Γ(initial state) for Auger transitions to the outermost levels; in molecules, Γ(Auger) $\approx$ Γ(final state) generally. In favorable instances, the vibrational structure of a stable state can be viewed through a window with width Γ of the initial state.

Auger spectra affording the best resolution originate in the K shells of first-row elements, 2p shells of second-row elements, 3d shells of third-row elements and so on. In these instances, the Auger transition rates are about 10^{15}/sec, corresponding to Γ = 0.1 eV since the radiative rates are negligible. Hence, M^{2+} states with a lifetime of 10^{-15} sec or greater are observable.

Under customary excitation conditions, normal Auger lines due to a single core vacancy are accompanied by various satellites whose nature must be understood to successfully utilize an Auger spectrum. By now, characteristics of satellites have been elucidated from studies of both atomic [7,8] and molecular systems [3,4,9].

Using N_2, the most thoroughly studied molecule [3,4,9,10], the interpretation of an Auger spectrum is given step by step describing an experiment that has not yet been done but is now possible with the use of the continuously variable synchrotron photon source.

In Fig. 1a, the entire N_2 spectrum is presented as it was measured by electron and light particle excitation [3,4,9-11]. A similar spectrum would be obtained if a white-spectrum photon source were used. Excitation by photons with $h\nu$ = 401 eV would result in the spectrum depicted schematically in Fig. 1b. At this energy, resonance absorption occurs, for example $\sigma_g 1s$, $^2\Sigma_g \rightarrow \pi_g, 2p, {}^1\Pi_g$, and in the subsequent Auger decay the lines A_a, A'_a, and A''_a are produced if the excited π_g,2p electron participates in the transition, and the structures A_s, A'_s, and A''_s if it does not. These satellites appearing at higher energies than the normal Auger lines correlate with a molecule left singly ionized.

When the K-ionization threshold at E = 410 eV is exceeded, the normal Auger spectrum depicted schematically in Fig. 1c emerges. It correlates with doubly ionized N_2. Structure B involves the least tightly bound valence electrons, corresponding to the 2p electrons in the atomic case; structure B" involves the most tightly bound valence electrons, corresponding to atomic 2s electrons; and B' involves s and p like electrons. The D lines indicate schematically the occurrence of double Auger processes. The B lines can be correlated with N_2^{2+} states whose potential curves have been calculated [3,12], allowing one to determine the low-lying energy states of N_2^{2+} from the B peaks. The other N_2^{2+} states can be obtained, in principle at least, from the regions B' and B". Of particular interest is the peak B1, since this peak with the highest Auger energy gives the (vertical) double ionization potential.

When the photon energy is increased above the shake<u>up</u> threshold, weak structures are added primarily on either side of the normal lines of Fig. 1c. Further increase of the photon energy well beyond the shake<u>off</u> threshold produces the Auger spectrum shown in Fig. 1d. In shakeup, a valence electron is excited to a bound state simultaneously with the ionization of a K electron, leading to the satellites S_a-S''_a if the excited electron participates in the subsequent Auger decay, and to S_s-S''_s if it does not. In shakeoff, a valence <u>and</u> a K electron are ionized producing the S-S" satellite structures. Shakeup results in N_2^{2+} and N_2^{2+*}, shakeoff in

N_2^{3+}. The S structures can be isolated by subtracting the normal Auger spectrum of Fig. 1c from the spectrum of Fig. 1d. Then the lowest ionization energy of the N_2^{3+} molecule can be obtained. The shoulder S1 was previously associated with this potential [4].

Figure 2 shows the potential curves that can be reached by an Auger process. As a rule one expects the stable states to correlate with narrow Auger lines and the unstable ones with broad peaks. Stable states should be associated with Auger spectra displaying a vibrational structure. Such a structure has in fact been demonstrated in the Auger spectrum of CO [4,10], but in general there is little likelihood of being able to delineate vibrational fine structure even with the best instrumental resolution. One reason is that the core level width is about 0.1 eV and therefore of the same order as the vibrational spacing; another reason is that upon core ionization the internuclear distance may change leading to several overlapping Auger decay series each arising from a different state

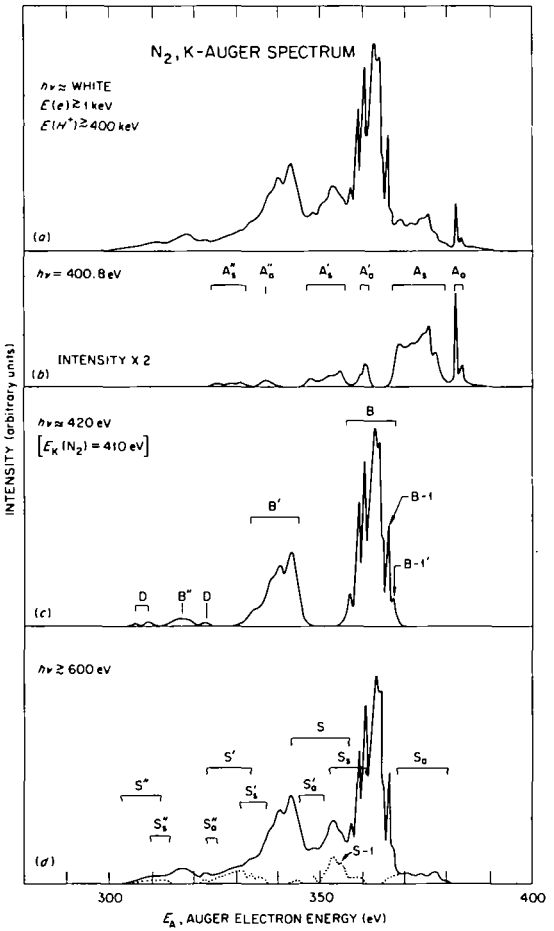

Fig. 1. Schematic representation of N_2 Auger spectra produced by photons of different energies. Approximate normalization to structure B. Spectra (a) and (d) have been measured, spectra (b) and (c) are predicted. Dotted structure in (d) is the difference between spectra (d) and (c).

of vibrational excitation of the innershell ionized molecule. Such internuclear relaxation has been demonstrated [13] by photoelectron spectrometry for CH_4 as shown in Fig. 3.

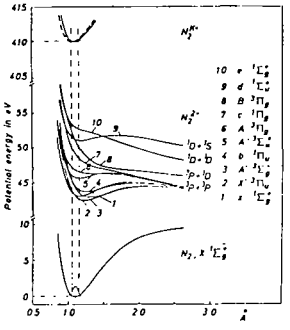

Fig. 2. Potential curves of N_2, N_2^{2+}, and N_2^{K+} [3].

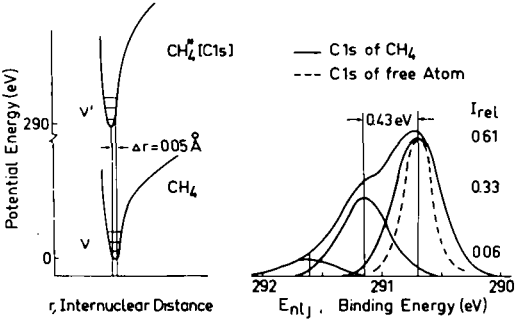

Fig. 3. Vibrational structure in the K-shell ionized CH_4 molecule as seen in a photoelectron spectrum (adapted from [13]).

It follows from this discussion that the energy of the peak B1 corresponds to the vertical ionization potential and that an accurate determination of the adiabatic ionization potential would presuppose an exact knowledge of, inter alia, the vibrational structures of the states of the doubly ionized molecule and the innershell ionized molecule. Otherwise, the adiabatic ionization energy can be determined with an accuracy of only a few tenths of an eV even from an experiment such as that illustrated by Fig. 1. Peak B1' presumably indicates the adiabatic energy.

In Table I, electron impact data [14] referring to the stable M^{2+} state of minimum energy are compared with Auger spectrometric data [4,15].

Table I. Minimum energy (eV)required for doubly and triply charged molecular ions. A: data from Auger spectra [4,15]; E: data from electron impact [14].

Ion	A	E	Ion	A	E
N_2^{2+}	42.9	42.7	NO^{2+}	35.7	39.8
N_2^{3+}	84	-		40.1(N)	
O_2^{2+}	37.4	36.5		34.7(O)	
CO^{2+}	39.9(C)	41.8	H_2O^{2+}	39.2	-
	40.2(O)		CO_2^{2+}	37.8(C)	36.4
$C_2O_2^{2+}$	29.7	33.0		37.4(O)	

In heteronuclear molecules, the Auger spectra originating from a K vacancy in the different atoms might be expected to be identical since in both cases the final states obtain to the same valence electrons. Indeed, this holds for the line spacing, but not for the relative intensities showing a rate dependence on the localization of the electrons [4,15]. Thus, it is possible to selectively double-ionize a molecule by creating an inner shell vacancy in one or the other atomic constituent.

A profitable use of Auger spectra would be to place an Auger electron of a given energy in coincidence with a mass and energy-analyzed fragment ion. Such an experiment would allow the unambiguous determination of the pathways to a certain fragmentation pattern and yield essential terms for the energy balance of a fragmentation process.

1.) See contributions to this Symposium.
2.) J. Appell, J. Durup, F. C. Fehsenfeld and P. Fournier, J. Phys. B, 6, 197 (1973).
3.) D. Stalherm, B. Cleff, H. Hillig, and W. Mehlhorn, Z. Naturf. 24a, 1728 (1969).
4.) W. E. Moddeman, T. A. Carlson, M. O. Krause, B. P. Pullen, W. E. Bull, and G. K. Schweitzer, J. Chem. Phys., 55, 2317 (1971).
5.) T. A. Carlson, "Photoelectron and Auger Spectroscopy," Plenum Press, N. Y. (1975).
6.) M. O. Krause, "Electron Spectrometry" in Atomic Innershell Processes, Vol. II, Academic Press (1975), p. 33-81, Fig. 1.
7.) M. O. Krause, T. A. Carlson, and W. E. Moddeman, J. Phys. (Paris), 32, C4-139 (1971).
8.) V. Schmidt, in "Proc. Intern. Conf. Inner Shell Ionization Phenomena," US-AEC Conf.-720404, R. W. Fink, et al., eds. (Jan. 1973), p. 548.
9.) T. A. Carlson, W. E. Moddeman, B. P. Pullen and M. O. Krause, Chem. Phys. Lett., 5, 390 (1970); F. Wuilleumier and M. O. Krause, in Proc. Intern. Conf. Inner Shell Ionization Phenomena, US-AEC Conf., 720404, R. W. Fink, et al., eds. (Jan. 1973), p. 773.
10.) K. Siegbahn, et al., "ESCA Applied to Free Molecules," North Holland Publ. Co., Amsterdam (1969).
11.) N. Stolterfoht and D. Schneider, Phys. Rev. A 11, 721 (1975).
12.) A. C. Hurley, J. Mol. Spectr., 9, 18 (1962).
13.) U. Gelius, E. Basilier, S. Svensson, T. Bergmark, and K. Siegbahn, J. Electr. Spectrosc., 2, 405 (1974); U. Gelius, J. Electr. Spectrosc., 5, 985 (1974)
14.) J. L. Franklin, et al., NBS Ref. Data Series, 26 (1969).
15.) L. Karlsson, L. O. Werme, T. Bergmark and K. Siegbahn, J. Electr. Spectrosc., 3, 181 (1974).

HIGH ENERGY ION/MOLECULE REACTIONS

R. G. Cooks, J. H. Beynon, T. Keough, T. Ast, L. Hendricks, J. F. Litton, D. L. Kemp, C. S. Hsu, M. Medved, T. L. Kruger, V. Franchetti and R. Kondrat, Department of Chemistry, Purdue University, West Lafayette, IN 47907

This paper is concerned with thermochemical and related information obtained by the study of ion/molecule reactions in the kilovolt energy range. The study of these reactions, particularly for polyatomic species, represents a growth point in mass spectrometry. Here an attempt is made to sketch the types of reactions which can be studied and the information so obtainable. Examples are taken chiefly from unpublished work of this laboratory.

Just a few types of reactions can occur when a high velocity ion interacts with a target atom or molecule. In the simplest inelastic processes, there is no change in charge or mass of either of the collision partners. Excitation of one partner occurs at the expense of their relative translational energy, and this reaction is shown in Eqn. 1. Excitation may be followed by unimolecular fragmentation and this overall process of collision-induced dissociation is shown in Eqn. 2. The other main class of reactions involves charge changing collisions, which may be of the stripping type (Eqn. 3) or the charge exchange type (Eqn. 4).

High Energy Ion/Molecule Reactions

Excitation

$$m^+ + N \rightarrow m^{+*} + N \qquad (1)$$

Dissociative Excitation (CID)

$$m^+ + N \rightarrow (m^{+*}) \rightarrow m_2^+ + m_3 \qquad (2)$$

Stripping

$$m^+ + N \rightarrow m^{++} + N + e^- \qquad (3)$$

Charge Exchange

$$m^+ + N \rightarrow m^- + N^{++} \qquad (4)$$

Most studies on high energy ion/molecule reactions have been concerned with collisions in which momentum transfer to the target is negligible and in which the fast product is detected at essentially zero scattering angle. Three measurements can be made on these reactions as listed below.

Types of Measurements

1. Relative cross-sections (σ)

   σ_{max} for $Q = 0$

2. Kinetic energy change (ΔE)

   $\Delta E \approx Q$ (high energy, small angle)

3. Kinetic energy release (T)

Relative cross-sections are measured from peak amplitudes, the kinetic energy change from the precise peak position and the kinetic energy release from the peak width. As a reaction approaches resonance or thermoneutrality (Q=0) the cross-section tends to maximize. The kinetic energy change (ΔE) in the fast species provides a good measure of the heat of reaction (Q) for high energy collisions at small scattering angle. The measurement of kinetic energy release applies only to fragmentations where the origin of the peak broadening is analogous to that for metastable ions.

The application of these measurements to some particular problems is indicated, with typical literature references, below.

<u>Thermochemical Measurements</u>

States present in ion beams (ΔE)

$m_1^+ + N \rightarrow m_1^{++} + N + e$ ref. 1

States of doubly charged ions (ΔE)

$H^+ + M \rightarrow H^- + M^{++}$ ref. 2

Fragment state assignments (ΔE and T)

$CS_2^+ + N \rightarrow CS^{+\cdot}\ (^2\Sigma) + S\ (^1D)$ ref. 3

Energy partitioning (T)

$H_2O^+ \rightarrow OH^+ + H$ ref. 4

$H_2O^+ \rightarrow OH^- + H$

Consider the use of energy loss measurements in obtaining thermochemical data on a neutral molecule, ethylene. Using 3keV He^+ ions and zero angle scattering, Moore[5] has shown that there are two energy loss peaks for the reaction

$$He^+ + C_2H_4 \rightarrow He^+ + C_2H_4^*$$

They fall at 4.3 and 7.8eV and correspond to $\pi \rightarrow \pi^*$ transitions which are very weak in conventional spectroscopy. Assignment of energy levels is accurate to ca. 0.1eV.

There is a close relationship between conventional mass spectral thermochemistry, as expressed in a breakdown curve, and energy loss measurements. Thus the molecular ion of ethanol undergoes collision-induced dissociations to yield fragment ions of m/e 31, 29 and 43.

Appearance potential measurements and QET calculations yield the breakdown graph[6] shown in Figure 1. The energy

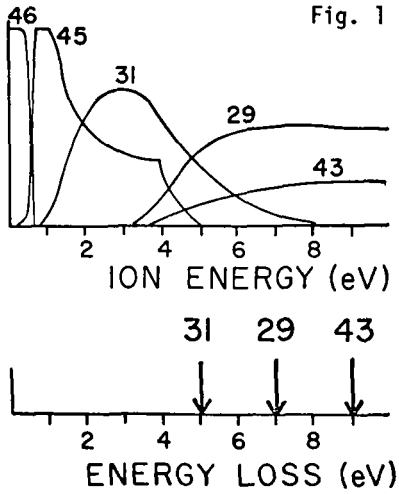

losses accompanying CID are consistent with this as shown by the fact that the energy loss in each case occurs somewhat above the thermochemical onset.[7] It is noteworthy that extremely large energy losses can be observed as in the reaction shown as Eqn. 5.

$$C_7H_7^+ + N \rightarrow C_4^+ + (C_3H_7) + (N) \quad \Delta E = 40eV \qquad (5)$$

The determination of kinetic energy releases for collision-induced dissociations has been considered in the literature.[7] However, there is an effect of pressure on the measured ion kinetic energy distributions which has apparently not been considered previously, either for CID or for metastable ion reactions. This concerns ions which have received components of momentum in the fragmentation process which disallow their collection. If such ions are involved in a subsequent collision, they may be scattered back on axis and collected. The analysis of metastable peak shapes[8] does not consider this effect which may have important effects on the energy resolution obtainable. An example of the probable operation of the effect is shown in Figure 2 for the metastable ion fragmentation

$$C_6H_6^{++} \rightarrow C_6H_3^+ + CH_3^+$$

Fig. 2

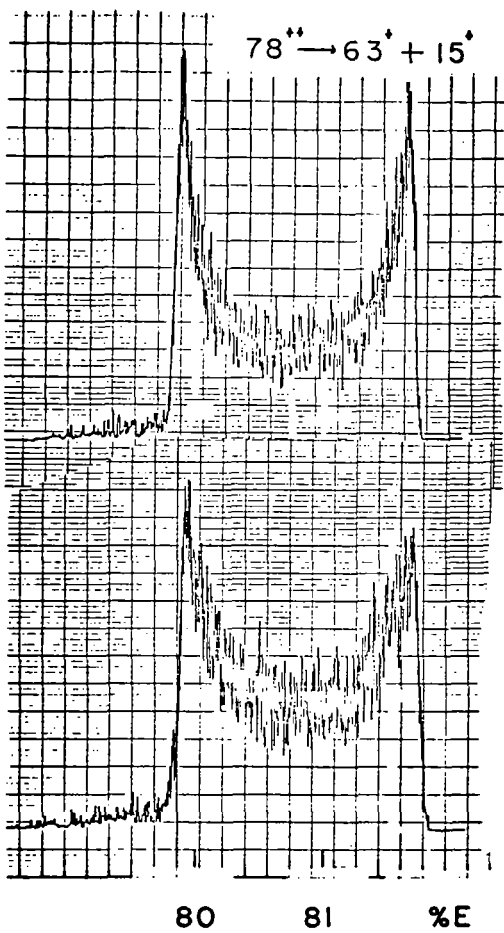

Note how extra ion signal appears in the inside wings of the peak as the target pressure is increased. This represents the scattering back on axis of ions which have directions corresponding to their just being discriminated against in the low pressure regime. Collisions subsequent to fragmentation are thus always to be avoided and this, with other factors[9] speaks for the use of short collision chambers in studying high energy ion/molecule reactions.

The remainder of this paper deals with particular studies made employing high energy ion/molecule reactions.

Independent Characterization of Ions Generated by CI

It is difficult to obtain evidence on the structures and thermochemistry of ions formed by CI (or ICR) except through the CI or ICR spectra themselves. By extracting these ions and studying their high energy ion/molecule reactions, information of this type is obtainable. This is best done using the reversed sector MIKE spectrometer. The principles of the method are illustrated in Figure 3 for the

case of the ethylated product of a disubstituted benzene. Figure 4 shows partial MIKE spectra for two particular cases; the observed fragmentations suggest that the p-cyanonitrobenzene is ethylated on the nitro group while the p-chloroaniline is ring-ethylated.

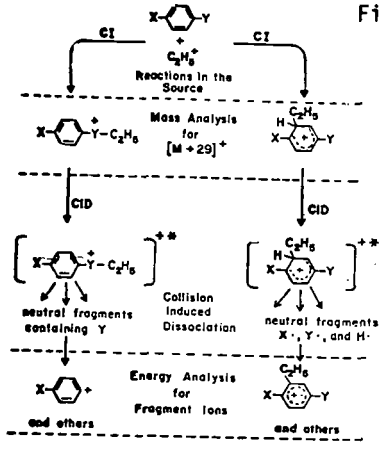

Fig. 3

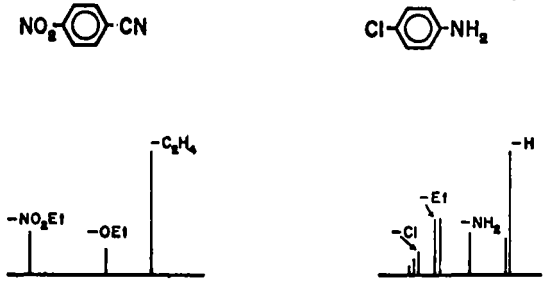

Fig. 4

Alternatives to CID in Ion Structure Determination

While collision-induced dissociation is an effective means of structurally characterizing ions, it could easily be supplemented by using other high energy ion/molecule reactions. Not only is this experimentally convenient, but the information obtained may refer to a different ion population. In particular, the occurrence of isomerism of an ion below the fragmentation threshold can be revealed by employing charge stripping in conjunction with collision-induced dissociation.[10] Figure 5 contrasts the sampling characteristics of these reactions.

Fig. 5

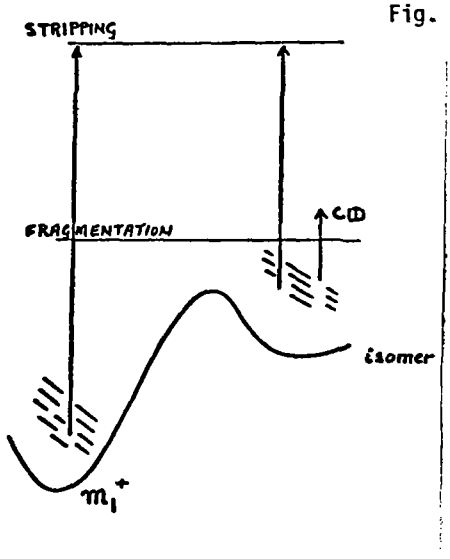

Because the energy loss for charge stripping is much larger than the differences in energy of the isomerized and non-isomerized structures, this reaction is expected to sample the entire stable ion population more uniformly than does collision-induced dissociation. In the latter reaction, the energy loss and hence the cross-section is very different for the two isomeric ions.

Spectroscopy of Organic Ions

By measuring the energy losses associated with ionic excitations which do not result in fragmentation, one can fix the energies of excited states of ions. To avoid overlap with the much more intense beam of elastically scattered ions, this measurement is best made at a non-zero scattering angle. This can be done using a modified mass spectrometer.[11] The best available methods for studying the states of ions either employ transitions from the neutral molecule as in photoelectron spectroscopy, or they refer to dissociative states of the ion as in photodissociation spectroscopy. The present approach, although still limited in accuracy, has the advantage of characterizing excitations between stable states of an ion. The situation is summarized in Figure 6 which compares conventional spectroscopy, photoelectron spectroscopy (PES) and photodissociation spectroscopy (PDS). Figure 7 illustrates some results of the ion/molecule type of measurement and compares them (in brackets) with PES data. The ethylene case in which ions are formed in states above the dissociation limit and yet survive for times of the order of microseconds is of special interest.

Fig. 6

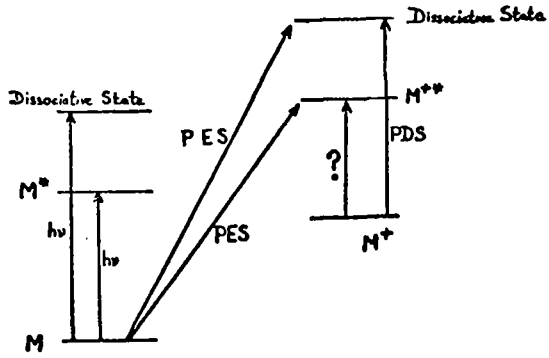

Fig. 7

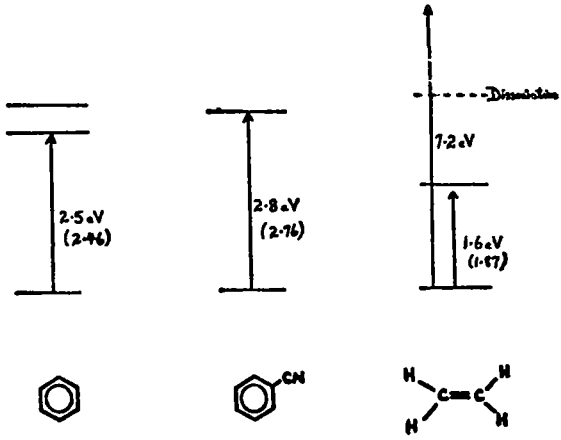

Ion/Surface Reactions

A whole class of phenomena, paralleling high energy ion/molecule reactions, involve ion/surface reactions. These offer structural and thermochemical information on ions and on surfaces.

It has previously been shown[12] that at grazing incidence the common excitation, stripping and charge exchange processes can occur at a surface. (See Figure 8) We now report[13] new

Fig. 8

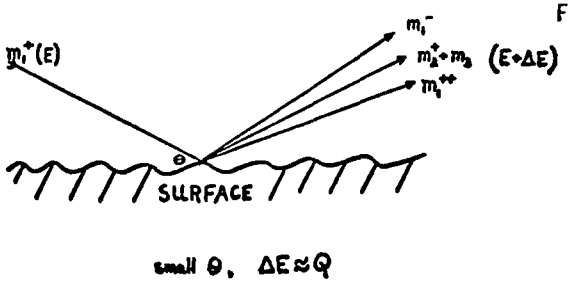

types of experiments involving larger scattering angles. We study here not the inelastic channels but the elastically scattered (reflected) ions. A mass spectrum can be run showing the relative abundances of all reflected ions from a particular sample. Comparisons of these reflection spectra with the corresponding mass spectra show striking differences. The reflection spectrum of benzene, reproduced in Figure 9, verifies this. The unique stability, to reflection, of $C_4H_2^{+\cdot}$ is dramatic.

Fig. 9

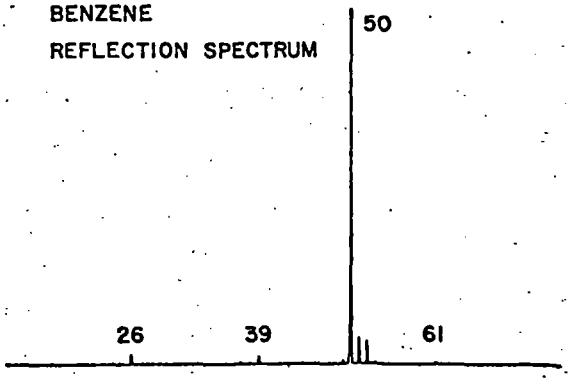

ACKNOWLEDGMENT

The support of the National Science Foundation is gratefully acknowledged.

REFERENCES

1. T. Ast, J. H. Beynon and R. G. Cooks, "Long-lived States of Rare Gas Ions. An Ion Kinetic Energy Study," J. Amer. Chem. Soc., 94, 6611 (1972).

2. J. Appell, J. Durup, F. C. Fehsenfeld and P. Fournier, "Double Charge Transfer Spectroscopy of Diatomic Molecules," J. Phys. B: Atom. Molec. Phys., 6, 197 (1973).

3. K. C. Kim, M. Uckotter, J. H. Beynon and R. G. Cooks, "Collision-Induced Fragmentation of Triatomic Ions," Int. J. Mass Spectrom. Ion Phys., 15, 23 (1974).

4. T. Keough, J. H. Beynon and R. G. Cooks, "Dissociative Double Electron Capture. Dynamics of Fragmentation of the Water and Hydrogen Sulfide Negative Ions," Chem. Phys., 12, 191 (1976).

5. J. H. Moore, Jr., "An Investigation of the Low Energy Singlet-Triplet and Singlet-Singlet Transitions in Ethylene Derivatives by Ion Impact," J. Phys. Chem., 76, 1130 (1972).

6. M. Vestal and G. Lerner, Fundamental Studies Relating to the Radiation Chemistry of Small Organic Molecules, Office of Aerospace Research, USAF, ARL 67-0114, 1967.

7. R. G. Cooks, L. Hendricks and J. H. Beynon, "Collision-Induced Dissociations of the Lower Alcohols. A Thermochemical Study," Org. Mass Spectrom., 10, 625 (1975).

8. D. T. Terwilliger, J. H. Beynon and R. G. Cooks, "Kinetic Energy Distributions from the Shapes of Metastable Peaks," Proc. Roy. Soc., (London) A, 341, 135 (1974).

9. R. G. Cooks and J. H. Beynon, "Ion Kinetic Energy Spectrometry," in A. Maccoll (Ed.) Mass Spectrometry, International Review of Science, Physical Chemistry, Series Two, Volume 5, 1975.

10. R. G. Cooks, J. H. Beynon and J. F. Litton, "Ion Structure Determination Through Collisions of Ions of High Kinetic Energy," Org. Mass Spectrom., 10, 503 (1975).

11. M. Medved, R. G. Cooks and J. H. Beynon, "Ion Kinetic Energy Losses and Excited State Population in Ion Molecule Reactions," Chem. Phys., in press.

12. R. G. Cooks, D. T. Terwilliger, T. Ast, J. H. Beynon and T. Keough, "Surface Modified Mass Spectrometry," J. Amer. Chem. Soc., 97, 1583 (1975).

13. V. Franchetti and R. G. Cooks, "Ion/Surface Reflection Mass Spectra," Int. J. Mass Spectrom. Ion Phys., in press.

Laser Photodetachment. W. C. LINEBERGER, Univ. of Colorado, Joint Institute for Laboratory Astrophysics and Dept. of Chemistry, Boulder, Colorado 80309

The techniques of tunable laser photodetachment of negative ions and laser photoelectron spectrometry of negative ions have been extensively utilized in the last four years to generate thermochemical data for a variety of atomic and molecular ions. In the atomic ion case, the interpretation of the experimental data is generally straightforward, and unambiguous atomic electron affinities are readily obtained.[1] Molecular negative ion photodetachment can be much more complicated as a result of 1) hot bands in the negative ion, 2) rotational structure, 3) large geometry changes between the negative ion and the corresponding neutral, and 4) the possibility of photodissociation. When such data are fully analyzed however, the structural information obtained is correspondingly more rich. In favorable cases, such as CH_2^-, one can deduce substantial portions of both the neutral and negative ion potential surfaces. The methodology of such measurements will be reviewed, and compared with other techniques for molecular electron affinity determinations.

[1] H. Hotop and W. C. Lineberger, J. Phys. Chem. Ref. Data (in press).

Electron Affinities of Polyatomic Species. JOHN I. BRAUMAN, Dept. of Chem., Stanford University, Stanford, Calif. 94305

We obtain estimates (generally upper limits) for EA's by observing thresholds for photodetachment of electrons from negative ions. Ion intensities (with and without light) are determined by ion cyclotron resonance. Major possible sources of error are excited ions (hot bands) and misidentification of the threshold due to (1) Franck-Condon problems and (2) small cross sections at threshold. These problems can partially be dealt with experimentally by lifetime and pressure dependence and theoretically by estimation of Franck-Condon factors and calculation of threshold shape. Possible discrepancies between these and other data will be discussed.

Determination of Ion Thermochemical Properties by Ion Cyclotron Resonance Spectroscopy.

J.L. BEAUCHAMP, California Institute of Technology, Dept. of Chem., Pasadena, CA. 91125

Ion cyclotron resonance spectroscopy is being widely applied to the determination of ion thermochemical properties. Studies of the generalized acid-base equilibria 1 and 2

$$AB_1 + B_2 \rightleftarrows AB_2 + B_1 \qquad (1)$$

$$A_1B + A_2 \rightleftarrows A_2B + A_1 \qquad (2)$$

have been carried out for a variety of acids A{e.g., H^+, Li^+, $CpNi^+$, R^+ (carbonium ions), $(CH_3)_3B$, etc.} and bases B{e.g., H^-, F^-, Cl^-, Br^-, n-donor, π-donor and σ-donor neutrals, carbanions, etc.}. The experimental methods utilized in these studies include variable pressure (drift mode) and variable time (trapped ion) techniques. These ICR studies will be critically reviewed and compared with other techniques which provide similar data. Several new research areas will be discussed, including the determination of acid-base properties of molecules in excited electronic states.

Thermochemical Results from Pulsed ICR Equilibrium Studies. R.T. McIVER, JR., and J.S. MILLER, Univ. of Calif., Chem. Dept., Irvine, Ca, 92717.

Since the time of the first measurement of equilibrium constants for proton-transfer reactions in the gas phase[1], there has been a great deal of interest in quantitative determinations of relative gas-phase acidities and basicities. Given a chemical reaction system and temperature, chemical equilibrium is a unique and well-defined state, and the validity of thermochemical results derived from Pulsed ICR studies is dependent on the conditions inside the ICR analyzer cell. This paper will carefully analyze the Pulsed ICR experiment in terms such as the number of ion-neutral collisions during the reaction period, the time scale for ion formation, reaction, and detection, and instrumental features which might alter the energy distribution of the ions. Numerous ICR results now available for bond dissociation energies and electron affinities will be presented and compared with the results of other techniques.

---

[1] M.T. Bowers, D.H. Aue, H.M. Webb, and R.T. McIver, Jr., J.A.C.S., 93, 4314 (1971); D.K. Bohme, E. Lee-Ruff, and L.B. Young, ibid., 93, 4609 (1971); R.T. McIver, Jr., and J.R. Eyler, ibid., 93, 6334 (1971).

FLOWING AFTERGLOW MEASUREMENTS BEARING ON THE THERMOCHEMISTRY OF GASEOUS IONS

D. K. Bohme and G. I. Mackay

Department of Chemistry and
Centre for Research in Experimental Space Science,
York University, Downsview, Ontario M3J 1P3, Canada

Flowing afterglow studies which origionally relied on the observation of the occurrence and/or non-occurrence of ion-molecule reactions to provide information on ion energetics have been extended in recent years to measurements of equilibrium constants, especially those for competitive solvation reactions of the type

$$X^{\pm}.\ Y_n + S \rightleftharpoons X^{\pm}.\ Y_{n-1}.\ S + Y \qquad [1]$$

termolecular association reactions of the type

$$X^{\pm}.\ Y_n + Y + M \rightleftharpoons X^{\pm}.\ Y_{n+1} + M \qquad [2]$$

and proton transfer reactions of the types

$$XH^+ + Y \rightleftharpoons YH^+ + X \qquad [3]$$

$$XH + Y^- \rightleftharpoons YH + X^- \qquad [4]$$

The results of these measurements have provided heats of formation of ions, bond energies of cluster ions and neutral molecules, electron affinities and proton affinities which have proven to be sufficiently accurate to be of both academic and practical value.[1,2] In this brief discourse we shall consider the quality of such equilibrium constant measurements as revealed from studies of proton-transfer reactions. Special attention will be given to possible errors introduced by the diffusion of ions in the flowing plasma and their sampling and detection.

Let us first examine how conditions for true equilibrium can be met with a flowing afterglow apparatus.

1. Sufficient time and concentrations are provided for the reaction to reach equilibrium. The reaction time which is fixed at ~ 5 or ~ 10 msec by the carrier gas flow velocity and the positions of the reactant inlet port and sampling orifice is quite sufficient for the fast reactions ($k \sim 10^{-9}$ cm^3 molecule^{-1} sec^{-1}) investigated at the concentrations of ions and neutrals usually available (~ 10^8 ions cm^{-3}, ~ 10^{10} to ~ 10^{14} molecules cm^{-3}). The dynamic range available for neutral concentrations (~ 10^4) and ion signals (~ 10^4) allow measurements of equilibrium constants $\lesssim 10^8$.

2. Both reactants and products are allowed to establish thermal equilibrium with their common surroundings prior to reaction. The thermalization of ions prior to their entry into the reaction region is ensured by the spacial separation of the ion production and reaction regions and the use of a buffer gas at ~ 0.3 torr. Within the reaction region one relies on collisions with molecules of the buffer gas which are in large excess (~ 10^{16} cm^{-3}) to thermalize both reactant and product

ions prior to reaction.

3. The process (whether a single or sequential reaction) which links two ions in equilibrium is unambiguously identified. The signals corresponding to the reactant and product ions and their ratio are monitored throughout the approach to and attainment of equilibrium as neutral reagent is added. Also care is taken to identify other source and loss processes for these ions: competing two-body channels and three-body association reactions. Finally, when the diffusion coefficients of the two ions are not nearly the same, preferential loss of one of the ions by diffusion is minimized by adding SF_6 into the reaction region. This changes the diffusion mode from ion-electron to ion-ion which is less rapid and less discriminating.

The equilibrium constants are obtained in practice either from a measurement of k_f/k_r determined from a fit to the decay of the reactant ion signal as the reaction approaches and attains equilibrium or from a measurement of relative concentrations of ions and neutrals once equilibrium is achieved.[3] Ion mass discrimination in the sampling region is accounted for by insisting that the sum of the reactant and product ion signals should remain constant and equal to the initial reactant ion signal. The stoichiometry of the reaction ensures this relationship in the absence of competing reactions and preferential ion loss by diffusion. A plot of the reactant vs. product ion signal should then yield a straight line with slope = -m, the mass discrimination factor.

A number of tests are usually carried out to establish confidence in the attainment of true equilibrium. The equilibrium constant is usually determined at different ion relaxation and reactant times, various flows of neutral back-reactant, in both directions of approach to equilibrium, in different buffer gases at various pressures, at various electron and ion densities and under different sampling conditions. Consider, for example, our studies[3,4] of the equilibrium

$$CO_2H^+ + CH_4 \rightleftharpoons CH_5^+ + CO_2 \qquad [5]$$

This equilibrium was approached from both directions at room temperature in a H_2 buffer at pressures ranging from 0.219 to 0.63 torr. The flow of back-reactant was varied by a factor of ~ 300 (flow of CO_2) in the forward direction and a factor of ~ 40 (flow of CH_4) in the reverse direction. Figures 1 and 2 show families of curves at various flows of back-reactant whose fits provided values for k_f/k_r. These experiments provided a unique value of 24±1 for the equilibrium constant. Figure 3 to 6 explore the affect of sampling conditions on these measurements. Fig. 3 shows a family of CO_2H^+ decays at various values for the nose cone (NC) potential (the potential of the nose cone with respect to the flow tube) at a fixed draw-in potential - the potential applied between the nose cone and the case of the quadrupole mass filter (QC). The fits to these decays all provided the same value for k_f/k_r within the experimental uncertainty. A similar result was obtained as the draw-in potential was varied at a fixed nose-cone potential as shown in Fig. 4. All the decays could be fit with the same value of $k_f/k_r = 23$. The mass discrimination between CO_2H^+ and CH_5^+ was observed to be independent of the NC potential at fixed QC potential but, as shown in Fig. 5, to depend on the QC potential at fixed NC potential. Mass discrimination decreases ($m \rightarrow 1$) at high draw-in potential as a result of the improved focussing of the high mass ion, CO_2H^+, into the mass filter. Fig. 6 displays the variation of the

measured ion ratio as equilibrium is achieved at various draw-in potentials. The measured equilibrium constant was observed to be independent of the draw-in potential within the experimental uncertainty when the correction was made for mass discrimination. Figures 7 to 9 explore the affect of diffusion on the equilibrium constant measurements. Fig. 7 shows the expected enhancement in ion signals as SF_6 is added. However, the shape of the CO_2H^+ decay and therefore the value of the k_f/k_r derived from a fit to this decay remains essentially unchanged as would be expected if CO_2H^+ and CH_5^+ have similar diffusion coefficients. The small change in the mass discrimination factor shown in Fig. 8 may reflect a genuine change in the sampling conditions at the orifice. The equilibrium constants derived from the ion-signal ratio at equilibrium again agree within experimental error when a correction is made for mass discrimination as is shown in Fig. 9.

Serious complications may be introduced into the equilibrium analysis if the diffusion losses of reactant and product ions are unequal. Figures 10-12 illustrate such complications for the reaction

$$H_3^+ + Kr \rightleftharpoons Kr\ H^+ + H_2 \qquad [6]$$

studied in a helium buffer.[5] A change in the difference in the diffusion coefficients of H_3^+ and KrH^+ as the diffusion mode is altered from electron-ion to ion-ion results in a definite change in the shape in the primary-ion decay and the value derived for k_f/k_r (Fig. 10), the shape of the mass idscrimination plot and the value derived for m (Fig. 11) and the value derived for the equilibrium constant from the equilibrium ion ratio (Fig. 12). Since the diffusion losses for H_3^+ and $Kr\ H^+$ will be more equal in the ion-ion mode, the apparent value derived for K in the presence of SF_6 will be closer to the true value of the equilibrium constant.

The final 6 figures serve to illustrate the role of competing two-body and three-body association reactions in equilibrium constant determinations. The occurrence of such reactions can of course influence the shapes of the primary ion decay, the mass discrimination plot and the ratio plot and therefore must be taken into account in a meaningful analysis of the data. Alternatively, operating conditions may be adjusted to minimize the rates of such reactions. Curvature in the mass-discrimination plot provides a sensitive indicator for the presence of such complications. Figures 13 to 18 provide some examples which have been encountered in a recent study of proton transfer reactions of type [4]:

1. Further reaction of the product ion with the neutral reagent by three-body association (Figs. 13 and 14).
2. A competing two-body channel in both directions of the reaction (Figs. 15 and 16).
3. Further reaction of the product ion with the neutral reagent by a two-body reaction followed by reaction with the neutral back-reactant to regenerate the primary reactant ion (Figs. 17 and 18)!

These results (especially example 3 in which the intermediate ion could easily have gone unnoticed) emphasize the caution which must be excercised in the gathering and analysis of data in equilibrium studies of this type. An extension to the standard analysis which takes into account competing source and loss processes under typical flowing afterglow conditions has recently been reported.[6]

Notwithstanding the complications which may be introduced by competing reactions, diffusion and sampling, the general quality of the equilibrium constant measurements with the flowing afterglow technique has proven to be sufficient to provide standard free energies for reactions of types [1] to [4] with an accuracy $\lesssim$ 0.5 kcal mole^{-1}. The accuracies of thermochemical values for proton affinities, electron affinities etc. derived from these standard free energy changes are generally limited by the uncertainties in the required supplemental data for neutral species.

Detailed comparisons of the measured equilibrium constants for proton-transfer reactions and the derived thermochemical quantities with those determined with other equilibrium (Ion-Cyclotron-Resonance, High Pressure Mass Spectrometry etc.) and non-equilibrium (Photodetachment, Photo ionization, Electron-Impact Ionization etc.) techniques have appeared[7] and will be reported elsewhere[8] in the near future.

References

1. E. E. Ferguson, in 'Ion-Molecule Reactions', J. L. Franklin (Ed.), Vol. 2, Plenum Press, New York, 1972, Ch. 8.
2. (a) H. I. Schiff and D. K. Bohme, Int. J. Mass Spectrom. Ion Phys. 16, 167 (1975). (b) D. K. Bohme, in 'Interactions Between Ions and Molecules', P. Ausloos (Ed.), Plenum Press, New York, 1975, P. 489.
3. D. K. Bohme, R. S. Hemsworth, H. W. Rundle and H. I. Schiff, J. Chem. Phys. 58, 3504 (1973).
4. R. S. Hemsworth, H. W. Rundle, D. K. Bohme, H. I. Schiff, D. B. Dunkin and F. C. Fehsenfeld, J. Chem. Phys. 59, 61 (1973).
5. J. D. Payzant, H. I. Schiff and D. K. Bohme, J. Chem. Phys. 63, 149 (1975).
6. G. I. Mackay, R. S. Hemsworth and D. K. Bohme, Can. J. Chem. 54, 1624 (1976).
7. D. Betowski, G. I. Mackay, J. D. Payzant and D. K. Bohme, Can. J. Chem. 53, 2365 (1975).
8. To be submitted to J. Chem. Phys and Can. J. Chem.

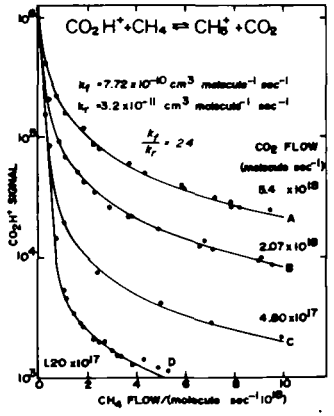

FIG. 1

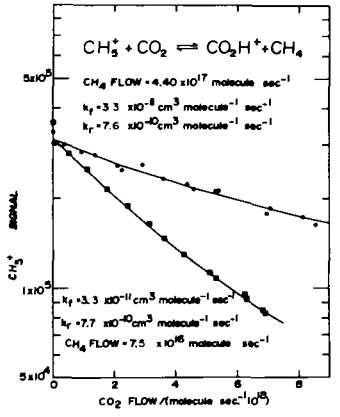

FIG. 2

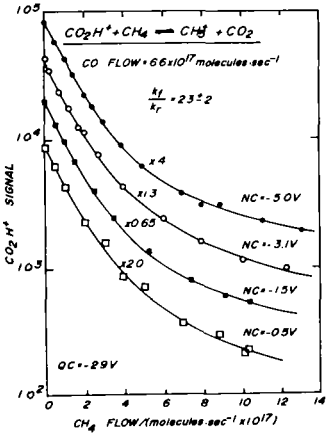

FIG. 3

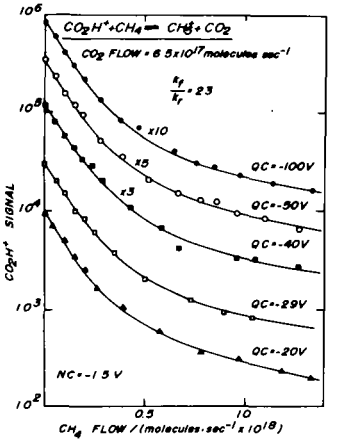

FIG. 4

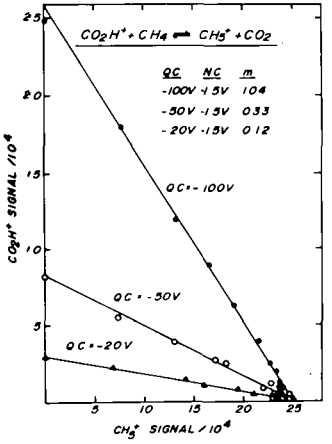

FIG. 5

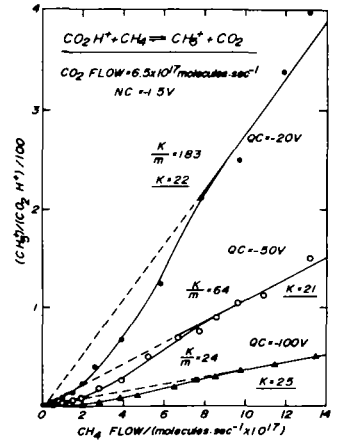

FIG. 6

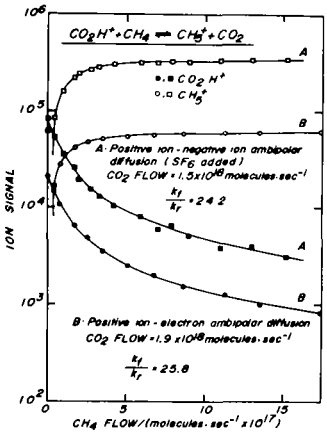

FIG. 7

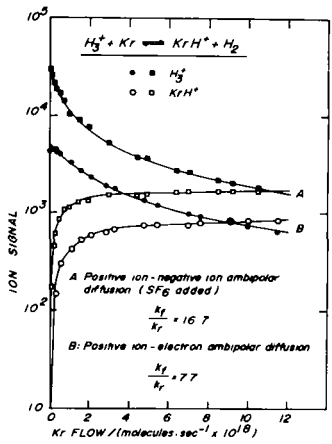

FIG. 10

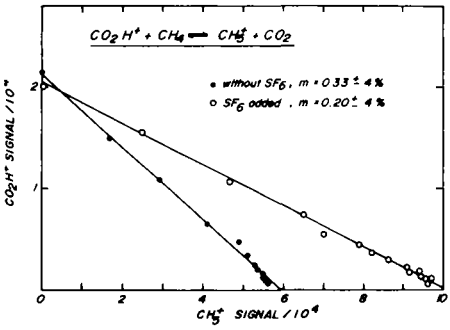

FIG. 8

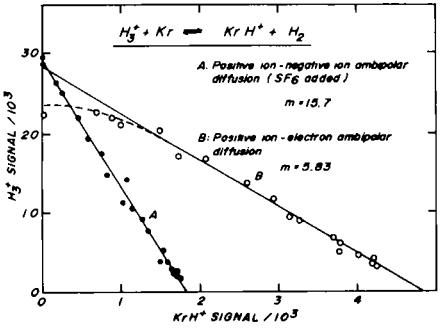

FIG. 11

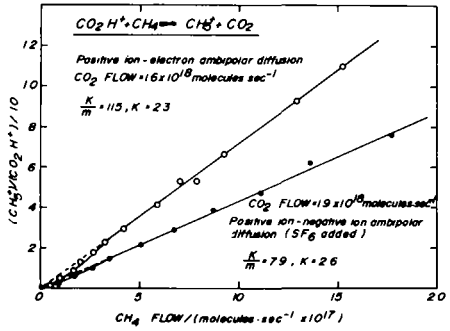

FIG. 9

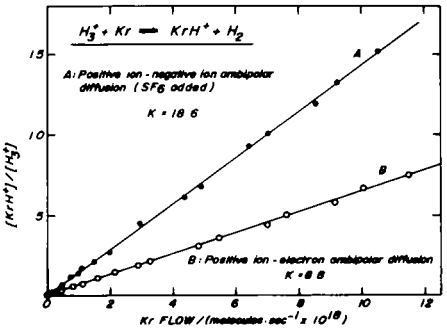

FIG. 12

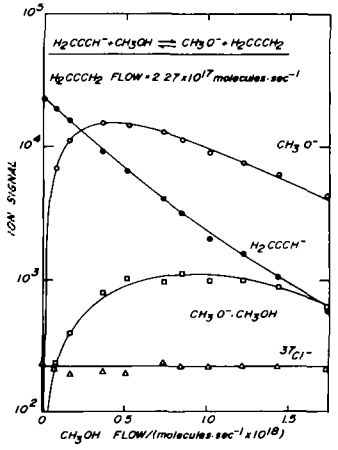

FIG. 13

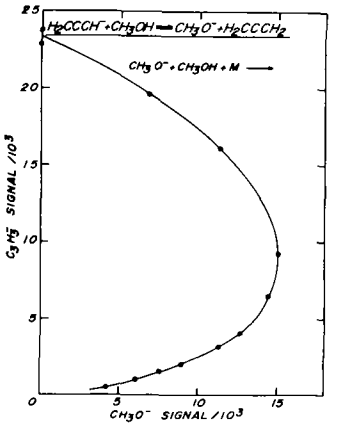

FIG. 14

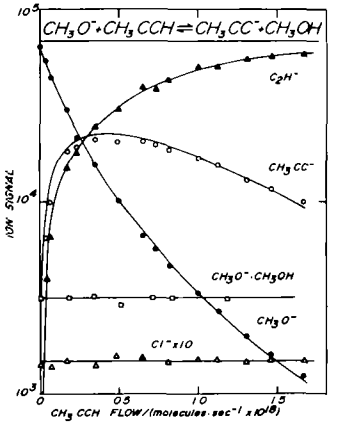

FIG. 15

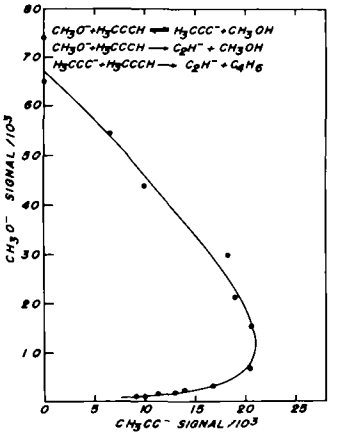

FIG. 16

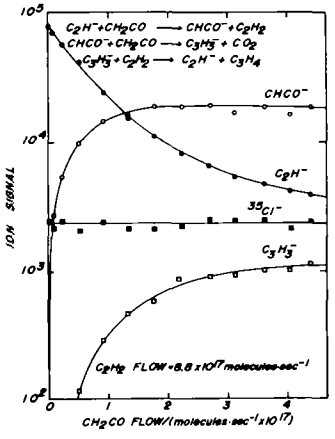

FIG. 17

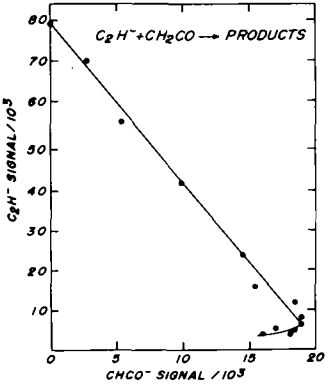

FIG. 18

Ion thermochemistry by pulsed high ion source pressure mass spectrometry, K. HIRAOKA and P. KEBARLE, Chem. Dept. Univ. of Alta. Edmonton, Alta, Canada, T6G 2E1

The measurement of ion equilibria in the gas phase is the major new source of ion thermochemical information. The method was initiated and developed with use of a high ion source pressure mass spectrometer. Fortunately ion equilibria can be measured also with other experimental arrangements like ICR and flowing afterglow. Each of these methods have their specific advantages and are complementary. The specific advantages of the high pressure method are: thermal ions and thermal activation due to high pressure, facile continuous ion source temperature control from -190° to 700°C, allowing determination of a wide variety of reactions, Van't Hoff plots leading to ∇H and ∇S, ability to study reactions which are too slow to be measured with other techniques. Examples of types of reactions and thermochemical information obtained will be given on basis of recent work. An assessment of the accuracy of the values obtained from the different types of measurement will be made.

The Thermochemistry of Carbonium Ions by MS Equilibrium Measurements. F. H. FIELD, The Rockefeller University, New York, N.Y. 10021.

The hydride transfer equilibria $R_1^+ + R_2H \rightleftarrows R_1H + R_2^+$ where R_1 and R_2 are C_4-C_7 hydrocarbon groups have been investigated by pulsed electron beam high pressure mass spectrometry. The equilibrium constants for the reactions and the temperature coefficients of the equilibrium constants have been determined and are used to establish a network of thermodynamic quantities for the several ionic entities. Trends in stability are related to structural aspects of the entities. Reaction kinetics pertinent to the establishment of the equilibria are discussed.

Ion Thermochemistry in Ionospheric Problems. ELDON E. FERGUSON, Aeronomy Laboratory, NOAA, Boulder, CO 80302

In recent years much of the interest in ionospheric chemistry has centered in the D-region, the lower altitute region of the ionosphere below ~ 80 km. There also is some current concern about destruction of atmospheric trace constituents by ion reactions in the stratosphere and troposphere which lie below the ionosphere. In all these relatively high pressure regimes, thermochemical information plays as vital a role as kinetic information for an understanding and predicting of ion composition. The most pressing need for the positive ion chemistry of the D-region is cluster bond energies and entropies. In negative ion chemistry, the electron affinities of several species are of interest, and also cluster bond energies, particularly for higher hydrate ions. In the troposphere and stratosphere there is a need to know proton affinities of such species as HNO_3 and H_2O_2 and other minor constituents. Some recent results will be presented and some of the current problems will be discussed.

Systematics of Organic Ion Decompositions

Maurice M. Bursey

William Rand Kenan, Jr.- Laboratories of Chemistry
The University of North Carolina
Chapel Hill, North Carolina 27514

There are a number of threads tying together many aspects of fragmentations of organic molecules in the mass spectrometer. In this presentation I attempted to trace such common features of a variety of reactions, sometimes drawing on data supported by detailed experiment, less frequently on conjecture of those skilled in devising complex mechanisms. In most cases, however, it would be appropriate to gather further information, particularly thermochemical data to relate to the supposed structures of ionic products, before one can consider the matter well understood.

The common feature of all the examples discussed is that they involve hydrogen rearrangements. The archetypal processes proceed through six-membered activated complex geometries. Some of these processes apparently involve shifting of double bond and some do not. The first category is exemplified by a McLafferty rearrangement:

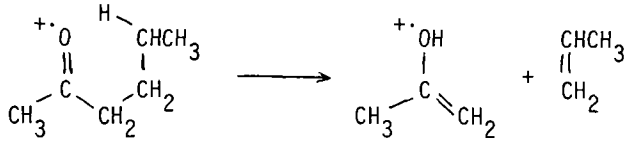

The second, by loss of water from an alcohol:

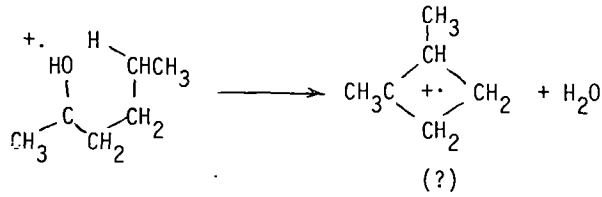

(?)

Other variants of the processes are best understood in relation to these models.

Energetic considerations related to structures of reactants and products have been partially developed. All of the material presented in this talk, and more, may be found in the following review articles (reprints unfortunately not available):

D. G. I. Kingston, J. T. Bursey, and M. M. Bursey, Chem. Rev., 74, 215 (1974).

D. G. I. Kingston, B. W. Hobrock, M. M. Bursey, and J. T. Bursey, Chem. Rev., 75, 693 (1975).

Use of Gaseous Ion Thermochemistry in Physical Organic Chemistry

by
R. W. Taft, Dept. of Chemistry, University of California, Irvine 92717

Although no effects of molecular structure have been identified which are entirely unique to the gas phase, the relative contributions of structural effects may be so different from those observed in solution that there has been difficulty in understanding the relationships involved. Gaseous proton transfer equilibria offer important new insights and clarifications of intrinsic structural and bonding effects.[1]

Entropy effects, which tend to be quite complex in aqueous proton transfer equilibria, are small and can generally be anticipated nearly quantitatively from molecular rotational symmetry numbers in gas phase proton transfer. This is shown by comparison of ΔG^0_{300} values obtained from high pressure mass spectroscopy by Yamdagni and Kebarle[2] with corresponding ΔG^0_{300} values obtained by low pressure pulsed ion cyclotron resonance spectroscopy.[3]

Steric effects in gas phase proton transfer equilibria are frequently very small. This is shown, for example, by plots of the proton affinities of primary amines vs. corresponding symmetrically substituted secondary and tertiary amines. Linear relationships are observed which are independent of the steric requirements of the alkyl substituent. This indicates that steric interactions in the free base and its conjugate acid are very nearly identical. The large increments in base strength resulting from alkyl substituents are due predominantly to the polarizability effects, as first identified by Brauman and Blair.[4] However, the severe non-additive relationship[1] $1^0:2^0:3^0 = 1.00:1.70:2.21$ indicates that there is also in the cations some charge transfer through the sigma bonds into the alkyl group.

In solution, the simple electrostatic models of the polar effects and polarizability effects have been conceptually useful but difficult to apply because of solvent effects. Gas phase proton affinities of corresponding substituted alcohols and ethers and 1^0 and 2^0 amines show a differentiation between these two effects.[1,3,5] Proton affinities of the oxygen compounds plotted vs. the nitrogen compounds form two separate lines. For hydrogen and increasingly polarizable alkyl groups, the proton affinity increase is 1.35 times greater for the oxonium than for the ammonium

ions. For dipolar substituents, proton affinity increases in oxonium than for the ammonium ions. For dipolar substituents, proton affinity increases in oxonium ions with the decreasingly unfavorable dipole by a factor of 1.05 times that for the ammonium series. Since the distance factors are less for oxonium than for ammonium ions, these results are explained qualitatively by the simple electrostatic model in terms of the $\frac{1}{R^4}$ dependence of the polarizability effect compared to the $\frac{1}{R^2}$ dependence of the polarizability effect.

Recently advances in ab initio molecular orbital calculation of energy changes for isodesmic processes make this approach of great interest for comparison with appropriate proton affinities.[6] In collaboration with Prof. Hehre, calculations for a series of substituted methyl amines with dipolar and polarizable substituents have been carried out and found to compare rather satisfactorily with the experimental results.[7] For eight substituents covering a range of 20 kcal in proton affinity, the average deviation between experimental and calculated values is 0.8 kcal. In view of these results, calculations were carried out for a series of hypothetical β-substituted ethyl amines and ammonium ions in which a fully extended (all trans) configuration was maintained to eliminate chelation effects and to minimize hyperconjugation and polarization effects.[7] That is, while experimentally it is difficult to find a reaction series for which only the polar substituent effect is strongly predominant, the STO-3G calculations readily allow calculations of this kind. The results offer the first quantum mechanical calculation of a polar substituent constant scale and do accord reasonably well with the empirical σ_I scale.

The applicability of the σ^+ scale of Brown[8] has been tested for two series of gas phase proton transfer equilibria, 4-substituted α-methyl styrenes and benzaldehydes. Since this parameter scale is based upon kinetic data in solution, it is considered particularly significant that the results are well fitted by the σ^+ parameters. The slopes (13.2 and 16.5, respectively, in kcal/σ^+) may be compared to that ($\sim$ 23) obtained by Harrison, Kebarle, and Lossing for the ionization potentials of benzyl radicals.[9]

The question of site of protonation in a polyfunctional molecule is not a trivial one in the gas phase. A simple approach which we have

found useful is based upon the observation that substituents which exert only polar and polarizability effects give rise to fall-off factors through a methylene group of approximately one-half.[1,3] Deviations from this proton affinity relationship for substituents which are directly substituted at the usual protonation N center in the series $X—N(CH_3)_2$ (in comparison to the corresponding $XCH_2N(CH_3)_2$ series) may be due either to resonance stabilization in the free base (negative deviation), the conjugate acid (positive deviation) or to a change in site of protonation due to resonance stabilization of this conjugate acid (positive deviation).

Making use of such a comparison, it can be estimated that the protonation of N,N-dimethylformamide is favored in the gas phase at oxygen over nitrogen by ~8 kcal. This result is in accord with the evidence found in anhydrous[10] and aqueous acid[11] solutions.

Comparison of substituent effects on proton affinities for the $X-\overset{O}{\overset{\|}{C}}-OC_2H_5$ family vs. the corresponding $X-CH_2N(CH_3)_2$ family gives the following magnitudes of resonance effects:[3,5] CH_3, 5.; CH_3O, 10.; $(CH_3)_2N$, 19 kcal. These figures refer to the increased resonance stabilization of the conjugate acid over that of the free base.

In collaboration with Profs. E.M. Arnett and G. Scorrano,[12] we have evaluated free energies and/or heats of solution of gaseous cations in aqueous solution and in solutions of the superacid, FSO_3H, using a thermodynamic cycle. In aqueous solution, the free energies of solution are used to minimize structure-making effects of alkyl groups.[13] Compared with carbocations having largely physical solvation (free energy of hydration 40-45 kcal), 'onium ions with protonic acid sites have appreciably greater hydration energies. The difference between the hydration energies for these two types of cations may be regarded as an estimate of the chemical binding of water to the ion.[14] The chemical binding energies obtained are related to both the number and kind of protonic acid sites. With increasing internal stabilization of positive charge, the binding of water to the cation is decreased.

Regarding CH_3 and C_2H_5 substituents as blocking groups, the average heats or free energies of chemical hydration of 'onium ions per protonic acid site are found to be very close in magnitude to the average

binding energy of single water molecules in the gas phase to the protonic acid sites of these cations, as obtained by Kebarle.[15] The average chemical binding per protonic acid for oxonium ions and ammonium ions in FSO_3H is much reduced, especially for the former, as compared with water. This result is readily understood in terms of cation solvation by H-bonding, but not in terms of expectations from bulk dielectric constants.

References

1. For a review, cf. R. W. Taft in "Proton Transfer Reactions," E. F. Caldin and V. Gold, Ed., Chapman and Hall, London, 1975, p.31.
2. R. Yamdagni and P. Kebarle, J. Amer. Chem. Soc., 48, 1320 (1976)
3. J.F. Wolf, R.H. Staley, I. Koppel, M. Taagepera, R.T. McIver, Jr., J.L. Beauchamp, and R.W. Taft, ibid., in preparation.
4. J. I. Brauman and L. K. Blair, ibid., 90, 5636, 6501 (1968).
5. unpublished results of Dr. J. L. Abboud.
6. W.J. Hehre, R.F. Stewart, and J.A. Pople, J. Chem. Phys., 51, 2657 (1969).
7. M. Taagepera, W.J. Hehre, and R.W. Taft, unpublished results.
8. H.C. Brown and Y. Okamoto, J. Amer. Chem. Soc., 79, 1913 (1957); 80, 4964 (1958).
9. A.G. Harrison, P. Kebarle, and F.P. Lossing, ibid., 83, 777 (1961).
10. R.J. Gillespie and T. Birchall, Can. J. Chem., 51, 148 (1963).
11. A.J. Kresge, P.H. Fitzgerald, and Y. Chiang, J. Amer. Chem. Soc., 96, 4698 (1974).
12. J.F. Wolf, R.W. Taft, E.M. Arnett, G. Scorrano, G. Perdoncin, R.H. Staley, and J.L. Beauchamp, J. Amer. Chem. Soc., in preparation.
13. D.H. Aue, H.B. Webb, and M.T. Bowers, ibid., 98, 318 (1976).
14. J.F. Wolf, P. G. Harch, and R.W. Taft, ibid., 97, 2904 (1975).
15. (a) P. Kebarle, S.K. Searles, A. Zolla, J. Scarborough, and M. Arshadi, ibid., 89, 6393 (1967).
    (b) J.D. Payzant, A. Cunningham, and P. Kebarle, Can. J. Chem., 51, 3242 (1973).
    (c) H. Hiraoke, E. P. Grimarud, and P. Kebarle, J. Amer. Chem. Soc., 96, 3359 (1974).

GC-MS Development in Forensic Science. Bryan S. Finkle, Center for Human Toxicology, Univ. of Utah, SLC, Utah 84112.

This presentation is an introduction overview of GC-MS development and applications in forensic Science. Adoption of this analytical technique by medico-legal scientists dates only to about 1968, yet today approximately 40-50% of all Forensic Science laboratories have GC-MS and/or computer capability. The reasons for this remarkable growth range from changing more constraining law concerning admission of physical evidence in criminal trials to burden of quantitating and identifying with scientific certainty minute amounts of abused drugs, therapeutic agents and metabolites in biological extracts. The forensic toxicologist is besieged by cases involving misuse of drugs: suicides, fata automobile accidents, drivers under the influence of drugs, possession and use of narcotics, acute intravenous narcotism deaths, accidental deaths from ignorant use of multiple drugs, surveillance of offenders under legal control for drug abuse, and the whole gamut of crimes associated with the need to acquire, use, sell, or promote illicit drugs. Although there is a strong bias towards toxicology applications, mass spectrometry is being used in many other types of case investigation including rape, road accidents, burglary, and arson.

Differentiation of Window Glasses by Spark Source Mass Spectrometry. Max A. Haney, FBI Laboratory, Washington, D.C. 20535

Specimens of window glass having similar refractive indices and densities were examined for trace element content by spark source mass spectrometry. Three experimental techniques were tried: (1) Direct sparking of the sample mounted on a gold wire using a gold wire counter-electrode, (2) Grinding the sample and mixing with graphite or gold powder, and (3) Dissolving the sample in HF and doing isotope dilution on selected trace elements (K, FE, Sr, Zr, Ba). The trace element analysis is shown to be very useful for differentiating window glass samples such as are encountered in forensic work.

Chemical Ionization Mass Spectrometry in Pharmacology Studies.

Robert L. Wolen and Charles M. Gruber, Jr., Lilly Lab for Clin. Res., Wishard Mem. Hosp., Indianapolis, Indiana 46202

The advantages of CI-MS include (1) simplicity of instrumentation, (2) high specificity and sensitivity, and (3) variable fragmentation. Deuterium labeled internal standards permit development of sensitive procedures. Deuterium and other stable isotope labels can be used to provide doublet markers for drug metabolic studies, which, when used with ^{14}C marker, provides sensitive, specific systems for following absorption, distribution, metabolism, and excretion of drugs in man. Deuterium labeling on one of two isomeric forms of a drug makes possible comparative metabolism studies under identical conditions with a single administration of drug. Determination of pharmacokinetic parameters and of drug and metabolite pools during ongoing therapy is possible using stable labeled forms. Examples of the techniques will be presented with *in vivo* data. CI-MS techniques are computer compatible and readily adaptable to automation for processing the large numbers of samples required in clinical pharmacology studies.

ADVANTAGES OF CHEMICAL IONIZATION IN FORENSIC TOXICOLOGY

Ronald F. Skinner, Elaine Jones Heron Ph.D.

The technique of electron impact (EI) mass spectrometry has been in use for nearly 50 years, but the application of this technique to drugs has occurred only in recent years. In this short time its use has become widespread and now well over a hundred drug analysis laboratories throughout the world are using the technique of EI routinely to confirm the presence of drugs and to identify unknowns and drug metabolites.

The technique of chemical ionization, however, has not found such widespread use. This technique was first introduced by Munson and Field in 1966. However, the lack of availability of a commercial instrument until 1972, resulted in few applications being studies by this technique. Also, the lack of published "cookbook" procedures has caused many labs. which have EI capability to be cautious about acquiring CI capability. This paper will attempt to show by an illustrative case how this technique can be of great use to toxicologists.

Perhaps the major advantage of CI is the fact that the molecular weight of compounds which do not give stable positive molecular ions in EI can be determined. An example of drugs which fall into this class are the barbiturates, which, while they can be readily identified by their EI spectra, fail to give stable molecular ions by EI. In CI they give an m+1 (quasi-molecular ion) which represents the base peak of their spectrum.

CI can also provide increased sensitivity and specificity for many compounds. The amines such as amphetamines, local anesthetics (benzocaine, lidocaine etc.), propoxyphene, and others , have EI spectra which are characterized by large ions at mass 58, 72 or 86 and also little or no molecular ion. These ions represent a nitrogen with either 3, 4, or 5 methylene units respectively and in general represent 60 to 70% of the total ions produced from the compound. A recent survey of the Finnigan drug library shows that 50 compounds in the library had a base peak of 58, 15 had a base peak of 72 and 18 had a base peak of 86. These ions are therefore not very specific and it is necessary to resort to ions of low intensity to characterize these compounds. This makes it difficult sometimes to make an absolute identification. CI, however, provides strong quasi-molecular ions for most of the compounds and often more significant fragment ions.

Fragmentation processes in CI are generally characterized by hydride abstractions, proton additions or neutral losses of small molecules such as water, ammonia, etc. from the protonated parent molecule. These simpler fragmentation routes make the spectra much easier to interpret than those obtained by EI. Therefore, the less experienced mass spectrometrist is often able to identify unknowns by CI, while their EI spectrum would require many years of experience to interpret. In addition, the simpler fragmentation often make it possible to examine extracts

of complex samples such as stomach contents for the presence or absence of certain drugs using the solid probe. Saferstein in the journal of Forensic Sciences has reported using the solid probe technique on both blood and urine extracts.

Perhaps the greatest advantage of CI to the drug analyst is the fact that CI spectra tend to compliment EI spectra. The two ionization processes often produce two completely different sets of positive ions from the same compound. This, therefore, gives two sets of physical parameters by which the compound can be characterized and with the addition of GC data which is usually simultaneously obtained, is often sufficient to unambiguously establish the identity of a compound. A summary of these advantages in addition to other more general advantages is given in Table I.

TABLE I

Advantages of CI

1. The molecular weight of a considerable number of compounds which do not give stable positive molecular ions by EI can be determined.

2. Increased sensitivity and specificity can be obtained for many compounds.

3. More predictable energy distribution and less tendency towards rearrangements which simplifies spectral interpretation.

4. Decreased time for analysis and interpretation of results.

5. More sensitive to stereo and chemical isomeric differences than EI.

6. Selective ionization of compounds in a mixture can often be affected by choosing the correct reagent gas.

7. CI spectra are complimentary to EI spectra.

8. Allows direct coupling of GC and MS

A typical case study involves a patient who was admitted to the hospital with severe psychiatric disturbances. The patient was initially treated with valium and chlorpromazine. After one day, this treatment was failing to produce the desired results, so the patient was put on an intravenous drip with continuous administration of haloperidol. On the third day after admission, the patient was found dead due to respiratory arrest. Since there was a possibility of litigation involved, it was necessary to determine the levels of all of the drugs administered and if possible their metabolites so that estimation of when and at what levels drugs were administered could be made.

A chromatogram of an extract of hydrolyzed urine is shown in Figure 1. To identify possible metabolites of the chlorinated drugs, a program was written in Finnigan Basic to access the

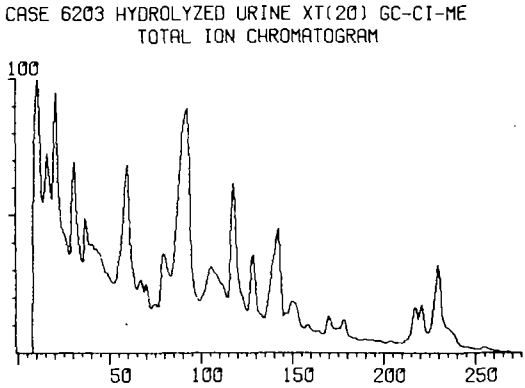

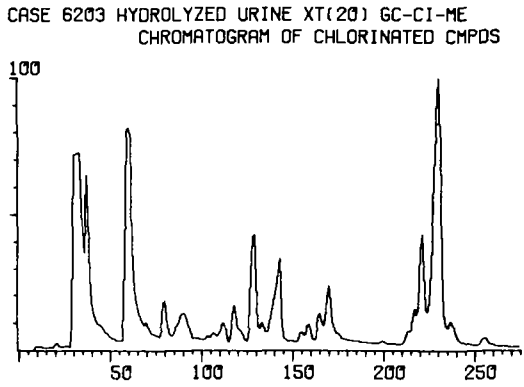

FIGURE 1

METABOLITE	m.w.	BASE PEAK	LIVER	KIDNEY	URINE
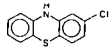	233	234	–	–	+
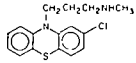	304	305	–	–	+
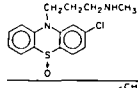	320	321	–	–	+
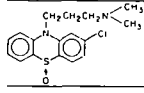	334	335	+	+	+

TABLE ONE

data and draw a chromatogram of those GC peaks which represented chlorine containing compounds. The program looked at the largest mass peaks in each spectrum and then checked them to see if they had the chlorine isotope peaks. The isotope peaks of the chlorine serve as a convenient "tag" to identify possible metabolites. Using this technique it was easy to determine which GC peaks represented possible metabolites of chlorpromazine and haloperidol.

Table 1 summarizes the metabolites of chlorpromazine which were tentatively identified.

Table 2 summarizes the postulated metabolites of haloperidol.

In summary, this paper has shown a number of advantages which CI has for the drug analyst. Perhaps its major disadvantage is the simplicity of the spectra generally obtained. (Many compounds may give only one fragment.) Even in the extreme case of a one peak CI mass spectrum, the data obtained in conjunction with the EI spectrum should serve to better characterize the compound in question. The predictability of CI spectra also makes it easier for the drug analyst to determine the presence or absence of reported metabolites even though he may not be able to obtain the standards necessary to determine them in other methods such as TLC or GC. These advantages make it apparent that CI will probably soon become as widely used in drug analysis as EI.

METABOLITE	m.w.	BASE PEAK	LIVER	KIDNEY	URINE
	189	190	+	+	+
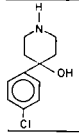	211	194	−	−	+
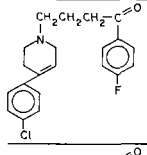	357	358	+	−	+
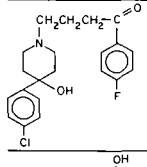	375	376	+	+	+
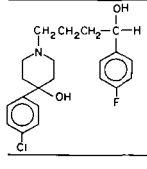	377	378	+	+	+

TABLE TWO

GC-MS of Simulated Gasoline Residues Suspected Arson Cases

Martin H. Mach
The Aerospace Corporation
El Segundo, California 90245

Computerized gas chromatography-mass spectrometry with methane chemical ionization has been used to characterize samples of simulated arson residue derived from gasoline by distillation, evaporation, and combustion. Virgin gasoline (Figure 1) contains chiefly the lower alkylbenzenes and naphthalene. A 35-times concentration by distillation shifts the "center of gravity" of the reconstructed gas chromatogram (RGC) to napthalene and methynapthalenes (Figure 2), while a 100-fold distillative concentration shifts the center of gravity to the methyl-and dimethylnaphthalenes (Fig 3). The evaporated sample, concentrated 480 times, has an RGC centered around di-and trimethylnaphthalenes (Fig 4). Finally,the burned sample (Fig 5) shows a relatively even distribution of polycyclic aromatic hydrocarbons (PAH) from methylnaphthalene to perylene (or an isomer). Specific compounds confirmed by their GC retention time and mass spectra, and numbered on the figures are naphthalene (1), 2-methylnaphthalene (2), 2, 3-dimethylnaphthalene (3), phenanthrene/anthracene (4), 2 - and 9-methylanthracene (5, 6), fluoranthene (7), pyrene (8), chrysene/benzo-[α]-anthracene (9), and perylene (10).

Fig. 6 shows five limited mass scans (LMS) for homologous methylated naphthalenes, anthracenes/phenanthrenes, $C_{16}H_{10}$ (pyrenes, etc.), $C_{18}H_{12}$ (chrysenes, etc.) and $C_{20}H_{12}$ (perylenes, etc.) derived from the RGC of Fig 5. This LMS technique should help to isolate gasoline residues in actual arson cases where interfering materials derived from the combustion and pyrolysis of wood, plastics and other debris might obscure their presence. If it can be shown that under a wide variety of test conditions the same distinctive compounds are always present, analytical techniques simpler and less expensive than GC-MS (e.g., TLC, IR, UV) could be used to assay for these specific components and thus verify the presence of gasoline residue.

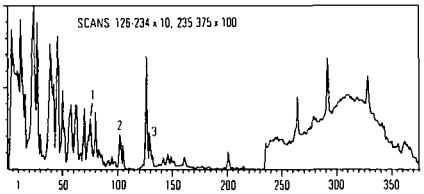

Fig. 1. Virgin Gasoline

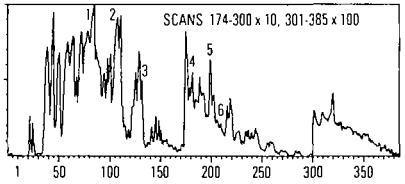

Fig. 2. First Pot Residue; Concentrated 35 Times

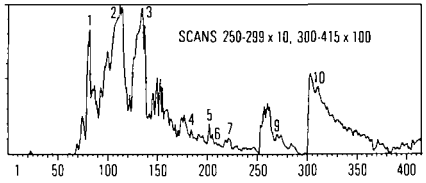

Fig. 3. Final Pot Residue; Concentrated 100 Times

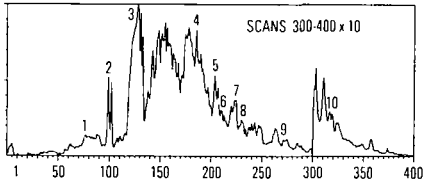

Fig. 4. Evaporated Gasoline; Concentrated 480 Times

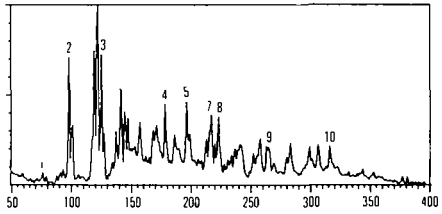

Fig. 5. Burned Gasoline

Fig. 6.

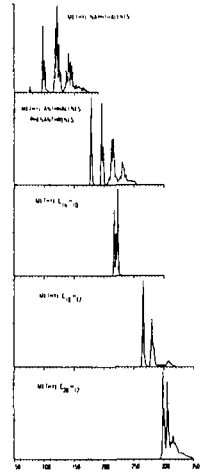

Limited Mass Scans of Burned Gasoline

CAMS-II, The Navy's Approach to Atmosphere Monitoring

J. R. Wyatt, J. J. DeCorpo, and F. E. Saalfeld

Naval Research Laboratory
Code 6110, Washington, D. C. 20375

CAMS stands for the Central Atmosphere Monitoring System used aboard nuclear submarines. The present system, CAMS-I, uses a mass spectrometer to monitor all the relevant atmospheric constituents except carbon monoxide. This unit is replacing the previous atmosphere monitoring systems that used either GC or a combination of IR, thermal conductivity and paramagnetic methods. We are currently in the development stage of CAMS-II which will be able to monitor a variety of trace atmospheric constituents.

The ability of a nuclear submarine to stay submerged for a long period of time depends upon maintaining a habitable atmosphere for the crew to breathe. In order to control the various species in the atmosphere, it is first necessary to monitor them. For a variety of reasons the systems used previously were not entirely satisfactory, hence the Navy interest in developing a new atmosphere monitoring system. The Navy and NASA in a joint project developed a mass spectrometric atmosphere analyzer. Two prototype units were constructed and employed aboard submarines. These units operated for about 25,000 hours (3 years) without a major failure. These tests showed that it was feasible to construct an atmosphere monitor using mass spectrometry that is sufficiently reliable for use aboard submarines.

Currently the submarine fleet is being fitted with CAMS units based upon the design of the prototype. The CAMS-I unit monitors the following atmospheric constituents: H_2, H_2O, CO, O_2, CO_2, F-11, F-12, F-114. All of these gases are monitored by mass spectrometry except CO, which is monitored by IR. The mass spectrometer is a single-focusing magnetic instrument. Separate collectors for an ion characteristic of each gas are placed on the focal plane of the instrument. In this way, a constant magnetic field (permanent magnet) and ion energy can be used.

Each collector has an electrometer of the appropriate gain. The output from each electrometer is divided by a signal proportional to the total pressure and multiplied by the appropriate factors to correct for interference fragments and to be output in the desired units (torr or millitorr). The system is pumped with an ion pump. Therefore, no consumable gases are required; the mass spectrometer unit has no moving parts, and the readings are continuous.

The major limitation of the current CAMS unit is its lack of flexibility. The particular ions which are monitored are determined by the placement of the collectors. Clearly by monitoring all of the ions between 2-200 AMU, it should be possible to measure a wide variety of atmospheric constituents and trace contaminants. Therefore, we are in the developmental stages of CAMS-II, a programable mass spectrometric atmosphere analyzer. A variety of mass spectrometer designs are possible--the final design is presently undecided.

In conjunction with designing CAMS-II, we have set up a laboratory model that is depicted in the Figure. We are using this model system to evaluate the ability of a mass spectrometer to measure trace constituents in air. The system is operated under similar conditions to those expected for CAMS-I. The pressure, measured by the ion pump current, is 2×10^{-6} torr. At this pressure, the ion pump should have a lifetime of about two years. Two years is the current expected operating time for CAMS-I before major overhauling. This is certainly much longer than we are use to with laboratory type mass spectrometers.

The present laboratory system uses a quadrupole mass spectrometer with a mass range of 2-300 AMU. The quadrupole electronics have been interfaced to a GC-MS data system. All of the programs we have written to control the mass spectrometer are FORTRAN, and therefore, are easy to understand and modify.

A program has been written to calibrate the mass scale of the spectrometer. The program does a linear fit to the mass centroids for AMU 18 and 44. It was found this procedure resulted in the system being accurate over the mass range 2-200 to ± 0.1 AMU. Therefore, no external calibrating gases are needed for this system.

Mass spectra were recorded of two calibrated mixtures of typical atmospheric contaminants. A summary of these results is given in the Table. With no air admitted to the system, the intensities were all zero. The column labelled background is the intensity sampling air (ion pump pressure ~2×10^{-6} torr). The columns labelled 10 ppm and 100 ppm represent the intensity when mixtures of 10 ppm and 100 ppm are sampled. Each mixture contained 10 ppm and 100 ppm respectively of the following: R12, R113, R114, methane, carbon monoxide, vinylidene chloride, trichloroethylene, methyl chloroform, hexane, benzene, and toluene. Using data from this table, one can infer sensitivity limits for various gases. For benzene, 1 ppm is readily detectable. Greater than 200 ppb of total freons were observable using m/e 85; however, specification of a particular freon would probably require 3-5 ppm. Certainly all of the species, except toluene, produce sufficient intensity to be identified at the 10 ppm level. The low sensitivity to toluene compared to benzene is believed to be due to toluene condensing

on surfaces prior to entering the vacuum system. This is surprising, since the leak valve was heated to 80°C and the gas sampled was flowing through the leak valve at 500 cc/min. Another unexplained phenomenon is the background intensity. As can be seen from the Table, the intensity increases with increasing mass. One explanation would be that it is due to photons striking the electron multiplier. The photons would be produced by collisions of the ions with the quadrupole rods. At higher mass, the increased RF and DC fields of the rods would produce more photons. It has to be assumed that the photons somehow are reflected from various surfaces onto the multiplier.

During the next year, we will obtain more quantitative limits for the sensitivity of the laboratory system. Algorithms will be evaluated for determining the concentration of various contaminants in presence of larger concentrations of other contaminants.

FIGURE

CAMS-II LABORATORY MODEL

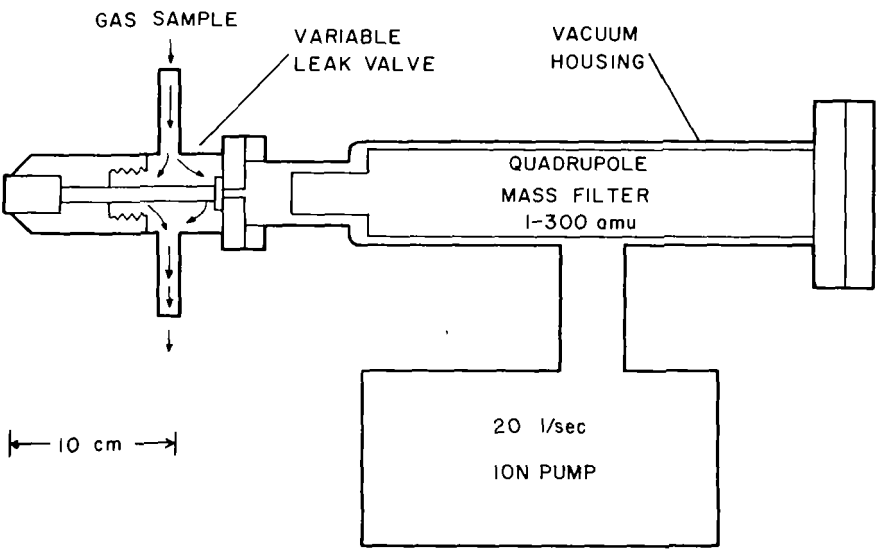

TABLE

ION CURRENT FOR VARIOUS CONTAMINANTS

m/e	BGRD	10 PPM	100 PPM	SPECIES
43	640	670	1570	HEXANE
57	5	65	886	"
61	4	115	1511	V.C.
78	15	62	796	BENZ.
85	17	250	2582	R12,113,114
92	8	10	87	TOL.
95	14	36	390	$CHClCCl_2$
96	15	44	535	V.C.
97	15	34	340	CH_3Cl_3
101	18	98	820	R113,12
130	24	34	234	$CHClCCl_2$
135	30	53	450	R114
151	32	46	324	R113

$100 \sim 5 \times 10^{-16} A$

QUANTITATIVE ANALYSIS OF TRACE ENVIRONMENTAL SAMPLES USING COMPUTER CONTROLLED HIGH RESOLUTION SCANNING MULTIPLE ION DETECTION (SMID)

by

D. Schuetzle, Research Staff, Ford Motor Company,
Dearborn, Michigan 48121 and
D. E. Hagge, Incos Corporation, Berkeley, CA. 94710

Multiple ion detection (MID) techniques have been developed by several investigators over the past several years to improve the sensitivity of scanning mass spectrometry (1). In such cases, the analysis of complex mixtures requires moderate to high resolution operating conditions. A new scanning multiple ion detection (SMID) technique is described which maintains the sensitivity of MID while gaining the accuracy of high resolution mass spectrometry. Up to 25 ions many be monitored at one time with mass accuracies of 10 ppm or better.

Quantitative analysis by direct sample insertion in medium and high resolution instruments was described in a recent paper (2) and at last years ASMS conference (3, 4). It was reported that it was necessary to resolve the complex spectra using moderate to high resolution instrumentation. A limitation of the technique was that much greater MS sensitivity was needed in order to cut down on the time required to collect a sample. This paper will briefly describe the SMID technique and its application to the rapid analysis of subnanogram quantities of PNA's and aliphatic hydrocarbons in air particulate matter.

A Micromass MM16-CI/EI mass spectrometer was interfaced to an INCOS 2000 data system. Sixteen bit D/A converters were used to control the accelerating voltage and magnetic field. A magnetic field-time scale was derived in the magnet scanning mode while holding the accelerating voltage constant at 5kv. The magnetic field was set at the initial mass M and the accelerating voltage dropped until 2M was reached within a specified scan interval (usually three seconds). A voltage-mass scale was derived using 6 PFK standard peaks within the range M to 2M. In the MID scanning mode, the high accuracy ($\pm$ 0.001 mass units) mass ions to be monitored were selected with the desired integration time. All of these operations were undertaken by software control and executed in less than five minutes.

The MID technique was applied to the rapid analysis of subnanogram quantities of PNA's and aliphatic hydrocarbons in air particulate matter. The average atmospheric concentration of PNA's in some urban areas is 1 ng/m^3. The sensitivity of the direct technique for PNA's was 10ng using exponential scanning from m/e : 15-600 at a cycle time of four seconds. Previously, atmospheric sampling times of 24-48 hours or more were required to obtained enough sample for the direct PNA analysis technique. For many air pollution studies much shorter sampling times were required. In addition, the rural concentration of PNA's are lower than that of urban areas. In the SMID mode the sensitivity was increased by 10 to 1000 times, depending upon the peak integration time. The increase in sensitivity was directly proportional to the increase in peak integration time as shown by Table 2. No loss in quantitation accuracy or precision was observed over a dynamic range of 10^3.

Air particulate matter was collected on suitable filter media such as fluoropore or quartz. A portion of the filter was punched and inserted into a specially designed direct insertion probe and the sample heated from 20°C to 390°C at 20-30°C/min.

The mass spectrometer was set up in the SMID mode over the mass range: 130-260 AMU with a total scan cycle time of 3000 msec. The loss in sensitivity over this mass range was 30%. This change in sensitivity is not considered significant when compared to the large gain in sensitivity obtained by the SMID technique (up to 1000 times). Eight ions were selected to represent eight groups of PNA's as follows: I. Methylnaphthalenes (142.078), II. Acenaphthalenes (154.078), III. Dimethylnaphthalenes (156.094), IV. Trimethylnaphthalenes, V. Anthracenes (178.078), VI. Pyrenes (202,078) VII. Benzanthracenes (228.094), and VIII. Benzopyrenes (252.094). A hold time of 200 msec. was used for each peak which represented a sensitivity gain of one hundred times over conventional scanning techniques. Figure 1 gives a three dimensional high accuracy mass chromatogram obtained for seven of the eight classes of PNA's. Isomers were not separated in this analysis because of poor insertion probe temperature control. Operation of the instrument at 1500 resolution was necessary in order to separate the peaks of interest from other peaks present at the same nominal mass. Figure 2 gives high accuracy mass chromatograms for $C_{16}H_{10}^{+}$ (202.078) and $C_{15}H_{22}^{+}$ (202.172) which occur at the same nominal mass. In the SMID mode, deconvolution of ion peaks was performed while scanning and ion fragment information for both of the deconvoluted peaks were recorded.

Table II. gives an elemental composition printout for the eight selected ions as well as resolved fragments. It might be noted that the interferring fragments are of much lower intensity than the selected ions (i.e. m/e:142.163 vs. m/e: 142.078) as a result of the short integration times (< msec) for these peaks. The mass accuracies for the ions of interest was good, ranging from 4 ppm for the most intense fragment (m/e: 154.078) to 46 ppm for the least intense (m/e: 252.082). However, masses calculated from an average number of scans give much better mass accuracies as shown by Figure 3 for the $C_{14}H_{10}^{+}$ ion (m/e: 178.078). The SMID technique was used in chemical ionization mass spectromstry as well as electron impact mass spectrometry. Figure 4 gives the methane-chemical ionization spectrum of four aliphatic hydrocarbons identified in air particulate matter using the SMID technique. This figure shows the high accuracy SMID mass chromatograms used to identify hexadecane ($C_{16}H_{34}$), heptadecane ($C_{17}H_{36}$), octadecane ($C_{18}H_{38}$) and nonadecane ($C_{19}H_{40}$). The methane CI spectrum gave large P-1 peaks which were used to identify each hydrocarbon. These chromatograms were obtained with a mass accuracy to better than 20 ppm.

REFERENCES

1. N. D. Young, J. F. Holland, J. N. Gerber and C.C. Sweeley, "Proceedings of the 23rd annual conference on Mass Spectrometry and Allied Topics." Houston, Texas, May, 1975 and references therein.

2. D. Schuetzle, Biomedical Mass Spectrometry 2, 288 (1975).

3,4. D. Schuetzle and T. J. Prater, "Proceedings of the 23rd Annual Conference on Mass Spectromstry and Allied Topics", Houston, Texas, May, 1975.

TABLE I

The Relationship between Peak Area and Peak Integration Time in Scanning Multiple Ion Detection (SMID)

Peak Hold Time msec.	Area of Peak[1] Observed	Calculated	%Error
2	283	299	-5.4
20	2881	2988	-3.6
50	7971	7670	+3.4
100	14939	14939	—
500	75398	74695	+1.0
1000	151066	149390	+1.1
1500	229430	224085	+2.4

[1]Area of 99.989 peak averaged for ten scans

TABLE II

Elemental Composition Printout for Mass Spectra Obtained In The SMID Mode (Scan #100 from Figure 2)

Peak No.	% RA	Mass	-Delta- MMU	PPM	Composition C	H	N	O	PNA Group
1	60.92	142.0775	-0.7	5	11	10	0	0	Methylnaphthalenes
2	0.30	142.1633	-8.8	62	10	22	0	0	
3	100.00	154.0787	0.5	4	12	10	0	0	Acenaphthalenes
4	43.01	156.0837	*-10	65	12	12	0	0	Trimethylnaphthalenes
5	33.40	170.1071	-2.4	14	13	14	0	0	
6	0.93	170.2017	-1.6	10	12	26	0	0	
7	75.32	178.0823	4.0	23	14	10	0	0	Anthracenes
8	48.06	202.0763	-1.9	10	16	10	0	0	Pyrenes
9	0.71	202.1791	7.0	35	15	22	0	0	
10	19.17	228.1024	8.5	37	18	12	0	0	Benzanthracenes
11	5.86	228.1857	-2.0	9	17	24	0	0	
12	27.57	252.0824	*-11	46	20	12	0	0	Benzopyrenes
13	14.42	252.2362	-9.0	36	17	32	0	1	

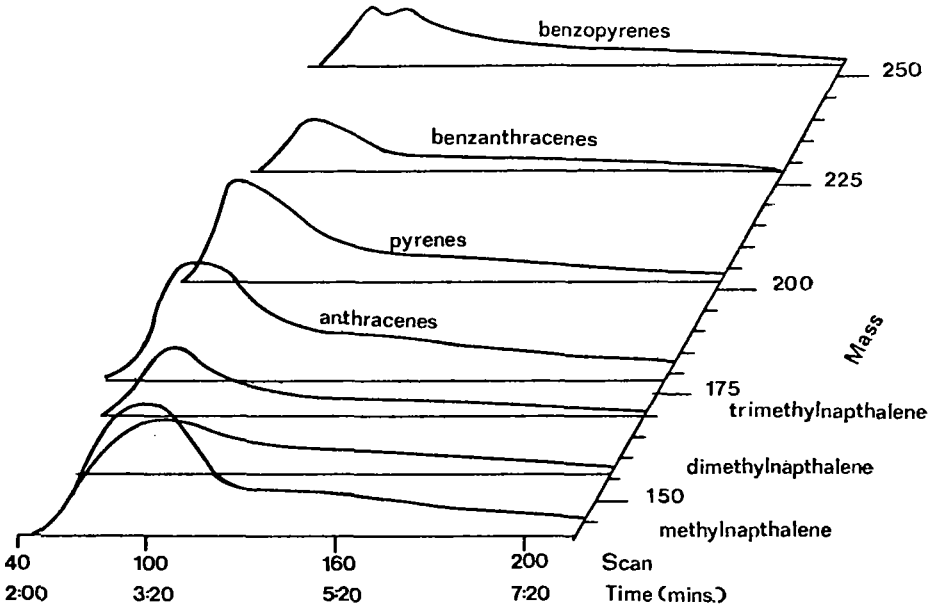

Figure 1. High Accuracy Mass Chromatograms for Seven Classes of PNA's Found in Air Particulate Matter Collected from The Alleghany Mountains.

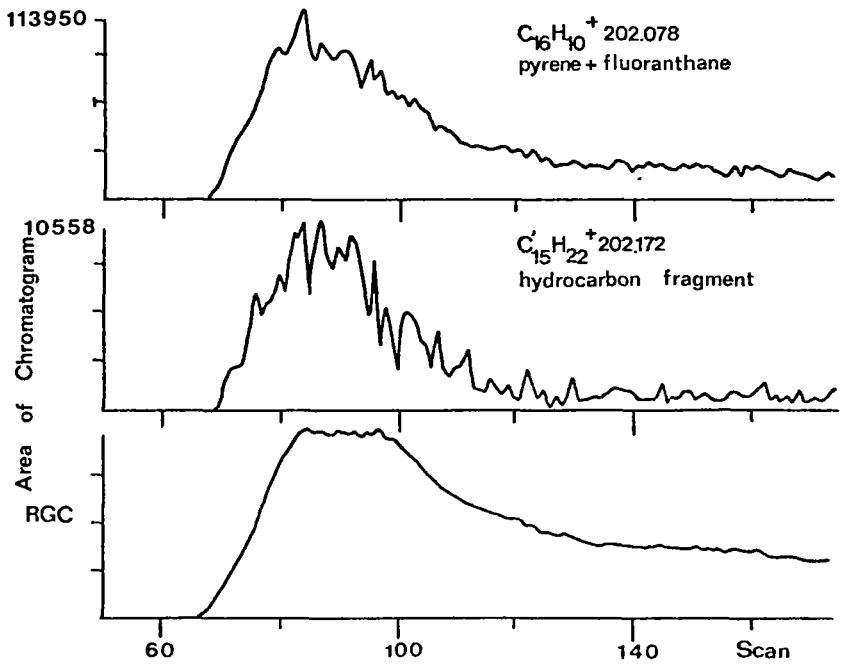

Figure 2. High Accuracy Mass Chromatograms for $C_{16}H_{10}^{+}$(202.078) and $C_{15}H_{22}^{+}$(202.172) Resolved in The SMID Technique.

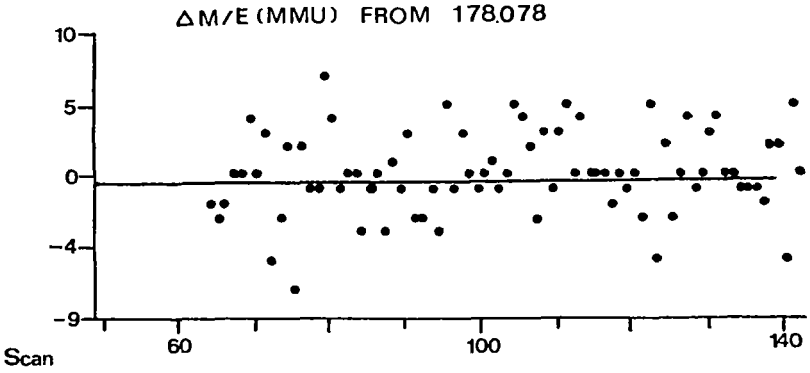

Figure 3. The Variation in Mass Accuracy as A Function of Scan for The $C_{14}H_{10}^{+}$ Ion (m/e: 178.078).

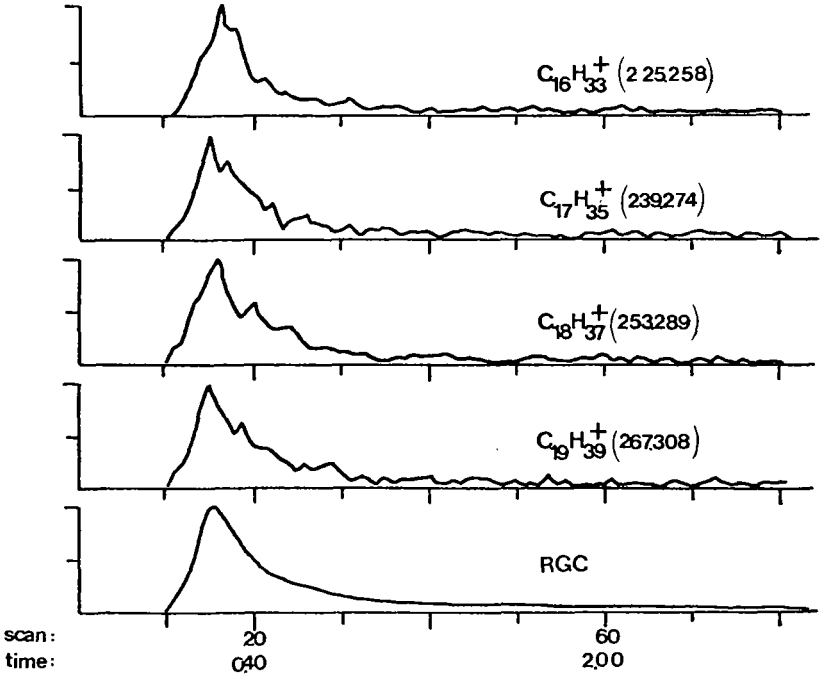

Figure 4. High Accuracy Mass Chromatograms for Four Aliphatic Hydrocarbons Found in Air Particulate Matter Collected From The Alleghany Mountains.

ANALYSIS OF TRACE LEVELS OF ORGANIC VAPORS IN AMBIENT AIR BY GLASS CAPILLARY GAS-LIQUID CHROMATOGRAPHY-MASS SPECTROMETRY-COMPUTER

E. D. Pellizzari, J. E. Bunch, R. E. Berkley, and J. Bursey
Research Triangle Institute, Research Triangle Park, NC 27709

The atmosphere contains numerous vapor phase organic compounds at ppm-ppt concentrations. It is difficult to detect such small amounts of materials, and this has discouraged their investigation until recently. They pass through glass fiber filters. Cryogenic trapping at -196° collects them efficiently, but collects water also, which complicates recovery for analysis. Use of solvent trains leads to similar difficulties.

At the Research Triangle Institute, a system for identifying and measuring atmospheric vapors is being developed which is based on the use of a sorbent cartridge for collection and GC/MS for analysis (1-6). This method offers important advantages: It is applicable to most volatile organics and suitable for positive identification as well as quantitation. Since thermal desorption is used for recovery, the entire sample can be delivered for analysis.

Vapors are collected by drawing air through a 1.5 x 6 cm bed of Tenax GC. Particulates are first removed by a glass fiber filter. After passing through the cartridge, the air is drawn through a suction pump, then passes through a flow meter and a calibrated gas meter. The flow rate is adjustable from one to ten liters/minute. Water and inorganic gases have very low retention volumes on Tenax. Organic vapors are collected quantitatively until they begin to elute from the back of the sorbent bed. Breakthrough volumes must be known for compounds that are quantitated. Loaded cartridges are sealed in airtight containers pending analysis. Vapors are thermally desorbed in a helium stream at 270° and collected in a capillary trap at -196°. Then the carrier gas stream is routed through the trap and it is heated to 175°. Glass SCOT columns are interfaced to a Varian MAT CH-7 mass spectrometer with a single stage glass jet separator. Mass spectral scans (30-300 amu every 2.5 sec) are taken during chromatographic separation. A total ion current chromatogram is recorded while chromatographic and mass spectral data are accumulated on magnetic tape by an on-line Varian 620i computer, which is later used to retrieve the data, plot normalized mass spectra, and generate a reconstructed gas chromatogram which can be used to correlate mass spectra with retention times.

Non-polar phases, usually OV-101, are used to obtain pollutant profiles. Polar phases, such as OV-225 and diethylene glycol succinate are also used for quantitative analysis. Ion plots for quantitation can be obtained by monitoring one ion or by generating mass fragmentograms from mass spectral data stored on tape.

Typically 80 to 150 compounds are found. Many alkane and alkene isomers from C_5 through C_{14} and large numbers of alkyl benzenes are detected. Most of these arise from engine exhaust. Specific structural identification of many of these hydrocarbon isomers could be made, but this has not been given priority. Instead, emphasis has been placed on identification of compounds which may be biologically hazardous. In addition to the hydrocarbons, ketones, aldehydes, alcohols and esters are usually found. Methylene chloride, chloroform, tetrachloroethylene, and the chlorobenzenes are common, and carbon tetrachloride, trichloroethylene, and bromoform are often observed.

Table 1 summarizes the compounds, other than the background of engine exhaust, which were collected at a rubber plant near Houston.

Among these compounds, chloroprene and chloroform have been cited as suspected carcinogens.

Table 1. COMPOUNDS COLLECTED IN HOUSTON AIR NEAR A RUBBER PLANT

Halocarbons	
chloromethane	tetrachloroethylene
dichloromethane	2-chloro-1,3-butadiene
chloroform	1,4-dichloro-2-butene
carbon tetrachloride	1-chlorobut-1-ene-3-yne
chlorofluoromethane	chlorobenzene
trichlorofluoromethane	m-dichlorobenzene
chloroethane	o-dichlorobenzene
1,1,1-trichloroethane	1,3,5-trichlorobenzene
Oxygen and Sulfur Compounds	
acetaldehyde	benzaldehyde
acetone	acetophenone
methyl ethyl ketone	diphenyl ether
furan	furfural
2-methylfuran	dimethyl furan isomer
carbon disulfide	
Hydrocarbons	
styrene	phenylacetylene
naphthalene	1-methylnaphthalene
biphenyl	2-methylnaphthalene
4-vinylcyclohexene	alpha-pinene

1500 liters collected 10 am to 2:30 pm, August, 1975.
42 meter OV-101 glass SCOT programmed 20-220°.

Table 2 summarizes the potentially hazardous compounds found in a sample collected at the Patapsco Sewage Treatment Plant in Baltimore. This facility processes large quantities of industrial waste. A trace of dimethylnitrosamine (DMN) was found. It is a potent carcinogen which

Table 2. COMPOUNDS IN BALTIMORE AIR NEAR A SEWAGE PLANT

dichloromethane	chloroform
trichlorofluoromethane	dibromochlorofluoromethane
chloroethane	1,1,1-trichloroethane
tetrachloroethylene	chlorobenzene
m-dichlorobenzene	benzaldehyde
3,4-dimethoxybenzaldehyde	
N-nitrosodimethylamine	

300 liters collected 10 am to 2 pm, October, 1975.
100 meter OV-101 glass SCOT programmed 20-220°.

has readily produced cancer in every species on which it has been tested. It is also highly toxic, and has caused fatal liver damage in man. The sewage plant was located cross-wind from an industrial site where DMN was being produced. Samples taken at the plant and downwind of it, especially in daytime, contained as much as ten parts per billion of DMN (7-9).

Potentially hazardous vapors collected at the plant where DMN was being produced are shown in Table 3. DMN was not detected in this night-time sample. Note that dimethylvinylchloride, trichloroethylene, and chloroform were found in an area where substantial levels of DMN were often present.

Table 3. COMPOUNDS COLLECTED IN BALTIMORE AT A CHEMICAL PLANT

dichloromethane	trichlorofluoromethane
chloroform	chloroethane
carbon tetrachloride	1,1,1-trichloroethane
trichloroethylene	tetrachloroethylene
1,chloro-2-methylpropene	3-chloro-2-methylpropene
d,l-2,3-dichlorobutane	meso-2,3-dichlorobutane
1,2,3-trichloropropane	1,4-dichloro-2-butene
chlorobenzene	m-dichlorobenzene
1,1,3,3-tetrachloro-2-methylpropane	o-dichlorobenzene

300 liters collected 11 pm to 3 am, October, 1975.
100 meter OV-101 glass SCOT programmed 20-220°.

The health effects of long-term, low level exposure to carcinogens and other hazardous vapors in air are not known. The most practical means of determining health effects of such exposure would be epidemiological studies. To do this, long-term monitoring of identities and concentrations of vapors are required. Sorbent trapping with recovery by thermal desorption and analysis by GC/MS is a method well suited for this purpose.

ACKNOWLEDGEMENTS: This work was supported by EPA Contract Nos. 68-02-1228 and 68-02-2262 of HEW. Assistance by Mr. W. Cooney and Mr. G. Ferreri (State of MD Air Quality), Mr. G. A. DeMarrais, Dr. E. Sawicki, and Mr. K. Krost (EPA) and Dr. M. E. Wall (RTI) are deeply appreciated.

REFERENCES

1. E. D. Pellizzari, "Development of Method for Carcinogenic Vapor Analysis in Ambient Atmospheres", Publication No. EPA-650/2-74-121, Contract No. 68-02-1228, 148 pp., July 1974.
2. E. D. Pellizzari, "Development of Analytical Techniques for Measuring Ambient Carcinogenic Vapors", Publication No. EPA-600/2-75-076, Contract No. 68-02-1228, 187 pp., November 1975.
3. E. D. Pellizzari, J. E. Bunch, B. H. Carpenter and E. Sawicki, Environ. Sci. Technol., 9, 552 (1975).
4. E. D. Pellizzari, B. H. Carpenter, J. E. Bunch and E. Sawicki, Environ. Sci. Technol., 9, 556 (1975).
5. E. D. Pellizzari, J. E. Bunch, R. E. Berkley and J. McRae, Anal. Lett., 9, 45 (1976).
6. E. D. Pellizzari, J. E. Bunch, R. E. Berkley and J. McRae, Anal. Chem., 48, 803 (1976).
7. D. Fine, D. Rounbehler, N. Belcher and S. Epstein, Science, 192, 1328 (1976).
8. E. D. Pellizzari, J. E. Bunch, R. E, Berkley and J. T. Bursey, Biomed. Mass Spectrom., in press.
9. E. D. Pellizzari, J. E. Bunch, J. T. Bursey, R. E. Berkley, E. Sawicki and K. Krost, Anal. Lett., in press.

Sampling and Analysis of Submarine Atmospheres.* J. J. DECORPO, F. E. SAALFELD and J. R. WYATT, Physical Chemistry Branch, F. W. WILLIAMS and H. G. EATON, Chemical Dynamics Branch, Naval Research Laboratory, Code 6110, Washington, D.C. 20375 D. E. SMITH, Desmatics, Inc., State College, Pennsylvania 16801

Atmosphere sampling methods such as the personnel sampling tubes (charcoal absorption), critical orifice samplers, and the filling of an evacuated flask have been statistically compared and evaluated. The samples analyzed by g.c.-m.s. and g.c., provide reliable information on the contamination in the submarine atmosphere. The "split plot" or "analysis by variances" statistical approach was used for the comparison and evaluation of the sampling methods. Results indicate that there is a significant time factor in the accuracy of the sampling method. That is, the time between sampling and analysis is an important consideration in determining the accuracy of a sampling method.

*A detailed account of this work will be published at a later date.

MASS SPECTRA OF CARCINOGENIC PARTICULATE ORGANIC MATTER (POM) FOUND IN THE ENVIRONMENT by R. S. THOMAS and R. C. LAO, CHEMISTRY DIVISION, TECHNOLOGY DEVELOPMENT BRANCH, AIR POLLUTION CONTROL DIRECTORATE, ENVIRONMENT CANADA, OTTAWA, CANADA, KIA OH3.

A continuing programme was initiated two years ago to investigate the some 600 odd carcinogenic compounds in the environment and health toxic substance listing of NIOSH. This work contains mass spectral data on nine nitrogen containing heterocyclic compounds, their analogs in polycyclics regularly form major components of the organic moiety present in both urban and industrial atmospheres.

The compounds are:

1. 2-azafluoranthene
2. 13-azafluoranthene
3. 1-azapyrene
4. 2-aminofluorene
5. 2-aminoanthracene
6. 4-aminofluoranthene
7. 3-aminopyrene
8. 2-aminochrysene

and

9. 6-aminochrysene

Each of the compounds investigated is a known carcinogen and reported as present in environmental samples. The detailed analytical procedures and mass spectra will be published in the International Journal of the Science of the Environment.

Application of Direct Thermal Desorption GC-MS to the Analysis of Volatiles in Commercial Polymers. WOODFIN V. LIGON, Jr., General Electric Corporate Research and Development, Schenectady, New York 12301.

A new thermal desorption device[1] which was originally designed for use with commercial porous polymer adsorbents has been applied to the analysis of indigenous volatiles in high polymers. Entrained volatiles are extracted from a sample by passing a flow of helium over the sample with concurrent heating. The helium and liberated volatiles are then directed to a GC-MS where the various constituents are separated and mass spectra obtained. The volatiles most often identified include process solvents, unreacted monomer and various stabilizers.

[1]Woodfin V. Ligon, Jr. and Robert L. Johnson, Jr. 23rd Annual Conf. ASMS Houston, Texas, May 1975 and Anal. Chem. (In Press).

ANALYSIS OF BRAZILIAN NATURAL WATERS FOR ORGANIC POLLUTANTS BY GC/MS/COMPUTER

C. Herndon Williams Jr.

Institute of Chemistry, Universidade Estadual de Campinas
Campinas, Sao Paulo, Brazil

We have undertaken a survey of some of the rivers and lakes in the contiguous regions of Campinas and Sao Paulo for dissolved organic pollutants by GC/MS/COM and GC/FID. This is a report of our first results.

The area that we have chosen for study is heavily developed and populated, containing a wide variety of industries in and around the city of Sao Paulo and north of Campinas as well as intensive cultivation in a broad range of agricultural products, from cotton to wine grapes. In this report, we present preliminary results for samples of surface water taken from five sites, plus one sample of rain water.

Since DDT and other chlorinated pesticides are in use in Brazil and, in some cases, are fabricated here, our sample treatment procedures (1,2) were set up to extract the neutral compounds either dissolved in the water or adsorbed on the suspended matter. A diagram of our water sample treatment procedure and our instrumental configuration appears in Fig. 1.

The water samples were collected in clean glass jugs and either were extracted soon after their return to the laboratory or were kept refrigerated at 5° C. When necessary, the pH of the water was adjusted to 7 with hydrochloric acid before a 1 liter portion was extracted with three 50 ml portions of CH_2Cl_2. No filtering was done prior to this extraction, so any suspended matter present in the original sample was also extracted and sent along to the next step. This step consisted of passing the ~ 150 ml of extract through a solvent-washed anhydrous Na_2SO_4 column to remove any water. Any suspended matter was filtered in this step. Fresh solvent was used to rinse the separatory funnel and to wash any suspended matter on the column. The ~ 200 ml of CH_2Cl_2 were concentrated to 0.5 ml by low temperature distillation in a modified Kuderna-Danish apparatus. These procedures were tested with distilled water blanks and with prepared solutions of Lindane/Dieldrin/DDT in distilled water and in natural water, in the concentration range 25-250 ppb.

An injection of 1 to 5 microliters of the concentrated extract could be made on parallel GC/MS/COM and GC/FID systems: a Finnigan Model 9500 dual column GC with a flame ionization detector and a jet separator interface to a Finnigan Model 1015 MS with a Model 6100 data system. The two GC columns were identical: 2 mm ID x 6 ft glass, packed with 3% OV-17 on Gas Chrom Q and operated in a 200° C isothermal mode, with a 30 ml/min flow of He.

The mass scale was calibrated with perfluorotributylamine (FC 43) and the relative ion intensities in the range 50-450 amu using decafluorotriphenylphosphine (DFTPP) by the method of Eichelberger, Harris and Budde (3). Analysis of the pesticide standard solutions gave the following sensitivity information for Dieldrin: the recovery was about 50% and the detection limit was ~ 10 ppb in water; 50 ng of Dieldrin in a GC peak was sufficient to produce a "library-searchable" spectra.

All of the blanks showed two or three early-eluting GC peaks (RT = 1.0, 1.3, 1.8 min at 200° C), all with a base peak at mass 149 and tentatively identified (4) as phthalate impurities in the CH_2Cl_2. The rain water and, surprisingly, most of the rest of the ground water samples exhibited no other detectible GC peaks at our current levels of sensitivity.

We expected that the water samples collected from the Rio Atibaia at Paulina, north of Campinas and about 1 km downstream from a large industrial and petrochemical complex, would be the most likely to show organic pollutants. A reconstructed limited-mass (100-450 amu) chromatogram of a water sample from this site, spiked with 25 ppb of Dieldrin as an internal standard, is shown in Fig. 2.

The large peak labeled a is one identified as a phthalate and peak #4 (RT = 5.48 min) is Dieldrin. The seven other peaks, with retention times between 3.26 min (#1) and 10.89 min (#8), represent unknown peaks not present in the blanks. Peak #5 was verified by mass fragmentography using mass 266.

The positive identification of the seven unknown peaks has proved to be difficult with the resources at our disposition. Using the Library Search routine and the small pesticide file of the Finnigan data system on the background-subtracted spectra, we found that only peak #4, Dieldrin, gave a satisfactory match. A manual search through the 8 Peak Index of Mass Spectra (4) produced two further tentative identifications:

peak #2	2,4 dioxo-1,2,3,4 tetrahydro-5H-(1)-benzopyrano (2,3-D) pyrimidine	$C_{15}H_{20}O$,
peak #8	3-(p-dimethylaminophenyl) benzo-1,2,3-triazine-4-one	$C_{15}H_{14}ON_4$.

Since one of the other sites sampled was upstream of the industrial complex on the Rio Atibaia and did not show these extra GC peaks, it seems probable that these 7 peaks represent components of industrial discharge in the concentration range 10-100 ug/liter and warrant further study.

REFERENCES

1. R.G.Webb, A.W.Garrison, L.H.Keith and J.M.McGuire, EPA-R2-73-277 (August 1973).
2. J.M.McGuire, A.L.Alford and M.H.Carter, EPA-R2-73-234 (July 1973).
3. J.W.Eichelberger, L.E.Harris, W.L.Budde, Anal. Chem. 47, 995 (1975).
4. 8 Peak Index of Mass Spectra, First Edition (1970) and Second Edition (1975), Mass Spectrometry Data Center, Aldermaston.

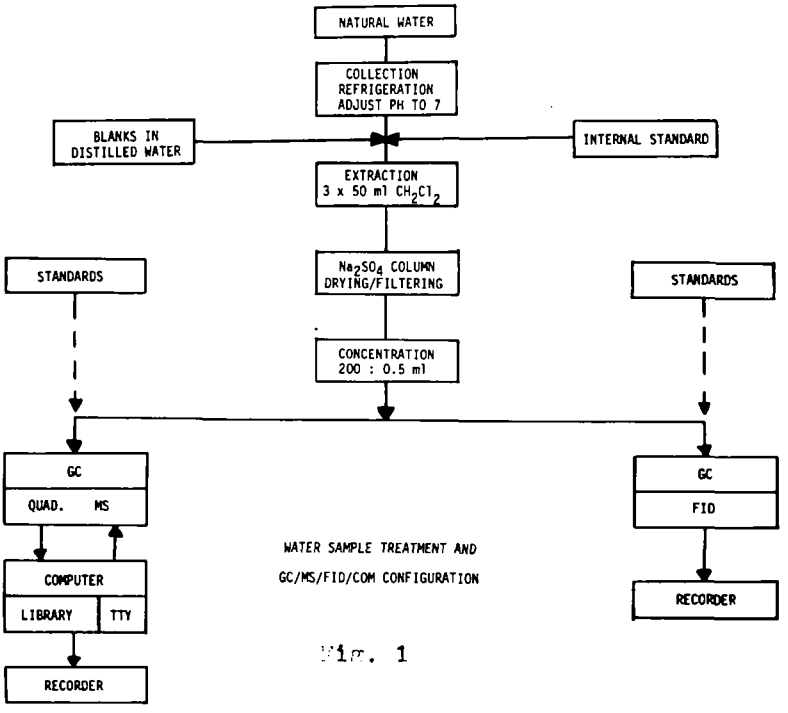

WATER SAMPLE TREATMENT AND
GC/MS/FID/COM CONFIGURATION

Fig. 1

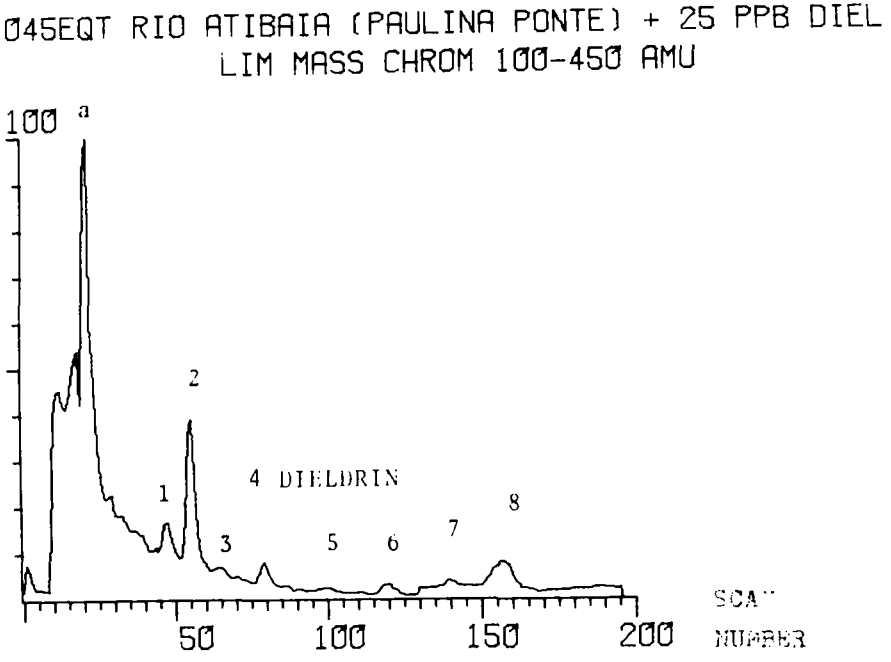

Fig. 2 Limited mass chromatogram (100-450 amu) of water from the Rio Atibaia + 25 ppb Dieldrin

USE OF HIGH SENSITIVITY GC-MS FOR IDENTIFYING ORGANIC WATER POLLUTANTS AT THE SUB-PPB LEVEL.*

R. M. Milberg and J. C. Cook, Jr.

School of Chemical Sciences and Institute for Environmental Studies, University of Illinois, Urbana, Illinois, 61801

In recent years there has been a great deal of concern about the effects of trace organic compounds in water supplies. Numerous surface water samples collected from across the country have been examined to identify previously unrecognized compounds at the PPB level. New technology and methodology have been developed for improving the sensitivity and chromatographic resolution of the analyses using GC-MS.

Volatile organic compound analysis is performed by purging 125 ml of water with helium and trapping the compounds on Tenax (Applied Science). The compounds are then desorbed onto a 12 foot by 2 mm ID glass column packed with 0.2% Carbowax 1500 on Carbopack C 60/80 mesh (Supelco, Inc.). This column is capable of separating the aliphatic alcohols up to C5, halogenated hydrocarbons up to C3, and aliphatic hydrocarbons up to C7 found in water. The column also works well for direct injection of water samples. The column has very little bleed even at 200° C and is ideally suited for GC-MS work.

Base extracts and methylated acid extracts of water samples are analyzed on a 12 foot by 2 mm ID glass column packed with 3% OV-17 on Gas Chrom-Q 80/100 mesh (Applied Science). This column is well suited for general purpose separations.

Samples were analyzed on a Varin-MAT 311A GC-MS and SS-100C data system. The ion source housing of the 311A is pumped with a 200 l/s turbomolecular pump which provides essentially zero background. The 311A with the turbomolecular pump provide the ability to routinely identify as little as 0.1 PPB of many compounds.

Our work has indicated that the use of high resolution capillary GC columns is necessary for the more polluted acid and base extracts. Some of the samples have several hundred components present at the 1 PPB level.

* Work supported by U.S. EPA contract 68-01-3234

GC/MS IDENTIFICATION OF SYNTHETIC ORGANIC POLLUTANTS IN INDUSTRIAL EFFLUENTS AND RECEIVING WATERS

Gregory Jungclaus, Larry M. Games,
M.L. Lee, and Ronald A. Hites
Department of Chemical Engineering
Massachusetts Institute of Technology
Cambridge, Massachusetts 02139

It is obviously important to identify potentially toxic organic compounds in the environment, isolate their sources, and determine their environmental fates. We are currently analyzing the wastewaters, receiving waters, and sediments of several cooperating companies to determine the fates of such compounds. One of the plants we are studying is a general-purpose chemical manufacturing plant located about 2 km from the mouth of a small river which empties into Narragansett Bay. The flow rate of the wastewater out of the plant is about 10^6 gal/day, and the flow rate of the river is about 10^7 gal/day. Prior to release into the river, the wastewater is neutralized in a one million gallon equalization tank, passed through a trickling filter for biological degradation, and freed of most solids in a clarifier.

Composite and grab water samples were extracted with dichloromethane, and sediment samples were extracted with 3:1 benzene-methanol. The sediment extracts were separated into hexane, benzene, and methanol fractions using column chromatography on alumina and silica gel. The samples were analyzed on a dual source (EI/CI) Hewlett-Packard 5982A

GC/MS system interfaced with a HP 5933A data system. The mass spectrometer was coupled to the gas chromatograph via a glass-lined jet separator held at 300°C and was operated in the continuous scanning mode under control of the data system.

A few representative compounds found in the plant wastewater, receiving waters, and sediments are presented in Table 1. Although the concentration of these compounds in the river water was generally only a few parts per billion, analysis of the river sediment revealed very high concentrations of some of the components; up to 0.3% for 2(2'-hydroxy-5'-methylphenyl)-2H-benzotriazole, for example. Some of the compounds were even found in Narragansett Bay sediment 5 km from the source; this may result from transport of the contaminated river sediment.

We have concluded that normally water insoluable industrial organic compounds can be accommodated in wastewater by interaction with high concentrations of dissolved and suspended organic material (e.g. solvents, biological sludge). Dilution of this effluent with river water seems to cause many of the organic compounds to precipitate and become incorporated into the underlying sediment. Low molecular weight compounds are apparently rapidly lost through volatilization. These findings lead to the concern that high concentrations of anthropogenic organic compounds in sediments may continually repollute the water even after effluent controls are implemented.

Table 1

Representative Compounds and Their Approximate Concentrations in the Wastewater and Receiving Waters and Sediments

Compound	Approximate Concentration (ppm)			
	Wastewater	River Water (30m)	River Sediment (30m)	Estuary Sediment (5 km)
Toluene	30			
Chlorophenol	0.5			
di-t-butyl phenol	5	0.03	500	8
methyl 3-(3',5'-di-t-butyl-4'-hydroxy phenyl)-propionate (I)	10	0.02	400	
2-chloro-4,6-bis (isopropylamino)-s-triazine (II)	7	0.02	10	
2(2'-hydroxy-5'-methyl-phenyl)-2H-benzotriazole (III)	12	0.05	3000	3.5
2(2'-hydroxy-3',5'-di-t-amyl-phenyl)-2H-benzotriazole (IV)	8	0.03	1900	20

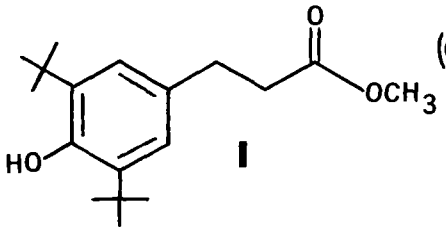

I

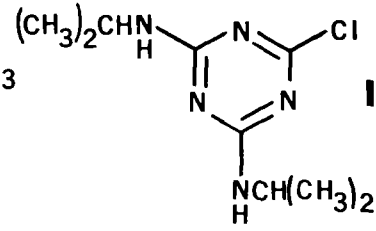

II

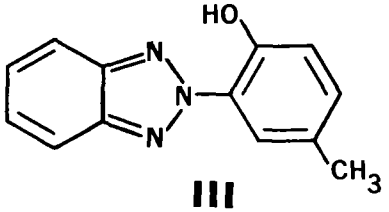

III

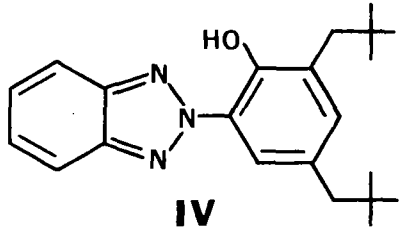

IV

COMPUTERIZED MASS SPECTROMETER DATA SYSTEM AT LLL*

R. D. Friesen, R. J. Dupzyk

Lawrence Livermore Laboratory, University of California
Livermore, California 94550

ABSTRACT

The data systems on the three mass spectrometers at LLL are computer-controlled, pulse-counting systems synchronized to a repeatedly-swept magnetic field. The data are accumulated in the memory of the computer or in a Nuclear Data ND 180 in a multi-scaler mode of operation. This mode of data acquisition allows a continuous check of the background stability and makes tune-up easier. But the main benefit is a reduction in the required ion emission rate stability. By the use of standards to set the system dead time, we have been able to utilize the sensitivity of a pulse counting system without the expense of exotic equipment.

Pulse Counting Equipment

The electron multiplier is an 18-stage EMI 9642/2B beryllium-copper venetian blind type. The socket is a specially made ceramic unit that forms the vacuum seal and electrical interface. Every stage is bypassed directly to ground. The first dynode is run at -3.5 to -6.0 kV (depending on the age of the multiplier). The last dynode, at ground potential, is dc coupled to the preamp.

Using an oscilloscope, the dead time of the multiplier was found to be 20 ns.

The preamplifier is an in-house design using a Fairchild 733 wide-band video amplifier. It is connected as a gain of 100 and performs the discrimination function also.

Using a fast double pulse generator, the measured dead time of the preamplifier was 13 ns.

The data counter was designed and built at LLL. It is a 100 MHz T^2L binary counter with switch selectable serial or parallel output. The serial output is used when the counter is connected to a Nuclear Data ND 180 and the parallel output is interfaced directly to the PDP-8. The counter's measured dead time is 10 ns.

The equation for combining the individual time components is:

$$DT = (M^2 + P^2 + C^2)^{1/2}$$

From this the system dead time should have been 25.8 ns.

To check our calculations, we ran several N.B.S. Uranium standards. We varied the emission rate over a .1% to 10.0% dead time correction range and adjusted the dead time correction until the isotope ratios remained constant over the entire range. The actual system dead time was approximately 40 ns. It varied with discriminator setting, multiplier voltage and the age of the multiplier.

*Work performed under the auspices of the U.S. Energy Research & Development Administration under contract No. W-7405-Eng-48.

Mode of Operation

Our instruments use a fixed high voltage and a swept magnetic field. The sweep is a linear ramp moving first up then down through the isotopic region of interest. The sweep times vary with sample requirements, but the average times are .25 to .5 seconds and the run times are 100 to 1000 seconds. Sweeping up and down through the spectrum tends to cancel long term emission drifts and repetitive sweeping improves the signal-to-noise ratio.

Computer System

The computer system CPU is a Digital Equipment Corporation PDP-8 with 16K of core. Bulk storage for the system is two Diablo disk drives, one fixed platter and one removable platter. Peripherals on the system are a 2400 baud Telray 3300 CRT terminal, a 100 character-per-second Centronics 306 printer, a 14 inch H-P 1300A display scope, a DEC high-speed paper-tape reader-punch, and an in-house fabricated joystick for operator data interaction.

The software for the system uses DEC's OS8/V3. The actual programs are written in FORTRAN II with assembly language subroutines for data acquisition, display, and control.

The system operation code is actually many small codes divided into levels and linked through a process called chaining. At the start, the code asks if this sample is an old or new type. If it is old, it uses a parameter file from a library. If it is a new type, the code asks questions until it has created a new parameter file which is then added to the library.

The parameter file sets the route through the nest of programs, it sets the type of data reduction, and it sets the data output format.

The nest of programs is divided into six basic levels of operation:

The first level establishes the initial parameters such as log number, sample identification, mass range, and system dead time. It also opens the variable file.

The second level does the data acquisition, either by reading the ND 180 memory or reading the data counter. When the data counter is being used, the program provides a linear or log display of the data as it accumulates. The program then writes the data into a temporary data file on the disk.

The third level allows the operator to correct any dropped channels or noise spikes that may have occurred. It then does data smoothing by an algorithm called a moving average. It then goes through the data a peak at a time, finding peaks and backgrounds. The computer's choice is displayed using cursors to mark the selected points. The operator may correct these choices and the program then calculates the peak heights and isotope ratios. These ratios and their errors are then printed. If the operator wishes to take more data, the chain goes back to the second level. If he is through, the chain goes on to the fourth level.

The fourth level calculates and prints the final ratios and errors from all the data accumulated. Then, depending on the experimental requirements, any further required calculations are performed.

The fifth level in the set gathers all the temporary data files into one permanent data file for long term storage and deletes all the temporary files.

The sixth level retrieves the permanent data files and creates new temporary data files, allowing the data to be reprocessed if needed.

Results

The on-line computer and pulse counting system has allowed us to increase our precision and dynamic range. We are now reporting the following results:

For routine samples in the 50 picogram to 300 nanogram range, a precision of $\pm$ .5% on minor isotopes is obtainable. By special request (and handling) we have been able to report $\pm$ 10% precision on 10^8 atoms of sample, $\pm$ .2% precision on 1500-to-1 adjacent mass dynamic range, or $\pm$ 10% precision on 10^7-to-1 adjacent mass dynamic range.

**Reference to a company or product name does not imply approval or recommendation of the product by the University of California or the U.S. Energy Research & Development Administration to the exclusion of others that may be suitable.

Sensitivity, Dynamic Range and Mass Accuracy Optimization In A Mass Spectrometer Data System.

Donald E. Hagge, Peter G. Blaney and Bernard M. Grinberg, INCOS Corp., 1332 6th St., Berkeley, Ca. 94710

A computerized data system provides many new features to the mass spectroscopists. It can rapidly acquire large volumes of data automatically, quickly retrieve, process, display and hard copy data, do library searches, etc. It is difficult if not impossible for a data system to compete with a trained mass spectroscopist and a multi-pen recorder in achieving sensitivity and dynamic range. The standard approaches to interfacing generally taken fall short of utilizing the information available from a mass spectrometer. Pulse or ion counting is optimum for sensitivity but suffers dynamic range limitations. Analog filtering with conventional sample and hold/analog-to-digital converter systems limits sensitivity and mass accuracy. A review of the critical parameters that determine sensitivity, dynamic range and mass accuracy in mass spectrometry will be made. A description of the data acquisition system developed for the INCOS 2000 data system will be given.

DA/CS-VII – A NEW DATA ANALYSIS AND CONTROL SYSTEM FOR 12-90-HT MASS SPECTROMETERS AND OTHERS USED FOR THERMODYNAMIC STUDIES

G. L. Brezler, Nuclide Corporation, 642 East College Avenue, State College, PA 16801

The DA/CS-VII MS data acquisition system embodies not only programs for Knudsen cell studies of chemical systems at equilibrium, using a Nuclide 12-90-HT mass spectrometer, but also GC/MS and isotope ratio software.

The core of DA/CS-VII is a G. A. SPC-16/45 minicomputer with 16k core and the usual ancillary equipment.

The 16-bit D/A produces a 0-to-10-V signal with a resolution of 1 part in 65,536. The analog output circuit is optically coupled to the digital signal lines of the computer bus to prevent ground loops which cause noise. The 16-bit D/A controls the magnetic field in this application; it could also be utilized to step the accelerating potential.

The 14-bit A/D measures the magnetic field when the mass spectrometer's internal scan circuitry is used. Its field measurements are used to calculate m/e values. It also is optically coupled.

The voltage-to-frequency converter produces a 0-to-100-kHz pulse train for a 0-to-10-V input. This frequency yields a resolution of 1 part in 100,000 for a one-second measurement. The amplifier has a relative accuracy of 0.01% and extends the dynamic range of the V/F converter to 10^7. The integration time for the V/F is programmable between 1 and 4095 milliseconds.

The multiplexer provides eight channels of differential analog input. Five channels are used by amplifiers having gains of 1, 4, 16, 64, and 256, respectively; their relative accuracies are $\pm$ 0.01%. Three spare channels are available for future use, for example, as temperature measuring channels. The input signal is presented in parallel to all amplifiers. Gain is programmed by means of multiplexer channel selection. The output of the multiplexer is fed to the input of the 12-bit unipolar A/D. The resolution of this converter is 1 part in 4096, and the amplifiers extend the dynamic range to 10^6. The 12-bit A/D is used whenever high-speed data acquisition is desired since it can initiate a new reading every 4 microseconds; its high speed permits programs to be written which incorporate a real time averaging process. In contrast, the 14-bit A/D can only make a measurement every 45 μs.

The signal input to the V/F converter and MUX can be switched between the outputs of the electrometer and the lock-in amplifier. [The LIA is a MS accessory used to subtract those spectrum signals resulting from ionization of residual background gases in the source (see paper Z8)].

DA/CS-VII uses flexible disks with 150,000 16-bit word storage capacity.

The high-speed paper tape reader is a 300-character-per-second device used for program generation and modification. It can also be used to reload the system software.

A digital plotter serves as the DA/CS-VII output device for the various graphs and spectral plots. Other options include Nuclide's Dynagraph MK-III graphic display system, and an interface to the MS's emission regulator for control of the electron acceleration, used to automate appearance potential studies.

The software package supplied with DA/CS-VII provides the analyst with the same capabilities to acquire and massage data included in our DA/CS-I.2 GC/MS data system, e.g., to acquire spectral data while the MS is scanning, to assign m/e values to peaks, and to store information on flexible disks. The data massage routines permit plotting or printing of mass spectra, spectral addition and subtraction, plotting or printing of the variation of operator-specified mass peak intensities, and plotting or printing of total ion intensities. GC/MS data systems typically render the resultant plots as a function of time or scan number. DA/CS-VII information is collected as a function of time or temperature. Since temperature is usually varied slowly, the system can be instructed to display every spectrum in real time but to store on disk every nth spectrum, thus saving storage space. DA/CS-VII can also automatically store a scan at each specified increment of temperature.

Slide 1 shows an ionization efficiency plot for a dimer of selenium. (Here the vertical axis is logarithmic, but DA/CS-VII software also accomodates linear scaling.)

Note that the measured appearance potential is 9.75 volts. If the measured appearance potential was several electron volts higher than the spectroscopic value of 9.75 eV, one could suspect that the ions were formed by the fragmentation process.

Ionization efficiency plots also make obvious slope or other changes which can provide information on the method of formation of the ions of interest.

Two or more ionization efficiency curves can be included on one plot, e.g., a standard and a sample, to determine a correction factor. Ionization efficiency curves for up to 10 masses can be obtained sequentially with DA/CS-VII. Each operator-specified mass is focused at the collector by computer-controlled peak stepping; the electron acceleration can be varied automatically or manually.

For this type of experiment the ion intensity is measured using the voltage-to-frequency converter because it is not necessary to acquire data rapidly; the V/F converter acts as an integrator and effectively filters noise.

Another capability of DA/CS-VII is the calculation of heat of vaporization and sublimation. Up to 10 masses can be magnetically focused by the computer at specific increments of

temperature. Peak intensities are measured at each temperature level and stored along with the measured or controlled temperature. After the designated temperature range of interest has been traversed, the plot is generated. The best straight line through the data points is calculated using a linear least squares fit. The slope of this line gives the heat of vaporization or sublimation.

DA/CS-VII software also permits the analyst to request the isotopic distribution pattern of any molecular species such as dimers, trimers and higher polymers. The system will then compute and print out the calculated and the measured relative abundances.

A basic library search system is also provided. It is comprised of 100 "groups," with up to 10 masses per group; the species are arranged in order of intensity. The portion of the spectrum to be compared against the library is specified by the operator.

Programs to expand the capabilities of DA/CS-VII are under development at Nuclide. However, we know from experience that individual laboratories will desire specific program modifications. Therefore, in the development of DA/CS-VII, emphasis has been placed on insuring that the hardware provided will readily permit the expansion of software capabilities. Since source listings for the system software are provided, program modifications can be done in the user's laboratory, if desired.

Inclusion of the Disk Based Operation System (DBOS) software permits DA/CS-VII to also be used as a general purpose stand-alone laboratory computer with Fortran and BASIC language programming capabilities. This capability might be used, for example, for supplementary thermodynamic calculations of equilbrium constants.

Note: the complete version of this paper may be obtained from the author (request Nuclide publication no. 1588-1275).

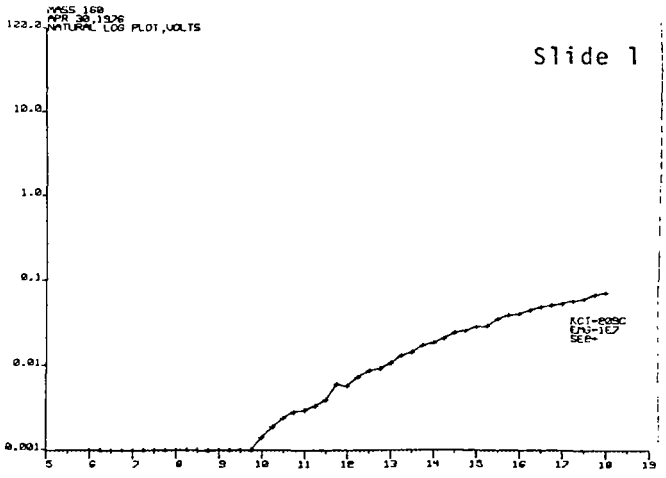

Slide 1

Solutions to Some Problems in Computerized Data Analysis of Multicomponent Mass Spectra, M. E. Scolnick, Stanford Research Institute, Mass Spectrometry Research Center, Menlo Park CA 94025

Introduction. The identification of complex mixtures by the use of field ionization mass spectra requires a technique for measuring the degree of similarity between two spectra. Spectrograms can be ranked in order of their similarity to a reference spectrogram by counting the number of positions in the spectral range at which the relative peak heights are approximately equal. If Z_j is a measure of the difference between two spectra at the jth mass number and t is a fixed threshold value, the number of values of j for which $Z_j \leq t$ can be used as a measure of similarity. The threshold value t should be chosen so that comparison between spectra of the same specimen rank high on the similarity scale while comparisons between spectra of different mixtures result in low similarity scores.

A mass spectrum can be represented by a vector X with components $x_1, x_2, \ldots, x_j$, where x_j is the height or area of the peak at the jth mass number. The vector representation of a spectrum can be normalized so that the sum of all the components or of all the squared components equals unity. The difference between two spectra X and Y can be computed as the difference between their normalized J-dimensional vector representations. The jth component, $x_j - y_j$, of this vector difference is one way to define X_j.

For the purpose of deciding whether or not two spectra represent the same oil, an identification criterion must be chosen. The latter may be defined as an artibrary lower limit for the degree of similarity. To be concise, H_o is the null hypothesis: spectra X and Y represent the same oil. Reject H_o when $Z_j \geq t$ for at least R values of j, $j = 1, 2, \ldots, J$. The degree of similarity is given by J-R. Clearly, if a small value for t is chosen, H_o will be rejected in a large number of cases where X and Y represent the same oil. Conversely, if a large value of t is chosen, H_o will be accepted in a large number of cases where X and Y represent different oils. A prudent decision on the value of T can be made on the basis of a statistical model or empirically, as a result of the analysis of a set of spectra of known identity.

Statistical Models. Assume H_o is true and suppose that for a prescribed probability α a threshold t can be determined such that

$$P\left[\,|Z_j| > t\right] = \alpha, \text{ for } j = 1 \text{ or } 2 \text{ or } \ldots \text{ or } J \quad (1)$$

Assume that the spectral differences Z_j and Z_k are stochastically independent for $j \neq k$. The requirement $Z_j \leq t$ for all J values of j as the identification criterion, implies

$$P\left[\text{accept Ho} \,\middle|\, \text{Ho is true}\right] = (1 - \alpha)^J \quad (2)$$

$$P\left[\text{reject Ho} \,\middle|\, \text{Ho is true}\right] = 1 - (1 - \alpha)^J \quad (3)$$

Equation (3) describes the probability for incorrectly rejecting H_o. Suppose we are willing to tolerate this error in 100 A% of the spectrum pairs analyzed. Then

$$1 - (1 - \alpha)^J = A \quad (4)$$

Solving for α obtains

$$\alpha = 1 - (1 - A)^{1/J} \tag{5}$$

Combining equations (1) and (5) yields

$$P\left[\left|Z_j\right| > t\right] = 1 - (1 - A)^{1/J} \tag{6}$$

Equation (6) enables us to choose a threshold t so that the risk for error is equal to A when the number of possible spectral differences is J and when the identification criterion requires zero spectral differences greater than t. In general, the identification criterion: $Z_j \leq t$ for at least J-R values of j, implies

$$P\left[\text{accept } H_o \mid H_o \text{ true}\right] = \sum_{r=0}^{R} \frac{J!}{(J-r)!\,r!} \alpha^r (1-\alpha)^{J-r} \tag{7}$$

$$A = 1 - \sum_{r=0}^{R} \frac{J!}{(J-r)!\,r!} \alpha^r (1-\alpha)^{J-r} \tag{8}$$

Note that 1-A is the confidence level of this test for the null hypothesis: X and Y represent the same oil.

The statistical model elucidates two characteristic properties of spectral fingerprinting. First, the significance of a spectral difference decreases as the number of possible differences increases. In comparisons of spectra of the same oil, the chances for a large difference to occur at random are greater when the mass range spans 400 amu than where threr are only 20 possible places for differences to occur. Second, the spectral difference threshold, required for a given confidence limit, decreases as the number of allowable differences in the identification criterion increases. These two characteristics are demonstrated in Table 1.

The threshold values in Table 1 were obtained in the following way: (a) the confidence level 1-A = 0.98 was chosen; (b) equation (8) was solved for α for the cases R = 0, 1, 2 and J = 10, 20, 40; (c) a normal distribution with unit variance was assumed for Z_j; (d) the threshold values for t were found by using

$$\alpha = 1 - \frac{1}{\sqrt{2\pi}} \int_{-t}^{t} \exp\left(-Z^2/2\right) \, dZ \tag{9}$$

or

$$\alpha = 2(1 - F(t)).$$

where F(t) is the cumulative normal distribution found in most statistics tabels.

R \ J	10	20	40
1	3.09	3.29	3.48
2	2.28	2.54	2.78
3	1.87	2.18	2.45

Table 3. Threshold values t as functions of J, the maximum number of spectral differences possible, and R the maximum number of differences acceptable for the identification test at the 98% confidence level. Errors are assumed to be normally distributed and independent.

In cases where the spectral differences Z_j and Z_k are correlated for $j \neq k$, a statistics model based on a distribution such as the generalized Student-t statistic[1] must be used instead of the above analysis. The number of spectra required for the computation of a covariance matrix, however, must be larger than the dimensionality of the spectral vector representations, which in most cases makes this approach economically unattractive.

A nonparametric statistical model[2] based on the use of the Wilcoxon test[3] has been used successfully for finding significant differences between classes of field ionization urine spectra[4].

Empirical Model. The empirical approach differs from the statistical model in the way in which threshold values are chosen. The definition of an identification criterion or "discriminant function" is essentially the same in both models with the exception that in the empirical case, threshold values are usually not restricted to a single value (i.e., the usual case is $t = t(j)$). Empirical techniques are described in the literature under the headings "Pattern Recognition" and "Learning Machine Techniques." [5,6,7] The literature has become extensive in recent years.[8,9]

Discriminant functions differ from the identification criterion used in the statistical model primarily in the use of J threshold values t_j. Note, however, that the use of a single threshold value in the statistical model was merely a methematical convenience and not a logical necessity. In an ideal empirical case the t_j are simply chosen so that $Z_j \leq t_j$ for all X and Y that represent spectra of the same oil. As additional spectra are acquired, the t_j are adjusted so that the condition $Z_j \leq t_j$ is maintained for all vector pairs in the set. If, by applying this empirical method to the sets of spectra representing many classes, we find that every spectrum can be unambiguously identified with its respective class, we say that the data are "separable." The assumption is made that if sufficiently large sets of data are used - they are referred to as "training sets" - the values of t_j will converge to their respective limits. At this point the vector representation of an unknown spectrum can be classified correctly by applying the discriminant functions iteratively to differences between the unknown spectrum and spectra from each of the training sets.

Two problems that can arise are: The unknown spectrum may not be a member of any of the training classes, in which case correct identification is impossible. Secondly, the training sets may not be completely separable, in which case a spectrum will sometimes be identified with more than one class. The latter problem is often acceptable, however. For example, a conceptually simple discriminant function has been applied to the classification of 154 oil spectra into 35 classes with ambiguities in only 5% of the cases.[10]

Conclusions. There is no "best" criterion for identifying oils by the use of their mass spectrometric fingerprints. Identification criteria can be evaluated in terms of the frequency with which either of two kinds of errors are made: (a) the common identity of a pair of spectra is incorrectly rejected and (b) the common identity of a pair of spectra is incorrectly accepted. The significance of the

total difference between two spectra is dependent on (a) the number of possible differences (i.e., the number of peaks in the spectra or the dimensionality of their representations), (b) the definition of a spectral difference (i.e., the threshold values), (c) the number of spectral differences, (d) how well the true spectra are known and (e) the dispersion of the data as measured by the variances or the ranges, etc. The relationship between these five parameters and the two kinds of error that determine the success or failure of an identification criterion can be described precisely by assuming that errors in measurements are random and independent and applying a statistical model. Notwithstanding the fact that these assumptions may be invalidated experimentally, the conclusions of the statistical model provide guidelines for constructing an empirical discriminant function.

References

1. T. W. Anderson, An Introduction to Multivariate Statistical Analysis, John Wiley & Sons, Inc., New York, 1958.
2. A. B. Robinson and F. C. Westall, J. Orthomol. Psychiat. 3, 1 (1974).
3. F. Wilcoxon, Biometrics 1, 80 (1945).
4. M. Anbar, R. L. Dyer, M. E. Scolnick, Clin. Chem., in press.
5. R. O. Duda and P. E. Hart, Pattern Classification and Scene Analysis, John Wiley & Sons, New York, 1973) .
6. N. J. Nilsson, Learning Machines, McGraw-Hill, New York, 1965.
7. J. T. Tou and R. C. Gonzalez, Pattern Recognition Principles, Addison-Wesley Publishing Co., Reading, Mass, 1974.
8. B. R. Kowalski, Anal. Chem. 47, 1152A (1975).
9. P. S. Shoenfeld and J. R. DeVoe, Anal. Chem. 48, 403R (1976).
10. M. E. Scolnick, A. C. Scott and M. Anbar, 24th Annual Conference on Mass Spectrometry and Allied Topics, San Diego, pager PSBIIa.

Extraction of Mass Spectra Free of Background and Neighboring Component Contributions from GC/MS Data.

Thomas C. Rindfleisch, R. G. Dromey, Mark J. Stefik and Alan M. Duffield, Stanford Univ., Dept. of Genetics, Stanford, California 94305

A computer method has been developed for the systematic generation of mass spectra free of background and contributions of unresolved components from GC/MS data of biomedical samples. A pair of histograms which characterize the positions and intensities of singlet mass fragmentogram peak modes are used to detect each component. Tabular models of singlet peak profiles are then used for the least squares resolution of multiplet fragmentogram complexes, removal of background contributions and correction of peak saturation. The method can detect and resolve reliably components that elute from the gas chromatograph within 1.5 to 2 mass spectral scan times of each other. The program is written in FORTRAN and operates with a DEC PDP 11/45 computer (28K core).

A Method for the Automatic Detection of Isotopic Clusters In Repetitive GC-MS Scans. Joseph A. Steinborn and Donald J. Jenden, Dept. Pharmacology and Brian Research Institute, University of California, Los Angeles, California

Ion clusters resulting from natural or artificial abundances of stable isotopes have been previously used as signals for identification of the source of compounds in biological fluids as a precursor with a corresponding label (Knapp, D. R. & Gaffney, T. E.: Clin. Pharmacol. Therap. 13: 307, 1972). A program has been written which allows a rapid computer search of continuous repetitive GC-MS scans for doublets of user-defined mass separation and relative intensity, and for components eluting from the GC which contain one or more doublets with these characteristics. This program allows an efficient search of a very large data base with a sensitivity approaching 1 pmol, identifying those components of a complex mixture which arise as metabolic products of a labelled drug, and yielding normalized mass spectra of doublet-containing compounds.
(Supported by NINDS # N01 NS 4-2330).

CODIFICATION OF MASS SPECTRA BY FUNCTIONAL GROUP CLASSIFICATION

D. H. Robertson, R. A. Graham & C. Merritt, Jr.

US Army Natick Research & Development Command, Natick, MA 01760

Over a period of time we have talked at these meetings about a binary encoding procedure[1,2] which we term octal coding, designed to facilitate coding of a data library in limited space and to aid searches therein for purposes of identifying unknown spectra.

The mass range of interest is divided into multiple groups of seven. The number representing the spectrum peak of highest intensity in the group is encoded as a three-bit binary number. Zero is used to denote the absence of a peak within the grouping, hence a total of eight possible values and the term octal code. The octal code is a string of digits each with possible values between 0 and 7 which represent a pattern that may be recognized by the computer.

We have chosen a 7 mass window and the starting masses for these octal groups in order to incorporate functional group and structural information into the octal code[3]. A series of masses corresponding to a series of ions such as 29, 43, 57,71, etc., represents alkanyl fragments and will each be encoded as the 7th digit in an odd-numbered window, thereby indicating the skeletal formula for the compound. Another ion series coded as 2 and representing masses 31, 45, 59, etc., is an example of a code appearing in even-numbered windows, which leads to information about functionality; in this case an alcohol or other oxygenated compounds.

Such a pattern of codes shows the recurring octal digit patterns for various series of ions which correspond to several common functional groups. The hydrocarbon fragments will always be coded in odd-numbered windows and when the skeletal structure is a saturated aliphatic hydrocarbon, the most abundant peaks represent a series of alkanyl fragments that are coded as octal 7. If the compound is unsaturated the octal code is 2 less than 7, or 5. Ions still more saturated, such as the alkyne series of formula, C_nH_{2n-3} will be represented by octal digit 3 in odd-numbered windows. Oxygen-containing peaks such as those arising from ketones and alkehydes are isometric with the alkyl ion fragments and will be coded concomitantly as octal 7.

Generally speaking, the appearance of a particular digit as a series in an odd-numbered window may be correlated with a particular skeletal feature. Octal patterns from even-numbered windows are related more commonly to functionality. Experience with octal coding as a means for searching a large data library (Registry of Mass Spectral Data) demonstrates that numerous structural features are indicated by the octal code. In a search the code is not ordinarily seen, but upon printout of the library in octal code, it is easy to see periodicity within the octal digit string. In addition to ion

series there are individual masses occurring in specific windows which relate as well to structure. We believe that an investigator may be easily trained to analyze the octal digit strings for various compounds and abstract structural information without specific knowledge of the masses which have been coded. Some examples follow.

Table 1 shows the octal codes for several C_7 compounds in which the functionality varies. For n-heptane the alkyl ion series is represented by the periodic appearance of 7s in odd-numbered windows. The terminal 1 in an even window as seen for the first two compounds represents the molecular ion. Ion groups as well as ion series also may be diagnostic, i.e., branching in a saturated alkane is indicated by a characteristic 101 sequence for the iso compounds compared to a terminal 001 for the corresponding n-alkane.

The periodicity of 5 indicates an olefin. Further structural features may be discerned as in the case of heptene-1 and heptene-3, where a strong ion of formula C_nH_{2n}, i.e., m/e 56, is observed in window 5, indicating the position of the double bond. In the case of the alkynes a periodicity of 3 occurs. In the low mass region however the alkenyl ions tend to be stronger than the alkynyl ions. The numbers in parentheses indicate the appearance of peaks in even-numbered windows which have no significance. Frequently peaks recorded in these windows may be due to background.

In the case of alcohols and aldehydes, the occurrence of a 2 in window 2 indicates oxygenation. The periodic sequence of 2s in heptanol-1 supports the presence of oxygen in continuing the series begun in window 2. A similar isometric series exists for sulfur-containing ions, but the first ion of this series is at mass 45. Accordingly, absence of a 2 in window 2 shifts the diagnosis from oxygenated compounds to thiocyclo compounds and other S containing compounds.

The parent ion, as is well known for alcohols, is very small or does not exist. Unlike the case for an alkene, the appearance of 6 in a terminal odd-numbered window of an oxygenated compound corresponds to the M-18 ion rather than the parent. Thus a 2 in window 2 in combination with 6 as terminal code number is indicative of an alcohol. The alkyl ion series usually found in alcohols of course corresponds to those found in alkenes although the series C_nH_{2n} indicated by 6s is frequently stronger than the series C_nH_{2n-1} indicated by 5s. The appearance of 5 instead of 7 in window 1, even though the alkyl chain may be saturated, tends to indicate that the alcohol is secondary rather than primary. The code for an aldehyde is seen in row 10. The appearance of 2 in window 2 and the appearance of strong ions in the unsaturated series in odd-numbered windows identifies it as an oxygenated compound. The presence of strong alkanyl ions of low mass indicates the alkyl chain to be saturated. The appearance of a 4 in a position 3 windows away from the parent indicates a strong M-18 ion expected for an aldehyde.

Other functionalities may be represented by specific ion series; e.g., a sequence of 4s in odd-numbered windows

represents a nitrile, whereas a series of 4s in even-numbered windows is diagnostic for alkanethiols and thiaalkanes. A series of 1s in even-numbered windows indicates an amine.

Another feature of the code which helps to indicate the presence of functional groups is the separation of the last digit of the code, representing the highest mass, from the next highest mass by several zeros. A determination of the parent ion as odd or even is also useful as in the case of amines where the series of 1s in even-numbered windows might be confused with the appearance of this series as trivial ions in an alkane series except for the fact that the parent mass is odd.

The binary method of encoding is highly successful in our laboratory for searching[4], and consideration of these structural features of the code enables us both to facilitate the search and to evaluate the results. We expect further application of pattern recognition and learning techniques will aid in the identification of compounds not in the library.

REFERENCES

[1] Proc. ASMS 20th Meeting, Dallas, 1972, p359
[2] Proc. ASMS 21st Meeting, San Francisco, 1973, p65
[3] Proc. ASMS 22nd Meeting, Philadelphia, 1974, p447
[4] J. Agr. Food Chem. 22, 750, 1974.

Table 1

Window Number	1	2	3	4	5	6	7	8	9	10	11	12	13	14	15	16
Carbon Number	2		3		4		5		6		7					
n-heptane	7	1	7	1	7	1	7	1	7	0	0	1				
2-methylhexane	5	1	7	1	7	1	7	1	7	1	0	1				
heptene-1	7	1	5	0	6	0	5	0	5	0	6					
heptene-2	5	1	5	(7)	5	(6)	5	0	5	0	6					
heptene-3	5	1	5	0	6	0	5	0	5	0	6					
heptyne-1	7	1	5	(7)	5	(5)	3	0	3	0	3					
heptyne-2	5	1	5	(1)	4	(6)	3	0	3	0	4					
heptanol-1	7	2	7	2	6	2	6	2	5	0	6					
heptanol-2	5	2	7	2	5	1	6	0	5	2	6					
heptanal	7	2	7	1	5	1	6	1	3	1	4	0	6	1		
heptane nitrile	5	1	5	1	4	0	4	0	4	0	4	0	4			
heptyl amine	7	1	5	1	6	2	6	1	7	1	6	0	0	2		
heptanethiol	5	6	5	4	6	4	6	2	5	4	6	4	0	0	0	5

LOW RESOLUTION MASS SPECTRA SEARCH BY MINI COMPUTER

William G. Urban, John A. Thompson and Paul V. Fennessey

University of Colorado Medical Center
Denver, Colorado 80220

This paper presents a brief description of our mini computer system as it relates to library search of low resolution mass spectra. The data acquisition system is shown in Figure 1. The DEC tapes are used for both saving any runs that may be of future interest, and also for transferring the file to the analysis system which consists of a PDP 8/E with 20K of core memory, 2 DEC tapes and an ASR33 teletype.

DATA ACQUISITION SYSTEM

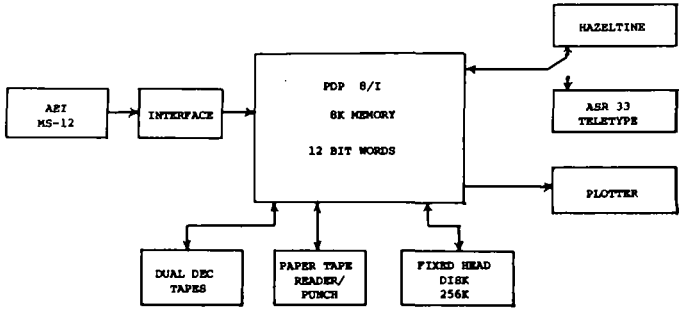

There are several ways of generating the compressed library files that one needs for the search program (Figure 2). In our case, the entire disk monitor (DM) file, which represents a complete gas chromatogram, is to be used as a library with possibly a few minor editing changes. Our nominal data flow is to use program DM20S8 to convert the DM file into a OS8 ASC II file. Then by processing this file via program GLIB, we generate a library file (LB). The entire library file, in turn, can be converted by program CLIB into the compressed format required for analysis by SLIB (the actual search program). An alternate route to generate the library data is to use a tabular listing or Aldermaston paper tape to update via the GLIB program (Figure 2).

DATA FLOW FOR CREATING OR UPDATING OF THE LIBRARY

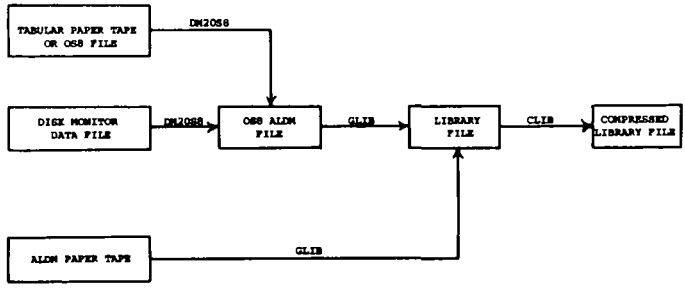

The compression method is shown in Figure 3. Each window is 14 AMU wide, starting with mass 15. The most intense peak in each window is converted to a 4 bit relative mass for that window. The intensity of the peak is quantized to four levels, which can be saved in two bits. Therefore, all the information of interest for each window is compressed into 6 bits or one-half a computer word (the PDP 8 has 12 bit words). To calculate the relative mass for the window, subtract the mass from the start of window mass and add 1; example, 39 - 29 + 1 = 11. Convert this number to octal (or binary) and this is the actual code saved by the computer.

COMPRESSION METHOD

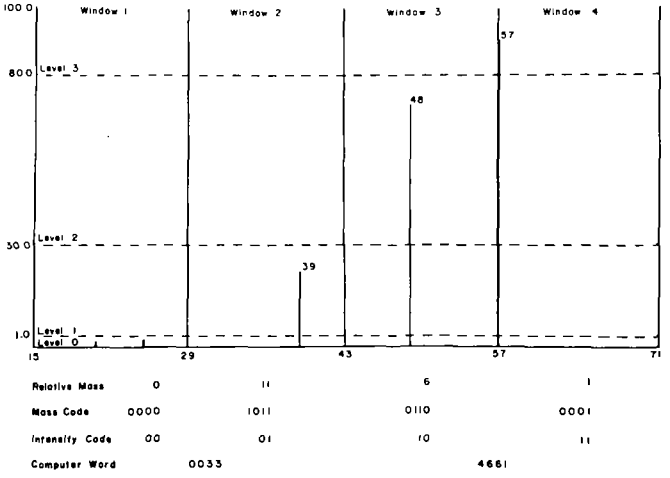

To demonstrate the amount of space saved by this method, let us look at Figure 4. We can see that the most inefficient way of storing the data is in tabular ASC II format and the next is the Aldermaston format. The most efficient method of saving a full spectra is in a binary format, if we assume masses can be represented in a single word (no fractions) and intensities in two words. If we are willing to accept the single most intense mass every 14 AMU, then the space reductions are very dramatic. Still further space reductions are made if the intensity level quantizations are accepted. This reduction in computer memory aids in both the speed of the search as well as in the required bulk storage capability needed (i.e. from 720 12 bit words to 11 - see Figure 4).

COMPUTER STORAGE REQUIREMENTS

(FOR COMPOUND BFS-253)

FULL SPECTRA	COMPUTER WORDS
ASCII TEXT STRING TABULAR FORMAT	720
ASCII TEXT STRING ALDERMASTON FORMAT	603
BINARY NUMBERS	231
COMPRESSED SPECTRA	
ASCII TEXT STRING TABULAR FORMAT	168
ASCII TEXT STRING ALDERMASTON FORMAT	164
BINARY NUMBERS	54
CODED BINARY	11

The search capabilities available are very flexible. We can search an unknown file (one individual compound) against any library file[1], or visa versa (the library against the unknown). Also, we can consider any file as a library. For instance, if we desire to check for differences (or for similarities) of two mass spectral files, we only have to designate one of them as the library and search against it.

The diagreement criteria used is the one proposed in the literature[2] (Figure 5), which gives a value to Co of zero for a perfect fit. The largest value Co can have depends upon the maximum number of windows compared (M). Similarly, we have allowed for calculation of two different intensity criteria; the normalized least squares fit and also the absolute difference criteria. These intensity criteria can be used either in place of the mass criteria (Co) or in addition to other selection processes in order to provide the interpreter with more discriminate data.

CONFUSION CRITERION

$$C_o = \mu N + \sum_{i=1}^{M} \delta_i$$

$$\delta_i = 0 \qquad m_{xi} = m_{\ell i} = 0$$

$$\delta_i = -\mu \qquad m_{ix} = m_{\ell i} \neq 0$$

$$\delta_i = 1 \qquad m_{ix} \neq m_{\ell i}$$

Figure 6 shows a sample output of searching an "unknown" against our library (this library consists of 280 compounds, and the amount of time required for the five best fits is 19.5 seconds on the teletype or 10 seconds on the Hazeltine). In this example, we have searched for a known compound (Myristic Acid-TMS), which is in the library against the library. As can be seen in the output (Figure 6), the compound is found with a perfect fit (i.e., Co = 0000). The other compounds found with close fits are homologs (straight chain acids as mono or di-TMS derivatives).

SAMPLE OUTPUT

$\mu = 2$

```
ARE THE FILES ON SYS:? Y
LIBRARY? BFSTMS.CM
BFS LIBRARY .GENERATED AUG,13,73

UNKNOWN? TEST.CM
IDENTIFY UNKNOWN 253

PLEASE INPUT SCANS
? 1

STD. CRITERIONS? Y
UNKNOWN?  0001
0253     0000
0210     0013
0252     0017
0249     0022
0125     0022

ARE THE FILES ON SYS:? N
```

We have produced a searching system which is presently running in only 12K of core on a 12 bit computer. The system is in a minimum and inexpensive configuration, yet provides a very sophisticated set of library search algorhythm.

REFERENCES

1. Mass Spectra of Compounds of Biological Interest, edited and compiled by S. P. Markey, W. G. Urban, S. P. Levine; report TID-26553-P2.

2. Automatic Identification of Chemical Spectra: A Goodness of Fit Measure Derived from Hypothesis Testing, S. L. Grotch, Anal. Chem., 47 (75), p. 1285-1289 and references cited therein.

Forward and Reverse Library Search Methods Applied to Mass Reconstructed GCMS Data

P Powers, A J Hopkinson, J D Robinson and M J Wallington, VG Data Systems Limited, Altrincham, England.

At the 1975 meeting we described an important extension to minicomputer data system operation which implemented the principles of Mass Reconstruction of GCMS Data as originally outlined by Biller & Biemann in 1974. A particular feature of our development was the operation of this process in real time, so permitting the on line reporting of concealed GC components in Interscan Reports. This paper discusses two further improvements we have made to provide valuable assistance to the GCMS chemist in areas where there is GC component overlap.

In cases where poor GC resolution can be anticipated the best approach may be to use capillary columns and to pay special attention to the chromatographic analysis. To accommodate the latest developments in this application we have implemented a very fast scan extension to the VG 2000 series of data systems to allow scan cycle times (i.e. scan plus reset) of 0.7 seconds or less to be accommodated whilst still permitting all present real time facilities, including MassMax and full Interscan Reporting. When such fast scans are being used many spectra can be acquired across a GC run and so the fast scan extension also permits 6500 scans to be stored in one named run. Even though the use of capillary columns increases the GC resolution, Mass Reconstruction or Mass Max yields an enhanced resolution TIC and automatic subtraction of interfering background components.

The second major improvement involves sophisticated Reverse Library Searching. Conventional, or forward, searching merely takes a group of the more prominent peaks of the sample and compares them with each library entry in turn. If the sample was itself a mixture then a good library match is often not possible, since prominent peaks may have come from more than one component of the mixture. In reverse searching all entries in the library are compared against all peaks of the sample so two, or more, constituent parts can be readily identified. The reverse search process is usually quite lengthy, since the detection of small components requires a separate renormalisation of the sample spectrum each time a different potential base peak is being considered.

An interesting question is whether or not the use of Mass Reconstructed data would allow the faster forward search to give equivalent results. The process of Mass Reconstruction correlates all masses which maximise at a particular retention time and therefore eliminates interference from background or other neighbouring peaks. It should therefore be sufficient to use forward searching on such data .

Figure 1 shows the effect of Mass Reconstruction on a GC run of an Industrial Perfume Sample. The top trace shows the original TIC trace and the bottom that produced by the Mass Maximising process. In this example the computer also automatically identifies the new maxima as scans of interest (see arrows) and subsequent library searching (or other data system functions) can, if required, be restricted to such identified

scans.

Two regions of especial interest are those between scans 280 and 320 and between 120 and 150. Taking the right hand region first, Figure 2 shows successful identification of the two fairly well resolved, higher intensity peaks but no fits at all for the small yet well resolved component which has been adversley influenced by a high relative background.

Figure 3 shows how prior use of the MassMax process improves this. Not only is a good matching factor obtained for this small component but that for the third component is actually increased.

The use of MassMax, Scan of Interest Marking and Forward Searching has, we believe, an important place in fast and accurate library identification.

Turning now to the left hand region, scans 120-150 in this GC run, identification of the scans of interest is again possible by forward searching on the MassMax data, although this trace is representative of those occasions when it is convenient to be able to confirm the presence of both spectra on one side of a peak or even in a valley. By its very nature Mass Reconstructed data does not lend itself to this sort of work and it is here that Reverse searching comes into its own.

Figure 4 shows again how no fits are found with forward searching on the first peak and how only the second component is found (with a poor fit) in the valley.

Figure 5 shows the success of reverse searching in this area. Both components are identified and both are reported in the valley area as well.

Reverse searching, although more time consuming, provides comparable results to those obtained with forward searching after use of MassMax, so allowing a very useful confirmation of such work. Furthermore, reverse searching allows all spectra across a GC profile to be identified.

The library searching software provided on the VG range of systems also incorporates a number of additional powerful facilities. Searching can be followed by extensive reporting - even to the extent of listing the complete library spectrum if this has been stored, and the chemist can introduce search parameters of his own by specifying elemental compositions or any combination of up to 8 filter values. Such filters can be operator defined and potential matches accepted or rejected by comparison with them. In this way retention time, retention index, molecular weight, IR information, sample origin, analysis date or any other numerically definable parameter can be used. The use of such filters can give dramatic results, since, for the first time, they allow a user of a dedicated data system to introduce into the search process other information he may have about his sample.

It is difficult to illustrate all of the improvements possible when using filters but Figure 6 shows the application of a single filter, based on retention time. A unique fit obtained without filters is retained at the top of each list. A succession of poor matches caused because the compound had no entry in the library is entirely rejected on scan 148 when filters are used.

It is our experience that the use of only a single filter can improve search times by up to a factor 2, as well as allowing the chemist to interact in the search process with the other information he may have.

The table below lists comparative search times for different library sizes. Naturally the use of filters will speed up these times significantly.

Library size	Forward Search	Reverse Search with Renormalisation
225	0.5 sec.	8 sec.
2000	4 sec.	64 sec.
20000	36 sec.	9 min.

Forward: 8 Largest peaks from unknown.
Reverse: 50 Largest peaks from unknown with intensities > 10% considered as base peaks.

VG 2000 - Eight Peak Library Search Times

Our conclusions from this work are that Forward Searching on Mass Reconstructed Data is reliable and that when this is combined with the automatic marking of Scans of Interest by the MassMax process, Library Identifications can even be obtained from very large libraries in true Real Time, not merely on line as with other systems. Full reverse search on the original data provides confirmation of these identifications and also allows a presentation of the way in which each component of an unresolved GC peak varies over the original TIC profile.

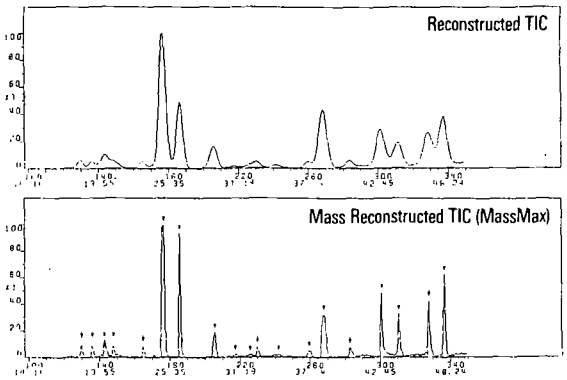

Industrial Perfume Sample - Figure 1

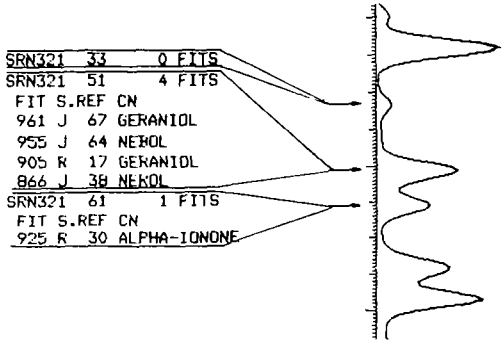

VG 2000-Forward Library Searching - Figure 2

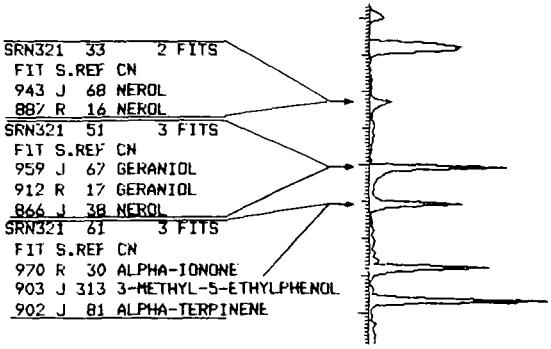

VG 2000-Forward Searching after MassMax - Figure 3

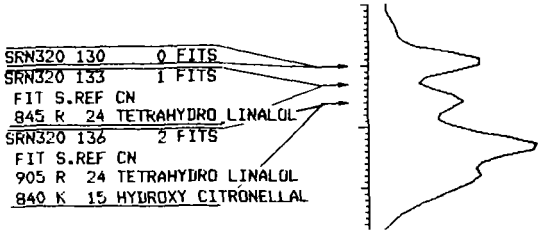

VG 2000–Forward Library Searching – Figure 4

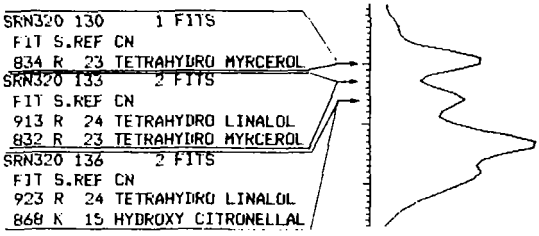

VG 2000–Reverse Library Searching – Figure 5

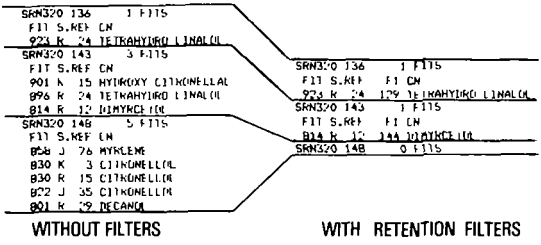

VG 2000 Library Searching–The Use of Filters – Figure 6

A Chemical Analysis Information System. James J. Downs, James L. Spigarelli, Michael J. Serrone, and Joe B. High, Midwest Research Institute, Kansas City, Mo. 64110

Environmental surveys involving chemical analysis are made more useful by putting analytical results and interpretations in a survey data base. The survey data base is used with a reference data base containing analytical data for pertinent chemicals. Infrared and mass spectra, together with TLC and sample preparation data have been stored for survey samples and organophosphorus compounds. System 2000* software was used for file management computer matching programs for infrared and mass spectra are used to identify compounds in analytical samples. Data components are similar but hierarchical structures differ for survey and reference data bases. "Reverse Search"[1] methods are used for computer matching. The information system has been used for large sample surveys.

*Copyright, Management Research International, Austin, Texas
[1]Abramson, F. P., Anal. Chem., 47, 45-49 (1974).

AN IMPROVED SELF-TRAINING INTERPRETIVE AND RETRIEVAL SYSTEM

Henry E. Dayringer, F. W. McLafferty, and Rengachari Venkataraghavan

Cornell University, Department of Chemistry, Ithaca, New York 14853

The STIRS[1] system for computer-aided interpretation of unknown mass spectra is now available on the Cornell computer over the TYMNET international computer network. Its performance for total unknowns has been substantially improved by a 70% expansion of the data base (reference spectra of over 32,000 different compounds), restriction of reference spectra to those of the common elements and isotopes, use of data classes containing groups of homologous series, and combinations of data class rankings to give new "overall match factors". A computer program utilizing a "random-drawing" model allows STIRS predictions of the presence of 200 substructural groups with a recall of >50% at the 98% confidence level.[2-4]

[1]K.-S. Kwok, R. Venkataraghavan, and F. W. McLafferty, J. Am. Chem. Soc., 95, 4185 (1973). [2]H. E. Dayringer, G. M. Pesyna, R. Venkataraghavan, and F. W. McLafferty, Org. Mass Spectrom., 11, 529 (1976). [3]H. E. Dayringer and F. W. McLafferty, Org. Mass Spectrom., 11, 543 (1976). [4]H. E. Dayringer, F. W. McLafferty, and R. Venkataraghavan, Org. Mass Spectrom., in press.

The Use of Mass Spectrometric Data in Computer Assisted Structure Elucidation. Raymond E. Carhart and Dennis H. Smith, Stanford Univ., Depts. of Comp. Sci. and Chem., Stanford, Calif. 94305

Recent additions to the COGEN[1] computer program allow the generation of structures which are consistent with a given set of mass spectral peaks, where "consistency" is determined by a user-defined theory of mass spectroscopy. Initial work has focussed upon a simple theory to be described which is independent of the chemical class of structures under investigation. Though simple, this theory is capable in many cases of extracting a significant amount of structural information from the mass spectra of unknowns.

The mass spectral information can be utilized either as a retrospective filter on candidate structures obtained for an unknown using other sources of structural information, or as input to a new generation scheme we have developed for constructing possible structures directly from observed mass spectral peaks. In either case, the full power of the CONGEN constraint language is available to express structural requirements inferred from other sources.

[1] R. E. Carhart, D. H. Smith, H. Brown and C. Djerassi, J. Amer. Chem. Soc., 97, 5755 (1975).

STRUCTURAL INVESTIGATION OF NARASIN AND RELATED IONOPHORES

by

D. Berg and J. L. Occolowitz

Lilly Research Laboratories
Division of Eli Lilly and Company
Indianapolis, Indiana 46206

As a result of a mass spectrometric investigation of narasin, A28086B, A28086-1, salinomycin,[1] and their derivatives, structures were deduced for the first three compounds. The structures are as follows:

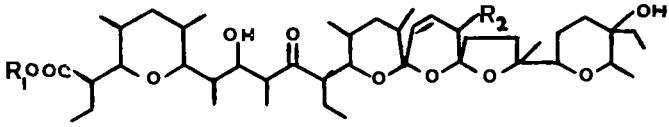

	R_1	R_2
Narasin	H	H, OH
A28086B	H	O
A28086-1	CH_3	H, OH

[1]H. Kinashi, N. Ōtake, H. Yonehara, S. Sato, and Y. Saito, Tetrahedron Letters, 4955 (1973).

A full account of this work is scheduled for publication in Biomedical Mass Spectrometry.

Sterospecificity of Eliminations From Arylcyclohexyl Derivatives under Electron Impact. Joseph Sharvit, Miriam Weissdorf and Asher Mandelbaum, Dept. of Chemistry, Technion Israel Institue of Technology, Haifa

The elimination of H_2O, CH_3OH, and CH_3CO_2H from steroisomeric 3- and 4-arylcyclohexyl alcohols, methyl ethers and acetates under El

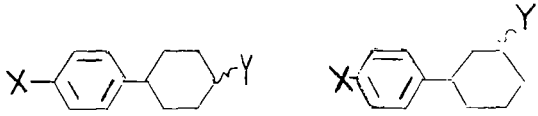

X= NO_2, H, CH_3, OCH_3, NH_2
Y= OH, OCH_3, OAc, NH_2, NHEt, $NHCH_2Ph$
$NHCOCH_3$, NHCOPh, $NHCOC_6H_4NO_2$

is stereospecific occuring to a much greater extent in the trans-isomers. Deuterium labeling and substituent effect measurements show that these eliminations of the trans-isomers take place by similar mechanisms involving the benzylic hydrogen atom. Cis-alcohols and ethers undergo these eliminations by different mechanisms. No stereospecificity has been observed in the analogous eliminations from the corresponding amines and amides. A mechanistic explanation based on substituent effects, deuterium labelling and analogies will be presented.

STERICALLY CROWDED TRIALKYLSILYL DERIVATIVES IN THE ANALYSIS AND CHARACTERIZATION OF STEROIDS

Michael A. Quilliam and J. B. Westmore,
Department of Chemistry, University of Manitoba
Winnipeg, Manitoba R3T 2N2, Canada

The electron-impact mass spectra of sterically crowded silyl* ether derivatives of hydroxy steroids have some important features which give them certain advantages over the widely studied trimethylsilyl analogues. There is significantly less extensive fragmentation, and abundant ions at $(M - \underline{t}Bu)^+$ or $(M - \underline{i}Pr)^+$ serve as indicators of molecular weight and should be useful for selected ion monitoring. From various precursors, the ease of elimination of HX_2SiOH, via a proposed multicenter transition state, appears to depend upon conformational and stereochemical factors, as well as the position of the parent silyloxy group, RX_2SiO, an the steroid skeleton. This particular fragmentation appears to be a powerful diagnostic method for distinguishing between stereoisomers, being especially useful for differentiation between epimers. In addition, elimination of silanol, RX_2SiOH, at various stages in the fragmentations of bis- or tris-silylated steroids is also an important process, but other familiar features of the mass spectra of steroid trimethylsilyl ethers, though usually present, are very much suppressed.

* RX_2Si represents the sterically crowded silyl group, where R = $\underline{t}Bu$ or $\underline{i}Pr$ and X_2 = Me_2 or $-C_4H_8-$

Manuscript to be submitted to STEROIDS

The Temperature Dependence of an Electron Impact Induced Stereoselective Rearrangement Reaction

Mark M. Green, Thomas J. Mangner,
F.J. Brown, and Stuart P. Turner

Department of Chemistry
Michigan State University
East Lansing, Michigan 48824

In spite of the enormous energies utilized in the ionization process, rearrangement reactions occuring from organic molecular ions in mass spectrometers exhibit remarkable stereosensitivity to energetically small conformational differences.[1] Moreover, intramolecular transfer of diastereotopic hydrogens in parallel rearrangement reactions of chiral substrates in mass spectrometers and in solution actually show quantitatively similar stereoselectivities.[2] The question immediately arises as to the source of this similarity. The reacting molecules in solution are subject to a Maxwell-Boltzmann energy distribution defined by their temperature. On the contrary, in the mass spectrometer the molecular ions are not only of uncertain energy distribution because of their mode of formation by electron impact, but as well the temperature cannot be experimentally defined because of the absence of intermolecular or wall collisions for the detected ions.[3]

The source of this kinetic similarity[2] may be understood by a few simple considerations centered around the quasi-equilibrium theory of mass spectrometry.[4] The theory predicts, and experiments bear out, that rearrangement reactions in mass spectrometers occur from molecular ions of the lowest internal energies.[5] Photoelectron spectroscopy demonstrates that in molecules with non-bonding electrons these lowest internal energy ions, in focus here, are produced by removal of an electron from these non-bonding orbitals and furthermore that such ionization gives rise to discrete and relatively narrow bonds often separated by an energy space from the broader bonds involving higher energy ionization of bonding

electrons.[6] As has been pointed out by D.W. Turner[7] such promotion of nonbonding electrons will produce an ionized state which within reasonable approximation will have the same bonding parameters as the neutral precursor. This is a key point with regard to our inquiry because it follows from the Franck-Condon principle that such a circumstance of equivalent potential surfaces for the ion and its neutral precursor will lead to producing the ionized molecule with the same vibrational and rotational energy as the neutral.[7,8] In other words, the temperature of the ion produced by removal of a nonbonding electron, within the limits of the above approximations, will be the same as the temperature of the neutral from which it is formed.[9] It thereby becomes clear why quantitatively similar rearrangement stereoselectivities[2] are observed in solution and in mass spectrometers. We can, though, go a step further.

If the temperature of the neutral is an accurate measure of the immeasurable temperature of the ions produced it would follow that the rearrangement rate constant for the electron impact induced reaction should depend on the temperature of the neutral precursor in the form of the Arrenhius expression. The precision of the Arrenhius dependency would moreover constitute a measure of the assumptions leading to the prediction of temperature equivalence in the ionization process producing the rearranging ions. Because a stereoselectivity involves a rate ratio which cancels out temperature dependent instrumental parameters[10] and also obviates the otherwise extreme difficulty of measuring an absolute rate constante in a mass spectrometer, we were placed in a position to test for Arrenhius temperature dependency.[11] The reaction chosen for this purpose was the stereoselective rearrangement elimination of acetic acid from electron impact produced 2-butylacetate cation radical.[2] Figure 1 shows this process as well as a plot of the stereoselectivity (ka/kb) as a function of the temperature of the precursor neutral.

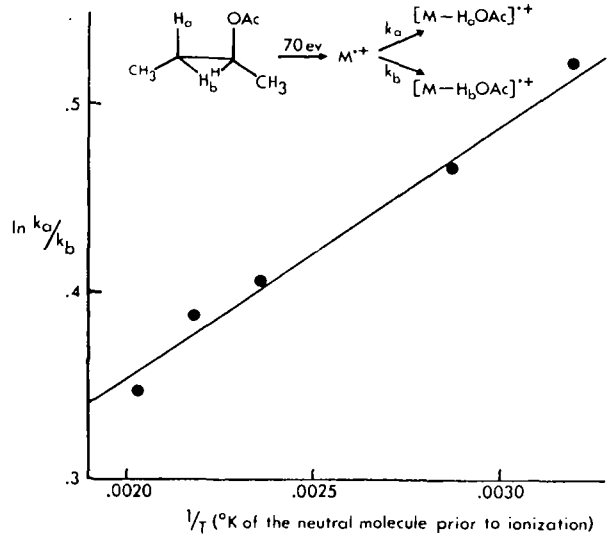

a. Measured on an MS-902 mass spectrometer at 70 ev beam energy and by varying in consort the temperature of the inlet, ion chamber and source walls. The temperature is accurate to ±2°C. The experiments were conducted four times over a period of six months and gave the same line within experimental error. Each experiment consisted of at least five measurements at each temperature of 2-butylacetate and the two deuterated diastereomers necessary to calculate ka/kb.[2] The data were handled by a computer program written here which yielded the stereoselectivities and the accuracy. Each point was calculated to 95% confidence (2σ) and then used to generate the linear least square line shown. The line has a correlation coefficient of 0.991. Another experiment varying only the ion chamber temperature and leaving the inlet system at ambient temperature gave the same line as above with the lowered correlation coefficient of 0.968. The elimination of acetic acid is known not to be pyrolytic under these conditions.[12] The experimental data here show no time dependency at the temperatures reported and as well we have subjected 2-butylacetate to gas chromatography on steel columns and throughout this temperature range there is no evidence for pyrolysis.

The Arrenhius equation may be derived from Boltzmann's Law[13] and thus the clear Arrenhius dependency exhibited in Figure 1 is strong evidence that the rearranging molecular cation radicals are in an at least approximate Maxwell-Boltzmann energy array defined by each temperature along the absicca. This is precisely in line with the arguments made (vide supra) and can be further supported by the data presented in Table I which gives the slope and as well, the intercept at infinte temperature, for the line in Figure 1 and for an equivalent experiment conducted at low beam energy (15 ev).

There are two expectations corellary to the ideas discussed here. First, the exact temperature dependency should be independent of beam energy if only the lowest energy ions are contributing to the rearrangements under observation. Sevond, the ratio of pre-exponential factors for two reactions differing only in abstraction of diastereotopic hydrogens (Ha or Hb) should be unity. Inspection of Table I shows that the experiments yield exactly these results. Moreover, in a further experimental test, we have determined the appearance minus ionization potentials for the lowest energy fragmentations of the 2-butylacetate cation radical. Loss of acetic acid, as demanded by the current proposal, is lowest (A.P.-I.P. equals 0.3 ± .05 ev) with cleavage loss of methyl and ethyl next highest by another 0.3 ev.[14,15]

In conclusion, therefore, persuasive experimental evidence is presented for the theoretically justifiable proposal that rearranging molecular ions in mass spectrometers when produced by ionization of nonbonding electrons maintain a close or perhaps exact correspondence to the thermal energy, that is, the temperature, of their precursor neutrals. Put in another way, the electron beam by simply ionizing without depositing energy, converts the molecules investigated here to a highly reactive state, charged radicals, rather than to the highly excited state which might be

imagined.

Clearly, the kind of experiment carried out here offers the possibility of a quantitative conformational analysis on charged free radicals reacting in the fascinating non-environment of molecular isolation.[16]

Table I[a]

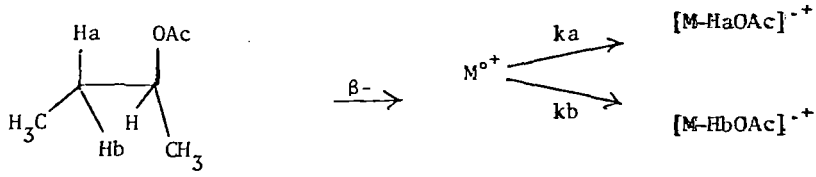

β^- (ev)	ΔΔEnergy of Activation (cal. $mole^{-1}$)[c]	Ratio of Preexponential factors[d]
70	264 ± 43	1.08 ± .06
15[b]	282 ± 22	1.02 ± .03

a. The errors (±) are presented within two standard deviations (2σ). See footnote to Figure 1.

b. 15 ev is the lowest nominal beam voltage on the mass spectrometer (MS-902) which would yield accurate data.

c. Calculated from the line slope which equals ΔΔ Eact/RT.

d. Calculated by extrapolation of the line to temperature equals infinity.

References

1. For general reviews see: M.M. Green in Topics in Stereochemistry, Vol. 9, edited by N.L. Allinger and E.L. Eliel, Wiley-Interscience Publ., New York City, 1976 (in press); A. Mandelbaum in Handbook of Stereochemistry, edited by H. Kagan, Georg Thieme Verlag, Stuttgart Publ., Paris, 1976 (in press); Z.V. Zaretskii, Mass Spectrometry of Steroids, Halsted Press, J. Wiley and Sons Publ., New York, 1976; S. Meyerson and A.W. Weitkamp, Org. Mass Spectrometry, 1, 659 (1968). In particular see: H.E. Audier, H. Felkin, M. Fétizon, and W. Vetter, Bull. Soc. Chim. France, 1965, 3236; M.M. Green, J. Amer. Chem. Soc., 90, 3872 (1968); M.E. Munk, C.L. Kulkarni, C.L. Lee, and P. Brown, Tetrahedron Lett., 1970, 1377; M.M. Green, R.J. Cook, J.M. Schwab, and R.B. Roy, J. Amer. Chem. Soc., 92, 3076 (1970) for earlier work and leading references.

2. M.M. Green, J.G. McGrew, II, and J.M. Moldowan, J. Amer. Chem. Soc., 93, 6700 (1971); M.M. Green, J.M. Moldowan, and J.G. McGrew, II, J. Org. Chem., 39, 2166 (1974); M.M. Green, J.M. Moldowan, M.W. Armstrong, T.L. Thompson, K.J. Sprague, A.J. Hass, and J.J. Artus, J. Amer. Chem. Soc., 98, 849 (1976).

3. For a description of the instrumental parameters of mass spectrometers see R.W. Kiser, Introduction to Mass Spectrometry and its Applications, Prentice Hall Publ., Englewood Cliffs, New Jersey (1965).

4. H.M. Rosenstock, M.B. Wallenstein, A.L. Wahrhaftig, and H. Eyring, Proc. Natl. Acad. Sci. U.S., 38, 667 (1952).

5. Excellent and comprehsneive discussions are found in: D.H. Williams and I. Howe, Principles of Organic Mass Spectrometry, McGraw-Hill Publ., London, 1972, Chapter 4; F.W. McLafferty, Interpretation of Mass Spectra, 2nd Edition, Benjamin Publ., Reading, Mass., 1973, Chapter 8, and numerous references therein.

6. See the following and references therein. See also reference 7 below. M.J.S. Dewar and S.D. Worley, J. Chem. Phys., 51, 263 (1969); P. Bischof, J.A. Hashmall, E. Heilbronner, and V. Hornung, Tetrahedron Lett., 4025 (1969); M.J.S. Dewar and J.S. Wasson, J. Amer. Chem. Soc., 92, 3506 (1970); A.D.Baker, D. Betteridge, N.R. Kemp, and R.E. Kirby, Chem. Commun., 286 (1970); A.D. Baker, D. Betteridge, N.R. Kemp, and R.E. Kirby, Anal. Chem., 43, 375 (1971); S.A. Cowling and R.A.W. Johnstone, J. Elect. Spectrosc. Rel. Phenomena, 2, 161 (1973); R.J. Boyd, J.C. Bünzli, J.P. Snyder, and M.L. Heyman, J. Amer. Chem. Soc., 95, 6478 (1973); A.H. Cowley M.J.S. Dewar, D.W. Goodman, and J.R. Schweiger, ibid., 95, 6506 (1973). W.-C. Tam and C.E. Brion, J. Elect. Spectrosc. Rel. Phenomena, 3, 467 (1974); R.J. Suffolk, ibid., 3, 53 (1974); D. Chadwick and A. Katrib, ibid., 3, 39 (1974); W.-C. Tam and C.E. Brion, ibid., 4, 139 (1974); N.S. Hush, A.S. Cheung, and P.R. Hilton, ibid., 7, 385 (1975); Y. Gounelle C. Menard, J.M. Pechine, D. Solgadi, F. Menes, and R. Botter, ibid., 7, 247 (1975).

7. D.W. Turner, C. Baker, A.D. Baker, and C.R. Brundle, Molecular Photoelectron Spectroscopy, Wiley-Interscience Publ., London, 1970, p. 7-10.

8. A.D. Baker, Acc. Chem. Res., 3, 17 (1970); F.H. Field and J.L. Franklin, Electron Impact Phenomena and the Properties of Gaseous Ions, Academic Press, New York, 1957, p. 57-62.

9. These arguments are in accord with representation of the total energy distribution of ions produced by electron impact by convolution of the neutral thermal energy with the energy deposited by the ionization process. See: G.G. Meisels, C.T. Chen, B.G. Giessner, and R.H. Emmel, J. Chem. Phys., 56, 793 (1972); F.W. McLafferty, T. Wachs, C. Lifshitz, G. Innorta, and P. Irving, J. Amer. Chem. Soc., 92, 6867 (1970); D.J. McAdoo, P.F. Bente, III, M.L. Gross, and F.W. McLafferty, Org. Mass. Spectrometry, 9, 525 (1974); P.F. Bente, III, F.W. McLafferty, D.J. McAdoo, and C. Lifshitz, J. Phys. Chem., 79, 713 (1975). See also: W.A. Chupka, J. Chem. Phys., 54, 1936 (1971); W.A. Chupka, ibid., 30, 191 (1959).

10. F.H. Field and J.L. Franklin, Electron Impact Phenomena and the Properties of Gaseous Ions, Academic Press, New York, 1957, p. 202-204; D.P. Stevenosn, J. Chem. Phys., 17, 101 (1949).

11. There has been a great deal of interest, extending over many years, on the temperature dependency of mass spectral fragmentation behavior. See reference 9 above as well as the following and numerous references therein: M. Spiteller-Friedmann, S. Eggers, and G. Spiteller, Monatsh, 95, 1740 (1964); A. Cassuto, Mass Spectrometry, Edited by R.I. Reed, Academic Press, New York, 1965, p. 283-ff; V.N. Komarov and M.V. Tikhomirov, Russian J. Phys. Chem., 40, 1594 (1966); M. Spiteller-Friedmann and G. Spiteller, Chem. Ber., 100, 79 (1967); M.V. Tikhomirov and V.N. Komarov, Russian J. Phys. Chem., 41, 561 (1967); S. Meyerson, Appl. Spectros., 22, 30 (1968); K. Hirota, Y. Niwa, and I. Fujita, Zeit. Phys. Chemie, 67, 244 (1969); J. Jullien and J.M. Pechine, Org. Mass Spectrometry, 4, 325 (1970); V.N. Komarov and M.V. Tikhomirov, Russian J. Phys. Chem., 46, 766 (1972); K. Levsen and H.D. Beckey, Int. J. Mass Spectrometry and Ion Phys., 9, 51 (1972); V.A. Pokrovsky, I.V. Goldenfeld, and E.N. Korol, ibid., 11, 1 (1973). B.H. Solka, J.H. Beynon, and R.G. Cooks, J. Phys. Chem., 79, 859 (1975); M. Medved, R.G. Cooks, and J.H. Beynon, Int. J. Mass Spec. Ion Phys., 19 179 (1976). See also: H.D. Beckey, Field Ionization Mass Spectrometry, Pergamon Press, New York, 1971, p. 180ff; Principles of Organic Mass Spectrometry, D.H. Williams, and I. Howe, McGraw-Hill, London, 1972, p. 156.

12. Reference 2 and G. Eadon, P. Gold, and E. Bacon, J. Amer. Chem. Soc., 97, 5184 (1975) and references therein.

13. E.A. Moelwyn-Hughes, Physical Chemistry, Second Revised Edition, Pergamon Press, New York, 1961, p. 1132-1137.

14. In line with this, the percent of total ionization of loss of acetic acid is increased by three times in going from 70 ev to 15 ev.

15. We are grateful to J.F. Litton and R.G. Cooks (Purdue) for making these measurements for us. Details will be presented in the full paper.

16. We are indebted to the National Institute of General Medical Sciences for generous financial support and to the Chemistry Department of the University of Michigan for the use of the MS-902 mass spectrometer. M.M.G. is grateful to Professor F.W. McLafferty for his important suggestions concerning this work.

Mass Spectrometric Study of Antipyrine and its Metabolites. J-P. THENOT, M. STAFFORD and K. D. HAEGELE Institute for Lipid Research, Baylor College of Medicine, Houston, Texas 77025.

The electron impact induced fragmentation of antipyrine (2,3-dimethyl-1-phenyl-3-pyrazolin-5-one) is discussed. High resolution mass spectra of antipyrine and of the N-CD_3, 3-CD_3 labeled derivatives were obtained. As expected in the pyrazole series, the base peak is the molecular ion. The major fragment ions are derived from the cleavage of the nitrogen-nitrogen bond. 4-Hydroxy, 3-hydroxymethyl and norantipyrine are the metabolites in the human and in animal species. These compounds were synthesized and labeled with deuterium. The influence of the substituents is discussed. Methane CI spectra of antipyrine and its metabolites were obtained. No significant fragmentation was observed. For quantitative measurements of antipyrine and its metabolites, the CI mode is recommended.

THE STUDY OF THE ISOMERISATION BEHAVIOUR OF ORGANIC IONS BY COLLISIONAL ACTIVATION SPECTROMETRY

K. Levsen, Institut für Phys. Chemie, Wegelerstr. 12, 53 Bonn, Fed. Rep. Germany

It has been shown by metastable ion characteristics, collisional activation (CA) spectrometry and isotopic labelling that alkyl ions, $[C_nH_{2n+1}]^+$, undergo complete isomerisation prior to decomposition. Introduction of a heteroatom, however, reduces the tendency for isomerisation considerably as demonstrated with n- and iso- dipentylketone, n- and iso- dipentylether, and n- and iso- dipentylamine: while the collisional activation spectra of the n- and iso- pentyl ions $[C_5H_{11}]^+$, from these compounds are identical within the reproducibility the CA spectra of the corresponding heteroatom containing ions, n- and iso- $[C_5H_{11}X]^+$ (X = CO, OCH_2, $NHCH_2$), differ considerably in the relative abundances of their collision induced fragments. The reduced tendency for isomerisation in the heteroatom containing species could be explained by the presence of additional decomposition channels with lower activation energy than in the corresponding pentyl ions. Appearance potential measurements show, however, that the lowest threshold for decomposition in the heteroatom containing species, $[C_5H_{11}X]^+$, is often higher than in the corresponding pentyl ions, suggesting that the predominant localisation of the charge at the heteroatom increases the energy barrier for isomerisation.

The influence of a phenyl ring on the isomerisation of a hydrocarbon chain has been studied with isomeric pentylbenzenes. Here the $[M - CH_3]^+$ fragments represent phenyl substituted butyl ions. While the CA spectra of the isomeric butyl ions are identical within the reproducibility the CA spectra of the corresponding phenyl substituted butyl ions, $[C_{10}H_{13}]^+$, show distinct differences demonstrating no or incomplete isomerisation. This result is supported by ^{13}C labelling data: although the loss of ethylene and propene from the $[M - CH_3]^+$ ion of n-pentylbenzene-δ-^{13}C does not occur

via a simple direct cleavage, it is also not preceded by a complete randomization of the side chain carbons, indicating incomplete interconversion between the various isomeric structures prior to decomposition. Appearance potential measurements reveal that the lowest thresholds for decomposition in these phenyl substituted butyl ions are lower than in the corresponding butyl ions which is one explanation for the reduced tendency of isomerisation.

[1] K. Levsen, Tetrahedron, 31, 2431 (1975)

[2] J. Heimbrecht, K. Levsen, and H. Schwarz, Z. Naturforsch., submitted.

An Analysis of the Electron Impact Mass Spectrum of Diphenylketenediphenyl Ketal.

WOODFIN V. LIGON JR., C.B. QUINN and T. TAKEKOSHI, General Electric Corporate Research and Development, Schenectady, New York 12301.

Diphenylketenediphenyl Ketal has been found to undergo an interesting rearrangement in which one of the phenyl groups on oxygen migrates to the carbon already bearing two phenyl rings. This arrangement occurs simultaneously with or is followed by cleavage of the C1-C2 bond, thereby producing a triphenylmethyl cation. This process constitutes the major fragmentation pathway for the compound under electron impact. Correlations of ion structure for this triphenylmethyl cation with ions of presumably the same structure from other sources have been made using Mass Analysed Ion Kinetic Energy Spectrometry (MIKES).

ISOBUTANE CIMS OF URETHANE PROTECTING GROUPS

G. Barany, A.L.C. Smit, D.V. Bowen, R.B. Merrifield, and F.H. Field

The Rockefeller University

New York, New York 10021

Urethane-protected amino acids are important intermediates in peptide synthesis. Therefore it was of interest to explore the utility of mass spectrometry in the analysis and quality-control of these derivatives. Urethane-protected glycine ethyl esters were examined since we predicted that these would be more volatile and would have fewer side-chain related reactions than other urethane derivatives. Subsequently, suitable spectra were also obtained with other urethane-protected amino acids and esters.

Almost all the urethanes examined gave an (M+1) ion with isobutane chemical ionization (Figure 1). The (M+1) ion could fragment by loss of alcohol from either the urethane or the ester end of the molecule to give respectively ions referred to as the isocyanate or the acylium ion. Each of these ions could lose carbon monoxide to give a corresponding imine ion. These pathways are analytically useful. (The ion structures reported are based on compositions deduced from accurate mass measurements and are chemically reasonable. They are not supported by specific structural evidence.)

The gas phase fragmentation pathway of most interest mimics the currently accepted reaction mechanism for acidolytic removal of urethane protecting groups in solution. First, the alkyl group of the protonated urethane is lost as the alkene to give a protonated carbamic acid ion. Such an ion has been postulated as a transient intermediate in acid solution, but its stability in the gas phase was unexpected. The protonated carbamic acid ion then loses carbon dioxide to give a protonated amino acid ester ion.

To further elucidate these fragmentations, d_9 t-butyloxycarbonyl

glycine ethyl ester was prepared and examined by electron ionization. The protonated carbamic acid ion contained two deuterons which must presumably have been transferred from the d_9 t-butyl group. The protonated amino acid ester ion also contained two deuterons which must have come from the same source. With isobutane CI, transfer of only one deuteron to each of these ions was observed. Presumably, a proton was derived from the reactant gas. It is of additional interest that the deuterium did not exchange with the reactant gas, nor did the deuterium become randomly distributed through the molecule.

Figure 2 shows a series of protecting groups that were examined, and indicates the qualitative hierarchy of solution phase acid stability. The extremely acid stable phthaloyl group, while not a urethane, provided a useful reference point for our gas phase study. The methoxycarbonyl group is removable only under acid conditions that effect cleavage of peptide bonds; whereas on the other end of the series, the biphenylisopropyloxycarbonyl group can be removed by acids as mild as 0.5% anhydrous trifluoroacetic acid in dichloromethane. The intensities of $(M+1)^+$ and of the protonated amino acid ester ion were determined, and are given in the Figure. The more acid stable compounds showed intense (M+1) ions, whereas the acid labile molecules fragmented readily to give the protonated amino acid ester ion. There is significant similarity in behavior between the gas phase and solution phase acidolysis of the urethane groups. The differences observed are those which might be expected in a change from a condensed phase to the gas phase. We feel there may be some interest in following up these observations and obtaining more quantitative data.

FIGURE I

ISOBUTANE CI FRAGMENTATION PATTERNS OF URETHANES

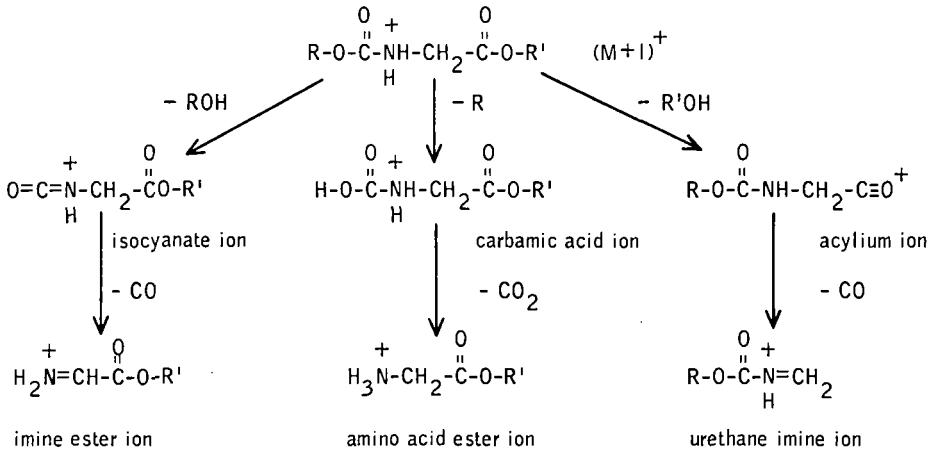

FIGURE 2

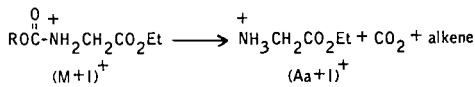

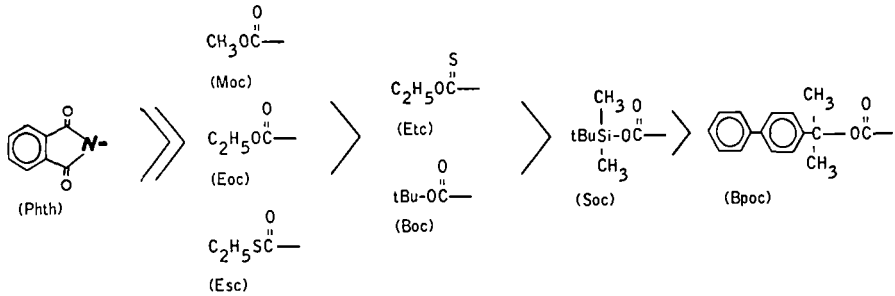

Relative Intensities in iC_4H_{10} CIMS

$(M+I)^+$	100*	100	Etc* 100	Boc* 5-50	100	0*
$(Aa+I)^+$	0	<1	10	100	15	100

* The protected amino acid, ROC-NHCH$_2$CO$_2$H, was examined and similar results obtained.

USE OF GAS CHROMATOGRAPHY/MASS SPECTROMETRY WITH CHEMICAL IONIZATION TO DETERMINE DOUBLE BOND POSITION IN COMPLEX OLEFIN MIXTURES

G. W. Mappes, O. E. Kinast, and M. W. Dietrich

Monsanto Company
800 N. Lindbergh Blvd.
St. Louis, MO 63166

Our laboratory has been searching for simple, effective ways of measuring double bond position in olefins for several years. The classic method using ozonolysis to cleave the olefin at the double bond position is time-consuming and cannot be used on complex mixtures.

The combination of gas chromatography and mass spectrometry could be an effective tool for determining structures of complex mixtures of olefins. However, the mass spectra of olefins with the same number of carbon atoms does not give very good evidence of the position of the double bond.

In 1974 Tumlinson, Heath and Doolittle at the U.S.D.A. in Gainesville, Florida measured the chemical ionization mass spectra of olefin epoxides. Their main interest was to analyze individual purified epoxide to establish a fragmentation mechanism and relate it to the epoxide structure. Our interest was in using their mechanistic data to analyze complex mixtures of olefins without prior separation. To do this we had to use:

1. Glass capillary columns to separate the complex mixtures;
2. Selected Ion Monitoring to measure characteristic ions;
3. $NaHCO_3$ to remove excess reagent.

The olefin epoxides are made by reacting the olefins with m-chloroperoxybenzoic acid in methylene chloride.

When these epoxides are ionized in a chemical ionization source, a major part of their fragmentation occurs according to Figure 1. This means that the protonated epoxide ion can fragment to give an ion characteristic of the alkyl groups on each side of the double bond.

In Figure 2 we show the characteristic ions for the linear octenes which would come from chemical ionization of the octene epoxides. These characteristic ions apply to other olefins. That is, the C_2 portion of 2 octene will give a 45 ion as will the C_2 portion of 2 hexene or 2 decene. The C_3 alkyl portion of alkenes will give a 59 ion.

Before we could analyze a complex mixture of olefins using epoxidation and GC/MS we had to find a GC column which would separate the olefin epoxides with the same number of carbon atoms. We made up a mixture of hexene and octene epoxides and tested long packed columns, SCOT columns and glass capillary columns. The best separation was obtained on a 50 M OV-101 glass capillary and this separation is shown in Figure 3. This figure shows the flame detector response for five hexene and seven octene epoxides.

During our experiments we found that the m-chlorobenzoic acid which remained in solution after epoxidation interfered with the GC separation. This was easily reduced to a suitable level by extraction with sodium bicarbonate.

To test our prediction of characteristic ions we injected octene 3 epoxide into our GC/MS system and monitored four characteristic ions (45, 59, 73, 87) using the selected ion monitoring mode of operation and methane as the CI reagent. The results of this experiment are shown in Figure 4. We would predict that the C_3 portion of the 3 octene would give a 59 ion and the C_5 portion of this epoxide would give an 87 ion. In all of the standards which we analyzed in this way, the predicted characteristic ions were the largest characteristic ions.

In Figure 5 we see the capillary column separation and the characteristic ions for a synthetic mixture of six of the linear octenes. The 128 ion or the 129 ion was used to monitor the six octene epoxides. The first peak is trans 4 octene. As predicted the 73 ion is the largest characteristic ion for this compound. The next peak is trans 3 octene and as predicted the 59 ion and 87 ion are the largest characteristic ions. The third peak is trans 2 octene and the 45 ion and the 101 ion are the largest characteristic ions. The next 3 peaks are cis 4 octene, cis 3 octene, cis 2 octene and they have the correct characteristic ions.

Figure 6 shows the 87 ion increase for trans 3 octene as well as the 45 ion increase for trans and cis 2 octene. These data were obtained on a Hewlett-Packard 5982 GC/MS system.

Although cis and trans isomers give the same characteristic ions, they can be distinguished by their GC elution order. For example, on our OV-101 capillary column the trans isomer always comes out before the corresponding cis isomer.

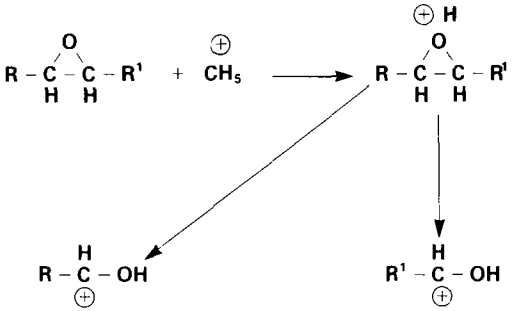

FIGURE 1

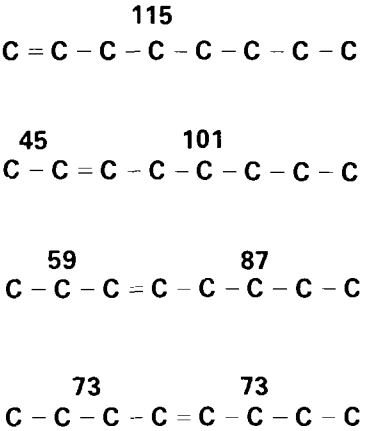

FIGURE 2

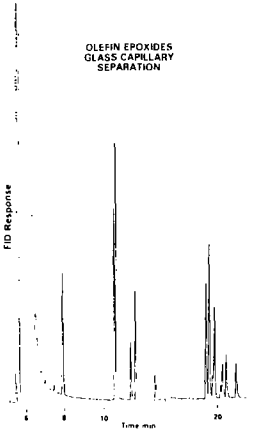

FIGURE 3

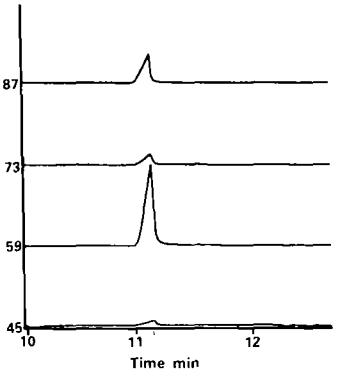

FIGURE 4

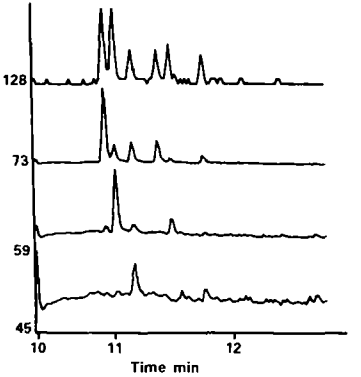

FIGURE 5

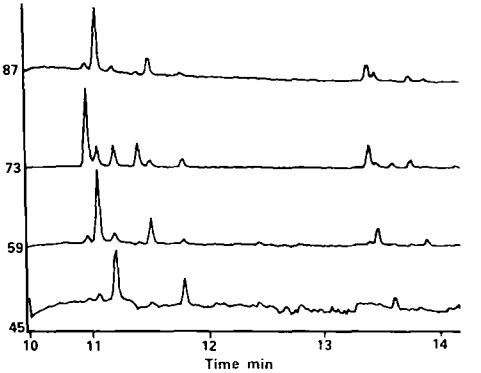

FIGURE 6

Reactions of Methyl Cations with Acetone Neutrals

R.D. Smith, T.A. Elwood, D.A. Herold and J.H. Futrell
Department of Chemistry
University of Utah
Salt Lake City, Utah 84112

The reaction and subsequent decomposition of CH_3^+ with acetone has been followed using a tandem Dempster-ICR mass spectrometer.

$$CH_3^+ + CH_3\text{-}\overset{O}{\overset{\|}{C}}\text{-}CH_3 \rightarrow CH_3\text{-}\overset{\overset{+}{O}\text{-}CH_3}{\overset{\|}{C}}\text{-}CH_3 \rightarrow$$

		Branching Ratio
$C_2H_5^+$	$+ C_2H_4O$	0.09
CH_3O^+	$+ C_3H_6$	0.07
$C_3H_5^+$	$+ CH_4O$	0.08
$C_3H_7^+$	$+ CH_2O$	0.12
CH_3CO^+	$+ C_2H_6$	0.28
CH_3OCH_2	$+ C_2H_4$	0.11
$C_3H_5O^+$	$+ CH_4$	0.05
$C_4H_7^+$	$+ H_2O$	0.06
$C_3H_6O^+$	$+ CH_3$	0.09
$C_3H_7O^+$	$+ CH_2$	0.05

Product Distribution

5%	Proton Transfer	+10 kcal
9%	Charge Transfer	- 4 kcal
15%	Hydrogen Abs.	-83 kcal
71%	Complex Formation	>>-83 kcal

Proton transfer being endothermic reveals that at least 5% of the CH_3^+ has 10 kcal of excess energy. The charge transfer processes have been given a cursory check via crossed beam studies in our laboratory by Dr. Calvin Blakley. It was shown that the production of mass 43 species specifically, acetyl, does not result from charge transfer.

Decomposition from complex formation form the majority of the products. The decomposition processes were examined using CH_3^+, and CD_3 reacting with acetone, acetone $-d_6$ and acetone-2-C^{13}. The examination of the results of the labelled studies enabled us to distinguish all product pathways.

The largest ion product was a result of a "olefinic disproportionation"

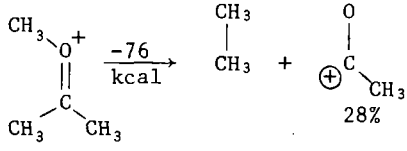

A second contribution to mass 43 was from the production of propyl ions:

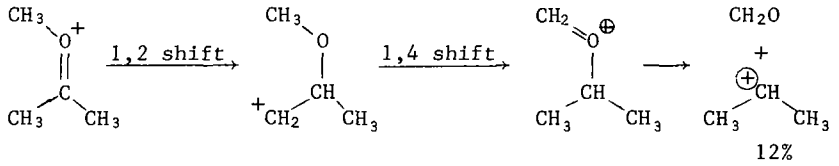

The 1,2 hydrogen shift followed by a 1,4 hydrogen shift from the methyl group allowed a bond cleavage to formaldehyde and propyl ion. While a 1,3 shift could also account for the observed data, this process is disallowed in a Woodward-Hoffmann sense.

The loss of ethylene and methanol are also explained by a series of 1,2 shifts supported by isotope labelling.

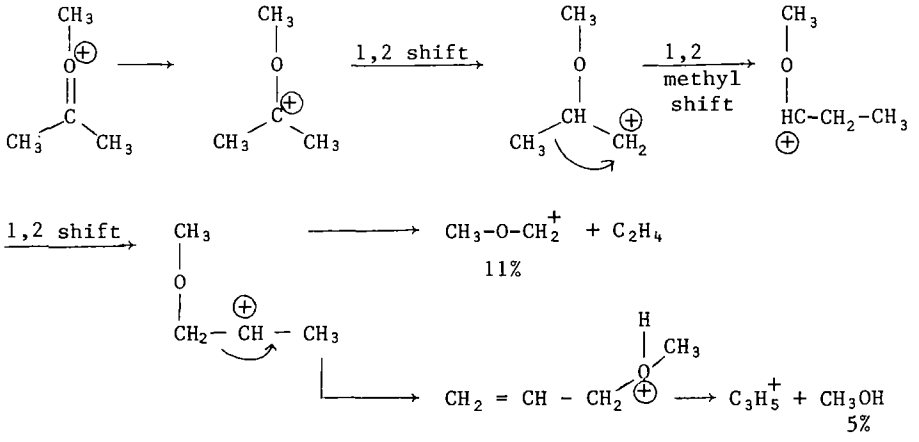

The loss of water from the complex is the most scrambled, but the product ratio of H_2O, HDO and D_2O adducts suggests that the CH_3^+ adds across the C=O bond as shown.

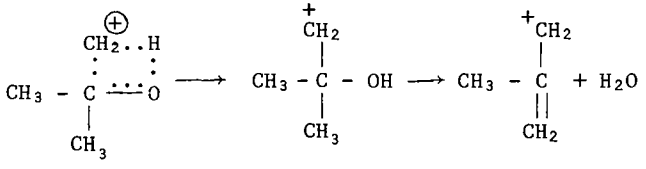

This is not surprising when one considers that CH_3^+ is isoelectronic with BH_3.

ORGANIC REACTIONS OF ANIONS IN A FLOWING AFTERGLOW

by

R. H. Shapiro, C. H. DePuy, V. M. Bierbaum and J. H. Stewart
Department of Chemistry, University of Colorado, Boulder, Colorado 80309

Gas-phase reactions involving hydrogen-deuterium exchange between organic anions and deuterium oxide have recently been investigated in this laboratory using the flowing afterglow technique.[1] The exchange process is broad in scope and seems only to require that the organic species have acidic or potentially acidic hydrogens. Several organic anions have been studied and found to exhibit exchange of a specific number of hydrogens depending upon the anion structure (Table I). A rate study has also been made to gain more information on the process involved.

The most interesting aspect of the reaction is that exchange can occur. Secondly, it is surprising that there are similarities between the number of hydrogens which exchange in solution and in the gas phase considering completely different mechanisms are involved. In basic solutions, exchange between organic anions and deuterium oxide occurs by a series of deuteron additions and deprotonations. This cannot be the mechanism taking place in our gas phase exchange studies. In the Flowing Afterglow, neutral reactant concentrations are greater than 1×10^{11} particles/cm^3 and ion concentrations in the reaction region are approximately 10^7 particles/cm^3. If an organic anion did abstract a deuteron from deuterium oxide, that deuterated neutral would be only one in 10^{11} particles/cm^3 so it would be extremely unlikely for this molecule to be reionized. In view of the acid strength of the organic molecules studied, it would also be unlikely that deuteron abstraction from deuterium oxide to form the neutral organic molecule would have any significance in these reactions. These facts imply that exchange must occur with the <u>charge always remaining on the organic species</u>.

For the reaction of allyl anion, up to four hydrogens will exchange with deuteriums much like the solution reaction of propylene. Two different mechanisms could account for exchange. First, the exchange may involve a concerted transition state where a hydrogen is abstracted from the organic ion with concomitant transfer of a deuterium from deuterium oxide to the organic ion as shown in Equation 1.

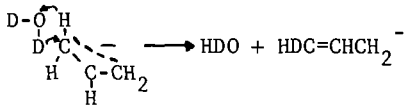

(1)

In the reaction of <u>cis</u> or <u>trans</u>-2-butene anion, where all hydrogens can exchange, this concerted mechanism must include adding a deuterium to one carbon while abstracting a hydrogen from another in order to account for allylic rearrangement of charge in the molecule. Another possible mechanism would involve formation of an intermediate complex between deuterium oxide and the organic anion. In the complex, the organic species may become neutral but must lose a proton to deuteroxide anion before the complex fragments. This is shown in Equation 2.

$$D_2O + CH_2{=}CHCH_2^- \longrightarrow [CH_2{=}CHCH_2D \cdot OD^-]$$
$$[CH_2{=}CHCHD^- \cdot HDO] \longrightarrow CH_2{=}CHCHD^- + HDO \qquad (2)$$

The intermediates must be short lived since the corresponding clusters are not detected for many organic ions.

A kinetic study was made of the reactions involving acetonitrile anion and deuterium oxide. The relevant equations are as follows:

$$CH_2CN^- + D_2O \longrightarrow CHDCN^- + HDO \qquad (3)$$

$$CHDCN^- + D_2O \longrightarrow CD_2CN^- + HDO \qquad (4)$$

$$CHDCN^- + CH_3CN \longrightarrow CH_2DCN + CH_2CN^- \qquad (5)$$

$$CD_2CN^- + CH_3CN \longrightarrow CD_2HCN + CH_2CN^- \qquad (6)$$

By studying the change of ion intensities versus time it was possible to determine that exchange occurs primarily with one hydrogen replacing a deuterium per reactive collision. If the exchange of deuteriums for hydrogens between deuterium oxide and acetonitrile anion proceeded by a series of transfers in one complex, on a statistical basis the monodeuterated ion concentration could never be greater than twice the dideuterated acetonitrile anion concentration. However, when monitoring this reaction, at one point the monodeuterated ion concentration was five times that of the dideuterated ion concentration. Though a portion of the exchange reactions may go through a long lived complex involving multiple transfers, this pathway must be minor. For this particular reaction, the rate of exchange was found to be twenty times slower than the reaction of the deuterated ions with acetonitrile to form the undeuterated product (Equations 5 and 6).

With deuterium oxide concentrations greater than 10^{13} particles/cm^3, collision rate constants of about 10^{-9} cm^3/particle sec, and reaction times of a few milliseconds, there may be several hundred collisions between the organic anion and deuterium oxide before the products are sampled. At these long reaction times it is possible to detect up to 9 hydrogens exchanging in the <u>cis</u>-2-pentene anion. Other anions which were found to exchange are shown in Table 1.

TABLE I

Neutral (HA) which produced anion (A^-)	Number of H-atoms present in A^-	Max. number of H-atoms in A^- which exchange
Propylene	5	4
cis-2-Butene	7	7
trans-2-Butene	7	7
cis-2-Pentene	9	9
2-Butyne	5	2
Acetonitrile	2	2
Glycol Aldehyde	3	1
Acetaldehyde	3	0
Acetic Acid	3	0
Ethylene Glycol	5	1
Methanol	3	0
Toluene	7	2

It is interesting that ethylene glycol anion and the anion of methoxide clustered to methanol each exchange one hydrogen for a deuterium. In each of these reactions, not only is a hydrogen-oxygen bond cleaved but hydrogen bonding is interrupted. In the gas phase, this type of hydrogen bonding would be approximately 25 kilocalories per mole for methoxide and somewhat less for ethylene glycol. For these particular ions, clusters with deuterium oxide are observed so it seems likely that exchange occurs through intermediate complexes.

The present work is critical for studying reactions involving deuterium labeled organic molecules. Unless the scope of exchange reactions is understood, information gained on mechanisms of fragmentation from labeled species may be misinterpreted. Deuterium exchange also aids in differentiating ions with the same charge to mass ratios, especially when natural isotopic abundance ratios cannot be determined. We are currently studying other aspects of this reaction.

[1] J. H. Stewart, R. H. Shapiro, C. H. DePuy, and V. M. Bierbaum, to be published.

Ion Molecule Reactions of the 1,3-Butadiene Ion--Possible Ionic Cyclo Additions.

M.L. Gross, P-H Lin and D.H. Russell
Department of Chemistry
University of Nebraska
Lincoln, NE 68588

We have found that the butadiene radical cation reacts with most simple alkenes from ethene to various isomeric pentenes. The results with neutral pentenes have been published.[1] The objective of this work is to understand the mechanism of the reaction by investigations with both carbon-13 and deuterium-labeled precursors. Specifically, it is of interest to determine whether this diene cation reacts with olefins via a cyclo-addition pathway.

Using various deuterium labeled butadienes and ethene, we observe extensive scrambling of H-atoms prior to methyl loss (equation 1).

$$C_4H_6^{\cdot +} + C_2H_4 \rightarrow [C_6H_{10}]^{\cdot +} \rightarrow C_5H_7^{+} + CH_3 \qquad (1)$$

Although extensive, we find a slight preference for elimination of methyl carrying deuteriums originally part of butadiene moiety. The results from carbon-13 labeling are more definitive. Using 1,3-butadiene-1-^{13}C, we find equal probability for loss of $^{12}CH_3$ and $^{13}CH_3$. We postulate that these results rule out formation of a Diels-Alder type adduct (i.e., the cyclohexene radical cation) because extensive hydrocarbon scrambling, by double bond isomerizations, would lead to statistical loss of $^{13}CH_3$. The highly-specific loss of $^{13}CH_3$ vs. $^{12}CH_3$ and the deuterium labeling results can be accommodated by formation of an acyclic intermediate, viz:

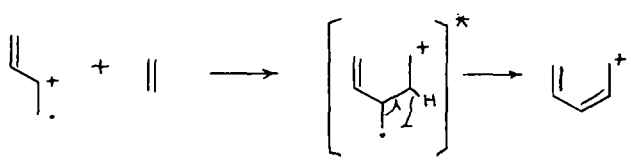

Further studies to measure the rate constants for the model reactions and to determine the effects of methyl substitution in the neutral olefin are underway. The completed investigation will be submitted to the "Journal of the American Chemical Society".

(1) M. L. Gross, P-H. Lin, and S. J. Franklin, Anal. Chem., 44, 974 (1972).

ANALYSIS OF A THREE-COMPONENT DEUTERIUM-LABELED MIXTURE BY MULTIPLE ION-MONITORING MASS SPECTROMETRY

W. K. Rohwedder, W. F. Kwolek, D. J. Wolf, and W. L. Everhart

Northern Regional Research Center, Agricultural Research Service, U.S. Department of Agriculture, Peoria, Illinois 61604

Accuracy of measurement of a three-component mixture by gas chromatographic-multiple ion-monitoring mass spectrometry was studied in association with the analysis of deuterium dual-labeled blood lipid samples from a human feeding experiment. The samples--mixtures of methyl oleate, methyl dideutero oleate, and methyl tetradeutero elaidate--were injected into a GC column connected through a membrane separator to a mass spectrometer operated in a multiple ion-monitoring mode. The mass spectrometer, under computer control, was stepped through six masses, 264 to 269. The integrated intensities for each mass under the GC curve, less the background, are combined with the relative mass intensities of the three pure components into six linear equations, which are solved by a least squares technique. The percentage relative standard deviation in test mixtures approached within a factor of 2 of the theoretical ion statistical limit.

Quantification of Prostaglandins in Human Seminal Fluid by Single Ion Monitoring.

DONALD L. PERRY and DOMINIC M. DESIDERIO,
Institute for Lipid Research and Dept. of Biochemistry, Baylor College of Medicine, Houston, Texas 77030.

The purpose of this paper is to present for the first time quantitative analytical data on the endogenous levels of the recently discovered 19OH PGE_1 and 19OH PGE_2 compounds (1,2) in human seminal fluid. The role that these novel 19OH PGE compounds play in biochemical processes is at the moment completely unknown. However, a promising avenue of investigation involves infertility, since previous workers have evidence that varying PGE levels correlate with human infertility. (3) Therefore we have begun studies to directly quantify endogenous levels of the 19OH PGE compounds together with PGE_1 and PGE_2.

Collection of seminal fluid and extraction procedures rigorously avoided chemical and/or enzymatic degradations of the primary PG's. Prostaglandin fractions were eluted from a silicic acid column with $CHCl_3$: MeOH (8:1). The 9-keto function was converted to the corresponding methoxime function while the carboxylic acid and hydroxyl groups were trimethylsilylated to the corresponding TMS ester and TMS ethers, respectively. An LKB 9000 instrument equipped with a 9 ft. x 0.25 in. silanized glass column packed with 1% SE 30 on Gas Chrom Q was used in this study. The accelerating voltage alternator was used to repetitively monitor and record the appropriate ion current at the following m/e values: 595, $(M-90)^{+\cdot}$ of 19OH PGE_2; 582, $(M-15)^+$ of PGE_2; 597, $(M-90)^{+\cdot}$ of 19OH PGE_1; 584, $(M-15)^+$ of PGE_1; 586, $(M-15)^+$ of 3,3,4,4-d_4 PGE_2, the internal standard for these measurements. The reproducibility of measuring the internal standard was 7.2%, while the error for each sample determination was estimated to be ±8%.

Seventeen samples were analyzed and the data categorized in the following three groups: (1) Azospermia Donors; (2) Fertile Donors, and (3) Fertility Status Unresolved.

	No. Samples	Ave. µg/cc E_1	E_2	19OHE_1	19OHE_2
Azospermia	(2)	9.0	15.4	42.9	71.9
Fertile Donors	(4)	30.7	45.5	101	169
Fertility Unresolved	(11)	20.7	41.2	37.3	88.2

Absence of any PGA, PGB and their corresponding 19OH analogues ensured that the collection and extraction procedures were performed satisfactorily. The range of the combined PGE levels of the first two groups correlates well with previous reports. (3,4) Direct measurement of the endogenous 19OH PGE levels indicate that these compounds are in much higher concentration than any of the other types of prostaglandins.

In addition, it is concluded that this method of quantifying endogenous

levels of prostaglandins is superior to other methods (ie. RIA, GC, and chemical treatment with base followed by UV detection) in terms of ensuring quantification of only that compound of interest.

(1) Taylor, P.L. and Kelly, R. W., Nature, 250 665 (1974).
(2) Jonsson, H. T., Middleditch, B. S., and Desiderio, D. M., Science, 187 1093 (1975).
(3) Bygdeman, M., Fredricsson, B., Svanborg, K., and Samuelsson, B., Fertility and Sterility, 21 622, (1970).
(4) Cooper, I., and Kelly, R. W., Prostaglandins, 10 975 (1975).

CHEMICAL IONIZATION MASS SPECTROMETRY OF URINARY COMPOUNDS FOR CLINICAL DIAGNOSIS

D. Issachar and J. Yinon
Department of Isotope Research
The Weizmann Institute of Science
Rehovot, Israel

Introduction

The urine amino acid excretion of normal healthy humans conforms to a fairly standard pattern which is usually different for children than for adults, and which is only changed by disease or by a change in dietary intake.

The screening of urine samples for amino acids has become a routine procedure in medical centers as a useful aid for the diagnosis of certain diseases.

There are two inherent problems in the analysis of amino acids in body fluids:

a) The large number of compounds which make up such fluids;
b) The low volatility of most amino acids.

In GC-MS the low volatility of the amino acids is solved by derivatization, which by itself causes new problems like increase in the number of components and increase in the mass number of the compounds. As all chromatographic techniques, GC-MS is inherently slow.

We would like to show how we have used chemical ionization mass spectrometry (CI-MS) without GC separation for semi-quantitative determination of amino acids and other nitrogeneous compounds found in human urine.

Experimental

Mass spectra were obtained with a Du Pont 21-490 B Single focusing mass spectrometer equipped with a dual EI/CI source. Isobutane at a pressure of 0.2 - 0.5 Torr was used as CI reagent. Source temperature was 200°C and probe temperature 160°C. Mass spectra were recorded 5 minutes after introduction of the probe into the source. These 5 minutes are necessary to evaporate and pump away most of the urea present in the sample which normally prevents protonation of the amino acids by the reagent ions. Both the temperatures and the timing were kept constant for all samples.

The urine samples we have used to demonstrate this technique were taken from seven children, four of them were healthy and three of them suffered from hereditary disorders in amino acid metabolism.

The urine samples were filtered and acidified to pH 2-2.5 and passed through a cation exchanger. The adsorbed nitrogenous compounds were then eluted with ammonium hydroxide. The eluate was evaporated and the residue introduced directly with the solid probe into the ion source of the mass spectrometer.

Results and Discussion

Figure 1 shows the CI spectra of the normal urine samples. In order to simplify the mass spectra the (M+1) urea peak at m/e 61 and the (2M+1) Creatinine peak at m/e 227 are not shown. The identification of the various compounds in the CI mass spectra is based on the $(M+1)^+$ ion or typical fragment ions of each compound in the mixture. The relative concentrations of the various compounds in the urine samples of the normal healthy patients exhibit the normal distributions (1).

Figure 2 shows the CI spectrum of a sample from a Phenylketonuria patient. We see clearly an increase of more than 25 times the normal concentration of Phenylalanine which has a base peak at m/e 166. The increase of Phenylalanine is characteristic to this disease.

Figure 3 shows the CI spectrum of a sample from a Cystinuria patient. An increase in the concentration of Ornithine (base peak at m/e 115) can be observed. Part of the peak at m/e 115 is due to the isotopic contribution of Creatinine. There is an increase in Lysine (base peak at m/e 147) by more than 50 times the normal concentration and an increase in amino butyric acid at m/e 104. An increase in Arginine has also been observed when the mass spectrum was recorded at higher probe and source temperatures (2).

Figure 4 shows the CI spectrum of a sample from a Maple-Syrup Urine Disease patient. Although this patient was under therapy, we could clearly see an increase in the peak at m/e 132 by more than 8 times the normal. The increased peak at m/e 132 corresponds to the increase in the Leucine/Isoleucine concentration. We did not observe an increase in Valine, probably because of the therapy.

Conclusions

It is well known that in order to obtain precise quantitation of amino acids concentrations in urine, the use of internal standards or the use of ion current integration is necessary.

However, our results can be defined as semi-quantitative because of the reproducibility of the mass spectra which are taken under controlled conditions. The advantages of this method for the screening of amino acids can be concluded as follows:

a. No derivatization is necessary.

b. A simple mass spectrum is obtained.

c. As the ratio of amino acids to Creatinine is fairly constant (3) it is necessary to know the amount of Creatinine. In our method, the relative amount of Creatinine is already given in the CI mass spectrum and no separate determination of Creatinine is necessary.

We intend to extend this technique also to other urinary compounds like carboxylic acids.

References

1. C.F. Consalazio, R.E. Johnson and L.J. Pecora in "Physiological Measurements of Metabolic Functions in Man", p. 448, McGraw Hill, New York, 1963.

2. D. Issachar and J. Yinon; to be published.

3. A.M. Lawson, R.A. Chalmers, P. Purkiss, F.L. Mitchell and R.W.E. Watts, Advances in Mass Spectr. 6, 235 (1974).

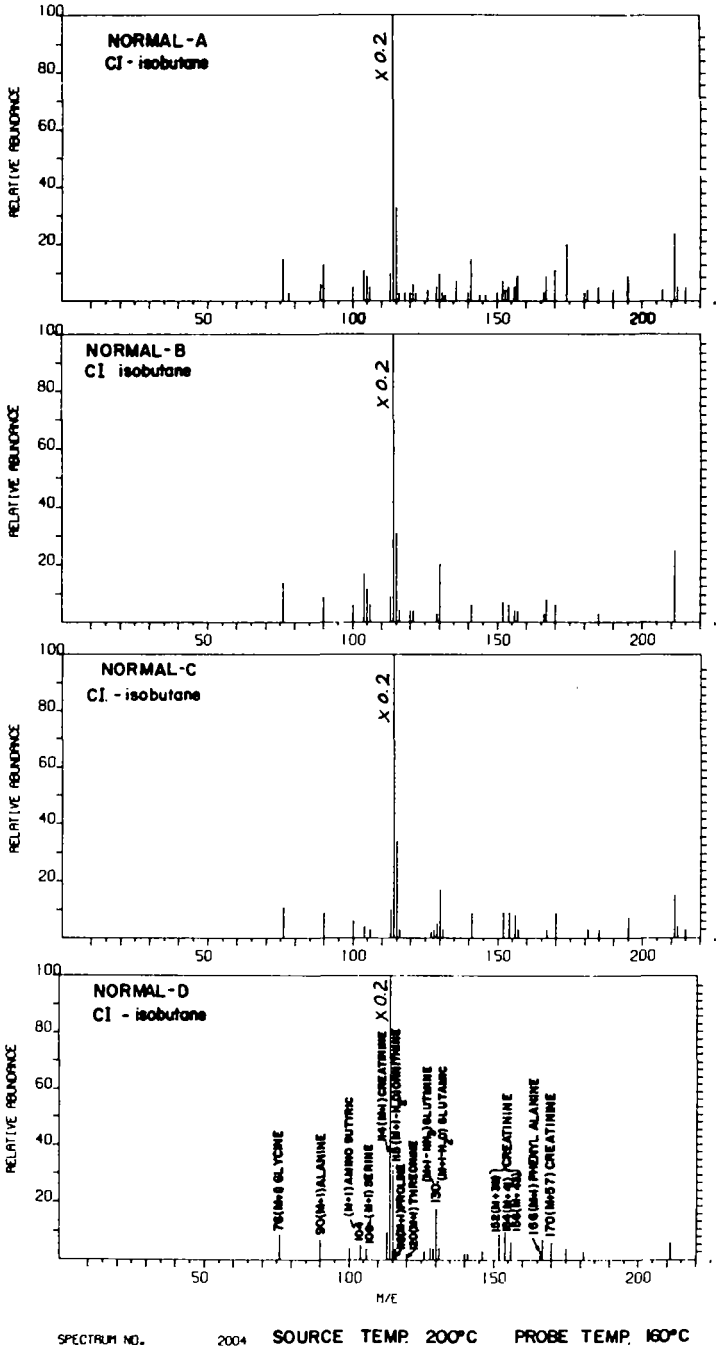

Figure 1. CI mass spectra of normal urine samples.

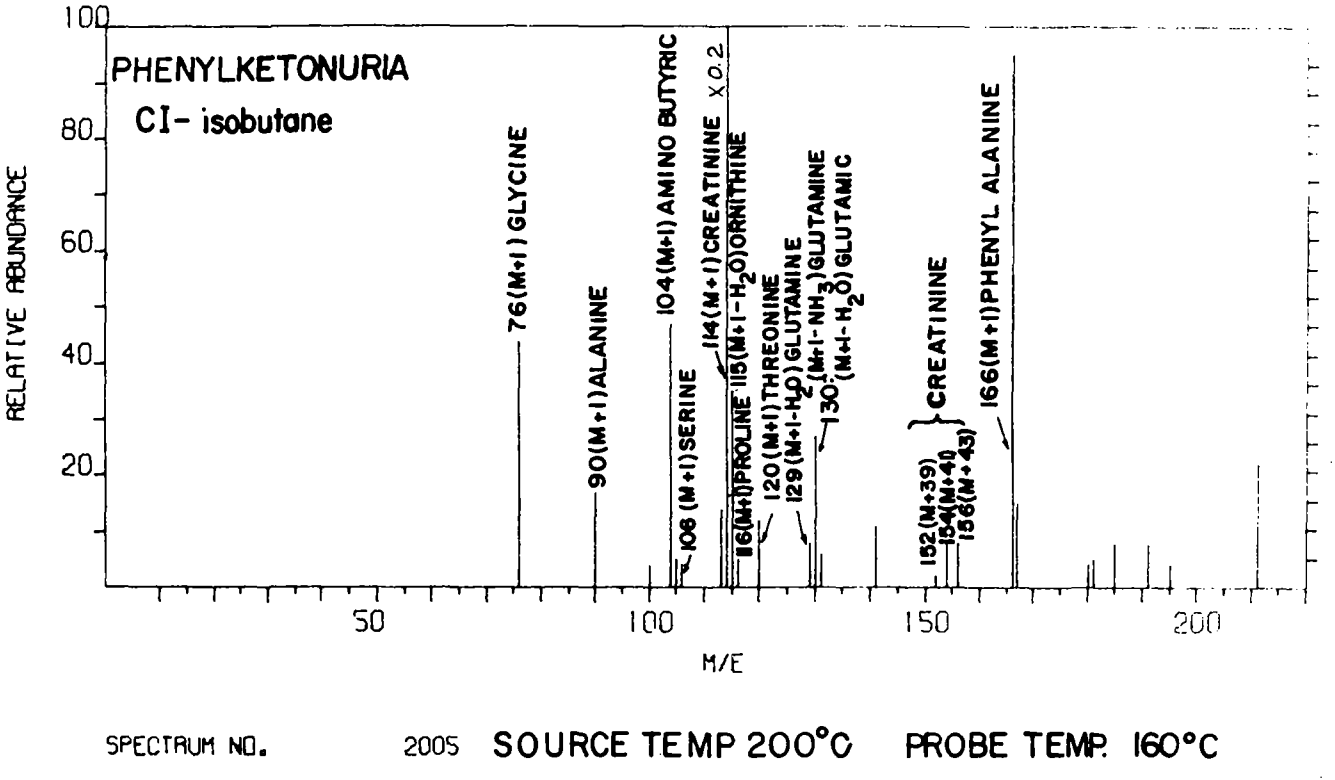

Figure 2. CI mass spectrum of Phenylketonuria patient sample.

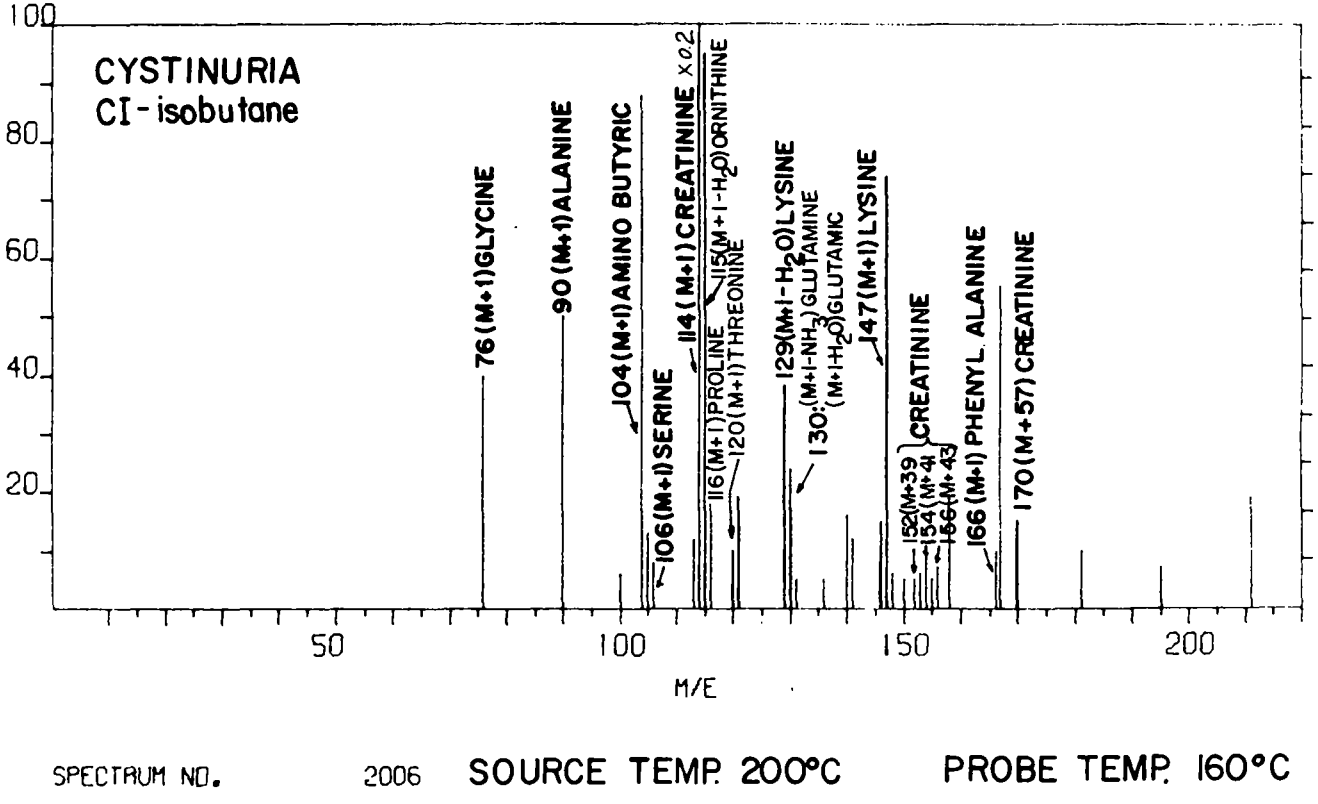

SPECTRUM NO. 2006 SOURCE TEMP. 200°C PROBE TEMP. 160°C

Figure 3. CI mass spectrum of Cystinuria patient sample.

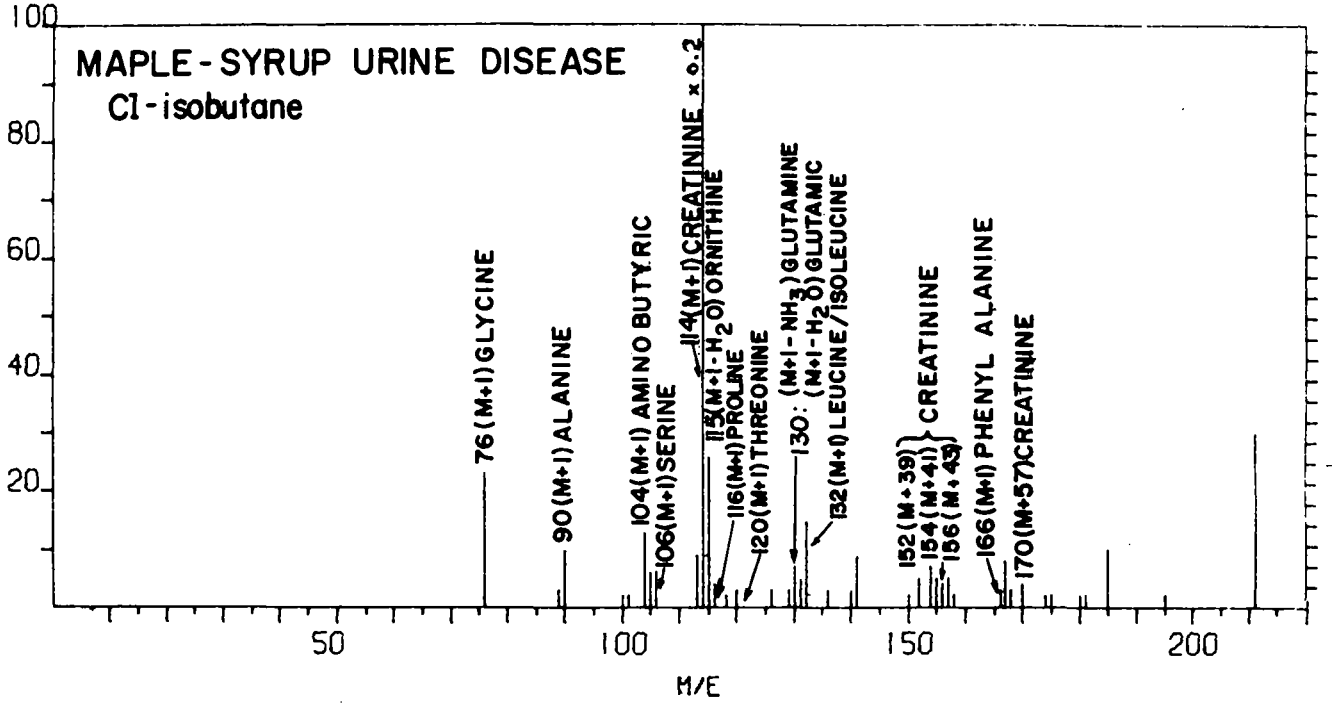

SPECTRUM NO. 2007 SOURCE TEMP 200°C PROBE TEMP 160°C

Figure 4. CI mass spectrum of Maple-Syrup Urine Disease patient

Analysis of Polyamines in Urine by Stable Isotope Mass Fragmentography. E. T. EVERHART, W. E. PEREIRA, T. C. RINDFLEISCH, and A. M. DUFFIELD, Stanford Univ. Med. Ctr., Dept. of Genetics, Stanford, Ca.94305.

A sensitive and specific method using mass fragmentography for the analysis of the polyamines putrescine, cadaverine, spermidine and spermine has been developed, along with a method of synthesis for their deuterated analogs. The procedure involves addition of a known amount of a standard solution of deuterated analogs to the urine, followed by acid hydrolysis, solvent extraction and ion exchange chromatography. The polyamine extract is trifluoroacetylated, and polyamine quantitation is achieved by measuring peak height ratios of specific ions characteristic of the trifluoroacetylated derivatives of indigenous and deuterated polyamines. The method is currently being investigated as a sensitive diagnostic tool in the screening of patients with cancer. Preliminary studies, however, indicate that within experimental error, the daily milligram excretion levels of putrescine, spermidine and spermine in patients with prostatic cancer are identical to the excretion levels found in controls. The daily mg excretion levels of cadaverine vary over a factor of 40-fold for controls, and the compound seems to be useless as a diagnostic marker for cancer. Complete results of this study will be published shortly.

This work was supported by National Cancer Institute Contract N01-CB-43902.

BIOGENIC AMINE DERIVATIVES FOR USE IN NEGATIVE CHEMICAL IONIZATION ANALYSIS

E. Anne Bergner and Ralph C. Dougherty

Department of Chemistry

Florida State University, Tallahassee, FL 32306

Negative Chemical Ionization (NCI) mass spectrometry offers many advantages for the analysis of selected trace components in complex mixtures. If isobutane is used as the "reagent gas" to develop the NCI plasma, and if the substrate mixture is not rich in halides the NCI spectrum will be dominated by ions that result from resonance capture and disassociative capture of electrons. The electron capture cross sections for most organic molecules are small and thus the "average" organic will be transparent to an isobutane NCI analysis. Molecules with high electron affinitives are on the other hand exceptionally sensitive to NCI analysis with nanogram and subnanogram detection limits for normal screening mass spectrometry. Thus, if the mixture under analysis contains traces of molecules that will efficiently capture electrons, these molecules will dominate the spectrum without interference from the bulk of the substrate. We have previously taken advantage of these features of NCI mass spectra in the analysis of complex mixtures for traces of chlorine containing toxic residues.[1]

The simultaneous and unequivocal quantitation of all known neuro transmitter substances in biofluids should be of research and diagnostic value in neural and affective disorders such as Huntington's chorea or schizophrenia. In addition to acetylcholine and several amino acids the postulated neurotransmitters include the following amines: dopamine, norepinephrine, serotonin, tyramine, octopamine and histamine. In order to simultaneously measure the amount of these amines in a mixture by NCIMS the amines must be converted to derivatives that have high electron capture cross sections and generally similar volatility for each of the amines in the group.

Table 1 lists the derivatives we have looked at in the development of this procedure.

TABLE I

Yields And Relative Sensitivities
For
Tyramine Derivatives

Derivative	Yield (%)	Relative Sensitivity		Yield x Sensitivity
Fluorescamine	92	NCI	1	.9
		CI	.05	.04
MDPF	76	NCI	.5	4.
		CI	.2	.2
2,4-DNP	55	NCI	2	1.
		CI	.05	.03
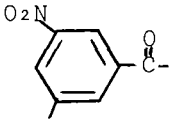	92	NCI	10	9
		CI	.05	.05
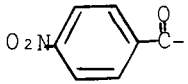	89	NCI	10	9
		CI	.1	.1
Dansyl	55	---		--

Didansyltyramine has an $M^{+\cdot}$ of only 3% relative intensity. 3,5-Dinitrobenzoyl, p-nitrobenzoyl and DNP derivatives have molecular anions of 100% but react with both phenols and amines to give mixtures of mono, di, and tri-derivatives whose volatility varies greatly. MDPF reacts only with primary amines but has numerous fragment ions. Fluorescamine is also specific for primary amines. Fluorescamine derivatives of tyramine, octopamine, norepinephrine, normetamephrine, and serotonin have molecular anions of 80-100%. The only fragment is 277,278 corresponding to loss of the amine side chain. The detection limits, which vary from 1 to 50 ng per injection depending on the condition of the ion source, are more than adequate for analysis of these amines in a 12 hour urine sample. NCI Spectral characteristics, reactivity and volatility make fluorescamine our reagent of choice for NCI studies of these primary amines.

The MDPF and fluorescamine used in this work were obtained from Manfred Weigele of Hofmann-La Roche.

References

1. R. C. Dougherty and K. Piotrowska, Proc. Nath. Acad. Sci. U. S., in press (1976).

Simultaneous Kinetic Studies and Quantitation of Catecholamines in Selected Areas of Rat Brain

Curt R. Freed and Robert C. Murphy
University of Colorado Medical Center
Department of Pharmacology and
Division of Clinical Pharmacology
Denver, Colorado 80220

The catecholamines dopamine (DA) and norepinephrine (NE) are synthesized in certain neurons in the central nervous system from precursor amino acids tyrosine and dihydroxyphenylalanine (DOPA). Norepinephrine turnover in rat brain has been customarily estimated by administration of tracer doses of radioactive NE or its precursors or by inhibition of NE synthesis and then observation of the decay of norepinephrine. These studies give an estimate of natural turnover rate of this catecholamine. We have been interested in the effect drug administration has on DA and NE turnover in rat brain; in particular, the effect of chronically administered L-DOPA on catecholamine metabolism in rat hypothalamus. The combined use of mass spectrometry and isotopic variants of these catecholamines has allowed us to measure both turnover and absolute concentration of dopamine and norepinephrine in rat hypothalamus during steady state infusions of L-DOPA.

Experimentally, conscious restrained rats are infused in the right jugular vein with L-DOPA for 20 hrs at a rate of 2-10 mg/kg/hr in an infusion volume of 0.5 ml/hr. A peripheral decarboxylase inhibitor, MK-486, is added to all infusions to block peripheral loss of drug. After 20 hrs, the infusion is switched to the identical dose of deuterated L-DOPA and animals sacrificed at intervals thereafter. The hypothalamus is rapidly dissected, and divided into halves and weighed. A known amount of side-chain deuterated catecholamine is added to one-half. This half is used to gauge total catecholamine concentration. The other half of the hypothalamus is analyzed for dopamine and norepinephrine synthesized from the deuterated L-DOPA. The brain samples are homogenized in cold, 5% TCA and catecholamines isolated by column ion exchange (Dowex 50, Na^+ form). The column fractions are lyophilized and catecholamines derivatized with pentafluoropropionic anhydride for GC-MS analysis.

The ring-deuterated L-DOPA is prepared in gram quantities by aromatic proton exchange in 6N DCl. Our present procedure yields 80% D_3-DOPA, and negligible D_1 and D_0. We have demonstrated that this compound can be metabolized *in vivo* to D_3-dopamine and D_3-norepinephrine without deuterium loss. This is critical for the use of this isotopic variant as a marker for new transmitter synthesis.

The combined enrichment-concentration determination is made possible by the electron impact mass spectral characteristics of the pentafluoropropionyl derivatives of the catecholamines. The mass spectrum of DA-PFP has two abundant ions at m/e 428 and 176 which come from the aromatic and side chain structural features, respectively. The ion at m/e 428 arises following transfer of a proton from the β-carbon to the carboxyl of amide function in a McLafferty type rearrangement. By contrast the deuterated dopamine, synthesized *in vivo*, from D_3-L-DOPA has the catechol ion at m/e 431 but the same side chain ion at m/e 176. The ratio of 428 to 431 will therefore give the portion of native to deuterated dopamine, or enrichment. The side-chain labelled dopamine (D_4-dopamine) has the side chain ion shifted to m/e 178. In samples with this internal standard

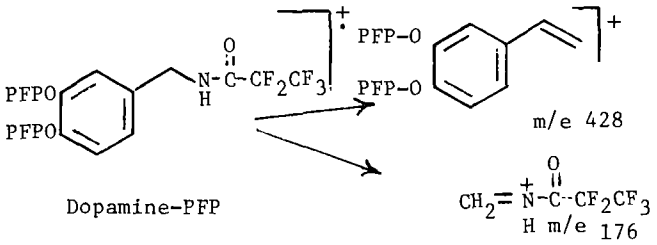

added, then, the total dopamine concentration is given by the ratio of 176/178. As one can observe, this internal standard also produces an ion at m/e 431 which would interfere with the enrichment measurement. It is for this reason that only one-half of the hypothalamus has internal standard added to determine concentration while the other half is used to measure enrichment.

The electron impact mass spectrum of norepinephrine-PFP is similar to that of dopamine-PFP, only the catechol ion is shifted to m/e 590 due to the β-hydroxyl moiety which carries an additional PFP. As before,

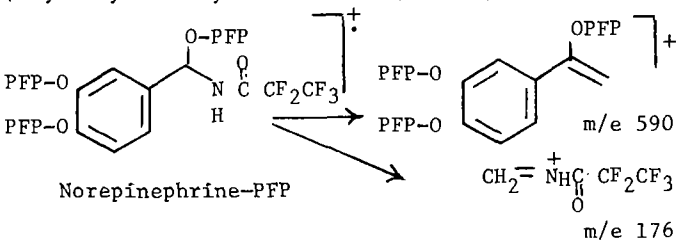

enrichment is measured by 590/593 ratio and total NE concentration by the 176/178 ratio. The gas chromatographic column provides a very nice separation of NE from DA and thus the identical ions at m/e 176 and 178 can be specifically measured for each catecholamine. The mass spectrum of side chain labelled norepinephrine was reported last year[1].

The Table shows some preliminary results of the application of this method to determine the turnover of dopamine and norepinephrine during a 5 mg/kg/hr infusion of L-DOPA. The L-DOPA was switched to D3-L-DOPA as described above and animals sacrificed at 2, 3, and 4 hour intervals. There is a progressive increase in the fraction of deuterated dopamine and norepinephrine, with a lag between the fractional enrichment of DA and NE. This is expected since dopamine is the direct precursor of norepinephrine by the action of the enzyme dopamine-β-hydroxylase. Since there are also neurons in the hypothalamus which contain dopamine as the end product of L-DOPA metabolism, further experiments are being carried out at different dosing levels to evaluate the effect chronic infusion of L-DOPA has on the turnover of norepinephrine in the hypothalamus.

References

1. R. C. Murphy, J. A. Zirrolli, K. Clay, S. E. Hattox, and R. Helbig: Proc. 23rd Ann. Conf. Mass Spectrom. Paper Q-5.

TABLE

Percent of Deuterated Dopamine and Norepinephrine Enrichment in Rat Hypothalamus After Infusion with D_3-L-DOPA Under Chronic Infusion (5 mg/kg/hr)

Catecholamine	Time After D_3-DOPA Infusion (Hours)		
	2	3	4
Dopamine	38 ± 1.5*	30 ± 3	65 ± 1
Norepinephrine	18 ± 1	24 ± 1.5	39 ± 1

* Standard error, n = 5

DEUTERIUM LABELLED INTERNAL STANDARDS FOR POLYAMINE ANALYSIS

Ronald G. Smith and G. Doyle Daves, Jr.
Oregon Graduate Center, Beaverton, Oregon 97005

Polyamines have received intense interest and study since it was found that rapid cell growth was accompanied by increased levels of urinary polyamines[1]. More recently some kidney disorders and other disease states have also been found to be accompanied by increased polyamine levels.

Because of their potential as biochemical markers[2] for these diseases a variety of methods for the quantitative measurement have been explored[3,4,5]. Their presence in relatively low amounts makes mass spectrometry, used in the selected ion recording (SIR) mode, an ideal choice.

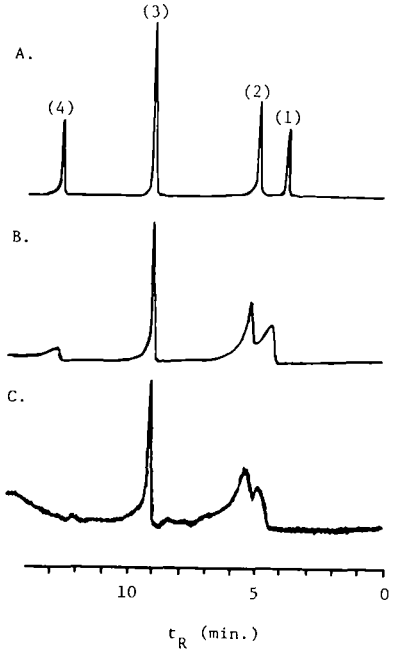

Figure 1. Effect of decreasing sample size on the chromatographic bands of the trifluoroacetylated polyamine derivatives. Mass fragmentogram recordings of the ion at m/e 126 ($F_3CCONH{=}CH_2^+$) in samples containing, A) 500 picomoles, B) 50 picomoles and C) 10 picomoles each of the trifluoroacetylated derivatives of putrescine (1), cadaverine (2), spermidine (3) and spermine (4).

In separate publications Gehrke[6], Walle[7] and Denton[8] have reported the GC and GCMS analysis of urinary polyamines after derivatization by trifluoroacetic anhydride (TFAA). The chromatographic properties of these derivatives appear ideal down to the lower levels reported, which is about 1 nmole.

Our interest in clinical studies dealing primarily with polyamine levels in blood serum require us to perform analyses at the 5-50 pmole level. The mass fragmentograms (m/e 126) of Fig. 1 illustrate the problem presented by low-level quantitative analyses of compounds with different chromatographic characteristics.

It was anticipated that deuterated internal standards would help to solve this problem. Namely, they should be good internal standards specific to each polyamine and, if large excesses can be used, should serve as a chromatographic carriers. Also, if added to the sample prior to separation or purification steps, all losses will be compensated by similar losses in the internal standards. The following deuterated polyamines were prepared by catalytic deuteration of the appropriate nitriles.

D_4-Putrescine	$H_2NCD_2CH_2CH_2CD_2NH_2$
D_4-Cadaverine	$H_2NCD_2CH_2CH_2CH_2CD_2NH_2$
D_6-Spermidine	$H_2NCD_2CH_2CH_2CD_2NHCH_2CH_2CD_2NH_2$
D_8-Spermine	$H_2NCD_2CH_2CH_2NHCD_2CH_2CH_2CD_2NHCH_2CH_2CD_2NH_2$
D_2-Acetylspermidine A	$CH_3CNHCH_2CH_2CH_2CH_2NHCH_2CH_2CD_2NH_2$

By measuring the intensities of the recorded ions at m/e 128 and m/e 126 (the base ions in the spectra of all deuterated and non-deuterated trifluoroacetylpolyamines, respectively) it was shown that D/H = 20 to 50 for the deuterated standards. To maintain a higher ratio of D/H higher mass ions were monitored. These ions, resulting from the loss of either CF_3 or CF_3CO, gave D_{max}/H >330 for all standards. This permits large excesses of internal standard to be used without significantly changing the peak height for the mass of the unlabeled polyamine. The "carrier effect" of a large excess of the internal standard is illustrated in Fig. 2.

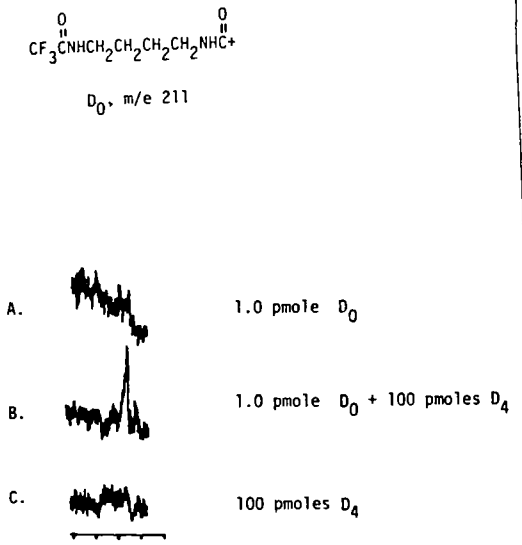

Figure 2. Sensitivity enhancement from the addition of excess deuterated analog. Mass fragmentograms of trifluoroacetylated putrescine recording the ion at m/e 211 (loss of CF_3 from D_0-putrescine).
A) 1.0 picomole of D_0-putrescine.
B) 1.0 picomole of D_0-putrescine with 100 picomoles D_4-putrescine added.
C) 100 picomoles of D_4-putrescine.

The response curves of all internal standards are linear from 1.0 nmole down through 1.0 pmole.

The high mass ions of the polyamines and their deuterated internal standards can be monitored from a single temperature programmed sample.

References

1. D. H. Russell, C. C. Levy, S. C. Schimpff and I. A. Hawk, Cancer Res., 31, 1555 (1971).

2. D. H. Russell, B. G. M. Durie and S. E. Salmon, The Lancet, p. 797, October 25, 1975.

3. L. J. Marton, D. H. Russell and C. C. Levy, Clin. Chem., 19, 923 (1973).

4. F. Abe and K. Samejima, Anal. Biochem., 67, 298 (1975).

5. T. Sugiura, T. Hayashi, S. Kawai and T. Ohno, J. of Chromatog., 110, 385 (1975).

6. C. W. Gehrke, K. C. Kuo, R. W. Zumwalt and T. P. Waalkes, Polyamines in Normal and Neoplastic Growth, D. H. Russell, Ed., Raven Press, p. 343 (1973).

7. T. Walle, Polyamines in Normal and Neoplastic Growth, D. H. Russell, Ed., Raven Press, p. 355 (1973).

8. M. D. Denton, H. S. Glazer, T. Walle, D. C. Zellner and F. G. Smith, Polyamines in Normal and Neoplastic Growth, D. H. Russell, Ed., Raven Press, p. 373 (1973).

ALDEHYDE CONDENSATION PRODUCTS AS DERIVATIVES FOR THE ANALYSIS OF BIOGENIC AMINES

Brian S. Middleditch

Department of Biophysical Sciences
University of Houston
Houston, Texas 77004

Few derivatives of β-phenylethylamines and β-indolylethylamines afford abundant molecular ions. Condensation of the amines with aldehydes yields tetrahydroisoquinolines and tryptolines, respectively, which generally afford abundant molecular ions, together with diagnostic fragment ions characteristic of the substituents both on the aromatic nucleus and the ethylamine moiety. There is some evidence that these compounds are produced in vitro by condensation of biogenic amines with acetaldehyde (derived from ethanol) or formaldehyde (derived from 5-methyltetrahydrofolic acid), and speculation that they are also present in vivo. Thus, a detailed study of their mass spectral fragmentations has been performed.

For further details, see:

B. S. Middleditch, J. Chromatog., in press.

GC-MS Studies of Thiocarbamic Acid Derivatives of Some Biologically Important Secondary Amines. N. Narasimhachari, ISPI, Chicato, P. Vouros, Northeastern University, Boston, D. E. Green, V. A. Hospital, Palo Alto, Cal.

In earlier communications we reported the GC-MS studies of isothiocyanate (NCS) derivatives of biologically active primary amines. Secondary amines of the general structure $R\text{-}NH(CH_3)$ also constitute a major class of biologically important compounds such as biogenic amines (N-methyltryptamine, N-methylserotonin, metanephrine), drugs and drug metabolites (methamphetamine, desipramine). Secondary amines react with CS_2 to form thiocarbamic acids $R\text{-}N(CH_3)\text{-}C(=S)\text{-}SH$ and these on methylation with diazomethane yield the methylesters $R\text{-}N(CH_3)\text{-}C(=S)\text{-}S\text{-}CH_3$.

We have now investigated the usefulness of these derivatives in the identification and quantitation of secondary amines in biological samples. The mass spectral data of the thiocarbamic acids and their methylesters will be presented and the fragmentation mechanisms based on HRMS and metastables will be discussed using NMT and methamphetamine as illustrative examples. The GC retention data of various compounds will be given.

SIMULTANEOUS ANALYSIS OF CHLORPROMAZINE AND ITS MAJOR METABOLITES BY STABLE ISOTOPE RATIO MEASUREMENTS USING IMPROVED VOLTAGE SWEEP INSTRUMENTATION

L. D. Gruenke and J. C. Craig

University of California, School of Pharmacy
Department of Pharmaceutical Chemistry
San Francisco, California 94143.

We have previously reported[1] the construction of a low cost analog selected ion recording system for the AEI MS-12 which in spite of its simplicity was capable of excellent precision in determining ion current ratios. The key feature of this system is the use of a 60 Hz a.c. sine wave voltage superimposed on the d.c. accelerating voltage of the mass spectrometer to sweep back and forth over a small mass range. The purpose of this voltage sweep is to minimize the effects of drift on the ion current ratio measurement, while allowing m/e peak shape and focus conditions to be continuously displayed on an oscilloscope.

We now report the construction of a more sophisticated version of this system and its use for the quantitation of chlorpromazine (CPZ) and CPZ metabolites. Figure 1 shows a block diagram of the updated selected ion recording/voltage sweep (SIR/VS) system we have designed for the AEI MS-12. By replacing the original AEI accelerating voltage supply we were able to decrease the dwell time from one second in the earlier prototype system to 33 ms in this system. The heart of the system is the Kepco OPS-2000 operational high voltage power supply which makes all the voltage changes. The output voltage of this supply is proportional to the reference voltage which is set for each channel by the resistors R_1. The Fluke 410-B power supply provides a fixed voltage which makes up the rest of the 8 KV accelerating voltage. The sweep voltage is obtained by modulating the current from the reference voltage for the OPS-2000 with 60 Hz a.c. from a 12 V transformer. The potentiometer R_2 is the sweep range adjustment. A sweep counter performs all the control functions for the system. It counts the number of sweeps and at the beginning of every fourth sweep switches the reference bank of high speed mercury-wetted relays to the next reference voltage. After a delay of one sweep time (8 ms) to allow the output voltage of the OPS-2000 to settle the sweep counter switches the recorder relay bank so that the appropriate channel of the multipen recorder is connected to the output of the mass spectrometer. The sweep counter also sends a sync pulse to a 2 channel oscilloscope at the same time that the recorder relay is being switched. In this way the oscilloscope is made to alternately display the m/e peaks at 2 masses on separate oscilloscope channels. Since the dwell time is so short, both displays appear <u>to be simultaneous</u> (Fig. 2a). In this system all four recorder channels use the sample- and -hold technique. A typical recorder output for 2 channel operation is shown in Fig. 2b. Because of the short dwell time, the hold periods are not visible and the result is a smooth curve for each ion current being monitored.

Ion current ratios can be determined with the updated SIR/VS system with even greater precision than those obtained using the prototype. In ideal cases average coefficients of variation of as low as 0.2% have been obtained for data used in the construction of standard curves. In cases of demonstrated interference from ion current at the same nominal but different exact mass, we have been able to overcome this problem

by operating at resolutions as high as 3000 with only a slight loss of sensitivity.

An assay has been developed for CPZ and its major metabolites using the updated version of the selected ion recording/voltage sweep system. In the past there has been considerable effort devoted to the measurement of CPZ and its metabolites in biological fluids, including some early work using SIR as a method of detection[2]. However, CPZ quantitation has proved to be an exceptionally tough analytical problem. Many of the methods tried in the past lacked the necessary specificity or sensitivity. We have found that by using the method of selected ion recording with stable isotope labelled standards many of the earlier analytical problems in this field can be overcome. We have synthesized for use as standards d_2 labelled CPZ and several of its major metabolites including the N-oxide, S-oxide, and the mono- and di-demethylated compounds.

In the mass spectra of labelled and unlabelled CPZ, the unlabelled compound shows a strong molecular ion at m/e 318 for the ^{35}Cl isotope and at m/e 320 for the ^{37}Cl isotope. The base peak at m/e 58 is due to the dimethylaminomethylene end of the side chain. In the labelled compound both the molecular ion and base peak show clean shifts to 2 mass units higher and thus either of these could be used for quantitation. Since there is less background interference in the mass spectrometer at higher masses, we elected to use the molecular ions for quantitation. The mutual interference which occurs at m/e 320 from the ^{37}Cl isotope of the unlabelled compound and from the ^{35}Cl isotope of the labelled compound was avoided by measuring the ion current at m/e 318 for the unlabelled compound and at m/e 322 for the labelled compound. Figure 3 shows the standard curve we obtained in this manner for d_2 CPZ enriched with known amounts of its natural analog. We normally add about 100 times the amount of standard as the expected amount of unlabelled drug. In this way the labelled compound not only serves as an internal quantitation standard but also acts as a carrier.

Our extraction procedure has been carefully designed not only to provide good separation and recovery of the desired metabolites but also to separate cleanly the N-oxide from the rest of the metabolites, since the major product obtained by injection of CPZ N → O onto a gas chromatograph is the allyl compound together with substantial amounts of CPZ as well as traces of desmethyl CPZ and 2- Cl- phenothiazine.

The results from the extraction of plasma thus far show that the recovery of all 5 d_2 standards is excellent and the gas chromatographic analysis also shows the expected clean separation of all metabolites, and particularly of CPZ N → O from the other metabolites. The SIR's of d_2 CPZ standard recovered from plasma show ion current records which are near 0% enrichment on the standard curve.

We plan to demonstrate the effectiveness of the technique in measuring levels of CPZ and its major metabolites in clinical samples from patients treated with chlorpromazine. We also plan to extend our analysis to the measurement of other CPZ metabolites using the appropriate labelled standards.

[1] Gruenke, L. D., Craig, J. C., and Bier, D. M., Biomed. Mass Spectrom., 1:418-423 (1974).
[2] Hammar, C. G., Holmstedt, B., and Ryhage, R., Analyt. Biochem., 25:532-548 (1968).

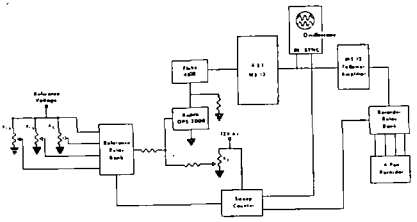

Fig. 1 Block Diagram of SIR/VS System.

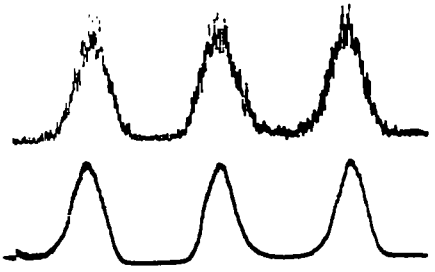

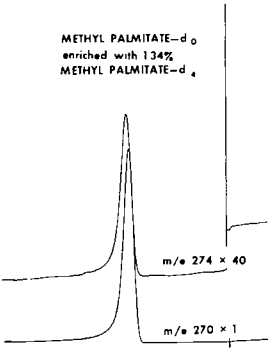

Fig. 2(a) Typical Oscilloscope Display and 2(b) Typical Selected Ion Record of 2-Channel SIR/VS System.

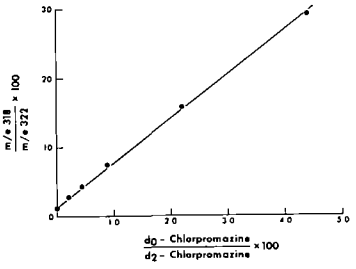

Fig. 3. Calibration Curve for d_2 chlorpromazine enriched with known amounts of its natural analog.

CHARACTERISTICS OF A DOUBLE BLADE FIELD IONIZATION SOURCE

William Aberth,* Arnold M. Falick, James T. Wilder and A. L. Burlingame
Space Sciences Laboratory,
University of California, Berkeley, Ca. 94720

A field ionization source has been constructed which consists of two razor blades separated by 4 microns and positioned at 60° relative to each other (Fig. 1). The sample material enters the field ionizing region of the blades via a 0.25 mm hole placed directly behind the blades (Figs. 1 and 2). Since the sample material must pass very close to the ionizing region of the blades, a high ionization efficiency is anticipated. In addition, the small dimensions of the aperture between the blades permits a higher operating inlet system pressure, thus increasing the source brightness. The source was designed to operate on a CEC 110B mass spectrometer but can be easily adapted to operate on most commercial mass spectrometers.

Perhaps the most difficult aspect of the source shown in Fig. 2 is the positioning of the two razor blades. The procedure is to place the double blade support in a jig which clamps one of the blades in a horizontal position. The jig with the blade and support is placed on the stage of a 100x microscope and the location of the blade relative to the outer edge of its support is trigonometrically calculated. The microscope eyepiece reticle is positioned at the calculated location and the blade is moved to this position by a tapping procedure. After the blade is in position it is held there by a few light spotwelds. Next, the blade support is rotated 180° in the jig and the second blade is brought into position and spotwelded. In practice, the blade positioning procedure must be repeated numerous times before the blades are correctly placed. A superior method for positioning, which is now being developed, involves changing the angle between the blades from 60° to 90°. With one blade in a horizontal position, the other blade edge is used as a reference for accurately positioning the horizontal blade. The jig is then rotated 90° and the positioning procedure is repeated with the positioned blade edge acting as the reference.

To obtain a better understanding of the double blade effect on the electric field in the ionizing region of the blades, a computer-assisted calculation was performed of the potential field in the region of the blade edges.[1] Fig. 3 shows the potential field structure in the region of the blades and the extraction cathode. The break in the angle near the double blade apex represents a 10° bevel in the blade edge.[2] The cathode slit is 0.25 mm wide and 0.50 mm deep and is spaced about 0.05 mm from the double blade tip. Fig. 4 is an enlargement of the tip region of Fig. 3 showing parabolic shaped blade edges separated by 0.004 mm. The electric field lines have been included in this figure and clearly show two important characteristics of this source. First, the electric field lines emanating from the inner region of the blades bend towards the plane of symmetry. This represents a focusing effect which can have important ion-optical advantages and will be studied further. Second, the most intense portion of the electric field (region of closest spaced field lines) is at the edge of the main stream of sample material. This effect will tend to limit the ionization efficiency and is consistent with a measured ionization efficiency of 10^{-4} for toluene at 8 kV blade-cathode

* Present address: Linus Pauling Institute of Science and Medicine, Menlo Park, Ca. 94025.

potential difference. The growth of microneedles in the region between the blades may greatly improve the ionization efficiency, but with accompanying deterioration of the ion optical characteristics. The razor blades used in the source described here were uncoated Gillette Super Stainless and do not provide as effective a substrate for microneedle growth as tungsten.

The ionization efficiency of the double blade source was up to a factor of ten better than that of a single blade for the same sample pressure change in the source chamber. It appears that an overall improvement in the double blade source can be accomplished by replacing the stainless steel razor blades with etched tungsten blades.[3] The etched tungsten is sharper than the commercial razor blades and consequently will shift the effective ionizing region closer to the gap. By using etched tungsten blades and closer blade spacing (made possible with the 90° geometry), improvements in ionization efficiency by one or two orders of magnitude should be effected.

The financial support of the National Science Foundation (Grant MPS-72-05129A02) and the National Aeronautics and Space Administration (Grant NGL 05-003-003) is gratefully acknowledged.

References

1. J.-P. Pfeifer, A. M. Falick and A. L. Burlingame, Int. J. Mass Spectrom. Ion Phys. 11, 345 (1973).
2. D. F. Brailsford and A. J. B. Robertson, Int. J. Mass Spectrom. Ion Phys. 1, 75 (1968).
3. R. E. Ardrey, D. B. Hibbert, A. J. B. Robertson, P. J. Derrick, M. A. Baldwin, J. T. Hill and R. P. Morgan, Int. J. Mass Spectrom. Ion Phys. 19, 415 (1976).

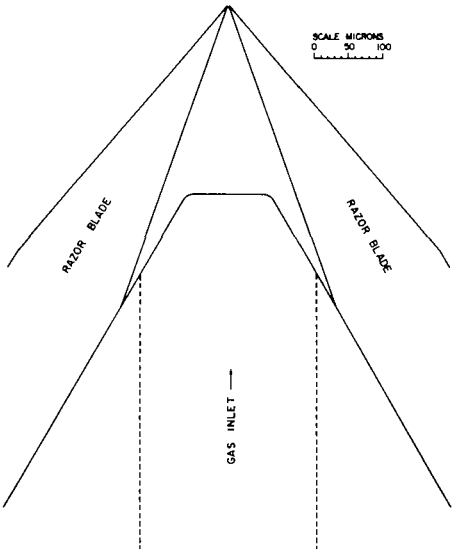

Fig. 1. Enlarged cross sectional view of double razor blade source.

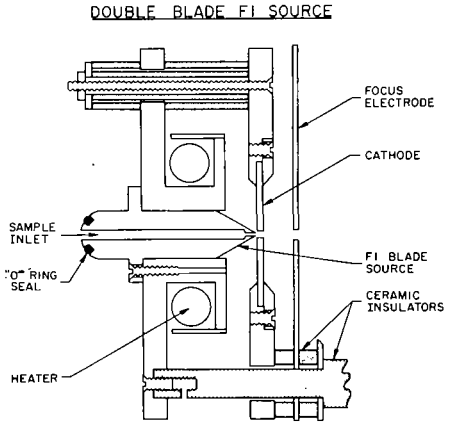

Fig. 2. Schematic of the same source.

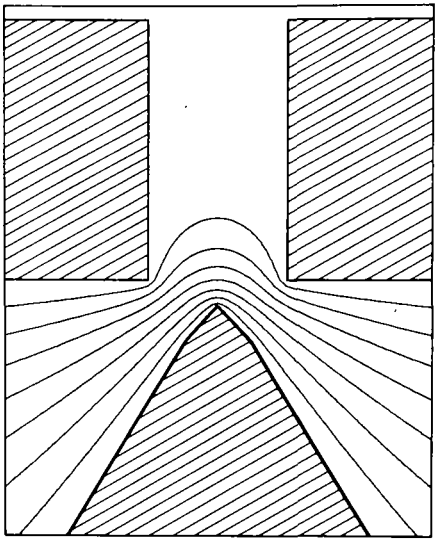

Fig. 3. Potential field plot of the region between the double blade source and extraction cathode.

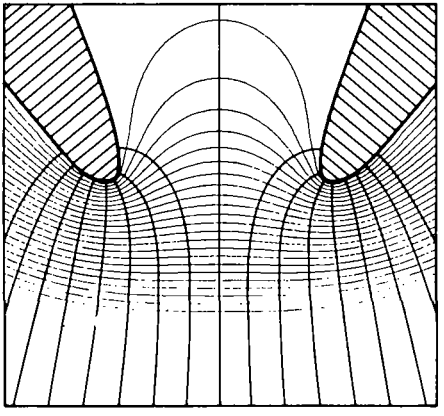

Fig. 4. Potential field plot of the double blade tip region. The electric field lines emanating from the blade edges have been added to show the focusing nature of the electric forces.

A Field Ionization/Field Desorption (FI/FD) Source for AEI-MS9 and MS50 Mass Spectrometers

G. K. Eigendorf and C. A. McDowell

University of British Columbia
Department of Chemistry
2075 Wesbrook Place
Vancouver, British Columbia
Canada V6T 1W5

Abstract

Initial results from the development of a FI/FD source for AEI-MS9 and MS50 mass spectrometers are presented.

****

Two basic source designs (Fig. 1) are presently under investigation. Type A utilizes a standard* source block through which a cylindrical passage (dia. 15 mm) has been machined. A filament anode, positioned 2 mm from the cathode, is operated at a potential of +8 KV, while the latter (standard slit plate) is maintained at -2 KV. A pair of standard half-plates operates at a variable potential of up to 1.8 KV, with a maximum gradient of 90V between the plates. The original slit at ground potential as well as the y- and z-deflectors have been maintained. This source can also be operated in the electron impact mode (EI filament and trap have been omitted in Fig. 1A) by replacing the filament anode with a circular repeller plate.

Source B has been machined in standard dimensions from DuPont Vespel SP1. To operate, an anode potential of +9 KV is applied while the cathode is operated at -3 KV. An additional lens (standard slit plate) is supplied with a maximum of +4 KV. The remainder of the source is identical to type A. Independent high voltage power supplies are utilized for the FI/FD experiments.

Using standard components, either source is mounted on a flange equipped with sixteen high voltage ceramic feed-throughs. A vacuum tight seal to the source housing can be achieved by utilising either a gold gasket or a Viton O-ring. With suitable modifications the standard AEI source endplate can also be employed.

The probe carrying the anode emitter is introduced via a vacuum lock attached to the flange. The lock has been fashioned after the Schulten-Beckey[1] design and incorporates a micromanipulator, a Goddard high vacuum valve and an axial adjustment permitting variation of the anode to cathode distance. Pumping for the probe lock is achieved via existing vacuum lines.

For this study commercially available emitters (Aurotech) have been used. Samples were applied by the dipping technique and in FI mode, the original inlet systems were employed. Data were recorded using the standard electron multiplier and recorder. Spectra have been successfully obtained on a variety of materials, and in particular members of the carbohydrate family (i.e. Fig. 2, D-glucitol-hexaacetate) and various porphyrins (Fig. 3, tetraphenylporphyrin) have been analyzed.

* Throughout this paper the term standard refers to original AEI parts.

ACKNOWLEDGEMENT

The authors would like to thank Dr. H.D. Beckey and Dr. H.R. Schulten for technical design information. We are also indebted to the National Research Council of Canada for very generous grants in aid of our research programme.

REFERENCES

1. H.R. Schulten and H.D. Beckey, Org. Mass Spec., 7, 861 (1973).

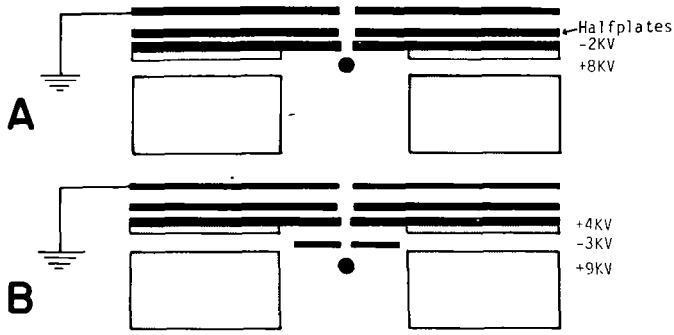

Fig. 1. FD source for use with AEI-MS9 and MS50 mass spectrometers.

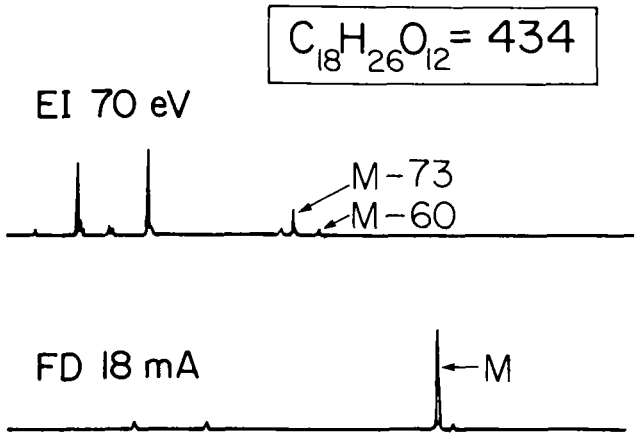

Fig. 2. EI/FD spectra of D-glucitol-hexaacetate.

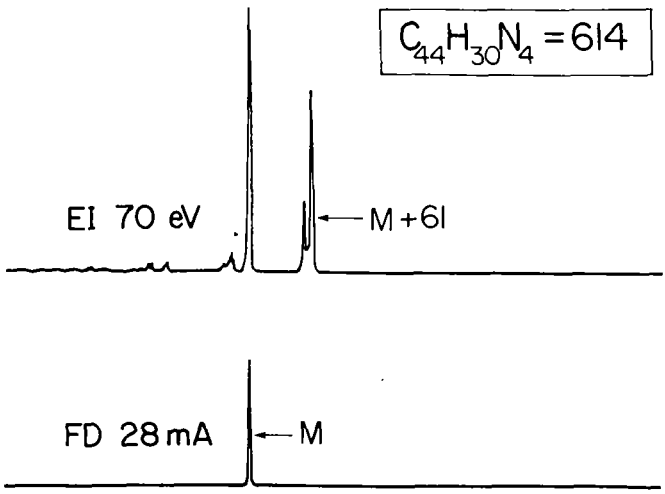

Fig. 3. EI/FD spectra of tetraphenylporphyrin, (M+61 due to capture of Cu within ion source).

Comparative Efficiencies of Various Types of Field Ionization Sources, H. L. Brown, R. H. Cross and M. Anbar, Stanford Research Institute, Mass Spectrometry Research Center, Menlo Park, CA 94025

We have measured the absolute ionization efficiency of multipoint FI sources and their relative efficiencies compared with activated wire sources and with a newly developed activated tungsten foil source.

The apparatus used consists of the following equipment. First is a gas sample feed system (Figure 1), which allows introduction of a well-known, steady sample feed to an ionizer through a heated probe containing a fixed leak calibrated in situ. The sample flow rate into the source is controlled by maintaining a given pressure in the ballast volume with a Baratron-APC combination.

Test sources are installed in the spectrometer shown in Figure 2. Mass separation is accomplished by a Colutron velocity filter with mass dispersion in the vertical plane. The ion beam is extracted at 5 keV and focused by a pair of einzel lenses. Horizontal and vertical deflectors are used for beam shims and to allow off-axis detection by either an electron multiplier or a microchannel plate image intensifier. The multiplier entrance is masked to a slit smaller than the beam image at that point, so that we determine relative current densities of sources, allowing a fixed collector geometry regardless of the size and shape of the source. Image areas and, therefore, total ion current, can be estimated using the image intensifier. Data are made absolute by determining the transmission of this instrument and others with a standard source whose total ion output was previously measured using a large faraday cup in a separate bell jar experiment. The probe, the source, and the inlet system were all transferred from the bell jar to the spectrometers.

Figure 3 shows the FI multipoint source presently in use in our laboratory. The counter electrode screen is stretched and clamped as shown with the spacing to the emitter points adjusted by shimming. The source is assembled with ruby ball insulators and heated by the peripheral heaters on the counter electrode fixture. The interior is chrome blacked to insure good radiative contact and nearly uniform temperatures over the entire source. For 1-butene absolute efficiencies range from 1.4×10^{-7} ions/molecule to 6.2×10^{-7} ions per molecule for this source. Weighed thymine samples yield absolute efficiencies of 4 to 10×10^{-5} ions/molecule.

We obtained wire emitters from Professor Beckey and mounted them in lieu of the multipoint pedestal shown in Figure 3, using the fixture shown in Figure 4. Our intent was to standardize as many operating parameters as possible. First, we placed the emitter $\sim 50\ \mu$ from a grid counter electrode; we directed sample flow to the activated area by means of the tube shown; and we used emitter-counter electrode potentials similar to those used for

multipoints. The ionizing fields developed at the tip of the activation were the same as for multipoint sources under similar conditions, and the same as those obtained in the conventional high voltage-large spacing operation of wire emitters.

Figure 5 summarizes the relative efficiency measurements. These data are uncorrected for the spectrometer transmission efficiency, which was 1.1×10^{-4}.

We conclude that the lower efficiency of the wire emitters is due to less effective sample feed both in our experiment and also in the conventional use of wire emitters, since ionization efficiency of sample which finds itself within the ionizing volume surrounding an emitter tip should not differ for the two styles of sources. Further, the activated wire emitters are known to be efficient FD emitters.

The conclusion led us to develop a new source shown in Figure 6 where two razor blades are mounted in an edge to edge wedge configuration with sample flowing between them. The source was found to achieve efficiencies within a factor of two of activated multipoint FI sources but it was necessary to activate this source by operating it for a period of several days.

Low temperature activation, however, is fragile and easily removed if electronegative compounds are introduced into the source; therefore, the razor blades have been replaced by tungsten shim stock whose ionizing edge has been high temperature activated using the techniques employed by Beckey, Barofsky and others for activating wire emitters. These sources are as efficient as well activated multipoint sources and as inexpensive and rugged as activated wire emitters.

In conclusion, the efficiency of multipoint FI sources was found to vary from 1.4×10^{-7} ions/molecule to 1×10^{-4} ions/molecule depending upon the source and substance ionized. Activated wire FI sources were found to be 10 to 100 times less efficient than multipoint FI sources. A new source has been developed combining the advantages of high temperature activated FI emitters with the high efficiency of the multipoint sample feed arrangement. The performance of this new source is exemplified in the analysis of coal liquefaction products, paper V2.

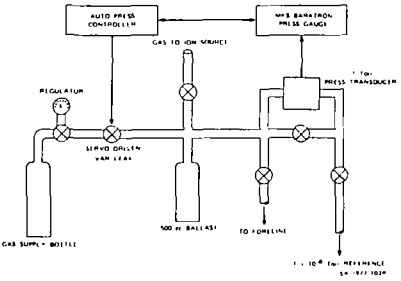

Figure 1

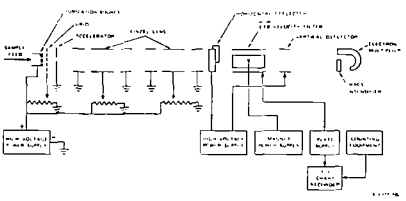

Figure 2

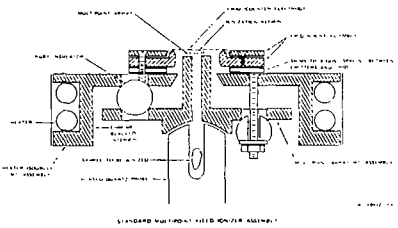

Figure 3

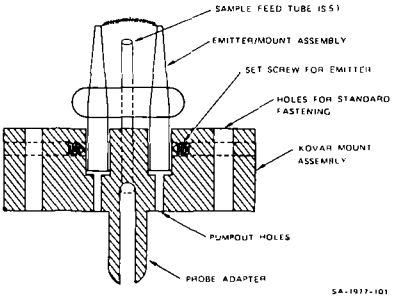

Figure 4

Figure 5

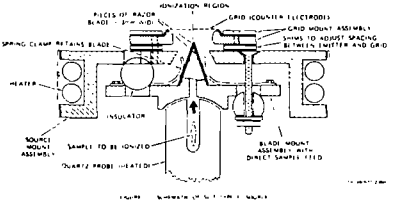

Figure 6

Structural Determination by Combined Field Ionization - Collision Induced Dissociation, J. H. McReynolds, M. Anbar and W. Aberth, Stanford Research Institute, Mass Spectrometry Research Center, Menlo Park, CA. 94025

A combined field-ionization-collision induced dissociation instrument has been constructed to allow the structural identification of individual components in a complex mixture. This technique promises to be especially useful in the field of chemical diagnosis where the molecular weight profiles of physiological fluids obtained by FIMS have been shown to have diagnostic value.[1]

An existing single focusing magnetic sector was modified by adding a differentially pumped collision cell and a spherical electrostatic sector designed according to parameters calculated by Ewald.[2] A schematic of the instrument is given in Fig. 1 with its ion optical parameters listed in Table 1. Both the magnetic and electrostatic sectors are stigmatic focusing so that a high transmission is achieved allowing collisional spectra to be recorded using sample sizes less than 1 μg per component.

Collisional spectra are recorded on a multichannel analyzer which sweeps the energy analyzer via the circuit shown in Fig. 2. This circuit uses two Kepco programmable power supplies to provide the sector voltages with a feedback circuit consisting of amplifiers 4 and 5 to maintain both voltages equal. Figs. 3, 4, and 5 show several spectra taken with the instrument using a multipoint field ionization source, ion energy of 5 kV and H_2 as the collision gas. These spectra are qualitatively similar to EI spectra and show that it may be possible to distinguish isobaric species in complex mixtures using FI-CD spectrometry. Complete details of this work have been submitted to the International Journal of Mass Spectrometry and Ion Physics. This work was supported by a NIH Grant GM 21835.

References

1. Anbar, M., Dyer, R. and Scolnick, M. E., Proceedings of the 24th Annual Conference on Mass Spectrometry and Allied Topics, San Diego, May 1976, paper J8.
2. Ewald, H., Z. Naturforschg. 14a, 680-681 (1959).

Table 1. Ion Optical Parameters

$r_m = 254$ mm $\phi_m = 90^\circ$ $\epsilon' = \epsilon'' = 26.5^\circ$

$r_e = 254$ mm $\phi_e = 90^\circ$; $c = 1.0$; $c' = 1.4$; $q'' = -0.167$ re

$l'_m = l''_m = 508$ mm, $l'_e = l''_e = 254$ mm

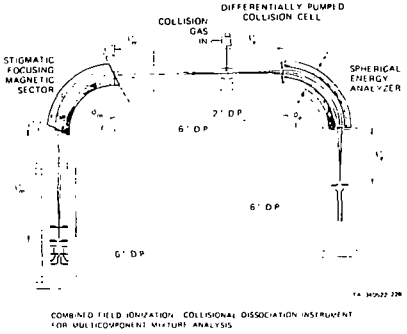

Figure 1

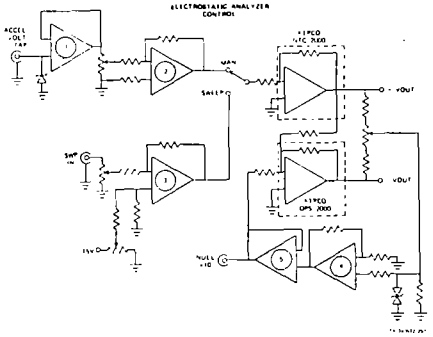

Figure 2

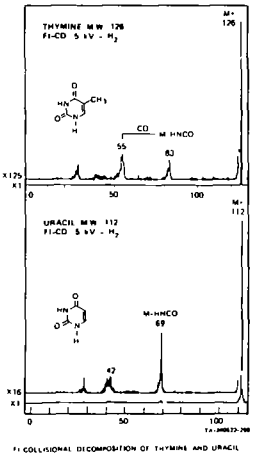

FI COLLISIONAL DECOMPOSITION OF THYMINE AND URACIL

Figure 3

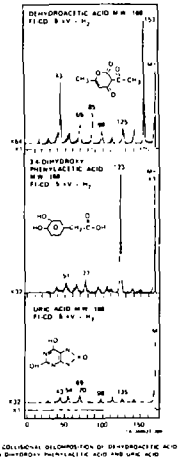

FI COLLISIONAL DECOMPOSITION OF DEHYDROACETIC ACID
3,4-DIHYDROXY PHENYLACETIC ACID AND URIC ACID

Figure 4

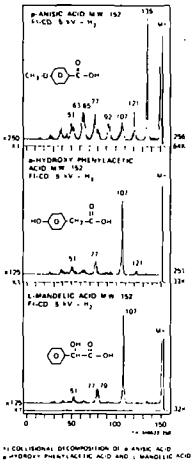

FI COLLISIONAL DECOMPOSITION OF p-ANISIC ACID
p-HYDROXY PHENYLACETIC ACID AND L-MANDELIC ACID

Figure 5

GC/MS Analysis of Low Level Contaminants in Tap Water by Direct Water Injection.

R. G. BEIMER, E. M. CHAIT, B. N. COLBY. E. I. Du Pont de Nemours, 1500 S. Shamrock Ave., Monrovia, CA 91016.

The determination of light hydrocarbons, aromatics and chlorinated materials in tap water can be most easily accomplished by direct injection thus eliminating the need for extraction. To accomplish this task a very sensitive GC/MS system is required since the levels of these materials in water are typically in the low PPM and PPB range. Water samples from several major U.S. cities have been analyzed using the Du Pont Dimaspec GC/MS system. Data will be presented to show the type of materials present and the approximate concentrations. The techniques used to obtain data on water samples will be discussed as well as the limits of detection for various materials. The types of GC columns which are compatible for water analysis will be discussed relative to their applicability and specificity to various types of impurities.

Elemental Composition Chromatography (ECC): The Characterization of Complex Mixtures of Organic Substances in Aqueous Effluents. A. L. BURLINGAME, B. J. KIMBLE, E. SCOTT and F. C. WALLS, Space Sciences Lab., Univ. of California, Berkeley 94720

Glass capillary gas chromatography/real-time high resolution mass spectrometry (HRGC/HRMS) has permitted the development of elemental composition chromatography (ECC).

This technique has been applied to the study of mixtures of organic substances of extreme complexity, especially the trace organic composition of aqueous effluents, cf. municipal and industrial waste waters, urine, etc.

The scope and limitations of its use will be contrasted with analogous data sets obtained using nominal mass spectrometry.

Acknowledgements: National Institutes of Health Grant RR 719 03 and National Aeronautics and Space Administration Grant NGL 05-003-003.

Studies of Volatile Metal Compounds with Chemical Ionization Mass Spectrometry. S. R. PRESCOTT, P. C. JURS, T. H. RISBY, Chem. Dept., Penn State Univ., Univ. Park, Pa. 16802

Various volatile compounds of several first row transition metals have been analyzed by chemical ionization mass spectrometry. The carbonyls of V, Cr, Mn, Fe, Ni, and Mo all have sufficient volatility to give spectra with large ion current intensities in the parent region. The spectra were recorded using methane and isobutane as reagent gases by subliming crystals of the compounds off the direct insertion probe at 100° - $130^{\circ}C$ depending on the volatility of the carbonyl. Gaseous carbonyls were run in ambient air to determine the feasibility of chemical ionization mass spectrometry for environmental analysis. A sensitivity study on $Ni(CO)_4$ was undertaken due to its extreme toxicity at low concentrations (1 ppm). Two other environmentally important metals, Pt and Pd, were analyzed by preparing volatile chelates with the ligand H(tfa) 1, 1, 1-trifluoro-2, 4-pentanedione. Modifications of literature syntheses were employed to prepare the chelates. Sensitivity studies on both chelates have been done. Direct injections of toluene solutions of the chelates were made into the ion source using successive dilutions starting with 10 ppm Pt and Pd. The results of these sensitivity studies will be discussed.

NATURE OF IONS OBSERVED IN PLASMA CHROMATOGRAPHY

F.W. Karasek, Univ. of Waterloo, Dept. of Chem., Waterloo Ont. N2L 3G1

Plasma chromatography (PC) allows observation of the characteristic positive and negative ionic mobility spectra of nanogram and picogram quantities of organic compounds at atmospheric pressure. The mobility spectra give qualitative and quantitative information for organic compounds. The method involves reaction of organic molecules with ions and electrons generated by a ^{63}Ni source in a nitrogen carrier gas, followed by mobility separation of the products in an ion-drift spectrometer. A recent review and its references describes the technique and summarizes its capabilities (1).

Plasma chromatography is particularly well-suited for selective detection of gas chromatographic effluents at sub-nanogram levels. To use PC as a qualitative detector it is very desireable to have available a large number of reference mobility spectra as well as a knowledge of the general type of spectra produced for different classes of compounds. A number of mobility spectra have been reported previously as part of a general study of the applicability of the plasma chromatographic technique to the detection of GC effluents. While the reference mobility spectra can be used alone as finger print patterns for identification, their value is enhanced by assigning identification to the ionic peaks involved. In previous spectra identity of the ionic peaks observed has been postulated based on an apparent relationship of positive mobility spectra to chemical ionization (CI) mass spectra, combined with information obtained from an approximate mobility - mass relationship. The procedure we have followed is to postulate ionic assignments in the mobility spectra by comparing these spectra to spectral patterns in their counterpart CI mass spectra. The CH_4CI mass spectra are generally the most available, but when CI spectra are not available, then the type of CI mass spectra produced by compound classes are used for guidance. The reasonableness of the ionic assignments made are then checked using an approximate mobility - mass curve. By application of this procedure the positive mobility spectra of most compounds are found to exhibit prominent ions of the MH^+, M^+, $(M-H)^+$, $(MNO)^+$ type, along with those fragment ions most abundant in the CI mass spectra.

Only those compounds undergoing electron attachment reactions producing stable ions exhibit negative mobility spectra. The ionic assignments made for these spectra are accomplished using data from studies of associative and dissociative electron capture for the gas chromatographic electron capture detector and mobility considerations of the observed ions. The negative mobility spectra appear to be primarily the ions of M^-, $(M-H)^-$, along with simple dissociated fragment ions.

Although ion identities postulated by these indirect methods are very useful in advancing our understanding and further development of the PC method and

instrumentation, the procedure does not give a positive identification to each ion. For identity of the exact mass associated with an ionic peak in the mobility spectra, an interfaced plasma chromatograph/mass spectrometer (PC/MS) system is needed. A directly coupled plasma chromatograph - mass spectrometer combination is capable of producing three types of spectra: mass spectra of all ions produced in the plasma chromatograph, ion mobility spectra using the total ion monitor of the mass spectrometer, and specific ion mobility spectra by tuning the mass spectrometer to selected m/e values. The combination of these spectra confirmed the masses associated with each ionic peak in the mobility spectrum of both the reactant ions and product ions of heroin, cocaine and p-nitrophenol (2,3). These identified ions agree closely with those predicted using the approximate method previously described. Figure 1 shows the comparison for heroin and cocaine. Of these compounds only p-nitrophenol showed a negative product ion of (M-H).

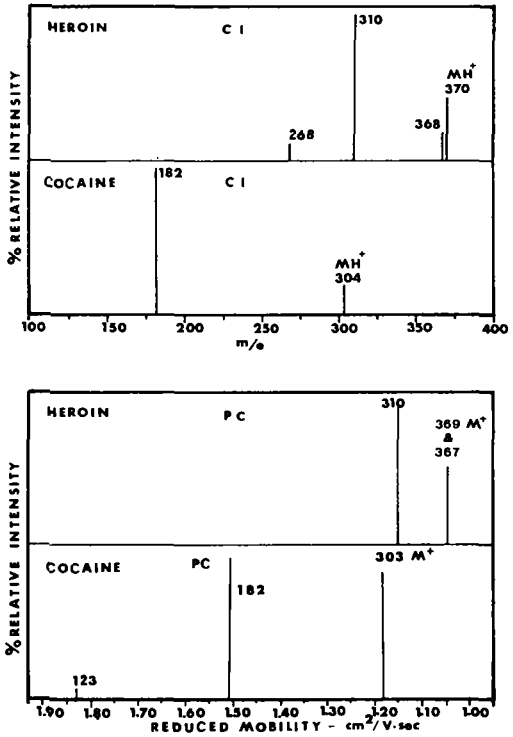

Fig. 1. Comparison of CH_4CIMS data with ion mobility data for heroin and cocaine. Spectra were normalized to the most intense peak. Reduced mobility values were obtained from the Beta/VI plasma chromatograph.

These data indicate that the indirect method can predict reasonably well the types of ions involved in ion

peaks in PC mobility spectra. Considering the relative simplicity of the PC instrument, compared to the PC/MS, an identity assignment of product ions by the indirect method gives sufficiently analytically useful results to justify its use.

Details of the work presented in this paper can be found in references 2 and 3.

This work was supported by the National Research Council of Canada, Grant No. A5433

References

1. F.W. Karasek, Anal. Chem., 45, 710A (1974)

2. F.W. Karasek, H.H. Hill, Jr., and S.H. Kim, J. Chromatogr., 117, 327 (1976)

3. Mass Identified Mobility Spectra of p-Nitrophenol and Reactant Ions in Plasma Chromatography, F.W. Karasek, S.H. Kim and H.H. Hill, Jr., ANAL. CHEM. (In Press)

LEVELS OF TETRACHLORODIBENZO-p-DIOXIN IN ENVIRONMENTAL AND BIOLOGICAL SAMPLES AS DETERMINED BY GAS CHROMATOGRAPHY-HIGH RESOLUTION MASS SPECTROMETRY

M. L. Taylor, R. L. C. Wu, C. D. Miller, and T. O. Tiernan

Department of Chemistry
Wright State University
Dayton, Ohio 45431

The development of analytical methodology for determining 2,3,7,8-tetrachlorodibenzo-p-dioxin (TCDD) present in biological samples at concentrations on the order of 10^{-12} g TCDD/g of sample (1×10^{-12} g/g = 1 part per trillion) has been prompted by literature reports of the extreme toxicity of this compound (1,2) as well as activity within the Environmental Protection Agency which is attempting to assess the environmental burden of TCDD and the threat TCDD may pose to human health. Since methods of sample preparation which are currently in use are incapable of completely isolating TCDD from constituents of the biological sample matrix and commonly encountered pollutants which are structurally very similar to TCDD, an instrumental method has been sought which will enable determination of TCDD in the presence of comparatively high concentrations (10^2- 10^6 that of TCDD) of potential interferences (polychlorinated biphenyls, DDE).

In our laboratory we have developed a method similar to that reported by workers at Dow (3) which employs gas chromatography-high resolution mass spectrometry to quantify TCDD in extracts from biological samples. Details of the method are given below.

Instrumentation: Varian 1440 Gas Chromatograph coupled thru an AEI Silicone Membrane Separator to an AEI Scientific Apparatus MS-30 Double Beam Mass Spectrometer.

Conditions for Chromatography: A 5' x 1/8" O.D. coiled glass column packed with 3% OV-101 on Chromosorb W H/P was used. Carrier gas, Helium @ 40 cc/min. Column Temperature, 230°. Injector Temperature, 220°.

Separator Temperature: 210°
Mass Spectrometer Source Temperature: 250°
Mass Spectrometer Resolving Power: 1:13,000 (Static, 10% Valley)
Data Acquisition: Nicolet 1072 Signal Averager

In order to accomplish high resolution mass spectrometric determination of TCDD the MS-30 was modified by introduction of a special scan circuit shown schematically in Figure 1. The circuit permits the ESA voltage to be scanned repetitively (20 scans/second) over a narrow portion of the mass scale (0.3 AMU) which brackets the base peak for TCDD at 321.8936. In practice, scanning is begun as the TCDD elutes from the gas chromatographic column and enters the mass spectrometer source and is continued until the peak has completely eluted. Other compounds eluting from the gas chromatographic column are, within the limits of the resolving power of the mass spectrometer, distinguished from TCDD mass spectrometrically. Figure 2 shows the resolution of mass peaks observed following injection of a standard solution containing Aroclor 1254,DDE and TCDD. It should be noted that the relative amounts of Aroclor 1254 and DDE are considerably greater than TCDD (96 nanograms of Aroclor were injected along with 76 nanograms DDE and 110 picograms of TCDD). Figure 3 (top) shows an accumulated signal for a liver extract which after comparison with a signal obtained for a TCDD standard (Figure 3 bottom) was found to contain no measurable TCDD. Results of a recovery study

performed on beef fat extracts are shown in Table 1. Here TCDD was added to these extracts and subsequently determined by GC-High Resolution MS in our laboratory.

In conclusion, the gas chromatographic-high resolution mass spectrometric method described above has been implemented in assaying approximately 100 extracts of beef adipose tissue and beef liver tissue and has been found to yield accurate results for samples containing parts-per-trillion concentrations of TCDD.

REFERENCES

1. B. A. Schwetz, J. M. Norris, G. L. Sparaschu, V. K. Rowe, P. J. Gehring, J. L. Emerson, and C. G. Gerbig in Chlorodioxins-Origin and Fate, American Chemical Society Advances in Chemistry Series #120. (E. H. Blair, Ed.). Washington, D. C., American Chemical Society, 1974, pg. 55.

2. J. L. Emerson, D. J. Thompson, C. G. Gerbig and V. B. Robinson, Toxicology and Applied Pharmacology 17, 317 (1970).

3. L. A. Shadoff and W. B. Crummett, Private Communication.

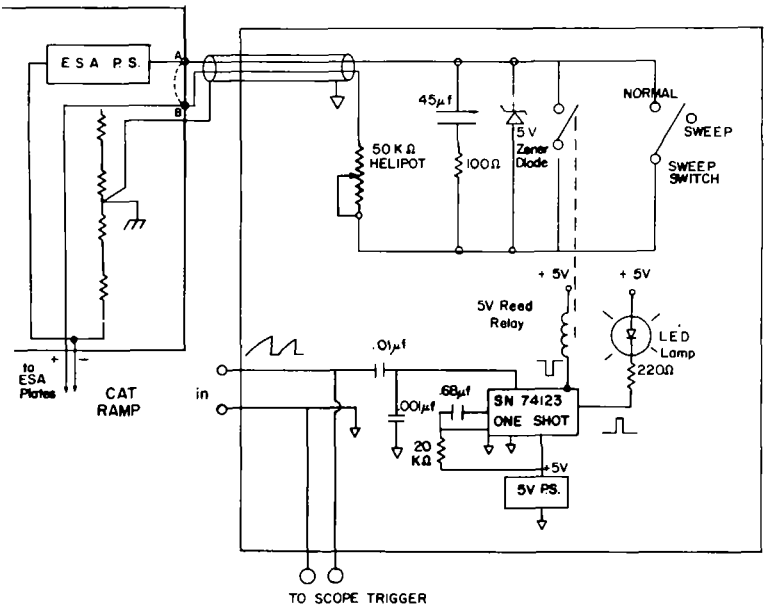

Fig. 1. Scan Circuit for Rapid Scanning of ESA Voltage

TABLE 1.

Results Obtained For Spiked Beef Fat Extracts

Sample I.D.	TCDD found (ppt)	TCDD added (ppt)	% Recovery
112	75	80	94
115	45	40	113
119	21	20	105

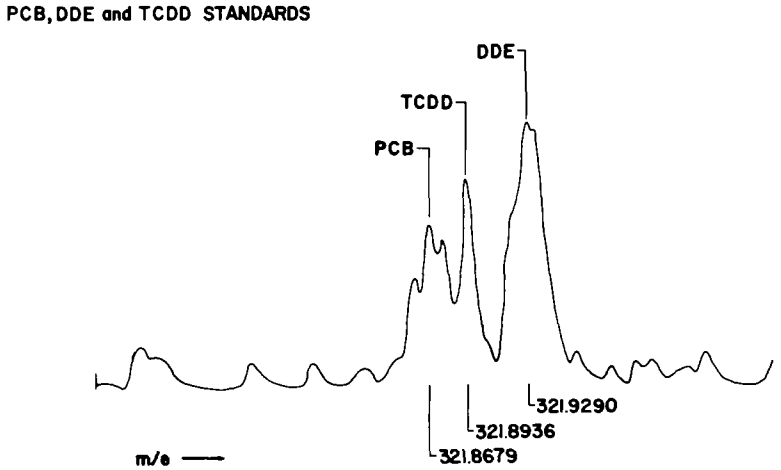

Fig. 2. Resolution of Mass Peaks Arising From Aroclor 1254, TCDD and DDE.

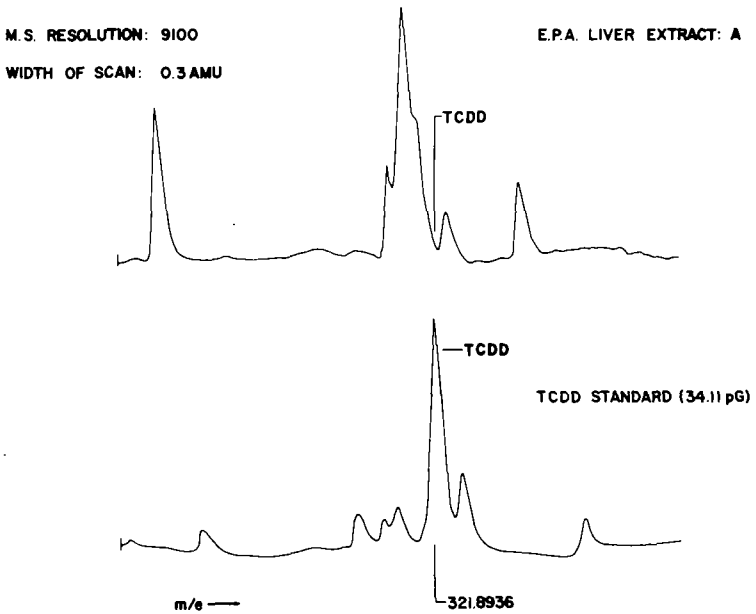

Fig. 3. Top: Accumulated Signal Obtained For EPA Liver Extract.

Bottom: Accumulated Signal Obtained For TCDD Standard.

The Application of New Techniques in GC/MS to the Analysis of Drugs and Complex Mixtures

P. Dobberstein, A. Zune, Varian MAT, Bremen, West Germany and W. A. Wolstenholme, Varian MAT Mass Spectrometry, Springfield, N.J.

Introduction

The use of capillary columns in GC work gives the chromatographer increased ability to separate very complex mixtures. The chromatograms are characterized by many sharp peaks the elution time of which is typically a few seconds. Furthermore, the sample quantities injected onto the columns are usually lower than for packed columns. Thus, for GC/MS studies capillary column work requires a combination of very high sensitivity and fast scan rate.

Recent work using a Varian MAT 311A high resolution GC/MS system for the analysis of tobacco smoke volatiles has shown that provided the basic performance of the spectrometer is high enough, the system can be operated at medium resolution with a combination of sensitivity and scan rate sufficient to provide molecular formulas from nanogram quantities eluted from capillary columns.

Experimental

A capillary column GC was interfaced directly to the ion source of a Varian MAT 311A mass spectrometer. This direct connection involves no molecular separator. The spectrometer used a turbomolecular pumping system which provided a very clean system with a pumping capacity sufficient to take the total He flow from the column.

In order to test the feasibility of analyzing the complex tobacco smoke mixture with sufficient sensitivity to analyze the minor components and obtain mass measurements with sufficient accuracy for molecular formula determination, two test mixtures were run. These mixtures contained from 1 to 10 ngm injected onto the column of compounds such as nicotine, phenol, limonene and furfuryl alcolhol. The spectrometer was scanned at a rate of 3 seconds per decade with a resolution of 3000 (10% valley). At this resolution the MAT 311A retains very high sensitivity since the instrument is capable of a resolution in excess of 25,000. The reference compound perflucrokerosene was admitted to the ion source throughout the run and spectra acquired by the SS 100 data system.

Following the successful runs with the test mixtures, a sample of the volatile constituents from tobacco smoke was run.

Results

Figure 1 shows a schematic of the GC and interfacing via the direct connection. Figure 2 shows the reconstructed GC trace from the tobacco smoke sample. The approximate quantities on the column for the furfuryl alcohol and dimethylphenol peaks were 5 ngm and 1 ngm respectively.

Figure 3 shows the element listing obtained from the data system for the furfuryl alcohol peak, and figure 4 shows similar data for the dimethylphenol. It can be seen that the accuracy of the mass measurements is very good and provides unambiguous assignments of the atomic compositions.

Summary

It is possible, using a high performance MAT 311A GC/MS system directly coupled to a capillary column GC, to obtain accurate mass measurements and thus molecular formulas from nanogram quantities in complex mixtures.

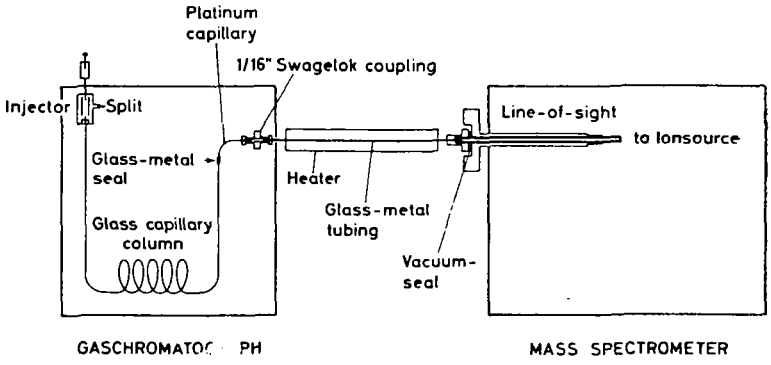

Figure 1: Schematic Diagram of Direct Coupling between GC and MAT 311A Mass Spectrometer

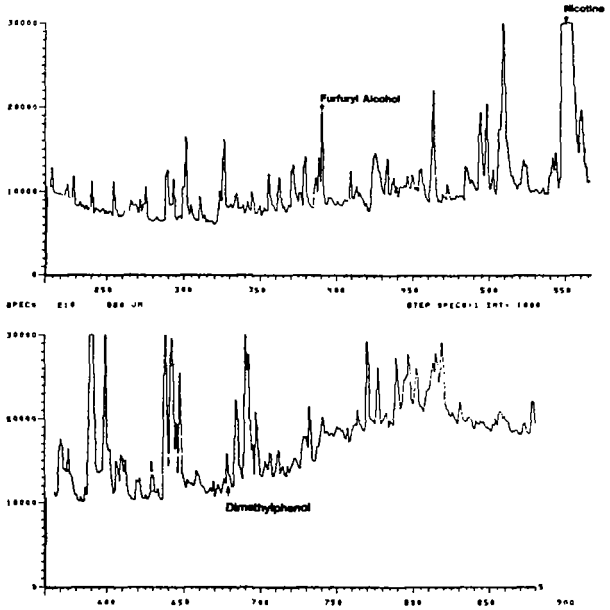

Figure 2: Reconstructed GC trace from Tobacco Smoke Condensate

>>DATE<<<SPEC# 390/FM/FURFURYLALCOHOL

BASE PEAK 5931 / MASS 98

PEAK	I/BASE	MASS	DIFF	C 12	H 1	O 16	
46	24.27 %	50.0133	-2.3	4	2	0	
50	85.19 %	53.0019	-0.8	3	1	1	
79	64.15 %	69.0201	-3.9	4	5	1	M-CH_2O
80	9.23 %	69.0662	-4.2	5	9	0	
88	3.77 %	72.0215	0.3	3	4	2	
99	14.19 %	81.0323	-1.8	5	5	1	M-OH
104	4.72 %	83.0487	-0.9	5	7	1	
107	4.88 %	85.0249	-4.0	4	5	2	
120	3.09 %	94.0464	4.5	6	6	1	
121	14.31 %	95.0175	4.3	5	3	2	
122	7.50 %	95.0867	0.7	7	11	0	
125	42.49 %	97.0292	0.2	5	5	2	M-H
126	5.05 %	97.0777	-1.8	7	13	0	
127	100.00 %	98.0375	0.7	5	6	2	M
130	7.25 %	99.0434	-1.1	5	7	2	

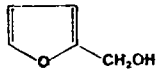

MW: 98

Figure 3: Element listing from approximately 5ngm furfuryl alcohol

>>DATE<<<SPEC# 678/FM/3,4 DIMETHYL PHENOL

BASE PEAK 10237 / MASS 107

PEAK	I/BASE	MASS	DIFF	C 12	H 1	O 16	
77	8.46 %	70.0426	0.7	4	6	1	
109	6.93 %	92.0475	0.2	7	8	1	
111	9.62 %	93.0724	2.0	7	9	0	M-CHO
125	6.08 %	101.0431	4.0	8	5	0	
126	5.55 %	102.0480	1.1	8	6	0	
127	12.57 %	103.0534	-1.3	8	7	0	
128	4.13 %	104.0687	0.1	8	8	0	
129	6.93 %	105.0675	-2.9	8	9	0	
131	100.00 %	107.0521	2.4	7	7	1	M-CH_3
133	12.41 %	108.0596	2.0	7	8	1	
135	23.65 %	110.0702	-3.0	7	10	1	
140	5.64 %	113.0389	-0.3	9	5	0	
143	7.83 %	115.0541	4.3	9	7	0	
144	6.44 %	116.0578	-4.7	9	8	0	
150	6.99 %	119.0676	-3.2	5	11	3	
153	32.85 %	121.0663	0.9	8	9	1	M-H
155	67.67 %	122.0738	0.6	8	10	1	M
156	7.31 %	123.0630	2.1	8	11	1	

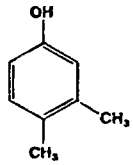

MW: 122

Figure 4: Element listing from approximately 1ngm dimethylphenol

QUANTITATIVE DETERMINATION OF PHENACETIN AND ITS METABOLITE ACETAMINOPHEN BY GC-MS

W. A. Garland, K.-C. Hsiao*, E. J. Pantuck* and A. H. Conney

Department of Biochemistry and Drug Metabolism
Hoffmann-La Roche Inc.
Nutley, N.J. 07110

and

*Department of Anesthesiology
College of Physicians and Surgeons
Columbia University
New York, N.Y. 10032

A gc-ms method has been developed that can measure 1 ng/ml of phenacetin and 0.1 μg/ml of acetaminophen in plasma or urine. Deuterated analogs of phenacetin and acetaminophen were added as internal standards to 1 ml of plasma, and the plasma extracted with 5 ml of benzene-dichloromethane (7:3). The solvent was evaporated, and the residue dissolved in methanol and treated with etheral diazomethane to methylate the acetaminophen. The mixture was then evaporated to dryness, and the residue reconstituted in 30 μl of ethyl acetate. An aliquot of this solution was analyzed by gc-ci-ms with the mass spectrometer (Finnigan 1015D) set by a Finnigan model 6000 data system to monitor m/e 180 (phenacetin), m/e 183 (phenacetin-d_3, $H_3C-\overset{O}{\overset{\|}{C}}-N-$ 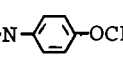 $-OCH_2CD_3$), m/e 166 (methylated acetaminophen, p-acetanisidine), and m/e 169 (p-acetanisidine-d_3, $D_3C-\overset{O}{\overset{\|}{C}}-N-$ 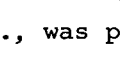 $-OCH_3$) in the gc effluent. The column, 1.2 in. x 2 mm i.d., was packed with 3% OV-17 on 100-120 mesh Gas Chrom Q and operated at 180-195°C.

Isobutane was used both as gc carrier gas and ci reagent gas. The isobutane ci mass spectra of phenacetin and acetanisidine are quite simple, consisting only of their MH^+ molecular ions.

For the determination of total acetaminophen (unconjugated and conjugated) in plasma, 0.1 ml of plasma and acetaminophen-d_3 were incubated at 37° for 16 hours with 0.4 ml of Glusulase (containing 16,000 units of β-glucuronidase and 64,000 units of sulfatase) in a final volume of 3.1 ml at pH 5.0. The sample was extracted with ethyl acetate, methylated with diazomethane and analyzed for p-acetanisidine and p-acetanisidine-d_3. For the measurement of conjugated and unconjugated acetaminophen in the urine, 0.1 ml of Glusulase was mixed with 0.1 ml urine, 1 ml of 0.2M sodium acetate buffer (pH 5.3), and acetaminophen-d_3 in a final volume of 3.1 ml. The sample was incubated at 37° for 16 hours, and the total acetaminophen was quantified as described above.

The curves relating the amount of phenacetin and acetaminophen added versus amount of phenacetin and acetaminophen found for 12 known phenacetin concentrations over the range 9.9 ng/ml to 246.6 ng/ml, and for 16 known acetaminophen concentrations over the range 0.52 μg/ml to 13.10 μg/ml, are straight lines with intercepts of nearly zero and with slopes of unity. Analyses of six separate plasma samples each containing 25 ng/ml phenacetin and 1.31 μg/ml acetaminophen had a precision of ± 1 ng/ml for phenacetin and ± 0.08 μg/ml for acetaminophen.

The benzene-dichloromethane (7:3) extracting solvent, used when both phenacetin and acetaminophen are to be simultaneously determined, was found to remove 95 ± 8% (n = 6) of the phenacetin and only 0.91 ± 0.12% (n = 6) of the acetaminophen. This allowed both compounds to be determined

from a single injection in spite of the commonly observed hundred to a thousand fold difference in their relative concentration. Ethyl acetate, used as an extracting solvent when only acetaminophen was to be determined, was found to extract 89 ± 18% (n = 6) of the acetaminophen.

For nine subjects, who received a 900 mg oral dose of phenacetin, the following data was obtained using the above assay.

1. average half life of phenacetin in plasma ± S.D. = 61 ± 4 minutes.
2. average phenacetin excreted in urine as % of the dose ± S.D. = 0.14 ± 0.02.
3. average acetaminophen (unconjugated) excreted in the urine as a % of the dose ± S.D. = 1.74 ± 0.23.
4. average acetaminophen (conjugated + unconjugated) excreted in the urine as % of the dose ± S.D. = 55.7 ± 2.6.
5. average phenacetin levels ± S.D. seven hours after dosing = 9 ± 3 ng/ml.

A manuscript fully describing the assay, including the synthesis of the stable isotope analogs, has been accepted for publication in J. Pharm. Sci.

A Single-Ion-Monitoring GC-MS Assay for Methylphenidate in Biological Media.* JOE GAL, BARBARA J. HODSHON, BRUCE L. FLAMM, ARTHUR K. CHO, and CAM PINTAURO, Univ. of California, School of Medicine, Dept. of Pharmacology, Los Angeles, Calif. 90024

A GC-MS assay based on single-ion monitoring has been developed for the determination of methylphenidate (MEPPA) in biological fluids and tissues. The internal standard used is the ethyl ester homolog (ETPPA) of MEPPA. The two compounds are extracted with hexane from the aqueous medium after saturation with ammonium carbonate (pH 8.8-9.0). The organic solvent is then evaporated and the residue is treated with trifluoroacetic anhydride. The resulting N-TFA derivatives of MEPPA and ETPPA are monitored at m/e 180 (N-trifluoroacetyl-Δ'-piperideinium ion), the base peak in the spectra of both compounds. The recovery of MEPPA is quantitative, and the limit of sensitivity is 1 ng/ml. The method was applied to the determination of the concentration of MEPPA in plasma and brain of rats treated with the drug intravenously.

*Supported by USPHS Grant DAQ-1057 and Contract ADM-45-74-178.

Quantification of Caffeine, Theophylline, Theobromine and 1,7-dimethylxanthine by Chemical Ionization Using N^+ and N_2^+. M. G. HORNING and J. NOWLIN, Baylor College of Medicine, Houston, Texas 77030

A method for the quantification of caffeine and the three dimethylxanthines in biological fluids has been developed based on chemical ionization using a 1:1 mixture of N^+ and N_2^+. Caffeine (M=194) can be separated by GC from the dimethylxanthines (M=208) following ethylation, but the three dimethylxanthines (theophylline, 1,3-; theobromine, 3,7-; and 1,7-dimethylxanthine) are not resolved, even on a capillary column. When chemical ionization is carried out with a 1:1 mixture of N^+ and N_2^+ (obtained by adjusting the voltages on the CI source), characteristic ions at m/e 95 (theophylline), m/e 109 (theobromine) and m/e 136 (1,7-dimethylxanthine) became the base peaks. Thus the three dimethylxanthines can be quantified in biological samples by SID although they are eluted in the same GC peak. Deuterated caffeine (7-trideuteromethyl-1,3-dimethylxanthine) was used as the internal standard for caffeine and the dimethylxanthines and a response factor was determined for each of the dimethylxanthines with respect to the internal standard.

DETERMINATION OF PHOSPHONOACETIC ACID IN SERUM BY CHEMICAL IONIZATION-MASS FRAGMENTOGRAPHY. JOHN ROBOZ, ROBERT SUZUKI, SHELDON SIVAKOFF, and GEORGE BEKESI, Mount Sinai School of Medicine, New York, New York 10029.

Phosphonoacetic acid (PAA) is a potent inhibitor of herpes simplex virus replication. Pharmacokinetic and metabolic data are needed because of possible implications in several types of cancer. Determination of PAA in serum: proteins are precipitated with cc $HClO_4$, lipids removed with methylenechloride, aqueous phase evaporated to dryness (N_2, 40°C), residue dissolved in BSTFA+1% TMCS: Pyridine (1:3), kept at 100°C for 5 min, and the unchanged intact circulating drug determined as tri-TMS derivative by monitoring the intensities and ratio of (M+1) and $(M-15)^+$ ions together with phosphonopropionic acid as internal standard. Detection limit: 100 ng/ml. Serum levels are presented for various therapeutic dosages for tumor-bearing mice, rabbits, owl and squirrel monkeys (virus-infected).

Supported by Grant #5P01-CA15936-03, from the National Cancer Institute, NIH.

Quantitative Analysis of Phenobarbital, Diphenylhydantoin and Clonazepam Using Atmospheric Pressure Ionization Mass Spectrometry. D. I. CARROL, I. Dzidic, R. N. Stillwell and E. C. Horning. Institute for Lipid Research, Baylor College of Medicine, Houston, Texas 77030

The quantitative analysis of several anticonvulsant drugs in human plasma extracts, using atmospheric pressure ionization mass spectrometry, will be discussed. Phenobarbital and diphenylhydantoin are relatively strong acids in the gas phase, and both compounds yield $(M-H)^-$ ions by reaction with Cl^-. The negative ions are used in the simultaneous quantification of these drugs using ^{13}C internal standards. The drug clonazepam forms a very stable negative ion by dissociative electron attachment which can be used for quantitative analysis. The fluorine analog of this drug, flunitrazepam, forms a related negative ion, and is used as an internal standard.

Identification of Drugs Using a GC/MS System Equipped with EI/CI and EI/FI/FD Ion Sources

A. Zune, K. H. Maurer, U. Rapp, Varian MAT, Bremen, West Germany and W. A. Wolstenholme, Varian MAT Mass Spectrometry, Springfield, N.J.

Abstract

A small double focussing GC/MS (Varian MAT 112) has been used to analyze biological extracts. The instrument is fitted with a combined EI/CI ion source which allows rapid changeover from one optimized ionization mode to the other. This is facilitated by an ion chamber, the geometry of which can be changed from outside the vacuum, and a duplicate set of source focussing controls.

Work has also been carried out using a combined EI/FI/FD source in the FI mode. It has been found that the FI spectra are very simple and exhibit some of the advantages of both EI and CI spectra. Thus, they exhibit intense peaks at the true molecular weight (rather than M+1 or M-1 in CI spectra). The sensitivity of the FI technique is in the nanogram range and has been shown to be well suited to the analysis of drugs in urine extracts.

The above results will be published in full in Journal of Chromatographic Science, 122, 365 (1976).

Clinical Diagnosis by Molecular Profiles of Metabolites in Urine, M. Anbar, R. Dyer and M. E. Scolnick, Stanford Research Institute, Mass Spectrometry Research Center, Menlo Park, CA 94025

Chromatographic separation techniques (e.g., GLC or HPLC) have been applied to multicomponent analysis of biological fluids with promising results.[1-4] Mass spectrometry, particularly non-fragmenting field ionization mass spectrometry, which produces molecular weight profiles of the analyzed sample, offers a number of advantages over the chromatographic techniques. It can provide quantitative and reproducible information on hundreds of nonpolymeric constituents of biological fluids in a relatively short time, and therefore at a relatively low cost.

We performed the field ionization mass spectrometric analysis of acid and/or neutral metabolites in human urine. Analyzing urine of patients with infectious hepatitis and comparing it with urine of normal subjects resulted in the demonstration of highly significant, distinctive patterns.

The extracted metabolites were analyzed by the multi-scanning field ionization mass spectrometric technique previously described.[5] The technique used in the present study was modified in the following respects: The multipoint ionization source was mounted on a low heat capacity mount which facilitates rapid heating and cooling of the ionization source structure. This feature facilitates the analysis of up to 2 samples per hour, including bakeout between each sample. The mass analyzer used was a modified 16 mm Extranuclear quadrupole (Model 270-9),[6] which simplifies considerably the multiscanning procedure. The analyzer was operated at a resolution $M/\Delta M$ of 250 at an overall efficiency of about 3×10^{16} detected ion counts/mole (i.e., 2×10^{14} counts/mole/amu when scanning over 150 amu) with a background of about 50 counts/amu. This sensitivity should allow the determination of 10^{-10} moles of a single substance in a multicomponent mixture. In general, spectra were reproducible to within ± 7% (relative standard deviation), about half of which was inherently due to counting statistics. The multiscanned spectra were accumulated in a multichannel analyzer, Nuclear Data ND 100 (4096 channels) and recorded on 9-track magnetic tape, which was used to transfer the data to a computer (Burroughs 6700).

The data were analyzed as follows: Each digitized spectrum was smoothed by the least squares procedure of Savitzky and Golay.[7] The threshold for peak detection was set at 2.5 times the noise level. Peak areas, corrected for noise level, were computed and normalized to unit total area.

The quality of the spectra of the neutral metabolites was uniformly superior to that of the acids. In both series we analyzed a total of 96 samples - duplicates of both normal and pathological specimens. These were treated as four separate groups: controls A and B and pathological A and B.

The Wilcoxon test was used to test the null hypothesis that two classes of data represent samples from the same population.

After normalizing each spectrum to unit total area, the areas of peaks at mass numbers where significant spectral differences occurred were then used as the variables in a diagnostic test. Our results indicate that in the molecular mass range 68 to 215 amu, we can use the areas of peaks at eleven different mass numbers in the case of acid metabolites and at twenty-four mass numbers in the case of the neutral metabolites.

In the series of the neutral metabolites, we were able to identify 113 peaks common to all four groups in the mass range 68 to 215 amu. The average spectra of one of the control (CA) groups and one of the pathological (PA) groups are presented in Figure 1.

The computation of p-values was performed as a measure of the pattern difference between the control and pathological spectra. To evaluate the significance of this pattern difference in terms of its diagnostic merit, weighted noncorrelation indices, WNI,[9] were computed for each spectrum. The WNI for comparing the ith spectrum to the average control spectrum is defined as

$$WNI_i(C) = 100 \sum_{j=1}^{J} \frac{\left| A_{ij} - \bar{A}_j(C) \right| r_j}{A_{ij} + \bar{A}_j(C)} \Bigg/ \sum_{j=1}^{J} r_j ,$$

where A_{ij} is the **normalized area of the** j^{th} **peak of the** i^{th} spectrum, $\bar{A}_j(C)$ is the jth average peak of the control group and r_j is a weighting factor. For peaks which have p values ≤ 0.1, a weight of 1.0 was assigned to r_j, otherwise $r_j = 0$.

The difference between weighted noncorrelation indices $D_i = WNI_i(C) - WNI_i(P)$, defines a discriminant function for distinguishing between two classes of data. D_i will be positive when the ith spectrum represents a pathological case and negative when it represents a control case. The differences D_i were computed for each of the control and pathological spectra. D_i represents a possible diagnostic criterion. For the case $D_i = 0$, the percent correct diagnoses averaged over pathological and control spectra was 91% in the case of the acid metabolites and 97.7% in each of the four neutral metabolite comparisons. However, for any value of D_i in the range of $0.027 < D_i < 2.8$, the percent correct diagnoses using neutral metabolites was 100% in all four comparisons, simultaneously.

Another figure of merit is the diagnostic power,[8] $0 \leq DP \leq 1$. The acid metabolite data yielded a DP of 0.82 while the more reliable neutral metabolite produced the maximum diagnostic power (DP = 1.00).

Our results with the neutral metabolites indicate that in the molecular mass range 68 to 215 amu, we can use the areas of peaks at twenty-four different mass numbers to distinguish between normal subjects and infectious hepatitis patients with correct diagnoses in all of the cases.

References

[1] A. Zlatkis, W. Bertsch, H. A. Lichtenstein, A. Tishbee, F. Shunbo, H. M. Liebich, A. M. Coscia, and N. Fleischer, Anal. Chem. 45, 763 (1973).

[2] R. Teranishi, T. R. Mon, P. Cary, A. B. Robinson, and L. Pauling, Anal. Chem. 44, 18 (1972).

[3] T. A. Witten, S. P. Levine, M. T. Killian, P.J.R. Boyle, and S. P. Markey, Clin. Chem. 19, 963 (1973).

[4] E. C. Horning and M. G. Horning, J. Chromatog. Sci. 9, 129 (1971).

[5] M. E. Scolnick, W. H. Aberth, and M. Anbar, I. J. Mass Spec. Ion Phys. 17, 139 (1975).

[6] M. Anbar and E. Kempster, I. J. Mass Spec. Ion Phys., in press.

[7] A. Savitzky and M.J.E. Golay, Anal. Chem. 36, 1627 (1964).

[8] F. Wilcoxon, Biometrics 1, 80 (1945).

[9] A. B. Robinson and F. C. Westall, J. Orthomol. Psychiat. 3, 1 (1974).

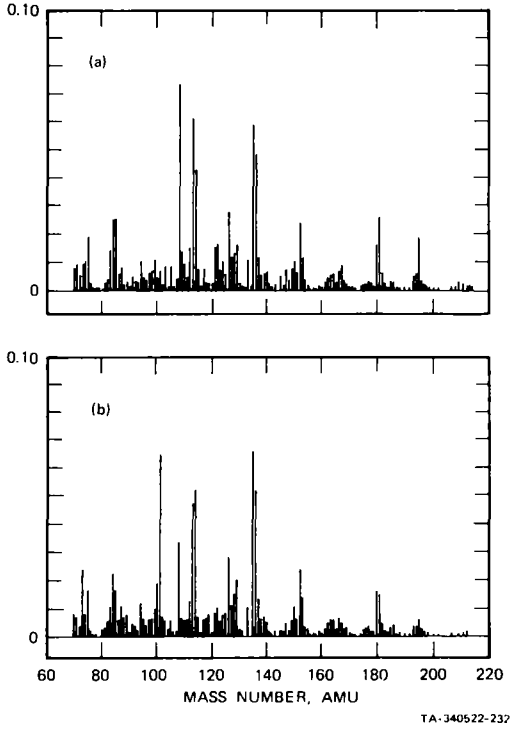

AVERAGE SPECTRA OF ONE OF THE CONTROL (CA) GROUPS (a) AND ONE OF THE PATHOLOGICAL (PA) GROUPS (b)

ACCURACY OF ORGANIC ANALYSIS BY ISOTOPE DILUTION-MASS SPECTROMETRY (ID-MS)

T. Sun, A. Cohen, H. S. Hertz, and R. Schaffer

Bioorganic Standards Section
Analytical Chemistry Division
National Bureau of Standards
Washington, D. C. 20234

In order to set up an accuracy basis for clinical laboratory measurements of organic constituents in blood serum, the National Bureau of Standards is participating in a program in which our laboratory is assigning accurate values for constituents in a series of serum samples. These samples are then used for evaluating the accuracy of the clinical results obtained by a group of clinical laboratories that perform a standardized clinical reference method for that constituent. The technique NBS is employing for assigning values is organic isotope dilution mass spectrometry. Thus far, techniques other than ID-MS are employed for the reference method measurements by the clinical laboratories.

The instrumentation being used in these measurements at NBS is a Varian CH-7A mass spectrometer with magnetic field switching capabilities for single ion recording. The instrument is interfaced to a Hewlett-Packard 9830 programmable calculator for data reduction. In measurements at m/e 250 with dwell times of 1 s, the reproducibility in magnetic switching over a 5 amu range is ±0.04 amu. Dynamic magnetic field drift over 0.5 h is ±0.02 amu and static field drift (obtained without magnetic field jumping) is -0.05 amu/h.

Initial determinations were made for glucose in serum. The sample handling consists of adding D-glucose-U-^{13}C (in H_2O) to the naturally occurring D-glucose in serum, at approximately a 3:1 ratio. (This gives an approximately 1:1 ratio of measured ions.) The serum is freeze-dried and the glucose is converted into 1,2:5,6-di-O-isopropylidene-D-glucofuranose (DAG). A purified mixture of DAG and DAG-^{13}C is isolated. The M-15 ions at m/e 245 and 250, respectively, are used for glucose determinations. In order to evaluate the possible occurrence of an isotope effect in the derivatization process, weighed mixtures of ^{13}C- and natural abundance glucose were converted to DAG and weighed mixtures of independently synthesized DAG and DAG-^{13}C were also prepared. The m/e 245/250 peak height ratios were measured for both sets of mixtures and plotted as a function of the known weight ratios. The results for both mixtures lay on the same straight line. The mixtures were used as standards.

In making measurements on unknown samples, each unknown is bracketed by a sample of the nearest higher and lower ratio DAG-^{13}C/DAG standard mixture, and these

measurements are rerun on several days. On consecutive days, the measurement sequence is alternated between high standard, unknown, low standard and low standard, unknown, high standard.

For the glucose in serum unknowns, the precision of our results is better than ±1%. More detailed measurements with glucose, and measurements with uric acid and other blood constituents are now in progress.

The authors wish to thank Dr. Don Ott, Los Alamos Scientific Laboratories for the D-glucose-U-^{13}C.

Identification of any commercial product does not imply recommendation or endorsement by the National Bureau of Standards, nor does it imply that the material or equipment identified is necessarily the best available for for the purpose.

Stereochemistry of Amphetamine Metabolism: A Study by Stable Isotope GC/MS.* JEREMY WRIGHT, JOSEPH GAL and ARTHUR K. CHO, Univ. of Calif., Dept. of Pharmacology, School of Medicine, Los Angeles, Calif. 90024

Inconsistent reports[1,2] concerning the metabolism of amphetamine type molecules prompted us to study the stereochemistry of R and S amphetamine metabolism. "Pseudo racemates" R-amphetamine-d_3: S-amphetamine-d_0 or R-amphetamine-d_0 : S-amphetamine-d_3 (2 mM) were incubated with 9000 g supernatant of rabbit liver homogenates and cofactors. Extracts (CH_2Cl_2) of 1 hr. incubations were derivatized with trifluoroacetic anhydride. Estimations of two of the major metabolites (N-hydroxyamphetamine, NHA, and phenyl-2-propanol, P_2P) by GC/MS using selective ion monitoring at masses 118 and 121 revealed that NHA and P_2P derived from S-amphetamine predominated by factors of 4 and 3 respectively, suggesting that S-amphetamine is the preferred substrate for deamination and N-hydroxylation reactions.

*Supported by USPHS Grant DAO-1057

[1] J. Gal, L. D. Gruenke and N. Castagnoli, Jr., J. Med. Chem., 18, 683 (1975).

[2] A. H. Beckett and S. Al-Sarraj, J. Pharm. Pharmacol., 24, 174 (1972).

Identification of New Meperidine Metabolites by Gas Chromatography-Mass Spectrometry. JAMES T. STEWART, M. G. HORNING, W. G. STILLWELL AND K. HAEGELE, Institute for Lipid Research, Baylor College of Medicine, Houston, Texas 77025 and School of Pharmacy, University of Georgia, Athens, Georgia 30602.

Studies on the metabolism of meperidine (I) were performed in rats and guinea pigs using unlabeled meperidine, the N-CD_3 and the $COOC_2D_5$ labeled drugs. In addition, samples of human urine containing meperidine were also investigated.

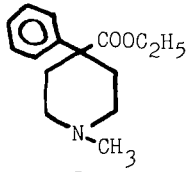

I

Following intraperitoneal injections of meperidine into the test animals, urines were collected, extracted and analyzed for metabolites by GC-MS. Mass spectra were generated on a LKB-9000 operated in the electron impact mode (70ev) Gas chromatrographic separations were performed using 5% SE-30 or 1% OV-17 on 80-100 mesh Gas Chrom Q. Sample introductions were via the GC inlet on the LKB-9000 and temperature programming was at 2-5° C/minute. Enzymic hydrolysis of the urine samples was accomplished with the use of Glusulase (Endo Laboratories, Garden City, N. Y.) for 16 hours at 37°C. The neutral and basic metabolites were isolated from the biological samples using the ammonium carbonate-methylene chloride extraction procedure of Horning et al.[1]

The following compounds have been identified from this study: meperidine N-oxide, p-hydroxyphenylmeperidine, N-hydroxymeperidine, N-formylmeperidine and meperidine N-carbamate. The latter two meperidine derivatives are believed to be artifacts arising from the use of methylene chloride and/or chloroform in the isolation procedures. Both compounds can be eliminated from the chromatograms by using other extraction solvents such as benzene.

Meperidine N-oxide (II) was found in human (trace amounts), guinea pig (major amounts), and rat (trace amounts) urine.

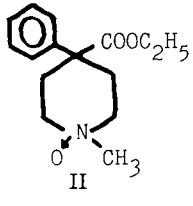

II

The mass spectrum shows parent ions at m/e 245 and 247 indicating loss of oxygen and water. The structure responsible for the m/e 245 has been shown to be a 4-ethoxycarbonyl-1-methyl-4-phenyl-1, 2, 3, 4-tetrahydropyridine (III).[2] Other investigators have reported the presence of the N-oxide in human urine.[2, 3]

The p-hydroxyphenylmeperidine (IV) metabolite was found in rat (major amounts) and guinea pig (minor amounts) urine. It was not found in human urine.

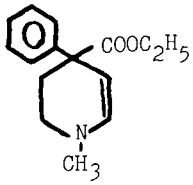

III

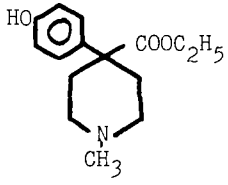

IV

A d_9-TSIM derivative (d_9-trimethylsilylimidazole) at m/e 335 proved the existence of the hydroxyl function. The assignment of the hydroxyl group to the para position is tentative and is based on analogy to the well known p-hydroxylation of other compounds. This metabolite has been recently reported to be in both rat and human urine.[4]

The N-hydroxy metabolite (V) was found in human, guinea pig (major amounts), and rat (trace amounts) urine after enzymic hydrolysis. The mass spectrum of the TMS derivative gives m/e 321. The compound was further verified by comparison with the mass spectrum of the derivative synthesized by the general procedure of Coutts et al[5] and by TLC using an ammoniacal nitrate spray.[5]

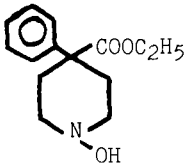

V

References cited

1. M. G. Horning, P. Gregory, J. Nowlin, M. Stafford, K. Lertratanargkoon, C. Butler, W. G. Stillwell and R. M. Hill, Clin. Chem., 20, 282 (1974).
2. C. Lindberg and C. Bogentoft, Acta Pharm. Scuec. 12, 507 (1975).
3. M. Mitchard, M. J. Kendall and K. Chan, J. Pharm. Pharmac., 24, 915 (1972).
4. C. Lindberg, C. Bogentoft, U. Bondessson and B. Danielsson, J. Pharm. Pharmac., 27, 975 (1975).
5. R. T. Coutts, R. Dawe and A. H. Beckett, Biomedical Mass Spectrometry, 2, 137 (1975).

GC-MS IDENTIFICATION OF p,p'-DIHYDROXYDIPHENYLHYDANTOIN AS A MINOR METABOLITE OF DILANTIN IN THE RAT AND HUMAN

Richard M. Thompson, Dept. of Peds., Ind. Univ. School of Medicine, Indianapolis, IN 46202; John Beghin and Wilmer K. Fife, Dept. of Chem., IUPUI, Indianapolis, IN 46218; and N. Gerber, Dept. of Pharmacol., Univ. of Ore. Med. School, Portland, OR 97201

Previously reported hydroxylated metabolites of Dilantin in the rat and human include p-hydroxyphenylphenylhydantoin (p-HPPH), 5-(3,4-dihydroxyphenyl)-5-phenylhydantoin, 5-(3-methoxy-4-hydroxyphenyl)-5-phenylhydantoin, and a dihydrodiol, 5-(3,4-dihydroxy-1,5-cyclohexadien-1-yl)-5-phenylhydantoin. In 1969 D.M. Woodbury (Epilepsia, 10, 121) postulated that p,p'-dihydroxydiphenylhydantoin (p,p'-dihydroxy-DPH) could also be a metabolite of Dilantin but he did not identify it rigorously.

We have now unambiguously characterized this compound as a metabolite present in the urine of the rat and human and in the bile from the isolated perfused rat liver by GC and GC-MS comparison of the permethylated derivative (MW=340) to the synthetic standard prepared from 4,4'-dihydroxybenzophenone by a standard hydantoin synthesis. In all cases this metabolite was excreted as the glucuronide and was determined after hydrolysis with either Glusulase, β-glucuronidase or acid. It comprised about 1% of the total hydroxylated metabolites, in human urine and rat bile. The hydroxyl group not involved in the conjugation was not methylated biologically. p,p'-dihydroxy-DPH was not a metabolite of p-HPPH in the rat.

Addition of synthetic p,p'-dihydroxy-DPH to the isolated perfused rat liver yielded the glucuronide, and minor glucuronides of a trihydroxy and a dihydroxymethoxy species. The position of conjugation in the latter two metabolites was undetermined.

An *in extenso* report of this work is being published in Drug Metabolism and Disposition.

The authors acknowledge financial assistance from the James Whitcomb Riley Memorial Association and the Public Health Service (NIH AM-17665, DA-00942, and NO-1-NS-5-2328).

MASS SPECTROMETER SENSITIVITY DATA FOR SELECTED COMPOUNDS, Bruce A. Petersen and Paul Vouros, Northeastern Univ., Boston, Ma. 02115 and Donald J. Marshall, Nuclide Corporation, Acton, Ma. 01720.

A knowledge of mass spectrometer sensitivity information is useful for several reasons including:

1) It facilitates the evaluation and monitoring of instrument performance on a continuing basis.
2) It is useful in making predictions of instrumental performance from one sample to another.
3) It is useful in making predictions of detection limits for small samples.
4) It facilitates the comparison of performance between different instruments.

A program of sensitivity measurement was undertaken with particular emphasis on the determination of relative sensitivities of the compounds (base peak in parentheses) cholesterol (386), cholestane (217), DDT (235), DFTPP (442), morphine (285), LSD (323), and methyl stearate (74).

Mass spectrometer sensitivity can be expressed in several ways. An important consideration in the choice of definition is the sample inlet (s) to be used. For the purposes of this study, we selected a definition which is generally useful when the solid probe inlet is used in the non-scanning mode.

$$\text{SENSITIVITY} = S = \frac{\text{Time integral of current of mass analyzed ion reaching multiplier input}}{\text{Total weight of sample introduced}} \qquad \text{I}$$

$$S = Idt/GW \text{ (coulombs per microgram)} \qquad \text{II}$$

where I = multiplier output current (amperes), G = gain, W = weight of sample (micrograms), and t = time (seconds). Any convenient mass anlyzed ion can be selected. For this study the base peaks were selected.

Based as it is on the ion current reaching the Faraday cup position, the definition takes into account the sample introduction process, the ion formation process, the extraction of ions from the ionization chamber and acceleration through the source electrodes, and the transmission through the slits and the mass analyzer.

A list of parameters affecting the sensitivity of a single focusing magnetic deflection instrument with a solids probe would include 30 or more entries and as many as 15 of these may be accessible to the operator and variable in routine operation. Some of the parameters also affect the relative sensitivities of different compounds. The values selected for some of the parameters in this study are Instrument Type - Nuclide 12-90G, El.Energy - 70eV, Trap current 50μamps, Ion Chamber Temp. 225-275 C, Ion Energy - 4.5kV, Source slit - 0.001", coll. slit - 0.025".

Data were collected over a period of several months. The same set of operating parameters was strived for in each of the measurements but otherwise the sensitivity comparison tests were fitted into the regular schedule of the instrument

which was used for a wide variety of types of samples and with an EI/CI or EI source.

The exact electron multiplier gain was measured for each beam using the retractable Faraday cup. We observed that the variation in gain above mass 28 to mass 442 was about 10-20%. We measured the gain at mass 181 from PFK and assumed this value thereafter for all of the ions. The gain was set between 1000 and 10,000.

Before each run, the ion source was tuned (repeller, source magnets, source electrodes) for maximum signal of mass 181 (PFK). The sample probe was introduced and the probe heater set to 3.5 amperes corresponding to a final temperature of 240°C. In this mode, the temperature increases at about 120°C per minute.

Relative sensitivities, defined as the ratio of the sensitivity of the compound to the sensitivity for cholestane (LH Scale of Fig. 1) measured in the same run are shown in Fig. 1. The absolute sensitivity varied by about 3 orders of magnitude over the period of data collection. Despite the large variations in absolute sensitivity, the variation of relative sensitivities is less than a factor of 3 in most cases. An important factor in the variation may have been the fact that source temperature settings varied over 50° C during the study.

The sensitivity of morphine, alone, varied drastically during the series of runs, presumably due to compound degradation, either thermally or in solution.

Obviously for quantitative analysis, careful attention to the parameters and especially temperature is crucial. But for the intended purposes of this study, as enumerated at the outset, the factor of 3 is a realistic value for the month-to-month reproducibility of relative sensitivities.

No particular attempt was made to maximize the absolute sensitivity but values of at least 8×10^{-9} coul/μgm, at a R.P. of 600 are attainable for cholestane (100μa, source slit = 0.005").

The value of S' (sensitivity in terms of ions per molecule is related to S as S' = 10.4 MS where M = mol. wt. in grams. Values of S' are in the vicinity of 10^{-6} to 3×10^{-5} ions per molecule.

The detection limits for LSD was studied and the preliminary results for a 10-30 picogram sample are a S/N of about 10/1 (noise = 6×10^{-16} amps, signal = 6×10^{-15}, τ = 10 millisec).

In a few runs a thyroxin derivative (mol. wt. 1183, base peak 972) was included and its relative sensitivity was about 2/3 that of LSD. If similar considerations apply, we would expect that detection limits in the low picogram range would be possible also for the thyroxin derivative.

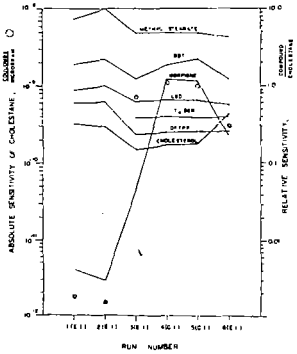

Figure I.

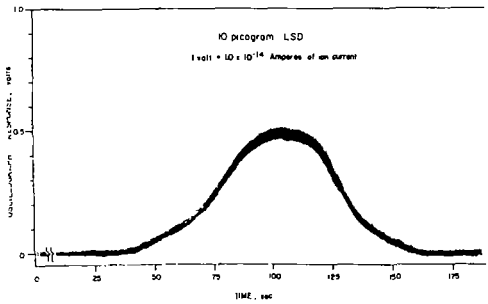

Figure II.

MASS AND MICROWAVE SPECTRAL STUDIES OF THE MECHANISM OF OZONOLYSIS

by

Robert P. Lattimer
The B.F.Goodrich R & D Center
Brecksville, OH 44141

Charles W. Gillies
Harvard University, Dept. of Chemistry
Cambridge, MA 02138

Robert L. Kuczkowski
University of Michigan, Dept. of Chemistry
Ann Arbor, MI 48104

The organic ozonolysis reaction has been used for many years as a means for identifying the locations of double bonds in structure analysis. The study of the mechanism of this important reaction spans the last two decades and is a continuing process. But that is a long story and only a few of the highlights will be given here.

In the ozonolysis reaction we take any alkene, dissolve it in a suitable solvent, pass a stream of ozone through the solution, and the final product is a five-membered ring called an ozonide. The reaction is remarkable in that the strong double bond is cleaved and three oxygen atoms are inserted to give a 1,2,4-trioxalane ring with one ether linkage (C-O-C) and one peroxy linkage (C-O-O-C). The initial adduct that is formed between ozone and the alkene is called the primary ozonide or molozonide. Several structures have been proposed, including the Staudinger oxetane ring, the σ-complex epoxide ring, and the favored 1,2,3-trioxalane. The five-membered ring molozonide is favored since this is the only structure for which spectroscopic evidence has ever been obtained.

There have been several mechanistic proposals through the years for the ozonolysis reaction. The simple Criegee mechanism was first proposed in 1957 in Germany. The key intermediates are the Criegee zwitterion (R_2COO) and a carbonyl (R_2CO) compound. Much evidence initially accumulated which supported the Criegee mechanism, but in the early 1960's workers started to separate ozonides by gas chromatography into their cis and trans isomers. The Criegee mechanism did not take into account the distributions of cis and trans ozonide isomers, so in 1966 Story, Murray, and Youssefyeh at Bell Labs came up with an entirely different proposal which attempted to solve the stereochemical consequences of the reaction. This new mechanism became known as the SMY or aldehyde interchange scheme.

Bauld, Bailey, and co-workers at the University of Texas didn't favor this abandonment of the simple Criegee mechanism, so a short time later they came up with a revision of the Criegee mechanism that attempted to account for the stereochemistry that had been observed. The key concept contributed here was the existence of two different stereochemical forms of the Criegee zwitterion - the syn and anti isomers. Finally in 1974, three of us at the University of Michigan proposed a different extension of the basic Criegee mechanism. Our analysis was based on

orbital symmetry considerations as the key factors in determining the stereochemical course of the reaction.

The basic Criegee mechanism assumes that the 1,2,3-trioxalane primary ozonide cleaves both an O-O and a C-C bond to give a zwitterion (or it could be a di-radical) and a carbonyl compound (an aldehyde or a ketone). These then recombine in a different manner to yield the final ozonide. The aldehyde interchange scheme assumes that the primary ozonide cleaves only a single O-O bond. Then an aldehyde, formed either via the Criegee mechanism or else added to the reaction mixture, inserts itself into the opened ring to form a new seven-membered ring intermediate. This intermediate, according to the authors, has a preferred conformation, and this conformation is what ultimately explains the observed stereochemistry of the ozonolysis reaction. The seven-membered ring eliminates a different carbonyl compound than that which was inserted originally, and the ring closes to yield an ozonide.

This brings us to the labeled foreign aldehyde experiments that will be described here.[1,2] Several years ago it was found that if one added an aldehyde to an ozonolysis reaction mixture, part of that aldehyde would be incorporated into the final ozonide produced. One experiment that could be useful, then, would be to put an oxygen-18-labeled aldehyde into the reaction pot and let it incorporate into the final ozonide. It can be seen that a Criegee zwitterion will react with the foreign aldehyde to give a final ozonide with the O-18 label exclusively at the ether site. There will be no label in either of the peroxy positions. The SMY mechanism, however, predicts a different consequence. Following through the SMY scheme it can be shown that the O-18 label will appear exclusively at a peroxy site. Thus the position of the O-18 label allows one to distinguish between the SMY and a Criegee-type mechanism.

We have used both mass spectrometry and microwave spectroscopy to study the ozonolysis reaction mechanism. The use of mass spectrometry may be illustrated with the mass spectrum of propylene ozonide. There is a strong molecular ion (m/e 90), a methyl-loss fragment (m/e 75), and a strong fragment at m/e 58 due to the loss of two oxygen atoms. It is clear that one can determine the total O-18 enrichment of the ozonide from the molecular ion and its (M+2) ion, and the ether O-18 enrichment from the m/e 58 and 60 ions. Microwave spectrometry was also used to establish the site of O-18 enrichment. The very high resolution of microwave (rotational) spectroscopy enables one to easily distinguish transitions arising from different isotopic species of a molecule. Thus one can directly observe the presence (or absence) of a particular O-18 species.

Much labeled-aldehyde incorporation data was obtained. Several alkenes (ethylene, propylene, cis- and trans-2-butene, and cis- and trans-diisopropylethylene) were ozonized in the presence of added O-18 formaldehyde or acetaldehyde. In nearly all cases the total O-18 enrichment as determined by mass and/or microwave spectroscopy was identical within experimental error to the ether-O-18 enrichment. This indicated to us that a Criegee-type pathway was exclusively, or very nearly exclusively, occurring in the ozonolysis reaction. In summary we observed only ether O-18 incorporation in the experiments carried out. This was consistent with the Criegee mechanism or any of its revisions. The SMY mechanism, which predicts only peroxy incorporation, was therefore inoperative in the reactions studied.

References

1. C. W. Gillies, R. P. Lattimer, and R. L. Kuczkowski, J. Amer. Chem. Soc., 96, 1536 (1974).

2. R. P. Lattimer and R. L. Kuczkowski, J. Amer. Chem. Soc., 96, 6205 (1974).

LABELED FOREIGN ALDEHYDE INCORPORATION

Alkene	Aldehyde	Ozonide	Total O^{18} Enrichment	Ether O^{18} Enrichment
	CH_3CHO^*	Pr. Oz.	70.1 ± 1.5%	70.1 ± 2.3%
	CH_3CHO^*	Pr. Oz.	10.3 ± 0.9%	10.4 ± 1.5%
	CH_3CHO^*	2-Bu. Oz.	76.7 ± 1.0%	76.0 ± 2.0%
	CH_3CHO^*	2-Bu. Oz.	45.6 ± 0.5%	45.9 ± 0.7%
	CH_2O^*	Pr. Oz.	34.9 ± 0.7%	34.5 ± 0.8%
	CH_2O^*	Pr. Oz.	78.9 ± 0.6%	78.1 ± 0.7%
	CH_2O^*	Pr. Oz.	82.0 ± 0.4%	82.6 ± 1.1%
	CH_3CHO^*	Me. iPr. Oz.	54.7 ± 0.2%	52.1 ± 0.7%
	CH_3CHO^*	Me. iPr. Oz.	54.6 ± 0.5%	53.0 ± 0.6%

Acylated Fatty Acids in Commercial Fats From Natural Sources

Robert S. Ampulski
The Procter & Gamble Company
Miami Valley Laboratories
Cincinnati, Ohio 45247

A new type of dimer fatty acid was identified as a minor component in several natural animal and vegetable fats used for deep frying at 375°F for 120 hours. This new material was separated from the fats by first converting the triglycerides to methyl esters and then adducting with urea. Straight-chain esters form adducts with urea, while branched-chain and cyclic esters do not. The non-urea adductable (NUA) material, which comprised 2-5% of the heated fat, was column chromatographed using silica gel and a hexane-benzene gradient. Most of the NUA material consists of straight-chain esters and oxidative condensates. The latter are normally formed in the process of heating fats in air for long periods of time at high temperatures.(1) A minor material, comprising 1% or less of the NUA material (approximately 200 ppm of the fat) eluted from the column in the benzene fraction. This paper reports the spectral identification of that minor NUA isolate.

The mass spectrum of the column fraction containing the minor component from a beef tallow NUA isolate is shown in Figure 1. This low resolution spectrum shows evidence of a molecular ion at m/e 560, a methyl ester [$(M-OCH_3)^+$; m/e 529)], and an oleoyl group [$(C_{18}H_{33}O)^+$; m/e 265]. Exact mass measurement of the molecular ion at m/e 560.517 corresponded to $C_{37}H_{68}O_3$. The mass spectrum of this sample did not match that expected for any of the known heated-fat oxidative reaction products. The molecular composition and the significant ions in the mass spectrum of the tallow isolate suggested the structure I - methyl oleoyloleate [$(CH_3O)(OC_{18}H_{32})(OC_{18}H_{33})$].

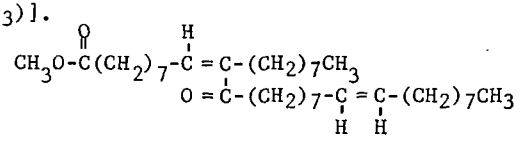

I M.W. 560.5168

A reference substance was synthesized by reacting methyl oleate with oleic anhydride at room temperature using a stannic chloride catalyst. The mass (Fig. 2), NMR, and IR spectra of the reference compound are entirely consistent with methyl oleoyloleate (I).

A comparison of Figure 1 with Figure 2 shows that all the major ions of the mass spectrum of the reference are also in the mass spectrum of the tallow isolate. However, there are many more intense ions in the spectrum from the tallow isolate than in the reference. These intense ions can possibly be accounted for by the fact that the tallow triglyceride contains palmitate, stearate, and oleate esters. The ions in Figure 1 in the mass range 502-508 could be due to a structure similar to I composed of two C-16 groups with various degrees of saturation [e.g., methyl palmitolyl-palmitate $(CH_3O)(OCH_{16}H_{30})(OCH_{16}H_{31})$; M.W. = 508].

The ions in the mass range 530-536 could be due to a structure also similar to I composed of mixed C-16 and C-18 groups with various degrees of saturation [e.g., methyl palmitolyl-oleate $(CH_3O)(OC_{18}H_{32})(OC_{16}H_{31})$; M.W. = 534]. The separation scheme was not sufficient to isolate these homologs.

To help eliminate the ambiguities in the mass spectra of mixed triglyceride isolates, glyceryl trioleate (triolein) was heated under the same conditions as the fats. Triolein is a pure unsaturated C-18 triglyceride. The mass (Fig. 3) and infrared spectra of the triolein isolate were consistent with that of the reference (Fig. 2). Intense ions in the 560 mass range were observed in the triolein isolate. No ions were observed in the 502-508 and 530-536 mass ranges. This is consistent with the hypothesis that the ions at 502-508 and 530-536 in tallow spectrum (Fig. 1) are acylated derivatives arising from the other fatty acids that make up the triglyceride.

High resolution mass measurements were made on the molecular ion of isolates from several fat sources (Table I). In all cases the measured mass was within ± .003 amu of the calculated mass for $C_{37}H_{68}O_3$ (560.5168).

The significant ions observed in the spectrum of the reference material are listed in Table II. Table II also lists ion intensities from the minor constituents found in several heated natural fats. From these data it was concluded that methyl branched-keto esters were present as trace components in the NUA material of heated fats. A possible fragmentation scheme for methyl oleoyloleate is shown in Figure 4.

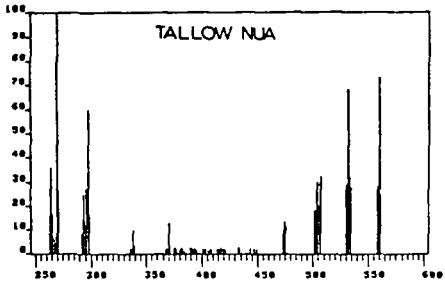

Fig. 1

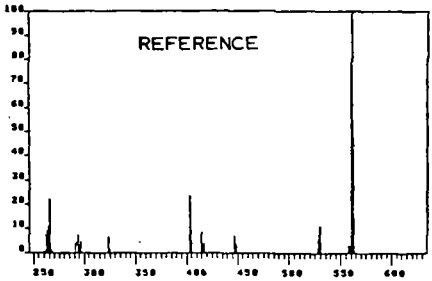

Fig. 2

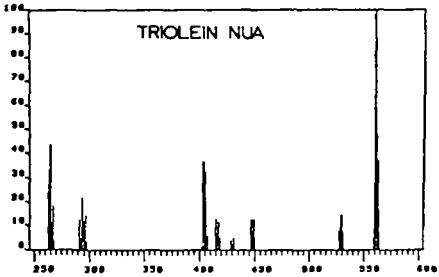

Fig. 3

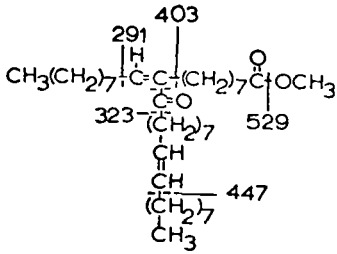

Fig. 4

Table I

Exact Mass Measurement
ON NUA ISOLATES

Calculated M.W. for ($C_{37}H_{68}O_3$)	560.5166
REFERENCE	560.516
Animal Frying Fat	560.516
Vegetable Frying Fat	560.520
Animal-Vegetable Frying Fat	560.516
Non-heated Vegetable Fat	560.515
Calculated M.W. for ($C_{36}H_{64}O_4$)	560.4804

Table II

Comparison of Mass Vs. Intensity

m/e	REFERENCE	Animal Frying Fat	Vegetable Frying Fat	Animal-Vegetable Frying Fat
560	100	100	100	100
529	11	20	28	18
447	7	15	29	16
415	8	5	9	13
403	23	13	27	17
323	7	3	10	8
294	7	60	326	172
291	4	6	24	16
265	22	52	40	115
264	11	116	91	243

1. Artman, Neil R., Advances In Lipid Research, 7 (1969), p. 245.

FIELD IONIZATION KINETICS STUDIES OF STEREOISOMERS

James S. Holler, Donald G. Patterson, Richard B. Scott,
Morton E. Munk and Peter Brown
Department of Chemistry, Arizona State University
Tempe, Arizona 85281

Our interest in the study of the differences in the retro-cycloaddition reaction lead to an investigation of the fragmentation of aminotriazolines I-III under conditions of electron impact and field ionization.

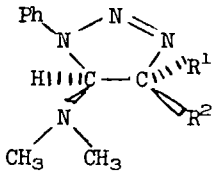

I-R^1=CH_3, R^2=Ph II-R^1=Ph, R^2=CH_3 III-R^1=R^2=CH_3

Epimerization studies in solution indicate I is more stable than II. This stability is consistent with a smaller steric requirement for the phenyl group than for the methyl group in this system.[1]

Metastable defocusing studies[2] suggest that the loss of nitrogen is the only fragmentation pathway from the molecular ion in electron impact. Measurements of the M-N_2 peak intensity relative to the base peak exhibit behavior consistent with the stability of the individual compounds.[3] This trend is accentuated when lower ionizing voltages are used.[4]

Plots of ion current versus blade potential are presented for the three compounds studied. The "normal" field ion spectra correspond to points in the scan just less than the normal accelerating voltage of 8,000 kv.[5] The trends observed in the electron impact spectra occur to a larger extent in the field ion spectra. Phenomenological rate constants have been calculated from the plots of ion current versus blade potential. Major fragmentations are loss of nitrogen, loss of nitorgen plus amine, and loss of substituted diazomethane. Compound II reacts faster than I at times less than 10^{-9} seconds in all the fragmentations studied. This increased reactivity is attributed to the relief of steric strain in the fragmentation process.

In summary, field ionization and field ion kinetics may be useful in the analysis of stereochemical problems. Problems of multiple step processes and thermal decomposition are minimized. Larger stereochemical effects are observed by these methods than by conventional electron impact mass spectrometry.

References:

1. M. Charton, J. Amer. Chem. Soc., 97, 1552 (1975).

2. M. Barber and R. M. Elliot, ASTM Committee E-14, 12th Annual Conference on Mass Spectrometry and Allied Topics, Montreal, June, 1964.

3. K. Bieman, "Mass Spectrometry. Organic Chemical Applications.", McGraw-Hill, New York, 1962, pp. 144-151.

4. J. M. Wilson, "Structure Determination in Organic Chemistry. Mass Spectrometry.", MTP Int. Rev. Sci.: Org. Chem., Ser. One, 1, 29 (1973).

5. A. J. B. Robertson and B. W. Viney, J. Chem. Soc. (A)1843 (1966).

REARRANGEMENT AND DECAY OF 1-HEXENE IONS: FIELD IONIZATION KINETIC (FIK) MEASUREMENTS

Arnold M. Falick and Tino Gäumann
Ecole Polytechnique Fédérale de Lausanne
Institute of Physical Chemistry, Lausanne, Switzerland

Recent studies of the molecular ions of some simple olefins have provided some unanticipated results concerning the behavior of these ions.[1-3] It has been demonstrated by means of labeling experiments that both hydrogen and skeletal rearrangements contribute abundantly to the overall scheme of decomposition of these ions.[4-7] Many of the specific details of these rearrangements remain obscure, however.

The work described here is an FIK study of 1-hexene and a number of ^{13}C labeled analogs of this molecule. The apparatus and experimental method were similar to those employed previously.[8] This particular compound is interesting for several reasons. First, methylcyclopentane has been shown to undergo ring-opening prior to decomposition, possibly to a 1-hexene structure.[5,9] Second, some recent EI work on a series of labeled 1-heptenes showed a remarkable degree of skeletal rearrangement in the molecular ion. As is shown below, 1-hexene also manifests a great deal of skeletal rearrangement prior to decomposition.

Following field ionization, the molecular ion of 1-hexene undergoes unimolecular decomposition via several pathways. The principal modes of decay for which we have evidence are shown in Fig. 1. Note that loss of ethyl can occur either as a two step process or in a single step. The transition 84 → 83 (loss of H from the molecular ion) is not directly observed in the gas phase, but it must occur since a strong metastable peak for the transition 83 → 55 is observed in the first and second field-free regions.

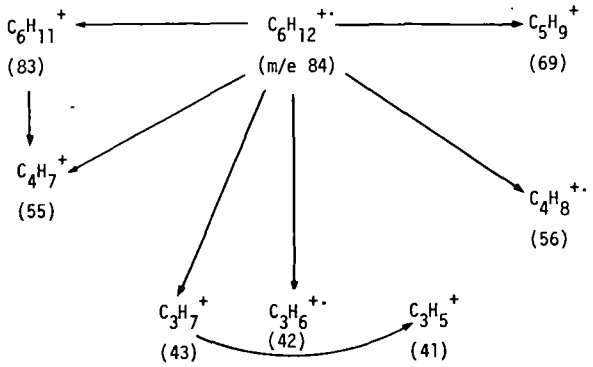

Fig. 1. Decomposition pathways of 1-hexene following FI.

The lack of any direct pathway to $C_3H_5^+$ is interesting, since the IP of $C_3H_5^+$ is probably slightly lower than that of $C_3H_7^+$. However, this result is in agreement with the EI study on ^{13}C labeled 1-heptanes in which it was concluded that $C_3H_5^+$ ions were mainly generated by loss of molecular H_2 from propyl ions, and not by direct β-cleavage.

The extent to which skeletal rearrangement is operative in the 1-hexene molecular ion is vividly demonstrated by the labeling results for loss of methyl and loss of ethylene from 1-hexene monolabeled with ^{13}C in various positions. Fig. 2 shows the results for the loss of a methyl radical from each of the labeled analogs. In this figure, the solid lines represent data which were taken continuously as a function of time. The additional two points at the right are data taken at the saddle point between the focusing electrodes and in the first field-free region, respectively. Consider the compound labeled in position 6. At short times, most of the ^{13}C is lost as methyl, but with increasing time, the percent loss of the labeled atom decreases until, at about 10^{-6} sec, it is not significantly different from the statistical value assuming complete mixing of all the C atoms. The compound labeled in position 1 shows a steep rise at short times, followed by a gradual decline again to the statistical value. The initial steep rise is probably due to a hydrogen transfer from one of the other C atoms to C-1, thus forming a methyl group which is subsequently lost as a unit. The H transfer is clearly rapid, since at the shortest measurable time ($\sim 5 \times 10^{-11}$ sec for this reaction) loss of C-1 already accounts for $\sim$30% of the total methyl loss. The loss of carbon 2 or 4 (and presumably C-3 and C-5 would be similar) does not become important until considerable time has elapsed, but the results at long times confirm that a great deal of skeletal rearrangement has occurred.

Fig. 3 shows the results for loss of ethylene. The data are even clearer than for the loss of methyl. There was essentially no difference observed between the compounds labeled in positions 1 and 2. We infer from the curves that loss of ethylene occurs initially almost entirely from the unsaturated end of the molecule. Transfer of a hydrogen atom from one of the other four positions is of course required prior to or simultaneously with loss of the neutral ethylene fragment. These results are in agreement with earlier EI studies on labeled 1-heptene[6] and 1-pentene,[10] which also tended to show that ethylene loss occurs preferentially from the unsaturated end of 1-alkenes. The fact that a seemingly unfavorable vinylic bond cleavage is occurring here might lead us to speculate that the appropriate mechanism to explain the C_2H_4 loss is more complex than simple transfer of an H atom followed by bond cleavage. Certainly our results show that more complex skeletal rearrangements cannot be excluded a priori. Further experiments on related compounds are in progress.

References

1. J. H. Bowie, in Mass Spectrometry, Vol. 3, Specialist Periodical Reports, The Chemical Society, London, 1975.
2. K. Levsen, Org. Mass Spectrom. 10, 55 (1975).
3. A. M. Falick, P. Tecon and T. Gäumann, Org. Mass Spectrom. 11, 409 (1976).
4. A. Stefani, Org. Mass Spectrom. 7, 17 (1973).
5. A. M. Falick and A. L. Burlingame, J. Am. Chem. Soc. 97, 1525 (1975).
6. A. M. Falick and T. Gäumann, Helv. Chim. Acta, in press.
7. P. J. Derrick, A. M. Falick and A. L. Burlingame, Adv. Mass Spectrom. 6, 877 (1974).
8. A. M. Falick, P. J. Derrick and A. L. Burlingame, Int. J. Mass Spectrom. Ion Phys. 12, 101 (1973).
9. S. Meyerson, T. D. Nevitt and P. N. Rylander, Adv. Mass Spectrom. 2, 313 (1963).
10. B. J. Millard and D. F. Shaw, J. Chem. Soc. (B), 664 (1966).

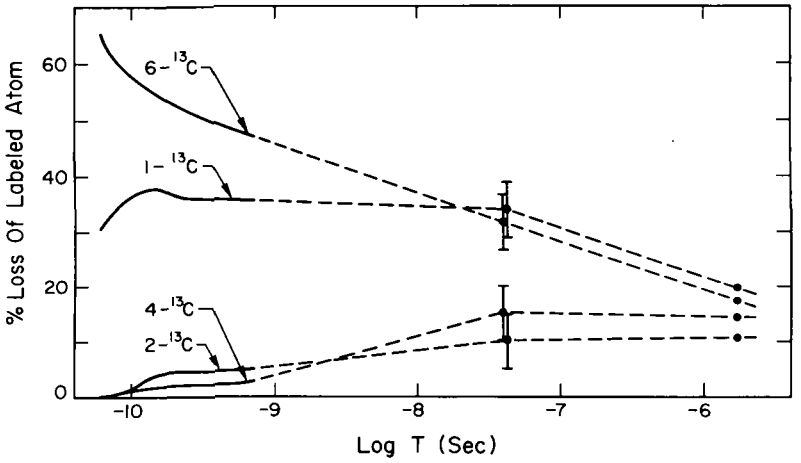

Fig. 2. Loss of methyl radical from several ^{13}C labeled 1-hexenes.

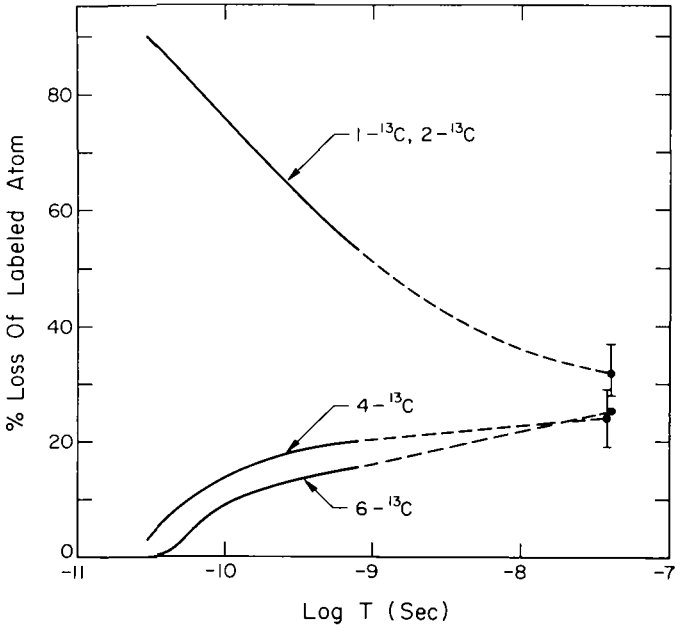

Fig. 3. Loss of ethylene from labeled 1-hexenes.

MIXTURE ANALYSIS BY COLLISIONAL ACTIVATION SPECTROMETRY

K. Levsen, Inst. f. Phys. Chemie, 53 Bonn, Fed.Rep.Germany

A direct analysis of mixtures by collisional activation spectrometry is possible using a double focussing instrument of reversed geometry and applying the following procedure: The magnetic field is successively adjusted to pass those peaks in the normal spectrum which characterize the various components of the mixture. Collision gas is introduced into a collision cell placed between the magnetic and electric sector. The electric sector potential is then scanned to obtain the individual CA spectrum of every component each time. As fragment ions do not reflect a given precursor unambiguously and, moreover, various components may contribute to a given fragment peak, it is desirable to produce the primary spectrum of the mixture under conditions which favour the occurrence of molecular ions. FI, CI, and low energy electron impact spectra are especially suited for this purpose.

The analysis of a simple pain reliever containing a 1:1 mixture of phenacitine and methylsalicylate (aspirin) with combined field ionization and collisional activation is reported. The close similarity between the published EI spectra and the CA spectra allows an unambiguous assignment of the components. In a more complex mixture of the pyrolysis products of DNA the following components were detected by low energy electron impact in conjunction with collisional activation: methanol, ethanenitrile, propargylalcohol, furan, 2-metnyl-furan, α - angelicalactone, and furfurylalcohol. The components were identified by matching their CA spectra with the CA spectra of known reference compounds. The structure assignment is, however, complicated by the occurrence of isomers.

[1] K. Levsen and H.D. Beckey, Org. Mass Spectrom. 9, 57o (1974)

[2] K. Levsen and H.-R. Schulten, Biomed. Mass Spectrom.,in press

INTERPRETATION OF THE FIELD DESORPTION MASS SPECTRA OF DIIONIC SALTS

C. N. McEWEN AND S. F. LAYTON
Central Research and Development Department
E. I. du Pont de Nemours & Co., Wilmington, Del. 19898

Field desorption mass spectrometry (fdms) has proven to be a valuable tool in the analysis of organic salts with singly-charged ions. The major peaks observed in the fd spectra of these salts have the formula $[\text{cation}_{x+1}\ \text{anion}_x]^+$ where ion intensity decreases as x increases from zero to higher integer values. Little work has been reported on field desorption of salts with doubly-charged ions.[1,2] We find the fd spectra of these salts to be structure- and temperature-dependent. (The few salts we have run with doubly-charged anions either do not field desorb or decompose into singly-charged anions and field desorb as a cluster ion; therefore, salts with doubly-charged anions will not be discussed further except to note that ion-exchange to produce an ammonium salt or the free acid generally allows desorption of the anion as the free acid.)

In salts with doubly-charged cations several competitive processes may occur simultaneously. Our interest here will be the processes favored at low emitter current and the relation to structure, but it is important to note that where alternate pathways for desorption are available, their relative intensities will often vary with changes in temperature. Relative intensities are given only in general terms since they vary greatly from scan-to-scan and are an estimated average of several scans.

Desorption of the cation as a doubly-charged ion is structure dependent. For example, in 1 the doubly-charged ion is the base peak but in 2 it is not observed. The

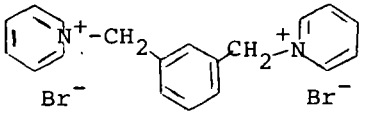

1

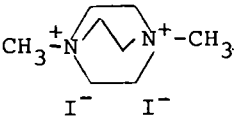

2

intensity of this ion also varies considerably from run-to-run, possibly indicating desorption occurs from a surface bonded species. Less intense ions of formula CtH^{++}, CtH_2^{++} and CtH_3^{++} (Ct=cation) are sometimes observed. These ions are likely formed by a surface reaction.

In general, desorption of the doubly-charged cation is not the favored process. Instead, field and thermally induced processes occur that produce singly-charged ions. Cluster ions, $[Ct^{++}An^{-}]^{+}$, comprise the base peak in the spectra of compounds such as 3 where both cationic centers can simultaneously be in the near vicinity of the anion; however, the major pathway for becoming singly charged will be fragmentation if several pathways for dealkylation exist as in 4, or if an excessively large ring is formed when the cation centers are simultaneously near the anion as in 5. For these compounds, cluster ion formation remains a significant part of the total ion current, but in 6 it is not possible for both cationic

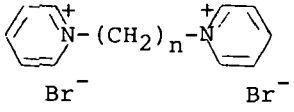

3 (n=3)

5 (n=12)

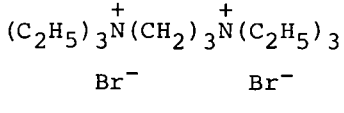

4

centers to be near the anion simultaneously, and thus cluster ions are not observed. Instead, 6 becomes singly-charged by thermally induced electron transfer producing the radical cation 7. (In eims the neutral compound 8 is observed and presumably involves transfer of two electrons.)

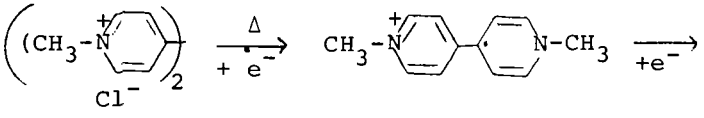

6 7

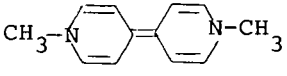

8

The base peak in the fd spectrum of 9 is also the radical cation produced by electron transfer, but the radical cation of 10 is not observed. The reducing agents for these reactions are not known.

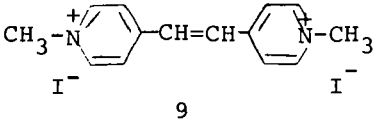

9

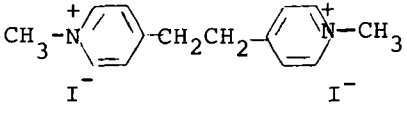

10

Thermal decomposition is generally observed to some extent with all doubly-charged cationic salts, especially at high emitter temperature, but compounds such as 2 which cannot form cluster ions, or easily be reduced by electron transfer, become singly-charged by Hofmann degradation or dealkylation type reactions.

Sometimes, distinguishing between cluster-ion formation and dealkylation is difficult. In 11 the anion can attack an α-methylene group to produce a singly-charged ion of mass $[Ct^{++}An^{-}]^{+}$, or the same mass is obtained by cluster ion formation with the anion included in the cage and in contact with both ammonium ions. In 11 the base peak has the mass of the

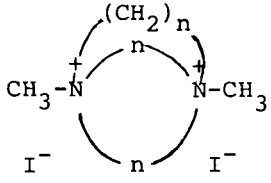

(n=14) 11

(n=8) 12

cluster ion but in 12 where the cage is too small to contain the anion the $[Ct^{++}An^{-}]^{+}$ ion is only about 10% the intensity of the ion formed by demethylation of the cation.

The study of salts, especially those with multiply-charged ions by fdms can provide basic information concerning the processes that occur before and during field desorption. Further work in this area will be reported elsewhere.

1. G. W. Wood, J. M. McIntosh and P-Y. Lau, J. Org. Chem., 40, 636 (1975).

2. M. C. Sammons, M. M. Bursey, and C. K. White, Anal. Chem., 47, 1165 (1975).

FIELD DESORPTION MASS SPECTROMETRY OF ORGANIC, INORGANIC AND ORGANOMETALLIC SALTS

David E. Games, John L. Gower and Leon A.P.Kane-Maguire,
Department of Chemistry, University College, PO Box 78, Cardiff.
CF1 1XL, Wales.

The involatile nature of coordination complex salts has precluded their characterisation by electron impact (EI) and chemical ionization (CI) mass spectrometry. Encouraged by the success of field desorption mass spectrometry (FD) in the study of organometallic salts,[1] we carried out a similar study with cationic coordination complexes. The FD spectra of the monocationic complexes $[Pd(Et_4dien)X]X$ (X = I, NCS), $[Pd\ diene\ X]X$ (X = Cl, I). $[CO\ en_2(NO_2)_2]I$, and $[Ru\ en_2Cl_2]Cl$ all showed the cation as the base peak in their spectra with no fragment ions. In many cases cluster ions were observed corresponding to $(Cation)_2$ Anion. The complex $[Co\ en_2\ Br_2]Br$ showed a weak ion for the cation and fragment ions corresponding to loss of en and en + X. In the case of the corresponding compound $[Co\ en_2\ Cl_2]Cl$ and the complex t - $[Co(\underline{1}\ pn)_2\ Cl_2]Cl$, ions for the cations were absent but ions corresponding to loss of the amine ligand and amine ligand + halogen were observed. One dicationic complex $[Co\ trien\ (H_2O)\ Cl]Cl_2$ was also studied and this only exhibited ions corresponding to loss of water from the cation.

We have also studied the FD spectra of different types of salts of drugs and other biologically important molecules. Chlorides, bromides, iodides metabromides, sulphates, phosphates and maleates have been investigated and in almost all cases their spectra exhibited ions which enabled identification of the base (B) portion of the salt and the anion (A). This latter portion of the molecule could be identified by the presence either of cluster ions in the spectrum or e.g. in the case of codeine phosphate and methotrimeprazine maleate by $(A + 2H)^+$ ions at m/e 99 and 117 respectively. Behaviour of this type was fairly unusual and appeared to correspond to a low ratio (less than 1) of the relative intensities of the $(B + H)^+/B^+$ ions. In most other cases, in addition to $(B)^+$ and $(B + H)^+$ ions, cluster ions corresponding to BHA, BH.BHA and BH2BHA, in accord with those previously reported[2] were present. However in the FD spectra of the sulphates (ephedrine, amphetamine, dexamphetine, tranylcypromine, hordenine, mephentermine, atrophine and quinine) and the chlorides of promazine and amytriptyline we found in many cases additional cluster ions see table 1. Although these ions are useful in that they characterize both the base and the anion, difficulties in spectral interpretation can ensure, particularly when they are the base peaks in the spectra. In an endeavour to ascertain some of the factors involved in the formation of these cluster ions we examined the effect of field strength, emitter current, solvent solution concentration and nickel dendrite emitters[3] on their formation. Variation of field strength and emitter had little effect on the spectra obtained, changes in emitted current caused changes in the relative intensities of ions but no discernable pattern could be ascertained apart from the loss of water from sulphate cluster ions at higher wire currents. Variation of solvent proved difficult to investigate in many cases, however for some sulphates a decrease in cluster ion formation was observed when spectra were run from water as opposed to methanol. The most effective parameter was solution concentration; at low concentration few or no cluster ions were observed, increasing concentration gave cluster ions of increasing dominance in the spectra.

e.g. the FD spectrum of amphetamine sulphate at a concentration of 1μg/μl showed only $(BH)^+$ ions but at 15μg/μl the spectrum was dominated by $(BH)_2 HSO_4^+$ & $(BH)_3(HSO_4)_2^+$ ions.

In the course of our studies of the effect of solvent on the FD spectra of salts, we examined choline chloride. FD spectra were obtained from methanol, dimethyl sulphoxide and dimethyl formamide solutions taking care not to remove all solvent from the emitter before obtaining spectra. Although no reproducible change in cluster ion formation was observed, a marked change in the intensity of the intermolecular methyl transfer[4] ion (m/e 118) was observed. The intensity of this ion in the spectrum obtained from dimethyl sulphoxide increased relative to that from methanol and was the base peak in some of the spectra from dimethyl formamide. The FD spectrum of the related compound (1) was also studied from methanol and dimethyl formamide. Instead of intermolecular methyl transfer occurring ions at m/e 204 and 202 indicate that a hydroxy ethyl group and an isopropyl group undergo transfer, the former ion is strong in the spectra while the latter is weak and not always present. In agreement with the spectra of choline the intensities of both these ions relative to other ions in the spectra, were enhanced in spectra obtained from dimethyl formamide.

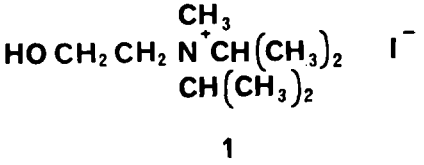

1

Rollgen and Schulten[5] have advocated the addition of small amounts of alkali metal salts to enable good FD spectra to be obtained of more difficult compounds. Previously we have utilized this technique in situ, by variation of solvent polarity,[6] more recently we have been able to obtain more reproducible and intense spectra of mono-, di- and trisaccharides by addition of small quantities of lithium, sodium and potassium salts to solutions of the sugar[7] e.g. melezitose gives an $(M + Na)^+$ ion as the base peak in its spectrum, as opposed to an $(M + H)^+$ ion which is 12% of the base peak when normal spectra are obtained.[8]

TABLE I Cluster Ion Formation in Organic Salts.

Salt	Ions observed
Sulphate	$BH.HSO_4$, $BH.2H_2SO$, $(BH)_2HSO_4$, $(BH)_2.(HSO_4)_2$ $(BH)_3.(HSO_4)_2$, $(BH)_4.(HSO_4)_3$, $BH.HSO_4$-18, $(BH)_2.HSO_4$-18, $(BH_2)_2.HSO_4$-36, $(BH)_3.(HSO_4)_2$-18.
Chloride	$BH.Cl$, $B.Cl_2$, $BHCl_2$, $(BH)_2.Cl$, $(BH)_2Cl_2$ $(BH)_2.Cl_3$, $(BH)_2.Cl_4$, $(BH)_2.Cl_5$.

REFERENCES

1. D.E.Games, A.H.Jackson, L.A.P.Kane-Maguire and K. Taylor J.Organometallic Chem., 1975, 88, 345.

2. e.g. G.W.Wood and N. Mak., Proceedings 23rd Annual Conference on Mass Spectrometry and Allied Topics, Houston, Texas, May 1975, 56.

3. R.M.Wightman, D.H.Hinton, M.C.Sammons and M.M.Bursey, J.Mass Spectrometry Ion Phys., 1975, 17, 208.

4. D.A.Brent, D.J.Rouse, M.C.Sammons and M.M.Bursey, Tetrahedron Letters, 1973, 4127; G.W.Wood and P -Y Lau, Org. Mass Spectrom, 1975, 10, 1147.

5. F.W.Rollgen and H.R.Schulten, Org. Mass Spectrom., 1975, 10, 660.

6. D.E.Games, Transactions of the Biochemical Society 556th meeting, London, 1975, 455.

7. This technique was first reported by J.C. Prome and G. Puzo, Centre de Recherche de Biochimie et de Genetique Cellulaires, Toulouse, France, at the 3rd meeting of the Mass Spectrometry and Gas Chromatography - Mass Spectrometry Group, Dijon, France, March 1976.

8. J. Moor and E.S.Waight, Org. Mass Spectrom., 1974, 9, 903.

FIELD DESORPTION MASS SPECTROMETRY OF CATIONIC AND ANIONIC DYES

C. N. Mc EWEN AND S. F. LAYTON
E. I. du Pont de Nemours & Co., Central Research and Development Dept., Wilmington, Del. 19898

Ionic dyes generally decompose before vaporization, thus, electron impact (e.i.) and chemical ionization (c.i.) which require vaporization before ionization fail to produce ions characteristic of the intact dye or its constituent ions. Cationic dyes (i.e., the chromophore in the cation portion of the dye salt) are usually more amenable to conventional mass spectrometric analysis, especially if the products of dealkylation or Hofmann degradation can be recognized. Unfortunately with unknown dyes this can be difficult, and especially so in view of our finding that amine substituted triarylmethane dyes and dyes of related structure sometimes undergo thermally promoted reduction before decomposition producing the leuco form of the dye (eq. 1). Presumably an oxidation-reduction reaction occurs between chromophores during heating of the dye in the mass spectrometer producing a free radical which abstracts a hydrogen atom from a nearby ion before vaporization. For example, the base peak in the e.i. spectrum of crystal violet, 1, is the molecular ion of the leuco form 2.

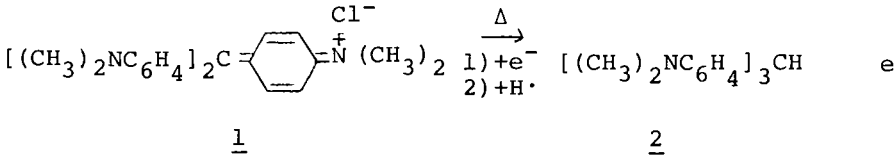

The difficulty associated with determining the mass of the cation is eliminated by using field desorption mass spectrometry (f.d.m.s.) where the base peak in the spectrum is the intact cation. This is also true for the amine substituted triarylmethane dyes where apparently the temperature required for field desorption is less than that necessary for thermally promoted oxidation-reduction.

Identification of the anion portion of high molecular weight cationic dyes is usually not possible by f.d.m.s.; however once identification of the cation is made by f.d.m.s., interpretation of the e.i. spectrum and subsequent identification of the anion is more manageable.

Dyes in which the chromophore is anionic are usually too nonvolatile to produce meaningful e.i. or c.i. spectra. Ion exchange of the cation for hydrogen greatly enhances volatility for most anionic dyes, but the free acids of many sulfonate substituted dyes remain too nonvolatile to vaporize intact. Field desorption, as has recently been reported[1,2] is capable of producing ions that characterize the anion and cation of certain anionic dyes. The major peaks observed by

f.d.m.s. are the $[cation_{x+1} anion_x]^+$ ions where the ion intensity decreases as x goes from zero to higher integer values. Our observations confirm that many anionic dyes field desorb readily even when complex structures such as 3 are involved; however, it is not uncommon for anionic dyes of relatively simple formulas such as 4 to fail to field desorb while closely related compounds such as 5 desorb readily. Anionic dyes that fail to field desorb will often produce ions characteristic of the free acid after ion-exchange with H^+ or NH_4^+ or if $(NH_4)_2SO_4$ is simply added to the dye. Finally, there are a few anionic dyes such as 6 that have eluded all our attempts at producing a meaningful spectrum by f.d.m.s.

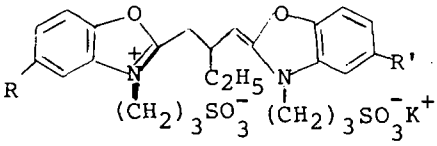

Ortho G 3

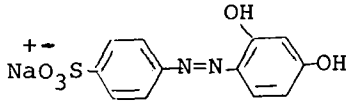

Tropaeolin O 4

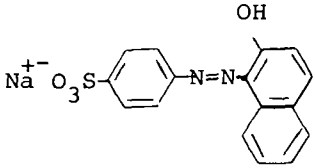

Orange II 5

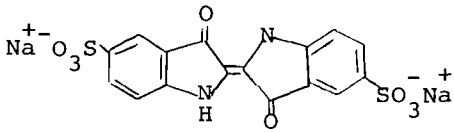

Indigo Carmine 6

1. H.-R. Schulten and D. Kummler, Z. Anal. Chem., 278, 13 (1976).

2. A. Mathias, A. E. Williams, D. E. Games and A. H. Jackson, Org. Mass Spectrom., 11, 266 (1976).

SOME QUANTITATIVE ASPECTS OF FIELD DESORPTION MASS SPECTROMETRY

Douglas F. Barofsky, Rosemarie Held and Elisabeth Barofsky
Oregon Graduate Center, Beaverton, Oregon 97005

An interest in applying FDMS to the analysis of airborne polynuclear aromatic hydrocarbons (PAH) has lead us to study several quantitative aspects of FDMS with respect to this class of compounds. As of the time of this writing, we have investigated some effects of sample handling, desorption rate and focusing on the quantitative parameters precision, accuracy and minimum detectable limit. In addition we have determined an absolute sensitivity curve for chrysene over several orders of magnitude of sample amount.

All experiments were conducted with a Hitachi RMU-7 single focusing mass spectrometer converted for use in the field desorption mode. Quantitative data was determined from experimental plots of total ion emission and specific ion currents versus heating current. These plots (thermograms) were produced by means of a programmable emitter heating current supply which has been more fully described elsewhere[1,2]. Standard solutions of PAH in dichloromethane were prepared from commercially available chemicals (purity $\geq$ 95%) at concentrations of about 10^{-3} M. Less concentrated sample solutions were obtained by dilution of the standard solutions.

A determination of precision was made by integrating several ion current plots of both the total emission and the transmitted parent ion using the same emitter. Integration was accomplished with both a compensating polar planimeter (K&E) and an Autolab Minigrator electronic integrator (Spectra Physics). Sample was applied to emitters by both the dipping and the microsyringe techniques. In the former case a highly concentrated solution of chrysene in methanol (8×10^{-4} g/μℓ) was used; the resulting integrated ion currents from several runs differed in area by only 1%. In the latter case the integrated ion currents from several runs at a given sample concentration varied by less than 5%. The amounts of sample applied to the emitter via the microsyringe technique were varied from 40 ng to 0.5 pg.

Accuracy was tested by recording several thermograms generated from the same amounts of material applied to different emitters. In the case of dipped emitters marked variations in the area of the ion current plots were observed as a function of needle length. Emitters having longer needles can hold larger amounts of sample and consequently desorb larger amounts of sample. When, however, equal amounts of sample were placed on different emitters by the microsyringe technique variations in the number of collected ions generally varied by less than 20%. An occasional emitter would exhibit markedly different (usually poorer) performance through other emitters, but this is definitely not the usual case.

A sensitivity curve for chrysene was measured for sample amounts ranging over 5 orders of magnitude (Fig. 1). The curve shows an increase in sensitivity for small sample amounts ($\leq$ 10 pg). This is presently thought to be an artifact of our sample handling procedure. Background subtraction substantially reduces the effect but does not eliminate it.

Future work will be concentrated on refining our present techniques for pure compounds and extending them to compound mixtures.

Acknowledgment: The authors are indebted to the Electric Power Research Institute for their support of this work (Contract RP 674-1).

References:

[1] D. F. Barofsky, L. Jacob and E. Barofsky, submitted to Int. J. Mass Spec. and Ion Phys. (1976).

[2] J. W. Maine, B. Saltmann, J. F. Holland, N. D. Young, J. N. Gerber and C. C. Sweeley, Analytical Chem. 48, 427 (1976).

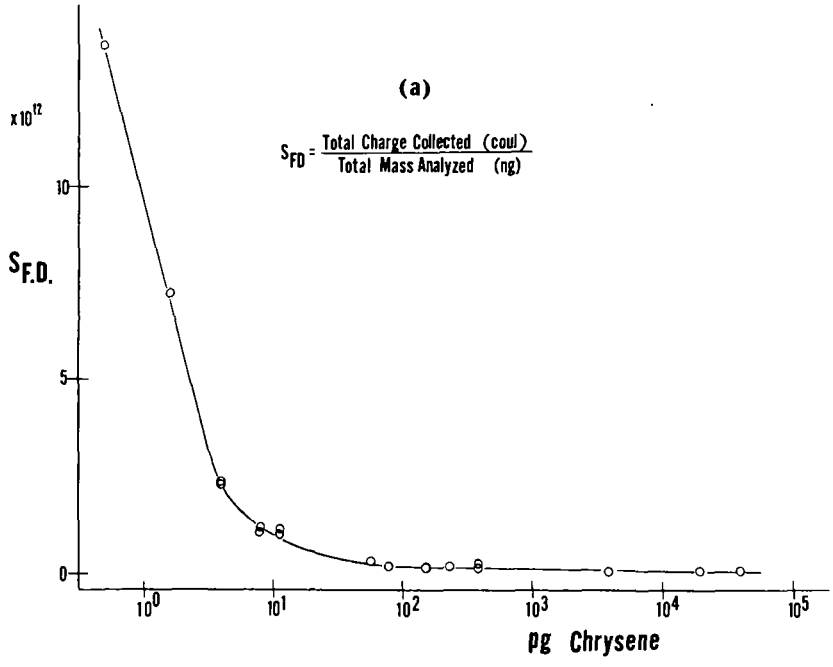

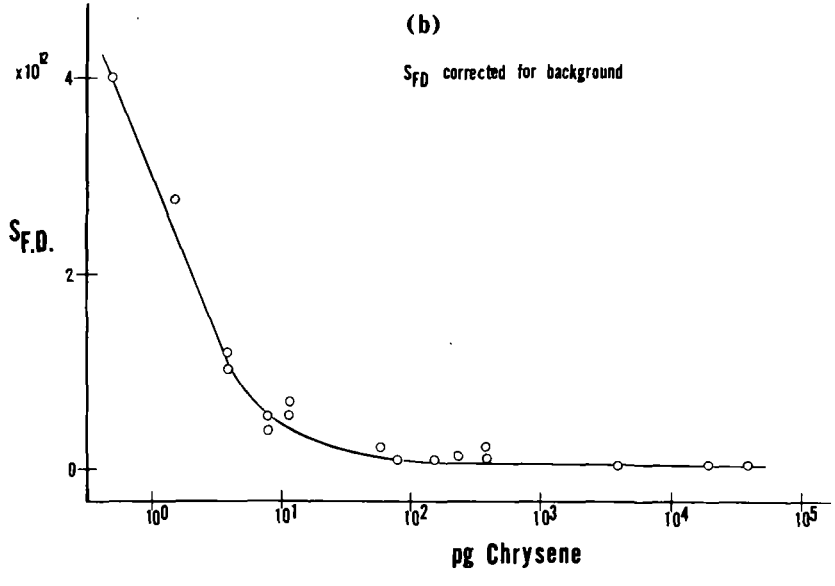

Figure 1. FDMS sensitivity curve for chrysene: a) uncorrected for background, b) corrected for background.

QUALITATIVE AND QUANTITATIVE FIELD DESORPTION MASS SPECTROMETRY OF MIXTURES

Hans-Rolf Schulten and Hans Dieter Beckey,
University of Bonn, Institute of Physical Chemistry,
5300 B O N N , Wegelerstr. 12 , West-Germany

The results obtained from the field desorption (FD)mass spectra of complex mixtures of the pyrolysis products of deoxyribonucleic acids (1) indicated that FD mass spectrometry (MS)is particularly well suited for the qualitative analysis of mixtures. The method has provided a good indication of the composition of complexes of antibiotics (2), of steroid conjugates (3), and the organic (4) and inorganic (5) components of aerosols. The utility of the FD technique for the examination of natural mixtures of bile acids from bile extracts (6) and of mycotoxins from food extracts (7) has been demonstrated.

Recently mixtures of pesticides (8), of parent pesticides together with their metabolites (9), of drugs (10), and of drugs and some of their metabolites (11) have been investigated successfully. Synthetic mixtures of oligopeptides have given FD spectra that consisted almost exclusively of molecular ions (12,13). As an example of the FD mass spectrum of such a mixture of a tri-,tetra-, and pentapeptide is shown in Fig. 1.

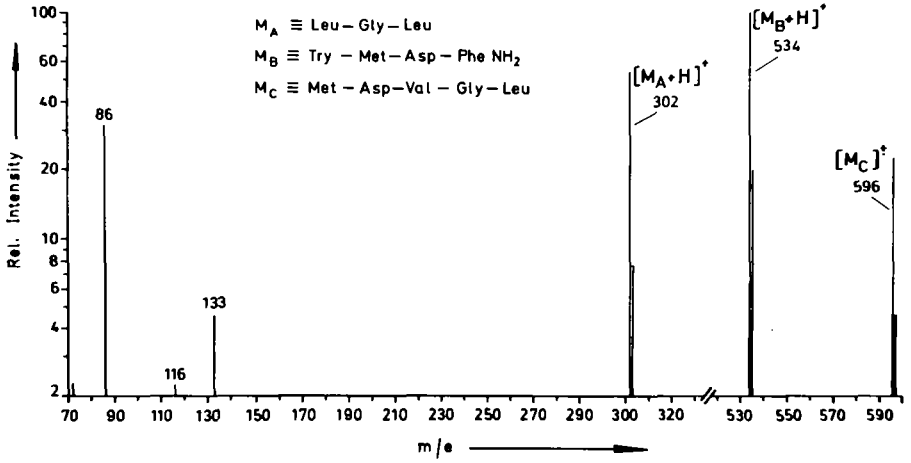

Fig.1: FD mass spectrum of an equimolar (10^{-2}M) aqueous solution of three oligopeptides. Photographic detection on vacuum evaporated AgBr-plates (12).

Using photographic detection and high resolution the potential of FD MS for mixture analysis was exemplified by means of synthetic mixtures of up to 15 PTH amino acids (14). The high molecular ion intensities , low fragmentation and the relatively small intermolecular interaction allowed the easy discrimination of individual components of these mixtures. The sensitivity and selectivity of the FD method was tested on PTH amino acids obtained from automated Edman sequenator degradations of a ribosomal protein. The FD spectra showed the molecular ions and significant fragmentation of the PTH-derivatives of all investigated ten degradation steps. Even in the cases where conventional EI (and in special cases CI) fails to to show the molecular ions and only characteristic fragment ions are found, the FD method gave rise to the molecular ions in high yields (e.g. PTH-arginine, PTH-(ε-PTC-lysine). There-

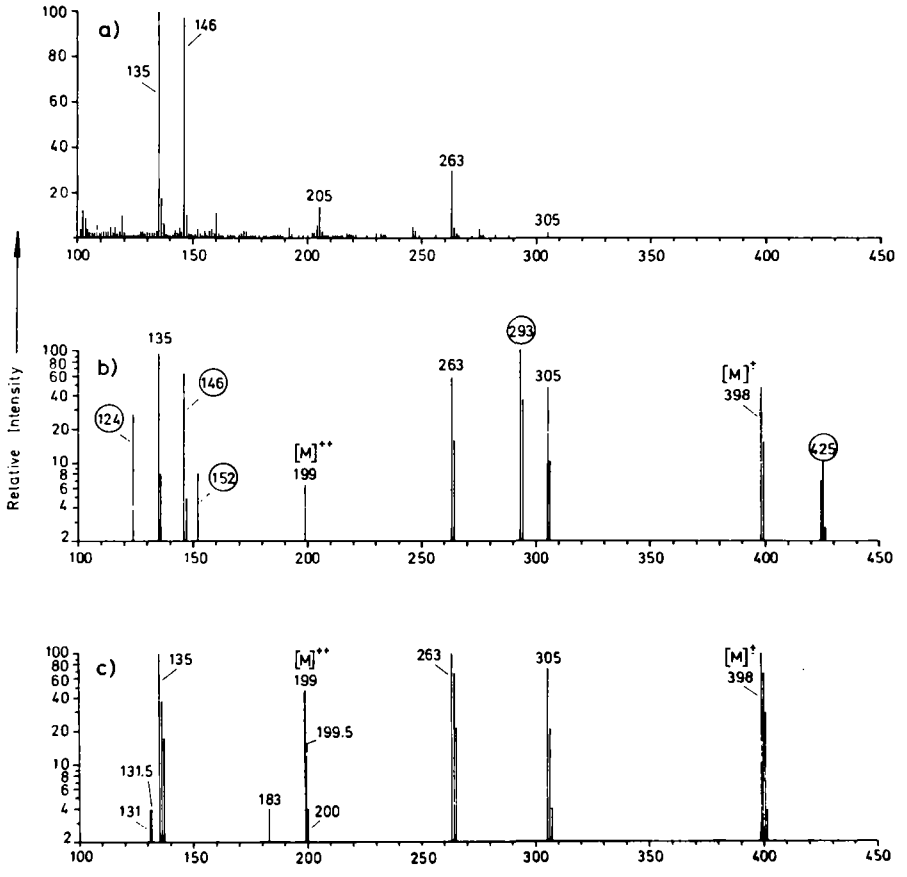

Fig.2: EI(a),FD(b) MS of PTH-Lys from Edman sequenator(14).

fore the use of the method as a complimentary technique for the confirmation of PTH amino acids released in the Edman sequenator appears to be advantageous. In Fig. 2 the EI mass spectrum (a, 400-600 ng) of a genuine sample is contrasted with the FD mass spectrum of the standard (c, 500 ng) and the sample (b, 200 ng) (14).

Quantitative determinations by FD MS are handicapped because of the following variable factors:

- (1) The quality of the field desorption emitter,
- (2) the adjustment of reproducible desorption conditions,
- (3) the transfer of the sample onto the FD emitter, and
- (4) the influence of the chemical properties of the compound under investigation on the desorption process.

However, these difficulties can be solved in the following way:

- (1) The production of emitters of similar field desorption characteristics can be achieved by high temperature activation in a multiple activation apparatus, control of the shape, distribution, and length of the microneedles under a light microscope, and testing of the ionisation efficiency of the emitter in the field ionisation mode.
- (2) Reproducible desorption conditions can be achieved when emission-controlled FD MS (15,16) is employed.
- (3) In our experience the syringe technique enables the reliable transfer of defined amounts of sample onto the emitter (17).
- (4) The virtual identity in the chemical properties between sample molecules and their isotopically labelled analogues allow quantitative FD MS using the isotope dilution technique (16,18).

With electric detection the field desorption mass spectra of dopamine-d_0/-d_4 (molar ratio 1:1) were averaged over 22 scans and gave a molar ratio d_0/d_4 (expt.) of 1:0.970 $\pm$ 0.05. The error for this estimation was -3%. In general at low resolution and electric detection accuracy of $\pm$ 5% was easily obtained (18).

With photographic detection for mixtures (5:100,20:100,100:100, 500:100) of d_0/d_6 cyclophosphamide the FD data gave errors between $\pm$ 5 and $\pm$ 10% (18). A typical FD spectrum of a mixture

of cyclophosphamide and its d_6 analog containing the d_0 and d_6 forms in the molar ratio of 1:0.85 is shown in Fig. 3.

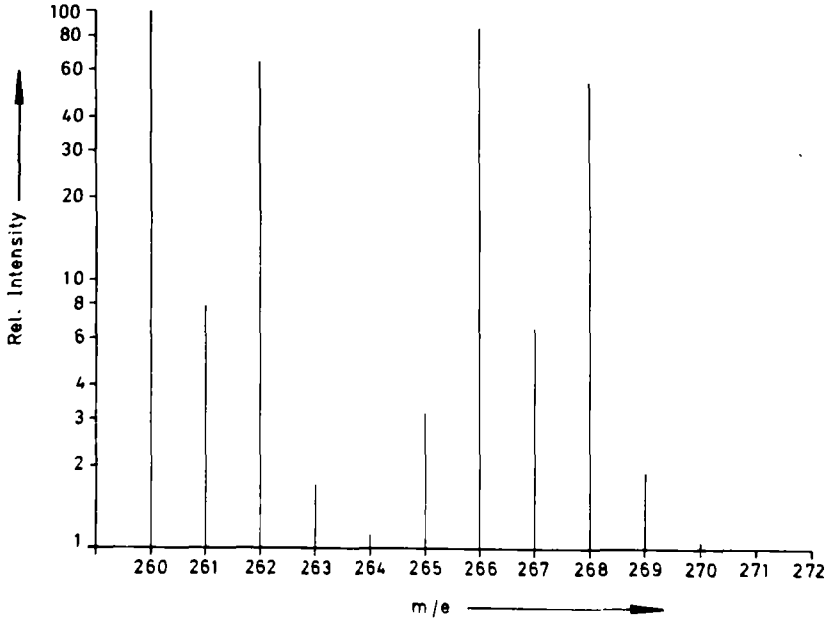

Fig.3: FD mass spectrum of cyclophosphamide d_0/d_6(100ng each), solvent acetone,emission threshold $1X10^{-8}$A, (16).

References:

1)H.-R. Schulten,H.D.Beckey,A.J.H.Boerboom,H.L.C.Meuzelaar, Anal. Chem. 45, 2358 (1973).
2)K.L.Rinehart,J.C.Cook,K.H.Maurer,U.Rapp,J.Antibiot.27,1(1974)
3)H.Adlercreutz,B.Soltmann,M.J.Tikkanen,J.Steroid Biochemistry, 5, 163 (1974)
4)H.-R.Schulten,U.Schurath,J.Phys.Chem. 79, 51 (1975).
5)H.-R.Schulten,U.Schurath,Atmos.Environ. 9, 1107 (1975).
6)D.E.Games,A.H.Jackson,M.Rossiter,Biomed.Mass Spectrom.i.press
7)J.A.Sphon,P.Dreifuss,H.-R.Schulten, J.A.O.A.C. i.press.
8)H.D.Beckey,H.-R.Schulten,Angew.Chem.87, 425;Angew.Chem.internat. Edit 14, 403 (1975).
9)H.-R. Schulten, J.Agr.Food Chem. in press.
10)H.Gierlich,H.J.Heinen,H,D.Beckey, Biomed. Mass Spectrom.2 , 31 (1975).
11)H.-R.Schulten,Biomed.MassSpectrom. 1, 223 (1974).
12)H.D.Beckey,H.-R.Schulten,in"Applied Spectroscopy Series",Eds. T.Pugh,C.Merritt,Marcel Dekker Inc.,New York, i.press.
13)H.-R.Schulten,in"Methods of Biochemical Analysis",Ed.D.Glick Interscience Publ.,J.Wiley&Sons,New york,Vol.24,1977.
14)H.-R.Schulten,B.Wittmann-Liebold,Anal. Biochem.i.press.
15)H.-R.Schulten,N.M.M.Nibbering,Biomed.Mass Spectrom.i.press.
16)H.-R.Schulten,Cancer Treat.Rep. 60, 501 (1976).
17)H.D.Beckey,A.Heindrichs,H.U.Winkler,J.Mass SpectromIonPhys. 3, App.9-11 (1970).
18)W.D.Lehmann,H.D.Beckey,H.-R.Schulten,in"Int.Symposium on Quantitative Mass Spectrometry in Life Sciences",Eds.DeLeenheer,R.Roncucci,Elsevier Scientific Publ. Amsterdam,i.press.

EMISSION-CONTROLLED FIELD DESORPTION MASS SPECTROMETRY OF LARGE ORGANIC SALTS

Hans-Rolf Schulten and Hans Dieter Beckey,
University of Bonn, Institute of Physical Chemistry,
5300 B O N N, Wegelerstr. 12 , West-Germany

One focal point in the analytical application of FD MS is the use of the method in investigations of inorganic(1-3) and organic salts (4).Since salts often produce weak and fluctuating ion currents a careful control of the desorption process is a basic requirement for the FD analysis of highly polar, nonvolatile material. An electronic device has been introduced that allows the registration of the emitter heating current and the total emission simultaneously (5).The monitoring of these two parameters prior to the evalution of the data from the photoplate proved to be particularly useful. The FD mass spectrum of a drug that consisted of a mixture of inorganic and organic salt was recorded in this manner.The sample was drawn from an injection vial which contained 5.48 mg methotrexate and 17.2 mg sodium chloride.

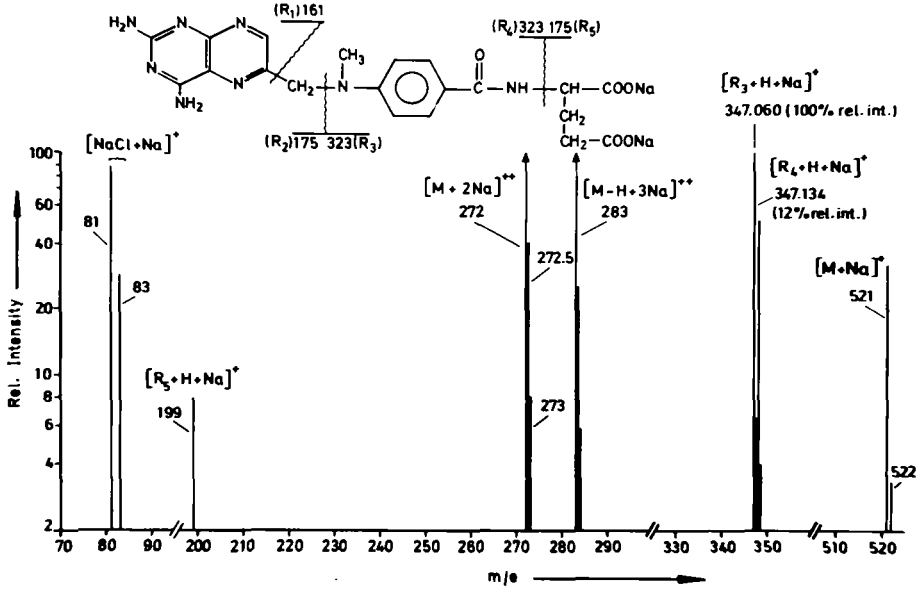

Fig. 1: FD mass spectrum of a mixture of methotrexate and sodium chloride.Solvent water, 1 µg of sample material was applied via the syringe technique. Emission-controlled FD, threshold 4×10^{-9} A,exposure time 26min.BAT 29-31mA.

Emission-controlled FD MS was used also for quantitation of biogenic amines which were present as hydrochlorides (6). The profiles of the emitter heating current and total emission during three different runs of an FD spectrum using three different emitters are shown in Figure 2. The emitter heating current e.h.c. (——) and total emission t.e. (----) of a mixture of dopamine d_0/d_4 hydrochlorides are plotted versus the desorption time. The $(C\text{-}H)^+$ ion intensities of the FD runs 1-3 are displayed in Table 1. The resulting molar ratio(expt) was d_0/d_4 1: 0.490 corresponding to an error of +5% from the theoretical value.

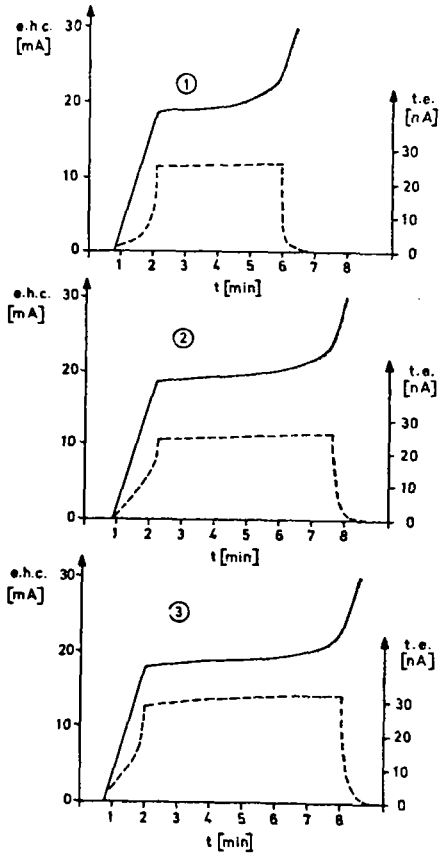

Fig.2 : Thermograms of the FD runs ① - ③ (6).

Table 1 : Quantitation of dopamine hydrochlorides (6).

	rel.int. ①	rel.int. ②	rel.int. ③
m/e 153	100	100	100
m/e 154	36.5	56.2	41
m/e 157	46.6	47.7	48.8
m/e 158	22.2	27.9	19.3

molar ratio d_0/d_4 (expt.) 1:0.490 error: + 5 %

References:
1) H.-R.Schulten, F.W.Röllgen, Org. Mass Spectrom. 10, 649 (1975)
2) H.-R.Schulten, F.W.Röllgen, Angew.Chem. 87, 544 (1975); internat.Edit. 14, 561 (1975).
3) M.Anbar, G.A.St.John, J.Am.Chem.Soc., 97, 7195 (1975).
4) H.-R.Schulten, W.D.Lehmann, Anal.Chim.Acta i.press (+ref.cit)
5) S.Pfeifer, H.-R. Schulten, unpubl. results.
6) W.D.Lehmann, H.D.Beckey, H.-R.Schulten, in "Int.Symposium on Quantitative Mass Spectrometry in Life Sciences", Eds. DeLeenheer, Roncucci, Elsevier Scientific Publ., Amsterdam

A Device for the Direct Measurement of Atomic Weights.*

WALTER H. JOHNSON, School of Physics and Astronomy, University of Minnesota, Minneapolis, Minnesota 55455.

A modification of the collector slit system of a mas spectrometer will be described which allows the direct measurement of the atomic weight of a multi-isotopic sample. Measurement of the atomic weight can be made relative to a standard sample or to the atomic mass of one of the isotopes by a modified peak-matching method.

*Work supported by the Office of Naval Research and the National Science Foundation.

ACCURATE MASS MEASUREMENT WITH THE AEI MS5074 MASS SPECTROMETER

S.Evans, D.Hazelby, K.R.Compson, and A.E.Holme

AEI Scientific Apparatus Ltd. Manchester, England

High resolution and high mass measurement accuracy are becoming increasingly important, and we reported last year, together with Aczel and Lumpkin of Exxon Research, on the special requirements of petrochemical analysis. Aczel and Lumpkin are reporting on further progress with this work at this meeting (V5).

Another application where exceptionally high performance is required is the analysis of compounds of high molecular weight and containing a large number of heteroatoms. In this case, high mass measurement accuracy is a pre-requisite, with resolution a secondary factor, in order to obtain unambiguous identification of fragment peaks.

This is illustrated by the analysis of a tri-methyl silyl derivative of adenosine-5-phosphate recently carried out using the MS5074.This sample has a molecular weight of 707 and was analysed at a resolution of 30000 and a scan rate of 100 seconds per decade. The mass measurement accuracy for a single scan was determined as 1.37ppm r.m.s., measured for 21 important peaks in the spectrum, ranging in intensity from 1% to the base peak. Fig.1 shows the errors in mmu for 8 of these peaks. In terms of confidence, the accuracy obtained implies that 2 out of 3 peaks will be measured within this error, and only 1 in 400 measurements will lie outside 3 times the r.m.s. error. i.e. 4.1 ppm.

The fragment ion at m/e 315 is clearly significant,and the importance of high mass measurement accuracy is illustrated in Fig.2, which shows the number of possible compositions, excluding isotopic peaks, at this mass as a function of the error tolerance used for the elemental composition calculations. Even at 5ppm, 19 possible combinations were found, several of which were structurally possible, but all involving some rearrangement.

A further complication was that all the isotope peaks were multiplets due to combinations of ^{13}C, ^{29}Si, ^{30}Si, or ^{18}O. However, by calculating the theoretical centroid and abundance for the isotopic peaks of each possible elemental composition of the fragment peak, isotopic information can be used as an aid to identification. Fig.3 shows the result of such an analysis on the m/e 316 isotopic peak of m/e 315, and it can be seen that the isotopic information clearly confirms that $C_9H_{28}O_4Si_3P$ is the true composition of m/e 315. Similar calculations on the m/e 317 and 318 peaks, the latter being a multiplet with 8 closely spaced components, gave equally good agreement. Weighted abundance calculations could be used alone, but the additional information derived from accurate mass measurements reduces ambiguity significantly.

Isotopically labelled compounds, usually using ^{13}C or D, provide a third and equally important application for high resolution mass spectrometry. An example of this is the analysis of a deuterated nucleoside, uridine, in which a sample of a few micrograms was evaporated from a direct inlet probe over a period of several hours. In this case, the MS5074 was used in the narrow scan mode due to the extremely high resolution, 70000 plus, necessary and the very wide dynamic range over which mass measurements and quantitative abundance measurements were required. Also, measurements were only required over the parent mass group extending from $^{m}/e$ 113 to $^{m}/e$ 116 so a wider mass range scan was inappropriate.

The narrow scan is a highly linear voltage scan of the electrostatic analyser voltage, the source accelerating voltage and other beam control supplies following the esa. The scan can be calibrated either by using known reference peaks, or by using the decade box to introduce a known voltage step during the scan. This voltage step allows a particular peak to be recorded twice with an accurately known separation between the two recordings. Mass measurements are then made direct from the u.v. chart, or by acquiring centroid times on a computer.

Three separate and overlapping narrow scans at 100ppm/second were carried out, covering the 113 to 114, 114 to 115, and 115 to 116 groups of peaks. Figs. 4 and 5 show the relevant sections of the first of these scans which illustrates the quality of information which was obtained. Mass measurements were obtained by introducing p.f.k. together with the sample, and using the $^{m}/e$ 113 peak from p.f.k., and its isotope at $^{m}/e$ 114, as references. The major peak in the 113 sample group was measured by peak matching, and these three known peaks were then used to calibrate the narrow scan. All the remaining peaks were the measured from the u.v. chart using the time marking trace shown at the bottom of the figures.

The elemental composition and abundance measurements obtained are summarized in Fig.6. Accurate mass measurements on components with an intensity of less than 0.1% are clearly possible using this technique.

SUMMARY OF MASS MEASUREMENTS OF ADENOSINE PHOSPHATE

5 microgrammes from direct insertion probe

Resolution 30.000 100 seconds per decade

Mass	Composition	Intensity %	Error (mMU)
707	$C_{23}H_{54}N_3O_7Si_3P$	1·8	1·8
692	$C_{24}H_{51}N_3O_7Si_3P$	12·7	0·1
466	$C_{19}H_{36}N_3O_3Si_3$	6·7	0·6
382	$C_{13}H_{31}O_3Si_3P$	22·8	0·6
337	$C_{13}H_{23}N_3O_2Si_2$	8·0	0·2
315	$C_9H_{28}O_4Si_3P$	85·8	0·0
258	$C_{11}H_{22}O_3Si_2$	33·3	0·0
73	C_3H_9Si	100·0	0·0

Fig 1

ACCURACY OF MASS MEASUREMENT

Effect of Confidence

Error limit (parts per million)	Number of possibilities
1	3
5	19
10	31
15	45

Fig 2

Resolution 30.000 Rate 100 s/decade

Sample TMS adenosine phosphate $C_{23}H_{54}N_3O_7Si_3P$

Isotope composition $^{13}C-^{29}Si$ doublet with 3·8 mmu separation

Measured Mass		Measured Mass	Measured Abundance %
315·1033		316·1048	25·3
Calculated Mass	Composition	Calculated Weighted Mass	Calculated Abundance
315·1033	$C_9H_{28}O_4Si_3P$	316·1044	25·28
315·1030	$C_8H_{21}N_3O_6Si_2$	316·1053	16·87
315·1029	$C_{10}H_{24}O_7SiP$	316·1036	16·22

MS50 USE OF ISOTOPES AS AN AID TO IDENTIFICATION AEI

Fig 3

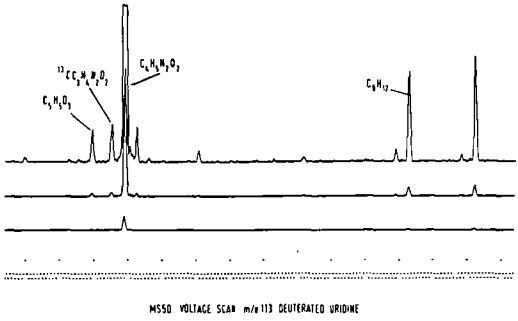

Fig 4

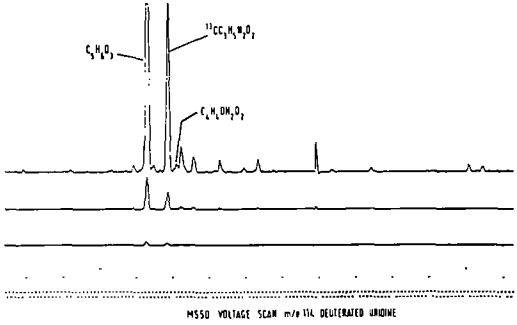

Fig 5

MASS	OBSERVED COMPOSITION	INTENSITY RELATIVE TO 113	ERROR MMU
113	$C_4H_5N_2O_2$	100%	0
	$C^{13}C_4H_4O_3$	0.10	0.3
	$C_5H_5O_3$	1.25	0.2
	$C^{13}C_3H_4N_2O_2$	1.02	0.2
114	$C_4H_4DN_2O_2$	0.21	0
	$C^{13}C_4H_5O_3$	0.08	0.4
	$C_5H_6O_3$	12.08	0
	$C_2^{13}C_2H_4N_2O_2$	0.12	0.1
	$C^{13}C_3H_5N_2O_2$	6.67	0.1
	$C_4H_6N_2O_2$	0.44	0.1

Fig 6

Precision of Relative Abundance Measurements as a Function of Mass Difference

W.R.Sherman,Washington University Medical School,St.Louis,Mo.
W.J.Fies and E.J.Heron, Finnigan Corporation,Sunnyvale,Ca.

Precision and accuracy data for isotope ratio measurements made with quadrupole GC/MS systems has been reported by several authors in the past five years, (1-3) but there is little data available on the precision that may be obtained when the ions whose abundance ratio is being measured are of different elemental composions. Since parameters such as source temperature, election energy, and ion energy are known to affect relative abundances of ions of different elemental compositions, this study was undertaken to determine the precision that was attainable for such measurements. Previous work indicated that the use of a homolog rather than an isotopically labelled analog as an internal standard for quantitation by selected ion recording could result in a significant loss of precision. (3) In order to determine whether this loss was unique to a single instrument or substance and to ascertain the specific causes of the increased error, several experiments were undertaken.

The work was carried out on two Finnigan model 3200 GC/MS systems, each with a 6000 data system, one in St.Louis and the other in Sunnyvale. Sufficiently large samples were used so that uncertainties which could be attributed to ion statistics were small compared to the standard deviations actually observed. Samples were analyzed in sets of ten and the coefficients of variation (cv) were determined for the various ion ratios.

The ratios of three pairs of ions in the electron impact mass spectrum of hexatrimethylsilyl myo-inositol (300 ng) were examined under various instrumental conditions over several months. The mean cv's obtained in 12 sets of runs were m/e 432/433, 1.55%; 305/432, 2.03%; 305/507, 3.43%. Some of the sets of runs were carried out with no ion energy programming and some with the compound dissolved in pure solvent rather than TMS reagent, but these changes did not consistently alter the performance.

The trend toward degradation of precision at large mass intervals seen in this data has several possible explanations. It was thought that such a trend might be the result of increased variation in the mass set voltages with increased mass interval. On the other hand, this trend could be the result of actual changes in the relative abundances of ions produced by the ion source. It is well known (4) that relative ion abundances depend on many factors including source temperature and it is not unreasonable to expect that this dependence could often appear to be a function of the mass difference of the ions. Several experiments were conducted in an attempt to distinguish between the two possible explanations for the observed mass dependence of the coefficient of variation. In order to compensate for possible lack of accuracy in the refocusing of the mass filter after a large mass change, a 1000 Hertz dither was used to sample the

ions over a ± 0.1 amu window. The runs sampled in this manner were made alternately with runs during which the dither was not used. No significant difference was found between the two sets of runs in which the average cv's were: 432/433, 0.26%; 305/432, 1.16%; 305/507, 2.98%.

To determine if this effect was unique to the quadrupole analyzer, we tested the same sample on an LKB-9000/PDP-12 system. The mean of the coefficients of variation obtained from three sets of ten samples were: 432/433, 1.75%, 432/507, 3.30%.

In order to compare the precisions attainable with both isotope ratios and ratios of ions of different elemental compositions, four ions in the mass spectrum of decachlorobiphenyl were measured. Six sets of ten runs each were analyzed on the Finnigan system and the cv's were: m/e 358/356, 0.56%; m/e 358/500, 2.15%. As expected the cv was less for the isotope ratio (m/e 358/356) than for the ion ratio (m/e 358/500). Since all four ions were measured in each run in the order: m/e 356, 358, 498, 500, the intensity of m/e 356 was measured after a large change in mass set voltage, while the intensities of m/e 358 and m/e 500 were sampled after relatively small changes. Thus the results suggest that possible lack of accuracy in refocusing the mass filter is not the primary cause of the observed error in the ratio of m/e 358/500.

In the course of continuous run of 50 samples of decachlorobiphenyl a trend toward improvement in the precision of the m/e 358/500 ratio was observed. When this experiment was repeated with the source temperature and filament power monitored it was found that the source temperature could be affected by simply introducing helium carrier gas or solvent into the source. A plausible explanation for this change is a change in the filament work function. In Figure 1 is shown the effect of accidently allowing a small amount of solvent from the GC solvent front to enter the source. The resulting increase in filament power and source temperature appears to change the ratio of m/e 358 to m/e 500. Since such fluctuations in source temperature may occur during a set of runs, experiments were carried out to measure the temperature dependence of the ratios of m/e 356/498 and 358/498. The source temperature was changed by heating with the direct probe black body coupled to the source through a copper heat collecter. As shown in Figure 2, these ion ratios show variation if the source temperature changes during a set of runs. The slopes for the plots of the various ratios as functions of temperature (^{o}K) are given below:

Ion Ratio	Slope
358/356	-50.60
500/498	45.34
356/498	691.23
358/500	602.60

Clearly the ratios of ions with different elemental compositions show much more dependence on source temperature than do the isotope ratios.

These findings have important consequences which should be considered when designing a quantitative experiment which

utilizes GC/MS. If ions produced by different processes are used for the quantitation, it is especially necessary to maintain constant source conditions by diverting the solvent and leaving the filament on at all times. Work is underway to design and evaluate an ion source with temperature control for those applications which require more precision than can be obtained with the standard system. When greater precision is required the use of an isotopically labelled standard is often prefered to the use of a homolog standard because flucuations in source temperature have little effect on isotope ratio measurements.

Acknowledgement

This work was supported, in part, by grants RR-00954 and AM-17904.

References

(1) Caprioli, R. M., W. J. Fies, and M.S. Story, Anal. Chem. 46, 453A (1974)

(2) Wolen, R.L., E. A. Ziege, and C.M. Gruber, Clinical Pharmacology and Theraputics 17, 15 (1975)

(3) Murphy, R.C., J.A. Zirrolli, K. Clay, S.E. Hattox and R. Helbig, Proc. of the 23rd Ann. Conf. on Mass Spectrometry and Allied Topics, P. 427 (1975)

(4) Beynon, J. H. , Mass Spectrometry and its Applications to Organic Chemistry, eg pp. 428-31, Elsevier, 1960.

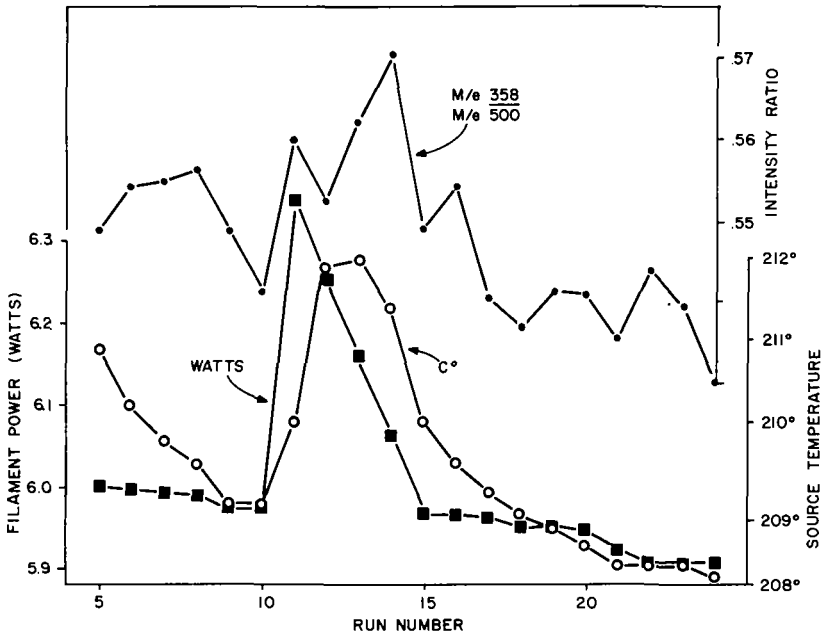

Figure 1

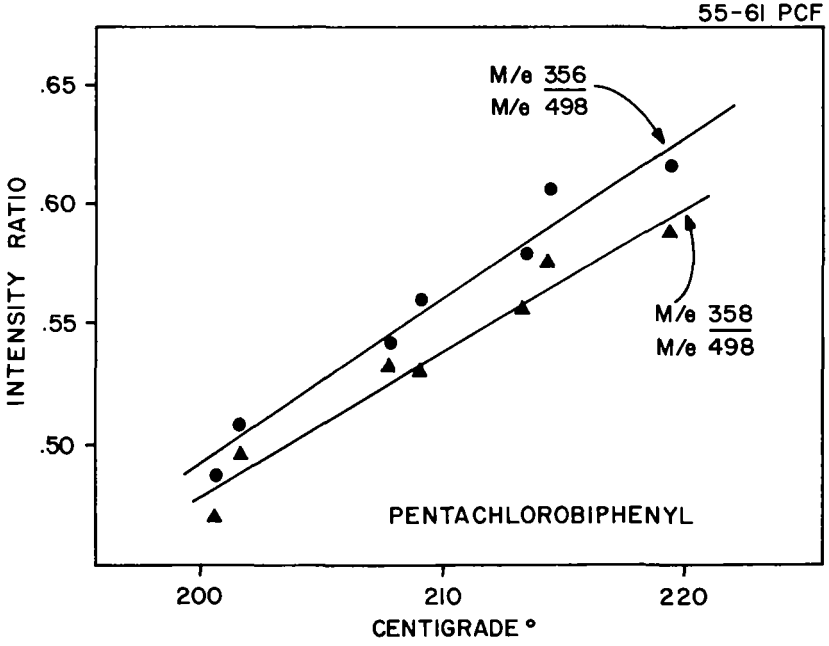

Figure 2

Mass Measurement Accuracy in the Trapped ICR Mass Spectrometer. EDWARD B. LEDFORD, JR. and R. T. McIVER, JR., Dept. of Chem., Univ. of Calif., Irvine, CA 92717.

A trapped ion cyclotron resonance mass spectrometer which features frequency sweep mass scanning has been developed. A study of the mass measurement accuracy of this instrument has been undertaken to determine whether it is suitable for identifying the elemental compositions of ions on the basis of exact mass measurements. Mass scale calibration and frequency measurement methods, as well as the factors which limit mass accuracy, will be discussed.

A Simple Approach to Quantitative SIMS. GENE R. SPARROW. Analytical Systems, 3M Company, St. Paul, Minnesota 55101.

Highly sensitive analytical instruments for Surface Analysis are being developed at a rapid rate to provide the data needed in todays research. A major advance has been the adaptation of mass spectrometry (SIMS) into analytical instruments for routine applications. Although a wealth of information has been obtained the general opinion has existed that SIMS is not readily amenable to giving good quantitative results. Quasi-equilibrium theories have been prepared and extensive, highly complicated and cumbersome computer programs have been written. However, reliable quantitative results from SIMS are not easily nor routinely obtained by more than a few surface scientists. This paper presents a simple approach to calculating quantitative results from most SIMS data utilizing some basic chemical and physical properties of the elements. Several samples of its application are presented.

A SIMPLE APPROACH TO QUANTITATIVE SIMS

G. R. SPARROW 3M ANALYTICAL SYSTEMS 3M Center, St. Paul, Minn. 55133

Highly sensitive analytical instruments for Surface Analysis are being developed at a rapid rate to provide the data needed in todays research. A major advance has been the adaptation of mass spectrometry (Secondary Ion Mass Spectrometry) into surface instruments. SIMS utilizing low energy primary ion beams especially 50 to 5000 eV is presently recognized as the most sensitive surface analysis tool available and is being used routinely to solve surface and bulk problems not previously amenable to other types of analysis. However, the general opinion exists that reliable quantitative SIMS data are not readily obtained. This paper discusses some of the existing quantitative techniques and presents a simple, easily applied technique applicable to SIMS data obtained at low energy from a variety of samples.

A diagram showing the essential components of a common SIMS apparatus is shown in Figure 1. This is commercially available as Model 620 Secondary Ion Mass Spectrometer from 3M Company. A leak valve admits a suitable inert gas into the electron bombardment type ion source where the ions produced are extracted. Focusing using a series of electrostatic lenses provides a beam size (full width at half maximum intensity) of less that 100μm to greater than 1 mm. Beam currents can range from a few nanoamps to over 1μ amp. Beam rastering and signal gating are also incorporated through the use of deflection plates to control the sputtering rate, obtain maximum depth resolution[1] during profiles, and for scanning SIMS images.

The low energy sputtered secondary ions from the specimen surface are extracted from the target area and admitted into a quadrupole mass spectrometer to provide high signal to background levels and good mass resolution for either positive or negative ions. An active gas enhancement system permits directing a flow of gas, such as oxygen, at the specimen surface to yield higher secondary ion yields,[2] and more constant signals during depth profiles.

Virtually all of the elements are detectable by the SIMS technique; however, elemental sensitivities vary by nearly five orders of magnitude. Such extreme variations of sensitivities, i.e., roughly 30 to 1 for Na compared to Si can give rise to spectra that are very misleading in appearance.

Quantification of SIMS data requires that relative ion yields be reasonably constant or that absolute ion yields can be calculated for each element. McHugh[3] has shown that relative ion yields are quite constant. Several methods of calculating quantitative data from SIMS data have been proposed using the Saha-Eggert equation. A model based on local thermal equilibrium (LTE)[4],[5],[6], a well documented highly theoretical approach, has achieved success with a small number of surface chemists. However, it requires use of a somewhat cumbersome, lengthy computer program not easily utilized by many analytical laboratories. A much simpliefed version of this LTE model has been developed and achieved similar results.[7] Another highly theoretical treatment is offered by Schroer.[8] The technique presented by McHugh[3] is based on an empirical method applicable to most SIMS systems.

The technique proposed in this paper is a rapid, easily applied procedure which yields reproducible approximations and does not require extensive calculations, cumbersome computer programs or time consuming reference analyses. An approximate relationship is assumed, based on chemical and physical properties and is applied to several problems. Figure 2 illustrates a simple diagram of the SIMS process. It is assumed that the number of ions detected by a system is determined by the ease of formation of the ion, (ionization potential), the relative energy required to separate that ion from the matrix and surface, and the transmission efficiency of the system for that particular ion. The energy required to separate an atom from a matrix is directly dependent upon its bonding to other surface atoms. This could be a complex function in itself, however, for simplicity the direct correlations between bond ionicity and electronegativitv is used. Hence, it is assumed that the electronegativity of the element will give good indication of its bonding characteristics. This is strongly supported from the known direct correlation of bond ionicity to electronegativity. There is also a direct linear correlation between electronegativity and work function, a frequently used physical property.

Due to differences in removal of ions from the source region, transmission of ions through a mass analyzer and differences in detector responses, absolute transmission efficiencies may vary greatly for different instruments. But Fralich et.al.[10] have shown that the relative

transmission efficiencies for high mass or low mass ions are roughly invariant for two types of SIMS instruments. It is assumed here that the overall transmission efficiency of the instrument to a given element is inversely dependent upon the mass of that atom. The following simple relationship produces useful quantitative approximations which should be similar for most SIMS systems. The relative sensitivity of each element for a particular ion beam energy is calculated by the simple assumed relationship:

$$S_R = A_I C/(nMX^2 e^{-I/kT})$$

where S_R = relative sensitivity for a given element

A_I = isotopic abundance of the particular mass

X = electronegativity of that element

M = mass to charge ratio of the ion used for measurement

I = ionization potential of the element

n = the number of bonds formed by the element

C = a correction constant obtained empirically from measured sensitivities if desired

For this particular presentation it is assumed that $C = 1$

Sensitivities for most of the elements have been calculated. The function $S = 1/MX^2e^{-I/kT}$ is shown plotted in Figure 3. This is a valuable guide to estimate the sensitivity one can expect for a particular element. Figure 4 illustrates the calculated sensitivities for a number of elements as well as a comparison to several sensitivities marked by an X measured by Andersen.[2] These sensitivities are intended for use in low energy 500 to 5000 eV applications not involving a reactive primary beam.

Several examples illustrating the validity of the application of this technique are discussed. Other data such as ISS (Ion Scattering Spectrometry) measurements made simultaneously and known bulk analysis were in good agreement. Prior to treatment of the data by this technique

only the raw spectral data were available. Other quantitative techniques were not readily applicable.

An untreated piece of 2024 Al sheeting was analyzed to a depth of approximately 1000Å and the results subjected to the procedure. Table I illustrates these results. Bulk analysis clearly shows much higher Cu. However, the surface analysis technique clearly demonstrates the contaminated outer surface is especially high in Mg, and substantially increasing Cu concentration as the bulk sample is approached. At about 3000Å the Cu eventually reached a concentration of 4.3% calculated using this technique.

Figure 5 illustrates quantitative SIMS depth profiles of a glass before and after heat treatment. Note the excellent correlation with the quantitative results for bulk analysis. Many other techniques cannot be applied to this typical problem due to surface charging which can cause ion migrations, extreme signal fluctuations, erroneous signals, beam wander, or even complete loss of the signal. Charge neutralization was utilized for the above measurements.

Several applications of this technique to catalysts have been made. Figure 6 illustrates results for one of these applications. Small Al_2O_3 beads approximately 1 mm. in diameter homogeneously treated with Ni and Mo were analyzed to determine the cause of failures to rejuvenate spent catalyst. It is obvious that the spent catalyst is contaminated with Fe and low in Ni. Quantitative data obtained from SIMS analysis of numerous other samples have been extremely useful over the past year.

These applications have covered integrated circuits, photoconductive powders and crystals, corroded and contaminated metals, and polymeric surfaces. Quantitative results for most elements have given excellent quantitative approximations from a few parts per million to nearly 100%. The most reliable information is obtained from ionic or covalent bonded materials. The least reliable information obtained is from pure, clean metals although the calculated values have not departed seriously from actual known values. The nature of the bonding in these cases is not as easily characterized. The calculated sensitivities of the more electronegative elements are also least accurate although they serve as a useful rough approximation to quantitative calculations.

The assumed relationship used to calculate these sensitivities has been found to be extremely valuable for general use in providing reliable quantitative approximations for most materials. Further more accurate relationships can be used for each specific problem; however, this relationship is reasonably accurate, simple, and convenient for general applications.

REFERENCES:

1. T. W. Rusch, J. T. McKinney, J. A. Leys, J. VAC. SCI. TECHNOL., Vol. 12, No. 1 Jan/Feb 1975.

2. C. A. Andersen, INT. J. MASS SPECT. & ION PHYSICS 2 (1969).

3. J. A. McHugh, "EMPIRICAL QUANTITATION PROCEDURES IN SIMS" in Secondary Ion Mass Spectrometry, edited by K. F. J. Heinrich, and D. E. Newbury, NBS Special Publication 427 Oct. 1975.

4. C. A. Andersen, J. R. Hinthorne, SCIENCE 175, 853 (1972).

5. C. A. Andersen, J. R. Hinthorne, ANAL. CHEM. 45, 1421 (1973).

6. C. A. Andersen, "A CRITICAL DISCUSSION OF THE LTE MODEL FOR THE QUANTITATIVE CORRECTION OF SPUTTERED ION INTENSITIES" in Secondary Ion Mass Spectrometry, edited by K. F. J. Heinrich, and D. E. Newbury, NBS Special Publication 427 Oct. 1975.

7. D. S. Simons, J. E. Baker, C. A. Evans, Jr., "TEST OF A QUANTITATIVE CORRECTION PROCEDURE FOR SIMS ANALYSIS", to be published in ANAL. CHEM.

8. J. M. Schroer, T. H. Rhodin, R. C. Bradley, SURFACE SCIENCE 34, 571 (1933).

9. Linus Pauling, The Nature of the Chemical Bond, Cornell University Press, p. 98, (1960).

10. R. D. Fralich, H. J. Roden, J. R. Hinthorne, "ANALYSIS OF SOLIDS USING A QUADRUPOLE MASS FILTER", APPLIED RESEARCH LABORATORIES, personal communication.

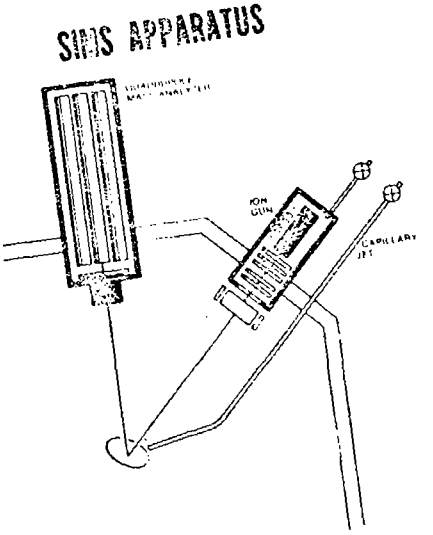

FIGURE 1
SCHEMATIC DIAGRAM OF SIMS APPARATUS

Some Practical Applications of SIMS. GENE R. SPARROW and J. A. LEYS, Analytical Systems, 3M Company, St. Paul, Minnesota 55101.

Secondary Ion Mass Spectrometry (SIMS) is rapidly becoming a routine analytical instrument to satisfy the demands of research and development for surface analysis. Its extremely high sensitivity, especially for low Z elements such as H, Li, C, O, F, Na, Etc., has made it useful and productive for a variety of applications. Its ease of operation and interpretation make it an excellent surface analysis tool that is readily adaptable to other analytical tools such as the SEM. Its application to analysis of trace surface contaminants in catalysts, metal surfaces, and treated polymers will be discussed. Application of this technique to determine elemental variations with depth (depth profile) of organic coatings and contaminants will also be discussed.

SIMS ANALYSIS OF Cu_2S/CdS SOLAR CELL SAMPLES *

FRANK G. SATKIEWICZ and Harry K. Charles, Jr.
The Johns Hopkins University APPLIED PHYSICS LABORATORY
Laurel, Maryland 20810

Three typical Cu_2S/CdS solar cell material samples[1] were analyzed by using sputter-ion source, secondary ion mass spectrometry (SIMS). The samples included: (a) an as deposited CdS layer (No.1), (b) a Cu_2S/CdS specimen (No.2) removed immediately following the topotaxial growth of the Cu_2S layer (barrier formation) by dipping in a solution of Cu_2Cl_2, and (c) a Cu_2S/CdS specimen (No.3) subjected to simulated gridding and encapsulation (lamination) processes. A typical cell cross section is illustrated in Figure 1.

SIMS analysis was accomplished by directing a defocused primary beam of 10 keV Ar^+ ions at the target. Positive ions from the secondary beam are then focused onto the entrance slit of the double focusing mass spectrometer (GCA Corporation Model IMS101B). By adjusting the energy window, simple spectra of elemental ions are transmitted (Figure 2). When bonding or structural features are desired, a polyatomic ion spectrum can be obtained (Figure 3). Since the beam produces a large flat crater (2x3 mm) as shown in Figure 4, intensity-time data arise from a consistent surface regression. Scanning electron microscope (SEM) analysis showed that the original surface topography was essentially preserved after the removal of ~9 μm, dispelling fears of preferential sputtering. Since a large area, homogeneous beam was used, the resulting profiles represent an averaging of about a million grains (grain size from SEM 1-3 μm). Relatively minor variations in the profiles result from a finite depth resolution (~5%), shadowing from asperities, and memory. Memory was minimized by obtaining data at a high energy window.

Continuous intensity-time data of a single species is relatively valueless in a polycomponent system (unless the species is present in relatively low concentration and the matrix intensities do not vary with time (e.g. boron in silicon)). To provide a material balance in polycomponent systems, the intensity-time profiles of the major matrix species must be taken simultaneously, or as in this study by alternate peak sitting. Intensities can be converted into surface fractions (f) by the application of appropriate yield factors with the use of a two component sputtering model.[2] Basic assumptions for the Cu_2S/CdS system are that the yield factors of Cu (and S) from Cu_2S and Cd (and S) from CdS are independent of depth and that the sulfur stoichiometry is consistent throughout.

Figure 5 shows Cu and Cd surface fraction vs time profiles for samples No. 2 and 3. The depth figure estimates arise from a determination of the average neutral sputtering yield of single crystal CdS sputtered perpendicular and parallel to the C axis, and the assumption that the neutral yield for Cd_2S is approximately the same. The initial fall in Cu (rise in Cd) occurs at the main interface between the Cu_2S and CdS (~0.2 μm.) The slower fall (0.2 - 2 μm) can be explained by interpenetration of the two phases, by original CdS topography, by changes in sputtering rate, or by impurity inclusions. Additional profile analysis combined with SEM surface studies will hopefully resolve some of the former possibilities. Since both samples started with the same amount of Cu_2S per unit area, the integral under both profiles should be identical. They are not and since no losses can occur the conclusion is that the

sputter ion yield for Cu (or Cd) in the region 0.2 - 2 μm is not quite the same.

These profiles were the result of using a constant set of yield factors. To examine the deviation from the assumption, the calculated total sulfur intensity was compared to the experimental intensity as shown in Figure 6. The region just before the pure CdS shows a statistically significant difference in the expected S intensity. The most likely explanation for this is the presence of a component which enhances the S^+ yield or lowers the Cd^+ yield.

In the definition of the surface fraction of atoms, the term $\sum(I/Y)$ is proportional to the total concentration of atoms in a fixed surface element and was found to be inversely proportional to the molar volume of a phase. A plot of the deviations of this factor also revealed differences as a function of depth, accordingly compounds of Cd, S, Cu, and O can be examined to obtain likely candidates for the suspected components. These include high molar volume compounds such as $Cu_2SO_3.H_2O$ and lower molar volume compounds such as CuS, CuO, and CdO. The latter also satisfies the deviation of sulfur stoichiometry due to yield enhancement as well as deviations of the $\sum(I/Y)$ factor in the vicinity of 2 μm. The presence of these components can be studied through a suitable calibration and a SIMS depth profile analysis of selected polyatomic species such as CdO^+ and CuO^+.

Other impurities were present at both the surface and the Cu_2S/CdS interface and include: Li^+, C^+, Na^+, Mg^+, Al^+, Si^+, Cl^+, K^+ and Ti^+. Most of these were probably introduced from the Cu_2S dipping process and were localized at the interface. Evidence of ambient interaction was found in a sample re-analyzed after approximately two months exposure to laboratory air. The $CuOH^+/Cu^+$ intensity ration at a depth near the CdS layer increased by a factor of three in this time interval.

---

* This work supported by the Naval Sea Systems Command under Contract N00017-72-C-4401

1 The authors wish to thank J. Meakin at the Institute for Energy Conversion, University of Delaware, Newark, Delaware for supplying the samples.

2 F. G. Satkiewicz and H. K. Charles, Jr. "Sputter Ion Mass Spectrometer Analysis of Copper Sulfide/Cadmium Sulfide Solar Cell Samples" APL/JHU Technical Memorandum TG-1284, October 1975.

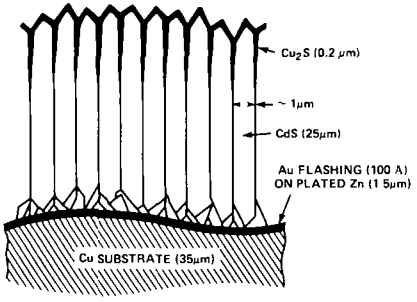

Fig. 1 Typical Cu_2S/CdS Solar Cell Cross Section

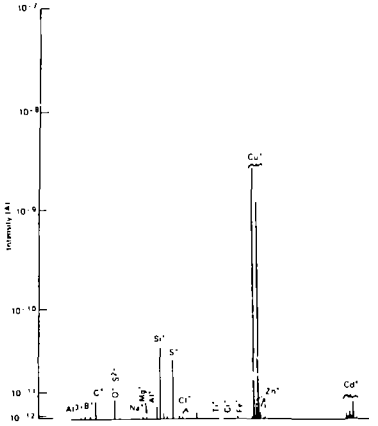

Fig. 2 Atomic Spectrum of Cu_2S Layer Sample No. 3

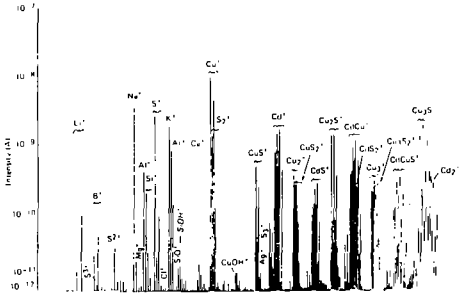

Fig. 3 Polyatomic Spectrum at 3 μm Depth Sample No. 3

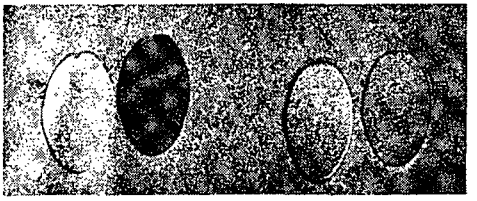

Fig. 4 Cu_2S/CdS Sample No. 3 Illustrating SIMS Craters (Craters ~ 2 x 3 mm)

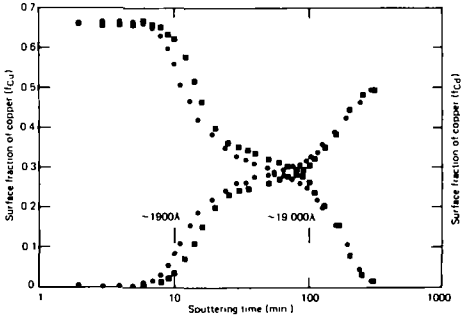

Fig. 5 Averaged Cu and Cd Profiles Cu_2S/CdS Samples ● No. 2 ■ No. 3

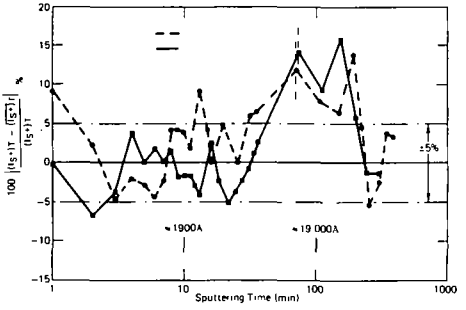

Fig. 6 Sulfur Stoichiometry Deviations versus Depth ● No. 2 ■ No. 3

A SIMS INVESTIGATION OF HETEROEPITAXIAL SILICON ON SAPPHIRE

W.L. Harrington, C.W. Magee,
G.W. Cullen, and J.F. Corboy

RCA Laboratories
Princeton, New Jersey 08540

Transistors fabricated in silicon on sapphire (SOS) are capable of operation at higher speed and with lower power consumption than are similar devices in bulk silicon[1]. The semiconducting properties of the heteroepitaxial silicon are influenced by contamination of the film as the result of reaction between silicon and sapphire at the growth temperature[2]. This contamination can result in degradation in the crystallinity of the deposit and the introduction of electrically active species (autodoping). The distribution of Aℓ and other species in these epitaxial films has been determined by SIMS depth profiling, and correlations are shown with growth conditions and heat treatments.

SOS samples were 0.5-1 μm films of (100) Si deposited on $(1\bar{1}02)$ sapphire substrates. Heteroepitaxial growth using silane in a hydrogen ambient was carried out with both constant growth rates and a rapid-early-growth or "burst" technique[3].

Since Aℓ is the most important contaminant in question, calibration of SIMS response was performed on known dosages of Aℓ implanted into bulk Si wafers. Since these studies were done with a Cameca IMS-300 as well as with a secondary ion quadrupole mass spectrometer (SIQMS) constructed at RCA Laboratories, a comparison of results for an Aℓ-implant standard is shown in Figure 1. In addition to the remarkable agreement of the data taken on the two rather different instruments, this figure also shows that our sputter rates are well calibrated (agreement with the projected range of distribution) and that we can obtain simultaneous high sensitivity (down to 10^{16} atoms/cm^3) and good depth resolution necessary for SOS characterization.

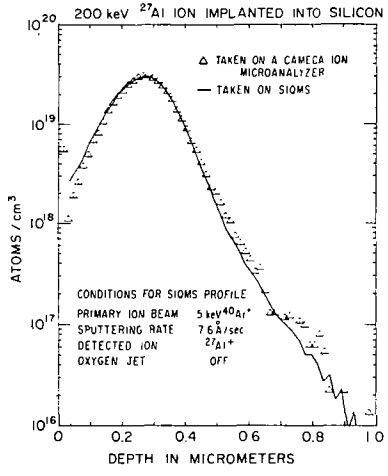

FIGURE 1.

Figure 2 shows Aℓ distributions in SOS films prepared using different growth conditions. The first two films, grown at a constant rate of 2 μm/min at two deposition temperatures, show a relatively flat Aℓ distribution. The higher temperature deposition results in an increase in the level of Aℓ contamination. The burst technique (initial growth of 600 Å at 5 μm/min with the remainder of the 1 μm film grown at 0.5 μm/min) results in a very low Aℓ concentration for most of the film, but the surface or end of growth is characterized by a large increase in Aℓ concentration. In most cases, these high surface concentrations have been shown to be reproducible and not due entirely to surface oxide yield enhancement.

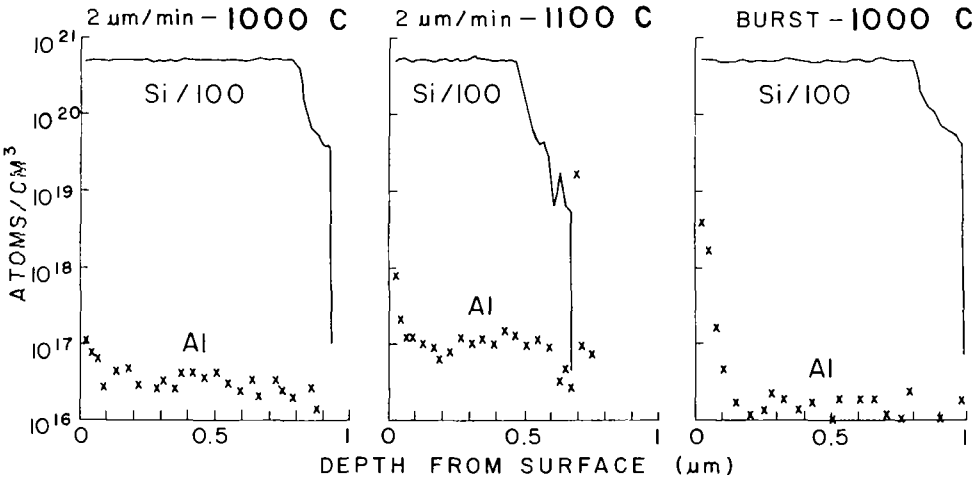

FIGURE 2.

Figure 3 shows changes in the Aℓ distribution as a function of thermal treatments after growth. The "as grown" sample was intentionally "N"-doped with As, but Hall measurements indicated that the resulting Si was "P-type". Heating this sample in an O_2 ambient was shown to cause a change in the Si from P to N-type. This change can be associated with an order of magnitude drop in overall Aℓ concentration. Although the concentration gradient is complicated by the possibility of oxide enhancement near the surface, the change in distribution and the loss of Aℓ is evident. H_2 annealing after O_2 treatment further smooths out the Aℓ distribution to a relatively low, uniform value throughout the film.

Also plotted in Figure 3, is a quantity indicative of the hydride content of the film. Since 28 is the large Si isotope, the response at 29 can be much too large if SiH^+ ions form from a large amount of hydrogen present. Thus, the $^{29}/30$ ratio, corrected for isotopic abundance and multiplied by 5×10^{20} to correspond to the Si value plotted, should coin-

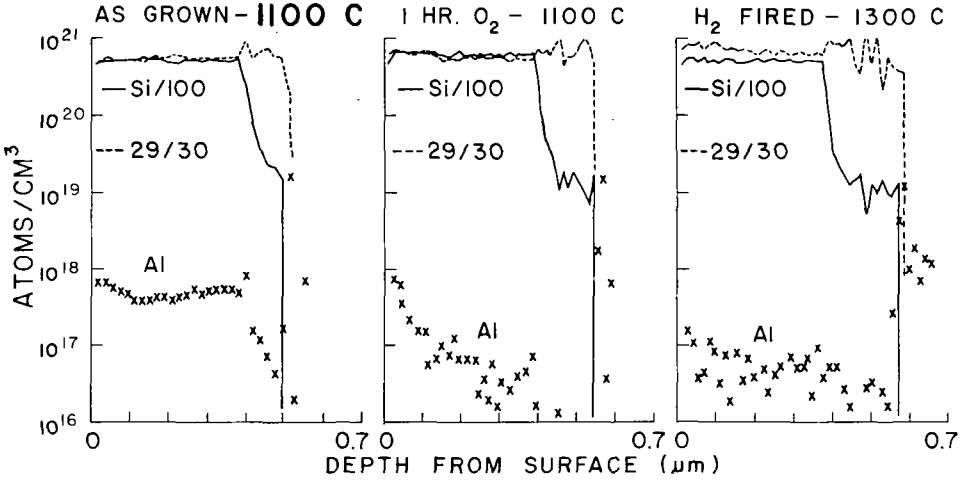

FIGURE 3.

cide with the raw Si response with no hydride present and rise above the raw Si response where hydride formation is prevalent. Notice that after H_2 annealing, the level of the $^{29}/30$ ratio indicates the presence of hydride throughout the film.

For films showing low contamination levels, the interfacial region generally appears as shown in Figure 4. The apparent Aℓ content decreases to bulk level within a distance of 300-500 Å from the silicon/substrate interface. There appears to be no significant redistribution of Aℓ between the interface layer and the remainder of the deposit. It is interesting to note that the thickness of the interface region as measured by SIMS is in excellent agreement with the thickness at which the substrate is completely covered with silicon during film growth[4].

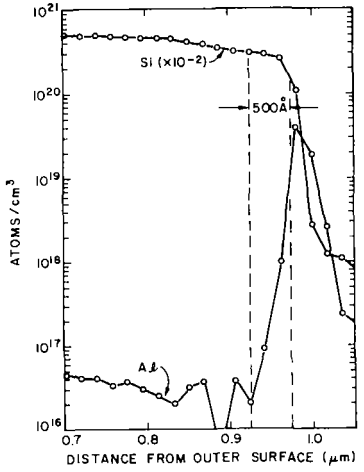

FIGURE 4.

In the above SOS profiles, taken with the Cameca instrument, one can notice a drop in the Si signal before the abrupt fall-off at the Si/sapphire interface. Figure 5 shows a burst-grown film profiled on both the Cameca and SIQMS instruments. The rise (SIQMS) or fall (Cameca) before the interface is reproducible in both instruments and is independent of primary beam density. The magnitude of the change and the overall shape of the change depend on the sample, but are reproducible for any one sample. With SIQMS, where we have had the opportunity to investigate this feature in more detail (conditions A, B, and C in Figure 5), there are several observations which suggest that this phenomenon is characteristic of the sample and not just a changing or anomalous yield effect. (A) All Si species (Si^+, Si^{2+}, Si_2^+, etc.) show the same effect, but there is no corresponding change in oxygen signal in the vicinity of the interface. (B) Secondary ions leaving the sample at higher energy (57 eV as compared with 14 eV at the distribution maximum) result in a decreased Si^+ signal, but the interface rise is relatively the same. (C) Even with a jet of O_2 on the sample during bombardment with Ar^+, which increases the Si^+ response by a factor of at least 100, the same relative rise at the same distance from the interface is observed. Because oscilloscopic ion images can be observed in real time during sputtering, and because this image is very sensitive to sample voltage and shows no change in the region 1000-2000 Å before the interface, we feel that the effect is not caused by sample charging. At this point we have no explanation of the difference between SIQMS and Cameca.

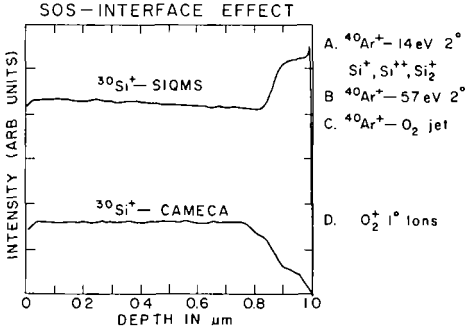

FIGURE 5.

The positive secondary ion variation must be associated with a yield effect, but one that likely can be correlated with a property of

the sample. We are currently investigating this effect as a function of Si crystal orientation, and will report on this aspect at a later time.

References

1. E.J. Boleky and J.E. Meyer, IEEE J. Solid State Circuits SC-7, 135 (1972).

2. D.J. Dumin, P.H. Robinson, G.W. Cullen, G.E. Gottlieb, RCA Rev 31, 620(1970).

3. G.W. Cullen, J.F. Corboy and R.T. Smith, J. Crystal Growth 31, 274 (1975).

4. G.W. Cullen, and J.F. Corboy, J. Electrochem. Soc. 121, 1345(1974).

STUDY of NEGATIVE SECONDARY ION SPECTRA PRODUCED by CS^+ PRIMARY BEAM on METAL TARGETS

Marcel Baril et Pierre Vallerand

Département de Physique
Université Laval
Québec, CANADA G1K 7P4

The mechanism of secondary ion emission produced by ion bombardment on metals and alloys is not well understood. Therefore it seems useful to provide new experimental facts and data. They are based on our results obtained by bombarding appropriate targets by positive Cs ions.

Figures 1 and 2 are typical spectra of a Nickel Chromium steel alloy; it contains much of the peculiarities which caracterised peak nature and intensities obtained by $Cs^{\pm}$ ion bombardment.

In the positive spectrum shown in fig. 1, the alcaline peaks Rb^+ and Cs^+ come from the primary beam. Peaks coming from the target are: $A\ell^+$, Mg^+, Ti^+, Cr^+, Fe^+, Ni^+, TiO^+, TiO_2^+

The negative spectrum of the same target which is shown in fig. 2 exhibits four main features:

1) production of ion clusters such as Ni_2^- and Ni_3^-
2) production oxygenated polyatomic ions such as NiO^- , $A\ell O^-$, FeO^-, $A\ell O_2^-$, CrO_2^-, NbO_2^-, CrO_3^-, NbO_3^-
3) production of metallic complexes such as $NiCr^-$, Ni_2Cr^-
4) production of hydride ions such as Ni_2H^-

For pure metals such as Copper and Aluminum, we have observed clusters up to Cu_7^- and $A\ell_6^-$ respectively. The relative intensities of peaks Cu^- to Cu_7^- and $A\ell^-$ to $A\ell_6^-$ seem to contain a precious piece of information concerning the emission process of the clusters. For Copper, for example, the peak intensity is distributed as following: $I_3 > I_1 > I_2 > I_4 > I_5 > I_6 > I_7$.

Enhancement of polyatomic oxygenated peaks comes from the fact that it is a chemical emission process instead of the standard kinetic process. This fact could be used to increase the detection limit of trace element in a matrix. We have done it for Arsenic, Indium and Antimony in lead matrix. Polyatomic oxygenated ions could also be used to evaluate the degree of oxygenation of the surface in regard to that of the bulk material.

Finally, metallic complexes, hydride ions and hydroxyde ions may be used to gain information on the chemistry of the surface and on the molecular complexes that are formed in metals and alloys.

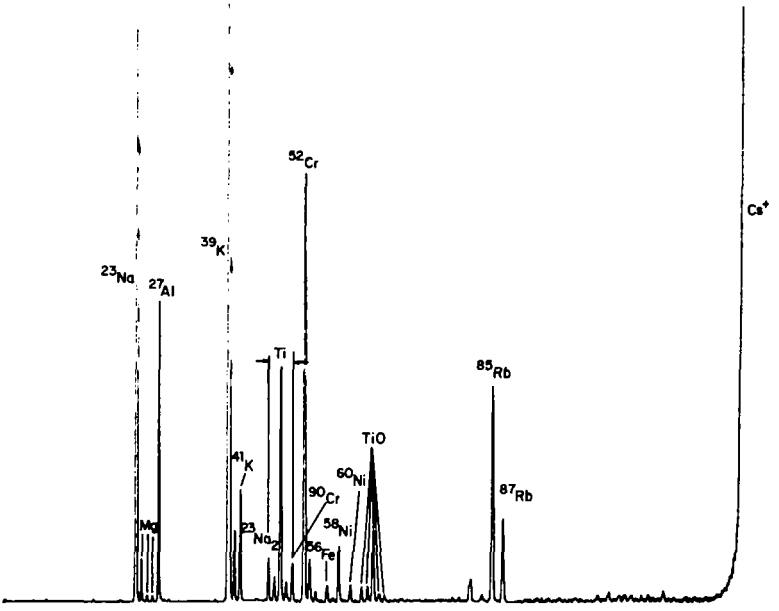
52Cr
Cs+
39K
23Na
27Al
Ti
85Rb
TiO
41K
60Ni
90Cr
87Rb
Mg
23Na2
58Ni
56Fe

FIGURE 1

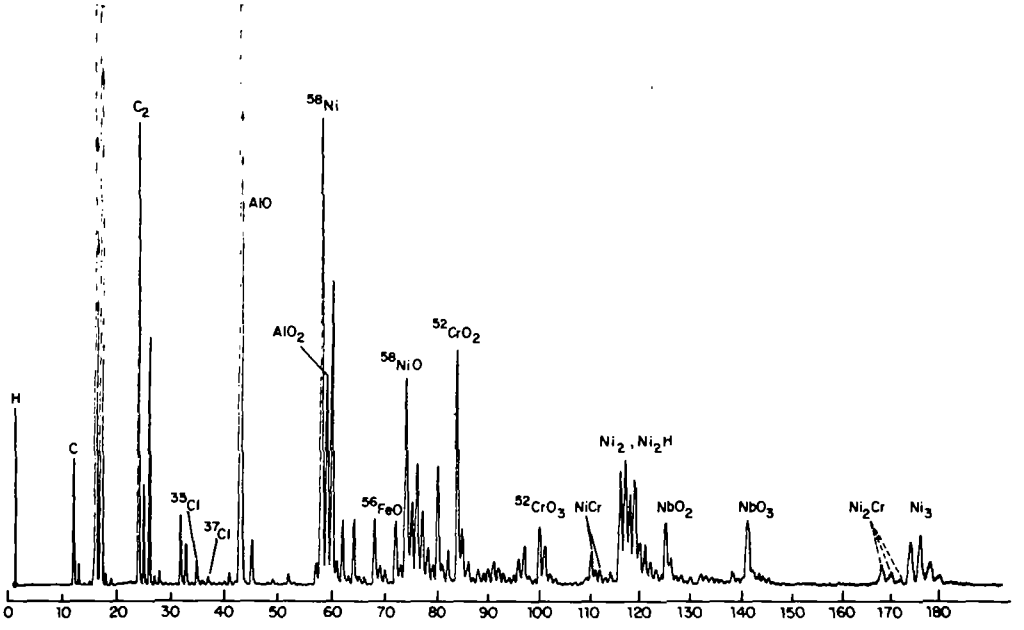
H
C
C2
35Cl
37Cl
AlO
AlO2
58Ni
56FeO
58NiO
52CrO2
52CrO3
NiCr
Ni2, Ni2H
NbO2
NbO3
Ni2Cr
Ni3
0
10
20
30
40
50
60
70
80
90
100
110
120
130
140
150
160
170
180

FIGURE 2

Study of an Iodine Discharge in a Duoplasmatron,

W. W. HARRISON* and H. LIEBL, Max-Planck-Institut für Plasmaphysik, 8046 Garching b. München, EURATOM-Association, West Germany.

An iodine discharge in a Duoplasmatron hollow cathode ion source allows the extraction of negative iodine species for possible application in SIMS. The electro-negative character of iodine produces efficient negative ion formation with a simple resultant mass spectrum. Iodine vapor from a reservoir containing solid iodine must be delivered to the discharge in a controlled and reproducible manner. Discharge stability is enhanced by the use of a carrier gas. Argon is particularly advantageous in that it contributes no additional negative ions which would complicate the primary beam in a SIMS application. The intensity and stability of the iodine discharge depend upon several parameters, including choice of carrier gas, the pressure ratio between iodine and carrier gas, the discharge current, zwischen-electrode offset, and the Duoplasmatron magnet fieldstrength. Stainless steel cathodes have been used at discharge currents to 100 ma.

*On leave, 1975-76 from: Depart. of Chemistry, Univ. of Va., Charlottesville, Va. 22903, USA

The Measurement of Isotopic Ratios with Sputtering-Ion Source Mass Spectrometers, J. R. HINTHORNE, R. L. CONRAD, R. D. FRALICK and C. A. ANDERSEN, Applied Research Laboratories, Hasler Research Center, 95 La Patera Lane, Goleta, California 93017

Applications of the sputtering-ion source for the isotopic analysis of solid samples will be described utilizing data obtained from a quadrupole mass spectrometer (QMAS) and from a double-focusing magnetic mass spectrometer (IMMA). In both instruments accurate ratios are obtained on elements, such as Li, Ti, Sr, Mo, Ag and Pb, without changing instrument operating conditions and without normalization to standards. The important characteristics of this type of ion source are a lack of mass fractionation and the simplicity of sample preparation and presentation. The high absolute sensitivity of the technique makes it possible to measure isotope ratios of many elements at the trace concentration levels.

ION IMAGING AND ION COUNTING: COMPLEMENTARY TECHNIQUES FOR DIFFUSION STUDIES

George Sweeney
Westinghouse Research Laboratories
Pittsburgh, Pennsylvania 15235

The techniques of Secondary Ion Mass Spectrometry (SIMS) have been most successful with studies of diffusion in semiconductors and thin films where diffusion depths are consistent with reasonable sputtering times.[1] In these applications sputtering takes place in the direction of diffusion. In metallurgical samples, diffusion takes place on a much larger scale and requires a different approach. In a study of nickel activated recrystallization of doped tungsten, the specimen is cut along the axial plane containing the direction of diffusion. Concentration gradients are observed by ion imaging and/or ion counting along the direction of the diffusion front. By comparing tungsten and nickel images of a given area, complete coincidence between nickel penetration and the recrystallization front was observed. It appeared that nickel was concentrated along the recrystallized grain boundary with a small amount within the recrystallized grain. These observations were confirmed by ion counting, i.e., plots of nickel intensity vs. distance obtained with the sample slowly traversed under the ion beam.

---

1. "Analysis of Metal-GaAs Schottky Barrier Diodes by Secondary Ion Mass Spectrometry", H. B. Kim, G. G. Sweeney, and T.M.S. Heng, Inst. Phys. Conf. Ser. No. 24, 1975, Chap. 5.

THE ROLE OF SAMPLING IN ION PROBE ANALYSIS

G. J. Scilla and G. H. Morrison
Department of Chemistry, Cornell University
Ithaca, N. Y. 14853

INTRODUCTION

In any chemical analysis, the analyst must be concerned with the introduction of error into the final results. Error may be generally classified into three categories: sampling error, error associated with physical and/or chemical pretreatment, and finally, measurement error. The overall variance of the method is given by the sum of the variance terms shown in the equation:

$$S_t^2 = S_s^2 + S_p^2 + S_m^2 \qquad \text{Eq. 1}$$

where S is the standard deviation and the subscripts s, p, and m associated with each variance represent sampling, physical and/or chemical pretreatment and measurement error, respectively. (1) In concise terms, sampling error is defined here as the error associated with the selection of an analytical sample from a heterogeneous material. There can be no sampling error from a homogeneous material.

In microprobe analysis, the analyst is presented with unique sampling problems. The main objective of the various probe techniques is to provide *in situ* chemical information on microfeatures in solid samples and thus establish their chemical identity. Unlike most analytical techniques, no physical or chemical pretreatments such as grinding, dissolution or mixing are employed. The probist, therefore, has no opportunity for homogenization of the sample in order to reduce sampling error. A second problem exists in the fact that the analytical volume sampled in probe analysis is extremely small, typically much less than a few cubic microns.

It is apparent, therefore, that because the analytical sample volume is small,and that steps to insure homogenization are precluded, sampling error in microprobe analysis of a heterogeneous material may be a serious problem.

ESTIMATION OF SAMPLING ERROR

As was previously stated, the objective of microprobe analysis is the *in situ* characterization of a microfeature. If that microfeature is homogeneous in the constituent of interest, and if it is large enough so that the only signal collected originates from within its boundaries, then there will be no sampling error. If it is small enough so that the entire microfeature can be sampled, the sampling error will be minimal if the background area does not contain the constituent of interest. (Even if the background contains the constituent of interest, a simple correction for background approach will minimize sampling error, as long as the sampling requirements of the background are considered.) Finally, if the microfeature is heterogeneous and so large that collection of signal from the entire microfeature is impractical, there will be a certain amount of sampling error in the final result.

It would be helpful to the analyst to be able to obtain an estimate of the expected sampling error as a function of the degree of heterogeneity of the sample and the parameters he wishes to use in the analysis. For these purposes, one may usually represent the distribution of hetero-

geneities as either point masses, or for a more exact estimate of sampling error, spherical particles in space. Also, since the area sampled in ion probe analysis is usually much greater than the depth sampled, it is convenient to limit our discussion to areal analysis only. One may easily convert to 3-D space, however, by replacing area terms with volume terms and by considering the number of particles/unit volume rather than number per unit area. With these simplifying assumptions in mind, the following two equations were derived:

$$S_s = \frac{100}{(\bar{N}a_o)^{1/2}} \qquad \text{Eq. 2}$$

$$S_s = \frac{100(1-\bar{N}\bar{A}_p)^{1/2}}{(\bar{N}a_o)^{1/2}} \qquad \text{Eq. 3}$$

where S_s = % Relative Standard Deviation due to sampling alone. Equation 2 was derived making use of the Poisson distribution law and estimates sampling error when the heterogeneities are approximated by point masses. Here $\bar{N}$ = the number of points per unit area and a_o = area sampled. Equation 3, derived employing the Binomial distribution is an estimate of sampling error for the case where one wishes to consider the average area of the heterogeneities, $\bar{A}_p$, in order to obtain a better estimate. It should be noted that the term $\bar{N}\bar{A}_p$ is equivalent to the fraction of surface covered, thus, as the surface coverage approaches 1, the sampling error goes to zero, as would be expected. Also, as the particle size $\bar{A}_p$ approaches zero i.e., point masses, Equation 3 becomes identical to Equation 2, as also is expected.

RESULTS

The accuracy of these equations has been tested experimentally for systems of small, moderate, and large numbers of heterogeneities using a CAMECA IMS-300 ion probe. The total experimental error was determined by taking 20 sets of data for each system, at varying field aperture or sample area sizes. Sputtering rate for each system was approximately 20 Å/sec, and data collected for one second.

Table 1a shows the results for the case of a small number of particles. Here $\bar{N}$ is approximately equal to 8.2×10^{-5} particles per μ^2 which corresponds to an average of four particles in a field of view of a 250 μ diameter. $\bar{N}$ was estimated by taking a number of ion images and counting the number of inclusions. S_s was calculated using the equation for point masses and the experimental vs. calculated results are shown.

The results for a system of a moderate number of particles are shown in Table 1b. $\bar{N}$ was estimated by the same method as above and was determined to be approximately 2.5×10^{-3} particles/μ^2 or 123 in a 250-μ diameter area. Again, S_s was calculated using the point mass equation and the results are also displayed. As in Table 1a, it can be seen that the sampling error becomes a serious problem as the sample area decreases.

The second equation was used to calculate the sampling error for Cr in NBS 661 steel and the results are shown in Table 1c. Here, $\bar{N}$ is approximately equal to .233 which corresponds to 12,000 heterogeneities in a 250 μ diameter area. $\bar{N}$ was estimated using the 250 μ data and the coverage estimated by combining the 250 and 63 μ data. The worst sampling situation in this case occurs when the diameter of the area sampled is 9 μ and gives rise to an 18% sampling error. If the sampling area diameter were 1 μ, the second equation predicts an error of 83%.

CONCLUSIONS

In conclusion, it is apparent that in certain cases, sampling error in microprobe analysis is potentially a serious problem. In any case, the smaller the sampled area, the larger the sampling error that is incurred in the analysis. In using a small beam probe technique, consideration must be given to the homogeneity of the microfeature under study.

Also, while there has been considerable effort to make SIMS a quantitative technique, insufficient attention has been given to the important role of sampling to the quality of results. Most treatments of quantitation have assumed homogeneous sampling; however, we must realize that this situation is far from reality.

REFERENCES

R. K. Skogerboe and G. H. Morrison, Symposium on Trace Characterization - Chemical and Physical, NBS, Gaithersburg, Md., 1966. Proceedings, p 589.

A more complete paper based on this study will be submitted for publication to ANALYTICAL CHEMISTRY.

TABLE 1. EXPERIMENTAL RSD vs. CALCULATED SAMPLING ERROR.

(a) Zr in Metal Alloy

$\bar{N} \approx 8.2 \times 10^{-5}$ Particles/μ^2

$\bar{N}$ estimated by counting

Sampled Area Diam.	Expt. RSD(%)	Calc S_s(%)
250μ	42	50
63μ	195	198

(b) Ti in NBS SRM 664

$\bar{N} \approx 2.5 \times 10^{-3}$ Particles/μ^2

$\bar{N}$ estimated by counting

Sampled Area Diam.	Expt. RSD(%)	Calc S_s(%)
250μ	5	9
63μ	39	36
33μ	67	68

(c) Cr in NBS SRM 661

$\bar{N} \approx .233$ Particles/μ^2

$\bar{N} A_p \approx .5$

$\bar{N}$ estimated by calculation from 250 μ data

$\bar{N}\bar{A}_p$ estimated by calculation from 250μ and 63μ data

Sampled Area Diam.	Expt. RSD(%)	Calc S_s(%)
250μ	.94	(.94)
63μ	2.7	2.6
34μ	4.3	5.0
9μ	17	18

A New Laser - Arc Milliprobe Mass Spectrometer

Spark source mass spectrometry has enjoyed only limited success in its use as a milliprobe instrument. This will describe some initial work on a new milliprobe which will retain the advantages of SSMS but will improve considerably its capabilities.

We have found the r-f spark source to be useful as a milliprobe by using a 7 mil diameter gold (in some cases 20 mil diameter graphite) probe as a counter electrode to a metal sample. This ion source has been applied to the measurement of concentration profiles of trace level solutes which can be measured conveniently by r-f spark excitation between the probe and the sample rod by moving the sample rod from site to site under the probe. This application of the spark source mass spectrometer as a milliprobe is very useful but it is far from ideal. This is due to the lack of control over the location of excitation as well as the diameter of the excited spot and the lack of control over the power dissipated in the excitation. However the technique could be extremely powerful if these difficulties were overcome. The idea of a laser probe or of a laser ignited arc is not new. However laser techniques alone have not enjoyed much success either. They have usually relied upon very high energy pulses for sample excitation, upon time-of-flight mass analysis, and the application of low repetition rate lasers. We believe that a powerful milliprobe can be developed by careful selection and combination of laser, excitation source and mass spectrometer.

Before describing the development, let us consider some of the characteristics indicated in Fig.1 for 3 different means of sample excitation: the r-f spark, the low voltage d.c. arc, and the laser. The laser is the only one yielding the kind of site selection needed to improve lateral resolution. The laser also produces an ion beam with a low energy spread although the d.c. arc is much lower than the r-f spark in this regard. The d.c. arc provides more controlled power for production of positive ions than the laser or the r-f spark. It also produces more stable ion currents than the other two. Laser excitation produces more neutrals than the other two sources. Multiply charged ions are more intense with the d.c. arc and least intense with the laser sources. Perhaps the r-f spark has the more convenient levels in this regard. Both the d.c. arc and the laser produce low levels of molecular ions compared with the r-f spark as well as all sputtering ion sources. The duty cycle of the r-f spark ion source is largely unknown due to the erratic nature of the ion current as is the case with the laser. However the d.c. arc can be operated with a quite dependable duty cycle. The range of relative sensitivity coefficients (RSC), should be small. The range is smallest for the arc and greatest for the laser. Sputtering ion sources also have a large range of relative sensitivity coefficients. Laser excitation does not require a counter electrode. However the d.c. arc provides preferential analysis of one electrode. Our general plan is to combine the spot selection capability of the laser with the favorable features of the d.c. arc as indicated conceptually in Fig. 2.

A site to be analyzed is selected by viewing through the laser optics and then a short duration focused laser pulse is fired to that site. Sample excitation occurs with vaporization and plasma formation. However this excitation is kept to a minimum, only that necessary to initiate a d.c. arc which runs under steady state conditions for a preset time after which the sample is allowed to cool. The laser we have chosen is a Nd doped yttrium aluminum garnet which has a 1.06 μm wavelength. (Holobeam Laser, Inc. model 255QT) It has an acousto-optic-Q switch which permits external control of the laser pulse in single shots from 0 to 24 kilohertz. Each pulse is about 300 ns long and contains several hundred microjoules of energy. This is about one kilowatt peak power. The laser beam is focused to a spot 12 μm in diameter which gives a power density of about 10^8 watts per square cm. The position of the focused spot can be controlled electronically over an area of ~1 square mm. The reproducibility of a setting is within 12 μm. The laser beam may also be rastered within this square millimeter.

The working distance from the objective lens to the focused spot is approximately three inches which allows the complete laser system to be located outside the vacuum chamber as shown schematically in Fig. 3.

The sample (cathode) and the counterelectrode (anode) are located just in front of an ion accelerating plate. A co-axial-tube cylindrical lens has been designed to provide mechanical support for the source and for focusing the ion beam at the object slit of the instrument. The outer tube is approximately 6 cm in diameter and is at ground potential. The inner tube is about 2 1/2 cm dia and is at ~18 kV with the accelerating plate at 25 kV. The overall length is ~40 cm. Ion beam adjusting electrodes are located just in front of the object slit of the mass spectrometer, a double focusing mass spectrograph. Figure 4 gives the flow diagram for <u>electronic control</u> of the ion source. The gap voltage is applied prior to a preset <u>wait</u> period (repetition rate) after which the laser is triggered to give a single pulse. If an arc is not sensed the laser is fired again 100 μs after the first pulse. If the "No" cycle is followed 4 times in succession the system stops and indicates this information to the operator. When an arc is sensed, the ion gate is turned on to sample the arc for a preset period after which the arc is turned off. An arc counter is incremented and the system decides whether the number of arcs requested by the operator (preset) has been obtained. The system has been designed to provide a given number of arcs, i.e., an arc count. If the system has been switched to a continuous mode then the system cycles until stopped by the operator.

Figure 5 is a <u>block diagram</u> of the <u>controlling circuit</u>. The items at the left are switch settings of parameters under control by the operator. The logic circuitry is at ground potential and it communicates digitally thru optical couplers providing voltage isolation for the arc power supply which floats at 25 kV. The logic circuit controls the ion gate and the laser.

The system has been assembled and tested. The laser works well as does the control circuit and we are able to initiate a d.c. discharge. However the power supply, as yet, has failed to provide a reliable d.c. arc. The present supply is a high speed high power circuit and tends to oscillate when the arc is ignited. This is the stage at which we are presently.

Some of the advantages we hope to gain within the next few months over the r-f spark ion source milliprobe are as follows. The lateral resolution is expected to be improved, perhaps by a factor of 10. The overall system should be faster since the d.c. arc has a better defined and more intense ion current. It should be relatively insensitive to surface effects that may be encountered, e.g., with sputtering techniques. In general, we hope to gain most all of the advantages of the low voltage d.c. arc in comparison with the r-f spark ion source.

Some of the immediate applications for the new milliprobe are given below. We have been successful in using the SSMS to measure concentration profiles of trace level solutes in the study of chemical diffusion and electrotransport and thermotransport in metals. However the limited lateral resolution of the SSMS required that the profile extend over a centimeter or more in order to be measured accurately. We hope to be able to reduce this profile to one millimeter. This will give much more flexibility to the metallurgical experiments.

We intend to apply the probe to diagnostic work on surfaces and inhomogenities where the r-f spark ion source didn't quite have adequate finesse and resolution to provide more definitive information.

The development should permit taking advantage of the analytical features of the d.c. arc both for metals and for non-metals. The case of non-metals may have some interesting possibilities. For example, it may be possible to identify and measure elemental impurities in coal with direct excitation.

The important aspects of this development are:

1. A high repetition rate laser is used to select the site to be analyzed.
2. Laser energy-per-pulse is minimized being only that necessary for desired excitation. e.g. for ignition of an arc.
3. The analytical advantages of a d.c. arc are utilized.
4. The mass spectrum is integrated with a double focusing mass spectrometer.

R. J. Conzemius and H. J. Svec
Ames Laboratory-ERDA
Iowa State University
Ames, Iowa 50011

	R F SPARK	D C ARC	LASER
SPOT SELECTION [illegible]	300	300	0.5-300
ENERGY SPREAD	HIGH	MEDIUM	LOW
PULSE POWER	ERRATIC	CONTROLLED	VARIES
ION CURRENT	ERRATIC	HIGH STEADY	VARIES
MULTIPLE IONS	REL HIGH	HIGH	LOW
MOLECULAR IONS	MEDIUM	LOW	LOW
DUTY CYCLE	0.0001 - 0.0001[illegible]	0.01	0.01 (VARIES)
REP RATE	30	10	10^3

Fig.1 Characteristics for three means of sample excitation.

Fig.4 LASER-ARC ION SOURCE FLOW DIAGRAM

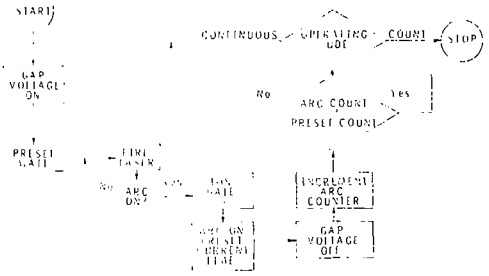

Fig.2 STAGES OF OPERATION

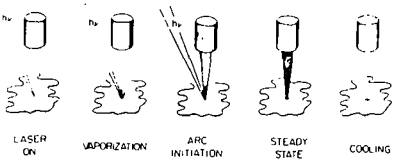

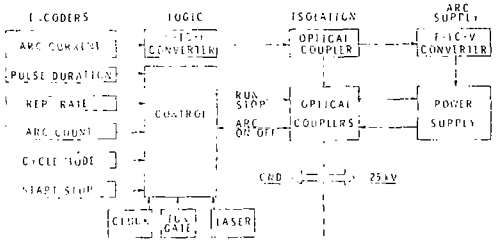

Fig.5 Block diagram of controlling circuit.

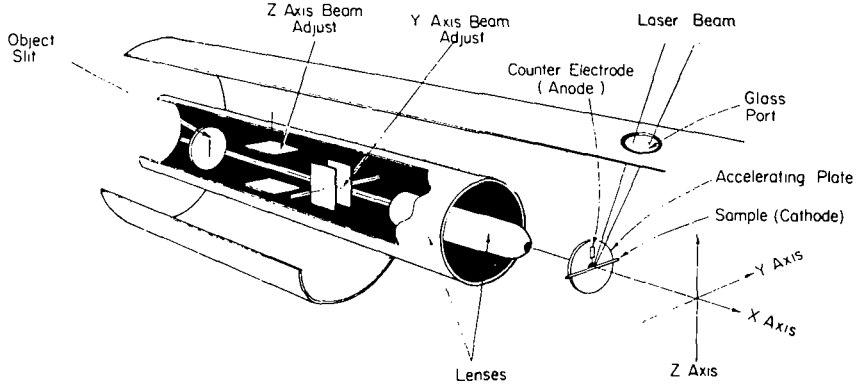

Fig.3 SCHEMATIC VIEW OF LASER-ARC ION SOURCE

SYSTEM FOR QUANTITATION OF ION MICROGRAPHIC IMAGES

J. D. Fassett, J. R. Roth, and G. H. Morrison

Department of Chemistry
Cornell University
Ithaca, N. Y. 14853

This study involves the analysis of the chemical information contained in ion micrographic images. The CAMECA IMS-300 ion microscope is a unique tool producing an isotopic distributional image of a solid surface. The typical ion image has a 250-micron diameter circular field of view with point-to-point resolution of one micron or better. Thus, there are 49087 information bits in a typical ion image. Each information bit represents the total number of ions of a particular mass being extracted from a particular one-micron squared area of a sample's surface. The analysis of all the information bits in an ion image is readily accomplished via computerization. Where previously the image information could be utilized only semiquantitatively, computerization allows the quantitative handling of the information bits in an ion image. This study describes the development of a computerized system for analyzing ion micrographs.

Quantitation of an ion micrograph is achieved by the digitization of the image and conversion of film darkening per information bit to ions extracted per information bit. The first step in computerization is the digitizing of the image. Digitization is accomplished by a Photomation Mark II microphotodensitometer which has a density range of either 0-2D or 0-3D and a density resolution of 8 bits or 256 levels. Effective film point size read by the densitometer is 25, 50, or 100 microns square. The densitometer is interfaced with a PDP-11 computer. The ion micrograph, which is 28 mm in diameter, is conveniently digitized onto magnetic tape into 512 × 512 matrices using the 50-micron square aperture of the microphotodensitometer. If centered, this results in the loss of about 6% of the total ion image with no loss of point-to-point resolution. There is also digitized about 6% of the background to the image. This background allows background correction made on image points. However, since there is presently a maximum limit to the size of the image matrix storable on the disk at 128 × 128, to transfer this image completely into one disk file necessitates the reduction of resolution to two microns, or quarters the number of information bits. If this loss of resolution can be tolerated in the image, this is the most convenient method to handle the image. However, if resolution must be preserved, the image can be quartered and each quarter image transferred into separate disk files.

The conversion of film darkening per information bit to ions extracted per information bit is accomplished after the determination of the characteristic curve of the film used in the image making. The secondary ions are converted to monoenergetic electrons prior to photographic detection with the ion microscope. Therefore, as opposed to the photographic detection as practiced by other analytical techniques such

as emission spectroscopy and spark source mass spectroscopy, the determination of the characteristic curve and its application to experimental images are simplified. The film darkening process is equivalent at all points on an image and there are no corrections necessary for mass effects or wavelength differences. The characteristic curve is straightforwardly analyzed, the linear range extended by use of Seidel densities and the results applied directly to conversion of darkening to ion intensity for the image.

The experimental determination of the characteristic curve is done for each roll of film by the taking of a series of standard images with set densities that range from saturation to background. The number of information bits in the standard image is fixed, and the ion photomultiplier current is monitored. This photomultiplier current is corrected for the transmission efficiency of the instrument and thus converted to an absolute ion intensity. Since the number of image bits is fixed, the ion intensity per information bit is directly determined. The standard images are digitized along with the experimental images.

The actual formation of the characteristic curve and conversion of density to ion intensity for experimental images is done by a series of software routines. The background corrected points of the H and D curve are determined from the standard images. The linearity of the curve is improved by the use of Seidel densities and the best line is fit to the data. A conversion file is computed from the characteristic curve data where each density is assigned an ion intensity. This conversion file is applied to experimental images for the final conversion. The operator inputs the analytical range of densities and any points below or above this range are labeled "background" and "saturation," respectively. The useful range is typically 5-70% transmittance. This range represents a factor of about 50 in ion intensities. The image data is conveniently displayed by contour plotting at set ion intensity levels, or by tabulation in a histogram of ion intensity *versus* total number of points with that intensity.

Digitization and computerization of ion images has a tremendous potential in future applications. A storehouse of information is accessible. The isolation and analysis of microfeatures is possible from images. The potential exists for cross-correlation of similar images. Multielemental analysis, three dimensional analysis, and extension of the dynamic range of the film can be done by combining the information from different images. The ultimate goal for ion microscopy, as well as SIMS, is quantitation in terms of concentration instead of ion intensity. This problem is a very difficult one and is caused by the highly complex and poorly understood nature of the secondary ion emission process. Potentially the most important result that digitization and quantitation of ion micrographs could produce is the unravelling of the mechanism behind secondary ion emission and true elemental quantitation of a sample's surface.

A more complete paper based on this study will be submitted to *Analytical Chemistry*.

Low Pressure Chemical Ionization of Some Complex Biological Molecules. EDWARD B. LEDFORD, JR., and ROBERT T. McIVER, JR., Univ. of Calif., Dept. of Chem., Irvine, Ca., 92717.

The trapped ion cyclotron resonance mass spectrometer has been shown to be useful for low pressure chemical ionization studies of compounds with very low vapor pressures.[1] The significant features of the technique include ultra low vapor pressure capability, small sample size, controlled fragmentation of target compounds using a wide variety of reagent ions for chemical ionization, and selective ionization of the components of mixtures. This paper will discuss the ion-molecule chemistry of a number of compounds of biological importance. Applications of low pressure chemical ionization to structure elucidation and the analysis of compounds encountered in biological fluids will be considered.

[1] R. T. McIver, Jr., E. B. Ledford, Jr., and J. S. Miller, Anal. Chem., 47, 692 (1975).

^{252}Cf-PLASMA DESORPTION MASS SPECTROMETRY - NUCLEAR PARTICLES TO PROBE BIOMOLECULES*

by

R. D. Macfarlane and D. F. Torgerson
Cyclotron Institute and Chemistry Department, Texas A&M University
College Station, Texas 77843

Introduction

^{252}Cf-plasma desorption mass spectroscopy (PDMS) is a new method which has particular application to the study of involatile large biomolecules.(1) The method utilizes techniques from nuclear science technology to measure mass spectra. The basic phenomena which result in the formation of quasimolecular ions from their solid films is the interaction of nuclear fission fragments (from ^{252}Cf decay) with a solid medium. Linear energy deposition is large (~1000 eV/A) resulting in the formation of a thermal pulse in the sample reaching temperatures of ~20,000 K for 10^{-12} sec.(2) A cylindrical microvolume of the sample (25 Å radius) is transformed into a hot gas at high pressure in which fast chemical reactions can occur between sample molecules and atoms. Some of the reaction products are ions which can be extracted by an external electric field and analyzed.

Chemical Reactions in the Thermal Pulse

There are two main reactions that occur that are of mass spectroscopic interest because they can be used to identify the molecular weight of the parent molecule. The first of these is fast proton transfer between two neutral molecules:

$$2MH \rightarrow MH_2^+ + M^-.$$

The mechanism has been determined by deuterium-labeling experiments. The H-transfer is from an acidic site of one molecule to the basic site of another. Thus, molecules that are zwitterionic, e.g., peptides, nucleotides, readily undergo this reaction. In the presence of alkali atoms, exchange reactions can also occur. Thus,

$$MH + Na \rightarrow MNa + H$$
$$MNa + MH \rightarrow MHNa^+ + M^-.$$

These reactions thus give a signature in positive and negative ion mass spectra from which M can be elucidated.

Application

We are participating in some collaborations which give us the opportunity to examine interesting, unusual molecules which test the applicability of PDMS in research problems of current interest. We include here some examples which also illustrate the reactions discussed above.

Figure 1 shows the positive and negative ion spectra of a new, modified nucleoside, Q*, which was isolated from the anti-codon portion of rabbit liver t-RNA.(3) The quasimolecular ions observed were $(M + Na)^+$ and $(M - 1)^-$. We have observed that with increasing Na^+ concentration

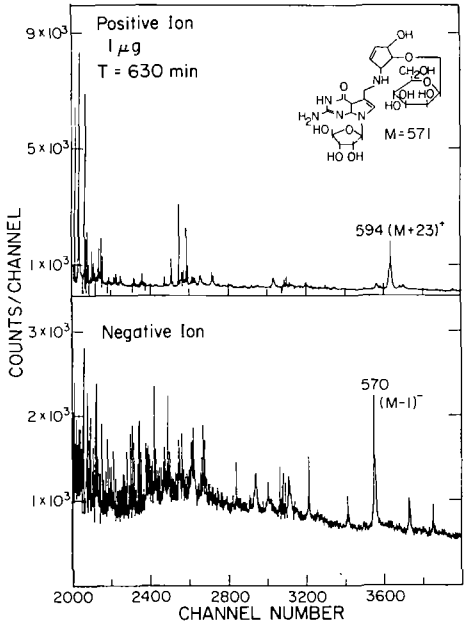

Fig. 1 ^{252}Cf-PDMS spectra of Q^{+}-nucleoside which is the first position of the anti-codon for rabbit liver t-RNA. This is the first modified tRNA nucleoside to carry sugars on its side chain.

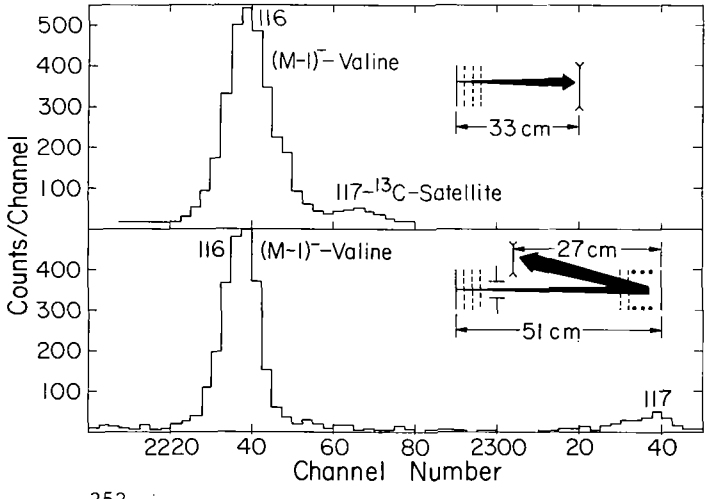

Fig. 2 ^{252}Cf-PDMS spectra of the negative quasimolecular ion of valine and its ^{13}C--satellite for a 33-cm flight path and a 51-cm flight path using a reflectron to achieve second-order energy focusing.

in the sample, the $(M + 1)^+$ intensity is transferred to the $(M + Na)^+$ channel. The significance of this work is that it is the first example of a nucleoside with a second nucleoside in the substituted position.

There is considerable interest in determining whether PDMS can be adapted to larger biomolecules. This depends on whether the reaction volume in the thermal pulse is large enough to vaporize an intact large molecule and on the probability for a reaction to occur that leads to free ions. Gramicidin-A, a 15-residue peptide, the natural form blocked at both ends, gives a strong $(M + Na)^+$ ion.(1) Vitamin B-12 gives good yields of negative quasimolecular ions. We have evidence that quasimolecular ions in excess of 5000 MW can be produced but the experimental problem also involves the detection of these large ions.

System Development

The ^{252}Cf-PDMS system that we have developed utilizes the time-of-flight (TOF) principle.(4) We feel that it is the best scheme for the application of PDMS although alternate modes of mass measurement are certainly valid. The most severe problem in TOF is loss of mass resolution at higher masses due to the initial velocity distribution of the ions. This problem has recently been solved by Mamyrin with the reflectron principle.(5) Second-order time-energy focusing is achieved by electrostatically reflecting the ions at the end of the flight tube and detecting the reflected ions in a plane near the ion source. Figure 2 shows a valine spectrum with and without the reflectron which demonstrates the enhanced resolution. The Mamyrin work is clearly an important development for TOF work and is a timely contribution to the utilization of PDMS for high resolution mass spectroscopy.

References

*Supported in part by U. S. ERDA and the Robert A. Welch Foundation.

(1) R. D. Macfarlane and D. F. Torgerson, Sci. 191, 920 (1976).
(2) R. D. Macfarlane and D. F. Torgerson, Phys. Rev. Lett. 36, 486 (1976).
(3) H. Kasai, K. Nakanishi, R. D. Macfarlane, D. F. Torgerson, Z. Ohashi, J. A. McCloskey, H. J. Gross, and S. Nishimura, J. Amer. Chem. Soc. (in press).
(4) R. D. Macfarlane and D. F. Torgerson, Int. J. Mass Spec. and Ion Phys. (in press).
(5) B. A. Mamyrin, V. I. Karataev, D. V. Shmikk, and V. A. Zagulin, Zh. Exsp. Teor. Fiz. 64, 82 (1973); Eng. trans.: Sov. Phys. JETP 37, 45 (1973).

Atmospheric Pressure Ionization (API) Mass Spectrometry. E. C. HORNING, D. I. CARROLL, I. DZIDIC, K. D. HAEGELE, and R. N. STILLWELL, Baylor College of Medicine, Institute for Lipid Research, Houston, Texas 77025.

The ionization of organic compounds in an API mass spectrometer occurs in a reaction chamber at atmospheric pressure external to the mass analyzer region. Two types of primary ionizing conditions have been used: a ^{63}Ni foil and a corona source. Ionization of compounds under study occurs by secondary reactions; both positive and negative ion spectra may be utilized. Samples may be introduced in solution in organic solvents, or in a gas stream with or without added reagents to generate reactant ions. Prototype LC-MS-COM and GC-MS-COM systems have been tested, and high sensitivity of detection has been demonstrated. Potential biologic applications will be discussed.

Techniques and Applications of Precise Isotope Ratio Measurements. J. M. HAYES, DWIGHT E. MATTHEWS, DAVID W. PETERSON, ZVI SOFER, and ERWIN VOGLER. Indiana University, Depts. of Chem. and Geol., Bloomington, Indiana 47401.

Different approaches (Faraday cup vs. electron multiplier, steady state inlet vs. GCMS) to isotope ratio measurements will be compared and contrasted. The utility of precise isotopic abundance measurements in biomedical and biogeochemical systems will be considered in terms of tracer experiments dependent on stable isotopic labels in physiological systems and dependent on natural isotopic abundance variations in geological systems. In the latter case, it is interesting to investigate intramolecular patterns of isotopic order, in which $^{13}C/^{12}C$ ratios at various atomic positions within molecules are determined by careful degradative procedures. These procedures are considered together with more routine techniques for the preparation of CO_2, N_2, and H_2 for isotopic measurements.

Studies of Rydberg-State Reactions*

CORNELIUS E. KLOTS
Health Physics Division
Oak Ridge National Laboratory
Oak Ridge, Tennessee 37830

In the normal operating mode of a time-of-flight mass spectrometer, a grid is pulsed to allow a burst of electrons to enter the ion chamber. After a variable delay a second grid is pulsed to drive the ions of a given charge sign down the flight tube. In the experiments described below, an intermediate pulse, immediately following the electron burst, is used to drive the ions to the chamber wall.

Curve (a) of the figure shows the He^+ signal obtained, as a function of electron energy, in the ordinary operating mode. Curve (b) is obtained in the modified mode. We interpret these ions as coming from high Rydberg states of helium, largely unaffected by the intermediate pulse but field-ionized by the larger collection pulse. The shape and magnitude of the signal is consistent with the known efficacy of field ionization and the cross-sections for ejecting slow electrons from helium.[1] This connection between creating Rydberg states and slow electrons follows from the correspondence principle.

This interpretation is confirmed by curve (c), obtained with some SF_6 present. The increase arises from the reaction $He^* + SF_6 \rightarrow He^+ + SF_6^-$. Examination of the SF_6^- current shows identical behavior.

The cross-section for generating Rydberg states is nearly a step function. This follows from the Wannier formula for ionization cross-sections near threshold. We plan to use this technique, with improved energy resolution, as a direct test of the Wannier formula.

The first step in the charge transfer reaction is thought to be a simple attachment by SF_6 of the nearly-free Rydberg electron, at large radial separation.[2,3] In order for the dissociation to ionic products to be possible, however, a vibrational relaxation, momentum-exchanging collision with the rare gas ion must occur. Our observation that the final SF_6^- is not susceptible to autoionization confirms this. What is remarkable is that SF_6^- is observed at all. Penning ionization by the helium metastable states is observed to give largely SF_5^+. The more highly excited Rydberg states eschew this very exothermic reaction channel. Likewise we see no sign of the exothermic reaction channel leading to $SF_5^- + F^+$ (or HeF^+). Similar remarks pertain to the formation of CS_2^-, $CH_3NO_2^-$ and CH_3CN^-. These charge transfer reactions, then, are bafflingly simple.

The stable ions CCl_4^-, CF_3Br^-, and CF_3I^- have been reported in the literature. We have attempted to use Rydberg states to prepare them, but see only the dissociative products Cl^-, Br^- and I^- respectively, together with the rare gas counter-ion. There is no sign of the exothermic products such as CCl_3^+, CCl_2^+, or CCl_4^+ for example. Dissociative attachment here can

(and evidently does) occur at a large radial separation with release of enough kinetic energy to throw each fragment from the field of the rare gas ion.

*Research sponsored by the U. S. Energy Research and Development Administration under contract with the Union Carbide Corporation.

[1]J. T. Grissom, R. N. Compton and W. R. Garrett, Phys. Rev. A6, 977 (1972).

[2]J. A. Stockdale, F. J. Davis, R. N. Compton and C. E. Klots, J. Chem. Phys. 60, 4279 (1974).

[3]W. P. West, G. W. Foltz, F. B. Dunning, C. J. Latimer, and R. F. Stebbings, Phys. Rev. Lett. 36, 854 (1976).

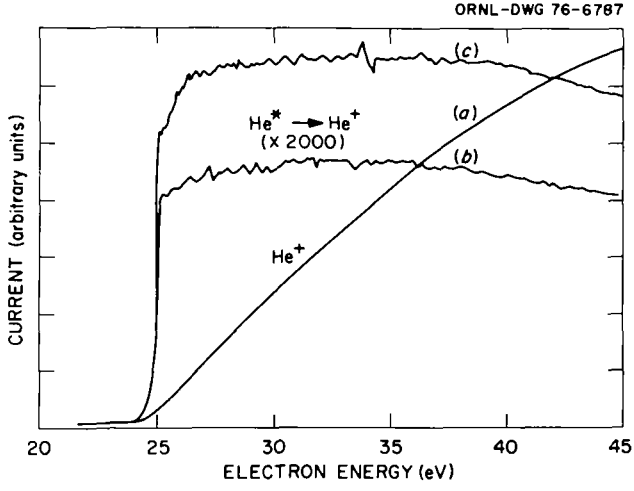

Figure 1. He^+ current, a function of electron energy, obtained as described in the text.

Variable Fragmentation Mass Spectrometry Using Chemiionization

by

James B. Laudenslager and Lowell P. Theard

Jet Propulsion Laboratory
4800 Oak Grove Drive
Pasadena, California 91103

Chemiionization (Penning ionization) is a process whereby a neutral substrate molecule is ionized by a collision with an electronically excited neutral metastable atom or molecule. There are several unique features of chemiionization which make this process an attractive alternate ionization method for analytical mass spectrometry.

Chemiionization at thermal collision velocities occurs only when the excitation energy of the metastable is greater than or equal to the ionization potential of the substrate molecule and, normally, all fragment ions which are energetically accessible in the reaction will be produced. A variety of long-lived atomic metastables can be produced by electron impact of the rare gases. These rare gas metastables have discrete excitation energies ranging from 8.3 eV for Xe^* to 20.61 eV for He^*. This energy range covers the region of interest for controlled ionization and fragmentation of most organic molecules. With use of selected low energy metastables such as Xe^*, Kr^*, and Ar^*, it is possible to obtain an upper limit for the ionization potential of an unknown compound. This information along with the molecular weight of a compound provide valuable information concerning the identity of an unknown compound.

The chemiionization method can also be used to ionize selective low ionization potential components in a mixture containing molecules with ionization potentials greater than the energy of the ionizing metastable.

Also, the cracking pattern of a complex organic compound can, in favorable cases, be varied using chemiionization with different metastables from a single peak spectrum consisting of the molecular ion peak to a complex cracking pattern in discrete and reproducible steps. These spectra, in some cases, provide unique structural information which cannot be obtained from high energy electron impact or chemical ionization methods.

We have utilized these features of chemiionization to generate mass spectra of isomeric compounds with different degrees of fragmentation. The particular systems studied were the C_5H_{10} geometrical isomers, several of which are indistinguishable by ordinary mass spectral methods, and several derivatized amino acids. The soft ionizing metastables, Xe^* and Kr^*, produced simplified mass spectra of these compounds consisting of essentially only the parent ion peak. The higher energy metastables, Ar^*, N_2^*, Ne^*, and He^*, produced spectra with various degrees of fragmentation, which provided unique structural information about the compounds. For example, cis and trans 2-pentene could be distinguished from each other from their Ne^* chemiionization spectra.

The Ar^* spectra of the C_5H_{10} compounds contained only three peaks, but from these spectra 4 of the 7 C_5H_{10} compounds could be distinguished. The N_2^* spectra was used to uniquely identify the others. The Ar^* chemiionization spectra of PTH-leucine was clearly distinguishable from that of PTH-isoleucine, yet each spectrum contained only three major peaks.

The Kr^* spectrum of an equimolar mixture of PTH-leucine, PTH-isoleucine, PTH-valine, and PTH-alanine consisted of essentially only the molecular ion peaks. The Ar^* spectrum of this mixture provided an analogous simplified spectra with intense molecular ion peaks but also provided two additional peaks clearly distinguishing PTH-leucine from PTH-isoleucine which have the same parent ion peak. Because the excitation energies of rare gas metastables are specific and the chemiionization reaction is independent of the accelerating potentials in the

ion source region, the various fragmentation patterns can be reproducibly generated in any ion source.

The ability of chemiionization to provide simplified mass spectra provides an additional mass spectral method for analyzing complex mixtures. The ability to distinguish isomeric compounds is an added benefit which might find use in clinical mass spectrometric applications.

Experimental Breakdown Curves of Propane and Deuterated Propane Molecular Ions

Roger Stockbauer
National Bureau of Standards
Washington, DC 20234
and
Mark G. Inghram
Department of Physics
University of Chicago
Chicago, Illinois 60637

ABSTRACT

The fragmentation of C_3H_8, $CH_3CD_2CH_3$, $CD_3CH_2CD_3$ and C_3D_8 molecular ions has been studied using the threshold photoelectron-photoion coincidence mass spectrometer at the University of Chicago. Detailed experimental breakdown curves have been obtained from 0 to 6 eV of parent ion internal energy. Where possible, the results are compared with previous photoionization and metastable ion studies and with calculations based on QET. The breakdown curves of the partially deuterated compounds show that some of the fragmentation mechanisms assumed in the calculations are incorrect. In particular, the high energy plateau on the H (D) atom loss curve is due to the formation of sec-propyl rather than n-propyl ions as had been assumed. Fragmentation preceded by hydrogen scrambling shows an intensity greater than 10% in the data. Hence, this effect should be included in future calculations.

A detailed account of this work has been submitted for publication in the Journal of Chemical Physics.

KINETIC ENERGY RELEASE DISTRIBUTIONS FOR THE DISSOCIATION OF INTERNAL ENERGY SELECTED CH_3I^+ AND CD_3I^+ IONS.* Donald M. Mintz and Tomas Baer, W. R. Kenan, Jr. Laboratory of Chemistry, University of North Carolina, Chapel Hill, North Carolina 27514.

Product translational energy distributions have been measured from an analysis of symmetrically broadened time-of-flight peaks of CH_3^+ and CD_3^+ ions in photoion-photoelectron coincidence spectra of CH_3I and CD_3I respectively. The reactions were investigated at various precursor ion internal energies, up to 1.7 eV above the dissociation threshold. We found that the experimentally obtained kinetic energy release distributions can be fitted accurately by simple exponential functions over the energy range considered. The experimental results are compared to predictions of the statistical theory of unimolecular reactions. An angular momentum conserving version of the quasi-equilibrium theory, formulated in terms of the Langevin collision cross section model for the reverse association reaction, predicts kinetic energy release distributions which agree very well with the experimental results at precursor ion energies up to .65 eV above the dissociation onset. At approximately this energy, the average kinetic energy released begins to deviate sharply from the theoretically predicted average, possibly indicating the accessibility of a new reaction channel.

*This work was supported by the National Science Foundation. The complete study has been submitted for publication in the Journal of Chemical Physics.

Photoionization of Ozone: Formation of O_4^+ and O_5^+ *

Morris J. Weiss, J. Berkowitz and E. H. Appelman, Argonne National Laboratory, Argonne, IL 60439

Ionization yields of O^+, O_2^+ and O_3^+ have been studied as a function of wavelength in the photoionization of ozone from threshold to 600 Å with the primary process being the production of O_3^+. The ratio O_3^+: O_2^+: O^+ at 600 Å is 1.00: 0.36: 0.05.

The adiabatic ionization potential of O_3^+ is 990.32 ± 0.3 Å (12.51 ± 0.004 eV). Steplike structure occurs near threshold, at wavelengths corresponding to vertical ionization potentials reported in photoelectron spectroscopy studies. A weak onset for O_2^+ production appears at 13.08 eV (947.7 Å), followed by more intense O_2^+ production at 13.43 eV (932.2 Å).

The onset for O^+ formation appears weakly at 15.21 eV, rising continuously with decreasing wavelength.

The formation of O_5^+ via the ion-molecule reaction $O_3^+ + O_3 \rightarrow O_5^+ + O$ was also observed and measured as a function of wavelength. The O_4^+ ion was also detected. Pressure dependences and enthalpy considerations make the reaction $O_3^+ + O_2 \rightarrow O_4^+ + O$ a highly probably mechanism for O_4^+ formation.

* Work performed under the auspices of the Energy Research and Development administration.

Measurement of Angular Distribution and Energy of Ionic Fragments from Photodissociation of Molecular Ions

R. Orth and R. C. Dunbar
Department of Chemistry
Case Western Reserve University
Cleveland, Ohio 44106
M. Riggin
Department of Physics
University of New Brunswick
Fredericton, Canada

ABSTRACT

The unique anisotropy in the trapping efficiency of the ion-cyclotron resonance (ICR) spectrometer offers a unique method for estimating the kinetic energy and anisotropy parameter describing the angular distribution of ionic photofragments. The spatial symmetry of the ICR trapping cell was used to measure the parameter for characterizing the angular distribution of the H^+ fragments from the photodissociation of H_2^+ at wavelengths of 5790 Å and 4358 Å. The results were found to agree with the theoretically expected value for the angular distribution parameter of 2.0. The average kinetic energy of the fragments at 5790 Å was 0.7 eV and at 4358 Å was 1.0 which agree with the theoretical kinetic energies. The technique was used to examine the less well understood cation CH_3Cl^+. The results indicate that at a wavelength of 3725 Å the angular distribution parameter β is approximately 2.0 and the CH_3^+ fragment average kinetic energy is 0.58 eV. The ICR theory utilized for the H_2^+ photodissociation and the experimental results have been submitted to Chemical Physics for publication.

Laser Photodissociation Spectrum of Hexatriene Cation

Robert C. Dunbar

Department of Chemistry
Case Western Reserve University
Cleveland, Ohio 44106

Abstract

The first photodissociation band of gas-phase 1,3, 5-hexatriene cation was investigated at 10 Å optical resolution from 5350 to 6700 Å using Ion Cyclotron Resonance detection and a CW tunable dye laser source. Extensive resolved vibrational structure was observed, with progressions corresponding to a skeletal bending mode and at least one carbon stretching mode. The Franck Condon factors may be compared with the neutral photoelectron spectrum, and the observed differences are reasonable in terms of the expected geometry changes upon ionization.

A description of this work is scheduled to appear in the Journal of the American Chemical Society.

Photodissociation of Ion Beams in a Tandem Mass Spectrometer Using a Tunable Dye Laser

Timothy F. Thomas* and John F. Paulson
Air Force Geophysics Laboratory (AFSC)
Hanscom AFB, Massachusetts 01731

We have constructed an apparatus, shown in block diagram by Figure 1, which is capable of determining both absolute photodissociation cross-sections as a function of wavelength(the photodissociation spectrum) and the kinetic energy spectrum of product ions by time-of-flight analysis. A pulsed laser beam, ~ 2½ mm in diameter, crosses a mass-selected ion beam whose energy can be varied between ~ 10 and 200 eV by the decelerating plates shown in Figure 1. The quadrupole mass analyzer is set to pass only the product ion formed by photodissociation; in between photolyses it is also used to monitor primary beam intensity. The photo-diode triggers the time-of-flight logic (resolution down to 10 n secs) at the start of each laser pulse so that the time between the pulse and the arrival of a product ion at the electron multiplier can be measured. The polarization rotator shown in the laser beam permits determination of the direction of the electronic transition moment, as well as checking whether product ions ejected at large angles to the flight axis are accepted by the quadrupole mass analyzer.

Initial experiments were done on the D_2^+ ion so that the experimental cross sections could be compared with those of von Busch and Dunn.(1) The results obtained with a primary ion energy of 173 eV, so that all product ions pass through the entrance aperture of the quadrupole mass analyzer, are shown in Table I.

Table I. Cross Sections for $D_2^+ + h\nu \rightarrow D^+ + D$

λ(nm)	≈ 600	595	590	585	445	307.5
$\sigma \times 10^{19}$ (cm^2)	≈ 5.2	5.7	5.1	5.3	9.5	18.5
v.Busch & Dunn (interpolated)	≈ 5.5	5.6	5.7	5.8	9.9	20.7

The agreement of the two sets of data is nearly within our estimated experimental error (±0.3, ±0.7, ±2.5 x 10^{-19} at 600, 445, and 307.5 nm, respectively), which is especially noteworthy since von Busch and Dunn used a bandwidth of 200Å compared to ours of < 1Å.

Figure 2 shows the time-of-flight spectrum at primary ion energies so low (17.5 eV) that only D^+ ions ejected in the forward direction enter the quadrupole mass analyzer. Product ions produced from different vibrational levels of the $1s\sigma_g$ state possess different kinetic energies and thus show different flight times, as indicated on the figure.

The case of HD+ has been briefly investigated, with the following results at 590 nm and $E_{primary}$ = 173 eV;

$$HD^+ + h\nu \rightarrow H + D^+, \sigma = 2.0 \times 10^{-19} cm^2$$

$$\rightarrow H^+ + D, \sigma = 2.0 \times 10^{-19} cm^2.$$

*NRC Senior Research Associate - On leave from University of Missouri-Kansas City, 1975-6

The most extensive study on our apparatus to date has been the process:

$$N_2O^+ (\chi^2\pi_i) + h\nu \rightarrow N_2O^+(^2\Sigma^+) \rightarrow NO^+ + N.$$

A nearly complete photodissociation spectrum is shown in Figure 3. Based on a partial analysis of a high resolution spectrum of the $^2\Sigma^+ \rightarrow 2\pi_i$ emission by Callomon,[2] we have identified a progression in the symmetric stretch (ν_1 = 1345 cm^{-1}) in the $^2\Sigma^+$ state as well as the spin-orbit splitting in the ground, $^2\pi_{3/2,\ 1/2}$, state. Additional data at 173 eV are being obtained to complete the vibrational analysis, and T.O.F. spectra at lower primary ion energies will be obtained to determine the electronic states of the dissociation products.

References:

1. F. von Busch and G.H. Dunn, Phys. Rev. A5, 1726 (1972).
2. J.H. Callomon, Proc. Chem. Soc., 313 (1959).

Figure 1

ION PHOTODISSOCIATION APPARATUS

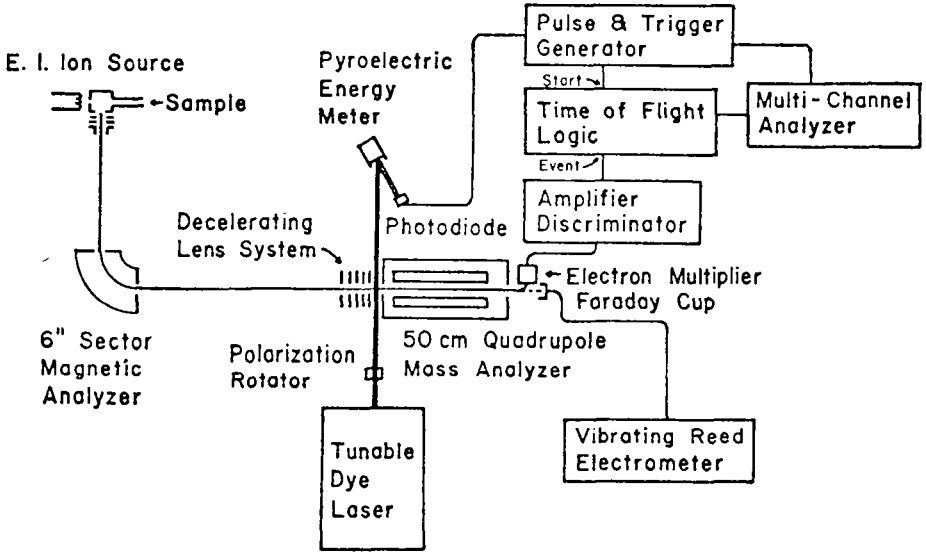

Figure 2

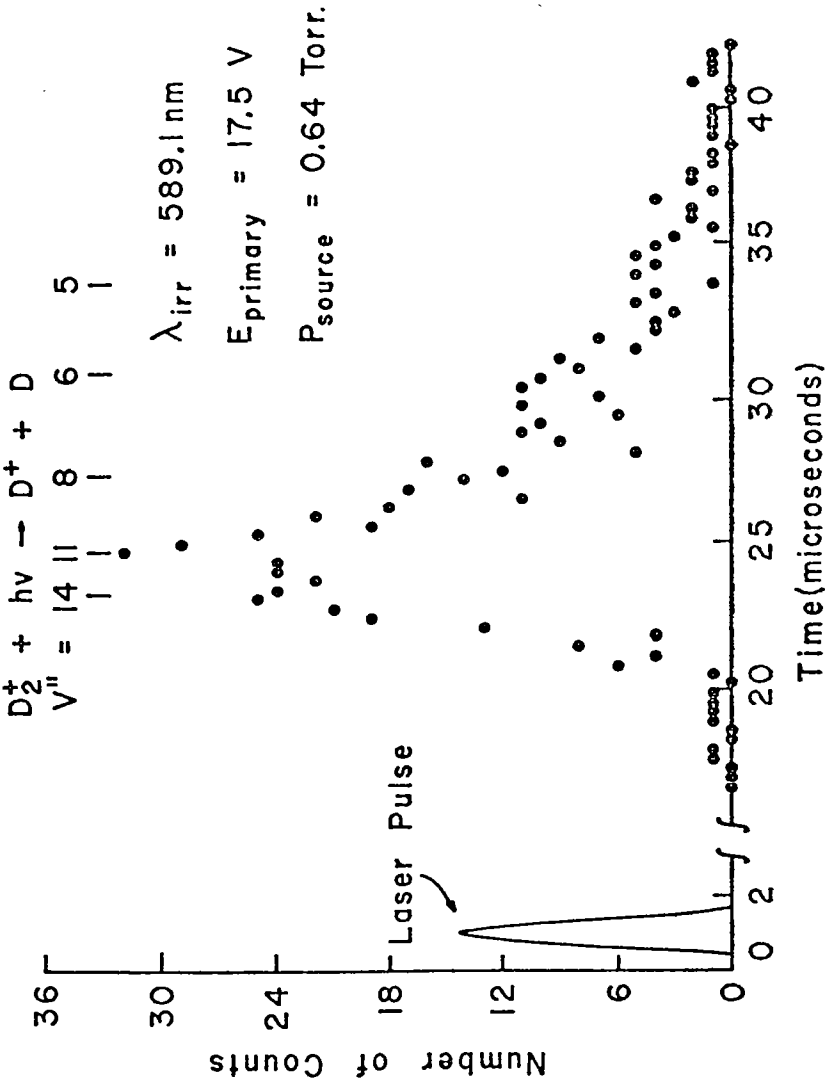
$D_2^+ + h\nu \rightarrow D^+ + D$
$V'' = 14 \quad 11 \quad 8 \quad 6 \quad 5$
$\lambda_{irr} = 589.1$ nm
$E_{primary} = 17.5$ V
$P_{source} = 0.64$ Torr.
Laser Pulse
Number of Counts
36
30
24
18
12
6
0
0
2
20
25
30
35
40
Time(microseconds)

Figure 3

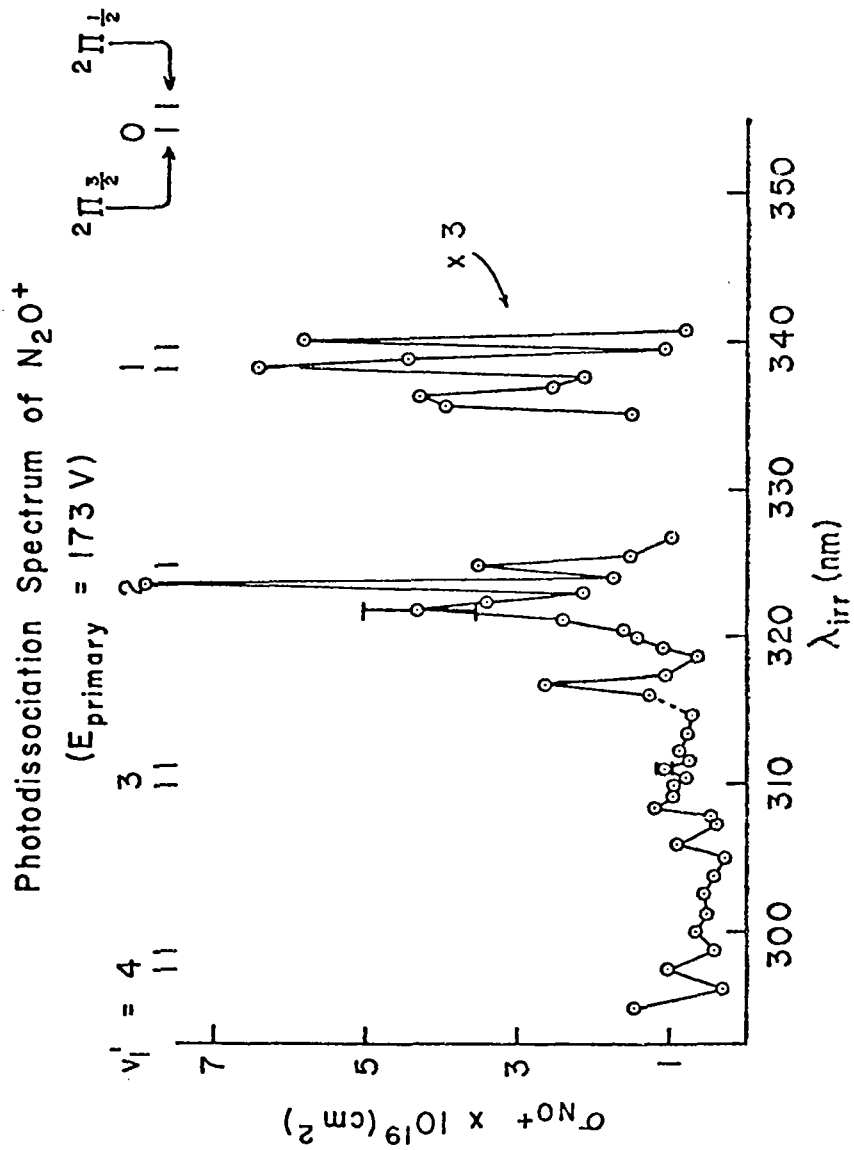
Photodissociation Spectrum of N_2O^+
($E_{primary}$ = 173 V)
$v_1' = 4$
3
2
1
0
$^2\Pi_{3/2}$
$^2\Pi_{1/2}$
x 3
$\sigma_{NO^+} \times 10^{19}$ (cm^2)
7
5
3
1
300
310
320
330
340
350
λ_{irr} (nm)

PHOTOIONIZATION OF HALOCARBONS*

F.P. Tully†, E.J. Darland, G.W. Ray, P.L. Kronebusch, C.G. Enke, and G.E. Leroi
Department of Chemistry, Michigan State University, E. Lansing, MI 48824

A new, computer-controlled photoionization mass spectrometer has been developed, and is being used to obtain information dealing with the thermodynamics and energetics of small molecules involved in atmospheric chemistry.

The vacuum-ultraviolet light source consists of a high-voltage pulsed dc discharge through helium or argon, or a continuous dc discharge through low pressure hydrogen. The radiation is dispersed by a one-meter near-normal incidence McPherson 225 monochromator equipped with a 1200 l/mm concave diffraction grating. Photoions formed in the source region are extracted and focused by a lens system, analyzed by a quadrupole mass filter and detected by an electron multiplier. Transmitted photon intensity is monitored by a second electron multiplier.

This instrument has several novel, but highly desirable features. An extensive interlock system which protects the instrument in the event of failures in the vacuum system or other utilities has been designed and installed. The safety interlock prevents valves from being opened or power from being turned on in an incorrect sequence. It also monitors foreline pressures, water flow rates, lamp gas pressure, etc., and will automatically shut down the endangered sections of the instrument when an error condition is detected.

In addition, the instrument is interfaced to a Digital Equipment Corp. PDP8/I minicomputer which controls the wavelength selected by the monochromator and acquires data on photon and ion intensities and other operating parameters. The computer optimizes the parameters of data acquisition, such as the integration time required to produce a preset signal/noise ratio at each wavelength, in real time. A photoionization efficiency curve, approximately corrected for drifts in sample pressure, detection electronics, etc., is also generated and plotted in real time. This allows the quality of the data to be monitored as it is collected.

An example of the value of variable integration time is shown in Fig. 1. The upper curve plots the photoionization efficiency curve (PIE) for the process $CF_2Cl_2 \rightarrow CF_2Cl^+$ using a constant integration time. The middle curve displays data for the same process obtained using variable integration time, and the bottom curve shows the helium Hopfield continuum in the region of interest. Clearly the constant integration time which would be required to produce low noise data in the threshold region would far exceed that time necessary in the region where the Hopfield continuum is intense. Use of constant integration time thus implies either very long experiments or spectral regions of low quality data. Experiments performed with variable integration time face the same tradeoff between experiment duration and signal/noise ratio, but at least the available time is being used as efficiently as possible. When using the hydrogen many-line spectrum, with its rapidly varying spectral intensities, variable integration times are especially valuable.

Photoionization efficiency data for selected ions produced upon photoionization of $CFCl_3$, CF_2Cl_2, and CF_3Cl illustrate our recent results. These data must be considered preliminary as they have not yet been corrected for either the effects of scattered light or the wavelength response function of the electron multiplier to transmitted light. The data analysis is therefore also in its early stages.

Table I lists the ionic fragments which we have observed upon photoionization of $CFCl_3$. A very small amount of parent ion is observed, but the dominant process results in formation of the chlorine-loss ion $CFCl_2^+$. Indeed, chlorine loss is favored over fluorine loss throughout the fragment

series. That is, $CFCl_2^+ > CCl_3^+$, $CFCl^+ > CCl_2^+$, and $CF^+ > CCl^+$.

The observation of stable parent ions for all three mixed halomethanes, illustrated for $CFCl_3^+$ in Fig. 2, presents an interesting interpretive problem. Neither CCl_4^+ nor CF_4^+ were detected in previous photoionization studies of CCl_4(1) and CF_4(2,3). These ions have thus been considered unstable with respect to dissociation. Werner, Tsai, and Baer (1) also studied CBr_4 and found a stable parent ion, of sufficient intensity that a large distortion in the equilibrium geometry between the molecule and ion seems unlikely. While we do observe parent ions from $CFCl_3$, CF_2Cl_2, and CF_3Cl, they are formed only rarely. If a small distortion in equilibrium geometry is assumed, then even if the ionic well is so shallow that it contains only the ground vibrational level, parent ion formation, at least over a small wavelength interval, should be fairly intense. Also, although ionization and appearance potentials have not yet been assigned, comparison of Figs.2 and 3 clearly show that $CFCl_3^+$ appears at longer wavelengths than the dominant $CFCl_2^+$ ion, and that the post-threshold decrease in parent ion intensity coincides with the onset of the dissociative channel. Our energy and intensity data are thus more consistent with a model in which the equilibrium configuration of $CFCl_3^+$ is quite different from that of $CFCl_3$, and in which nearly all of the vertical transitions sample the repulsive portion of the parent potential curve above the $CFCl_2^+$-Cl dissociation limit. Finally, an assumption of a similar distortion in CF_4 and CCl_4, coupled with the resonance stabilities of dissociated CF_3^+ and CCl_3^+, could result in a well too shallow to support even the zero-point energy, and thus the absence of a stable parent ion.

Also evident in Fig. 3 are two broad peaks at about 985 and 907 Å, which correspond in energy to peaks found in the absorption spectrum of $CFCl_3$ reported by Gilbert, Sauvageau, and Sandorfy (4). These absorptions were assigned to Rydberg transitions of a C-Cl bonding electron to excited 4p and 5p levels. It seems certain from our data that these discrete excited levels are subsequently autoionizing to the dissociative region of the $CFCl_3^+$ potential curve.

Figure 4a depicts the PIE for formation of CCl_3^+, the fluorine loss ion, from $CFCl_3$. The appearance potential for this ion is clearly higher than those of the parent ion or the chlorine loss ion, as expected from relative C-F and C-Cl bond strengths and the corresponding photoelectron spectrum (5). The spectrum is also rich in autoionization structure.

Figure 4b displays the PIE for formation of $CFCl^+$, and is representative in its features of the corresponding curves for CCl_2^+, CF^+, and CCl^+ (not shown). All these fragment ions show peaks in their PIE's at high photon energies, substantial autoionization structure, and very long tails toward as yet undetermined thresholds. The tails have been proven to be due to fragmentations induced by the longer wavelength light, and not to scattered light contributions, since long wavelength impurity lines superimposed on the helium continuum are exactly mirrored in the ion intensity data at the same impurity wavelengths. A likely explanation for the existence and structure of these long tails involves ion-pair formation, and negative ions will be searched for in the near future.

Figure 5 shows the PIE for the two principal fragments, CF_3^+ (a) and CF_2Cl^+ (b), obtained upon photoionization of CF_3Cl. Both spectra display peaks at about 920 Å and further well-defined structure at higher energies. The relative intensity of the chlorine-loss ion peak to the fluorine-loss ion peak at 920 Å is about 75:1. Gilbert, Sauvageau, and Sandorfy (4) tentatively assigned the corresponding peak in the absorption spectrum to either a C-Cl→5s or a C-F (or F lone pair) → 3s Rydberg transition. While both of these excited Rydberg states are apparently formed, our intensity data implies that the C-Cl→5s transition, followed by autoionization to the dissociative region of the parent curve, dominates.

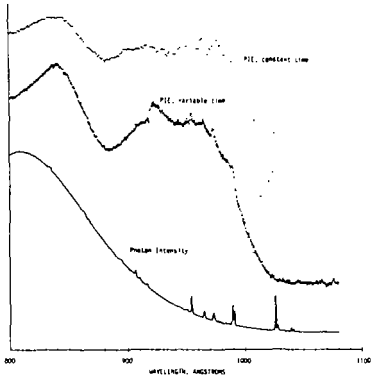

Figure 1

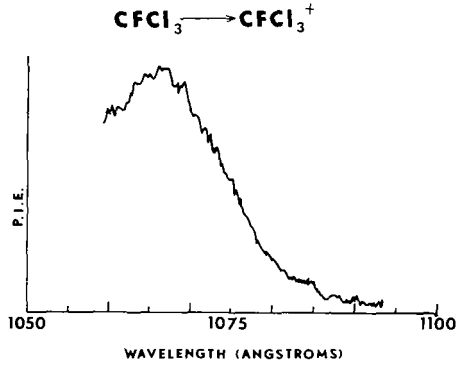

Figure 2

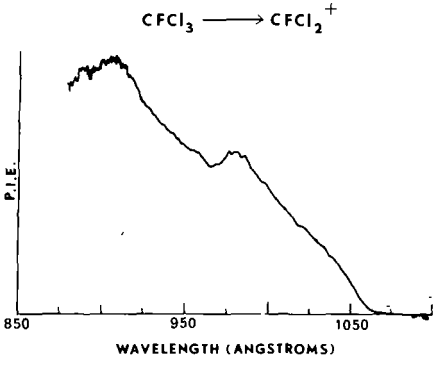

Figure 3

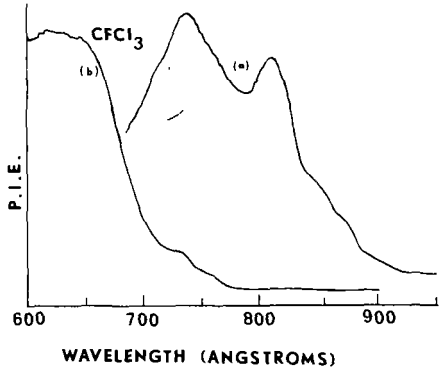

Figure 4

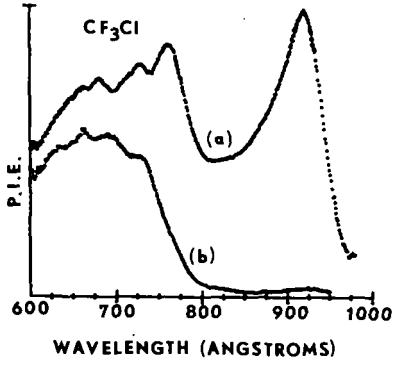

Figure 5

Table I. Photoionization Fragments of $CFCl_3$ at 815 Å (15.2 eV)

$CFCl_3^+$	$<10^{-4}$
$CFCl_2^+$	1.0
CCl_3^+	0.024
$CFCl^+$	9.3×10^{-3}
CCl_2^+	1.9×10^{-3}
CF^+	3.2×10^{-3}
CCl^+	1.1×10^{-3}

*This research was supported in part by the Office of Naval Research and The National Science Foundation.

†Present address: Engineering Experiment Station, Georgia Institute of Technology, Atlanta, Georgia 30332

1. A.S. Werner, B.P. Tsai, and T. Baer, J. Chem. Phys. 60, 3650 (1974).
2. C.J. Noutary, J. Res. Natl. Bur. Std. 72A, 479 (1968).
3. T.A. Walter, C. Lifshitz, W.A. Chupka and J. Berkowitz, J. Chem. Phys. 51, 3531 (1969).
4. R. Gilbert, P. Sauvageau, and C. Sandorfy, J. Chem. Phys. 60, 4820 (1974).
5. J. Doucet, P. Sauvageau, and C. Sandorfy, J. Chem. Phys. 58, 3708 (1973)

PHOTO-ASSISTED IONIZATION*

Arthur B. Denison, John M. Phillips, John M. Knox
Department of Physics and Astronomy
Laramie, Wyoming 82071

James H. Weber
Laramie Energy Research Center, ERDA
Laramie, Wyoming 82070

The introduction of light into the ionization chamber of a mass spectrometer in addition to the normal electron impact adds another dimension to mass spectroscopy. The benefit of separating molecules of the same nominal mass with selective radiation has been shown in some of our earlier work with carbon dioxide and carbon monosulfide.[1] In more complicated systems such as larger organic molecules we have also seen that fragment ratios can be modified with light.[2] By using different electron impact energies and different wavelengths one may develop a double spectroscopy which can help clarify complicated systems.

This optically modified mass spectroscopy also provides a tool for studying molecular excited states and molecular excited state dynamics. In this report we discuss the results of our work on carbon dioxide. This molecule shows an intense photo-assisted ionization spectrum which possesses structure indicative of vibrational transitions.

If carbon dioxide, which has been excited to high Rydberg levels by electron impact, is irradiated with light near 3000 Å, the ion intensity is observed to increase markedly, proportional to intensity of the light source.[3] Generally, the optical modification of ion intensity begins at about 4400 Å and increases to a maximum effect near 2900 Å. This wavelength region, active in producing ion enhancement, is the same as that observed for emission spectra from electron impact excited CO_2^+ ions.[4] Within this broad "resonance" local ion intensity maxima occur which correspond to particular vibrational bands. The ion enhancement between 3700 Å and 3100 Å agrees with the reported vibrational transitions between the $^2\pi_g$ to $^2\pi_u$ ion electronic levels. The maximum near 2900 Å agrees with the strong emission doublet reported for the $^2\Sigma_u$ to $^2\pi_g$ transition.

The mechanism proposed for this effect involves a two step excitation followed by autoionization. This mechanism is consistent with the experimental constraints and with known molecular parameters. The first step is excitation of the most loosely bound electron to a high Rydberg level leaving

behind essentially an ionic core. The cross section of such an excitation near the ionization threshold is known to be at least as large as 10^{-16} cm^{-2}. This electron which is in a hydrogenic type orbit has a long lifetime ($t \sim n^3$), and our measurements have shown the lifetime is really collision limited in our instrument and has a value $\sim 10^{-5}$ sec. The fact that this electron is far away allows to a first approximation that the core is nearly the same as the actual CO_2^+ ion and therefore, the excited ionic core levels are the same as those for the free ion. During the time the neutral but excited CO_2 lives, a photon of the correct energy can excite the ionic core. The cross section for this process is a little harder to estimate but various considerations allow a number on the order of 10^{-17} cm^{-2}. The photons which are active in producing the ion enhancement are of the same energy as the lower observed ionic excited states. This doubly excited system has too much energy to be stable and autoionizes, a process which is known to occur very fast. Such a process is not strictly photoionization and we would expect to see a resonant type behavior in the optically modified spectrum.

The optically modified mass spectral technique shows promise for detailed studies of the molecular excited state. In addition to energy resolution, relative level population may be obtained. By varying the repetition rate of our time-of-flight mass spectrometer we have been able to obtain certain excited state lifetimes. Combining the information obtained from various types of optically modified mass spectroscopy experiments one may obtain information about excited states including energy partition and rate phenomena leading to ionization and fragmentation.

---

[1] R. E. Ellefson, B. A. Osterlitz, J. M. Phillips, A. B. Denison, J. H. Weber; Chem. Phys. Lett. 31, 364 (1975)

[2] R. E. Ellefson, A. B. Denison, J. H. Weber; Chem. Phys. Lett. 37 1975, (1976)

[3] A. B. Denison, J. M. Phillips, J. H. Weber; Proceedings 23rd Ann. Conf. Mass Sepctrometery and Allied Topics, May 25-30, 1975 Houston Texas

[4] J. M. Ajello, J. Chem. Phys. 55, 3169 (1971)

*Supported in part by The National Science Foundation Grant CHE-75-17817

A Time-resolved Study of the Fragmentation of 1,5-Hexadiyne. P. P. DYMERSKI and A. G. HARRISON, Dept. of Chem., Univ. of Toronto, Toronto, Canada.

A significant amount of fragmentation involving loss of H from the molecular ion of 1,5-hexadiyne in the time range between 10^{-6} and 10^{-3} sec. has been reported[1] from a comparison of the conventional mass spectrum and the ICR mass spectrum. Using trapped ion mass spectrometry a time-resolved study of the fragmentation of the molecular ion of 1,5-hexadiyne has been carried out. The results confirm that significant fragmentation occurs between 0.01 and 0.5 msec. The dependence of the phenomenological rate coefficient and the population of the slow-fragmenting state (s) on the ionizing electron energy will be reported and discussed in terms of the QET.

[1] M. L. Gross and R. J. Aerni, J. Amer. Chem. Soc., 95, 7875 (1973).

PREPARATIVE MASS SPECTROMETRY

V. Franchetti and R. G. Cooks, Department of Chemistry, Purdue University, West Lafayette, Indiana 47907

In this paper we show that mass spectrometric methods can be used in the preparation of materials, specifically surfaces. The ability to prepare surfaces with desired characteristics has applications in catalysis, electrochemistry, textiles and solid state electronics, among others. We report results of high energy (1KV) and low energy (10eV) CS_2^+, CS^+, S^+ and S_2^+ reactions with Pb targets which indicate that low energy atomic and polyatomic ions may be used as synthetic reagents.

A Colutron Ion Beam Kit BK-1-D is used to produce and deliver ion beams. Ions are produced with a plasmatron ion source. They are extracted through a 1KV potential and focused with a three element einzel lens. Vertical deflection plates direct the beam through a Wien velocity filter which mass selects the reactant ion. The ion translational energy is chosen by proper selection of voltages on a six element decelerator. The target region allows reaction of metals, frozen vapors and non-conducting as well as conducting substrates. The system delivers mass selected, decelerated ion beams of 10^{-6} amps. High mass resolution (100) is attainable when lower ion currents are used (10^{-8} amps).

Ions formed from CS_2 were selected and reacted with Pb targets. The surface was analyzed using ESCA. In particular the S(2p) and Pb(4f) binding energy regions of the ESCA spectra were examined to detect reaction and determine variations with ion type and energy.

Figure 1 illustrates the S(2p) region of targets reacted with 1KV and 10eV S^+, CS^+, and CS_2^+ ions. The high and low energy spectra resulting from reactions of the same ion are superimposed for contrast. The high energy reaction spectra are nearly identical, characterized by two bands appearing close to 161 and 162eV. This implies that the ions are reacting similarly regardless of their structure. The lower binding energy peak is representative of metal sulfides; the higher binding energy peak may indicate the formation of an organic sulfide. The S(2p) spectra of 10eV ion reactions show more complicated spectra than the 1KV ion reactions. In general, there is a shift to higher binding energies. In addition, the spectra show differences depending upon the ion used in the reaction. This shift to higher binding energy indicates that binding to oxygen is occurring, forming more positively valent sulfur; notably, contribution to higher binding energy species increases with the complexity of the ion.

Fig. 1

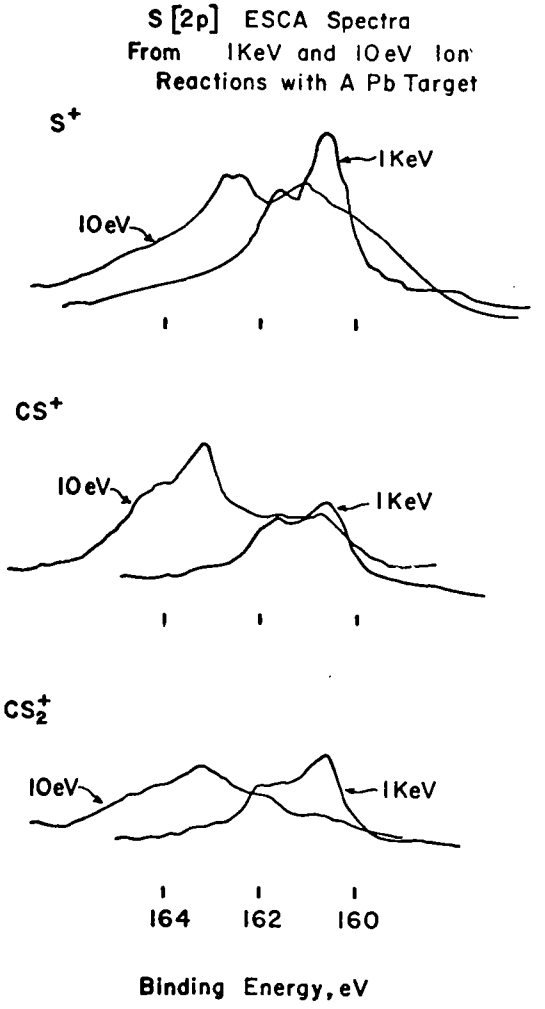

Figure 2 illustrates the Pb(4f) region of the ESCA spectrum from reaction of 1KV and 10eV S_2^+ ions with Pb. These spectra typify those obtained when S^+, CS^+ and CS_2^+ are used as reactant ions. The lead blank spectrum shows the 4f spin doublet (7/2, 5/2) split into two components. The larger component is due to the oxide and the shoulder at lower binding energy represents the pure metal. The spectra taken after reaction again indicate that the Pb surface has been altered, the 4f binding energy shifts toward lower values, between the oxide and the pure metal.

Fig. 2

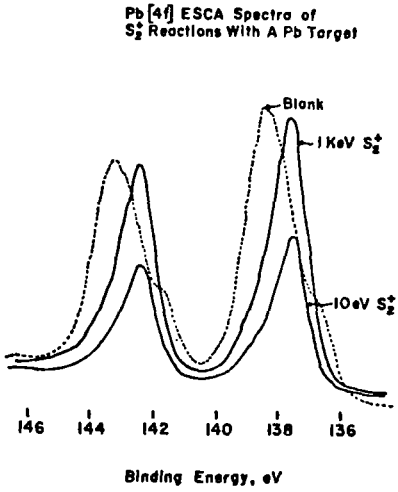

These data show that low energy ions react differently than high energy ions with metal surfaces. In addition, the nature of the species produced from reaction of 10eV ions varies as the ion is varied, implying that low energy polyatomic ions may be used as reagents for surface reactions. We are extending this study to reactions with condensed organic substrates as well as other metals.

This work will appear in Int. J. Mass Spectrom. Ion Phys.

MASS SPECTROMETRIC DETERMINATION OF WATER USING CRYOGENIC CONCENTRATION AND ACETYLENE CONVERSION

Gerald L. Carlson and William M. Hickam
Westinghouse Research Laboratories
Pittsburgh, Pennsylvania 15235

The routine mass spectrometric determination of moisture in gas samples is plagued with severe difficulties due to incomplete and non-reproducible transport of the water molecules through the spectrometer inlet system. These difficulties can be overcome by heating of the inlet system to above 100°C, but this requires precise thermostatting of the entire inlet and usually some other inlet modifications. For gas mass spectrometers not equipped with heated inlets and for laboratories where moisture analysis is called for only occasionally, these necessary modifications can be a sizeable undertaking. There is also evidence that water vapor reacts with the ion source filament and/or impurities collected on surfaces in the source region which may influence the accuracy of determining small amounts of water.[1]

In this paper a technique is described where moisture is cryogenically concentrated and quantitatively converted to another gas which can be conveniently determined by routine gas mass spectrometric techniques. The conversion is carried out external to the mass spectrometer system, and the method requires no modification of the instrument or inlet system.

A variety of chemical reagents are known to react with water generating a simple gaseous product, e.g., Na or CaH_2 giving H_2, Mg_3N_2 or $NaNH_2$ giving NH_3, and CaC_2 giving acetylene, C_2H_2. In this work, the CaC_2-acetylene conversion was chosen primarily because the most intense peak (m/e 26) of the analytical gas (C_2H_2) falls in a region which is usually free from interference by other sample gases or instrument background gases. Other considerations were that the CaC_2 reagent is readily available and convenient to handle, and the product acetylene is relatively stable and presents minimal hazards from the small quantities generated.

CaC_2 has been used extensively for moisture analysis with the evolved acetylene measured by a variety of techniques,[2] including a gas chromatographic procedure.[3] In the gas chromatographic method, it was determined that the use of uncalcined CaC_2 was advantageous and that saturation of the CaC_2 with CO_2 was necessary to prevent adsorption of the generated acetylene.

In the present work it was found that a dynamic system for conversion of H_2O to C_2H_2, where the sample gas is passed through a bed of CaC_2, did not yield reproducible results. Thus, a cryogenic concentration procedure was devised where the moisture is condensed onto the CaC_2 by the use of a refrigerated trap. This procedure not only greatly increases the sensitivity of the method, but also forces quantitative conversion of H_2O to C_2H_2 by providing intimate, prolonged contact of the moisture with CaC_2.

The moisture concentration and acetylene conversion is accomplished in a 1/4 in. stainless steel U-tube trap which is fitted with isolating valves. The trap is charged with a few grams of CaC_2 (Electrolite grade, 20-30 mesh) and "activated" by heating to ∿90°C while pumping to remove adsorbed C_2H_2 and other gases. At this stage only vestiges of the C_2H_2 peak at m/e 26 are present in the trap background spectrum. Once activated, the trap can be used for a large number of analyses unless it is opened to the atmosphere or a very wet sample is encountered. The sample is attached to the back end of the trap, and if desired, a preliminary mass spectrum of the sample can be obtained via a trap by-pass. The trap is then cooled with the appropriate refrigerant (usually liquid N_2 or dry ice bath) which is selected to efficiently condense all of the water while allowing the bulk of the gas sample to pass through. After all of the gas sample has been pumped slowly through the trap, the trap contents are isolated and heated to ∿90°C for 1/2 hour to promote the carbide reaction. The gaseous contents of the trap are then quantitatively analyzed by conventional mass spectrometric procedures to yield the absolute quantity of C_2H_2 produced, which, from the stoichiometry of the reaction:

$$CaC_2 + 2H_2O \rightarrow C_2H_2 + Ca(OH)_2 ,$$

is equivalent to one-half of the water content of the sample.

The accuracy of the method was determined by analyzing gas samples of known moisture content as determined with an Alnor Dewpoint Meter. The comparative results are given in Table 1.

TABLE 1
Determination of Moisture in Gases

Gas	ppm H_2O by Volume Alnor Method	CaC_2-MS Method
Nitrogen	<5	2
Nitrogen	28	25
Nitrogen	90	92
Air	650	655
Air	8600	7950

The sensitivity of the method is about 2 ppm of water vapor in a 300 cc-atm gas sample or approximately 1 μg of water.

The procedure can also be used to determine the amount of moisture desorbed from solids. In this case the solid sample is placed in a small furnace-enclosed container attached to the trap. The liberated moisture is vacuum transferred to the CaC_2 trap or could be swept into the trap with a dry carrier gas. Two hydrated salts of known water content were analyzed in this manner with the results:

Salt, mg	H_2O Analysis, mg	wt % H_2O Found	Theor.
$BaCl_2 \cdot 2H_2O$, 53.18	7.63	14.35	14.74
$K_2Fe(CN)_6 \cdot 3H_2O$, 155.14	19.33	12.46	12.78

The time required for moisture analysis by the described method is very dependent on the type and volume of the sample, but 1-2 hours per sample should be typical. However, in that same time, a complete mass spectrometric analysis of the sample can also be accomplished. It should also be noted that a simple manometric measurement of the amount of acetylene generated is usually not sufficient and could lead to serious errors for samples with low moisture concentration. The C_2H_2 content of the trap following the concentration and conversion steps has been found to vary between 10 and 95%, depending on the amounts of other residual gases caught in the trap. Thus, the mass spectrometer is needed to determine the composition of the trap gases. This method is obviously not intended as a replacement for the more rapid methods of moisture determination. It has, however, been found very useful as a complement to mass spectrometric gas analysis where the total composition of the sample, in addition to the moisture content, is of interest.

References

1. Y. Masuda, Shitsuryo Bunseki 1971, 19 (2), 150.

2. J. Mitchell, Jr. and D. M. Smith, Aquametry, Interscience Publishers, Inc., New York, 1958.

3. E. P. Chicherina and M. F. Prokop'eva, Uzb. Khim. Zh. 1968, 12 (5), 23.

Scope and Limitations of Mass Spectrometric Determination of Carbon 14, R. Schnitzer and M. Anbar, Stanford Research Institute, Mass Spectrometry Research Center, Menlo Park, CA 94025

In the last two meetings, we have described the mass spectrometric approach to carbon dating. C-14 is to be measured in the form of $^{14}C^{15}N^-$- (mass 29). Therefore, any background contribution to this mass is a critical interference and should be avoided. This paper describes our modifications made, in an effort to reduce some of these low-level background contributions. The background contributions arise from different sources: (1) hydrocarbons producing $C_2H_n^-$ (general form for all isotopic substitutes); (2) water-producing COH^-; and (3) silicon-producing $^{29}Si^-$ and $^{28}SiH^-$.

The reduction of hydrogen-containing species requires the removal of water and hydrocarbons, whereas reduction of the silicon-containing species requires that construction materials in the plasma zone have minimal silicone content.

We have modified the gas inlet system (Fig. 1), the hollow cathode duoplasmatron ion source (Fig. 2), and lens system (Fig. 3). The ion source can now be readily pumped out (5×10^{-8} torr) and baked together with the lens system up to 300°C.

The feed gas ($N_2 + CO_2$) is purified by passing over CuO + Pt at 600°C to oxidize hydrocarbons to CO_2 and H_2O. The H_2O present in the gas is effectively removed by conversion over $BaCl_2$ at 600°C to HCl and the latter is trapped by ZnO at 300°C. This procedure facilitates removal of H_2O in the presence of CO_2. At present, various construction materials must be tested before performance of the system can be evaluated.

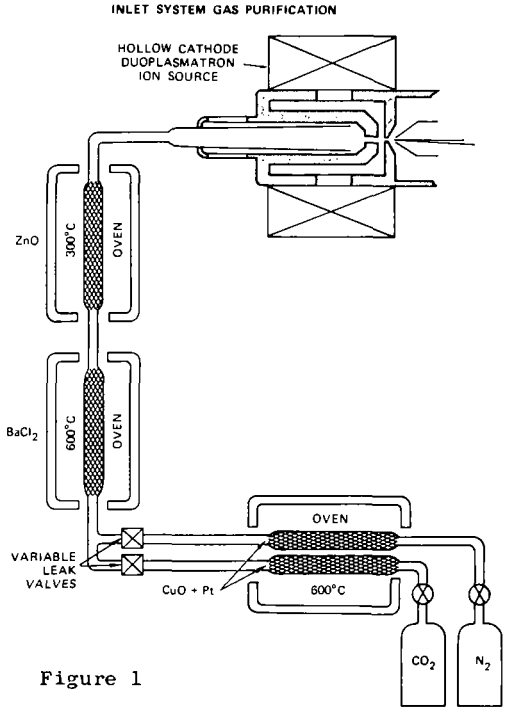

Figure 1

BAKEABLE HOLLOW CATHODE DUOPLASMATRON

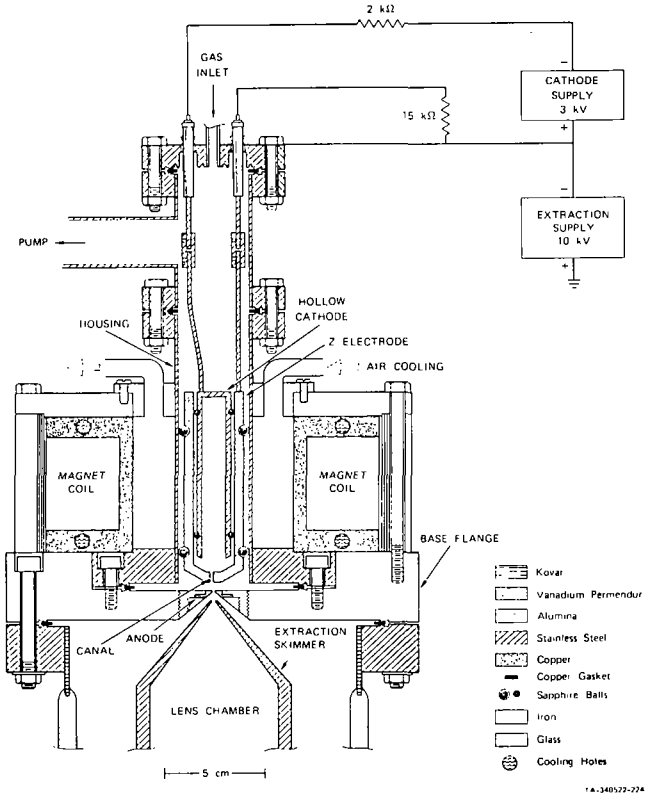

Figure 2

BAKABLE LENS SYSTEM

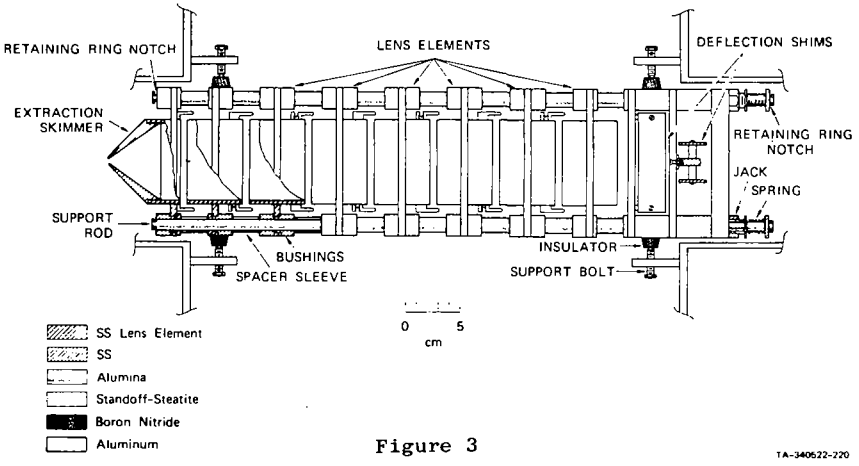

Figure 3

Polyatomic Phase Space Theory: Applications to Bimolecular and Unimolecular Reactions. WALTER J. CHESNAVICH and MICHAEL T. BOWERS, Univ. of California, Dept. of Chem., Santa Barbara, California 93106.

Rigorous, semiclassical expressions have been derived for the sum and density of momentum states of pairs of molecules containing one spherical top and either a linear molecule or a spherical, prolate, or oblate top molecule as a partner. Calculations are compared to experiment for the following examples: (a) $C_2H_4^{+\cdot} + C_2H_4 \rightarrow C_3H_5^{+} + CH_3\cdot$; both the energy dependence of the cross section and the product kinetic energy distribution indicate this reaction is statistical for $C_2H_4^{+\cdot}$ in its ground electronic state with energies of up to a few eV. (b) $C_6H_5CN^{+\cdot} \rightarrow C_6H_4^{+\cdot} + HCN$; the product kinetic energy distribution in this system indicates the reaction is statistical. Values of k(E) vs E are also given. (c) $C_4H_6^{+\cdot} \rightarrow C_3H_3^{+\cdot} + CH_3\cdot$; the product kinetic energy distribution in this system suggests the reaction is not statistical. Values of k(E) vs E are also given. Other applications will be discussed.

A Theoretical Approach to Ion Polar Neutral Momentum Transfer Collision Frequencies*

D. P. Ridge and R. A. Barker
Department of Chemistry
University of Delaware
Newark, Delaware 19711

Recently, momentum transfer collision frequencies for ions in polar neutral gases have appeared in the literature. An understanding of this data is essential to understanding the dynamics of ion polar neutral collisions. A simple statistical theory is proposed from which collision frequencies may be calculated. The results, which agree well with experiment, are compared to those of other theories. Effects of approximations and possible improvements in the theories are discussed.

*A full account of this work is in J. Chem. Phys., 64, 4411 (1976).

Vibrational Energy Dependence of Ion-Molecule Reaction Cross Sections. ASHLEY D. WILLIAMSON, Health Physics Div., Oak Ridge Natl. Lab., Oak Ridge, TN 37830.

The effects of internal energy on ionic reactions are of interest, especially since molecular ions are generally formed in a distribution of internal states. Using photoionization techniques, it is possible to prepare reactant ions with well characterized vibrational populations, allowing quantitative measurements of the dependence of reaction cross sections on reactant ion vibrational state. Data will be presented for both endothermic and exothermic reactions, including measurement of the distribution of products among competing reaction pathways. In the case of ion-molecule reactions in ketene, energy deposition in the primary product may be studied by its subsequent decomposition.

CROSSED-BEAM STUDY OF THE REACTION $ArH^+(H_2,Ar)H_3^+$

M.L. Vestal, C.R. Blakley and J.H. Futrell
Department of Chemistry, University of Utah
Salt Lake City, Utah 84112

Proton transfer reactions comprise a class of very simple ion-molecule reactions which have received much attention in our laboratory and elsewhere. The reactions

$$ArH^+ + H_2 \rightarrow H_3^+ + Ar \qquad R1$$

$$H_3^+ + Ar \rightarrow ArH^+ + H_2 \qquad R2$$

have been studied recently in our laboratory using the tandem ICR-Mass Spectrometer[1] where it was found that at near thermal energies, reactant internal energy had little effect upon the rate of R1, but large effects upon the rate of R2. This paper reports recent kinematic data on these reactions obtained with the Utah crossed-beam machine.

The crossed-beam apparatus, described in detail elsewhere[2], consists of an ion gun which produces a nearly monoenergetic beam of the desired ion which is then crossed at right angles with a beam of neutral molecules. Ionic reaction products are energy and mass analyzed in a moveable detector assembly. A chemical ionization source is used to produce the reactant ions, and a differentially pumped free jet is used to produce the neutral beam. Time averaged, phase sensitive pulse counting is used to obtain the energy spectra of the mass resolved product ions which are then processed off line on a computer.

Reaction R1 is quite well characterized by the elastic spectator model[3] which assumes that hydrogen strips the proton with elastic scattering of the products. The center of mass angular distributions show behavior similar to that reported[4] for the reaction $H_3^+(D_2,H_2)D_2H^+$. At low relative energies, below ca. 0.2 eV, there is considerable large angle scattering, suggesting the onset of orbiting collisions. At intermediate energies, up to a few electron volts, the product is strongly peaked at the spectator stripping point. Above a few electron volts, large angle scattering again occurs as one might expect for a hard, rebounding collision. Energetic data are summarized in Table 1; the observed most probable Q is close to that predicted by the spectator stripping model. Overall, the reaction exhibited behavior quite similar to the thermoneutral reaction of H_3^+ with D_2.

The reaction $H_3^+(Ar,H_2)ArH^+$ exhibited quite unexpected behavior. Using Henglein's recent value for the proton affinity of argon[5], this reaction is endothermic by about 0.6 eV, thus for ground state reactants, no products should be formed at Q values greater than -0.6 eV. Since the reactant ions in our machine are produced in a CI source, we expected to have vibrationally relaxed H_3^+ and therefore, no product at high Q values. We found, however, as shown in Figure 1, product was in fact being produced at high Q values implying that some of the H_3^+ had several quanta of internal energy.

Previous studies in this laboratory[6] and elsewhere[7] have suggested that H_3^+ is rapidly relaxed within about ten collisions. Our data clearly show that H_3^+ formed at moderate source pressure still have considerable internal energy. At 0.1 torr H_3^+ ought to undergo on the order of 100 collisions. The fact that we see direct evidence of remaining internal energy after this many collisions seems to contradict the previous work.

To further study this apparently slow relaxation process, we obtained data at a source pressure of 0.5 Torr, where the average number of

collisions is tens of thousands. These data are also summarized in Figure 1, where it is evident that the most probable Q does indeed agree with expectations. Detailed examination of the Q distributions, though, shows that there is product intensity formed at larger Q values, although not nearly to the extent of the lower pressure.

Clearly, the data show that a substantial fraction of H_3^+ retains at least a few quanta of internal energy after hundreds or even thousands of collisions. The suggestion that H_3^+ is rapidly relaxed was based upon the closing out of an endothermic reaction channel in competition with an exothermic channel, where it was assumed the endothermic reaction would occur if there was enough total energy available. This work suggests that this assumption may not be valid. Indeed, it appears that when endothermic and exothermic channels are competing, the endothermic channel may be closed well before the total reactant energy reaches the threshold for reaction.

Summarizing, the elastic spectator model fits the data for the reactions $H_3^+(Ar,H_2)ArH^+$ and $ArH^+(H_2,Ar)H_3^+$ quite well at all energies studied. At energies below ca. 0.2 eV, the data suggest an onset of orbiting for the reaction of ArH^+ with H_2. Finally, the data suggest that a substantial fraction of H_3^+ retains a few vibrational quanta after hundreds or thousands of collisions.

References

1. R.D. Smith and J.H. Futrell, Int. J. Mass Spectrom. Ion Phys., 20, 33 (1976).
2. M.L. Vestal, C.R. Blakley, P.W. Ryan, and J.H. Futrell, Rev. Sci. Intrum., 47, 15 (1976).
3. D.R. Herschbach, Appl. Opt. Suppl., 2, 128 (1965).
4. M.L. Vestal, C.R. Blakley, P.W. Ryan, and J.H. Futrell, J. Chem. Phys., 64, 2094 (1976).
5. A. Henglein, J. Phys. Chem., 76, 3883 (1972).
6. D.L. Smith and J.H. Futrell, Dynamic Mass Spectrometry, 4, in press
7. J.J. Leventhal and L. Friedman, J. Chem. Phys., 50, 2928 (1969).

Table 1

$ArH^+(H_2,Ar)H_3^+$

Relative Energy	Stripping Q	Observed Q
0.13 eV	-0.04 eV	0.03 eV
0.55	-0.19	-0.21
1.0	-0.36	-0.29
1.9	-0.67	-0.40
6.9	-2.4	-2.2

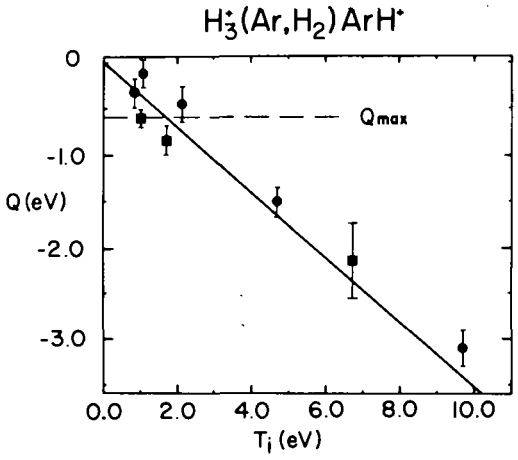

Fig. 1. Observed Q vs. initial relative energy T for $H_3^+(Ar,H_2)ArH^+$. The circles correspond to data obtained at 0.1 Torr source pressure and the squares to data obtained at 0.5 Torr. The solid diagonal line is the spectator stripping prediction. Q_{max} is the maximum allowable Q for ground state reactants.

Ion-Molecule Reactions Between Kr^+ and H_2, and HD.

JIDE IGE, Dept. of Chem., University of Ife, Ile Ife, Nigeria and M. J. HENCHMAN, Dept. of Chem., Drandeis Univ., Waltham, Mass. 02154.

Excitation functions for the formation of KrH^+ and KrD^+ have been measured in the energy range 0.014ev - 2.0ev. These have been transformed into absolute excitation functions by deconvoluting the effect of the thermal target motion, assuming a monoenergetic ion beam. Assuming a statistical population for the Kr^+ States and using the result that $k_{(2p_{1/2})} = 0.4\ k_{(2p_{3/2})}$, rate constants for the reaction of $Kr+(2p_{3/2})$ with hydrogen have been calculated for comparison with direct measurements using Afterglow and ICR techniques.

LUMINESCENCE FROM He^+/Cl_2 Collisions In The Energy Range 2-170 eV.

K. E. Siegenthaler

Air Force Materials Laboratory
Wright-Patterson Air Force Base, Ohio 45433

B. M. Hughes*, E. G. Jones and T. O. Tiernan

Wright State University
Department of Chemistry
Dayton, Ohio 45431

Spectral emissions in the 90 to 870 nm. region from collisions of He^+ with Cl_2 have been analyzed, and cross sections for excitation of specific product states have been determined over the He^+ kinetic energy range from 2-170 eV (lab). Ninety-six percent of total V. U. V. emissions were unambigiously identified to originate from excited Cl atoms. The cross section for total light emission in the 90 to 870 nm wavelength range was determined to be 5.0 A^2, with 1.2 A^2 of this total being due to cascading. Figure 1 shows the internal distribution of excited Cl atoms as a function of the energy levels. As it can be seen, after the emission cross sections are corrected for cascading, the major Cl atomic states that are formed are populated in reactions that are slightly exothermic or endothermic by as much as 1 - 2 eV. Figure 2 shows a Grotrian diagram for the Cl atom emissions, with the total cross section for emission of each state, summed over J-sublevels, given in parentheses. It can be seen that the only major violation of the $\Delta S = 0$ conservation rule for transitions involving this low atomic number atom occurs for the transition from the 4s ^4P J-levels to the ground state $^2P^o$ J-levels. This occurs since there are no lower energy quartet states. The lifetime of the 4s ^4P is estimated to be less than 10^{-6} sec., based upon the calculated atom residence time within the radiating region in our apparatus.

REFERENCES

*Present address: Flammability Research Center, University of Utah, Salt Lake City, Utah 84108

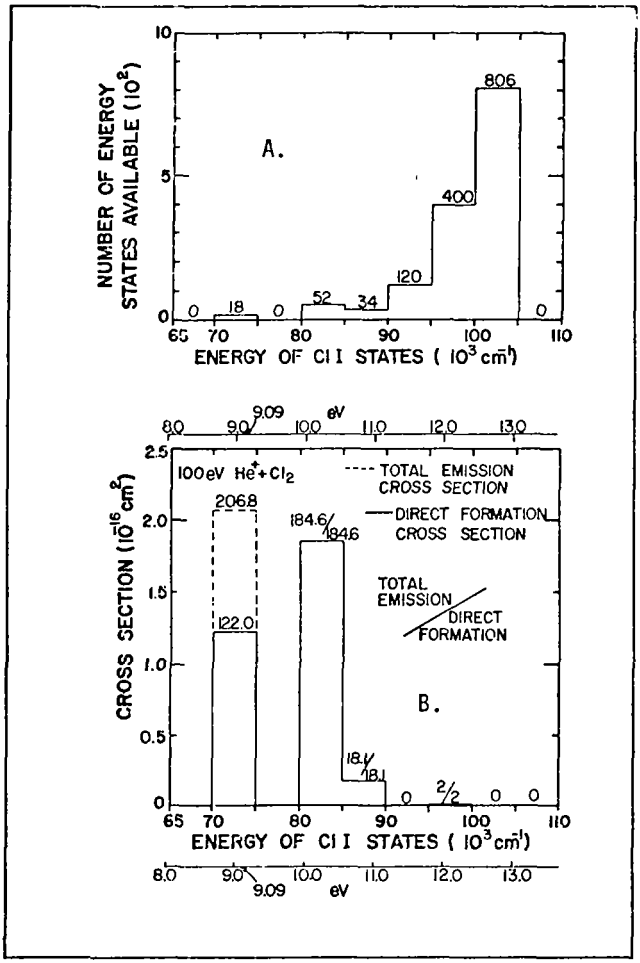

Figure 1A. Histogram of Density of States Available in the Chlorine Atom;

1B. Histograms of Cross Section for Total Emissions and Direct Formation in the He^+/Cl_2 Reaction.

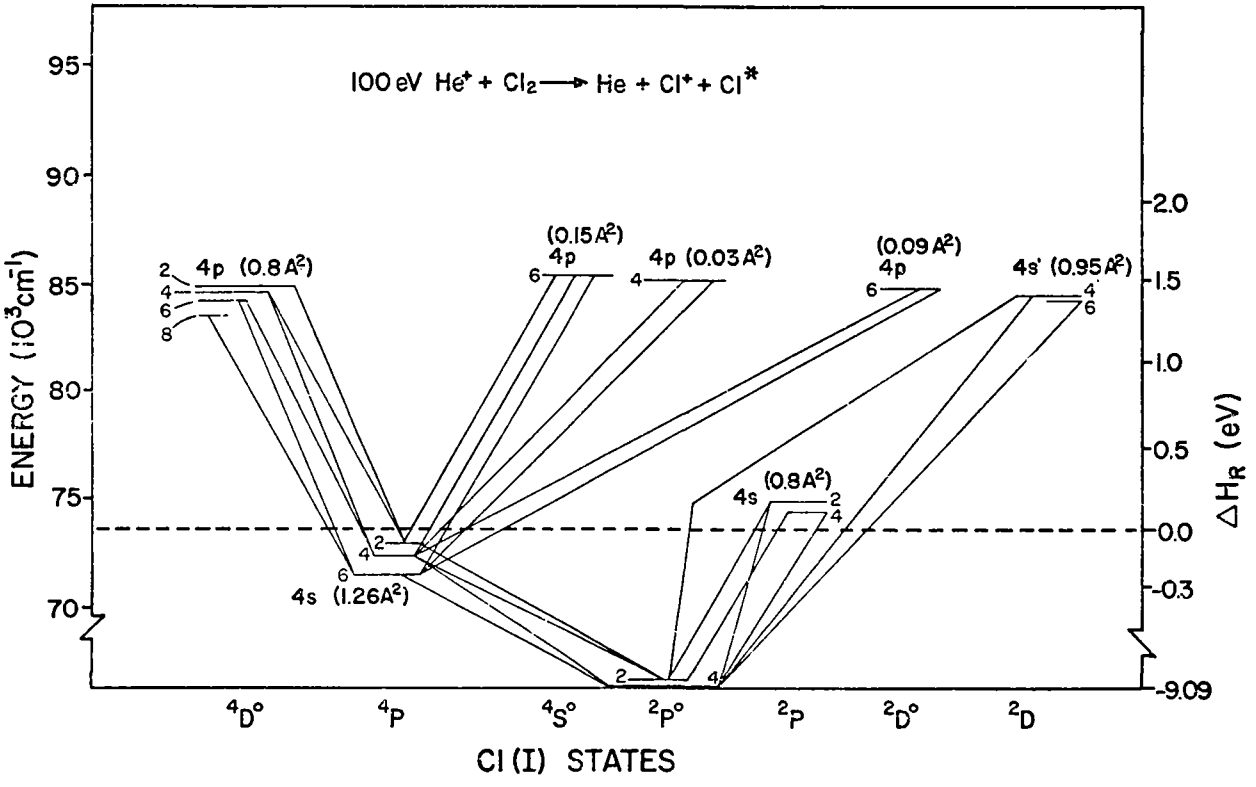

Figure 2. Grotrian Diagram of Cl Atom Emissions in the He^+/Cl_2 Reaction.

LIFETIMES OF INTERMEDIATE COMPLEXES IN ION-MOLECULE REACTIONS

G. G. Meisels, F. Botz[a] and E. F. Heckel[b]
Department of Chemistry, University of Nebraska-Lincoln, Lincoln, NE 68588

Relatively stable intermediate complexes in ion-molecule reactions were noted quite early;(1) numerous systems are now known where ionic intermediates are stabilized by collision and detected.(2-4) Lifetimes of intermediate complexes (τ_o) have been estimated on the basis of simplified mechanisms of collisional stabilization. These usually employ rate constants based on Langevin theory for the two coupled collision processes: the first which forms the complex (rate constant k_f), and the second which stabilizes it (k_s).(3-7) When one collision suffices for the quenching of dissociation, one arrives at the usual relationship(4-7) for the third order constant

$$k_1 = k_f k_s \tau_o = \nu_f \nu_s \rho_s \tau_o \qquad [I]$$

where ν is the collision frequency and $k_s = \rho_s \nu_s$ so that ρ is a stabilization efficiency of somewhat nebulous definition.

It is clear that all experimental studies to date have inseparably involved the formation and lifetime of the collision complex and the details of the deactivating collision. In order to gain insight into the nature of the complex and its reflection of the formation process, we have developed a model based on a retention of angular momentum, peculiar to ion-molecule collisions. Thereafter, however, we employ RRKM(8-10). Our model differs from that of Good(11) by assuming neither a classical unimolecular rate constant nor complete conversion of rotational angular momentum to internal degrees of freedom.

We combine r^{-4} polarization attraction with a hard core (Sutherland potential) and add the centrifugal potential defined for each collision by the initial relative energy and the value of the effective potential at the hard core separation r_e:

$$E_i = E_o(1 - b^2/r_e^2) + e^2\alpha/2r_e^4 \qquad [II]$$

where b is the impact parameter and α the polarizability. The barrier towards redissociation e_b is given by the effective potential at its maximum,

$$E_b = e_o^2 b^4/2e^2\alpha \qquad [III]$$

We now assume that E_i is randomly distributed and that redissociation can be described by RRKM.

Sample calculations for CO_3^-, chosen in spite of its smallness because of our previous interest(7) in the association reaction

$$O^- + CO_2 \rightleftarrows CO_3^{-*}$$

were performed using the method of steepest descent.(8,9) Vibrational frequencies were estimated from those of $CO_3^=$(12) and CO_3^-.(13)

The variation of $k(b,E_o)$ with b is shown in Figure 2 for three representative values of E_o. It is clear, particularly at the higher energies, that $k(b,E_o)$ varies substantially and increases with increasing impact parameter over most of the range. This reflects the reduction of the well depth at r_e, while the change in E_b is relatively minor. As b approaches the Langevin capture limit b_L, it passes through a maximum and then drops sharply to zero at b_L. This is to be expected from the model as the barrier height approaches the internal energy E_i.

$k(b_1,E_o)$ must now be folded into the appropriate distribution functions with the upper limits of b defined by the Langevin capture orbit, b_L.

$$k(T) = \langle k(b,E_o)\rangle = \int_{E_o=0}^{\infty} \int_{b=0}^{b_L} k(b,E_o)\ P(B)\ P(E_o)\ dbdE_o$$

where $P(E)_o$ is the Maxwell-Boltzman distribution and $P(b) = 2b\ b_L^{-2}$. The integration should be performed in two parts since the Langevin formalism does not apply at values of $b_L < \sqrt{2}\ r_c$(7) but we did not do so because $P(E_o)$ is small where this is required.

Typical results obtained after averaging over b only are shown in Figure 3. The small differences at 300 and 500° K. reflect the vibrational energy of the CO_2 precusor. Averaging over b and E_o leads to the overall rate constant which may be compared with experiment (Figure 4). The temperature effect now reflects both the change in $P(E_o)$ with T and the increased internal energy of CO_2 at higher temperature.

k(T) is perhaps most sensitive to the choice of r_e. Previous data on this system (7) can be matched for $r_e \simeq 0.14$ nm on the assumption that deactivation occurs with unit efficiency at the collision frequency calculated from Langevin theory. This is reasonable when compared to C-O bond lengths of 0.14 nm in carboxylic acids(14), 0.116 nm in carbon dioxide(15), or 0.129 nm in $CO_3^{=}$.(15) We may conclude that deactivating collisions indeed occur with near unit effectiveness.

Lastly, we note that this approach permits calculation of the temperature dependence. In the conventional form of an Arrhenius plot one obtains a small energy dependence or "activation" energy towards redissociation of ca. 0.4 kcal.mole, that is, redissociation is slightly faster at higher temperature; this is qualitatively consistent with preliminary observations.(6,16-18)

Alternately, one may calculate the apparent third order rate constant k_1 using approximate Langevin orbiting rate constants for k_f and k_s, the dissociation rate constant $k_{fo} = k(T)$ calculated here, and equation III, and evaluate the exponent of the relationship $k_1 = AT^n$; we find $n = -1.5$. In the interpretation of overall transition state theory(18) this corresponds to the conversion of one torsional oscillation to an internal rotation in the termolecular collision complex ($C_2O_5^-$) for a reaction without activation energy. Our model calculations show that a more detailed application of transition state theory using the RRKM formulation does not require untestable assumptions concerning internal degrees of freedom in the complex, and suggests that interpretation of n in terms of changes in internal degrees of freedom in the collision complex may be complicated by other factors.

LITERATURE CITED

1. R. F. Pottie, R. Barker, and W. H. Hamill, Radiation Research 10, 664, (1959). 2. G. G. Meisels, J. Chem. Phys. 42, 3237 (1965). 3. P. Kebarle, in "Ion-Molecule Reactions", J. L. Franklin, Editor, Plenum Press, New York, 1972; V. 1, p. 328. 4. E. E. Ferguson, Ibid., V. 2, p. 363. 5. V. G. Anicich and M. T. Bowers, J. Amer. Chem. Soc. 95, 1279, (1974). 6. A. G. Harrison, in "Interactions between Ions and Molecules" P. Ausloos, Ed., Plenum Press, New York; p. 263. 7. R. K. Mitchum, J. P. Freeman, and G. G. Meisels, J. Chem. Phys. 62, 2465 (1975). 8. W. Forst, "Theory of Unimolecular Reactions", Academic Press, New York (1973). 9. P. J. Robinson and K. A. Holbrook, "Unimolecular Reactions", Wiley-Interscience, New York (1972). 10. Y. N. Lin and B. S. Rabinovitch, J. Phys. Chem. 74, 3151 (1970). 11. A. Good,

Trans. Faraday Soc. 67, 3495 (1971). 12. K. Nakamoto, "Infrared Spectra of Inorganic and Coordination Compounds", Wiley, New York; 2nd Edition, 1970. 13. H. Gershinowitz and H. Eyring, J. Amer. Chem. Soc. 57, 985 (1935). 14. Handbook of Chemistry and Physics, Chemical Rubber Co., Cleveland, Ohio; 56th Edition (1975); p. F-155. 15. "Comprehensive Inorganic Chemistry", Bailar, Emeleus, Nyholm and Trotman-Dickenson, editors; Pergamon Press, New York (1973). Volume I., p. 1231. 16. L. I. Bone and L. Su, presented at the 24th Annual meeting on Mass Spectrometry and Allied Topics, San Diego, California, May 1976; Paper No. Q12. 17. M. T. Bowers, W. R. Davidson, T. Su, L. Bass, P. Neilson and D. H. Aue, Ibid., Paper No. Q10. 18. M. Meot-Ner, J. J. Solomon, F. H. Field and H. Gershinowitz, J. Phys. Chem. 78, 1773 (1974).

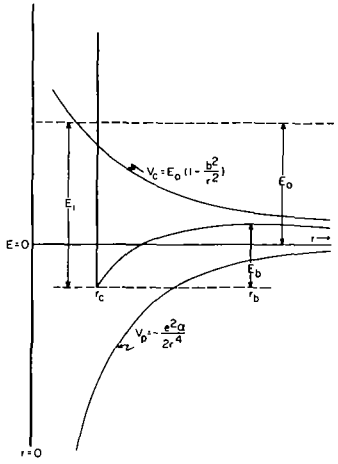

Figure 1. Diagram of effective potential for ion-molecule reaction leading to intermediate complex.

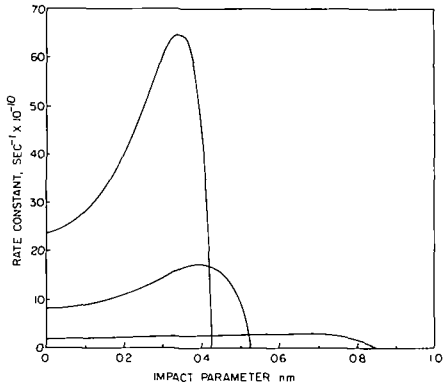

Figure 2. Variation of rate constant $k(b,E_0)$ with impact parameter b ($O^- + CO_2$). Top to Bottom: E_0 = 12 kT, E_0 = 5 kT, E_0 = kT.

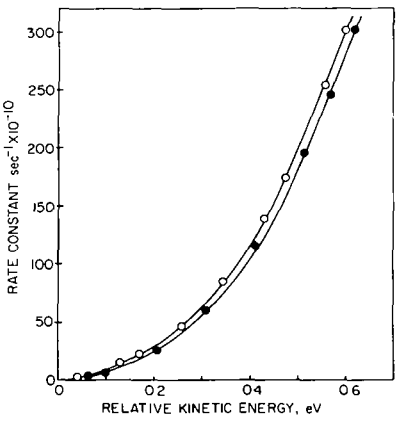

Figure 3. Dependence of $k(E_0)$, for the intermediate formed by reaction of O^- and CO_2, on relative energy. 500° K; 300°K.

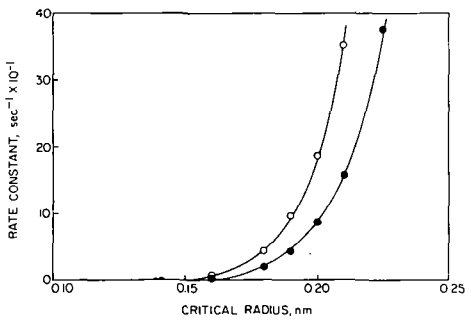

Figure 4. k for $CO_3^{-*} \rightarrow O^- + CO_2$ and its dependence on the choice of the hard core collision diameter r_c.

Unimolecular Decomposition of Protonated Methanol Ions from Metastable Peaks in Chemical Ionization Mass Spectrometry. W. T. HUNTRESS, JR., Jet Propulsion Laboratory, Pasadena, CA, M. T. BOWERS, Univ. of Calif., Santa Barbara, CA, and K. R. JENNINGS, Univ. of Warwick, Coventry, U. K.

The MS-50 mass spectrometer at the Univ. of Warwick has been used successfully to observe metastable peaks from the unimolecular decay of excited ions formed by ion-molecule reaction in a high pressure chemical ionization source. H_3^+ chemical ionization of methanol was used to produce excited protonated methanol ions, M/e = 33, for which metastables were observed for decomposition to protonated formaldehyde (M/3 = 31) and methyl cations (M/e = 15):

$$H_3^+ + CH_3OH \longrightarrow \{CH_3OH_2^+\}^* \begin{cases} \longrightarrow CH_2OH^+ + H_2 \\ \longrightarrow CH_3^+ + H_2O \end{cases}$$

The metastable peak for 33 → 31 is broad and dished-topped, and yields a kinetic energy release of 0.93 eV. The shape of the metastable for 33 → 15 is Gaussian and narrow, corresponding to an energy release of only 0.002 eV.

Thermal Energy Reactions of $^{12}C^+(^2P)$ and $^{13}C^+(^2P)$ Ions with Hydrocarbon Molecules

Richard D. Smith*
Code 6110, Naval Research Laboratory, Washington, D.C. 20375

and

Jean H. Futrell
Department of Chemistry
University of Utah, Salt Lake City, Utah 84112

The near thermal energy (~0.1 eV) reactions of $^{12}C^+(^2P)$ and $^{13}C^+(^2P)$ ions with methane, ethylene, ethane, propylene, and propane have been studied[1] utilizing a tandem Dempster-Ion Cyclotron Resonance mass spectrometer. The C^+ reactant ions are prepared by the charge transfer reaction of He^+ with CO.[1] Branching ratios for the reactions of the mass-selected reaction ion are obtained under conditions assuring the absence of secondary collisions and discrimination on the basis of product mass or momentum. Comparison of product distributions for reactions of $^{12}C^+$ and $^{13}C^+$ allows examination of mechanistic details.

The reactions of C^+ ions with simple hydrocarbons are more complex than suggested by previous work.[1] The results emphasize the striking differences in product distributions obtained at thermal energies and at only slightly higher energies (2-4 eV).[2] Undoubtedly the reactions are more complicated at thermal energies than at higher energies where all previous work has been done, and where the large excess of energy which must be disposed of favors the observation of direct processes.

The reaction of C^+ with methane exhibited the most dramatic changes between 0.1 eV and 3 eV. At thermal energies, this reaction occurs almost exclusively via complex formation. Indeed, breakdown curves for excited ethylene ions quantitatively rationalize the observed product distribution. At 3 eV several competing reaction channels such as hydride abstraction and dissociative charge transfer are observed.[2]

For the reactions of C^+ with ethylene and ethane at low energies we observe larger contributions of direct processes, such as charge transfer and hydride ion abstraction. For ethylene there were no C_2 products with detectable ^{13}C insertion; a mechanism involving attack at the C=C double bond and formation of a stable cyclic C_3 ion rationalizes this result.

---

*Present address: Radiological Sciences Dept., Battelle-Northwest
Richland, Washington 99352

The reaction of C^+ with ethane results in two C_2 ionic products with nearly complete (80%-90%) ^{13}C retention. Insertion at either a C-H or C-C bond is consistent with this result.

A model postulating C^+ insertion at the C-H bond or the C-C bond in combination with direct processes can rationalize the results. We favor C^+ insertion at the C-H bond by analogy with similar neutral reactions; moreover, the $C^+ + CH_4$ results demonstrate that C-H insertion is an important mechanism in the reactions of C^+ with hydrocarbons.

The reactions of C^+ with propylene and propane are more complex. In addition to the direct processes and complex formation (used to rationalize the reaction products with methane, ethylene, and ethane) it is necessary to postulate more complex mechanisms--either involving a very short-lived (on the order of a vibrational period) intermediate such that fragmentation preceeds equilibration of energy, or a combination of CH_2^-, CH_3^-, H_2^-, CH_2, and CH_3 abstraction reactions.

The need to postulate these more complex mechanisms on progressing to more complex neutrals indicates a congruence between the lifetime of the intermediates and the time required for equilibration of energy. This competition between equilibration and decomposition may be responsible for the decrease of the fraction of the total products which appear to result from complex formation as one proceeds to larger molecules.[1,3] This further suggests that the reaction energy is more slowly equilibrated in chemical activation by ion-molecule reaction excitation than by charge transfer or electron impact ionization where the randomization hypothesis assumptions appear adequate.

References:

1. R.D. Smith and J.H. Futrell, J. Chem. Phys., submitted.
2. P.S. Wilson, R.W. Rozett, and W.S. Koski, J. Chem. Phys., 52, 5321 (1970).
3. R.D. Smith, J.J. DeCorpo, W.N. Allen, and F.W. Lampe, Chem. Phys. Lett., submitted.

Vibrational Energy Transfer in Excited Ionic Species: Rates and Mechanism of Dimerization of Protonated Nitrogen Bases. M. T. BOWERS, W. R. DAVIDSON, T. SU, L. BASS, P. NEILSON and D. H. AUE, Univ. of California, Dept. of Chem., Santa Barbara, California 93106.

The rates and mechanisms of dimerization reactions of a series of protonated alkylamines will be presented. The validity of the energy transfer mechanism

$$AH^+ + A \rightleftharpoons \{A_2H^+\}^* \xrightarrow{M} A_2H^+$$

will be discussed in light of our experimental results and phase space theory calculations. Comparison will be made with recent results of Meot-Ner and Field[1] on similar systems.

---

[1] M. Meot-Ner and F. H. Field, J. Amer. Chem. Soc., 97, 5339 (1975).

Reaction of Ground State C^+ Ions

by

V. G. Anicich and W. T. Huntress

Jet Propulsion Laboratory
4800 Oak Grove Drive
Pasadena, California 91103

and

J. H. Futrell

Department of Chemistry
University of Utah
Salt Lake City, Utah 84112

The discussions of this conference have ranged over wide dimensions. These extend from solution reactions in test tubes to atmospheric chemistry encompassing very large volumes. The topic presented here is on reactions of C^+ ions, and the implications of these reactions in the extremely large volume of dense interstellar clouds. In these dense clouds there is an abundance of atomic species and a constant flux of light and high energy particles. The result is the formation of a large fraction of atomic ions. The reactions of these ions may lead to the formation of the interstellar molecules observed by radio astronomers, who have been recording the microwave spectra of large molecules and ions present in these dense clouds. In this laboratory study we have been able to answer a few questions and suggest possible test measurements for the radio astronomers. This research is part of an extensive investigation of interstellar chemistry being conducted at the Jet Propulsion Laboratory.

The experiments described were conducted using two separate instruments. Absolute rate constants were obtained from trapped ion ICR experiments at JPL. The branching ratios were obtained from tandem mass spectrometric experiments at the University of Utah.

The C^+ ions were produced by electron bombardment of a mixture of helium and carbon monoxide. He^+ charge transfer to CO produces C^+ ions in the ^2P ground electronic state. C^+ ions are the sole product of the charge transfer reaction. C^+ ions do not react further with carbon monoxide. By maintaining a 6/1 mixture of He and CO in the source it is insured that more than 90% of the C^+ ions are in the ground electronic state.

The tandem mass spectrometer at the University of Utah is a combination of a Dempster mass spectrometer and an ICR mass spectrometer. An experiment is performed at constant magnetic

field; the field being defined as that necessary to focus the desired reactant ion into the ICR. To observe ions in the ICR, the frequency of the marginal oscillator is scanned and the relative sensitivity of the marginal oscillator is measured using a Q-spoiler, or reference load. The measurement of the C^+ branching ratios were made at between 10 and 20% conversion to reaction products.

The absolute rate constants were determined by observing the C^+ ion abundance as a function of time with and without the reactant gas. Reaction times of from 0 to 100 msec were observed. The typical additive pressure used was about 3×10^{-7} torr in 1×10^{-5} total He + CO pressure. Kinetic plots indicate that the He^+ ions have almost completely reacted after 30 msec. A log plot of the ratio of the C^+ signal (with and without the reactant gas) was used to determine the limiting slope and the rate constant for the disappearance of the C^+ ion. The rate constants were found to compare well with those predicted by either the Langevin or the ADO theory, and with rate constants previously reported in the literature.

In the reaction of C^+ with oxygen, observation of the O^+ channel was somewhat surprising, since it has not been detected in previous studies.[1] The branching ratio measured for the C^+-NH_3 reaction differs markedly from that reported by Schiff *et al.*[2] These workers did not observe HCN^+ and reported the H_2CN^+ channel as only 5% of the total reaction. The reaction of C^+-NH_3 is of possible importance in the synthesis of HCN in interstellar space.[3] HCN can be produced by recombination of H_2CN^+ with electrons or by reaction of H_2CN^+ with NH_3. Together with the identification of the C^+-HCN reaction as a loss channel of HCN, we have been able to predict HCN/NH_3 of ≥ 0.4 for interstellar media. The reported interstellar ratios vary between 0.1 and 10. Reaction R7 is possibly an important mechanism for the formation of "X-ogen", HCO^+, in interstellar clouds by reaction of C^+ ions with H_2O. Reaction of C^+ with H_2S produces the sulfur analog, HCS^+. The CCl^+ ion is produced by reaction of HCl with C^+.

Using a mixture of He with ^{12}CO and ^{13}CO the carbon atom isotopic exchange rate[4] in collisions of C^+ with CO was measured. This was done by observing either the $^{12}C^+$ or $^{13}C^+$ ion signal both with and without ejection of the other C^+ isotope to prevent back reaction. From the ratio of these signals, the rate constants for isotope exchange were both measured as 2.0×10^{-10} cm^3/sec. If in cold interstellar clouds it is assumed that rate constant for isotope exchange is the same as observed at 300°K, the difference in zero point energies between ^{13}CO and ^{12}CO will tend to fractionate the carbon isotopes to enhance the ^{13}C abundance in CO. This is in agreement with observations.

References

1. F. C. Fehsenfeld, A. L. Schmeltekopf, and E. E. Ferguson, J. Chem. Phys. 45, 23 (1966).

2. H. I. Schiff, R. S. Hemsworth, J. D. Payzant, and D. K. Bohme, Astrophys. J. 191, L49 (1974).

3. W. T. Huntress and V. G. Anicich, Astrophys. J. (in press, 1976).

4. W. D. Watson, V. G. Anicich, and W. T. Huntress, Astrophys. J. (in press, 1976).

C^+ Ion Reactions

		$K(cm^3/sec) \times 10^9$	
$C^+ + O_2 \xrightarrow{0.36} O^+ + CO$ $C^+ + O_2 \xrightarrow{0.64} CO^+ + O$		1.22	(R1)
$C^+ + CO_2 \longrightarrow CO^+ + CO$		1.1	(R2)
$C^+ + CH_4 \xrightarrow{0.29} C_2H_2^+ + H_2$ $C^+ + CH_4 \xrightarrow{0.71} C_2H_3^+ + H$		1.45	(R3)
$C^+ + NO \longrightarrow NO^+ + C$		0.85	(R4)
$C^+ + NH_3 \xrightarrow{0.50} NH_3^+ + C$ $C^+ + NH_3 \xrightarrow{0.47} H_2CN^+ + H$ $C^+ + NH_3 \xrightarrow{0.03} HCN^+ + H_2$		2.3	(R5)
$C^+ + HCN \longrightarrow C_2N^+ + H$		3.2	(R6)
$C^+ + H_2O \longrightarrow HCO^+ + H$		2.7	(R7)
$C^+ + HCl \longrightarrow CCl^+ + H$		Fast	(R8)
$C^+ + H_2CO \xrightarrow{0.48} CH_2^+ + CO$ $C^+ + H_2CO \xrightarrow{0.21} HCO^+ + CH$ $C^+ + H_2CO \xrightarrow{0.31} H_2CO^+ + C$		4.4	(R9)
$C^+ + H_2S \xrightarrow{0.28} H_2S^+ + C$ $C^+ + H_2S \xrightarrow{0.72} HCS^+ + H$		2.0	(R10)
$(C^{12})^+ + C^{13}O \longrightarrow (C^{13})^+ + C^{12}O$		0.20	(R11)
$(C^{13})^+ + C^{12}O \longrightarrow (C^{12})^+ + C^{13}O$		0.20	(R12)

THE TEMPERATURE DEPENDENCE OF A THIRD ORDER RATE CONSTANT AS A FUNCTION OF THE COMPLEXITY OF THE THIRD BODY

Lily Su and Larry I. Bone
Department of Chemistry, East Texas State University,
Commerce, Texas 75428

We have used the East Texas State Photoionization Mass Spectrometer to investigate the ion clustering reaction,

$$NO^+ + H_2O + M \rightarrow NO(H_2O)^+ + M, \qquad (1$$

as a function of temperature and third body. Mixtures of H_2O, NO, and the third body are photolyzed in a field free source by radiation from a Kr resonance lamp. The energy of the radiation (10.03 and 10.63 eV) is such that NO^+ is the only ion produced. It then reacts with H_2O in the presence of the third body and the rate constant is calculated by measuring the relative abundance of NO^+ diffusing from the source as a function of the pressure in the source.

Experiments are conducted with SF_6 and NO as third bodies at four different temperatures between 25°C and 180°C. Monatomic third bodies, Ar and Xe, were tried but they were found to be so inefficient that even when they were in a 9 to 1 excess, the large majority of the reaction proceeded with NO or H_2O as the third body. In experiments where SF_6 was the principal third body, the ternary mixtures consisted of $X_{H_2O} = 0.125$, $X_{NO} = 0.125$, $X_{SF_6} = 0.75$ and $X_{H_2O} = 0.063$, $X_{NO} = 0.187$, $X_{SF_6} = 0.75$. In experiments where NO is the third body, $X_{H_2O} = 0.125$, $X_{NO} = 0.875$ and $X_{H_2O} = 0.25$, $X_{NO} = 0.75$.

The rate constant for reaction 1 was calculated from the rate of disappearance of NO^+ by correcting for clustering with the third body. In every case the rate constant decreased as the temperature was increased. A variation in the rate constant with temperature and third body was found to agree with absolute rate theory, ie.,

$$k = \frac{kT}{h} \frac{Q^{\ddagger}}{\prod_i Q_i} e^{-Eo/RT} = AT^n e^{-Eo/RT}$$

where n is estimated from the number of translational and rotational degrees of freedom and therefore depends upon

the complexity of the third body. When NO is the third body the pre-exponential factor for reaction 1 is predicted to vary as $T^{-4.5}$ and as $T^{-4.0}$ with NO as the third body. Figure 1 shows a plot of log k vs. log T with SF_6 and NO as the third bodies. If the activation energy for the reaction is assumed to be zero, the values of n obtained from Figure 1, are -4.1, when SF_6 is the third body and -3.4 for NO as the third body. Agreement with theory is reasonably good, but a much larger temperature range would be needed to observe any departure from linearity. This would entail working at subambient temperatures which at the present is beyond our capability.

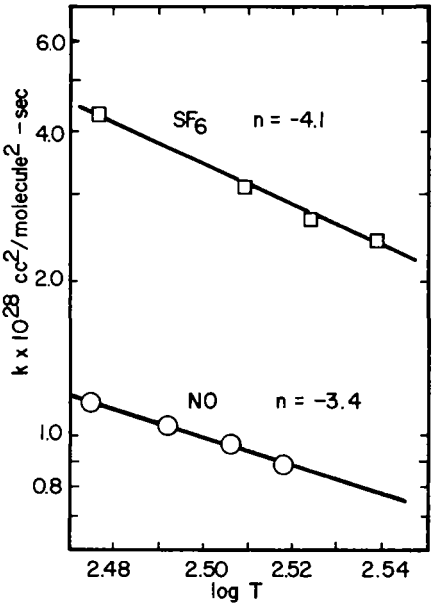

Figure 1. Rate constant of reaction 1 as a function of temperature and third body.

This work was supported by the Robert A. Welch Foundation.

QUANTITATIVE FIELD DESORPTION MASS SPECTROMETRY (FDMS) USING COMPUTER CONTROLLED SELECTED ION MONITORING

G.W. Wood and R.C. Charlton
Department of Chemistry, University of Windsor
Windsor, Ontario, Canada N9B 3P4

D.E. Hagge
INCOS Corporation
1332 6th St., Berkeley, Calif. 94710

Difficulties with sensitivity and reproducibility in f.d.m.s. employing electrical detection can be partially overcome by averaging several scans(1). In one example a synthetic mixture of cyclophosphamide-d_0 and -d_4 containing 89.71% d_0 gave the following results (%d_0 $\pm$ 95% confidence limits); 5 scans: 89.1 $\pm$ 3.0; 10 scans: 90.5 $\pm$ 1.9; 20 scans: 90.0 $\pm$ 1.1. Ion statistics are thus shown to be a major source of poor quality in field desorption spectra obtained by continuous magnet scanning.

Since selected ion monitoring of two peaks should allow a duty factor of 0.9 compared to 0.006 under limited range slow scanning conditions (200 amu in 10 sec), we set out to establish whether this expected 150-fold improvement in sensitivity would be reflected in improved isotope peak ratios. The compounds chosen for this preliminary work were uridine and thymidine nucleosides containing in their f.d. spectra fragrament peaks corresponding to sugar and base components.

The measurements were made with a Varian MAT CH5 DF mass spectrometer and an INCOS 2000 data system. Both the magnet scanning and SIR(Selected Ion Recording) were under computer control. The desired peaks, the mass window scanned and the scan times are selected under keyboard control. The single ion sensitivity necessary for these measurements is achieved by the interfacing technique of the data system (2).

A typical single scan of thymidine (base-deoxyribose) taken at 19 mA gave (m/e (rel. int.) assignment): 117 (4) deoxyribose; 126(1) base + H; 242(100) M; 243(11) M + 1. Selected ion monitoring of m/e 117, 118, 125, 126, and 127

for 150 2-second scans with time divided equally among the five ions gave (m/e, rel. int.): 117, 100; 118, 5.88; 125, 10.79; 126, 35.30; 127, 9.80. Statistical analysis of the base-related peaks is complicated by the presence of an unknown amount of hydrogen transfer to these ions. In contrast, the deoxyribose peak at m/e 117 is accompanied by an isotope peak of normal intensity (m/e 118 = 5.88, calc for $C_5H_9O_3$ 5.66). A more detailed analysis of the intensity of this peak is presented in the Table. Single scans (120-130) show extreme fluctuations in relative intensity of

Reproducibility of Deoxyribose Isotope Peak (m/e 118) in Thymidine

Scans	rel.int. (m/e 117 = 100)
120-130	0-50
Σ50-55	3.93 ± 0.59
Σ56-61	7.54 ± 1.05
Σ62-67	6.02 ± 1.04
Σ68-73	9.53 ± 1.56
Σ50-73	6.04 ± 0.47
Σ50-200	5.86 ± 0.33

m/e 118. Summation of 6, 24 and 150 scans yields values of m/e 118 which are improved in reproducibility and which progressively approach the expected value of 5.66. Similar treatment of the ribose isotope peak at m/e 134 in uridine gave similar results.

The theoretically expected gain in sensitivity in f.d.m.s. by using S.I.R. relative to conventional magnetic scanning has been demonstrated. In addition, measurement confidence has been increased by verifying reproducibility of the results from the analyses of a large number of scans.

---

[1] I. Jardine, M.-N.N. Dam, C. Fenselau, R. Brundrett, M. Colvin, G. Wood, P.-Y. Lau and R. Charlton, Proceedings of Second International Conference on Stable Isotopes, Oak Brook, Illinois, Oct 20-23, 1975. In Press.

[2] Donald E. Hagge, Peter G. Blaney, and Bernard M. Grinberg, The Twenty Fourth Annual Conference on Mass Spectrometry, May 1976.

Field Desorption and Chemical Ionization Analysis Using Double Beam Mass Spectrometers

H.R. Morris, Department of Biochemistry, Imperial College, London, England.
K.R. Compson, R.A. McDowell, D. Hazelby,
AEI Scientific Apparatus Ltd., Manchester, England.

Double beam mass spectrometry is now a well established technique (I), although its full capabilities in both mass marking and accurate mass measurement are only now becoming apparent. In particular we have found that this method of mass marking is particularly valuable with high molecular weight compounds such as those encountered in field desorption work. Double beam mass measurement has considerable advantages for GC work and when working with other methods of ionization than electron bombardment in which the spectrum of the reference compound is changed and may not provide a suitable calibration.

An example of double beam mass measurement is shown in figure 1 which is an atomic composition report obtained from a double beam scan of the chemical ionization spectrum of the drug amitriptyline.

Double beam mass spectrometry is ideal for field desorption work because it is possible to employ chemical mass marking of the FD spectrum, or use the second source for electron beam work. Consequently it is still possible to carry out gas chromatography on a field desorption instrument without changing sources.

The following examples illustrate the use of double beam mass spectrometry for field desorption research on compounds not previously reported in the literature. They were all obtained on an AEI MS3076 mass spectrometer.

Figure 2 is a spectrum of the dimethyl ester of protoporphyrin. This has a molecular weight of 590 and is mass marked with PFK. The small difference in mass due to the mass sufficiency of the protoporphyrin and mass deficiency of the PFK is easily seen.

Figure 3 is a portion of the spectrum of heptamethylcobyrinate. This has a molecular weight of 1088 and is mass marked with perfluoroheptyl triazine. This illustrates the simplicity of calibration above mass 1000 and other work has shown that the mass range is limited only by the availability of suitable reference compounds, e.g. perfluorononyl triazine.

Figures 4 and 5 are spectra of the anti cancer drug methotrexate which illustrate the effect of different wire currents. The spectrum in figure 4 was taken with a wire current of 16 milliamps and shows a strong M+1 ion at mass 455, however, the next spectrum used a wire current of 18 mA and shows a smaller M+1 peak at mass 455 but also peaks at $^{m}/_{e}$ 454, 436 and 437 (M^+, $M^+ - H_2O$, $M^+ + H - H_2O$). When working with repetitive scanning as the wire current is increased, it is relatively easy to obtain comparison spectra such as these.

Figure 6 shows the first field desorption spectrum of Leucine-Enkephalin a naturally occuring analgesic substance found in the brain, whose structure was determined by mass spectrometry (II).

The spectrum has been mass marked with PFK. On this instrument the reference beam had a logarithmic display, which is very useful

for mass marking purposes since effectively the small peaks have a higher amplification than the larger ones.

The final illustration, figure 7, shows the spectrum of bacteriochlorophyll having a molecular weight of 910. This was mass marked with a mixture of PFK and perfluorohephyltriazine. Further data on the usefulness of these studies in biochemistry will be reported elsewhere.

These examples of the use of the MS3076 for Chemical Ionization and Field desorption show the value of double beam mass spectrometry when working with soft methods of ionization. The technique has the advantages of providing accurate mass marking at all masses and scan speeds, of permitting accurate mass measurements to be made without adding reference compound to the sample beam and increasing the flexibility of a field desorption instrument by allowing the instrument to be used for GC work without having to make changes to the source.

References

I M.L. Aspinal, K.R. Compson, A.A. Dowman, R.M. Elliott, D. Hazelby. Proc. ASMS 1975 no. C-2.

II J.F. Hughes, T.W. Smith, H.W. Kosterlitz, L.A. Fothergill, B.A. Morgan and H.R. Morris. 1975, Nature 258, p.577.

FIG.1

DP1:30D0012.MS
10/14/75 14: 6

NO. PEAKS: 46
BASE/NREF INT: 6561./ 6561.
TIC: 13087.
MASS RANGE: 70.0676 - 320.2293
RETN TIME/MISC: 22: 0/ 60/ 0

C	C13	H	N	DEV	MEAS MASS	#PTS	%INT
25	1		1				
20	0	24	1	-1.2	278.1896	102	100.00
20	0	23	1	-5.7	277.1774	40	2.88
19	1	22	1	-1.2			
20	0	22	1	0.1	276.1753	47	15.55
17	0	17	0	-1.0	221.1320	34	1.87
16	1	16	0	3.4			

LIMIT OF DATA

MS30 CI(CH_4) Double beam mass measurements on amitriptyline ($C_{20}H_{23}N$)

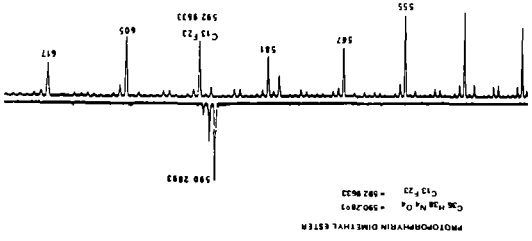

FIG.2

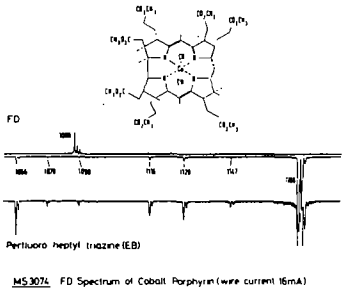

FIG. 3

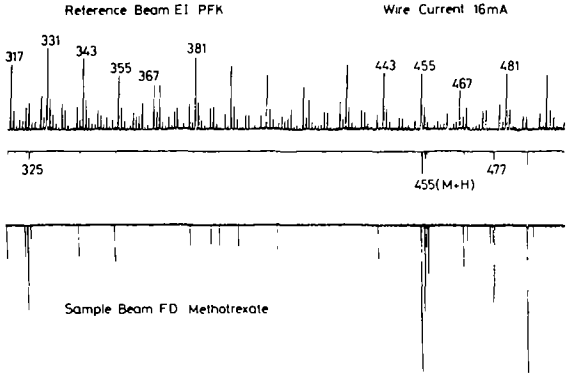

FIG. 4

FIG. 5

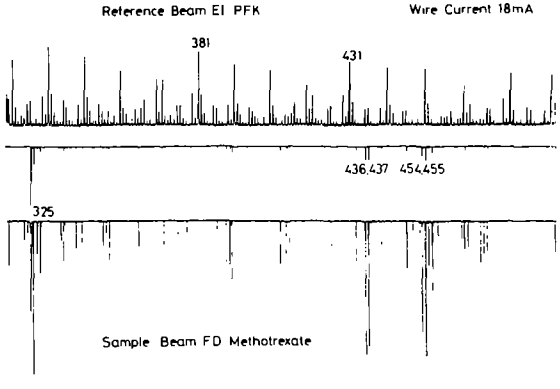

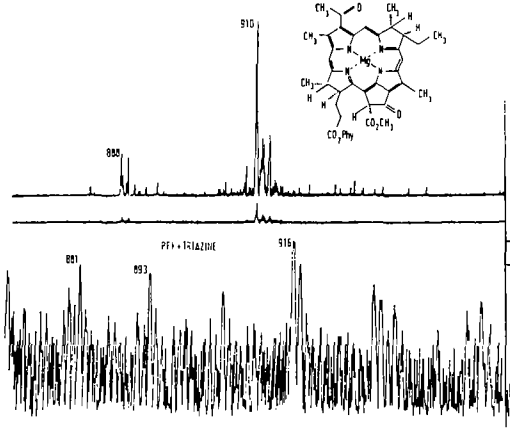

FIG. 7

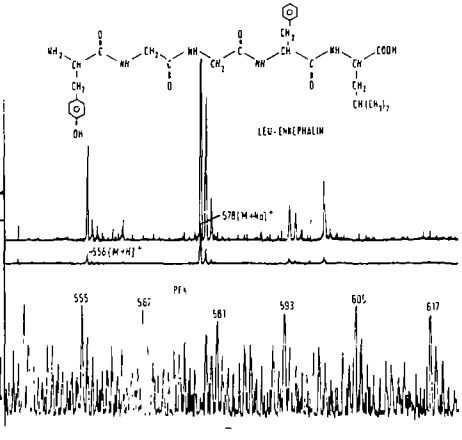

FIG. 6

APPLICATION OF QUANTITATIVE FIELD DESORPTION MASS SPECTROMETRY (FDMS) TO DETERMINATION OF HUMAN FETAL LUNG MATURITY

R.C. Charlton, K.-L. Kan, P.-Y. Lau, L. Linnell, G.N.S. Rao and G.W. Wood
Department of Chemistry, University of Windsor, Windsor, Ontario, Canada N9B 3P4

In two previous collaborative projects we have shown the feasibility of quantitative f.d.m.s.(1,2). Here we report our progress in applying f.d.m.s. to quantitation of dipalmitoyl-phosphatidyl choline (I) in amniotic fluid.

The major fragmentation pathways for I have been worked out from comparison of spectra obtained from I-d_0 with those from analogues incorporating choline trimethyl-d_9 and choline dimethylene-d_4(3). When anode temperatures are maintained near the minimum value for smooth desorption, the base peak in these spectra corresponds to M + H. Under these conditions, intensities of ions in the molecular region are reasonably reproducible. Isotope peaks at M + 2 and M + 3 obtained on a single scan (scan rate ca 44 amu/s) agree with calculated values (M + 2 = 44.8 ± 2.5%, calc 44%; M + 3 = 9.0 ± 2.2%, calc 11%).

Spectra of I-d_0 and I-d_4 show no detectable ions at m/e values which would interfere with measurement of M + 1 for each species in mixtures. One loading of a 1:1 mixture of synthetic I-d_0:I-d_4 was sufficient for 15 scans of the molecular ion region (10 s/scan, ca 25 amu/s) with anode current gradually increasing from 22 to 24 mA. The 10 most intense scans yielded 100 ± 5.3% / 96.7 ± 6.7% (I-d_0 ± SD / I-d_4 ± SD from 734/738 ratios). Reproducibility was poorer for the less intense scans or for M + Na ions (m/e 756, 760 with intensity 10% of base). Averaging five scans of the latter peaks gave 93 ± 13/100 for I-d_0/I-d_4.

Isolation of the phosphatidyl choline (PC) fraction of amniotic fluid in a sodium-free state for f.d.m.s. provides a significant technical challenge. Our current procedure involves extraction ($CHCl_3$:MeOH), centrifugation, and TLC purification on Bio-gel HTP. With this procedure it is

possible to obtain an essentially sodium-free spectrum from 50 ml of amniotic fluid, but reduction to a more realistic sample size(10 ml) typically produces a spectrum in which M + Na peaks are at least as intense as M + H. The larger sample has allowed the first estimate of the major intact PC species in term amniotic fluid. As expected, dipalmitoyl PC (16:0, 16:0) is the major component(80%) with ions corresponding to 16:0, 14:0 and 16:0, 18:1 accounting for about 10% each.

Typical data from a 10 ml sample of amniotic fluid to which 1 mg of I-d_4 was added as internal standard are shown in the Table. The precision is low, but our experience suggests

Table

Dipalmitoylphosphatidyl Choline in Amniotic Fluid from I-d_0/I-d_4[a]

scans	anode	ions	result (mg)
9-15	20 mA	734/738	0.41 ± 0.08
1-16	18-22	734/738	0.46
1-16	18-22	756/760	0.40

[a]10 ml of amniotic fluid + 1 mg I-d_4

that this is primarily a function of ion statistics and improvement can therefore be expected from further averaging of scans, or better, from selected ion monitoring. Although it may prove to be possible ultimately to use the ratio of M + Na ions (either alone or in combination with M + H) for this determination, we are continuing our efforts to remove sodium ions. Incorporation of a crown ether into the sample prior to TLC has been shown to increase the M + H/ M + Na ratio seven-fold and experiments of this kind are continuing.

1. N. Sukenik, J.A.P. Bonapace, N.S. Mandel, R.G. Bergman, P.-Y. Lau, G. Wood, Enhancement of a Chemical Reaction Rate by Proper Orientation of Reacting Molecules in the Solid State, J. Amer. Chem. Soc., 97, 5290-5291 (1975).
2. G. Wood, R. Charlton, R. Brundrett, M. Colvin, I. Jardine and C. Fenselau, Pharmacologic Studies of Chemotherapeutic Alkylating Agents Using Chemical Ionization and Field Desorption Mass Spectrometry, Proceedings of Second International Conference on Stable Isotopes, Oak Brook, Illinois, Oct. 20-23, 1975, In Press.

3. G. W. Wood, P.-Y. Lau, and G.N.S. Rao, Field Desorption Mass Spectrometry of Phospholipids II. Fragmentation of Dipalmitoyl Phosphatidyl Choline from Comparison of d_0, d_4, and d_9 Species, Biomed. Mass Spectrom., 3, 000 (1976).

Field Desorption Sensitivity Measurements. J. CARTER COOK, JR., KEITH L. OLSON, and KENNETH L. RINEHART, JR., School of Chemical Sciences, Univ. of Illinois, Urbana, Illinois 61801

Our quantitative method of sample loading makes field desorption (f.d.) sensitivity measurements possible.[1] We have used this technique to make f.d. sensitivity comparisons for a variety of compounds including steroids, amino acids, nucleosides and antibiotics of several classes. We have also employed quantitative sensitivity measurements in the comparison of metal dendrite emitter wires[2] with carbon emitter wires activated at high temperature.[3] The relationship between f.d. sensitivity and the quantity of sample deposited on the emitter is also examined.

[1] K. L. Olson, J. C. Cook, Jr., and K. L. Rinehart, Jr., Biomed. Mass Spectrom., 1, 358 (1974).

[2] R. M. Wightman, et al., Int. J. Mass Spectrom. Ion Phys., 17, 208 (1975).

[3] H.-R. Schulten and H. D. Beckey, Org. Mass Spectrom., 6, 885 (1972).

GC-CI-MS Multiple Ion Monitoring Quantitative Analysis of 1- -acetyl methadol (LAAM) in Biological Samples.

Thomas A. Jennison & Bryan S. Finkle, Center For Human Toxicology, Univ. of Utah, SLC, Utah 84112.

The objective of this paper is to present a new analytical method suitable for the routine detection and quantitation of 1- -acetyl methadol (LAAM) and its two principal metabolites nor-LAAM and dinor-LAAM, in small volume blood and urine samples. The method is currently being applied to biological samples taken from humans and animals in order to accurately determine the pharmacokinetics and human metabolism of LAAM. In addition, it is envisaged that the method used at the Center For Human Toxicology will provide analytical support to other researchers who haveongoing research programs involving LAAM. The analytical method has been fully developed and all aspects will be discussed. These include sample preparation and extraction, derivatization and gas chromatography chemical ionization-mass spectrometry-selected ion monitoring, using methane as carrier and amonia as reagent gas. The deuterated stable isotopes of LAAM and its metabolites are used as internal standards. The development, rationale , accuracy and precision of the method will be presented along with preliminary findings from biological test samples.

Phosphazenes: High Molecular Weight Reference Compounds. KEITH L. OLSON, J. CARTER COOK, JR., and KENNETH L. RINEHART, JR., School of Chemical Sciences, Univ. of Illinois, Urbana, Illinois 61801.

Field desorption mass spectrometry places special requirements on mass markers. Commercially available reference compounds are inadequate in the field ionization (f.i.) mode due to poor sensitivity or insufficient fragmentation and are limited to about m.w. 1500. In 1966 Fales proposed the use of polyfluoroalkoxyphosphazenes as high molecular weight reference compounds.[1] We have now synthesized a series of cyclotriphosphazene homolgoues ranging in m.w. from 729 to 2121 according to Rätz, et.al.[2] Mixtures of phosphazenes should provide an adequate number of intense reference peaks in either the electron impact or f.i. modes. F.i. spectra of s-triazines are included for comparison.

[1]H. M. Fales, Anal. Chem., 38, 1058 (1966).

[2]R. Rätz, et al., J. Amer. Chem. Soc., 84, 551 (1962).

HIGH RESOLUTION FIELD DESORPTION MASS SPECTROMETRY OF OLIGONUCLEOTIDES

Hans-Rolf Schulten
Institute of Physical Chemistry
University of Bonn
53 Bonn, Wegelerstr. 12, West-Germany

Hans Martin Schiebel
Institute of Organic Chemistry
Technical University of Braunschweig
33 Braunschweig, Schleinitzstr. 2, West-Germany

As recently reported[1] the complete high resolution spectra of unprotected dinucleoside phosphates could be obtained by field desorption mass spectrometry. In all cases these spectra contained the protonated molecular ions and - depending on the conditions of desorption applied - structural information about the building blocks of the dinucleoside phosphates, i.e. their nucleobases, nucleosides, and mononucleotides. In addition the corresponding cyclophosphates were formed by a thermally/field induced process (Figure 1).

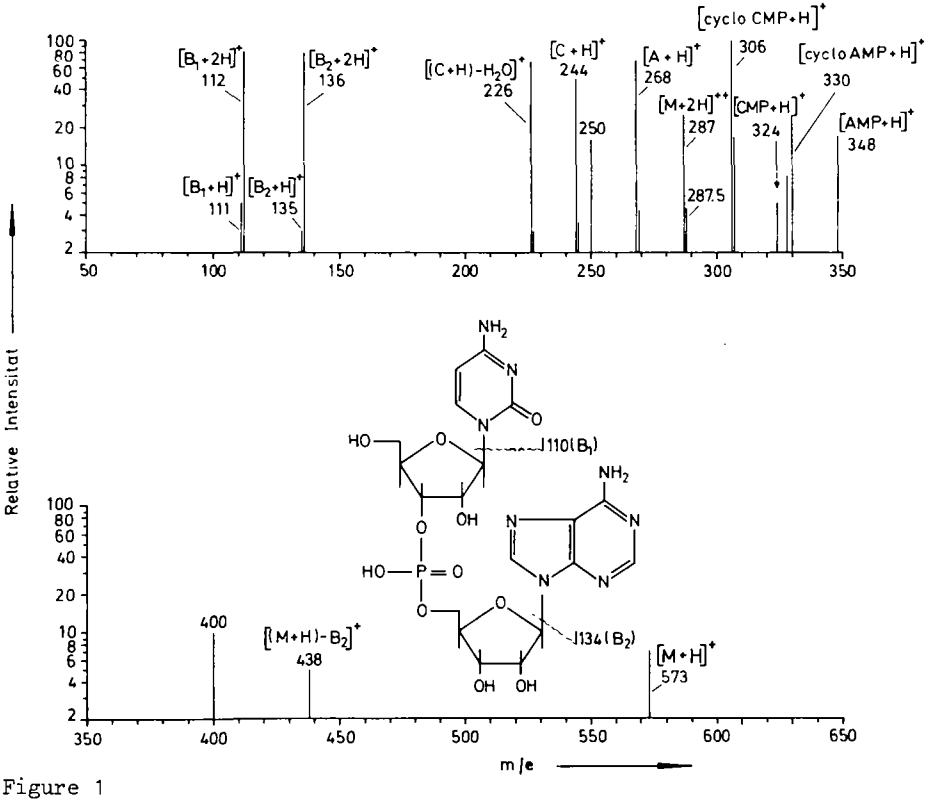

Figure 1

	ApC	CpA	ApG	GpA	ApU	UpA	CpU	UpC	GpU	UpG
base 1	++++	++++	+++	++++	+++++	++++	+++++	++	+++++	++++
base 2	+++++	++++	+++++	+++++	+	+++++	++	+++++	+++	++
nucleoside 1	+	+++		+	+++	+	++	+		
nucleoside 2	+++	++++		+	+++++	+++++	+++++	+++	++++	+
cyclophosphate 1	+	+++++	++	+	+++++	++++	+++++	+++	++++	++
cyclophosphate 2		++			+++	++	++	+	+	
nucleotide 1		+			+	+	+	+		++
nucleotide 2		++			++++	+	+	+	+++	

TABLE 1

The major types of ions observed in the FD mass spectra of ribodinucleoside phosphates (mass range m/e 100 to m/e 400). The relative intensities of the signals are given in five degrees of blackening of the photoplate: Very high rel. int. = +++++, high rel. int. = ++++, medium rel. int. = +++, low rel. int. = ++, and weak rel. int. = + [2].

As shown in Table 1 the formation of cyclophosphates is independent of the polarity of the investigated dinucleoside phosphates and in all cases its formation preferentially takes place by the nucleotide in position 1 (5'-end). In the first instance this behaviour could be explained purely statistically, for cleavage of the 5'-ester bond the nucleotide in position 1 can react to the 5'-OH under formation of a six membered ring as well as to the 2'-OH under formation of a five membered ring. The nucleotide in position 2 (3'-end), after cleavage of the 3'-ester bond, has only the possibility of a ring closure to the 3'-OH group (Scheme 1).

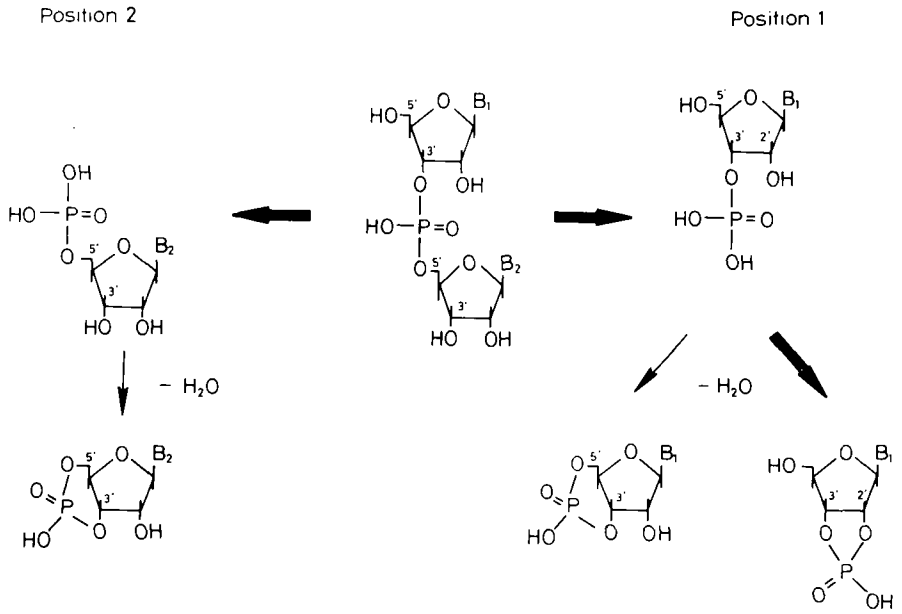

Scheme 1: Sequence-specific formation of nucleoside cyclophosphates in field desorption mass spectrometry[2].

However, more probable and in agreement with chemical results[3] is that after cleavage of the 5'-ester bond the cyclisation preferentially takes place to the vicinal 2'-OH group. The cyclisation to the 5'-OH group is much less favoured. Only the nucleotide in position 1 can react to the favoured 2',3'-cyclophosphate. Thus the first step to accomplish sequence information of unprotected oligonucleotides by mass spectrometry has been made and future applications of FD-MS to large subunits of nucleic acids are one of the most promising areas of the technique.

REFERENCES

1 Schulten, H.-R., Schiebel, H.M., Z. Anal. Chem. 280, 139 (1976)

2 Schulten, H.-R., Schiebel. H.M., Nucl. Acids Res., submitted for publication (1976)

3 Michelson, A.M., in "The Chemistry of Nucleosides and Nucleotides", pp 119-122, Academic Press, London and New York (1963)

MASS SPECTRAL ANALYSIS OF THE CARBOHYDRATE PORTION OF CEA*

William C. Schnute, Jr., John E. Coligan, David G. Pritchard, and Charles W. Todd, City of Hope National Medical Center, Department of Immunology, Duarte, California, 91010

ABSTRACT

The carbohydrate structural units of carcinoembryonic antigen (CEA) samples were quantitated using GC-MS after methylation and subsequent conversion to their alditol acetates. Using specific ion chromatograms the partially methylated alditol acetates were identified from their characteristic masses. From these data the relative proportion of the structural carbohydrate units in CEA were tabulated. The results indicate that a large portion of the fucose residues in the glycoprotein were linked to N-acetylglucosamine, and that most of the branching mannose residues were probably linked to three N-acetylglucosamine residues.

EXPERIMENTAL

The entire molecule of CEA was subjected to exhaustive methylation using the technique of Hakomori (1). All of the free hydroxyl groups present in the oligosaccharide structures on the CEA molecule were methylated. Following this treatment the molecule was hydrolyzed to liberate the individual saccharide units as their partially methylated derivatives. After reduction of the aldehyde group with sodium borohydride, which generates a fresh hydroxyl group, the product is exhaustively acetylated. In the resulting alditol acetates the carbons formerly carrying free hydroxyl groups are methylated, whereas those on which hydroxyls were generated in subsequent manipulations are acetylated.

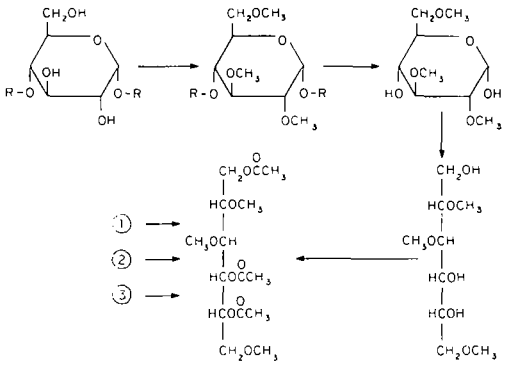

The established fragmentation rules (2) are as follows: A methylated alditol acetate prefers to fragment between two methoxylated carbons. In this case the positive charge can go with either of the daughter fragments. A secondary mode of splitting is between a methoxylated and an acetoxylated carbon. In this case the positive charge resides with the methoxylated fragment. The least preferred cleavage is between two acetoxylated carbons.

A Varian Model 2740 gas chromatograph connected to a Dupont Model 21-492B double-focusing mass spectrometer was used for these analyses. Isothermal runs at temperatures between 150-160° were used for the neutral sugars and at 180° for the amino sugars. Scans were taken every 9 sec, and the E.I. spectra were processed using a Dupont 21-094B disc-based data system.

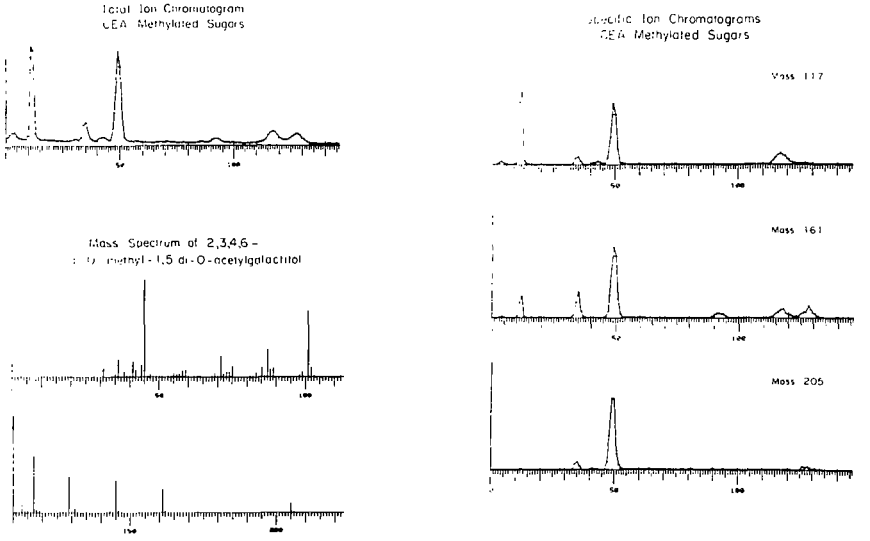

RESULTS

The results of methylation analysis of CEA samples are shown in Table 1. Methylation results indicated that all the

Carbohydrate residues	Glycosidic linkage	moles/10⁵g of CEA: CEA_1[a]	CEA_2	CEA_3	CEA_4	CEA-14[b]
N-Acetylneuraminic acid	Terminal	13	6	19	7	10
Fucose	Terminal	57	57	58	53	61
Mannose	Terminal	5	8	5	7	2
	2	5	4	5	4	8
	6	Trace	Trace	Trace	Trace	Trace
	2,4	11	10	12	7	10
	2,6	9	10	11	10	13
	3,6	13	14	6	12	10
Total		43	44	39	40	43
Galactose	Terminal	24	40	32	35	20
	3	34	12	25	10	6
	2	3	10	10	5	20
	6	6	1	6	2	7
	3,4 and 2,3	3	1	1	2	
Total		70	64	74	54	53
N-Acetylglucosamine	Terminal	Trace	9	18	11	3
	4	51	52	49	61	46
	3,4	35	42	32	46	23
Total		86	103	99	118	72

[a] The subscripts 1 to 4 indicate CEA purified from different tumors. All tumors were liver metastases that had originated in the colon.
[b] Data from Hammarström *et al.*

Table 1. Structural units of the polysaccharide portion of CEA.

fucose residues in CEA were terminal. In each of the five CEA preparations compared, fucose and N-acetylneuraminic acid account for more than one-half of the sugar residues at the nonreducing termini. Periodate oxidation studies (3) showed that N-acetylneuraminic acid was linked to galactose since prior treatment of CEA with neuraminidase led to increased

destruction of galactose by periodate. To our knowledge, the terminal fucose residues of mammalian glycoproteins have never been found linked to mannose. Since there are not enough galactose linkages available to accommodate all the fucose, it would appear, therefore, that a large portion of the fucose residues in CEA must be linked to N-acetylglucosamine. Three-quarters of the mannose residues in all the CEA samples studied were linked to three other sugars. It is a general characteristic of mannose residues in mammalian glycoproteins to be linked only to other mannose residues or hexosamines (4). On the basis of this observation, four possible linkage configurations for the branching mannose residues in CEA are illustrated in Chart 1. Branching mannose units such as those in a and b, cannot be present to any great extent, since they would require a much higher ratio than that observed of nonbranching mannose to branching mannose. On the average, the ratio of N-acetylglucosamine to branching mannose is close to three. In one of our CEA preparations and in the preparation of Hammarström *et al.* (5) this ratio was less than three. This would imply that at least some of the branching mannose units were linked to other branching mannose units as in Chart 1, d.

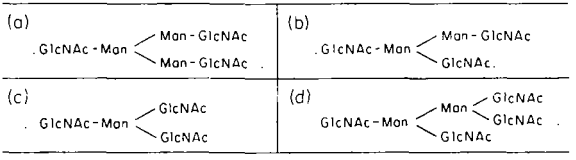

Chart 1. Possible Mannose Linkages

Further delineation of the carbohydrate structure of CEA will require methylation and periodate studies on purified glycopeptides. This work is now in progress.

This research was supported by Grants CA 12631, CA 16434, and Contract N01-CB-23877 from the National Cancer Institute and by the Stuart L. Bernath Cancer Research Fund.

REFERENCES

1. Hakomori, S., J. Biochem. Tokyo, 55:205-208, 1964.
2. Björndal, H., Hellerqvist, C.G., Lindberg, B., and Svensson, S., Angew. Chem. Intern. Ed. Engl., 9:610-619, 1970.
3. Coligan, J.E., and Todd, C.W., Biochemistry, 14:805-810, 1975.
4. Heath, E.C., Ann. Rev. Biochem., 40:29-56, 1971.
5. Hammarström, S., Engvall, E., Johansson, B.G., Svensson, S., Sundblad, G., and Goldstein, I.J., Proc. Nat. Acad. Sci., USA, 72:1528-1532, 1975.

*A detailed description of this work is scheduled for publication in "Cancer Research" in June, 1976.

STRUCTURE ELUCIDATION OF ALKYLATED NUCLEOSIDES

Catherine Fenselau
Department of Pharmacology and Experimental Therapeutics
The Johns Hopkins University School of Medicine
Baltimore, Maryland 21205

Adjunct to several collaborative programs studying alkylation of purine nucleosides by chemotherapeutic antitumor agents and by laboratory mutagens, we are attempting to correlate electron impact fragmentation patterns with the nature of substituent side chains and with the location of attachment of the side chain on the purine base. Examples of nucleosides with substituents more complex than ethyl groups are rare in the literature and we have begun to accumulate mass spectra of a number of authentic compounds of this type.

Spectra and fragmentation patterns were summarized in the presentation of the trimethylsilyl derivatives of two isomeric ethylthioethylene derivatives of deoxyadenosine in which the positions of substitution had been defined by ultraviolet spectroscopy and nuclear magnetic resonance. Spectra of two β-hydroxyethylene derivatives of guanosine, three ethylthioethylene derivatives of deoxyguanosine and two alkylated cytidines were also examined. On the basis of these spectra, correlations were suggested among fragmentation patterns that will permit substituents on exocyclic heteroatoms to be distinguished from substituents on ring heteroatoms. Electron impact mass spectra of more authentic compounds must be obtained and studied before it will be possible to distinguish mass spectrometrically which position in the ring is substituted.

Human Vaginal Secretions: Identity and Cyclical Changes in Small Organic Constituents by GC-MS. George Preti, George R. Huggins and Richard L. Doty, Monell Chemical Senses Center and Dept. of Obst. and Gyn., Univ. of Pa., Phila., PA 19104.

Anecdotal information in the literature, along with scientific reports, has stimulated speculation on the role of odors in human reproductive biology. Gas chromatography-mass spectrometry were used to serially study changes in the nature and abundance of small organic molecules in human vaginal secretions during the menstrual cycle. In addition to identifying compounds contributing to the vaginal odor profile at various times in the cycle, changes in these moleucles could reflect changes in circulating harmone levels and be diagnostic of the ovulatory period. The secretions were found to contain a complex mixture of short and long chain acids, alcohols, hydroxy-ketones and aromatic compounds. Small chain, volatile C_2-C_5 aliphatic acids which have been reported to induce mating behavior in male rhesus monkeys were consistently found in only 4 subjects; in addition, acetic acid, lactic acid and urea were found in all subjects and cyclical changes demonstrated.

MIXTURE ANALYSIS BY MASS SELECTION AND COLLISION INDUCED DISSOCIATION

T. L. Kruger, On leave from Department of Chemistry, Ball State University, Muncie, Indiana 47306 and J. F. Litton and R. G. Cooks, Department of Chemistry, Purdue University, West Lafayette, Indiana 47907

Mass selection followed by ion kinetic energy analysis (MIKES) in a reversed sector mass spectrometer[1] has been used to analyze multicomponent mixtures. A qualitative study of the alkaloids contained in the phenolic extract from the cactus, Dolichothele uberiformis, showed the presence of significant amounts of compounds producing molecular ions at m/e=193 and 235 in addition to the B-phenylethylamines, hordenine (m/e=165), methyl tyramine (m/e=151), and synephrine (m/e=167) and the tetrahydroquinoline (I) that had previously been identified. Structures II and III were deduced from the CID-MIKES results (Figure 1). The B-phenyl-

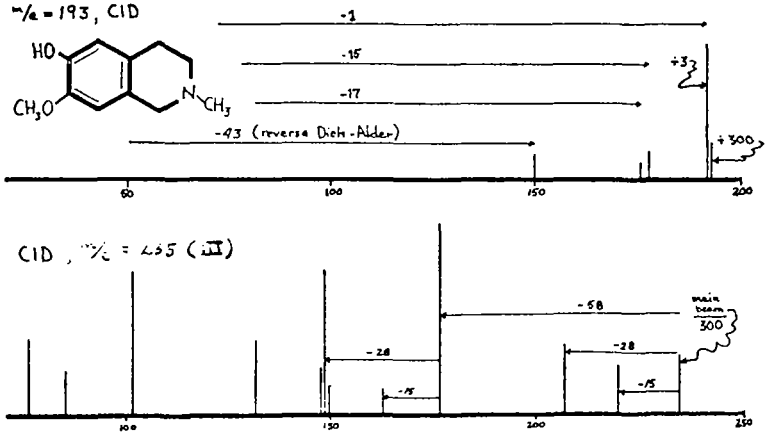

Fig. 1 MIKE/CID spectra of alkaloids II and III from the crude phenolic extract of Dolichothele uberformis.

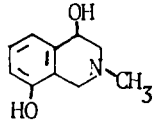

I

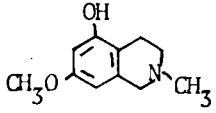

II

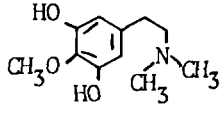

III

ethylamines are clearly characterized by cleavage between C_1 and C_2 in the side chain while tetrahydroisoquinolines exhibit H· loss and a reverse Diels-Alder fragmentation as the prominent processes. Thin-layer chromatography followed by NMR confirmed independently the structure indicated as II

In an application of the MIKES method to a mixture of isomeric $C_5H_{10}O$ ketones it was found that the amounts of the isomeric components of a mixture could be determined quantitatively (ca. 5%) by using either CID or unimolecular fragmentations of the m/e=86 ions. The plot of relative peak height versus mole fraction with known amounts in each mixture forms Figure 2. With CID conditions ($5x10^{-5}$ labora-

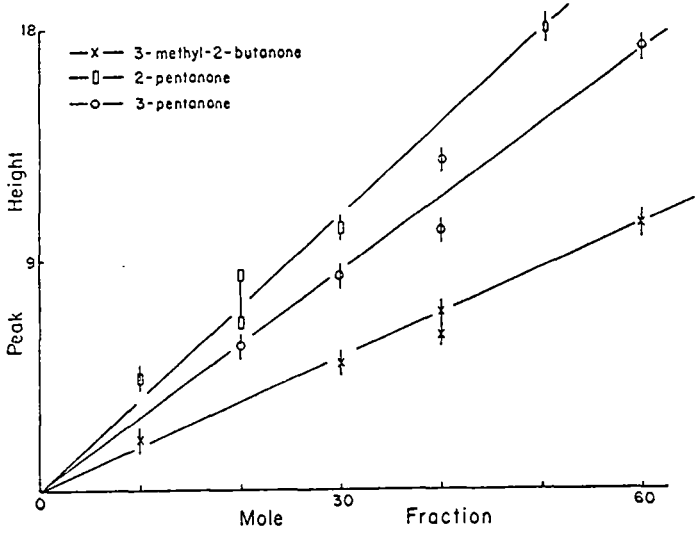

Fig. 2 MIKE/CID adjusted peak height plotted versus mole fraction for mixtures of $C_5H_{10}O$ ketones.

tory air in the second field-free region) the peak at M-29 was used for determining 2-pentanone, at M-28 for 2-pentanone, and at M-15 (less a small contribution from 2-pentanone) for 2-methyl-3-butanone.

Extension of these methods to mixtures arising in the permethylation of 2-butanone (excess methyliodide in glyme with sodium hydride) show clearly the complete spectrum of products. The variation in composition as reaction time is increased is consistent with the known chemistry of enolate anions (Table I).

TABLE I

Mole Fractions of Ketones in Crude Reaction Mixture at Various Times

Structure	m/e	ALIQUOT 1	2	3	4
	72	.15	-	-	-
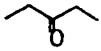	86	.20	.01	-	-
	86	.16	.03	-	-
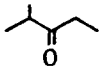	100	.35	.40	.04	.04
	100	.02	.05	-	-
	114	.10	.47	.93	.92
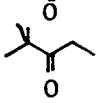	114	.02	.03	.03	.02
	128	-	-	.01	.01

COMPARISON OF TECHNIQUES OF COLLECTING BREATH CO_2 FOR ISOTOPIC ANALYSIS

D. A. Schoeller and P. D. Klein
Argonne National Laboratory
Division of Biological and Medical Research
Argonne, Illinois 60439

Recently we have developed $^{13}CO_2$ breath tests for the evaluation of intestinal absorption and hepatic microsomal function (1). The CO_2 breath test measures the oxidative utilization of ^{13}C-labeled substrates by quantitating the increase in $^{13}CO_2$ excretion in the breath following substrate administration. The CO_2 collection is a crucial step in the test, first, because the isotopic enrichment of $^{13}CO_2$ in the breath is small, typically less than 20‰ or 0.02 atom percent excess; and second, because the samples must be transported from the collection site to the central analytical facility for isotopic analysis.

The ideal CO_2 collection would have the following characteristics: the carbon isotopes should not be fractionated during collection; the collection apparatus should be easily carried to the patient; the samples in their final form after collection should be easily transported, stable during storage, and amenable to automated analysis; and finally, the cost of performing the collection should be small.

METHODS

Three techniques of collecting breath CO_2 were tested and compared. The first was cryogenic CO_2 trapping. The subject exhaled through an 8-mm ID spiral trap that was immersed in liquid nitrogen (-196°C), and the expired CO_2 was frozen out on the trap walls. After 30 seconds of collection, the trap was evacuated, isolated, and warmed to -78°C (dry ice-methanol), vaporizing the CO_2, but not H_2O. The CO_2 was then cryogenically transferred to a gas sample bulb for mass spectrometric analysis.

The second technique was chemical trapping. Here, the subject exhaled for 5 minutes through a 250-ml flask containing 10 ml of 2 N NaOH. The CO_2 dissolved in the NaOH solution and was trapped as $CO_3^{=}$. This solution was transferred to a plastic or teflon lined screw capped glass vial for transportation and storage. Later, the CO_2 was released from solution by acidifcation in vacuum, and the CO_2 was trapped in a liquid nitrogen cooled trap. The CO_2 was then transferred to the gas sample bulb as described above.

The final technique was collection of whole breath. Since 5 ml of breath contains approximately 400 μg of CO_2--an amount sufficient for analysis on most isotope ratio mass spectrometers--only a small sample of whole breath need be collected. For this collection, the subject exhaled into a 3-liter collapsible latex bag. A 50 ml, "red cap" Vacutainer^R (an evacuated, septum cap test tube commonly used for blood collection)(Becton-Dickinson, Rutherford, N. J.), was filled from the bag by piercing the septum with a 20-gauge needle. The "red cap" indicates that the tube walls are coated with silicone and the septum is lubricated with glycerin. The filled Vacutainers^R were transported to the mass spectrometer laboratory where a 10-ml aliquot was withdrawn by again inserting a 20-gauge needle through the septum and drawing the

aliquot into a vacuum purification train through a 7.5 μm x 50 mm viscus leak. The CO_2 was cryogenically trapped and purified as described above.

RESULTS AND DISCUSSION

Using the nonfractionating cryogenic trapping as a reference method, the two remaining techniques were tested for isotope fractionation. The collection in 2 N NaOH was found to fractionate the CO_2 by -13‰; however, the fractionation was nearly constant for each sample (standard deviation - 0.2‰) and was therefore easily corrected for during the calculation of enrichment. The fractionation was similar to that reported by Craig (2) (for collection yields of 10-20%) and was attributed to a kinetic isotope effect. The collection of whole breath did not isotopically fractionate the CO_2 (the precision of the measurement was 0.1‰).

The resistance to sample degradation was determined by collecting CO_2 by each of the methods and isotopically analyzing them during a period of 10 weeks of storage. After several weeks of storage, the cryogenically collected samples stored in ground glass stopcock sealed bulbs were contaminated with small amounts of air due to leakage across the stopcock. The samples collected and stored as carbonate or whole breath did not show any change over the period of storage. The absolute values of the slopes of the isotope abundance versus days stored were less than 0.002‰/day and were not significantly different from zero. Thus, there was no contamination or exchange with atmospheric CO_2.

Of the three techniques, only cryogenic collection was inconvenient to use. The vacuum station was not easily carried to the patient and liquid nitrogen was not always available.

The collection and storage of whole breath in Vacutainers^R was found superior to the other two methods. CO_2 was not isotopically fractionated during collection and the samples were not degraded during storage. The collection apparatus, weighing less than 2 lbs., was readily portable, and the sample containers were small enough to be mailed. Since the CO_2 is in the gas phase and stored in a septum capped tube, the purification can be easily automated in the future. Finally, the materials used were inexpensive.

The authors wish to acknowledge A. Engelkemeir who performed the isotopic analysis.

Work supported by the U. S. Energy Research and Development Administration and by the National Institutes of Health (AM 18741).

---

1. D. A. Schoeller, P. D. Klein, J. F. Schneider et al., Proc. of the 24th Ann. Conf. on Mass Spectrometry and Allied Topics, PSA 13.
2. H. Craig, Geochim. Cosmochim. Acta 3, 53-92 (1953).

Design Considerations of a GC/MS System Incorporating Glass Capillary Columns. G. W. FAVES, Finnigan Corporation, Sunnyvale , J. R. Reeher, Finnigan Corp., Sunnyvale, Calif.

The use of glass capillary columns in GC/MS provides the organic chemist with perhaps the most powerful analytical tool available today. This paper describes the necessary considerations for designing a GC/MS optimized for use with glass capillary columns. Some of the major considerations are: Optimization of ion source conductance for typical flows encountered; a GC/MS interface with minimal dead volume and active surface; a gas chromatograph that has accurate temperature programming capabilities; an injector that limits sample contact to glass components only; a column oven design that minimizes thermal gradient; and design of special low dead volume fittings for connecting the column to the gas chromatograph.

The new and unique design of the capillary GC/MS results in an extremely sensitive system.

A New Integrated Real-time Glass Capillary GC/MS: Performance Specifications and Biomedical and Environmental Applications. T. TAYLOR and A. L. BURLINGAME, Logos Spectrotek, Inc., Kensington, California 94707, Y. KATOH and T. NODA, Hitachi, Ltd., Naka Works, Mito, Japan.

A new low-cost-high performance real-time glass capillary GC/MS instrument has been developed which integrates a Hitachi, Ltd. Model M52 GC/MS with a LSI Model 2000 real-time GC/MS computer system.

Salient operational features include high chromatographic resolution with minimized adsorption/decomposition of labile bio-organic substances, high sensitivity, optimized rapid-cycle-time mass spectrum acquisition and display, versatile software processors for setting instrument parameters, display of reconstructed TIC chromatograms, spectral library and search facilities, and electrostatic printer-plotter hard copy graphics. Multiple ion detection and chemical ionization accessories are available.

Analysis of mixtures of substances from body fluids and environmental sources (water, organisms and sediments) will be presented and discussed.

Thermogravimetric (TG) - Gas Chromatographic (GC) - Mass Spectrometric (MS) Instrumentation for Material Evaluation. David L. Geiger and Gerd A. Kleineberg, Aerospace Medical Research Laboratory, Toxic Hazards Division (AMRL-THE), Wright-Patterson AFB, Ohio 45433.

A third generation TG-GC-MS system is currently being used in our laboratory for the identification of thermal decomposition products from non-metallic polymeric materials. The instrument combination employed can be used for the discontinuous simultaneous technique of TG-GC-MS as well as for the coupled simultaneous technique of TG-MS. The instrumentation employed will be discussed in detail and samples of the data obtained will be presented.

An In-Situ Sampling System For Thermo-Head-Space-Analysis of Non-Volatile Materials Using a GC/MS/Data System. JACOB SHEN, Standard Oil of Ohio, Research Center, Cleveland, Ohio 44128

To look into the thermostability of polymers at their processing temperatures, it often necessitates the analysis of their off gases. While samples can be prepared exterior to a gas chromatograph and then transferred using a gas syringe, it is more desirable if the off gases can be transferred in-situ. This paper describes a sampling system which transfers the off gases and/or decomposition products in situ onto a GC column to be analyzed by a GC/MS Data System. The solid samples are introduced through a quartz probe (3½" x ¼") into a heated chamber which also serves as a GC injection port and can be isolated from the GC stream. The atmosphere in the chamber can be controlled. Mass chromatogram and MID are very useful in this application. The system can be used in the quality control of polymers, identification of polymer additives, thermodegradative study of polymers and monitoring the off gases of other non-volatile materials such as solid samples from natural resources.

An Efficient Interface for Combined Liquid Chromatography/Mass Spectrometry Analysis. W. H. McFADDEN, Finnigan Corp., Sunnyvale, Ca. H. L. Schwartz, Finnigan Corporation, Sunnyvale, California 94086.

This paper will describe an interface method for LC/MS which is an extension of the moving wire technique proposed by R.P.W. Scott and co-workers. Effluent from the LC column runs directly onto a stainless steel belt in a preliminary evaporation chamber. The belt passes through two vacuum lock chambers and into the mass spectrometer where the sample is flash vaporized into the ion source. When the belt is driven at a rate of 1-2 cc/sec, it can carry up to 1 cc/min of effluent and hence has potential for full utilization of sample. However, sample losses can occur by spray evaporation, azeotrope formation, preliminary vaporization in the vacuum locks, or inefficient vaporizor. Depending upon the characteristics of the sample and control on the physical parameters that affect these losses, sample yields of 25-50% can be attained.

The versatility of this interface will be illustrated with a few LC/MS examples from typical liquid chromatography analyses.

LC/MS/COM USING AN UNCHANGED COMMERCIALLY AVAILABLE QUADRUPOLE MASS SPECTROMETER

J. D. Henion
Department of Chemistry
Cornell University
Ithaca, NY 14853

The application of LC to a variety of important problems is severely limited by the refractive index and ultraviolet detectors now commonly used. The performance of a mass spectrometer as a sensitive and unique detector for a gas chromatograph is well known today in the field of gc/ms. A flurry of interest has developed recently in efforts to interface mass spectrometers to a liquid chromatograph.[1-5] To date no simple, effective LC/MS/Com interfacing has been reported on an unchanged commercial mass spectrometer.

The interface used in this report utilized an approach that has been described.[5] The mass spectrometer was an unchanged Finnigan Model 3300 chemical ionization instrument interfaced to a System 150 data system from System Industries. This combination of equipment allows rapid scanning and continuous monitoring of LC effluent as is customary in routine gc/ms work. MID allows one to detect substantially lower levels of material with no additional difficulty.

The system consists of a glass capillary (0.250 in. O.D. x 10.0 in.; 0.003 in. I.D.) with a terminal restriction (∿5-15 microns) so that approximately 12 microliters/minute of solution (∿1% of the total LC effluent) continuously enters the CI ion chamber. This interface fits directly into the standard Finnigan solid probe inlet. The tip of the glass capillary (probe) is carefully positioned 1.5 cm. away from the electron beam, and the solid probe inlet is heated to approximately 130°C with heating tape. Both of these features significantly effect the sensitivity of the technique. All ion source and electronic parameters are exactly as those used for CI/CH_4 except for the indicated (uncorrected) source pressure. Optimum pressure for CH_3OH/H_2O was 850μ and 550μ for CH_3CN/H_2O.

Initial studies were performed on a series of 2-alkylanthraquinones and polynucleararomatic hydrocarbons. After establishing optimum sensitivity conditions on these materials, LC/MS/Com separation and analysis of several mixtures were conducted. Using aqueous solutions of acetonitrile CI mass spectra were obtained on several vitamins, vitamin acetates, drugs, drug metabolites, and high molecular weight keto esters. The mass spectra all displayed intense quasi molecular weight information and substantial fragmentation behavior. The latter was particularly prevalent when CH_3CN/H_2O mixtures were used as the mobile phase and reagent gas.

This LC/MS/Com system has successfully demonstrated that the technique should be readily ammenable to any CI quadrupole mass spectrometer with sufficient high speed pumping. The marriage of the LC to the mass spectrometer requires only the respective instruments and readily available materials. The choice of mobile phase for LC separation should be limited to exclude only highly chlorinated and caustic materials. It would seem we are only on the threshold of the opportunities for LC/MS!

BIBLIOGRAPHY

1. R.P.W. Scott, C. G. Scott, M. Munroe and J. Hess, Jr. Journ. Chrom., 99, 395 (1974).
2. P. R. Jones and S. K. Yang. Anal. Chem., 47, 1000 (1975).
3. R. E. Lovins, S. R. Ellis, G. D. Tolbert, and C. R. McKenny. Anal. Chem., 45, 1553 (1973).
4. F. W. McLafferty, R. Knutti, R. Venkataraghavan, P. J. Arpino, and B. G. Dawkins. Anal. Chem., 47, 1503 (1975).
5. P. J. Arpino, B. G. Dawkins, and F. W. McLafferty. Journ. Chrom. Sci., 12, 574 (1974).

A Very Rapid Heating CIMS Probe for the Evaporation of Fragile Molecules*, ROBERT C. PIERCE† and LEWIS FRIEDMAN, Dept. of Chem., Brookhaven Nat'l Lab., Upton, NY 11973

A very rapid heating device (∿1000°/sec) has been developed for the evaporation of fragile molecules. It is compatible with existing commercial and research type CI mass spectrometers. Heating is produced by the thermal generation and acceleration of electrons into a stainless steel foil onto which the sample material has been deposited on the opposite side. Characteristically a 5-10 nmol sample evaporates completely from this heated surface in ∿0.3 sec. Past investigations by this laboratory have indicated that heating of fragile molecules at 10-12°/sec reduces the extent of decomposition accompanying their evaporation[1]. The observations of protonated parent species for the dipeptide Arg-Pro and for sucrose at the ∿1000°/sec rate but not at the 12°/sec rate serve as examples of the probe's effectiveness in decomposition reduction.

*Work carried out under auspices of U.S. ERDA.
†Present address: Colgate-Palmolive R&D, Piscataway, New Jersey 08854.
[1] R. J. Beuhler *et al.*, J. Amer. Chem. Soc., 96, 3990 (1974).

Design and Performance of an Advanced Dual-Purpose EI/CI Ion Source for a Quadrupole GC/MS. J. R. Reeher, Finnigan Corp. Sunnyvale, Ca., R. D. Smith, Finnigan Corp., Sunnyvale, Ca., M. S. Story, Finnigan Corp., Sunnyvale, California 94086.

A dual purpose EI-CI ion source designed for use in quadrupole GC-MS is described. The ion source incorporates a unique high pressure lens system which allows rapid switch over from EI to CI (and reverse) mode of operation with no change in mechanical configuration. Additionally the lens system design reduces significantly the dependence of sensitivity on ion source pressure in the CI mode of operation. A cooling device on the ion source enables feedback control of the ion source temperature as low as 50° C with the filament on, so that less-fragmented EI and CI spectra of certain compounds can be obtained. A variable conductance device enables the gas conductance of the ionizer to be optimized to handle flows of 0-1.5 cc-atm/min He or 1.5 - 2.5 cc-atm/min He in the EI mode of operation.

Analysis of Mixtures by Collisional Activation (CA-DADI) of Ions by Chemical Ionization.

S. Meier, U. Rapp, Varian MAT, Bremen, West Germany and
W. A. Wolstenholme, Varian MAT Mass Spectrometry, Springfield, New Jersey

Introduction

It is well known that metastable ions can provide a great deal of significant additional information in structural and kinetic studies. Also, techniques which have been developed for recording "pure" metastable spectra by using double focusing mass spectrometers in the 'defocussed' mode provide increased sensitivity for the detection of metastable peaks and the unambiguous assignment of the corresponding decompositions. (1, 2)

More recent work has shown that more extensive fragmentation in the desired field-free region can be induced by allowing the ions to interact or "collide" with gas molecules introduced into that region of the spectrometer flight tube.

Experimental

A collision chamber has been added to a Varian MAT 311A mass spectrometer. This instrument has "reverse" Nier-Johnson geometry and "DADI" or "MIKES" spectra can be recorded by scanning the electrostatic sector. Metastable decomposition occuring in the field-free region between the magnetic and electrostatic analysers are studied, a typical scan giving directly the "daughter" ions from a chosen precursor.

Figure 1 shows diagramatically the arrangement of the collision chamber. A bellows assembly allows the chamber to be withdrawn from the flight path for conventional mass spectrometry. A valve in the gas inlet line to the collision chamber is regulated so that, typically, a pressure of 10^{-4} - 10^{-5} torr is maintained in the chamber. The pressure in the flight tube is maintained at the normal approximately 10^{-7} torr.

Figure 2 shows a photograph of the collision chamber assembly.

Results

In all cases studied, the use of the collision chamber increased the intensity of metastable peaks present before

collisional activation. In addition, in several cases other previously undetected peaks were identified, thus providing further information.

The system has been used to study and compare ion structures by comparison of pseudomolecular ion species in CI spectra with the equivalent ions formed by fragmentation in electron impact spectra of different molecules. Detailed results will be published elsewhere.

References

1. Barber, M., and Elliott, R. M., Proc Twelfth ASTM E-14 Conf, Montreal (1964)

2. Beynon, J. H., and Cooks,R.G., Int. Journal of MS and Ion Physics, 19/1, 107, 1976

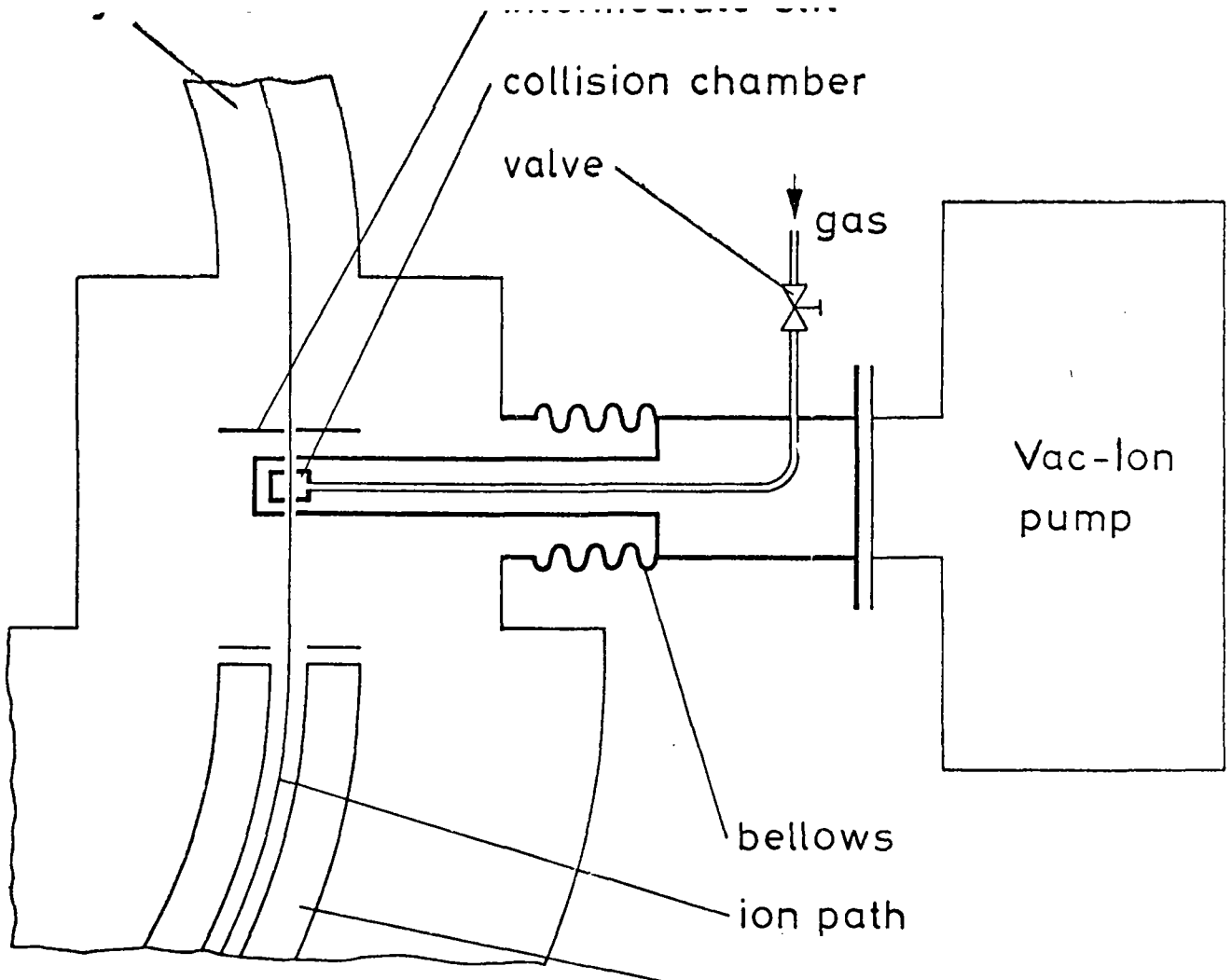

Figure 1: Schematic Diagram of Collision Chamber Arrangement in MAT 311A Flight Tube

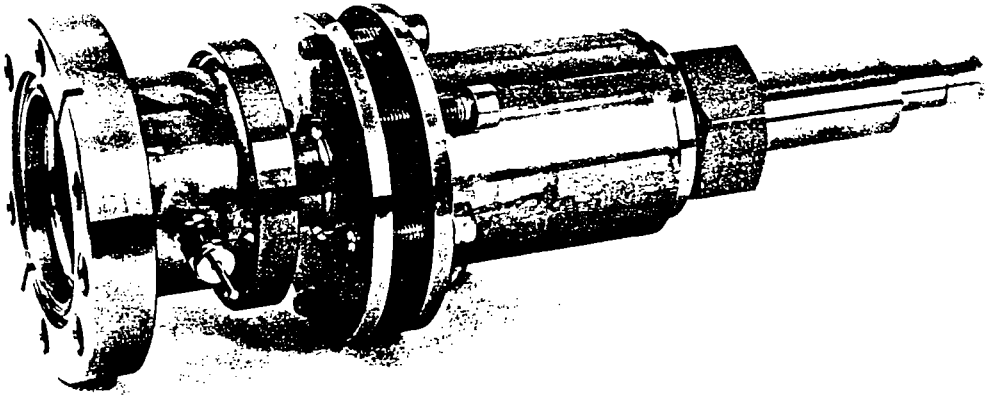

Figure 2: Collision Chamber Assembly

ATMOSPHERIC PRESSURE CHEMICAL IONIZATION STUDIES USING A HYPERSENSITIVE TRACE GAS ANALYSER. N. M. REID, J. B. FRENCH, C. C. POON. Univ. of Toronto, Inst. for Aerospace Studies, and J. A. BUCKLEY, Sciex Ltd., Toronto, Canada.

A new instrument, the TAGA 2000, based on positive and negative ion mass spectrometry combined with atmospheric pressure chemical ionization (API), has been developed for the hyposensitive detection of trace gases in ambient air or other applications where large sample volumes but very low concentrations are involved.

To use mass spectrometry for the identification and quantification of traces in ambient air in the parts ratios in the range of interest between 1 in 10^6 and 1 in 10^{14}, it is necessary to produce a massive degree of pre-separation or pre-selection of the trace gas molecules from air molecules before their introduction into the mass spectrometer. This is done by an extremely rapid preferential ionization, at atmospheric pressure, of the trace gas molecules using ions produced in primary ionization processes involving the major and minor constituents of air (reactant ions). This is thus an application of atmospheric pressure chemical ionization, or what is commonly called "API mass spectrometry". It is also equally necessary to maximize all the sequence of transfer coefficients that exist between the original "signal" trace molecules in air and their final arrival as mass-analyzed ions per second at the detector.

A continuous stream of 5 to 100 liters per minute of air is drawn through the inlet and passes through the API reactor. In this region primary ion production from the air occurs using, for example, a corona discharge, as is depicted, or a β-emitting radioactive foil, rapidly followed by secondary ion molecule reactions with trace gas molecules present containing hetero-atoms or having a significant polarity. The end result of this is the formation of staple product ions from many important and interesting trace compounds in air with an unusually high efficiency. Typical reactant ions found in ambient air are proton hydrate clusters in the positive mode and negatively charged oxygen hydrates and electrons in the negative mode. These ions, produced at atmospheric pressure, are then concentrated and introduced with high efficiency into the vacuum chamber. The trace gas ion mixture is allowed to expand into the vacuum system where the neutral gas is pumped using an ultra-high capacity pump and the ions are focussed using a series of ion lenses, and mass analyzed using a quadrupole mass-spectrometer with unit resolution up to m/e = 550. Ion detection is carried out using a high gain channel electron multiplier followed by a discriminator and ion counter. Both positive and negative ions can be analysed and detected. The output signal from the electrometer and counter can be handled in various ways - either by display on an oscilloscope, on an X-Y or chart recorder or most efficiently by a dedicated mini-computer with a suitable interface.

These three features, that is, high efficiency atmospheric pressure ionization, concentration and high efficiency ion transfer contribute to the unusually high sensitivity obtained with this instrument. Another feature of the instrument is its extremely fast dynamic response due to the high volume throughput used, and lack of memory effects which plague all ultrasensitive gas analysis techniques, allowing the real time monitoring of rapidly changing conditions such as, for example, the real time monitoring of metabolites in expired air.

An extensive application study program in several areas, including the

area mentioned above has been carried out during the last twelve months. Areas covered include environmental air monitoring geochemical prospecting.Compounds detected and response characteristics studied include, ammonia and other amines, nitrogen dioxide, nitric oxide, N-nitrosodimethylamine,acetone, aliphatic alcohols, iodine, dimethylsulphoxide, dimethylsulphide, alkyl halides. However, the detection of explosive vapours in air has been chosen here to demonstrate these features desoribed above.

Detection of trinitrotoluene (TNT) has been chosen as representative of the TAGA sensitivity to aromatic compounds containing nitro groups, a class of compounds of obvious interest in explosives detection. Due to TNT's high electron affinity (> 1.70 eV) the molecular ion M^- at 227 a.m.u. can be formed by associative electron capture from reactant ions such as O_2^- (H_2O) or directly from electrons in the corona discharge of the API source. TNT is also strongly acidic in the gas phase and therefore can also be ionized by proton transfer to an ion like O_2^- which is strongly basic in the gas phase. Denoting the TNT molecular ion as AH, the reaction is

$$O_2^- + HA \rightarrow A^- + HO_2$$

The ion A^- would appear at 226 a.m.u. Detection of TNT as a positive ion MH^+ has been shown in the plasma chromatograph , where

$$M + H^+ (H_2O)_n \rightarrow MH^+ + nH_2O$$

and a positive ion would appear at 228 a.m.u. This reaction would proceed slowly because of the low proton affinity of TNT and is therefore not ideal as a means of producing TNT product ions. The protonated molecular ion of TNT has been produced in a chemical ionization source using H_2 as a reagent gas .

Fig. 1 shows the detection of less than 1 ppb of TNT in an ambient air carrier. The mass range 226-231 a.m.u. was scanned at a rate of .5 sec/a.m.u. A trade-off is required between signal strength and adequate resolution to attain best detectability. In this example the peak (panel 2, top) is slightly wider than 1 a.m.u. and appears to contain both 226 a.m.u. and 227 a.m.u.

The vapor pressure of TNT at 20°C is only 10^{-6} torr. Detection of TNT in ambient air therefore involves detection at the ppb level and lower. Commercial TNT is known to contain dinitrotoluene (DNT) as a manufacturing impurity. DNT is more volatile, having a vapor pressure of 10^{-4} torr, and has been proposed by some as a suitable indicator for the presence of TNT. However, it contains one less nitro group and therefore has a lower gas phase acidity and lower electron affinity, thus decreasing the reaction rate with negative reactant ions. This factor obviously offsets the higher volatility because the DNT molecular peak at 182 a.m.u., seen in the lower half of Fig. 1 is 30 times smaller than the TNT molecular ion at 227 a.m.u.

The response shown in Fig. 1 was obtained by sampling the air from a plastic bag containing a small piece of solid TNT. If the TNT had come to equilibrium with the air in the bag, the carrier gas contained 10^{-9} parts TNT, by volume. Otherwise the concentration of TNT is below the ppb level. For the peak at 227 a.m.u., S/N = 100. The detectability limit at S/N = 2 is at least 2×10^{-11} parts or 2×10^{-13} gm/cm^3.

The high noise level (1000 cps) in the negative ion mode is thought to be due to electrons from the discharge which are reaching the detector. Reduction of the noise using a weak deflecting magnetic field is currently under study. Reduction of this noise by a factor of 100 (positive mode noise is 2 or 3 cps) to 10 cps would push the TNT detectability limit to 10^{-13} parts by volume, or into the femtogram/cm^3 range.

Figure 2 is a sequence demonstrating presence and absence of TNT. Note that solid TNT placed near the inlet does not produce an inlet air stream saturated in TNT vapor. Also observable is the presence of the experimenter's hand that had touched the TNT and subsequently been washed.

Fast dynamic response is shown (panel 7) by passing solid TNT quickly across the inlet as the molecular peak is being monitored. Scan speed is .5 a.m.u./sec. For this example, rise time in response to a discrete input of TNT vapor was less than .2 sec.; clearout was equally fast.

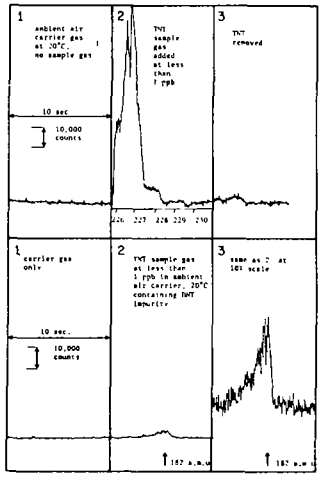

Fig 1- TNT detection at less than 1 ppb by repeated scans of 5 a.m.u. range. TNT molecular ion M^- is observed at 227 a.m.u. DNT molecular ion M^- is observed at 182 a.m.u.

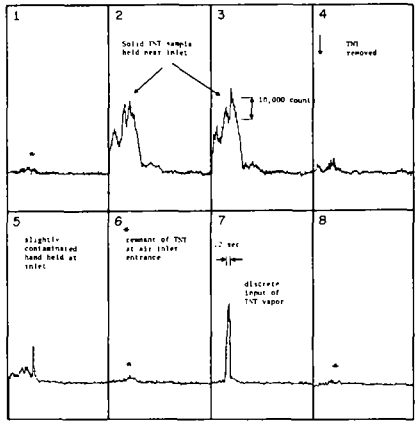

Fig 2- Detection sequence demonstrating presence and absence of TNT using repeated scan of 5 a.m.u. range. Molecular ion, M^- is observed at 227 a.m.u.

APPLICATIONS OF ATMOSPHERIC PRESSURE IONIZATION TO SPECIES OF ATMOSPHERIC INTEREST

M. W. SIEGEL
Extranuclear Laboratories, Inc.
Pittsburgh, Pennsylvania 15238

Atmospheric pressure ionization mass spectrometry research to date has largely concentrated on demonstrating very high sensitivity to a small number of compounds of immediate biological interest, e.g., drugs and pesticides. This perhaps premature emphasis on clinical applicability has led to a serious gap in the experimental literature: there is little or no data on response to simple molecular species, many of which are of atomspheric interest. Fundamental investigation directed at such species is now in progress. Three ends are planned: (1) comparison with theoretical sensitivity and scaling relationship predictions based on the reaction rate literature, (2) the generation of new or improved reaction rate data, particularly for three body processes which may prove better accessible at higher pressures, and (3) elucidation of the prospects for using API in direct atmospheric monitoring applications.

Our research to date has concentrated on technical goals aimed at simplifying the positive reactant ion spectrum by reducing the H_2O impurity level in the carrier gas (generally N_2, and occasionally Ar or air), and at calibrating the system response to a number of gaseous species. With respect to the first goal, we are now able to demonstrate that the H_2O impurity level can be reduced to the point where in N_2 the pseudo-primary ions N_3^+ and N_4^+ dominate the reactant ion spectrum. Residual impurity ions are then primarily connected with O_2 traces, the majority impurity ions being O_2^+ and NO^+. Very small residual H_2O traces then appear in the spectrum as $O_2^+ \cdot H_2O$. With respect to the second goal, we have observed and calibrated API-MS response to NO, SO_2, SF_6, vinyl chloride (HC=CCl), and the sequence of Freons CF_4 (F14), CHF_3 (F23), CHF_2Cl (F22), $CHFCl_2$ (F21), CCl_2F_2 (F12) and CCl_3F (F11).

Present indications are that with strongly responding compounds, e.g. SF_6 as SF_6^- and the Freons $CF_{4-n}Cl_n$ as $CF_{4-n-1}Cl_n^+$ and $CF_{4-n}Cl_{n-1}^+$, sensitivity extends below the part-per-trillion level and remains linear to the few part-per-billion level, in good agreement with theoretical estimates based on expected reaction and recombination rate constants. Sensitivity to vinyl chloride as C_2HCl^+ and $C_2HCl \cdot H^+$ has been demonstrated at the 50 part-per-billion level and, based on the observed signal-to-noise, can be extrapolated to the one part-per-billion level. Sensitivity to species of fundamental atmospheric interest, such as NO and SO_2, tend to have detection limits set by interfering reactant ion mass peaks, but sensitivities below the one part-per-million level are still easily demonstrated, and may be extrapolated to the tens of part-per-billion level with appropriate integration and background subtraction techniques.

A Negative Ion Source for Detection of Trace (PPT) Electrophilics in Air.* R. K. GOULD and W. J. MILLER, AeroChem Research Labs., Inc., Princeton, New Jersey 08540

A novel, repetitively pulsed, low pressure discharge tube has been designed and tested for use as a mass spectrometer negative ion source for the detection of very low concentrations of electrophilic tracer gases in the atmosphere. The instrument is intended for application to studies of meteorological phenomena. Sensitivity to less than 1 part SF_6 in 10^{12} parts air has been obtained with linear response and no detectable interferences from the common air gases. The ion source operates, typically, at 2 to 10 Torr and (for optimum SF_6 sensitivity) 300 HZ. Under such conditions, low energy electron attachment produces SF_6^- predominantly. Comparative tests indicate that this source is 100 to 1000 fold more efficient than corona or radio-iso-tope sources. The negative ion mass spectrometer is also applicable, with somewhat reduced sensitivity, to the detection of a number of high molecular weight Freons, but so far has proven non-specific with respect to the simpler Freons including F-11 and 12, both of which produce predominantly Cl^- and F^-.

*This work was conducted under EPA Contract 68-02-1443

Formation and Dissociation of Hydrogen Negative Ions H_2^-, H_3^-, and H^{2-}, R. Schnitzer and M. Anbar, Stanford Research Institute, Mass Spectrometry Research Center, Menlo Park, CA 94025

Introduction. The observation of H_2^-, H_3^- and H^{2-} has been facilitated by our mass spectrometric system.[1,2] The experimental setup is shown in Figure 1. These ions have been found in the ion beam extracted from a duoplasmatron ion source fed with H_2 or D_2. Since the ion currents of the species of interest are low, a high abundance sensitivity mass spectrometer is necessary for the analysis.

H_2^-, H_3^-. The mechanism of formation is concluded from the pressure dependence of the diatomic and triatomic ion currents.[3] The diatomic and triatomic negative hydrogen ions exhibit a first and second order pressure dependence, respectively. The suggested mechanism of formation of the diatomic ions X_2^- (X = H, D) assumes the atomic ion X^- as precursor,

$$(1) \quad e + H_2 \rightleftarrows H^- + H$$

$$(2) \quad H^- + H_2 \rightarrow H_2 + H$$

while the formation of the triatomic ions proceeds via an excited molecule and a diatomic ion as precursor

$$(3) \quad H_2 + M \rightleftarrows H_2^* + M \qquad (M = Ar, H_2)$$

$$(4) \quad H_2^- + H_2^* \rightarrow H_3^- + H$$

The collision-induced fragmentation patterns of the molecular ions were observed. In this experiment, the fragmentation takes place in the region prevailing between the einzel lens and the Wien velocity filter. The Wien filter analyzes the ions by velocity only, regardless of mass and charge. Therefore, fragment ions that are formed with a negligible change in velocity are analyzed by the Wien filter according to the parent ion velocity. However, the momentum carried by the fragment ions is only a fraction and therefore by scanning the sector magnet, the difference in mass can be detected.

Figure 2 demonstrates fragmentation spectra of mass 2 ion beams extracted from (a) hydrogen and (b) deuterium plasma. Mass 2 ion beam from hydrogen (Figure 2a) comprises H_2^- and D^- (from the deuterium naturally abundant in hydrogen). The collisional fragmentation results in a fragment H^- ion (H_f^-), thus demonstrating the existence of H_2^-. In a parallel experiment (Figure 2b) where a mass 2 ion beam from a deuterium plasma is momentum analyzed, no fragment ion has been detected.

Figure 3 demonstrates fragmentation spectra of mass 3 ion beams extracted from (a) hydrogen and (b) hydrogen-deuterium plasma. Mass 3 ion beam from hydrogen (Figure 3a) comprises mainly H_3^- ions that result upon collision in H_f^- ions carrying 1/3 of the initial momentum. Mass 3 ion beam from hydrogen-deuterium plasma (Figure 3b) comprises mainly HD^- ions instead of H_3^-. Upon collision, these HD^- ions yield H_f^- and D_f^- carrying 1/3 and 2/3 of the initial momentum, respectively.

H^{2-}. The existence of H^{2-} (D^{2-}) has been concluded from the detected 20 keV H^- ions when the extraction voltage is only 10 kV (ref. 2). It has been shown that the H^{2-} is formed on the plasma surface at the extraction orifice. Following a single electron autodetachment process, $H^{2-} \rightarrow H_a^- + e$, the H_a^- ions are detected with twice the nominal kinetic energy. However, H^{2-} ions surviving the einzel lens (EL) are focused at the regular voltage (SV), while autodetached H_a^- ions are focused at double the focusing voltage (DV), thus behaving as H^- ions extracted by 20 kV.

Charge Transfer Processes (CTP). 20 keV H^- ions involved may also be formed by two consecutive collisional CTP. The first CTP takes place along the drift distance between the extraction skimmer electrode and the einzel lens assembly and the second CTP may proceed at a high yield and a discrete energy inside the einzel lens region.

The first step occurs when the H^- ions extracted from the ionization source lose one or two electrons by collision with the residual gas in the field free drift space

$$H^- + M \rightarrow H^+ + 2e \quad (M = H_2, He, Ar) \qquad (1)$$

$$H^- + M \rightarrow H^o + M + e \qquad (2)$$

While in the second step inside the einzel lens region H^o and H^+ can be reconverted to H^- ions by electron capture reactions:

$$H^+ + M \rightarrow H^- + M^{2+} \qquad (3)$$

$$H^o + M \rightarrow H^- + M^+ \qquad (4)$$

These four reactions are well known and their cross sections have been measured by a number of investigators.[4]

An illustration of the gain in kinetic energy (KE) in these CTP is shown in Figure 4. Figure 4a shows the variation of the axial potential along the EL. Figure 4b shows the KE variation of H^- and H^+ traversing the EL. While the H^- ion beam is focused upon leaving the EL the H^+ ion beam is defocused (because of H^+ ions traversing the EL faster than the H^- ions, their focusing is not effective). Figure 4c shows the KE gain of the secondary H^- ions undergoing the reactions sequence (1) and (3) and Figure 4d the reactions sequence (2) and (4). These H^- ions emergy from the EL defocused with a continuum of KE. Therefore, kinetic energy continuum of defocused H^- ions ($E_o \leq KE \leq E_o + 2V$ for (1) and (3); $E_o \leq KE \leq E_o + V$ for (2) and (4)) emerges from the EL.

Figure 5a shows the H_a^- ion current variation with the EL voltage. If the first maximum in H_a^- ions current, SV, resulted from reactions (1) and (3) occuring with a high yield at the EL potential saddle of -5 kV and the second maximum, DV, corresponded to reactions (2) and (4) at a saddle of -10 kV, then lowering the EL potential would eliminate the H_a^- maxima at SV and DV.

The potential saddle of the EL can be lowered by extending the EL configuration as shown in Figure 6, thus predicting a shift of H_a^- maxima to 5 and 10 kV settings of the EL. Figures 5a and 5b show the H_a^- ion currents for the above configurations. The invariance in the H_a^- maxima under these conditions shows that the

contribution of of CTP is insignificant under our experimental conditions and confirms our earlier interpretation of the fast H_a^- ions originating from the autodetachment of H^{2-}.

References

1. W. Aberth, R. Schnitzer, and M. Anbar, Phys. Rev. Lett. 34, 1600 (1975).

2. R. Schnitzer and M. Anbar, J. Chem. Phys. 64, 2466 (1976).

3. R. Schnitzer and M. Anbar, J. Chem. Phys, in press (1976).

4. H. Tawara and A. Russek, Rev. Mod. Phys. A9, 2485 (1974).

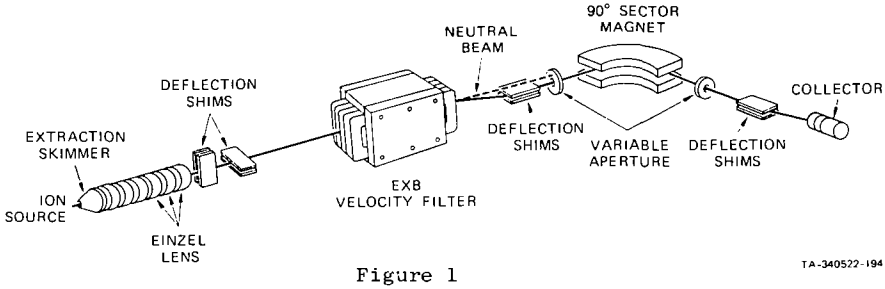

Figure 1

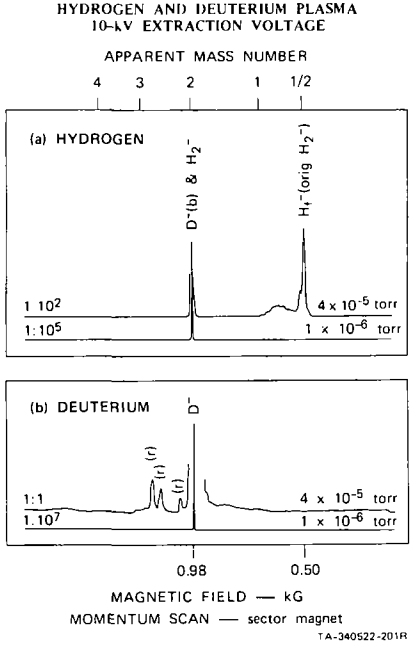

Figure 2

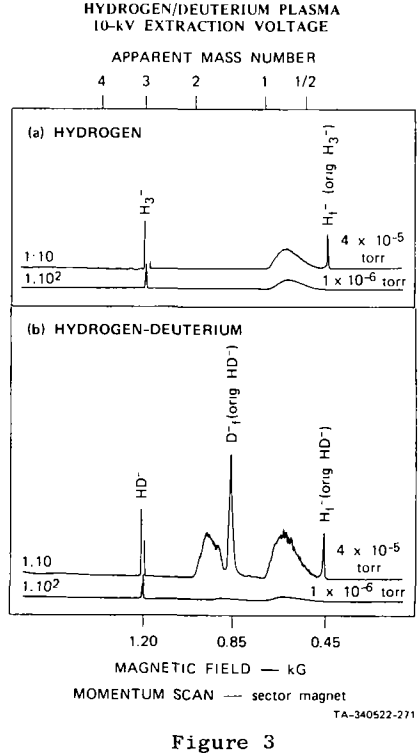

Figure 3

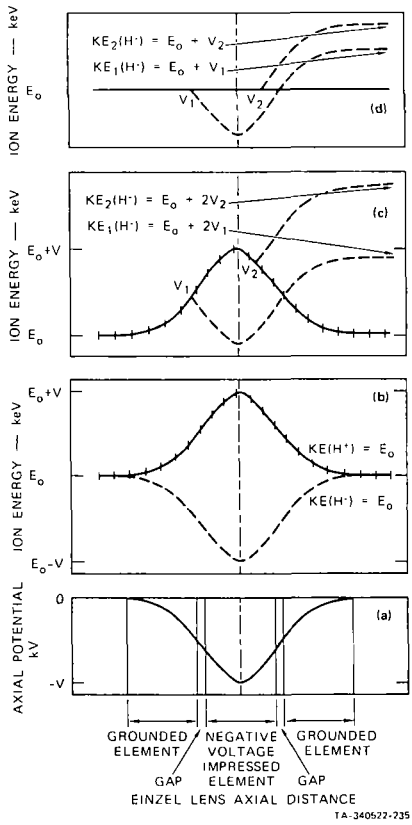

Figure 4

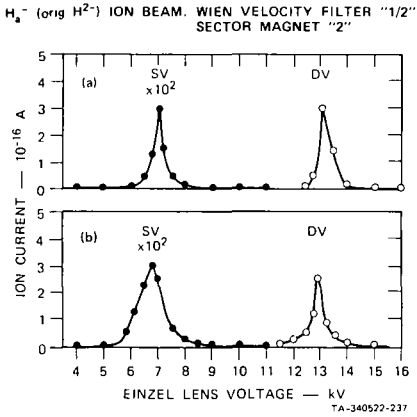

Figure 5

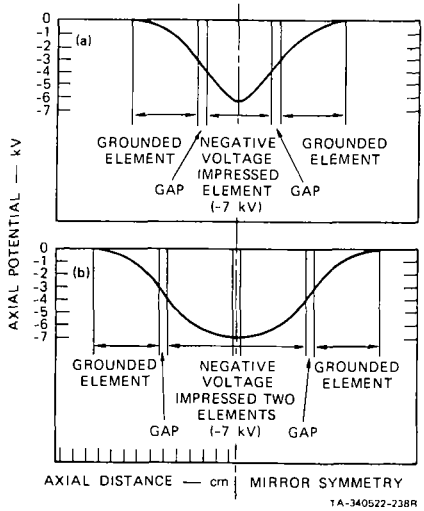

Figure 6

Structures, Exothermicities, Rates and Temperature Coefficients in H^- Transfer Reactions. M. MEOT-NER and F. H. FIELD, The Rockefeller University, New York, New York 10021.

H^- transfer reactions between C_2-C_{10} hydrocarbons and carbonium ions proceed with reaction probabilities (P) of $1 \geqslant P \geqslant 10^{-4}$. Fast Reactions ($P \approx 1$) are independent of temperature; slow reactions ($P < 1$) exhibit negative temperature dependencies with $k = AT^{-1}$ to $k = AT^{-7}$. Some reactions show a sharp transition from a region of fast kinetics at low temperatures to a region of slow kinetics at higher temperatures. Relations among complexity of the reactant, the exothermicity of the reaction, and the reaction rate and its temperature coefficient are discussed.

Orbital Ionization Energies and Molecular Properties. Proton Affinities and Photoelectron Spectra of Nitriles

Ralph H. Staley,* James E. Kleckner,** and J. L. Beauchamp
Department of Chemistry
California Institute of Technology
Pasadena, California 91125

Abstract

Proton affinities, defined for a base B as the heterolytic bond dissociation energy $D(B\text{-}H^+)$ for removing a proton from the conjugate acid BH^+, are determined for a series of nitriles using ion cyclotron resonance techniques. Photoelectron spectra of nitriles are also obtained. In previously examined series of bases, linear relationships have been established between proton affinities and adiabatic first ionization potentials which correspond to removal of an electron from a lone pair localized at the site of protonation. Nitrile proton affinities are found to be linearly related not to the first CN π ionization potentials but rather to the adiabatic N lone pair σ ionization potentials at higher energy. This relationship provides a useful chemical means for the assignment of bands in photoelectron spectra; specific examples are considered and assigned. A linear relationship is also found between nitrile (RCN) and primary amine (RNH_2) proton affinities for a range of substituents R. The results are discussed in terms of the intrinsic factors affecting molecular basicity.

A more detailed account of this work has now appeared in the Journal of the American Chemical Society.[1]

---

*Department of Chemistry, Massachusetts Institute of Technology, Cambridge, Massachusetts 02139.

**Department of Chemistry, University of California, Berkeley, California 94720.

[1] R. H. Staley, J. E. Kleckner, and J. L. Beauchamp, J. Amer. Chem. Soc., 98, 2081-2085 (1976).

Porton affinities of monosubstituted benzenes by Y. K. LAU and P. KEBARLE, U. of Alta. Chem. Dept. Edmonton, Alta, Canada.

The proton affinities of $X.C_6H_5$ (X = Cl, F, H, CH_3, C_2H_5, NO_2, OH, CN, CHO, OCH_3) were measured by proton transfer equilibria involving standard compounds with known PA's. The PA's were found to increase in the order given above and are in the range 182.4 - 198.3 kcal/mole. Correlation with σ values is observed only for X = (Cl, F, H, CH_3, C_2H_5, OH and OCH_3). This indicates ring protonation for the above compounds. The remaining benzenes must be protonated at the substituent. Measurement of the temperature dependence of the proton transfer equilibria, over a wide temperature range, was possible in some cases allowing good ΔS determinations. These could be explained on basis of symmetry number changes.

Hydrated carbenium ions, protonated alcohols ROH_2^+ and acid catalyzed dehydration of alcohols as studied in a pulsed high pressure ion source. K. HIRAOKA and P. KEBARLE Chem. Dept. Univ. of Alta. Edmonton, Alta.

In order to clear up the question whether hydrated carbenium ions ROH_2^+ are equivalent to the protonated alcohol ROH_2^+ studies of equilibria

$$R^+ + OH_2 = (ROH_2)^+ \qquad (1)$$

were initiated. Van't Hoff plots of K_1 lead to ΔH_1 and, provided that $\Delta H_f(R^+)$ is known, also to $\Delta H_f(ROH_2^+)$. This enthalpy of formation is compared with $\Delta H_f(ROH_2^+)$ obtained from the proton transfer equilibrium involving the alcohol ROH and a base with known proton affinity. Identical $\Delta H_f(ROH_2^+)$ testify to identical structure. This has been found to hold true for R = t-butyl$^+$, where ΔH_1 = -11.2 kcal/mole leading to PA(t-butanol) = 109 kcal/mole in agreement with PA measured by proton transfer. Interesting chemistry results on furthur addition of water to t-$C_4H_9OH_2^+$. The measured enthalpy changes indicate structural change in which the ion is converted to isobutene.$H_3O^+(H_2O)_n$ and then ultimately to $H_3O^+(H_2O)_n$ + isobutene. The above reaction is analogous to the acid catalyzed dehydration of alcohols to olefins in solution.

Charge Transfer Reactions in Alkane and Cycloalkane Systems
Estimated Ionization Potentials

S. G. Lias, P. Ausloos, and Z. Horvath*
Institute for Materials Research
National Bureau of Standards
Washington, DC 20234

Rate constants of charge transfer reactions, k_{CT}, involving C_3-C_9 alkanes and cycloalkanes have been determined in an ion cyclotron resonance mass spectrometer.[1] The rate constants are significantly lower than the corresponding rate constants for collision when the reaction is less than about 0.e eV exothermic for linear alkane ions, or less than about 0.2 eV exothermic for cycloalkane ions. In this region of low reaction efficiency, the efficiency of reaction with linear or branched alkanes seems to depend primarily on reaction exothermicity. (The efficiencies of reaction of a given ion with cyclic alkanes also depends on ΔH_{rn}, but are higher than for reactions with other compounds). Although the lowered reaction efficiencies probably result, at least in part, from unfavorable Franck-Condon factors in the energy range near the ionization onset, quanitiative correlations between reaction efficiency and estimated relative Franck-Condon factors were not observed. When the enthalpy of reaction is small (less than about -0.15 eV), it is seen that the reverse charge transfer can also occur, and equilibrium constants, values for the standard free energy change are derived, and values of ΔH_{rn} are estimated assuming that there are no contributions to ΔS except the differences in ion-molecule collision rates in the forward and reverse directions of the equilibria. In the case of the equilibria involving cyclohexane ion, these values of ΔH_{rn} lead to estimates of the ionization potentials of methyl-cyclopentane, 3-methylpentane, n-octane, 2,2-dimethylbutane, 2,3-dimethylbutane, and n-nonane which are lower than the I.P. of cyclohexane, i.e., <9.88 eV,[2,3] although all these compounds had previously been reported to have I.P. above 10.03 eV.[2] That the

ionization potentials are indeed lower than 10.03 eV is confirmed by determining the quantum yields of ionization with 10.03 eV photons.[1] Taking a value of 9.88 eV for the ionization potential of cyclohexane,[2,3] the values of I.P. given in Table I were obtained in the course of this work.

Table I

Ionization Potentials, eV

Compound	Watanabe et. al. (2)	This work
$n\text{-}C_7H_{16}$	10.08 ± ?	9.93
$c\text{-}C_6D_{12}$		9.90
$c\text{-}C_6H_{12}$	9.88 ± 0.02	9.88
$c\text{-}C_6H_5CH_3$		9.87
$(C_2H_5)_2CHCH_3$	10.08 ± ?	9.84
$n\text{-}C_8H_{18}$		9.81
$(CH_3)_3CC_2H_5$	10.06 ± ?	9.80
$(CH_3)_2CHCH(CH_3)_2$	10.02 ± ?	9.78
$n\text{-}C_gH_{20}$		9.72

(1) S. G. Lias, P. Ausloos and Z. Horvath, Intl. J. Chem. Kin., In Press.

(2) K. Watanabe, T. Nahayama and J. R. Mottl, J. Quant. Spectrosc. Radiat. Transfer 2, 369 (1962)

(3) J. W. Raymonda, J. Chem. Phys. 36, 3912 (1972).

Ion-Molecule Reactions Involving Halomethyl Ions; Heats of Formation of Halomethyl Ions

S. G. Lias and P. Ausloos
Institute for Materials Research
National Bureau of Standards
Washington, DC 20234

The reactions of $CH_5^+(CD_5^+)$ and $C_2H_5^+(C_2D_5^+)$ ions generated in CH_4 or CD_4, and of $C_3H_7^+$ ions generated in neopentane or propane with CH_3Cl, CH_2Cl_2, $CHCl_3$, CCl_4, CH_3F, CH_2F_2, CHF_3, CF_4, CH_2FCl, CHF_2Cl, $CHFCl_2$, $CFCl_3$, CF_2Cl_2, and CF_3Cl have been studied. In addition, the reactions of the various halomethyl ions with the halomethanes are investigated. Rate constants are reported for all reactions observed. The experiments were carried out on a pulsed ion cyclotron resonance mass spectrometer. In some cases, the identity of the neutral product formed in an ion-molecule reaction was verified by irradiating an appropriate mixture with gamma rays and analyzing the neutral products.

The $CH_5^+(CD_5^+)$ ion transfers a proton to all of these molecules. The protonated halomethanes (except CH_3ClH^+, $CH_2F_2H^+$, CHF_3H^+, and CF_4H^+) dissociate under the conditions of these experiments by losing a hydrogen halide molecule. When the original reactant ion was CD_5^+, it was seen that only DX loss, never HX loss, occurred (where X is Cl or F).

The ethyl, sec-propyl ions, and halomethyl ions abstract chloride or fluoride from the halomethanes. Chloride transfer always predominates over fluoride transfer when both channels are exothermic. Ethyl and sec-propyl ions do not undergo hydride transfer reactions with any of these molecules.

Making the assumption that an efficient ion-molecule reaction is exothermic, and that a reaction which can not be observed is endothermic,

it is possible from these results to establish upper and/or lower limits for the heats of formation of the halogenated methyl ions. The results indicate that the heat of formation of CF_3^+ is 4.18 ± 0.13 eV (96.3 ± 3 kcal/mole). The heat of formation of CCl_3^+ lies between the limits, 8.34-8.82 eV (192-203.5 kcal/mole), and therefore is lower than previously accepted values by at least 0.25 eV. The value obtained for $\Delta H_f(CFCl_2^+)$ is 6.72 ± 0.22 eV (155 ± 5 kcal/mole), and that for $\Delta H_f(CHFCl^+)$ is 7.76 ± 0.22 eV (179 ± 5 kcal/mole); the first of these is significantly lower than earlier determinations, and the latter has not been determined before. Previously reported values for the heats of formation of CF_2Cl^+, CF_2H^+, CH_2F^+, CCl_2H^+, and CH_2Cl^+ are confirmed.

STABILITIES OF UNSATURATED CARBOCATIONS

W. R. Davidson, D. H. Aue, and M. T. Bowers

Department of Chemistry, University of California,
Santa Barbara, California, 93106

Allyl, vinyl, cyclopropyl, and cyclopropylcarbinyl cations may be generated by proton transfer to appropriate dienes, acetylenes, allenes, cyclopropenes, and vinylcyclopropanes.

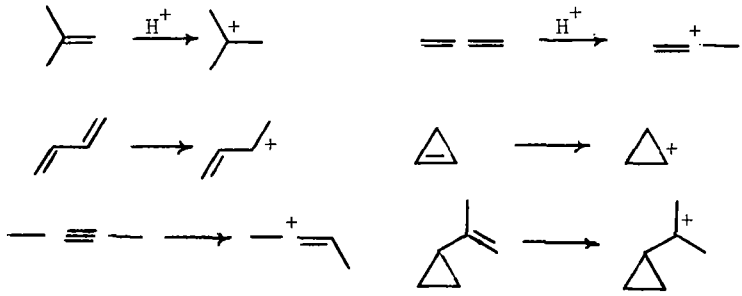

From the proton affinities of such hydrocarbons, the heats of formation of a number of derivatives of such carbocations have been measured by ion cyclotron resonance techniques. Double resonance, drift cell equilibrium, and low pressure trapped ion cell techniques have been utilized. Measured proton affinities (PA) of dienes and derived heats of formation (ΔH_f^o) and hydride ion affinities (HA) of corresponding allyl cations are shown in Table I. A comparison of the HA's of various carbocations

TABLE I - Thermodynamic Data for Allyl Cations (kcal/mol)

Olefin	PA	Cation	ΔH_f^o	HA
	-		226	254
	189		204	237
	197.4		187.7	227.5
	198.4		186.3	227.4
	205.0		173.0	222.2
	208.8		162.2	216.6

provides an evaluation of the relative stabilities of carbocations as derived from the standard reaction (1). As expected,

$$R\text{-}H \longrightarrow R^{+} + H^{-} \qquad \Delta H^{o} = -HA \qquad (1)$$

allyl cations show lower HA's and higher stabilities as the degree of methyl substitution increases at the termini of the allylic system.

Proton affinities of acetylenes give hydride affinities (HA's) for vinyl cations shown in Table II.

TABLE II - Hydride Ion Affinities (HA's) of Vinyl Cations (kcal/mol)

	HA
$CH_2{=}CH^{+}$	287
$CH_2{=}\overset{+}{C}\text{-}CH_3$	263
$CH_3\text{-}CH{=}\overset{+}{C}\text{-}CH_3$	254

Protonation of allene presents a particularly interesting problem since there are two possible modes of protonation (Fig.1).

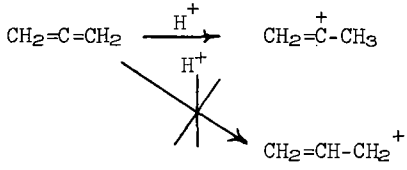

FIGURE 1

Allene is reversibly protonated by H_3S^{+} and exhibits an apparent proton affinity of 174 kcal/mol. This corresponds to a heat of formation of 237 kcal/mol for the ion formed. This heat of formation agrees exactly with that of the 2-propenyl cation derived from the PA of propyne but is 11 kcal/mol higher than the 226 kcal/mol heat of formation of allyl cation.[1] Furthermore, the ion formed on protonation of allene is capable of protonating methanol and H_2S, while the allyl cation derived from fragmentation of allyl chloride does not protonate methanol

or H_2S. Thus it is clear that the allyl cation neither forms on protonation of allene nor *via* subsequent rearrangement of the 2-propenyl cation formed.

Proton affinities of cyclopropenes, methylenecyclopropanes and vinylcyclopropanes have also been measured to give thermodynamic data related to cyclopropyl and cyclopropylcarbinyl cations.

---

1. F. P. Iossing, *Can. J. Chem.*, **50**, 3973 (1972); *ibid.*, **49**, 357 (1971).

Association of H_2O to $H^+(H_2O)_n$ between 80 to 120 K for I <n<60. ROGER THOMAS and RUDOLF R. BURKE, Centre de Recherches en Physique de l'Environnement terrestre et planétaire, C.N.E.T. et C.N.R.S. 45045 Orléans Cedex, France.

A cold plasma is obtained by expanding an ionized gas through a contoured supersonic nozzle. The static temperature of the resulting free jet is about 100 K, the static pressure is a few tenths of a Torr. The evolution of the ion concentration along the jet axis is monitored mass spectrometrically and interpreted in terms of reaction kinetics. The rate constants for the reactions:

$$H^+(H_2O)_n + H_2O\ (+\ M) \text{ ——— } H^+(H_2O)_{n+I}\ (+\ M)$$

have been determined as a function of pressure and temperature in several carrier gases M. Under our conditions these reactions are kinetically of second order: the rate constants of a few times 10^{-9} molecule^{-1} cm^3 s^{-1} are independent of pressure, temperature, and the nature of the carrier gas. Up to n = 60, the rate constants are nearly independent of n, except for m =21 and n = 28, where they are about three times smaller.

CONSERVATION OF SPIN ANGULAR MOMENTUM IN PROTON-TRANSFER REACTIONS INOVOLVING $C^-(^4S)$

K. Tanaka, L.D. Betowski, G. I. Mackay and D.K. Bohme

Department of Chemistry and
Centre for Research in Experimental Space Science,
York University, Downsview, Ontario M3J 1P3, Canada

It is now well established that the Wigner-Witmer spin conservation rule can account for the observed low probability of a number of exothermic ion-molecule reactions in which electronic spin angular momentum is not conserved through the intermediate state in going from reactants to products.[1] Spin-forbidden ion-molecule reactions usually proceed with rates at least 10 times slower than similar but spin-allowed reactions. In the course of our systematic measurements with the flowing afterglow technique of rate constants for proton-transfer reactions we have identified a series of such reactions which are also spin-forbidden, viz.

$$C^-(^4S) + SH(\text{singlet}) \rightarrow X^-(\text{singlet}) + CH(^2\Pi) \qquad [1]$$

However the violation of the spin conservation rule can be avoided for the more exothermic members of this series by the spin-allowed production of CH in the $^4\Sigma$ lowest excited state which has recently been shown to lie only 17.1 kcal mole^{-1} above the $^2\Pi$ ground state.[2] Consequently we chose to study a series of reactions of type [1] which allowed us to sweep the exothermicity from ~0 to ~ 30 kcal mole^{-1} with the expectation that reactions with an exothermicity larger than 17.1 kcal mole^{-1} would show a dramatic increase in reaction probability. The acids XH chosen for this study were CH_3COCH_3, SiH_4, H_2S, HCN and HCl.

$C^-(^4S)$ ions were produced by electron impact (70eV) on C_2H_2 in a helium buffer at ~ 0.4 Torr. Any $C^-(^2D)$ produced under these conditions should be collisionally detached prior to the reaction region because of the low binding energy of $C^-(^2D)$ relative to $C(^3P_o)$, viz. 35meV.[3] Also there was no evidence for the production of O_2^- by charge transfer from C^- when O_2 was added into the flowing C_2H_2 - He plasma. This result indicates that the C^- is present predominantly in its ground electronic ^4S state since Paulson[4] has found that $C^-(^2D)$ readily charge transfers with O_2 at low interaction energies. The rate constant measurements for the reaction of C^- with XH = CH_3COCH_3, SiH_4, H_2S, HCN and HCl were straightforward.[5] X^- was identified as the major product in each case.

The results of the measurements are summarised in Table I along with calculated reaction probabilities, k_{exptl}/k_c, and reaction exoergicities, ΔG°_{298}. The spin-forbidden production of $CH(^2\Pi)$ is exoergic in each case whereas the spin-allowed production of $CH(^4\Sigma)$ is exoergic or nearly so only for the reactions with H_2S, HCN and HCℓ. The measured rate constants and the calculated reaction probabilities are indeed low for the spin-forbidden reactions with CH_3COCH_3 and SiH_4 and increase sharply as the spin-allowed production of $CH(^4\Sigma)$ becomes energetically allowed. We can infer from these results that the reactions of $C^-(^4S)$ with H_2S, HCN and HCℓ involve the production of the lowest excited $^4\Sigma$ state of CH. The slightly lower reaction probability of the reactions with H_2S and HCN may be a result of a slight endoergicity.

TABLE I Rate constants (in units of 10^{-9} cm^3 $molecule^{-1}$ sec^{-1}) at 296±2°K for proton transfer reactions of the type $C^-(^4S) + XH \rightarrow X^- + CH$

XH	N[a]	$k_{expt\ell}$ [b]	k_c [c]	$k_{expt\ell}/k_c$ [d]	ΔG°_{298}/kcal $mole^{-1}$)[e]
CH_3COCH_3	3	0.071±0.010	3.7	0.019±0.005	-2.8±1.7 (14.3 1.9)
SiH_4	5	0.062±0.005	1.7	0.036±0.009	> - 6.9 (>10.2)
H_2S	4	0.58±0.12	2.0	0.29±0.07	-16.1±2.1 (1.0±2.3)
HCN	4	1.1±0.1	3.7	0.30±0.06	-18.1±3.8 (-1.0±4.0)
HCℓ	4	1.7±0.1	1.8	0.94±0.19	-32±1 (-15±2)

[a] N is the number of measurements [b] The mean value along with the precision of the measurements [c] Capture rate constant calculated from the Langevin or ADO theory (ref. 6, 7) [d] The limits reflect the estimated accuracy of $k_{expt\ell}$ [e] The values in parentheses correspond to the formation of $CH(^4\Sigma)$.

In conclusion, we have identified a new class of spin-forbidden ion-molecule reactions and measured their rate constants. The Wigner-Wintmer spin conservation rule accounts for the observed low probability of such reactions in the absence of competing spin-allowed channels. The measurements also provide an interesting example which illustrates how rate constant measurements at a single temperature can provide information about the electronic state of the neutral product formed in an ion-molecule reaction. This is a rare occurrence in ion-molecule chemistry where rate constants generally are not renowned for their information content, at least not when measured at a single temperature.

References

1. J.J. Kaufman in "Interactions Between Ions and Molecules" P. Ausloos (Ed.), NATO Advanced Study Institute, Plenum Press, New York (1975).

2. A. Kasdan, E. Herbst and W.C. Lineberger, Chem. Phys. Letters 31, 78 (1975).

3. V.A. Oparin, R.N. Il'in, I.T. Serenkov, E.S. Solov'ev and N.V. Federenko, JETP Lett. 13, 249 (1971).

4. J.F. Paulson, J. Chem. Phys. 52, 549/(1970).

5. D.K. Bohme, R.S. Hemsworth, H.W. Rundle and H.I. Schiff, J. Chem. Phys. 58, 3504 (1973)

6. G. Gionmousis and D.P. Stevenson, J. Chem. Phys. 29, 294 (1958).

7. T. Su and M.T. Bowers, Intern. J. Mass Spectrom. Ion Phys. 12, 347 (1973)

A HIGH PRESSURE MASS SPECTROMETRIC STUDY OF ION-MOLECULE REACTIONS IN C_2H_5F AND $C_2H_5C\ell$

by

H. S. Tan, M. J. K. Pabst and J. L. Franklin

Department of Chemistry
Rice University
Houston, Texas 77001

The gas phase ion-molecule reactions of $C_2H_5C\ell$ have been studied at 200 eV and those of C_2H_5F at 14 eV and 200 eV electron impact energies up to a pressure of one torr in a conventional magnetic-field-free single ion source quadrupole mass spectrometer. $C_2H_5C\ell^+$ and $C_2H_5^+$ mainly protonate $C_2H_5C\ell$ to form $C_2H_6C\ell^+$ which then condenses with $C_2H_5C\ell$ to produce $C_4H_{10}C\ell^+$ up to as much as 75% of total ionization at a pressure of one torr. In C_2H_5F, CH_2F^+ and $C_2H_4F^+$ mainly react with C_2H_5F by fluoride transfer to produce $C_2H_5^+$ which then reacts with C_2H_5F to form $C_4H_9^+$ up to as much as 70% of total ionization. As with $C_2H_5C\ell$, $C_2H_5F^+$ and $C_2H_5^+$ protonate C_2H_5F to form $C_2H_6F^+$ which then condenses to produce $C_4H_{10}F^+$. The mechanisms of ion-molecule reactions are quite similar in C_2H_3F, despite different electron energies (14 eV and 200 eV) having been employed. Reaction paths, product distribution and rate constants have been determined for the majority of ions in $C_2H_5C\ell$ and C_2H_5F.

Binding Energies of $(\eta^5\text{-}C_5H_5)Ni^+$ to n-Donor Ligands in the Gas Phase by Ion Cyclotron Resonance Spectroscopy.

REED R. CORDERMAN and J. L. BEAUCHAMP, California Institute of Technology, Dept. of Chem., Pasadena, California 91125.

Binding energies of $(\eta^5\text{-}C_5H_5)Ni^+$ to n-donor bases are obtained by measuring equilibrium constants for reactions involving transfer of $(\eta^5\text{-}C_5H_5)Ni^+$ between molecules using trapped ion cyclotron resonance techniques. The binding energies $D(C_5H_5Ni^+\text{-}B)$ range from ~48 kcal/mole (MeOH) to ~60 kcal/mole (Me_3P). A plot of $D(H^+\text{-}B)$ versus $D(C_5H_5Ni^+\text{-}B)$ gives an excellent correlation which is predictive value for determining $D(C_5H_5Ni^+\text{-}B)$. Several molecules, including NO, HCN, MeCN, MeNC, and Me_3As deviate from the correlation with anomolously large values of $D(C_5H_5Ni^+\text{-}B)$. This is the result of $L(p\pi) \rightarrow Ni(d\pi)$ electron donation for NO, HCN, and MeCN and $L(d\pi) \rightarrow Ni(d\pi)$ for Me_3As, which occurs in addition to the usual $L(p\sigma) \rightarrow Ni(d\sigma)$ bonding interaction.

Gas Phase Ion Chemistry of Chloromethanes and Chlorosilanes.

R. D. Kinser, A. H. Moskowitz, M. de Angelis and D. P. Ridge
Department of Chemistry
University of Delaware
Newark, Delaware 19711

Conventional ion cyclotron resonance techniques were utilized in this investigation of the effects of multiple chlorine substitution on Group IVA centers. Species studied included CH_2Cl_2, $CHCl_3$, CCl_4, SiH_2Cl_2, $SiHCl_3$, and $SiCl_4$.

Of the various ion molecule reactions observed in these systems, the one most indicative of substituent effects was the reaction of the protonated parent with the parent neutral to form a chloronium ion and eliminate HCl:

$$CH_2Cl_2H^+ + CH_2Cl_2 \longrightarrow (CH_2Cl)_2Cl^+ + HCl \qquad (I)$$

$$SiH_mCl_{4-m}H^+ + SiH_mCl_{4-m} \longrightarrow (SiH_mCl_{3-m})_2Cl^+ + HCl \qquad (II)$$

$$m = 0,1,2$$

An analogous reaction has been reported for methyl chloride (1). Analysis of double resonance results indicate that the chlorine in the neutral product comes randomly from either the ionic or neutral reactant in reactions of CH_3ClH^+ (1). The chlorine lost in reactions of multichlorinated ions, however, comes exclusively from the ionic reactant. A mechanism consistent with these results begins with attack on the charge bearing site of the ion, which is the proton in CH_3ClH^+, but carbon or silicon in the multi-chlorinated species.

A series of metathesis reactions were observed in mixtures of methyl fluoride and $SiCl_4$ and its Group IVB analog, $TiCl_4$. The net result of these reactions was the substitution of a fluorine for a chlorine on the reactant ion:

$$SiCl_3^+ + CH_3F \longrightarrow SiCl_2F^+ + CH_3Cl \qquad (III)$$

Multiply chlorinated species successively substitute fluorines for chlorines. Absence of analogs to this reaction or its reverse in chloromethyl systems suggests the presence of an intermediate which is inaccessible to carbon for electronic or steric reasons.

The proton affinities of CH_2Cl_2, SiH_2Cl_2, $SiHCl_3$, and $SiCl_4$ were determined by standard bracketing techniques. The chlorosilanes are seen to decrease in basicity with increasing chlorine substitution. The proton affinities of these compounds and of the reference bases used are shown in Tables I and II. The gas phase basicity of chloroform and carbon tetrachloride cannot be directly determined by these techniques. The observed reactions, available ΔH_f data, and the behavior of the other chloromethanes suggest the following limits:

$$160 \text{ Kcal/mole} < PA(CHCl_3),\ PA(CCl_4) < 170 \text{ Kcal/mole}.$$

Full details of this work will be published elsewhere.

We gratefully acknowledge Dr. T. Swanson of Union Carbide, Linde Division for the gift of the dichlorosilane.

Table I.

Species	PA (Kcal/mole)	Reference
CH_4	127	2
CH_3F	150	1
SO_2	155 ± 5	3
CH_3Cl	160	1
CH_2Cl_2	160 ± 2	this work
C_2H_4	160	4

Table II.

Species	PA (Kcal/mole)	Reference
CH_3F	150	1
SO_2	155 ± 5	3
$SiCl_4$	156 ± 4	this work
$(CF_3)_2CO$	157 ± 2	3
$SiHCl_3$	157 ± 2	this work
SiH_2Cl_2	158 ± 2	this work
C_2H_4	160	4

References:

1. J. L. Beauchamp, D. Holtz, S. D. Woodgate, and S. L. Patt, J. Am. Chem. Soc., 94, 2798 (1972).

2. W. A. Chupka and J. Berkowitz, J. Chem. Phys., 54, 4256 (1971).

3. D. Smith, Ph.D. thesis, University of Delaware, Newark, Delaware, 1976.

4. F. P. Lossing and G. P. Semelnk, Can. J. Chem., 48, 955 (1970).

Photochemistry of Weakly Bound Li^+ Complexes in the Gas Phase. A Novel Probe of Charge Distribution and Acid-Base Properties of Excited Electronic States. B. S. FREISER, R. H. STALEY, and J. L. BEAUCHAMP, California Institute of Technology, Dept. of Chem., Pasadena, California 91125

Information relating to electron distributions and acid-base properties of excited electonic states in the gas phase is derived from a comparison of excitation energies of the Li^+ complex of an n-donor base with the absorption spectrum of the corresponding neutral. Excitation energies for the Li^+ complexes are extracted from photodissociation spectra obtained using the methods of ion cyclotron resonance spectroscopy. As specific examples, the gas phase photodissociation spectra of Li^+ complexes with benzaldehyde, nitrobenzene, cyanobenzene, and aniline in the wavelength region 200-400 nm are reported and analyzed.

Ion-Molecule Reactions in Systems of Metal Carbonyls with Alkyl Halides and Alcohols - An ICR Study

J. Allison and D. P. Ridge
Department of Chemistry
University of Delaware
Newark, Delaware 19711

Reactions of alkali and transition metal ions with alkyl halides in the gas phase have been reported.[1,2] Table I indicates branching ratios for the reactions of a number of metal ions with methyl iodide. Reactions in systems of metal carbonyls and alkyl halides give insights into the mechanism through which these products are formed. An ion analogous to the intermediate in the reactions shown in Table I (Reactions (1) and (2)) can be formed as shown in (3). Further reactions (4) of the product of (3) indicate that $FeCH_3I^+$ exists as $I-\overset{+}{F}e-CH_3$ - the metal inserts into the C-X bond.

$$FeCO^+ + CH_3I \longrightarrow FeCH_3I^+ + CO \qquad (3)$$

$$FeCH_3I^+ + CD_3I \longrightarrow FeICD_3I^+ + CD_3 \qquad (4)$$

When β-H atoms are available, reactions of the type (5) are observed.

$$M^+ + RX \longrightarrow \begin{cases} MR^+ + X \\ MX^+ + R \\ MHX^+ + (R-H) \\ M(R-H)^+ + HX \end{cases} \qquad (5)$$

When RX is d^3-ethyl iodide, we see elimination of both HI and DI. The mechanism implyed is shown in (6). The metal inserts into the C-X bond. A D-atom shifts onto the metal. A dynamic situation exists between the D and the ethylene, resulting in DI as well as HI loss.

$$\begin{array}{l} Co^+ + CD_3CH_2I \rightarrow \left[\begin{array}{l} CD_3CH_2\overset{+}{-}Co-I \leftrightarrow \begin{array}{c} CH_2 \quad D \\ \| \quad\;\; | \\ CD_2 \quad Co-I \\ \quad\;\; + \end{array} \\ \qquad\qquad\qquad\qquad \downarrow \\ (CHDCD_2)Co^+ + HI \leftarrow \begin{array}{c} CHD \quad H \\ \| \quad\;\; | \\ CD_2 \quad Co-I \\ \quad\;\; + \end{array} \leftarrow CH_2D-CD_2\overset{+}{-}Co-I \end{array} \right] \rightarrow CH_2CD_2Co^+ + DI \end{array} \qquad (6)$$

This mechanism of metal insertion followed by H migration is consistent with reactions of metal ions and alcohols. Reactions of metal ions with bifunctional compounds (7) also are consistent with this mechanism, and are of use in obtaining thermodynamic data on interesting metal containing gas phase species.

$$Fe^+ + CH_2ClCH_2Br \rightarrow \begin{cases} FeCl^+ + C_2H_4Br & 17\% \\ FeBr^+ + C_2H_4Cl & 11\% \\ FeClBr^+ + C_2H_4 & 20\% \\ FeCl + C_2H_4Br^+ & 26\% \\ FeBr + C_2H_4Cl^+ & 26\% \end{cases} \quad (7)$$

[1] R. H. Staley, J. L. Beauchamp, J. Am. Chem. Soc., 97, 5920 (1975).

[2] J. Allison, D. P. Ridge, J. Organomet. Chem., 99, C11 (1975).

Table I.

		Li	Cr	Fe	Co	Ni	Hg	
$M^+ + CH_3I \rightarrow$	$MCH_3^+ + I$	--	0%	52%	27%	0%	0%	(1)
	$MI^+ + CH_3$	--	100%	48%	73%	100%	100%	(2)

GAS CHROMATOGRAPHY-MASS SPECTROMETRY OF BORONATE ESTERS OF SPHINGOSINES AND RELATED COMPOUNDS

S. J. Gaskell and C. J. W. Brooks
Department of Chemistry, The University,
Glasgow G12 8QQ, Scotland.

The 2-amino-1,3-diol and 2-amido-1,3-diol systems of sphingosines and ceramides, respectively, are suited to the formation of cyclic boronate esters (Ia,b,e). Such derivatives possess satisfactory GC properties,[1,2,3] which for the sphingosines are improved by a second derivatisation step to effect protection of the NH_2 group (Ic,f,g).

Salient features of the EI mass spectra of boronates of sphingosines and related compounds are shown in the Table. Ions arising by fragmentation of, and adjacent to, the boronate ring are designated as shown in Fig. 1. The abundance of the molecular ion in the spectrum of sphinganine methaneboronate contrasts with the very low intensities of the molecular ions in the EI mass spectra of the corresponding bis-OTMS[4] and N-acetyl bis-OTMS[5] derivatives. The spectrum of 4-sphingenine methaneboronate includes ions, m/e 225 (0.5%) and m/e 208 (0.3%), for which accurate mass determinations (AEI MS9) indicate the elemental compositions $C_{15}H_{31}N$ (calc.: 225.2456; found 225.2454) and $C_{15}H_{28}$ (calc.: 208.2191; found 208.2191), respectively. Metastable ions are observed for the transitions 323 → 225 → 208. The ions are attributed to loss of the boronate ring, with NH_2 migration to the hydrocarbon fragment, and subsequent loss of NH_3.

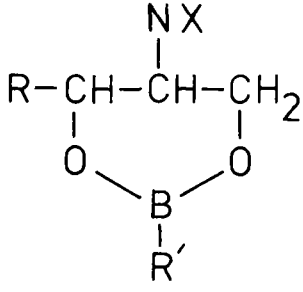

	X	R	R'
Ia	H_2	$C_{15}H_{31}$	CH_3
b	H_2	$C_{15}H_{29}$	CH_3
c	H, CH_3CO	$C_{15}H_{31}$	CH_3
d	H, C^2H_3CO	$C_{15}H_{31}$	CH_3
e	H, $C_{15}H_{31}CO$	$C_{15}H_{31}$	CH_3
f	$=C(CH_3)_2$	$C_{15}H_{31}$	C_6H_5
g	$=CHN(CH_3)_2$	$C_{15}H_{31}$	C_6H_5

Fig. 1. Fragmentations of sphingosine boronates and related compounds under electron-impact (cf. ref. 3).

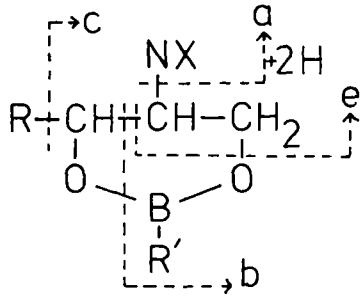

The intensities of molecular ions in the EI spectra of N-substituted sphingosine boronates are lower than that observed for sphinganine methaneboronate (Table). Quasi-molecular ions (M+1), however, constitute the base peaks in the isobutane CI spectra of all examples studied.

A bis-methaneboronate of phytosphingosine has been prepared. The probable structure and major modes of fragmentation under EI are as follows:

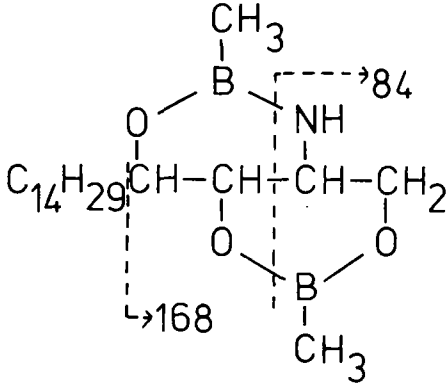

m/e	rel. intens.
365($M^{+\cdot}$)	8%
168	35%
84	100%

A full account of this work, which was supported by the Medical Research Council and the Science Research Council, will be published. We thank Dr. A. McCormick (A.W.R.E., Aldermaston) for high resolution mass measurements.

REFERENCES

1. S. J. Gaskell, C. G. Edmonds and C. J. W. Brooks, Anal. Lett., 9 (1976) 325.
2. S. J. Gaskell and C. J. W. Brooks, J. Chromatogr., 122 (1976) 415.
3. S. J. Gaskell, C. G. Edmonds and C. J. W. Brooks, J. Chromatogr., In press.
4. K.-A. Karlsson, Acta Chem. Scand., 19 (1965) 2425.
5. R. C. Gaver and C. C. Sweeley, J. Amer. Oil Chemists' Soc., 42 (1965) 294.

Table Electron-impact (70eV) mass spectrometric data for cyclic boronate derivatives of sphingosines and related compounds

Compound	EI mass spectrum						
	$M^{+\cdot}$	Base peak	Fragment ions : m/e (rel. intens.)*				
	m/e (rel. intens.)	m/e	$[M-R]^+$	a**	b	c	e
sphinganine methaneboronate (Ia)	325(40)++	43	310(1)	-	85(10) 84(11)+	114(2)	43(100)
4-sphingenine methaneboronate (Ib)	323(0.5)	43	308(0.1)	-	85(11) 84(13)+	-	43(100)
N-acetyl sphinganine methaneboronate (Ic)	367(2)	85	352(8)	60(60)	127(82)	156(3)	85(100)
N-[$^2H_3$]-acetyl sphinganine methaneboronate (Id)	370(2)	130	355(8)	63(70)	130(100)	159(3)	88(96)
N-palmitoyl sphinganine methaneboronate (Ie)	563(1)	256	548(13)	256(100)	323(9)	352(7)	281(2)
sphinganine benzeneboronate acetone Schiff base (If)	427(2)	58	412(3)	58(100)	187(29)	216(10)	83(47)
sphinganine benzeneboronate, N-dimethyl aminomethylene (Ig)	442(15)	98	365(87)	73(90)	201(43)+	231(13)	98(100)

* Fragmentation modes designated in Fig. 1. (cf. ref. 3)

** Fragmentation accompanied by double hydrogen migration to charge-retaining fragment

\+ Fragmentation accompanied by hydrogen loss from charge-retaining fragment

++ Becomes base peak if ions below m/e 50 are disregarded

GC-MS of Methylated Steroids

André L.C. Smit, Ad P. de Jong and Piet A. Leclercq

Laboratory of Instrumental Analysis

Eindhoven University of Technology

Eindhoven, The Netherlands 4500

In the gas chromotographic analysis of steroids, trimethyl silyl (TMS) derivatives are widely used. Methylation of steroids yields derivatives whose gas chromatographic properties compare favorably to TMS ethers. Methyl derivatives show an increased volatility, less sensitivity to hydrolysis, and excellent gas chromatographic and mass spectrometric behavior as described below.

For the permethylation of the steroids we used methylsulfinylcarbanion as base and methyliodide as methylating reagent. (1) With 17-keto steroids overmethylation occurs; the acidic protons at the C-16 carbon atom are both replaced by a methyl group. This overmethylation is quantitative if at least 5-fold excess of reagents is used.

The gain in volatility of the methyl derivatives over the TMS ethers is demonstrated in the following table:

Steroids	Kovats' Retention Indices	
	Me Derivatives	TMS Derivatives
Androstenediol	2425	2628
Etiocholanolone	2452	2498
Dehydroandrosterone	2457	
Androsterone	2468	2483
Dehydroepiandrosterone	2488	2551
Epiandrosterone	2502	
11 β-hydroxyetiocholanolone	2527	2700
Androstenetriol	2542	2873
11 β-hydroxyandrosterone	2547	

Fragmentation of permethylated steroids upon electron ionization is not directed from the methoxy groups because, unlike silyl ethers, the positive charge does not reside in the functional groups, but elsewhere in the molecule. As a result EI mass spectra of these methylated derivatives generally contain more information in the high mass region than the spectra of TMS ethers. The mass spectral fragmentation of the permethyl 17-keto steroids is very characteristic and leads to the formation of structually significant ions, by D-ring cleavage, by the loss of CH_3OH and $CH_3^{\cdot}$, or by combinations thereof. All spectra contain intense molecular ions.

Besides the steroids mentioned in the table we also succeeded in methylating the following steroids: 5β-pregnane-3α,20α-diol, 5α-pregnane-3α,20α-diol, estradiol-17β, estriol and the anabolic drug Demalon (1α,17α-dimethyl-17β-hydroxy-5α-androstan-3-one).

1) P.A. Leclercq, Biomed. Mass Spectrom., 1, 109 (1974).

Mass Spectrometric Studies of a New Mechanism of Drug Biotransformation in Rats.

Isamu Matsumoto, Tomiko Kuhara, Yoshito Inoue
and Shin-ichi Haraguchi
Kurume Univ., Sch. of Med., Kurume, Fukuoka 830, Japan

Applications of combined gas chromatography-mass spectrometry to the study of drug metabolism, offer remarkable advantages and have brought new aspects of drug biotransformation. In recent years we isolated a new metabolite of Mephenesin, 3-o-tolyloxy-1,2-propanediol, in rats and identified as N-acetyl-β-(o-tolyloxy)alanine by low and high resolution-mass spectrometries. As expected, from its estimated structure, acid hydrolysis of the metabolite yielded an aromatic amino acid, β-(o-tolyloxy)alanine not an aromatic carboxylic acid. Accordingly a new metabolic conversions involving introduction of nitrogen not due to conjugation with an amino acid in drug metabolism were demonstrated.

In order to investigate whether or not the new drug alteration is limited on this drug, we studied the metabolism of two Mephenesin analogues; 3-(p-tolyloxy)-1,2-propanediol and 3-phenoxy-1,2-propanediol. One group of male Wister albino rats were administered 150 mg per Kg body weight of 3-(p-tolyloxy)-1,2-propanediol and the other group of rats were given 150 mg per Kg body weight of 3-phenoxy-1,2-propanediol. After solvent extraction of the ruinary acids and trimethylsilylation with BSA and TMCS, the sample was analyzed by GC-MS.

The expected metabolite were found to exist. Fig. 1 and Fig. 2 show the mass spectra of the trimethylsilylated metabolites. These mass spectra were very similar to that of N-acetylphenylalanine derivatized with BSA and TMCS. The very intense peak occured at m/e 274 which was formed by the loss of aryloxy radical from the molecular ion. The removal of an aryloxymethyl radical from the molecular ion gave a peak at m/e 260. Characteristic fragmentation of N-acetyl compounds is elimination of ketene and this process produced the fragment at m/e 218 from the ion at m/e 260.

As we identified N-acetyl-β-(p-tolyloxy)alanine and N-acetyl-β-phenoxyalanine respectively as the metabolic products of 3-(p-tolyloxy)-1,2-propanediol and 3-phenoxy-1,2-propanediol in the urine of rats, we propose the new metabolic pathway which consists of preliminary oxidations, transamination and N-acetylation for the formation of the metabolites.

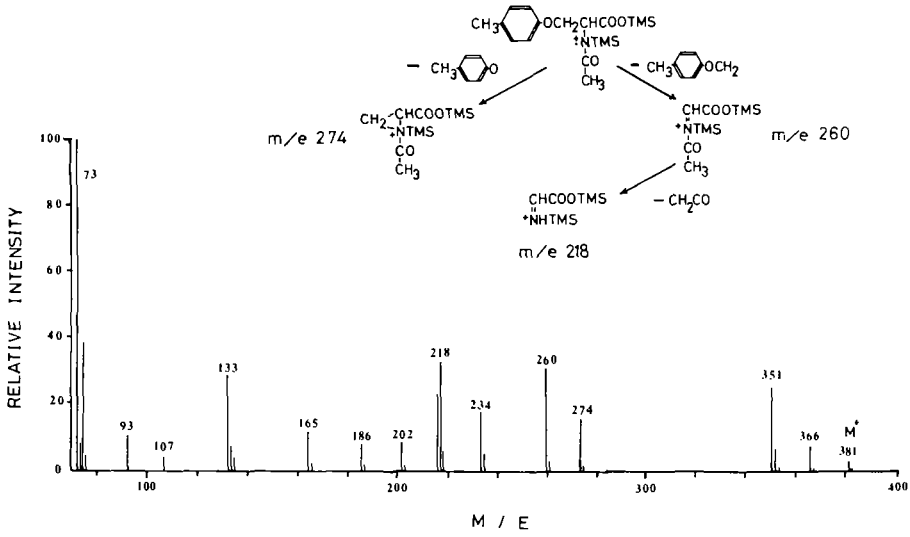

Fig. 1. The mass spectrum of the unknown metabolite from 3-(p-tolyloxy)-1,2-propanediol-treated rats.

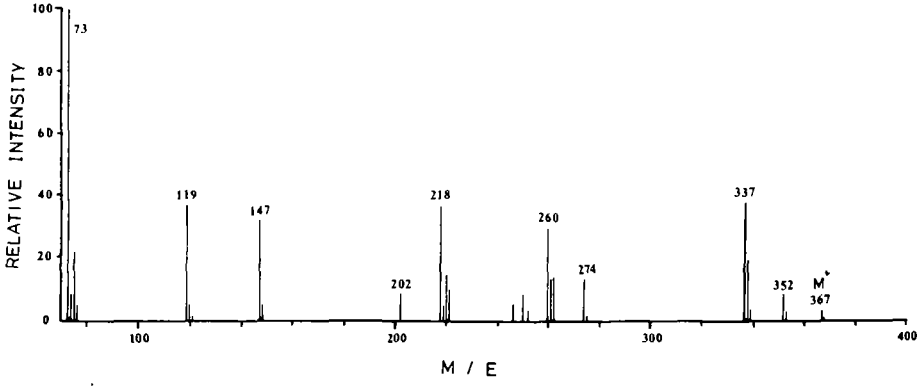

Fig. 2. The mass spectra of the unknown metabolite from 3-phenoxy-1,2-propanediol-treated rats.

The details of this work will be published in the near future.

Studies of Novel Dipeptide Derivatives with GC-MS

H. Frank, K. D. Haegele and D. M. Desiderio, Institute for Lipid Research, Baylor College of Medicine, Houston, Texas 77030

The applicability of dipeptidylaminopeptidases for sequence determination of peptides depends upon feasibility of separation and identification of the large number of possible resulting dipeptides. However, with none of the generally used derivatives can complete separation of all 400 dipeptides by GC be expected.

N-Acetylacetonyl dipeptide methyl esters (1,2,3) produce generally simple E.I.-mass spectra, which allows identification of dipeptides in a complex mixture, even if they are not totally resolved from each other by GC. An ion always present arises from cleavage between C_α and the carboxamide group of the N-terminal amino acid with retention of the charge at the N-terminal fragment (fragment A^+). The high intensity of this peak (in most cases 20-80% of the total ion current Σ) may be caused by a sterically favored six-membered transition state which may result in formation of a stable cyclic ether. The competing fragmentation, loss of the side chain of the N-terminal amino acid, is observed in all cases, however with a much lower intensity. The molecular ion is very intense compared to TFA-dipeptide methylesters.

According to their mass spectra, dipeptides are divided into three groups: (1) dipeptides containing N-terminal Ala, Gly, Glu, Ile, Leu, Phe, Ser, Thr or Val with fragment A^+ as the base peak and the molecular ion as second most abundant peak; (2) dipeptides containing N-terminal Arg, Asn, Gln, His, Met or Pro with fragment A^+ as base peak and one or more ions of high abundance originating from the side chain; (3) dipeptides with N-terminal Asp, Tyr or Trp or C-terminal His or Trp with mass spectra characteristic for the particular amino acid.

Accordingly a dipeptide is identified by (1) the base peak determining the N-terminal amino acid (except when His or Trp is C-terminal) and (2) the mass difference between base peak and molecular ion determining the C-terminal amino acid. All constituents of a mixture of 22 N-acetylacetonyl dipeptide methyl esters, separated on a GC column of 1% SE-30 on Gas Chrom Q (100-120 mesh), are identified. From all GC phases investigated (SE-30, OV-1, OV-3, OV-17, PZ-175) SE-30 has the lowest retention times.

As anticipated, N-trifluoroacetylacetonyl and N-hexafluoroacetylacetonyl derivatives have lower retention times, but their GC properties are not good: In both cases very broad, tailing peaks are obtained. Only for conversion of arginine-residues to the corresponding N^δ-pyrimidyl ornithine derivative is trifluoroacetylacetone advantageous, since the molecular ion is more intense compared to the 2,4-dimethylpyrimidine derivative.

Optimal conditions for complete derivatization of dipeptides are: (a) reaction of the dipeptide, dissolved in 2 equivalents of 0.1 N N-methylmorpholine in methanol, with acetylacetone at 100°C for 2 hours; (b) esterification with diazomethane in methylene chloride/methanol (1:1); (c) etherification of hydroxyl groups with hexamethyldisilazane in pyridine for 20 minutes at 90°.

References:

(1) R. A. Day, H. Falter, J. P. Lehmann and R. E. Hamilton, J. Org. Chem. 38, 782 (1973).

(2) G. M. Schier, P. D. Bolton and B. Halpern, Biomed. Mass Spectrom., 3, 32 (1976).

(3) H. Frank, K. D. Haegele and D. M. Desiderio, submitted for publication.

Quantitative Analysis of Biological Samples Using HPLC-MS Techniques.*

PAUL L. GUTSHALL, PAUL J. BRYANT, JIMMIE L. VALENTINE, OWEN H. M. GAN and HSIEN CHI NIU, University of Mo., Kansas City, Mo. 64110

A quantitative assay technology employing high performance liquid chromatography (HPLC) mass spectrometry (MS) has been developed and applied to determine drug levels in biological samples. A deterium labeled, stable isotope, of the drug is used as an internal standard. HPLC is employed for separation. Effluent droplets are dried and introduced to a mass spectrometer via a direct insertion probe. Quantitation is accomplished by rationing the molecular ion intensity to the isotopic standard. Ion counting is employed to obtain sensitivity values in the low nanogram per milliliter range. Experimental results from assays of human plasma, breath and saliva will be presented.

*Supported by the National Highway Traffic Safety Administration, Dept. of Transportation, under Contract No. DOT-HS-4-00968.

POLYPEPTIDE SEQUENCING USING LIQUID CHROMATOGRAPHY/MASS SPECTROMETRY

Bobby G. Dawkins, F. W. McLafferty, and Rengachari Venkataraghavan

Cornell University, Department of Chemistry, Ithaca, New York 14853

The liquid chromatograph/mass spectrometer/computer system described earlier[1] is the key part of a proposed scheme for automated sequencing of polypeptides. Conventional techniques for polypeptide degradation yield complex mixtures of oligopeptides which are derivatized, separated by LC, and continuously introduced into the MS. Direct chemical ionization of the solution gives complete sequence information on samples of a few nanomoles. A dedicated computer handles automated data acquisition, reduction, sequencing, and overlapping. Development of a micro LC column requiring a solvent flow rate of only 10^{-2} ml/min would make possible the automated sequencing of polypeptides in low picomole quantities.[2]

[1] F. W. McLafferty, R. Knutti, R. Venkataraghavan, P. J. Arpino, and B. G. Dawkins, Anal. Chem., 47, 1503 (1975).

[2] F. W. McLafferty and B. G. Dawkins, Biochem. Soc. Trans., 3, 856 (1975).

Mass Spectrometric Analysis of Anticonvulsant and Related Drugs After Separation by High Pressure Liquid Chromatography.

SHEN-NAN LIN, E. C. HORNING and M. G. HORNING, Institute for Lipid Research, Baylor College of Medicine, Houston, Texas 77025.

The estimation of anticonvulsant and related drugs in plasma or saliva in instances where the daily dosage is low requires high sensitivity and selectivity in detection. High pressure liquid chromatography is under investigation as a means of obtaining partially purified fractions for analysis. Direct injection in solution is possible with API techniques. Analysis by GC-MS-COM methods (CI mode) can also be used.

IDENTIFICATION OF LIQUID CHROMATOGRAPHY EFFLUENTS BY MASS SPECTROMETRY

by

Robert P. Lattimer, Kenneth R. Welch and Jerry B. Pausch

The B.F.Goodrich R & D Center
Brecksville, OH 44141

High performance liquid chromatography (HPLC) has proven to be an extremely valuable tool for many separations involving polymers and polymer chemicals. Single wavelength ultraviolet spectroscopy and differential refractometry are the techniques commonly used for the detection of effluents from the liquid chromatograph. While these are generally good for quantitative analysis of eluted samples, they provide little or no information on the chemical identity of effluents. It is generally recognized that the mass spectrometer holds the best chance for qualitative identification of LC effluents, and several elegant methods have been proposed and demonstrated to directly couple the mass spectrometer and liquid chromatograph. It seems apparent that it may not be too long before a commercial LC-MS interface becomes available, but it is not certain at this point which technique or techniques may ultimately prove to be the most feasible.

An interim technique has been developed in our laboratory that has been useful in several instances for trapping and identifying LC effluent peaks at the microgram level using the mass spectrometer. We have not seen this method in the literature. We have, of course, used the simple evaporation of solvent method to do some analyses. Some successes and some failures have been experienced with both evaporation of solvent and the method that will be described here.

Our trapping method uses a small capillary tube about 15 mm long and 1 mm inside diameter, and restricted slightly at one end. The tube size is such that it will fit into the solids probe of our mass spectrometer. A small plug of glass wool is forced into one end of the tube and the tube is then filled with a suitable porous silica packing such as is used in HPLC. A second small plug of glass wool is then forced into the open end of the tube to hold the packing.

Collections of effluent from the LC are then made using the packed tubes. The exit from the LC is fitted with a flexible 1/8" plastic tube to receive the packed capillary. The LC effluent is allowed to flow through the packed tube when one desires to trap a sample. Next the tube is allowed to air dry or is flushed with helium. Then the tube is fitted into the probe of the mass spec in the normal manner used for solid samples. Residual solvent is removed by the forepump before insertion into the source. The probe is then heated at near its maximum rate to drive off the LC effluent as quickly as possible. Spectra are recorded by oscillographic trace.

N,N'-diphenyl-p-phenylenediamine (DPPD), a common rubber antioxidant, was chosen for initial trials using the method. The material

gives a good mass spectrum with the molecular ion (m/e 260) as the base peak with little fragmentation. Several packing materials were tried. Twenty µg of DPPD in 2:1 methylene chloride/isooctane solvent were injected into the LC and then the effluent trapped on the packed tubes. The reverse-phase packing C_{18} on Porasil B was the only packing that was at all effective, giving a good signal/noise ratio of 900 on the base peak. As low as 0.1 µg DPPD gave a signal-to-noise (S/N) ratio of about 24. This doesn't sound very outstanding, but it is near the limit of sensitivity on our mass spectrometer, the P-E 270. The method is obviously not quantitative, but this is unimportant for chemical identification purposes. It is to be expected that with selective ion detection on a computerized mass spectrometer that greater sensitivity could be obtained. We were able to test this through the compliments of Hewlett-Packard, who ran one of our tubes on which a 0.1 µg DPPD sample had been trapped. The ion at m/e 260 was monitored on the HP 5982A system at Palo Alto, and the ion was very easily observed.

A second test compound studied was 2,2,4-trimethyl-1,2-dihydroquinoline (TMDQ). The mass spectrum shows a base peak at m/e 158 and a molecular ion (m/e 173) about 14 times weaker than the base peak. The trapping data showed a good S/N ratio for a one µg LC injection of TMDQ. This was for the molecular ion, so that one could go to a much lower quantity of TMDQ and still observe the base peak (m/e 158) with reasonable intensity. This the C_{18}/Porasil trapping was at least as effective for TMDQ as it was for DPPD.

One difficulty with the technique will be pointed out. That is the decomposition of some samples prior to evaporation into the mass spectrometer source. One example of this is the dimer of TMDQ. The mass spectrum of this compound shows a molecular ion at m/e 346 and the base peak at 331. After trapping on C_{18}/Porasil B, the spectrum showed a molecular ion at m/e 330 and a base peak at 315. The TMDQ dimer had lost a methane moiety to form the more stable quinoline structure which is called the demethylated TMDQ dimer. This sort of decomposition is probably due to acidity on the packing and perhaps partially due to the elevated temperature of the probe. Similar phenomena have been observed in a few other cases, usually with polymeric materials.

In summary the Porasil trapping technique has been found to be easier and faster than the traditional evaporation of solvent method. The sensitivity obtained is generally comparable to that of the UV detector on the LC, and the technique is not dependent on the LC solvent system used. Disadvantages are that the trapping is not quantitative, and the efficiency of trapping is dependent on the compound used. And finally decomposition is sometimes a problem, especially with polymeric materials.

Spectral Analysis of Coal-Derived Fuels: An Overview.

A. G. SHARKEY, JR.,
Pittsburgh Energy Research Center/ERDA
Pittsburgh, PA 15213

The development of processes for coal gasification, liquefaction, and solvent refined coal have presented new problems for the analyst. Petroleum and coal-derived liquid fuels differ in several respects and in many instances mass spectrometric techniques developed for petroleum products cannot be applied directly to coal-derived oils. Coal-derived oils are highly aromatic and in many instances have high concentrations of heteroatom species. A resume will be given of the process streams from current fossil energy processes to produce substitute gaseous and liquid fuels from coal. Data will be present for the feed coal, gaseous and liquid products, tars, and process waters. Problems of environmental concern, including the disposition of trace elements from coal gasification will be discussed. Analyses relevant to the possible carcinogens in coal-derived liquid fuels will be described.

Field Ionization-Field Desorption Determination of Molecular Weight Profiles of Coal Liquefaction Products, M. Anbar, E. Kempster, M. Scolnick and G. St. John, Stanford Research Institute, Mass Spectrometry Research Center, Menlo Park, CA 94025

Field ionization mass spectrometry, which produces fragmentation-free mass spectra, is being applied to the analysis of coal liquefaction products. Using a new highly efficient and sturdy field ionization source, samples of various coal liquefaction products have been successfully analyzed by the integrating multiscan technique.[1] A novel activated tungsten foil slit type field ionization source[2] shown in Figure 1 has been used. This source is superior to the now classical SRI multipoint source because of its insensitivity to deactivation in the presence of oxygen-, sulphur-, or halogen-carrying compounds. The new source comprises a tungsten foil on which carbonaceous dendrites are deposited from pyridine vapor at high temperature under high electrostatic fields.[2] The activated foil is mounted on a wedge-shaped hollow support, together with an auxiliary steel foil which directs the flow of the analyzed sample to the ionizing region.

The mass range of interest can be scanned repeatedly and synchronized with a 4096 channel multiscaler which integrates the spectra produced in each scan into a composite mass spectrum.[1] The integration over time is necessary since the sample is evaporated slowly and the composition of the vapor phase over it changes owing to the wide range of volatility of the different components. The detector is an electron multiplier operated in the pulse mode, the pulse rate of which is monitored with a pulse-rate meter in parallel to the pulses individually accumulated by the multiscaler. The sample is introduced in a heatable probe which is programmed manually or automatically according to the count rate obtained from the detector. This arrangement allows controlled evaporation of the analyzed sample into the field ionization source. This is continued until the sample is exhausted, or until no more ions are observed at the maximum temperature setting of the probe (e.g., 400°C).

The resolution of the mass spectrometer itself is 1600, but it deteriorates to about 800 due to the slight instabilities in the electronic circuitry during the 2 to 4 hours which are required to obtain a molecular weight profile of a complex coal liquefaction product. The resolution and reproducibility of the present system, when scanning over a wide mass range, is also limited by the limited number of channels available on the multichannel analyzer. These shortcomings of the present system are being overcome by interfacing the system with a PDP-11/10 minicomputer.

The molecular weight profile of an H coal product (fuel oil mode) is presented in Figure 2. The absence of any pyrolytic breakdown during the analysis is well demonstrated. Figure 3

shows a molecular weight profile of a fraction of H coal product produced in the syncrude mode. This fraction was eluted from a silica gel column by THF after removal of the hexane- and benzene-soluble components.

Figure 4 shows the molecular weight profile of the hexane extract from an SRC product. Figure 5 is a logrithmic display of the same spectrum presented in Figure 4. The interesting feature of this presentation is the observation that the abundance of the high molecular weight constituents declines linearly on the log display, indicating an exponential decline with molecular weight with no apparent cut-off up to mass 1100.

Figure 6 presents a molecular weight spectrum of the volatile fraction of SRC preasphaltenes. This spectrum is similar to the H coal syncrude preasphaltene fraction (Figure 3), although it is somewhat more volatile.

The molecular weight profiles of the different coal liquefaction products demonstrate one feature in common, namely a very high complexity. Even crude oil (Figure 7) has a relatively much simpler molecular weight spectrum in which homologous families of aliphatic, olefinic and aromatic compounds can be readily identified.

Of the SRC coal liquefaction products, the hexane extracts (the "coal oil") or the vacuum distillates are the fractions most amenable to quantitative field ionization mass spectrometry. On the other hand, preasphaltenes are the least suited for this technique, since only up to 50% of these fractions can be volatilized and mass analyzed.

The molecular weight profile determination is just the first step in the mass spectrometric characterization of coal liquefaction products. The present phase will be followed by the utilization of physical techniques, including collisional fragmentation and evaporation rate-temperature profiling, as well as by chemical procedures - primarily bulk derivatization.

The complete analysis of asphaltenes, and especially preasphaltenes, will become possible once field desorption techniques have been perfected. It is evident, however, that the equally powerful field ionization technique is capable already today of answering many open questions in the research and development of coal liquefaction processes.

References

1. M. E. Scolnick, W. H. Aberth and M. Anbar, Int. J. Mass Spec. Ion Phys. 17, 139 (1975).

2. R. H. Cross, H. L. Brown and M. Anbar, Rev. Sci. Instru., in press.

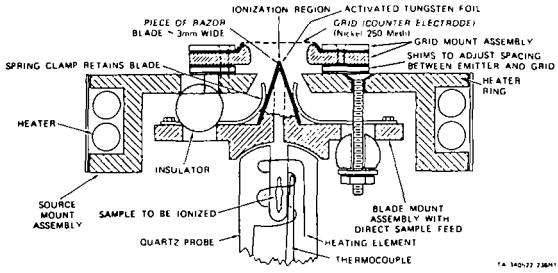

FIGURE 1 SCHEMATIC OF SLIT TYPE FI SOURCE

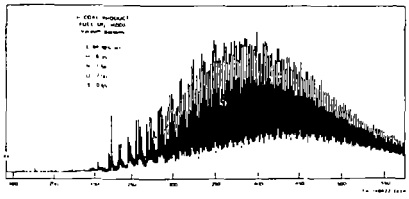

Figure 2

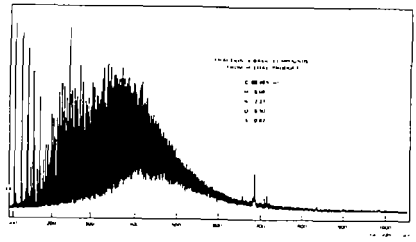

Figure 3

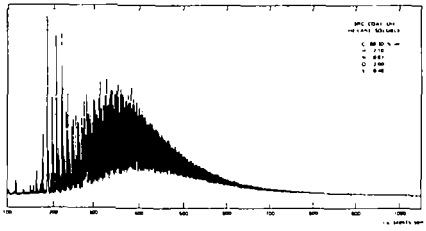

Figure 4

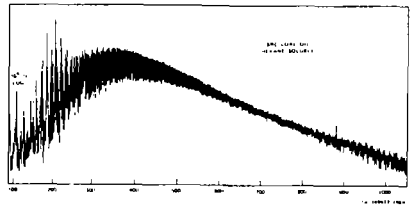

Figure 5

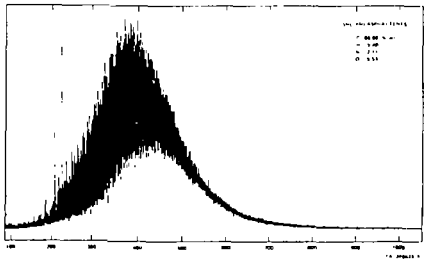

Figure 6

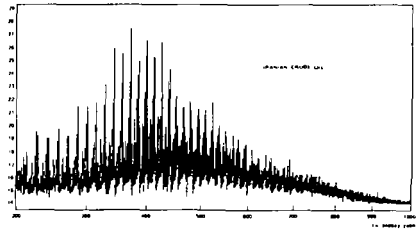

Figure 7

BIOMARKER HYDROCARBON IDENTIFICATIONS IN THE PYROLYSIS OIL OF HIAWATHA COAL USING GC-MS-C

Introduction

Three new $C_{15}H_{26}$ sesquiterpanes along with the usual pentacyclicditerpanes from C_{27}-C_{32} and low levels of the 5-α 5-β steranes from C_{27}-C_{29} were identified in the saturate fraction of the pyrolysis oil from Hiawatha coal. The aromatic fraction of this coal pyrolyzate revealed high concentrations of naphthalenes. Cadalene, $C_{15}H_{18}$, eudalene, $C_{14}H_{16}$, and other closely related diaromatics were identified. Multiple ion detection, MID, and isometric display of GC-MS data are used in this analysis.

Experimental

This work was done using a Hewlett-Packard 5700A gas chromatograph coupled directly to a Nuclide 12-90-G mass spectrometer using a 0.02 ID stainless steel column coated with Dexil 300. An INCOS computer system was used both to collect data and to control the mass spectrometer. The column was programmed from 150°C to 330°C at a rate of 2°C per minute. Data were collected onto a 4700-sector Wangko disk at magnetic scan intervals of 6.5 seconds. One-second intervals were used for MID acquisitions. The samples studied are the saturate and aromatic SiO_2 cuts of the pyrolysis oil from Hiawatha coal taken from King Mine, Hiawatha, Utah.

Results

Saturate Fractions

The saturate fraction is considered first in the study. Table I shows results from a 22-component group-type analysis of the saturate fraction from Hiawatha coal. Figure 1 shows the Alkane-only map of the saturate fraction along with the reconstructed gas chromatogram. The map was obtained by allowing display of the mass chromatograms of only the even mass peaks associated with Alkanes, i.e., 86, 100, 114... C_n C_{2n+2}. The darkened peaks are due to the parent ions of the n-Alkanes from n-C_{13} to n-C_{34}. The remaining array of peaks at low intensity is due to the isoalkane parents, i.e., pristane C_{19}, and to the ^{13}C $C_{n-1}H_{2n+1}$. These kinds of data provide access to molecular weight distribution of the Alkane. Figure 2 is the monocyclic saturates only map of the saturate fraction from Hiawatha coal. A close look at the m/e 83 mass chromatogram suggests two sets of homologous series of

one-ring components. The mass spectra further suggests that these are n-alkyl, 5- and 6-membered ring monocyclics. One of the sets of homologous cyclics elutes just before the corresponding n-Alkane GC peak and the other just after the corresponding n-Alkane peak. Figure 3 entitled the isoprenoid-only map of this fraction, in fact, represents an isometric map of all other possible parent and fragmentations in this fraction with the exceptions of the parent and fragment ions of the Alkanes and the monocyclic Alkanes. Note in Figure 3 that the greatest activity in this map appears between Scans 100 and 400 and 700 and over 1000. These, in fact, are due to the terpanes and steranes present in the sample. Figure 4 shows the mass spectrum of one of these C_{15}-sesquiterpanes identified in this coal. All three sesquiterpanes give similar mass spectra. Figure 5 is an isometric display of the pentacyclicditerpanes only map. Shown are the fragment 191 and the possible parent ions from 370, C_{27} to 454, C_{33}. Their location within the total sample can be determined by looking at the RGC also shown.

Aromatic Fraction

Table II shows the group-type analysis of the aromatic fraction of Hiawatha coal. Note that the monoaromatics and the diaromatics make up over 75% of this fraction. Figure 6 shows the alkylbenzene only map of the aromatic fraction. Revealed in this map is homologous series of alkylbenzenes reminiscent of the homologous series of cyclic components found in the saturate fraction. Mass spectra sugggests that these are n-alkylbenzenes. Figure 7 shows the naphthalene-only map of the aromatic fraction. Cadalene is indicated. The others are naphthalenes at m/e 184 and m/e 170 with some at 156 and 142. The mass spectrum this C_{15}-naphthalene corresponds identically to that of cadalene found in the literature. Coinjection of cadalene confirms the presence of the identification of cadalene. Coinjections of eudalene confirm that there is also small amounts of that compound in Hiawatha coal. Cadalene was first identified in a Loma Novia crude from the Eocene Jackson sands formation of South Texas.*

*J. C. Bendoraitis Advances in Organic Geochemistry ed. B. Tissot, F. Bienner 209, 1973.

TABLE I

HYDROCARBON GROUP TYPE ANALYSIS

SATURATE FRACTION	C(N)H(2N + 2) Paraffins	56.0
	C(N)H(2N) Monocycloparaffins	20.2
	C(N)H(2N - 2) Dicycloparaffins	9.2
	C(N)H(2N - 4) Tricycloparaffins	7.7
	C(N)H(2N - 6) Tetracycloparaffins	0
	C(N)H(2N - 8) Pentacycloparaffins	0
	C(N)H(2N - 10) Hexacycloparaffins	0
	C(N)H(2N - 11) Heptacycloparaffins	0
	Saturates	93.1
	Monoaromatics	
	C(N)H(2N - 6) Alkylbenzenes	3.0
	C(N)H(2N - 8)	0.6
	C(N)H(2N - 10)	0.4
	Diaromatics	
	C(N)H(2N - 12) Naphthalenes	0.6
	C(N)H(2N - 14)	0.4
	C(N)H(2N - 16)	0.4
	Triaromatics	
	C(N)H(2N - 18)	0.3
	C(N)H(2N - 22)	0.4
	Tetraaromatics	
	C(N)H(2N - 24)	0.3
	C(N)H(2N - 28)	0.1
	Aromatics	6.5
	C(N)H(2N - 4)S Thiphenes	0.1
	C(N)H(2N - 10)S Benzothiophenes	0.2
	C(N)H(2N - 16)S Dibenzothiophenes	0.1
	C(N)H(2N - 22)S Naphthabenzothiophenes	0
	Sulfur Compounds	0.5
	Thiphenic Sulfur	0.065
	Carbon	85.62
	Hydrogen	14.32

FIGURE 1

ALKANES ONLY
MAP OF THE SATURATE FRACTION FROM
HIAWATHA COAL

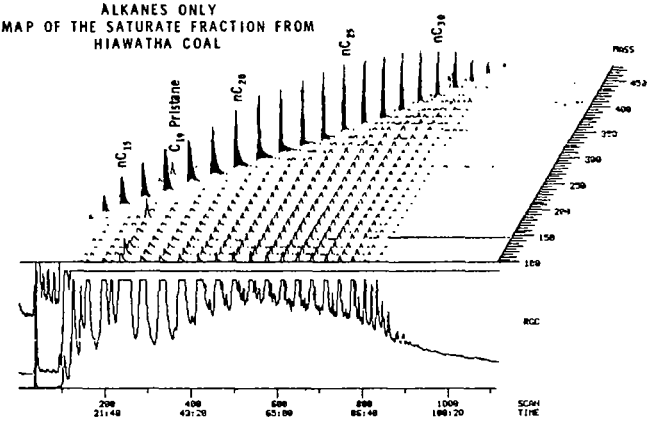

FIGURE 2

MONOCYCLIC SATURATES ONLY
MAP OF THE SATURATE FRACTION FROM
HIAWATHA COAL

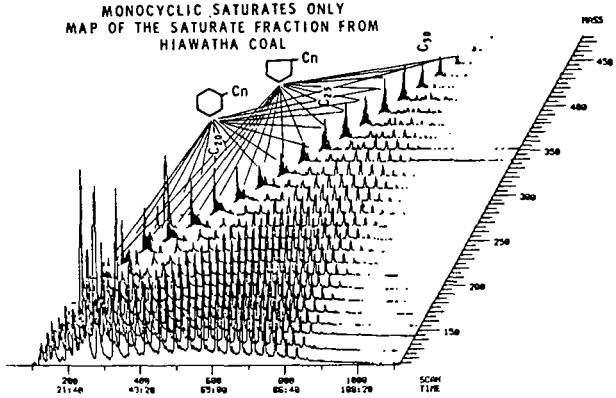

FIGURE 3

ISOPRENOIDS ONLY
MAP OF THE SATURATE FRACTION FROM
HIAWATHA COAL

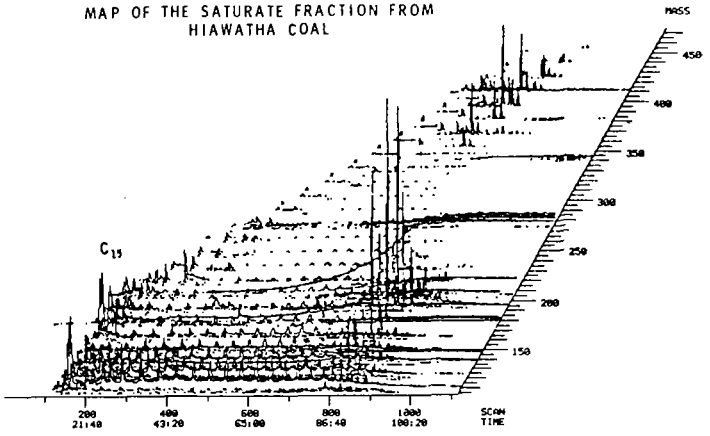

FIGURE 4

SESQUITERPANE B
MASS SPECTRUM

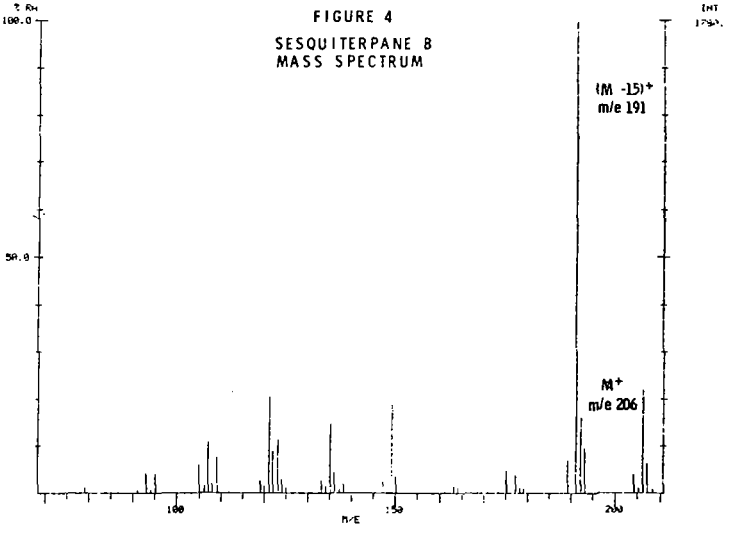

FIGURE 5
TERPANES PARENT AND FRAGMENT IONS MAP

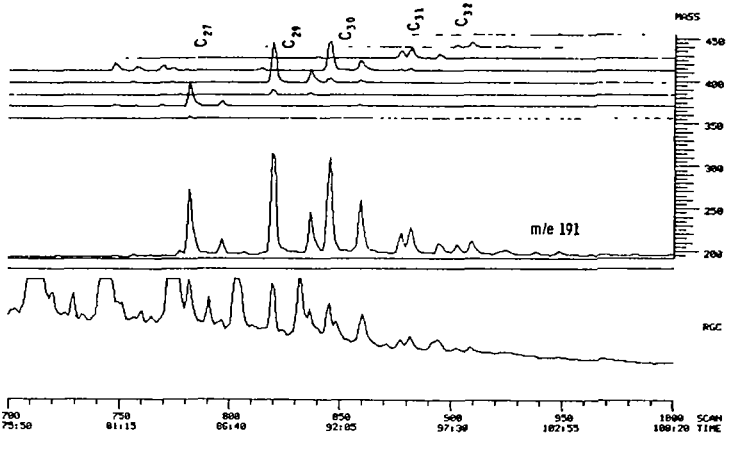

TABLE II

HYDROCARBON GROUP TYPE ANALYSIS

	C(N)H(2N + 2) Paraffins	1.2
	C(N)H(2N) Monocycloparaffins	1.4
	C(N)H(2N - 2) Dicycloparaffins	1.8
	C(N)H(2N - 4) Tricycloparaffins	2.4
	C(N)H(2N - 6) Tetracycloparaffins	0
A	C(N)H(2N - 8) Pentacycloparaffins	0
R	C(N)H(2N - 10) Hexacycloparaffins	0
O	C(N)H(2N - 12) Heptacycloparaffins	0
M	Saturates	6.8
A	Monoaromatics	
T	C(N)H(2N - 6) Alkylbenzenes	10.7
I	C(N)H(2N - 8)	9.8
C	C(N)H(2N - 10)	7.4
F	Diaromatics	
R	C(N)H(2N - 12) Naphthalenes	23.4
A	C(N)H(2N - 14)	11.3
C	C(N)H(2N - 16)	14.2
T	Triaromatics	
I	C(N)H(2N - 18)	5.5
O	C(N)H(2N - 22)	2.7
N	Tetraaromatics	
	C(N)H(2N - 24)	0.9
	C(N)H(2N - 28)	0.2
	Aromatics	86.2
	C(N)H(2N - 4)S Thiophenes	1.7
	C(N)H(2N - 10)S Benzothiophenes	3.6
	C(N)H(2N - 16)S Dibenzothiophenes	1.5
	C(N)H(2N - 22)S Naphthabenzothiphenes	0.2
	Sulfur Compounds	7.0
	Thiophenic Sulfur	0.989
	Carbon	89.23
	Hydrogen	9.78

FIGURE 6

ALKYLBENZENE ONLY MAP HIAWATHA COAL AROMATIC CUT

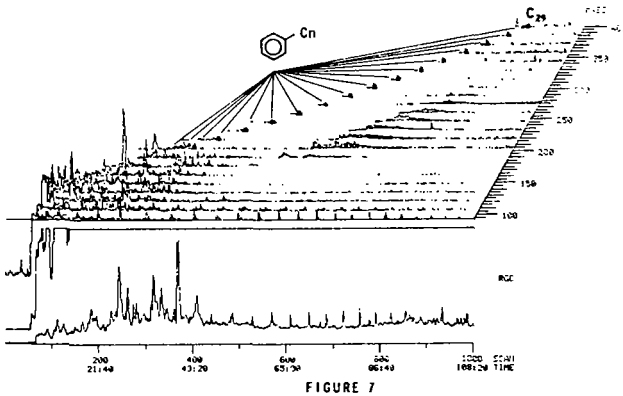

FIGURE 7

NAPHTHALENE ONLY MAP HIAWATHA COAL AROMATIC CUT

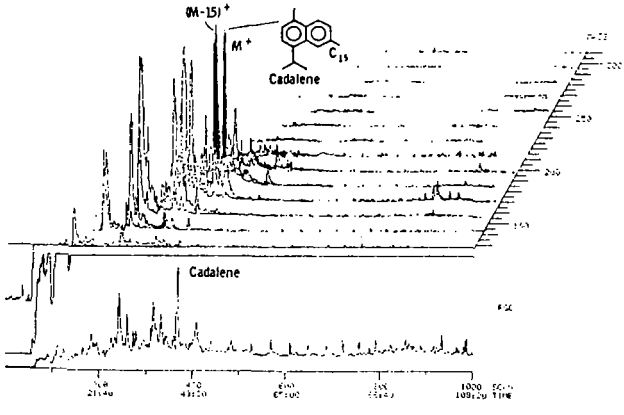

GROUP-TYPE ANALYSIS OF THE AROMATIC FRACTION OF PRODUCTS FROM THE CATALYTIC LIQUEFACTION OF COAL

by Harry T. Best and Alvin B. Marcus
Gulf Research & Development Co., Pittsburgh, PA 15230

A high concentration of hydroaromatic compounds and a low degree of alkyl substitution are found in the aromatic fraction of liquefied coal products. A group-type analysis tailored for this material and previously reported by this laboratory[1] has now been expanded to include 30 compound types. These are indicated by the filled circles in Fig. 1. Results are calculated from a low resolution mass spectrum obtained at standard ionizing voltage. A CEC model 21-103 equipped with a 350°C all-glass inlet and gallium frit was used. Prior removal of saturates, polar compounds, and hexane insolubles from the liquid coal product is required[2].

In the selection of calibration spectra, the unsubstituted molecule was emphasized. Calibration standards for some hydroaromatics were obtained by hydrogenating the corresponding aromatic compound followed by gradient elution chromatography of the product into monoaromatic and di+triaromatic fractions[3]. The group sum values obtained for each calibrant were divided by the observed total ionization and assembled into a 30x30 matrix for inversion.

Initially, the analysis was tested on the specially prepared concentrates. For example, the analysis of the di+triaromatics fraction of hydrogenated phenanthrene is shown in Fig. 2 (results in weight percent). The percentages of the expected compounds, phenanthrene, dihydrophenanthrene, and tetrahydrophenanthrene, total 86%. Fig. 3 shows the analysis of the monoaromatics fraction of hydrogenated chrysene. The percentage of the only expected compound, dodecahydrochrysene, is 85%. These results are considered satisfactory for the purposes of group-type analysis.

The analysis of the aromatic fraction of a typical catalytic coal liquid distillate is shown in Fig. 4.

---

1 J. T. Swansiger, F. E. Dickson, and H. T. Best, Anal. Chem., 46, 730 (1974).
2 J. C. Suatoni and R. E. Swab, J. Chromat. Sci., in press.
3 D. M. Jewell, R. G. Ruberto, and B. E. Davis, Anal. Chem., 44, 2318 (1972).

* included with dihydropyrenes

FIGURE 1.

AROMATICS & HYDROAROMATICS							
GROUP TYPE		+2H	+4H	+6H	+8H	+10H	+12H
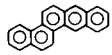	●		●	●	●	●	
	●	●	●	●	●	●	
	●		*	●	●		●
	●	●	●	●		●	
	●	●	●	●	●		
	●		●				
	●		●				
	●						

FIGURE 2.

PHENANTHRENE DI/TRIAROMATICS							
GROUP TYPE		+2H	+4H	+6H	+8H	+10H	+12H
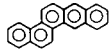							
	1	2		3			
	30	11	45	4	1		
	1						
	3						

FIGURE 3.

CHRYSENE MONOAROMATICS							
GROUP TYPE		+2H	+4H	+6H	+8H	+10H	+12H
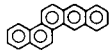							
		1	1				
			1		4		85
	1	1			1		
	1		1				
	2		1				

FIGURE 4.

CCL DISTILLATE 450-800°F							
GROUP TYPE		+2H	+4H	+6H	+8H	+10H	+12H
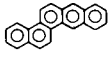	1		1	1	1	1	
	2	1	1	2	2	1	
	2				1		1
	17	12	3	8		3	
	13	5	14	1	5		
	1						
			1				

MASS SPECTRAL CHARACTERIZATION OF HEAVY COAL LIQUEFACTION PRODUCTS

Thomas Aczel and H. E. Lumpkin

Exxon Research and Engineering Company
Baytown, Texas

The mass spectrometric methods developed in our laboratories during the last few years have been summarized previously (Proceedings of the 23rd Annual Conference on Mass Spectrometry, May 25-30, Houston, Texas, pages 228-230). This paper illustrates some recent applications and the extension of this methodology to the "heavy ends" of coal liquefaction products.

Items discussed include the detailed characterization of narrow distillate fractions in the 600-1200°F boiling range, preliminary data on the usefulness of an ultra high resolution mass spectrometer, the MS50, in the analysis of heteroaromatics, analysis of the volatile portion of solid liquefaction bottoms, and MS contribution to the evaluation of the polyamantane hypothesis on the structure of coal.

Characterization of distillate fractions yields not only detailed composition data, but also calibrants which can be used for subsequent analyses without need for the expensive distillation and chromatographic separation steps. The simple separation scheme is shown in Figure 1 and the class distribution is shown in Figure 2. Saturates and aromatics decrease rapidly with increasing boiling point, polars reach a plateau, and the cyclohexane insolubles increase.

The saturates contain paraffins and 1 through 8 ring naphthenes. Molecular weights range up to 600. The isoprenoid paraffins pristane and phytane have also been identified.

Typical composition data on the aromatics are summarized in Figures 3-7. The capabilities of the MS50 are illustrated by the separation of multiplets and the large number of heteroaromatic compound types identified in a polar fraction (Figures 8-9). Although existence of most of these types was previously inferred on a non-routine basis from MS9 data, unequivocal identification was possible only with the MS50. Availability of this instrument will also allow the routine determination of these complex components.

The cyclohexane insoluble fractions, (technically identified as asphaltenes) are completely

volatile in the MS inlet system. They consist of entrained components, and/or low molecular weight asphaltenes and decomposition products. Components identified in these fractions include condensed ring hydroxyaromatics, pyrroles, and pyridines. Significant amounts of aromatic hydrocarbons, such as pyrene, phenanthrene, etc., are also present.

Analysis of the volatile portion of solid residue is made feasible by charging up to 100 mg of sample. The amount and the molecular weight distribution of the volatiles is a reproducible function of the temperature of the MS inlet system. No cracking is observed.

The next logical step after the characterization of the solid residue is that of coal itself. MS data were used in an indirect way (T. Aczel, M. L. Gorbaty, P. S. Maa, R. H. Schlosberg, Fuel, Vol. 54, 295 [1975]) to confute the polyamantane (polyadamantane-polytricyclodecane) model of coal structure. The use of mass spectrometry in this context was facilitated by the high stability of the adamantane skeleton under electron bombardment at both high and low voltage conditions (Figures 10 and 11).

The developments outlined in this presentation corroborate and extend the usefulness of mass spectrometry, in particular ultra high resolution mass spectrometry, for the analysis of coal liquefaction products.

OUTLINE OF SIMPLE SEPARATION SCHEME

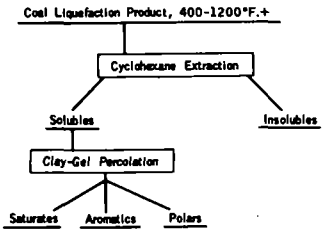

Separation is used only occasionally to obtain background information and calibration data.

768-3-98

Figure 1

CLASS DISTRIBUTION IN 600 - 1200°F RANGE

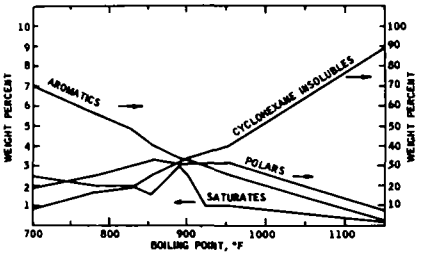

Figure 2

CHARACTERIZATION OF THE HEAVY ENDS OF COAL LIQUIDS
AVERAGE FEATURES OF AROMATICS IN DISTILLATION FRACTIONS

	Weight Percent or Value			
	814-844°F	869-896°F	915-937°F	975°F+ Bottoms
MOLECULAR WEIGHT	270	298	310	328
AVG. CONDENSATION (Z No.)	21.0	23.6	26.1	28.2
CARBON ATOMS IN SIDECHAINS	4.9	5.4	4.9	5.0
ATOMIC H/C RATIO	0.960	0.945	0.894	0.860
MS DISTILLATION				
10% off, °F	735	817	860	810
50% off, °F	808	899	944	1023
90% off, °F	895	985	1044	1125

768-3-101

Figure 3

CHARACTERIZATION OF THE HEAVY ENDS OF COAL LIQUIDS
AROMATIC RING DISTRIBUTION IN DISTILLATION FRACTIONS

	Weight Percent			
	814-844°F	869-896°F	915-937°F	975°F+ Bottoms
1-RING	0.2	0.2	-	-
2-RING	15.3	5.4	2.1	-
3-RING	30.3	15.5	6.1	6.8
4-RING	52.8	63.2	52.9	26.8
5-RING	1.1	14.4	32.0	34.0
6-RING	0.3	1.2	6.4	29.2
7+-RING	-	0.1	0.5	3.2

768-3-102

Figure 4

CHARACTERIZATION OF THE HEAVY ENDS OF COAL LIQUIDS
COMPOUND TYPE DISTRIBUTION OF AROMATICS IN DISTILLATE FRACTIONS I

	Weight Percent			
Compound Type	815-844°F	869-896°F	915-937°F	975°F+ Bottoms
C_nH_{2n-18}	7.3	3.8	1.2	-
C_nH_{2n-20}	19.5	7.4	3.6	5.3
C_nH_{2n-22}	29.1	18.9	8.3	6.7
C_nH_{2n-24}	19.0	25.1	15.1	5.8
C_nH_{2n-26}	2.2	13.3	22.5	8.8
C_nH_{2n-28}	0.4	11.5	21.0	12.5
C_nH_{2n-30}	0.5	1.8	6.3	14.6

768-3-103

Figure 5

CHARACTERIZATION OF THE HEAVY ENDS OF COAL LIQUIDS
COMPOUND TYPE DISTRIBUTION OF AROMATICS IN DISTILLATE FRACTIONS II

	Weight Percent			
Compound Type	815-844°F	869-896°F	915-937°F	975°F+ Bottoms
C_nH_{2n-32}	0.1	0.8	2.9	11.6
C_nH_{2n-34}	0.1	0.1	1.6	6.1
C_nH_{2n-36}	-	0.1	1.2	5.5
C_nH_{2n-38}	-	-	0.3	1.5
C_nH_{2n-40}	-	-	0.2	1.4
C_nH_{2n-42}	-	-	-	0.3
C_nH_{2n-44}	-	-	-	0.1

768-3-104

Figure 6

CHARACTERIZATION OF THE HEAVY ENDS OF COAL LIQUIDS
CARBON NUMBER DISTRIBUTION OF BENZOPYRENES IN DISTILLATE FRACTIONS

Carbon No.	Weight Percent 814-844°F	869-896°F	916-937°F	975°F+ Bottoms
20	0.1	2.4	1.1	-
21	Traces	2.8	3.0	-
22	Traces	1.7	4.2	1.0
23	-	1.5	3.7	1.5
24	-	1.0	3.3	2.1
25	-	0.8	2.3	2.3
26	-	0.5	1.3	1.4
27-34	-	0.8	2.2	5.1

Figure 7

MULTIPLETS SEPARATED BY MS 50 IN POLAR FRACTION OF A COAL LIQUEFACTION PRODUCT

Formula	Intensity	Precise Mass	Mass Measurement Error	RP Required
$C_{24}H_{16}O$	2340	320.1201	+0.0010	16500
$C_{23}H_{17}{}^{13}CN$	60	320.1395	+0.0007	18800
$C_{25}H_{20}$	279	320.1565	+0.0010	15200
$C_{22}H_{24}O_2$	676	320.1776	+0.0000	8800
$C_{23}H_{28}O$	236	320.2140	+0.0012	
$C_{23}H_{15}NO$	178	321.1153	+0.0005	39200
$C_{23}H_{16}{}^{13}CO$	452	321.1235	+0.0022	11380
$C_{24}H_{19}N$	2078	321.1517	+0.0002	94400
$C_{21}H_{23}NS$	154	321.1551	+0.0005	
$C_{24}H_{20}{}^{13}C$	37	321.1599	+0.0012	

Experimental data obtained by Messers Elliott, Evans, Hazelby of AEI, Ltd., Manchester, England

Figure 8

COMPOUND TYPES DETERMINED BY MS 50
IN POLAR FRACTION OF A COAL LIQUEFACTION PRODUCT

- HYDROCARBONS — C_nH_{2n-8} through C_nH_{2n-38}
- OXYGEN COMPOUNDS — $C_nH_{2n-6}O$ through $C_nH_{2n-38}O$
  $C_nH_{2n-16}O_2$ through $C_nH_{2n-32}O_2$
  $C_nH_{2n-8}SO$ through $C_nH_{2n-30}SO$
- NITROGEN COMPOUNDS — $C_nH_{2n-7}N$ through $C_nH_{2n-37}N$
  $C_nH_{2n-15}NO$ through $C_nH_{2n-33}NO$
- MISCELLANEOUS — S, SN, S_2, NO_2, O_3, S_2O

No. of Compound Types: 93

Smallest Peak: 90 ppm of Total Ionization

Experimental data obtained by Messers Elliott, Evans, Hazelby of AEI, Ltd., Manchester, England.

Figure 9

STABILITY OF ADAMANTANE SKELETON

COMPOUND	SKELETON IONS, % OF TOTAL IONIZATION	RELATIVE LV INTENSITIES
ADAMANTANE	32.1	52
ADAMANTANOL	13.2	26
2-ADAMANTANONE	20.5	33
ADAMANTANE-CARBOXYLIC ACID	54.4	5 (+25)
2-PHENYL-ADAMANTANE	27.0	79
DIAMANTANE	37.2	53
DECALIN	12.7	21
TETRALIN	26.5	100
NAPHTHALENE	75.3	165

Figure 10

FRAGMENTATION OF ADAMANTANE DERIVATIVES

ION	RELATIVE INTENSITY AD	AD-OH	AD-COOH	AD = O	AD - C_6H_5	DIAMANTANE
P	100	100	100	100	100	100
P-H	21	1	0	1	10	16
P-C_3H_7	44	17	0	6	5	5
P-C_4H_9	45	427	10	19	5	11
P-F	-	1	2043	0	1	1
F	-	-	-	-	43	-
(P-F)-C_3H_6	-	10	311	19	12	10
(P-F)-C_4H_8	-	28	419	89	29	20

AD. ADAMANTANE P. PARENT F: FUNCTIONAL GROUP

Figure 11

Mass Spectrometric Analysis of Coal Liquids and Their Hydrogenation-Hydrogenolysis Products.[1]

S. E. Scheppele, G. J. Greenwood, P. L. Grizzle,[2] T. D. Marriott, and N. B. Perreira, Department of Chemistry, Oklahoma State University, Stillwater, Oklahoma 74074.

Field ionization (FI) sensitivities were determined for 60 aromatic hydrocarbons and aromatic heteroatom-containing compounds relative to ethylbenzene.[3] The compounds studied are in general typical of those encountered in coal-derived liquids. Within the limits of experimental precision, the relative sensitivities for these compounds were found to be independent of sample composition. The relative sensitivities for ionization by electric fields and by low-voltage electrons[4] (EI) were converted to relative-cross sections for ionization by both techniques. For a representative number of compounds, Table I presents relative-cross

Table I. FI- and EI-Relative Cross Sections Relative to Benzene

Compound	m/e of M^+	FI-RCS	Ave. EI-RSC[a]
benzene	78	1.00	1.00
toluene	92	1.15	1.82
ethylbenzene	106	1.14	1.92
1,2-dimethylbenzene	102	1.25	2.81
naphthalene	128	1.45	5.57
1-methylnaphthalene	142	1.49	7.12
fluorene	166	1.74	5.57
phenanthrene	178	1.98	9.49
3-methylfluorene	180	1.75	6.75
pyrene	202	1.93	11.86
quinoline	129	1.83	3.29
carbazole	167	2.01	13.43
benzo[b]thiophene	134	1.31	6.23
dibenzothiophene	184	1.78	10.56
1,3-benzenediol	110	1.53	2.99

[a]Average of RCS(EI) calculated from EI sensitivities given in reference 4.

sections for FI, RCS(FI), and average relative-cross sections for EI, RCS(EI). As observed for ionization by low-energy electrons[4a,c,d] the cross sections for field ionization in the series benzene, naphthalene, phenanthrene, and pyrene are a function of the size of the aromatic nucleus. Substitution of one or more alkyl groups for hydrogen in benzene is seen to increase both EI- and FI-cross sections. The values in Table I for benzene, toluene, ethylbenzene, and propylbenzene suggest that the substituent effect on RCS(FI) and RCS(EI) is not strongly dependent on the nature and size of the alkyl group.

In the structurally related series fluorene, dibenzofuran, RCS(FI) = 1.69, dibenzothiophene, and carbazole replacement of CH_2 by O and SH is indicated to have little effect on the cross sections for FI whereas substitution of NH by CH_2 markedly increases RCS(FI). Substitution of OH for aromatic hydrogen increases both EI- and FI-cross sections.

Equation 1 shows that for the aromatic hydrocarbons a reasonable linear correlation exists between the relative-cross sections for FI and the average relative-cross sections for low-voltage EI.[3] For aromatic

$$RCS(EI)_{Ave.} = (9.52 \pm 0.62)(RCS(FI)) + 1.000 \pm 0.047 \qquad (1)$$

hydrocarbons equation 1 allows prediction of an RCS(FI) given as RCS(EI) or vice-versa. The relative-cross sections (sensitivities) for field

ionization of the parent aromatic hydrocarbons, parent thiophenes, and parent aromatic nitrogen-containing compounds are linearly correlated with -Z numbers.[3] These correlations can be used to predict FI relative-cross sections and relative sensitivities for various homologues upon suitably correcting the predicted value for the substituent.

Table II presents analytical data obtained from FI-MS and low-voltage EI-MS analysis of a synthetic blend containing compounds typical of those encountered in the hydrocarbon + ether fraction from a coal-derived liquid. The weight percents of each component calculated assuming unit relative-

Table II. Weight Percents of Components in Synthetic Blend

	Weight Percents and Percent Deviations by									
			FI				EI			
Compound	Grams	GLC[a,b]	S_i/S_1=1[a,c]	% DEV	S_i/S_1[a,c]	% DEV	S_i/S_1=1[a,b]	% DEV	S_i/S_1[a,b]	% DEV
2,3-dihydro-1H-indene	8.28	8.25	6.31	-23.8	7.73	-6.6	2.73	-67.0	8.90	7.5
1,3,5-trimethylbenzene	6.28	6.20	5.02	-20.1	5.83	-7.2	3.49	-44.4	6.35	1.1
naphthalene	4.46	4.93	4.10	-8.1	4.34	-2.7	3.12	-30.0	4.56	2.2
1,2,3,4-tetrahydronaphthalene	5.46		4.56	-16.5	5.30	-2.9	2.12	-61.2	5.44	-0.4
benzo[b]thiophene	3.21	9.01	2.62	-18.4	3.18	-0.9	2.70	-15.9	3.39	5.6
1-methylnaphthalene	11.78		11.25	-4.5	11.78	0.0	10.42	-11.5	12.03	2.1
6-methylbenzo[b]thiophene	4.35	17.13	4.17	-4.1	4.50	3.4	4.95	13.8	4.79	10.1
1,2-dihydroacenaphthylene	3.06	3.17	3.32	8.5	3.16	3.3	3.71	21.2	3.10	1.3
1,6-dimethylnaphthalene	9.43	9.17	9.94	5.4	9.15	-3.0	12.02	27.5	9.31	-1.3
1,2,3,4,5,5a-hexahydro-acenaphthylene	8.52	8.22	7.40	-13.1	8.72	2.3	4.65	-45.4	8.48	-0.5
fluorene	3.90	3.93	4.25	9.0	3.91	0.3	3.51	-10.0	3.62	-7.2
dibenzofuran	3.54	3.53	4.06	14.7	3.78	6.8	3.44	-2.8	3.86	+9.0
phenanthrene	4.05	4.14	4.95	22.2	4.02	-0.7	6.19	52.8	4.16	2.7
9,10-dihydrophenanthrene	9.11	8.44	10.24	12.4	9.29	2.0	9.37	2.9	8.88	-2.5
dibenzothiophene	2.13	2.31	2.42	13.6	2.25	5.6	3.42	60.6	2.21	3.8
4-methylphenanthrene	3.47	3.80	4.24	22.2	3.71	6.9	5.78	66.6	3.22	-7.2
pyrene	6.36	5.99	7.63	20.0	6.50	2.2	11.05	73.7	5.52	-13.2
2,6-dimethylanthracene	0.63	0.37	0.97	54.0	0.74	17.5	1.62	157.1	0.52	-17.5
chrysene	1.97	1.55	2.53	28.4	2.12	7.6	4.76	141.6	1.70	-13.7

[a]Uncertainty in values is *ca.* ± 5%. [b]Average of two determinations. [c]Average of three determinations.

sensitivities are shown in columns 4 and 8, respectively. The largest errors are observed for those compounds having the largest and smallest relative sensitivities as expected. The best agreement between known and experimental weight percents occurs for those components whose relative-gram-semsitivity approximates the average value across the distribution. However, it should be noted that the error in composition incurred by assuming unit relative-sensitivities is significantly worse for low-voltage EI than for FI. However, the data in columns 6 and 10 show that including relative sensitivities into the conversion of ion abundances to weight percents yields an excellent quantitative distribution by both techniques.

Raw anthracene oil and four mixtures obtained from its catalytic upgrading with molecular hydrogen were subjected[5] to separation using cation, anion, and complexation chromatography.[6] The acid, base, neutral nitrogen, and hydrocarbon + ether fractions were analyzed using low- and high-resolution FI/MS, high-resolution 70-eV EI/MS,[5] and GC-EI/MS.[5] Hydrocarbons containing three aromatic rings account for 40.1% of the raw anthracene oil. The parent member of the -18 Z series (mass = 178, formula = $C_{14}H_{10}$) was preparatively isolated using GC and identified as ≥ 98% phenanthrene. Thus, phenanthrene and assumably alkylated phenanthrenes comprise the Z = -18 series which accounts for 15.6% of the feedstock. The presence of phenanthrene rather than anthracene in anthracene oil has been previously suggested.[7] Upgrading of the anthracene oil increases the complexity of the hydrocarbon + ether fraction and shifts the maximum of the weight percent distribution to lower Z value.[5] This

result is consistent with the hydrogenation-hydrogenolysis of heteroatom containing compounds and probably higher-molecular aromatic hydrocarbons.

The elemental composition data for the acid fractions can be grouped into 19 major compound classes as shown in Table III. Possible structure assignments are based upon conclusions drawn from previous analyses of coal derived materials[4b,8] and from the compound types observed[5] in the

Table III. Possible Compound Types Present in Acid Fractions of KWT Anthracene Oil and Four Related Reactor Samples

Nominal Mass of Parent Compound	Empirical Formula of Parent Compound	Example of Possible Structural Type	Maximum Number of of Alkyl Carbons Alkylated Homologues
94	C_6H_6O	phenol	6
134	$C_9H_{10}O$	indanol	5
144	$C_{10}H_8O$	naphthol	4
170	$C_{12}H_{10}O$	acenaphthol	4
182	$C_{13}H_{10}O$	fluorenol	4
198	$C_{13}H_{10}O_2$	hydroxydibenzofuran, fluorenediol	4
194	$C_{14}H_{10}O$	phenanthrenol	2
210	$C_{14}H_{10}O$	phenanthrendiol	1
226	$C_{14}H_{10}O_3$	phenanthrentriol	1
218	$C_{16}H_{10}O$	fluoranthenol	2
220	$C_{16}H_{12}O$	dihydropyrenol	4
234	$C_{16}H_{10}O_2$	fluoranthendiol	2
117	C_8H_7N	indole	2
167	$C_{12}H_9N$	carbazole	3
207	$C_{15}H_{13}N$	indanylindanol	-
217	$C_{16}H_{11}N$	naphthlindanol	1
145	C_9H_7NO	hydroxyazanaphthalene	2
195	$C_{13}H_9NO$	hydroxyazaphenanthrene	1

hydrocarbon + ether fractions. The mass spectral data are consistent with the occurrence of extensive deoxygenation during the residence time of the coal liquid in the reactor. This conclusion is illustrated by the weight percents of phenol and alkylphenols in the feedstock and reactor samples in Table IV. Comparison of the data in columns 4-7 with those in column 3

Table IV. Weight Percent of Phenols Identified in Acid Fraction from Feedstock and Hydotreated KWT Anthracene Oil

Example of Structural Type	Molecular Weight	Weight Percent in				
		Feedstock	Reactor Sample			
			1	2	3	4
Phenol	94	0.91	0.00	0.10	0.04	0.11
Methylphenol	108	1.03	0.00	0.23	0.08	0.21
Dimethylphenol	122	1.06	0.00	0.28	0.08	0.23
Trimethylphenol	136	0.33	0.01	0.15	0.06	0.12
Tetramethylphenol	150	0.15	0.03	0.07	0.04	0.06
Pentamethylphenol	164	0.10	0.03	0.05	0.03	0.04
Reactor Temperature (°F)			700	600	700	700
Reactor Pressure (psig)			1000	1000	1020	507
Space Time (hrs.)			1.48	2.50	0.75	0.75
Catalyst			Nalco Sphercat 474		Harshaw HT 400	

suggests that the ease of deoxygenation is decreased with increasing number

of alkyl (methyl) substituents on the benzene nucleus. Comparison of the distributions for reactor samples 2 and 4 with those of 1 and 3 suggests that reduction in both temperature and hydrogen pressure reduce the extent of oxygen removal. The data in columns 4 and 6 suggest either a catalyst or space-time dependence or both on deoxygenation. Finally formation of partially-reduced oxygen-containing aromatics account for ≤ 5% of the acid fractions from the reactor samples. Although weight percents are not presented, the carbazoles were markedly resistant to denitrogenation.

For the base fractions obtained from both the feedstock and hydrotreated anthracene oil the high-resolution 70-eV mass spectral data reveal the presence of seven series of ions differing in mass by 14 amu. Although convergence of compound classes at various molecular weights in a given series complicates interpretation, the feedstock base fraction can be formally recognized as containing nitrogen analogs of the hydrocarbons, e.g., azabenzene, azaindane, azanaphthalene, azaacenaphthalene, azafluorene, azaphenanthrene, azafluoanthene, benza[a]acridine, etc.

Both the low-resolution FI and the high-resolution 70-eV EI mass spectral data demonstrate that the complexity of the base fractions is significantly increased upon hydrotreating the anthracene oil. Table V presents mole data for the reactant and product bases comprising the 129-135, 143-149, and 157-163 molecular-weight series. For purposes of the

Table V. Moles of Bases at Selected Molecular Weights Found in Feedstock and Hydrotreated Anthracene Oil

		Moles x 10^3 Present in				
Nominal Mass	Empirical Formula	Feedstock	Reactor Samples 1	2	3	4
129	C_9H_7N	6.6	0.39	0.23	0.08	0.46
133	$C_9H_{11}N$	0.15	1.1	1.7	0.68	1.2
135	$C_9H_{13}N$	0.15	1.8	0.89	3.0	1.4
TOTAL		6.9	3.4	2.8	3.8	3.1
143	$C_{10}H_9N$	4.1	0.63	0.35	0.21	1.0
147	$C_{10}H_{13}N$	0.41	2.0	1.5	1.6	1.9
149	$C_{10}H_{14}N$	-	0.67	0.33	1.3	0.20
TOTAL		4.5	3.3	2.2	3.1	3.1
157	$C_{11}H_{11}N$	2.6	0.76	0.45	0.45	1.3
161	$C_{11}H_{15}N$	0.37	1.8	1.2	2.0	1.2
163	$C_{11}H_{17}N$	-	0.35	0.12	0.67	0.25
TOTAL		3.0	2.9	1.8	3.1	2.8

present discussion and without attempt at justification, the elemental compositions in Table V are assumed to reflect primarily the presence of quinoline (1) and/or isoquinoline (2), mass 129, singly- (mass 143) and doubly-(mass 157)methylated 1 and/or 2, and compounds derived from reaction of these compounds with H_2. Hydrotreating is seen to effectively reduce the moles of compounds possessing molecular weights 129, 143, and 157. For the reactor samples compared to the feedstock the significant increase in the moles at mass a) 133 indicate formation of tetrahydro-1 and -2 and b) 135 indicate formation of 2-propylaniline (3). Consistent with the reaction of quinoline with H_2 catalyzed by MoS_2,[9] 1 and methylated-1 undergo addition of 2 moles of H_2 producing tetrahydroquinoline and its methylated homologues, respectively. These latter compounds react with hydrogen via hydrogenolysis of the N-C(2) bond producing 2-propylaniline. Isoquinoline and its methylated homologues would undergo the analogous hydrogenation-hydrogenolysis reactions. However, hydrogenolysis of the

N-C(3) bond in these tetrahydro compounds would produce either 2-ethylbenzylamine (4) or 2-(2-methylphenyl)ethylamine (5) and their methylated homologues. Since 4 and 5 contain a benzylic and an aliphatic NH_2 group, denitrogenation to 2-ethylmethylbenzene will be facile.[9] In contrast, the NH_2 group in 3 is aromatic and, hence, would, as observed,[9a] undergo hydrogenolysis less readily.

The sum of the moles at masses 129, 133, and 135 in each reactor sample divided by the number of moles at mass 129 in the feedstock suggest that the fraction of quinoline and/or isoquinoline denitrogenated under the experimental conditions given in Table IV was *ca.* 0.5. The extent of nitrogen removal from 1 and 2 is similar for both catalysts. Denitrogenation would appear to be facilitated by a reduction in both temperature and pressure. This result is clearly unreasonable and suggests that hydrogenation/hydrogenolysis of high-molecular-weight compounds is contributing to the moles of compounds at masses 133 and 135.

The corresponding trends are observed in the mole data for the 143 and 157 molecular-weight series. Possible contributions from members of the azaindane and aminonaphthalene have been neglected in this discussion. However, the mole data for the 129-135, 143-149, and 157-163 molecular-weight series are mutually consistent and reasonably suggest the synthesis of their constituents or other isomeric compounds from compounds of higher molecular weight.

References

[1]Research supported by The Energy Research and Development Administration; Contract Numbers E(49-18)-2011 and E(34-1)-0020.

[2]Present address Bartlesville Energy Research Center, Energy Research and Development Administration, Bartlesville, Oklahoma 74003.

[3]S. E. Scheppele, P. L. Grizzle, G. J. Greenwood, T. D. Marriott, and N. B. Perreira, submitted to *Anal. Chem.*.

[4]a) H. E. Lumpkin, *ibid.*, 30, 321 (1958); b) A. G. Sharkey, Jr., G. Wood, J. L. Shultz, I. Wender, and R. A. Friedel, *Fuel*, 38, 315 (1959); c) G. L. Kerns, N. C. Maranowski, and G. F. Crable, *Anal. Chem.*, 31, 1646 (1959); d) H. E. Lumpkin and T. Aczel, *ibid.*, 36, 181 (1964); e) T. Aczel and H. E. Lumpkin, 19th Ann. Conf. Mass Spectrom. Allied Topics, 328 (1971).

[5]S. E. Scheppele, G. J. Greenwood, and B. L. Crynes, 23rd Ann. Conf. Mass Spectrom. Allied Topics, 226 (1975).

[6]D. M. Jewell, J. H. Weber, J. W. Burger, H. Plancher, and D. R. Latham, *Anal. Chem.*, 44, 1391 (1972).

[7]Private communication from T. Aczel and A. G. Sharkey, Jr.

[8]a) H. C. Anderson and W. R. K. Wu, Bull. U. S. Bur. Mines, No. 606 (1963); b) J. L. Shultz, T. Kessler, R. H. Friedel, and A. G. Sharkey, Jr., *Fuel*, 51, 242 (1972).

[9]a) S. Landa, Z. Kafka, V. Galik, and M. Safar, *Collect. Czech. Chem. Comm.*, 34, 3967 (1967); b) H. A. Smith in "Catalysis", ed. P. H. Emmett, Reinhold, New York, N. Y., 5, 175 (1957).

COMPOSITIONAL ANALYSES OF SYNTHOIL FROM WEST VIRGINIA COAL

by

P. W. Woodward, G. P. Sturm, Jr., J. W. Vogh,
S. A. Holmes, and J. E. Dooley

Bartlesville Energy Research Center
Energy Research and Development Administration
Bartlesville, Oklahoma

A synthetic crude oil (synthoil) derived from West Virginia, Pittsburgh seam coal by the Synthoil process was separated into three distillates and a residuum fraction. The <207° C distillate was further separated and characterized by gas chromatography and spectral techniques. The 207° to 363° C and 363° to 531° C boiling distillates were separated and characterized by methods developed by the Bureau of Mines for characterization of heavy ends of petroleum, but with slight modifications. Each of the higher boiling distillates was separated by dual-pack adsorption chromatography into four concentrates: saturates, monoaromatics, diaromatics, and polyaromatic-polar. The saturates were characterized directly by mass spectrometry. Both the monoaromatic and diaromatic concentrates were further separated by gel-permeation chromatography (GPC) before characterization by GPC-mass spectral (MS) correlations and nuclear magnetic resonance spectrometry (NMR). Acids and bases were extracted from the polyaromatic-polar concentrates before GPC separation and mass spectral analyses.

The resulting data indicate compound type similarities among this synthetic crude oil (Synthoil syncrude), other syncrudes and petroleum crude oils. The similarities suggest that much of present petroleum processing technology, with some modifications, is applicable to processing syncrudes derived from coal.

The procedures and methods used are satisfactory for characterizing complex synthetic crude oils, as the data show, and will provide valuable information for developing efficient refining processes to utilize economically our vast coal resources.

The <207° C distillate made up only 4.4 percent of the original synthoil and was 61 percent hydrocarbons, the remainder being mostly acid type compounds.

The saturates in the 207° to 363° C and the 363° to 531° C distillates accounted for approximately 9.5 percent of the original synthoil. Monoaromatic hydrocarbons made up 13 percent; diaromatics, 15.4 percent; and polyaromatics, 14.6 percent. Other compound types in these two distillates accounted for approximately 17.4 percent and included heteroatomic types, weak acids, strong acids, and bases.

Approximately 26 percent of the original synthoil had a boiling point above 531° C. Our present methodology did not permit us to analyze this fraction, however we are working on an analytical scheme for analyzing such higher boiling fractions and plan to report the analysis at a later time.

This work has been published in more detail in an ERDA Report of Investigations, BERC/RI-76/2.

REFERENCES

1. Dooley, J. E., D. E. Hirsch, C. J. Thompson, and C. C. Ward. Analyzing Heavy Ends of Crude (Comparisons). Hydrocarbon Processing, v. 53, No. 11, November 1974, pp. 187-194.

2. Dooley, J. E., G. P. Sturm, Jr., P. W. Woodward, J. W. Vogh, and C. J. Thompson. Analyzing Syncrude From Utah Coal. ERDA, BERC RI-75/7, 1975, 24 pp.

3. Hirsch, D. E., J. E. Dooley, and H. J. Coleman. Correlations of Basic Gel Permeation Chromatography Data and Their Application to High-Boiling Petroleum Fractions. BuMines, RI 7875, 1975, 77 pp.

4. Hirsch, D. E., R. L. Hopkins, H. J. Coleman, F. O. Cotton, and C. J. Thompson. Separation of High-Boiling Petroleum Distillates Using Gradient Elution Through Dual-Packed (Silica Gel-Alumina Gel) Adsorption Columns. Anal. Chem., v. 44, No. 6, May 1972, pp. 915-919.

5. Sturm, G. P., Jr., P. W. Woodward, J. W. Vogh, S. A. Holmes, and J. E. Dooley. Analyzing Western Kentucky Syncrude. ERDA, BERC RI-75/12, 1975, 27 pp.

6. Yavorsky, P. M., S. Akhtar, and S. Freidman. Converting Coal Into Non-Polluting Fuel Oil. Chem. Eng. Prog., v. 69, No. 3, March 1973, pp. 51-53.

Spectral Characterization of Shale Oils Produced by In Situ Retorting,

J. H. WEBER, Laramie Energy Research Center, U.S. Energy Research and Development Administration, Laramie, Wyoming 82071

Production of oil by in situ or in place retorting of oil shale has many potential advantages over the more conventional mining/above ground retorting approach. One of the major advantages is that in situ retorting avoids the costly and disfiguring mining and spent shale disposal steps associated with the mining/retorting approach. This paper will describe the in situ experiments that were used to produce the oils and the spectral characterization of various fractions of the oil. Comparisons are also made between oil produced by in situ retorting methods and oils produced by above ground retorting methods.

ENERGETICS OF NEGATIVE IONS FROM THE GROUP VA PENTAHALIDES

by

R. E. Pabst, J. L. Margrave and J. L. Franklin

Department of Chemistry
Rice University
Houston, Texas 77001

Dissociative electron resonance capture processes have been studied for several Group VA pentahalides, including PF_5, AsF_5, SbF_5, $PC\ell_5$ and $SbC\ell_5$. The ions formed include X^-, X_2^-, MX_4^- and MX_3^- over the energy range of 0-15 eV. Translational energies of several ions were measured with accurate appearance potentials to determine the heat of the process. In several cases it has been possible to determine electron affinities of the Group VA halide radicals. From the processes forming X^- and X_2^- it has been possible to determine electronic transition energies for the radicals MX_4 and MX_3, respectively.

Endoergic Collision of I^- on Cyanogen and Nitrosyl Chloride.

KAMEL M. A. REFAEY, Phys. Dept., Cairo Univ., Cairo, Arab Republic of Egypt.

Endoergic collision of I^- on various target gas molecules has been successfully used[1,2] to obtain the thermodynamic properties of several species. Collision of I^- on $(CN)_2$ gives rise to the secondary ion CN^-. The onset obtained corresponds to the process

$$I^- + (CN)_2 \rightarrow CN^- + ICN$$

and give $\Delta H_f(CN^-) = 17.6$ kcal mole^{-1} which is in fair agreement with several reported values. Collision of I^- on NOCl gives the secondary ions Cl^- and ICl^-. The results indicate that Cl^- is accompanied by the formation of INO which as been suspected as a product in earlier measurements.[2] The results also indicate that $\Delta H_f(ICl^-) = -37$ kcal mole^{-1}.

[1] Kamel M. A. Refaey and J. L. Franklin. Accepted, Int. J. Mass Spectrom. Ion Phys.
[2] Kamel M. A. Refaey, Accepted, Int. J. Mass Spectrom. Ion Phys.

Electron Attachment in CBz-Amino Acid Methyl Esters

Costello L. Brown and Albert F. T. Chen

Department of Chemistry
California State University
Los Angeles, California 90032

The negative ion mass spectra of several CBz-amino acid methyl esters, including phenylalanine, tyrosine and aspartic acid have been studied. All of these derivatives give rise to a M-91 anion which is usually the base peak in the negative ion spectra obtained with electron energies of 4.2 eV. These low energy spectra are quite simple and do not contain a great deal of additional peaks due to extensive fragmentation.

Ionization efficiency curves for the M-91 ion in these compounds all showed a dissociative resonance capture maximum at 4.2 eV. It was also found that the 70 eV negative ion spectra of these CBz derivatives gave spectra which were not very different from the 4.2 eV spectra. Ionization observed at this higher energy is presumably due to electron capture of secondary electrons.

Although the negative ion sensitivity is not very good, from a practical analytical viewpoint, ions from possible volatile contaminents such as oil, grease, plasticizers, etc. are not formed with the 4.2 eV electron energy and thus would not produce interfering background.

Negative Ion Mass Spectrometry of Some Fatty Acid Derivatives

Costello L. Brown and Carcy L. Chan

Department of Chemistry
California State University
Los Angeles, California 90032

The p-nitrobenzyl ester derivative of nine fatty acids ranging from C_6 to C_{22} were synthesized and their negative ion mass spectra were obtained at 2.9 eV. The conventional positive ion studies of ester derivatives of fatty acids usually give numerous fragment ions and molecular ions of relatively low intensity. In this negative ion mass spectra study, p-nitrobenzyl esters were used and these ester derivatives gave intense carboxylate anion peaks (M-p-nitrobenzyl ion), with considerably less fragmentation.

From the spectra of the derivatives investigated only three peaks greater than 5% of the base peak were observed. These peaks were at m/e 46 due to the NO_2^-, m/e 136 due to the p-nitrobenzyl group, and the M-p-nitrobenzyl anion appeared as the base peak for all the derivatives except caproic and caprylic acids. In these two derivatives the relative intensity of the M-p-nitrobenzyl peaks were about 50% and the ion due to NO_2^- at m/e 46 was the base peak.

The ionization efficiency curves were determined for the carboxylate ions and the maximum was observed at 2.9 eV for all the p-nitrobenzyl ester derivatives. From these negative ion studies at 2.9 eV, it can be concluded that the p-nitrobenzyl esters of fatty acid do indeed give enhanced carboxylate anion peaks with little fragmentation.

APPARENT ACTIVATION ENERGIES IN GAS-PHASE REACTIONS OF ANIONS WITH HALOGENATED METHANES AT 297±2° K

K. Tanaka, G.I. Mackay, J.D. Payzant and D.K. Bohme

Department of Chemistry and
Centre for Research in Experimental Space Science,
York University, Downsview, Ontario M3J 1P3, Canada

Rate constants for exothermic displacement (S_N2) reactions of the type

$$X^- + CH_3Y \rightarrow Y^- + CH_3X$$

where $X^- = H^-, O^-, C^-, F^-, Cl^-, OH^-, C_2^-, CN^-, SH^-, S_2^-, C_2H^-, NH_2^-, NO_2^-, CHF^-, CH_2Br^-, CH_3O^-, CH_3S^-$ and CH_3NH^- where Y = F, Cl and Br, have been measured in the gas phase at 297 ± 2° K using the flowing afterglow technique. Comparisons with specific rates of capture indicate that several of these reactions may possess large activation energies $E_a > 2$ kcal mole^{-1}. In several instances energy barriers have been predicted by theoretical studies. Correlations were found between apparent activation energies and the heats of reaction.

The complete paper has now appeared in the Canadian Journal of Chemistry, Vol. 54, P. 1643 (1976).

Negative Ion Chemical Ionisation Spectra of Some Aromatic Compounds

Ronald K Mitchum, Alex G Harrison, Antonio J Ferrer-Correia & Keith R Jennings

Department of Molecular Sciences, University of Warwick, Coventry, England, CV4 7AL

Negative Ion Chemical Ionisation (NICI) mass spectrometry has recently been shown to have a sensitivity which equals or surpasses that of positive ion chemical ionisation mass spectrometry. Previous work on reactions of $O^{-\bullet}$ ions with a variety of organic compounds under ion cyclotron resonance (ICR) conditions suggested that these ions would be useful as a NICI reagent ion.

The work was carried out using a combined CI/EI source fitted to an MS50 double-focussing mass spectrometer (AEI Scientific Apparatus Ltd) which has been specially modified for high pressure work with negative ions. The source pressure is measured using an MKS "Baratron" Series 77 capacitance manometer, the output of which controls a Granville-Phillips automatic pressure regulator through which the CI reagent gas passes. N_2O was chosen as a source of $O^{-\bullet}$ ions but in order to minimise the reaction of $O^{-\bullet}$ ions with N_2O to form NO^-, the CI reagent gas consisted of a 9:1 mixture of N_2 and N_2O giving a total source pressure of 0.5 Torr. Ions were produced using 400 eV electrons and NICI spectra produced by reactions of $O^{-\bullet}$ ions were obtained at high sensitivity.

In addition to the formation of OH^- ions, the major reaction types found in the reaction of $O^{-\bullet}$ ions with aromatic compounds are as follows.

$$O^{-\bullet} + M \rightarrow (M-H)^- + \bullet OH \quad (1)$$

$$\rightarrow (M-H_2)^{-\bullet} + H_2O \quad (2)$$

$$\rightarrow (M-H+O)^- + H\bullet \quad (3)$$

$$\rightarrow (M-R+O)^- + R\bullet \quad (4)$$

$$\rightarrow (M+O-H-HX)^- + H\bullet + NX \quad (5)$$

The relative importance of these reactions depend on the substituents present in the aromatic compound, but reactions (4) and (5) were always less important than (1)-(3).

Benzene undergoes only reactions (2) and (3) and with 1, 3, 5-benzene-d_3 the ion $(M-HD)^{-\cdot}$ was essentially the only product of reaction (2), indicating 1, 2 or 1, 4 removal of hydrogen. Alkyl benzenes undergo reactions (1)-(4) and deuterium-labelling studies show that reaction (1) occurs very largely by the removal of a proton from an alkyl group, but that reaction (3) occurs by the displacement of a ring hydrogen atom. The mechanism of reaction (2) is less specific but this is the major reaction in compounds having two alkyl groups meta to each other when a hydrogen atom is removed from each alkyl group. The relative importance of reaction (3) varies widely with the substituents, the $(M-H+O)^-$ ion being of high abundance in spectra given by unsubstituted aromatic compounds such as pyridine and naphthalene, and in spectra given by fluorobenzene and acetophenone, but is always of low abundance if a methyl group is present in the aromatic ring.

In several cases, striking differences were found in the $O^{-\cdot}$ negative ion chemical ionisation spectra given by isomeric compounds such as the three xylenes and the three methyl pyridines. Both o- and p-xylenes yield $(M-H)^-$ ions as the base peak with low intensity $(M-H_2)^{-\cdot}$ peaks, but $(M-H_2)^{-\cdot}$ is the base peak in the m-xylene spectrum. Deuteration of the ring showed that the H atoms of the methyl groups are largely removed in these reactions. The spectrum given by m-$C_6H_4(CH_3)(CD_3)$ gave a large peak corresponding to $(M-HD)^{-\cdot}$ indicating that the $O^{-\cdot}$ ion removes a hydrogen atom from each of the methyl groups in forming the $(M-H_2)^{-\cdot}$ ion in the m-xylene spectrum. A similar variation in the spectra given by the methylpyridines was observed and further work is in progress to eludicate the mechanisms of $O^{-\cdot}$ reactions with these compounds.

The Effect of Sample Purity on Mass Spectrometric Isotope Ratio Measurements

John W. Gramlich

National Bureau of Standards
Institute for Materials Research
Analytical Chemistry Division
Washington, D. C., 20234

Isotope ratio measurements by solid sample thermal or surface ionization mass spectrometry can be seriously biased by the presence of impurities in the sample being analyzed. Attempts to compare high purity standards with impure samples are an exercise in futility, bacause the filament fractionation pattern of the sample and the standard will be the same only if the matrix and purity of the two materials are the same. Although replicate analyses of the same sample may show a high degree of precision, the results may be biased due to an altered fractionation pattern. The only sure way of eliminating this problem is to produce samples as pure as the standard. Modern isotope ratio mass spectrometers are capable of making measurements accurate to the parts in ten thousand level. The effects of chemical impurities can produce uncertainties which are orders of magnitude larger than this. Thus, the limiting factor for the accuracy of an isotope ratio measurement is often the quality of the pre-analysis chemistry.

Although every element that has been analyzed in this laboratory has exhibited at least some undesirable effects from the presence of impurities, further discussion of a few elements will suffice in describing the types of problems associated with impure samples. Chloride in blood serum has been analyzed in this laboratory routinely for several years [1], with agreement in the range of 0.2 percent for the analysis of multiple vials from the same lot of serum. Recently, two lots of serum were analyzed which showed variations between vials at the one percent level. Sample inhomogenity was ruled out as the source of the problem because of good inter-vial agreement for other electrolytes in the serum. Further chemistry, employing slow crystallization of large silver chloride crystals to exclude impurities, dramatically improved the precision and shifted the concentration values by several tenths of a percent.

A survey of potassium isotopic abundances in more than 70 minerals [2] shows a systematic shift of approximately 0.03 percent toward a higher $^{39}K/^{41}K$ ratio than has been found for a high purity reference sample [3]. Many of the mineral samples produced a slower rate of fractionation than was observed with the standard, yielding a higher $^{39}K/^{41}K$ ratio. This type of altered fractionation pattern has been observed with the standard after the addition of trace amounts of either organic or inorganic impurities.

Lead analyses by the silica gel method is one example where biases of up to one percent can easily be attained with impure samples. In addition to impurity induced altered fractionation patterns, small lead samples that are purified by ion exchange chromatography without subsequent electrodeposition [4] can often show the effect of isobaric interferences, presumably from leached organic resin.

Precision is relatively easy to obtain for mass spectrometric isotope ratio measurements, accuracy, however, requires both careful mass spectrometric technique and the highest quality chemical purification.

REFERENCES

[1] Garner, E. L., Machlan, L. A., Gramlich, J. W., Moore, L. J., Murphy, T. J., and Barnes, I. L., An Accurate Determination of Electrolyte Concentrations in Blood Serum by Isotope Dilution Mass Spectrometry, 7th IMR Research Symp., Gaithersburg, MD, Oct. 7-11, 1974. NBS Spec. Publ. 422, U.S. Government Printing Office, Washington, DC 20402 (In press).

[2] Garner, E. L., Goldich, S. S., Gramlich, J. W., Machlan, L. A., and Murphy, T. J., Absolute Isotopic Composition of Terrestrial Potassium (In preparation).

[3] Garner, E. L., Murphy, T. J., Gramlich, J. W., Paulsen, P. J., and Barnes, I. L., Absolute Isotopic Abundance Ratios and Atomic Weight of a Reference Sample of Potassium, J. Res. NBS 79A, 713-725 (1975).

[4] Barnes, I. L., Murphy, T. J., Gramlich, J. W., and Shields, W. R., Lead Separation by Anodic Deposition and Isotope Ratio Mass Spectrometry of Microgram and Smaller Samples, Anal. Chem. 45, 1881-1884 (1973).

Chemical Techniques for the Reduction of the Chromium Analytical Blank for Isotope Dilution Analysis

Lura P. Dunstan and Ernest L. Garner

National Bureau of Standards
Institute for Materials Research
Analytical Chemistry Division
Washington, D. C. 20234

In recent years there has been considerable interest in the determination of chromium in a number of environmental materials. Since chromium is often found at concentrations of less than 10 μg/g, it became necessary to develop a chemical procedure which would reduce the analytical blank so that high accuracy isotope dilution analyses could be performed.

Initial chromium determinations yielded analytical blanks averaging greater than 900 nanograms with variabilities as high as ±300 nanograms. To help ascertain the major sources of blank contribution, the chromium concentrations in the reagents used during the chemical separation procedure were determined by isotope dilution mass spectrometry. It was discovered that the two major sources of chromium contribution were the ceric sulfate, which was used to oxidize the chromium prior to extraction, and the methyl isobutyl ketone (MIKB), which was used as the extracting reagent. By using high purity (99.999%) ceric sulfate and MIKB which had been purified by sub-boiling distillation, the reagent blank for the chromium separation procedure was reduced from approximately 100 nanograms to less than 20 nanograms.

The major source of blank contribution from apparatus was found to be the borosilicate glass beakers which were used for the wet oxidation of the matrix. The analytical blanks determined in glass were three times larger than those determined in quartz, even though the glass beakers were new and had been rigorously cleaned. While it is well known that quartz is a purer material than glass, a difference of this magnitude was unexpected.

The reduction of the analytical blank from approximately 900 nanograms to less than 20 nanograms has permitted the determination of chromium with increased accuracy. The analysis of SRM 1570, Spinach, and SRM 1575, Pine Needles, yielded chromium concentrations of 4.47±0.05 μg/g and 2.63±0.02 μg/g respectively. Presently, samples containing one microgram of chromium can be determined with an estimated accuracy of 2 percent. Further reductions in the magnitude and variability of the analytical blank will be required to permit more accurate determinations at the submicrogram level.

Isotope Dilution Analysis of Synthetic Water Standards Using Electronic Detection Spark Source Mass Spectrometry

Paul J. Paulsen and John R. Moody

National Bureau of Standards
Institute for Materials Research
Analytical Chemistry Division
Washington, DC 20234

Table 1 shows the results of an analysis of a water standard by SSMS isotope dilution using both electronic and photoplate measurements of the altered isotopic ratios. With the exception of selenium where a large correction for a ZnC^+ interference caused difficulties, the photoplate precision is as good as can be routinely obtained. The standard deviation (S.D.) for electronic detection, however, was much higher than expected and not competitive when compared with the photoplate precision.

Table 1. SSMS Isotope Dilution Analysis of Synthetic Water.

	PPM by Weight				
	Cu	Zn	Cd	Se	Cr
Photoplate Detection, Graphite Mix	0.929 ±6.2%	5.49 ±4.1%	0.0145 ±6.0%	0.0118[a] ±12%	0.0465 ±5.8%
Electronic Detection, Graphite Mix	0.853 ±15%	5.55 ±12%	0.0157 ±19%	0.0106[a] ±19%	0.0500 ±11%

[a] Corrected for ZnC^+ interference.

Electronic measurement of an isotopic ratio requires the sequential measurement of the isotopes. Precision in the ratio measurements therefore depends on having a homogeneous sample, a controlled spark gap, controlled sample position, etc. The photoplate, which collects all mass simultaneously, has none of these requirements and its precision (±5% S.D.) is controlled only by the uniformity of the plate emulsion. Both the photoplate and electronic detection data suggested sample homogeneity variations as the source of the poor precision in the electronic detection analysis.

The water samples were prepared by spiking, evaporating to a small volume, slurring with graphite and ethanol, then drying. The dry graphite was then mixed in a plastic vial with several 1/8" plastic balls for 20 min on a Wig-L-Bug mixer. Since this procedure should have been adequate, we decided to examine other high purity powders as mixing medians to see if a more homogeneous final mixture could be obtained. Nine elements were added to various high purity powders. The samples were prepared and run under identical conditions. Isotopic ratios and precisions were calculated for each measurable element. Table 2 shows the result for a silver powder mixture. The average of all the S.D. (12.1%) is used as the criteria to evaluate the homogeneity of the mixture. Table 3 gives the average of the S.D. for each of the mixing powders used. The most significant improvement in precision of the

measurements was obtained with silver powder mixed in a stainless steel (SS) vial using a 1 g SS mixing ball. The use of a 1 g mixing ball is the key factor. Previous experience with the SS vials resulted in sample contamination with not only the major elements but also many minor constituents of the steel. This is the reason that plastic vials were used to mix the water sample (with graphite) reported in Table 1. Because of the significant improvement in the precision using the SS vial, the contamination problem was ignored and a mixing procedure with the SS vials developed. When a small sample is added to the silver, good homogeneity is obtained if mixed until the silver runs together to form 10X larger plateletts. Larger added amounts of sample may prevent the silver from forming large plateletts, however 5 to 10 min of mixing still will result in a sample giving good precision. Silver powder sometimes reacts chemically with certain samples to form a paste and proper mixing can only be obtained if a large excess of silver is used. The resulting dilution of the sample is usually not desirable. Gold powder will not react chemically and is the preferred mixing median for most samples.

Table 2. 100 mg "69" Ag Powder, 4 μg of Each Element Mixed in Plastic Vial, 3×10^{-10} Exposure.

	Measured Ratio	% Error	% S.D.
Pb 208/206	2.24	+1.2	10
Ba 138/137	6.07	-4.3	14
Mo 98/95	1.43	-5.4	9.8
Ni 58/60	2.56	-1.3	15
Cu 63/65	2.28	+1.7	11.4
		Average	12.1%

Table 3. Precision of Isotope Ratios Measured by Electronic Detection for Pb, Ba, Cd, Ag, Mo, Cr, Ni, Cu, Se.

	Wt. each Element	20 min Mixing	Average % S.D.
"69" Gold	4 μg	plastic[a]	8.8
"69" Silver	4 μg	plastic	12.1
"69" Silver	40 μg	plastic	12.8
"69" Silver	4 μg	stainless steel[b]	5.0
Pelletizing Graphite	4 μg	plastic	11.0
"69" Graphite	4 μg	plastic	15.9

[a] Plastic ball 1/8" diameter.
[b] SS ball 1/4" diameter, 1 gram.

The Wig-L-Bug mixer using the 1 g SS ball is equivalent to a high energy ball mill. It appears that the samples are being homogenized by a process of mechanical alloying of the added elements within the individual particles of the mixing powder (silver or gold). J. S. Benjamin [1] discusses this process in a recent review article on mechanical alloying of

high temperature alloys used in jet engine blades. Table 4 shows the precision and reproducability of the SSMS spike calibration done with electronic detection. These samples were mixed with silver in the SS vial using a 1 g SS ball. The precisions are considerably better than those reported in Table 1 using graphite mixed in plastic vials and are 2 to 3 times better than can be obtained by the photoplate. Table 5 gives the preliminary analysis of a new NBS synthetic water standard. The results are in error due to contamination from the SS vial during mixing, however there has been a significant improvement in analysis precision thru the proper homogenization of the samples.

Table 4. Spike Calibration for H_2O Analysis Silver Powder Mixed in Stainless Steel Vial.

	- - - #1 - - -		- - - #2 - - -	
	μg	% S.D.	μg	% S.D.
Pb	10.44	3.9	10.47	2.2
Ba	4.79	2.6	4.71	3.0
Cd	18.08	2.5	17.73	2.3
Mo	13.63	1.6	14.45	2.0
Sr	4.80	1.6	4.78	1.3
Se	18.10	2.7	---	---
Cu	10.34	3.5	10.20	3.5

Table 5. Preliminary Analysis of Synthetic Water Standard by Electronic Detection SSMS I.D.

	PPM Found	PPM Added
Pb	0.020	0.025
Ba	0.034	0.040
Cd	0.0080	0.0080
Mo	0.127	0.105
Sr	0.197	0.190
Se	0.011	0.012
Zn	0.064	0.065
Cu	0.014	0.015
Ni	$\leq$0.068[a]	0.050

[a] The samples show variable amounts of contamination from the stainless steel mixing vial.

Test of several types of mixing vials has indicated that sample contamination cannot be prevented easily. We have therefore adopted an approach of making mixing vials and balls out of a high purity material which will only contaminate the samples with a few elements. We are presently using oxygen free high conductivity copper (99.99% pure) to make mixing vials. These are being used for the analysis of the synthetic water shown in Table 5. The samples are mixed with gold powder and copper is the only detected contamination from the mixing ball and vial.

Reference

[1] Benjamin, J. S., Mechanical Alloying, Sci. Amer., 234, 40 (1976).

MODIFICATION OF AN A.E.I. MS7 SPARK SOURCE MASS SPECTROGRAPH FOR INCREASED PLATE RESOLUTION

M. L. Jacobs and S. L. Sweeney
Commercial Testing & Engineering, Golden, CO 80401
E. G. Kerfoot
Analytical Specialties Co., Lakewood, CO 80228

An A.E.I. Model MS7 spark source mass spectrograph has been updated by increasing the photoplate resolution of the instrument through a simple modification, without noticeably affecting the ion transmission.

The spark source mass spectrograph at Instrumental Analysis Division of Commercial Testing & Engineering Co., was originally built by A.E.I. in late 1963 and was not manufactured with a variable alpha slit or a later A.E.I. source modification which allowed increased plate resolution. The original instrument specifications called for 1000 resolving power at 208 m/e.

The modification consists of placing a fixed "alpha" slit at the entrance of the electrostatic analyzer housing by spot welding thin tantalum strips horizonally to the vertical 0.080" x 0.040" entrance slit to create a 0.040" x 0.040" opening. A marked increase in photoplate resolving power was obtained.

Densitometric measurements of resolution at m/e 207 and 208 (50% definition) were found to average 3000 to 4000 resolving power. The modified MS7 using a 0.002" No. 3 plate in the ion gun sufficiently separates hydrocarbon ion species and elemental ions into discreet and definable mass lines on the photoplate comparable to routine resolving power achieved by newer model instruments when operated at normal ion transmission rates.

Instrument modification was accomplished in one day with minimal expense and delay in normal analytical operations.

ANALYTICAL APPLICATIONS OF A DRIFT TUBE CI SOURCE

by

Philip Price, H. S. Swofford, Jr., and S. E. Buttrill, Jr.*
Department of Chemistry
University of Minnesota
Minneapolis, Minn. 55455

One of the most important characteristics of chemical ionization (CI) spectra is the high intensity of peaks containing molecular weight information. Often the $(M+1)^+$ ion is the only significant peak in the spectrum. While the molecular weight of an unknown sample is an extremely valuable piece of information, several fragment ions are generally required to identify an unknown. The extent of fragmentation in CI spectra can be increased by increasing the source temperature, but this method is too time consuming for routine work. One method of increasing the effective temperature of the ions in a CI source is to expose them to an electric drift field. The ion energy is then dependent on E/P which may be varied rapidly by changing the drift potential.

We have designed and built a chemical ionization source which incorporates a drift tube as shown in cross section in Figure 1. The shaded parts are polished rings machined from glass ceramic. The remaining parts are stainless steel. The electron beam enters at the rear at a 45° angle to the source axis, but electrons do not penetrate into the drift tube. The source has operated successfully at temperatures up to 250°C. Total distance traveled by ions leaving the 0.030 inch ion exit hole is about 6.5 cm.

Figure 2 compares the reagent ions observed in water and in isobutane as a function of E/P (volts/cm·torr). Isobutane has the obvious advantage of a simple reagent ion spectrum, but structurally significant propyl and butyl fragment ions cannot be detected in this reagent gas. At low E/P, the relative intensities of m/e 91, 73, and 55 in water $[H^+(H_2O)_n$, n = 5, 4, 3] are approximately those expected if the ions are in thermodynamic equilibrium. However, the ions at m/e 37 and 19 would be absent at true equilibrium. As the electric field in the drift tube is increased, the ions acquire increased amounts of translational energy between collisions. The ion neutral collisions result in the conversion of some of the translational energy into internal (vibrational, rotational) energy. There are two simple models of this situation: (1) the ions are broken apart as the result of energetic ion-neutral collisions and (2) the ion (but not the neutral) "temperature" is increased by the drift field. Both models are oversimplified.

---

*Present address: Mass Spectrometry Research Center, Stanford Research Institute, Menlo Park, CA 94025

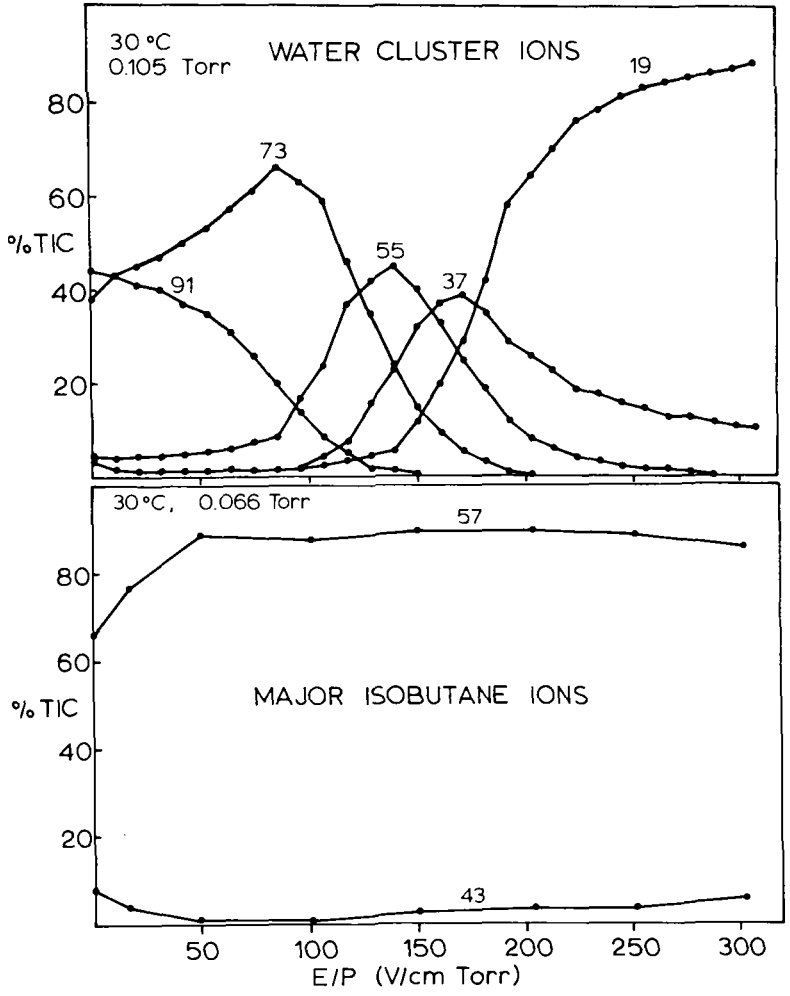

← Figure 2

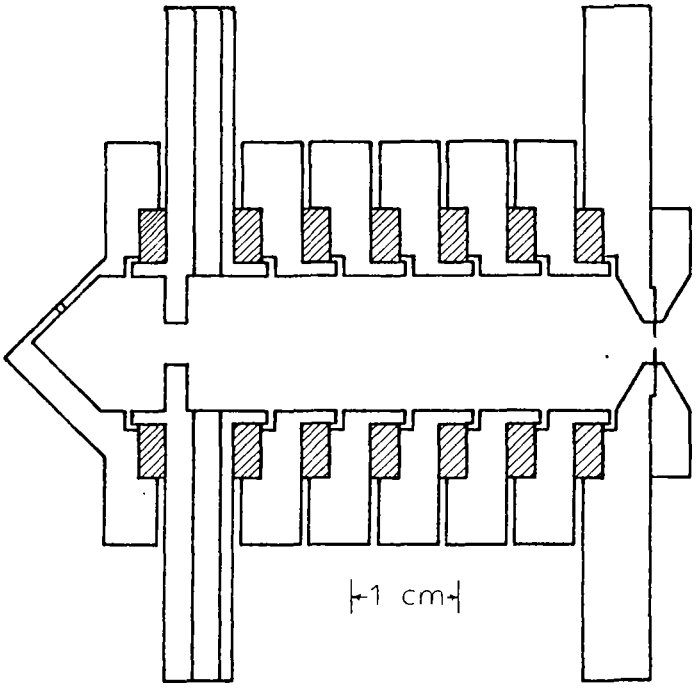

Figure 1

Figure 3 illustrates the similarity of the effects of raising the temperature and increasing the drift field strength on the water CI spectrum of ethyl acetate. The top spectrum at low E/P and 110°C shows only MH^+ at m/e 89 and the hydrogen-bonded cluster $MH^+ \cdot H_2O$ at m/e 107. At higher E/P, as shown by the middle spectrum, the cluster ion is completely gone and the MH^+ is about 80% fragmented. Raising the source temperature to 220°C as shown in the bottom spectrum produces about 50% fragmentation, but the high energy fragments at m/e 15 and 33 are not observed. The fragment ion at m/e 61 is protonated acetic acid formed by loss of ethylene from the MH^+ ion while m/e 43 is CH_3CO^+ formed by loss of ethanol.

In order to establish that the observed fragmentation is caused by energetic collisions between MH^+ ions and the reagent gas rather than a change in the reagent ion identity with E/P, ethyl butyrate was run as a function of E/P in both water and isobutane. Except for the cluster ion with water at low E/P, the spectra (Fig. 4) are qualitatively very similar even though the exothermicity of the proton transfer to the ester from H_3O^+ is about 25 keal/mole more exothermic than from $C_4H_9^+$. The situation is complicated, however, by the fact that, because of the difference in reduced mass, more energy is available for ion dissociation in collisions with isobutane than with water. A quantitative understanding of the processes occurring in the drift tube CI source will require further detailed studies.

The analytical utility of the drift tube CI source is obvious. From a single sample, one can obtain a CI spectrum at low E/P which provides both high sensitivity (single peak) and molecular weight information. By simply turning a knob, one can then go to a high E/P and obtain on the next scan a spectrum showing extensive fragmentation, and therefore containing a large amount of structural information. Furthermore, in future work it will probably be possible to relate the value of E/P at which a fragment appears to the thermochemistry of the MH^+ ion, thereby obtaining additional insight into the structure of the sample.

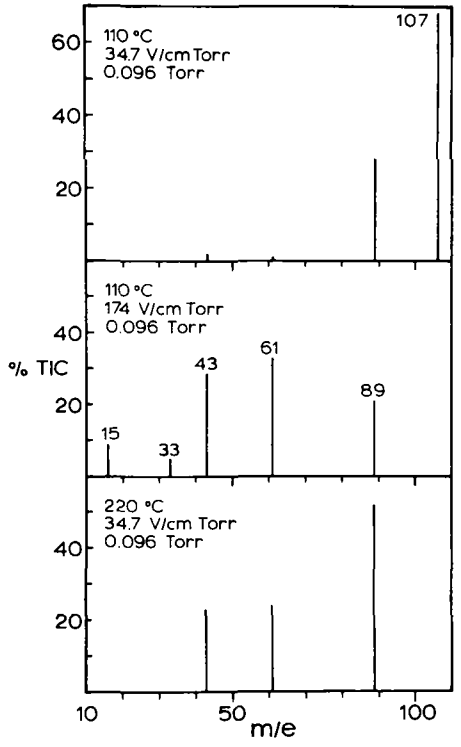

WATER CI SPECTRA OF ETHYL ACETATE

Figure 3

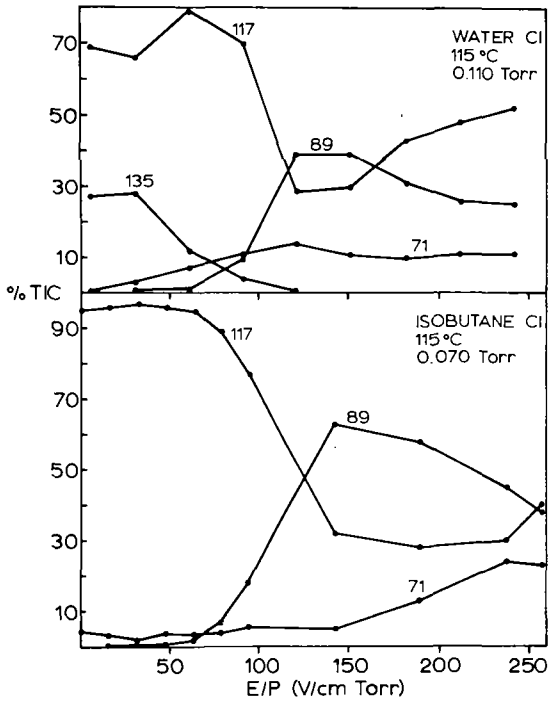

CI FRAGMENTATION OF ETHYL BUTYRATE

Figure 4

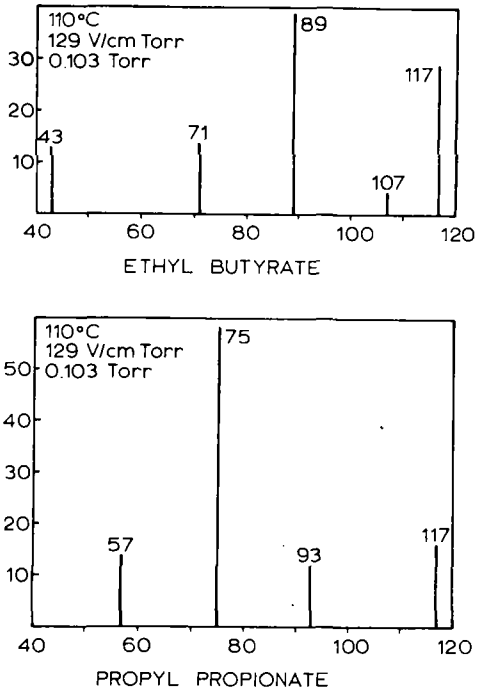

WATER CI SPECTRA

Figure 5

REAGENT GASES FOR NEGATIVE ION CHEMICAL IONIZATION MASS SPECTROMETRY *

Donald F. Hunt, T. Michael Harvey,
& Thomas Knudsen

Department of Chemistry
University of Virginia
Charlottesville, Virginia 22901

Bombardment of CH_3ONO in CH_4 at 1 torr with electrons from a hot metal filament or Townsend discharge[1] affords CH_3O^- in high abundance. This ion functions as a strong Bronsted base in the gas phase and produces abundant $(M-1)^-$ sample ions from most organics. If the sample molecule conc. reaches ca. 5% that of CH_4, the CH_3O^- ions are consumed and replaced by $(M-1)^-$ ions derived from the additive. With the above technique it is possible to generate a wide variety of ionic bases and nucleophiles for use as CIMS reagents. Ion molecule reactions of several negative ion reagents produced in the above manner will be discussed.

[1] D.F. Hunt, C.N. McEwen, and T. Michael Harvey, Anal. Chem., 47, 1730 (1975).

* to be published in Analytical Chemistry

AMMONIA CHEMICAL IONIZATION OF SOME FREE AMINO ACIDS AND UNDERIVATIZED PEPTIDES*

J. S. Gaffney, R. C. Pierce† and L. Friedman

Department of Chemistry
Brookhaven National Laboratory
Upton, New York 11973

Ammonia chemical ionization mass spectra of rapidly heated free amino acids and peptides provide an opportunity for a study of the competition between gas phase solvation and association reactions of these biochemically interesting species. Compounds investigated include methionine, phenylalanine, tryptophan , and peptides; Ala-Ala, Phe-Ala, Ala-Ala-Ala, Gly-Ala-Phe, Ala-Phe-Gly, Tetra-Ala, and PCA-His-Pro-NH_2 (Thyrotropin Releasing Hormone). Extensive formation of solvated-protonated species were observed and associated protonated peptides up to $(4M+1)^+$ in some cases. The observation of association reactions with rapidly heated samples presents problems in the analytical use of this technique. Investigation of the kinetic order of reactions leading to association of protonated species reveals a significantly more effective energy transfer process in collisions of protonated peptides with parent neutral molecules than with neutral solvent gas.

*Research carried out at Brookhaven National Laboratory under contract with the U.S. Energy Research and Development Administration.

†Present address: Research and Development Department, Colgate-Palmolive Co., Piscataway, New Jersey 08854.

REACTIONS OF LYSINE UNDER CHEMICAL IONIZATION CONDITIONS

ROBERT J. WEINKAM AND JAY D'ANGONA

Contribution from the Department of Pharmaceutical Chemistry
School of Pharmacy, University of California
San Francisco, California, 94143.

Reactions in a chemical ionization source occur at or near thermal equilibrium and at a sufficiently high pressure so that protonated molecular ions, once formed, undergo collisions before leaving the ion source. Under these conditions reasonably complex intra and intermolecular reactions can occur. The details of these reaction pathways are difficult to determine as only the molecular structure of reactants and mass of the products are known. This is an effort to use a series of related and model compounds to define reaction pathways and intermediates of protonated diamino acids in the gas phase.

Lysine, 2,6-diaminohexanoic acid, 1, fragments by loss of NH_3, H_2O and CO. An homologous series of diamino acids, 1 to 4, show large differences in the $MH-NH_3$ and $MH-H_2O$ ion intensities while the ions resulting from loss of H_2O, CO and subsequent fragmentation total about 25% Σ for each compound. Loss of NH_3 and H_2O proceed through bifunctional interactions as these ions are not formed in the simple model compounds 5 to 7. Loss of H_2O, CO, assumed to be a rapid sequential fragmentation, was prevalent in the 2-amino acid 7 and apparently occurs in 1 to 4 without interaction with the terminal amino group.

The fragmentation sequence for lysine was determined from its ion kinetic energy spectrum without interference from methane reagent gas. Losses of H_2O, CO from ($MH-NH_3$), m/e 130 to 84, and of NH_3 from ($MH-H_2O$, CO), m/e 101 to 84, were observed but no fragmentation of the ($MH-H_2O$) ion was detected.

Elimination of ammonia from the protonated diamino acids, 1 to 4, apparently occur by way of an intramolecular interaction between the amine groups. Lysine labeled as 2-$^{15}NH_2$ shows preferential loss of NH_3 from the terminal position. An homologous series of diamines $NH_2(CH_2)_nNH_2$, 8 to 14, show abundant loss of NH_3 for the lower homologs n = 3 to 6 while for n = 8 the protonated molecular ion is stabilized. This is consistent with an internal displacement and cyclization reaction. Subsequent loss of H_2O, CO will be dependent on the stability of the resulting cyclic immonium ion so that this ion would be less prevalent in 3 and 4. This is confirmed by the spectra of the cyclic amino acids.

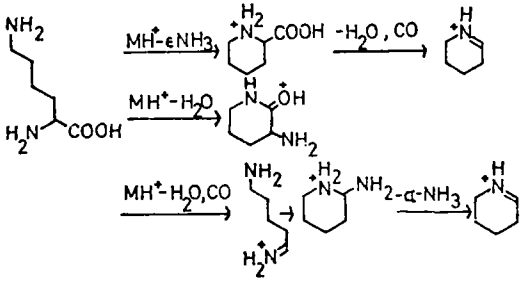

Loss of H_2O from protonated diamino acids apparently occurs through an interaction between the terminal amine and carboxyl groups. The MH-H_2O ion is prevalent in the amino acids $NH_2(CH_2)_nCOOH$, 15 to 18. This is consistent with internal displacement and lactam formation. No fragmentation of 2-amino lactams is observed under these ci conditions.

Loss of H_2O, CO is prevalent because of the ability of the 2-amino group to stabilize the resulting ion. This ion, however, shows a specific loss of the 2-NH_3 group. A cyclization elimination pathway had been proposed to explain this sequence. The prevalence of the NH_3 loss is dependent on the stability of the cyclic immonium ion and thus not seen in the lowest homologs.

It appears that the differences between the diamino acids 1 to 4 can be explained from the structures of the cyclic intermediates formed from the competing MH-NH_3 and MH-H_2O reactions, assuming some relation between activation energy and product stability, and from the stability of the MH-H_2O, NH_3, CO ion in determining the prevalence of secondary fragmentations. These results suggest that a reasonably detailed description of gas phase reaction mechanisms may be possible.

Table Methane Chemical Ionization Spectra Taken With An Ion An Ion Chamber Pressure of 0.6 torr and 200°C.

	Compound	MH	-17	-18	-17,18	-18,28	-18,28
1	2,6-Diaminohexanoic acid	30	24	4	2	2	29
2	2,5-Diaminopentanoic acid	1	3	44	3	3	34
3	2,4-Diaminobutyric acid	1	1	55	2	20	8
4	2,3-Diaminopropionic acid	30	31	2	2	29	1
5	1-Hexanoic acid	74		4			
6	1-Hexylamine	60	1				
7	2-Aminohexanoic acid	27	1	4		59	
8	1,3-Diaminopropane	22	63				
9	1,4-Diaminobutane	3	78				
10	1,5-Diaminopentane	5	72				
11	1,6-Diaminohexane	19	64				
12	1,8-Diaminooctane	62	8				
13	1,10-Diaminodecane	65	2				
14	1,2-Diaminododecane	79	2				
15	3-Aminopropionic acid	30	1	58			
16	4-Aminobutyric acid	12	20	57			
17	5-Aminopentenoic acid	26	17	49			
18	6-Aminohexanoic acid	24		50			

An Ion Cyclotron Resonance Investigation of Chemical Ionization Reactions of Ketones.

Douglas P. Ridge and Richard H. Dianich
Department of Chemistry
University of Delaware
Newark, Delaware 19711

The methane chemical ionization spectra of some steroidal ketones show significant (M+1 - H_2O) peaks.[1] The relative importance of water loss seems to depend on the structure of the ketone as indicated below:

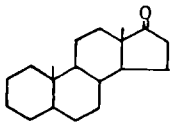

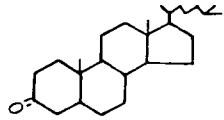

$\frac{M+1-H_2O}{M+1}$	1.36	.09

To better understand the water loss process we examined the reactions of CH_5^+ with a number of ketones using ion cyclotron resonance techniques.

Decalones and hexahydroindanones were selected as models for the steroidal systems. By analogy with the steroidal ketones it was expected that 1-hexahydroindanone would show considerable water loss but that 2 decalone would not. As indicated below both showed considerable water loss under icr conditions, although the high pressure chemical ionization spectra of the two compounds show little water loss.

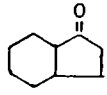

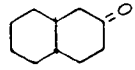

1 torr CH_4 [2] (CI conditions)	$\frac{M+1-H_2O}{M+1}$	0.15	0.06
5×10^{-5} torr CH_4 (icr conditions)	$\frac{M+1-H_2O}{M+1}$	3.8	0.96

A possible reason for the difference between the low pressure result and the high pressure result is the collisional stabilization of the protonated ketone at high pressure. A mechanism involving such a collisional stabilization is outlined below:

$$CH_5^+ + C_{10}H_{16}O \xrightarrow{k^*} [C_{10}H_{16}OH^+]^* + CH_4$$

$$CH_5^+ + C_{10}H_{16}O \xrightarrow{k} C_{10}H_{16}OH^+ + CH_4$$

$$[C_{10}H_{16}OH^+]^* + CH_4 \xrightarrow{k_s} C_{10}H_{16}OH^+ + CH_4$$

$$[C_{10}H_{16}OH^+]^* \xrightarrow{k_{uni}} C_{10}H_{15}^+ + H_2O$$

Applying the steady state approximation to this mechanism yields

$$\frac{[C_{10}H_{16}OH^+]}{[C_{10}H_{15}^+]} = \frac{k}{k^*} + \frac{k_s}{k_{uni}}\left(\frac{k}{k^*} + 1\right)[CH_4]. \qquad (1)$$

Thus if the assumed mechanism is correct a plot of $(M+1)/(M+1-H_2O)$ against methane pressure should be linear. From the slope and intercept of such a plot k_s/k_{uni} may be determined. If we assume $k_s=\varepsilon k_L$ where k_L is the Langevin collision rate and ε is the efficiency of the stabilization process, then $\varepsilon/k_{uni} = \varepsilon\tau$ may be determined from k_s/k_{uni}. Thus plots of $(M+1)/(M+1-H_2O)$ versus methane pressure provide us with a measure of the lifetime, τ, of the protonated ketone with respect to water loss. Such plots for several bicyclic ketones is shown in Fig. 1. The linearity of the plots indicates that the kinetic model is correct. Lifetimes derived from such plots assuming $\varepsilon=1$ are given for a number of protonated ketones in Table I.

The data in Table I suggest several conclusions. Position of the carbonyl determines the lifetime of protonated bicyclic ketones. Ring size is unimportant. Ring size is evidently important in the case of methyl cyclopentanone and methyl cyclohexanone. Straight chain saturated ketones have lifetimes similar to those of 2-bicycloketones. Straight chain unsaturated ketones have lifetimes similar to those of 1-bicycloketones. There seem to be at least two mechanisms for water loss from the protonated ketones as characterized by the lifetime data. These processes are under further study. Finally we note that the present results indicate the usefulness of icr for characterizing the dynamics of chemical ionization processes. The measurements would have been difficult by conventional means.

---

[1] J. Michnowicz and B. Munson, Org. Mass Spec., 8, 49 (1974).

[2] J. Michnowicz and B. Munson, unpublished results.

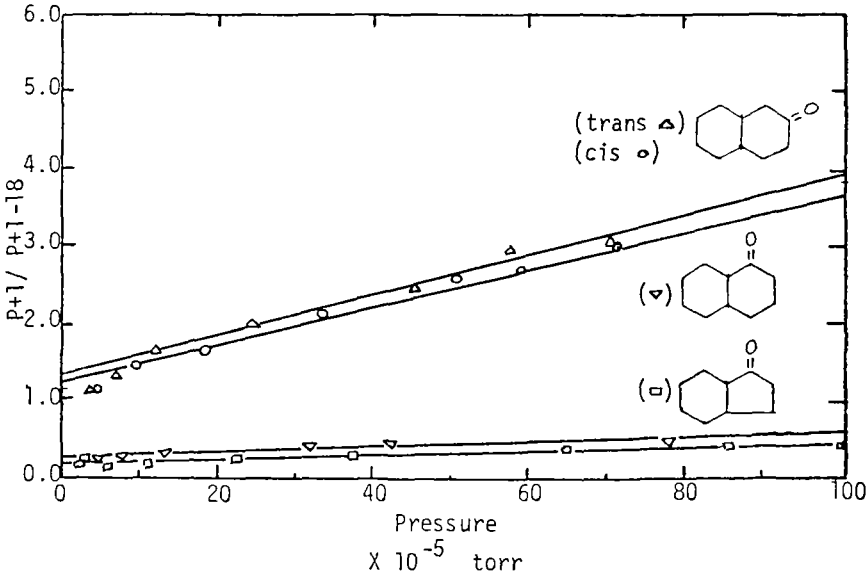

Figure 1

Table I.

Lifetimes of Protonated Ketones (μ sec)

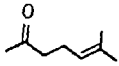

1

4.7

6.6

16

30

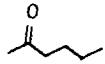

30

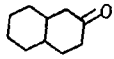

33

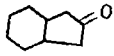

34

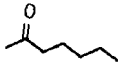

34

43

DETERMINATION OF THE SITE OF PROTONATION IN THE WATER CHEMICAL IONIZATION OF AROMATIC COMPOUNDS

by

D. P. Martinsen and S. E. Buttrill, Jr.*
Department of Chemistry
University of Minnesota
Minneapolis, Minn. 55455

In the D_2O CI spectrum of benzene, the $C_6H_6D^+$ ion undergoes a series of reactions with D_2O in which all six ring hydrogens are exchanged for deuterium.

$$C_6H_6D^+ + D_2O \rightarrow C_6H_5D_2^+ + HDO$$
$$C_6H_5D_2^+ + D_2O \rightarrow C_6H_4D_3^+ + HDO$$
$$\vdots$$
$$C_6H_6D^+ + D_2O \rightarrow C_6D_7^+ + HDO$$

Similar reactions are observed in toluene, the xylenes, and the halobenzenes. Although the relative rates of the exchange reactions vary widely, the number of hydrogens exchanged is equal in almost all cases to the number of unsubstituted ring positions. Hydrogen-deuterium exchange does not occur in either the molecular ion or the neutral molecules of these compounds, and we conclude that protonation of the ring is a necessary conditions for the exchange.

In contrast to the compounds listed above, no hydrogen-deuterium exchange is observed at the ring positions in aromatic compounds containing oxygen or nitrogen. Compounds studied include phenol, anisole, benzaldehyde, nitrobenzene, analine, the diaminobenzenes, and dihydroxybenzenes. The lack of exchange of ring hydrogens in these compounds indicates that they protonate on the substituent.

The formation of hydrogen-bonded clusters of the protonated molecule and one or more molecules of water is a second reaction which distinguishes between ring and substituent protonation.

$$MH^+ + H_2O \rightleftarrows MH^+ \cdot H_2O$$
$$MH^+ \cdot H_2O + H_2O \rightleftarrows MH^+ \cdot 2H_2O$$

It is our general experience that the formation of these cluster ions is to be expected when the molecule M contains oxygen or nitrogen and it is generally not observed if M is a hydrocarbon. In every case we have examined, compounds which undergo the ring hydrogen-deuterium exchange reaction show no $MH^+ \cdot H_2O$ ion formation, whereas aromatic compounds in which ring exchange is absent form $MH^+ \cdot H_2O$, $MH^+ \cdot 2H_2O$, etc. in "normal" amounts. This is the expected behavior since ring protonation results in extensive delocalization of the positive charge over the ring whereas protonation at oxygen or nitrogen leads to one or more hydrogens with the large positive charge required for the formation of strong hydrogen bonds.

A complete paper is in press in Organic Mass Spectrometry.

---

*Present Address: Mass Spectrometry Research Center, Stanford Research Institute, Menlo Park, CA 94025.

STRUCTURAL EFFECTS ON WATER CLUSTER ION FORMATION IN THE WATER CI SPECTRA OF SIMPLE AROMATIC COMPOUNDS

by

D. P. Martinsen and S. E. Buttrill, Jr.*
Department of Chemistry
University of Minnesota
Minneapolis, Minn. 55455

The water CI spectra of most compounds contain hydrogen-bonded clusters of general formula $MH^+\cdot(H_2O)_n$ (n = 1-4). Under carefully controlled conditions of source temperature and water pressure, the relative intensities of these cluster ions and the MH^+ ion are strongly dependent on the structure of the molecule M. It is often possible to distinguish the ortho, meta, and para isomers of disubstituted benzenes by this method. As examples, Table I gives the cluster ion distributions observed for four sets of substituted phenols at 120°C and 0.3 torr water pressure in our modified DuPont 21-490B mass spectrometer.

Table I: Water CI Spectra of Some Substituted Phenols

M	Isomer	Relative Intensities MH^+	$MH^+\cdot H_2O$	$MH^+\cdot 2H_2O$
chloro-phenol	ortho	1.0	0.10	
	meta	1.0	0.77	
	para	1.0	0.78	
hydroxy-phenol	ortho	1.0	0.18	0.16
	meta	1.0	0.58	0.06
	para	1.0	0.95	0.53
methyl-phenol	ortho	1.0	0.50	0.06
	meta	1.0	0.62	0.05
	para	1.0	0.85	0.30
ethyl-phenol	ortho	1.0	0.40	0.01
	meta	1.0	0.59	0.05
	para	1.0	0.78	0.20

In order to obtain quantitative information on the kinetics and thermodynamics of the processes which result in the structural dependence of the cluster ion intensities, we have built a special high pressure source designed to operate in the pulsed mode. The source mounting plate contains the ion exit hole and is electrically insulated from the source body as shown in Figure 1. A small extraction potential can be applied to the mounting plate to draw the ions out of the source. The source body and mounting plate are separately heated and the source pressure is measured through a 0.12 inch tube connected directly to either an MKS Baratron or Texas Instruments Bourdon Gage. The electron beam is provided by a

*Present address: Mass Spectrometry Research Center, Stanford Research Institute, Menlo Park, CA 94025

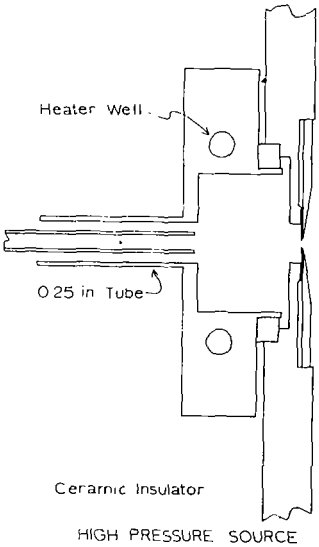

Figure 1

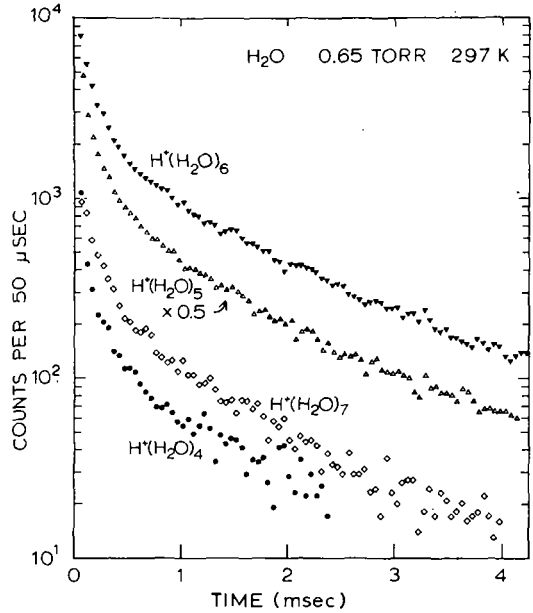

Figure 2

modified electron gun from an oscilloscope CRT. By using the oscilloscope controls, the electron beam may be rapidly positioned over the electron beam entrance hole in the source for a variable period of time as determined by the width of a TTL logic pulse. The experimental procedure is very similar to that of Kebarle (1). The electron beam is pulsed on, generally for 10 μs, and the mass analyzed ions reaching the multiplier are counted and stored by a PDP-12/30 computer as a function of the elapsed time. Data for pure water at 0.65 torr and 297K are shown in Figure 2. If the sum of all the ions detected within a 50 μs time window is used to normalize the ion count for each species counted, the data can be displayed as in Figure 3 as the percent of total ionization vs. time. In this way, the time dependence of the relative concentrations of the various ionic species in the source can be determined. Figure 3 shows that the concentrations of $H^+(H_2O)_n$, n = 4-7, rapidly come to equilibrium allowing us to measure the equilibrium constants K_n for the reactions

$$H_2O + H^+(H_2O)_{n-1} \rightleftharpoons H^+(H_2O)_n \qquad \text{(R1)}$$

$$K_n = \frac{[H^+(H_2O)_n]}{[H_2O][H^+(H_2O)_{n-1}]}$$

for n = 5, 6, and 7. All of our measurements to date of the equilibrium constants K_n for (R1) are in excellent agreement with Kebarle's data (1).

When ortho-chlorophenol is added in trace amounts to the water in the ion source, ions appear corresponding to protonated chlorophenol, MH^+, and the hydrogen-bonded cluster with one water molecule, $MH^+ \cdot H_2O$. From the data shown in Figure 4, we can calculate the

Figure 3

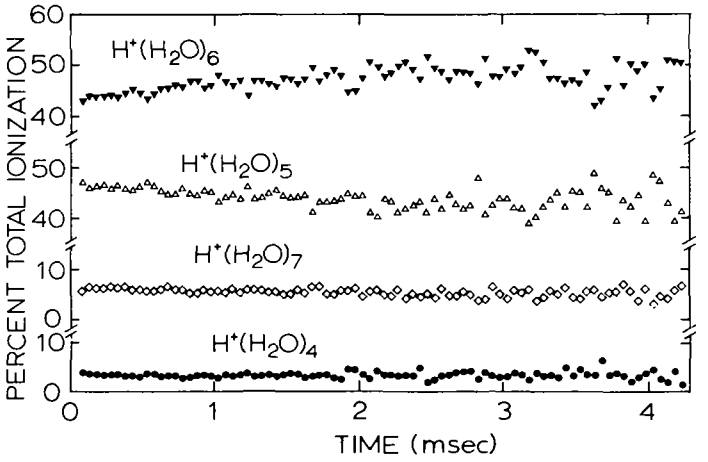

Figure 4

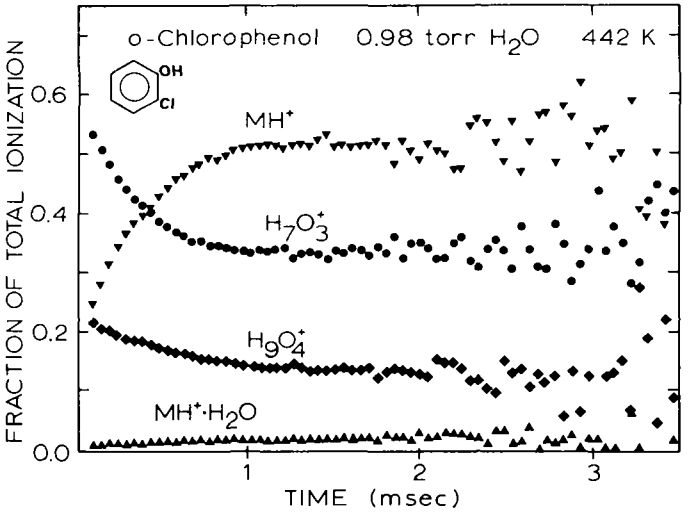

equilibrium constant for (R2)

$$MH^+ + H_2O \rightleftharpoons MH^+ \cdot H_2O \qquad \text{(R2)}$$

and from thence the free energy change, $\Delta G = -RT \ln K$. For the chlorophenols, our preliminary values for ΔG at 440K are ortho, -2.8; meta, -4.6; and para, -6.2 kcal/mole.

Measurements of ΔG for reactions such as (R2) are a potentially valuable analytical tool. In practice, the measurement can be quite simple since the partial pressure of water may be calculated from the known thermochemical properties of the reactions (R1). Thus, the only data required are the relative intensities of the peaks in the water CI spectrum of the compound after sufficient time has elapsed for the attainment of equilibrium.

(1) J. Amer. Chem. Soc. 94, 7627 (1972).

ION-MOLECULE REACTIONS OF COPPER ACETYLACETONATE (acac)

G. H. Weddle, T. C. Rhyne, and J. G. Dillard
Department of Chemistry
Virginia Polytechnic Institute and State University
Blacksburg, VA 24061

ABSTRACT

Ion-molecule reactions of copper acetylacetonate have been studied. Positive and negative ion reactions were examined. The important positive ion reactions involve the formation of polymeric copper-containing species according to the probable reactions:

$$Cu(acac)_2^+ + Cu(acac)_2 \rightarrow Cu_2(acac)_3^+ + acac$$
$$Cu(acac)^+ + Cu(acac)_2 \rightarrow Cu_2(acac)_2^+ + acac$$
$$CuH(acac)^+ + Cu(acac)_2 \rightarrow Cu_2(acac)_2^+ + Hacac$$

In mixtures of reaction gases with $Cu(acac)_2$ in a ratio of approximately 1000:1; reaction gas: $Cu(acac)_2$ a number of positive ion and charge transfer products were observed. The significant reactions are summarized below.

$$Cu(acac)_2 + M^+ \rightarrow Cu(acac)_2^+ + M$$
$$M = SO_2,\ N_2O,\ CO_2,\ SF_6,\ SO_2F_2$$
$$Cu(acac)_2 + SF_5^+ \rightarrow Cu(acac)_2F^+ + SF_4$$

Negative ion reactions of importance included the following.

$$Cu(acac)_2 + SO_2^- \rightarrow Cu(acac)_2S^- + O_2$$
$$\text{or} \rightarrow Cu(acac)_2O_2^- + S$$
$$Cu(acac)_2 + SO_2F_2 \rightarrow Cu(acac)F_2^- + acac + SO_2$$

The complete details of this work and a discussion of the results will be published in the near future.

Application of CI Fragmentation to Structural Elucidation. TED CHANG, Research Division, Wyeth Labs. Inc., P. O. Box 8299, Phila., Pa. 19101

Most organic compounds produce an intense MH+ ion in their CI spectra than the M+ ion in their EI spectra. Therefore the CI technique is mainly used for the determination of the molecular weights or for the analysis of mixtures. On the contrary to general misconception, many organic compounds do produce fragment ions in addition to the MH+ ion in their CI spectra. These fragment ions often provide useful structural information. The CI fragmentation can compliment the EI fragmentation in the following manners. The CI fragment ions are more pronounced and rarely show cruster ions thus making interpretation easier. Some weak EI fragment ions are more prominent in the CI spectra. Occasionally a fragment ion will appear in the CI but not in the EI because the fragmentation pathway is favored in the CI only. Finally, the neutral fragment ions which are not observable in the EI, can be protonated to offer additional information.

FORENSIC IDENTIFICATION OF DRUG MIXTURES BY CHEMICAL IONIZATION MASS SPECTROMETRY

S. Zitrin and J. Yinon
Department of Isotope Research
The Weizmann Institute of Science
Rehovot, Israel

Introduction

Drugs are often encountered as multicomponent mixtures, like commercial tablets or natural plants. The analysis of such mixtures is usually carried out by GC-MS techniques (1), producing large number of mass spectra, which makes forensic identification, without a data system, a complex and time-consuming process.

We have applied direct chemical ionization mass spectrometry as a technique for the identification of forensic mixtures using methane, isobutane and water as reagents.

This will be demonstrated by a few typical examples.

Experimental

Mass spectra were obtained with a Du Pont 21-490 B Single focusing mass spectrometer equipped with a dual EI/CI Source. The pressure of the methane and isobutane in the source was 0.3 - 0.5 Torr. The pressure of the water in the source was about 0.05 Torr, which is one order of magnitude smaller than normal CI with methane or isobutane. This pressure of water is obtained by injecting 20 - 30 µliter of water in the batch inlet system.

Results and Discussion

Figure 1 shows the CI mass spectra of Opium with isobutane and with water as reagents. We see the major alkaloids of Opium: Narcotine (M + 1 at m/e 414), Papaverine (M + 1 at m/e 340), Thebaine (M + 1 at m/e 312), Codeine (M + 1 at m/e 300) and Morphine (M + 1 at m/e 286). A non-alkaloid compound, Meconine, is also observed (M + 1 at m/e 195).

The base peak at m/e 220 is a fragment ion from Narcotine obtained from a fragmentation process which includes the protonation of the lactone oxygen, cleavage of the CH-O bond and rearrangement, so that the proton remains on the neutral species (2). This has been confirmed by analyzing pure Narcotine with deuterated methane.

Figure 2 shows the CI mass spectra of a drug suspected to be Scophedal. Two of its components, Dihydrohydroxycodeinone (Oxycodone) and Ephedrine

were easily identified from both CI isobutane and water mass spectra. A third component, Scopolamine, which should have been present in very small quantities, was not detected.

Figure 3 shows the CI (isobutane and water) mass spectra of a tablet suspected to be Velconal (or Wellconal), which was identified by its two components: Cyclizine (M + 1 at m/e 267) and Dipipanone (M + 1 at m/e 350). Both compounds undergo fragmentation processes following the protonation of the basic nitrogen atom, which give rise to the peaks at m/e 167 and m/e 265.

Figure 4 shows the CI mass spectra of an unknown tablet which has been given the name "Case No. 5522/1". Both spectra are with isobutane as reagent, but at different temperatures. The first spectrum, which is obtained at lower temperatures, shows two of the components of the tablet: Amobarbital (M + 1 at m/e 227) and Tetracaine (M + 1 at m/e 265). The third component appears only at higher temperatures: Fenethylline (M + 1 at m/e 342).

In figure 5, which shows the CI-water mass spectrum of the same tablet, we observe all 3 components in one single spectrum.

Figure 6 shows the CI (methane, isobutane and water) mass spectra of an unknown tablet which has been given the name "Case No. 306/76". It can be observed from the spectra that this tablet contains two components: 4-Methyl-5-Thiazoleethanol (M + 1 at m/e 144) and Pyridoxine (M + 1 at m/e 170).

Conclusion

Chemical ionization mass spectrometry can be used for forensic identification of drug mixtures by choosing the right reagent.

From the examples shown, water seems to be a good choice, because it gives simple CI mass spectra.

Acknowledgment

This work was supported by a grant from the Israeli Police.

References

1. R.M. Smith, J. of Forensic Sciences, 18, 327 (1973).
2. S. Zitrin and J. Yinon, to be published.

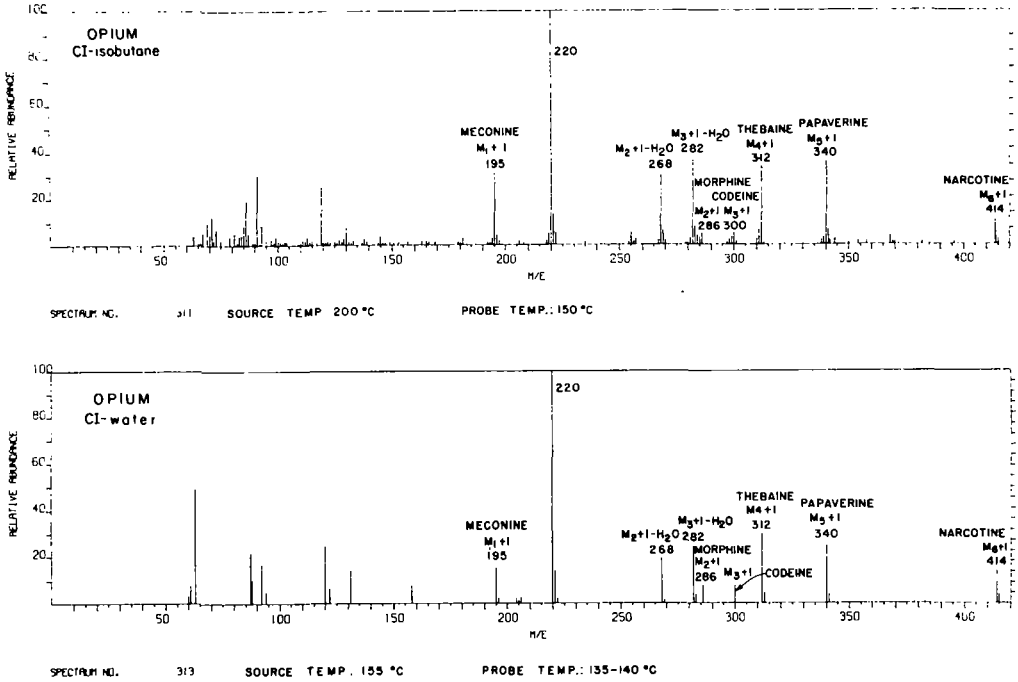

Fig. 1 CI mass spectra of Opium

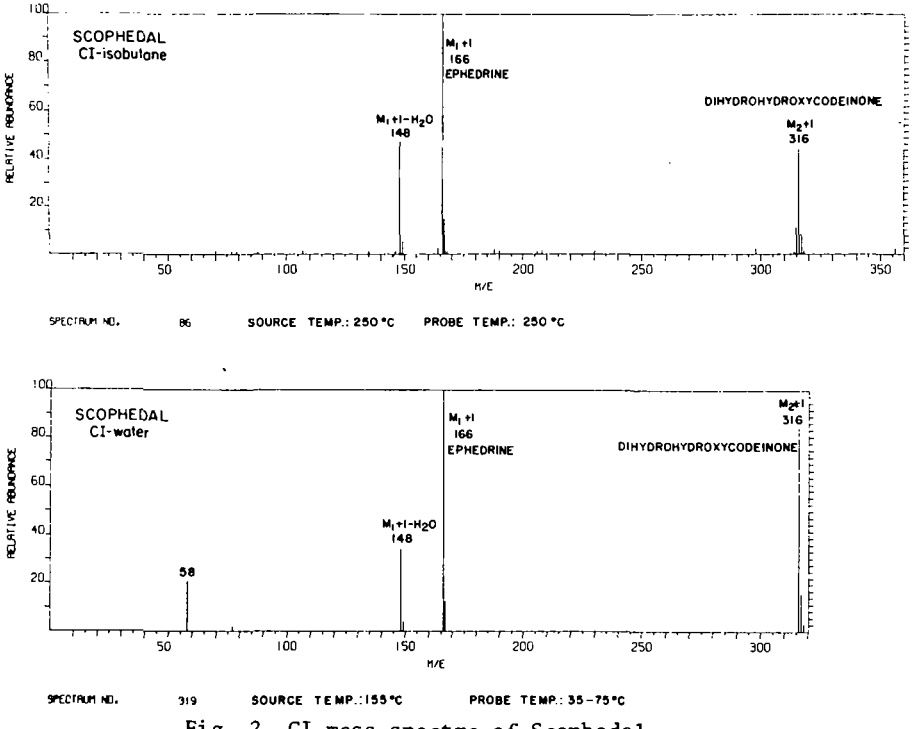

Fig. 2 CI mass spectra of Scophedal

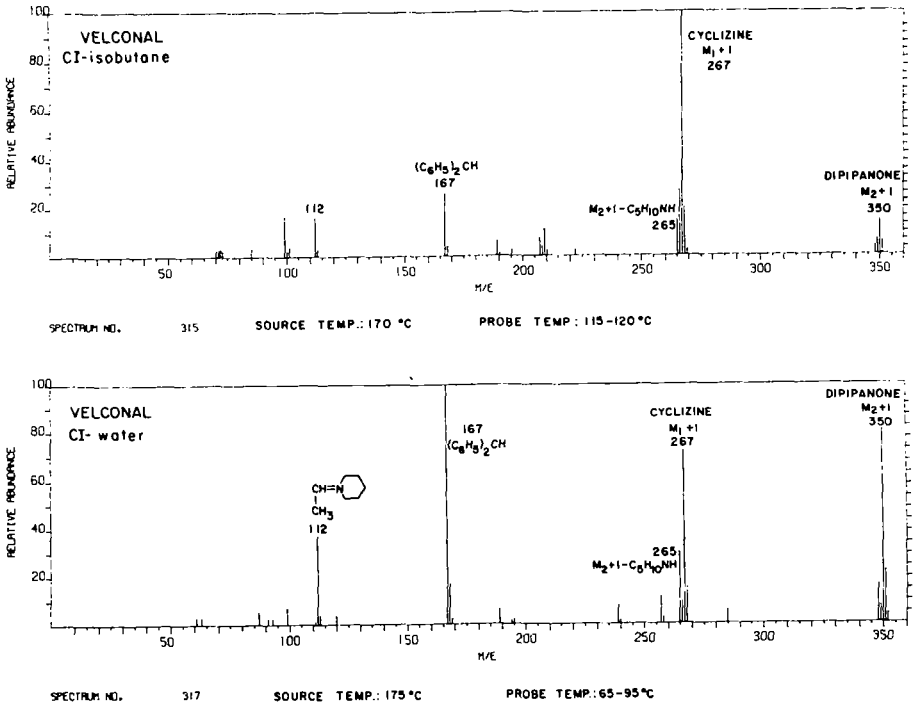

Fig. 3 CI mass spectra of Velconal

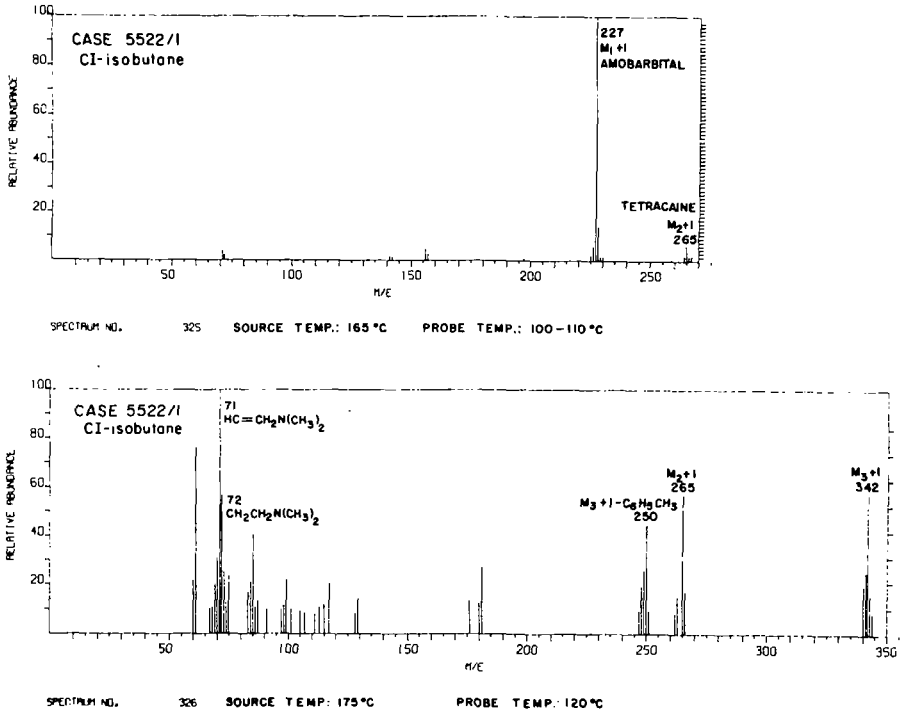

Fig. 4 CI-isobutane mass spectra of "Case No. 5522/1"

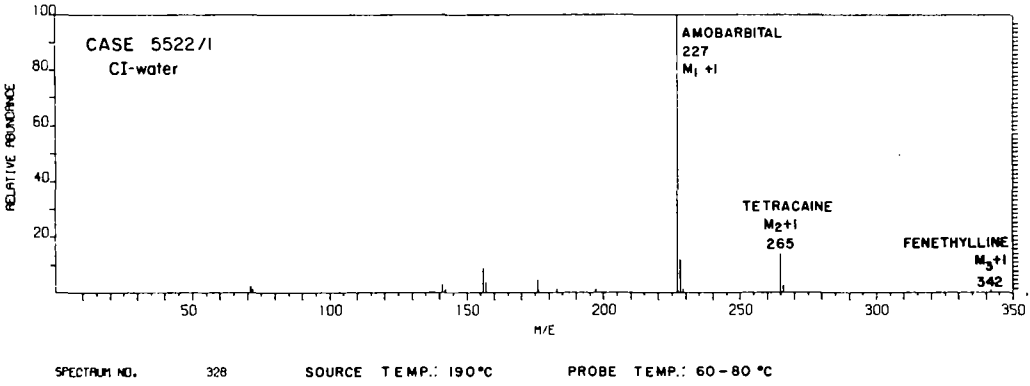

Fig. 5 CI-water mass spectrum of "Case No. 5522/1"

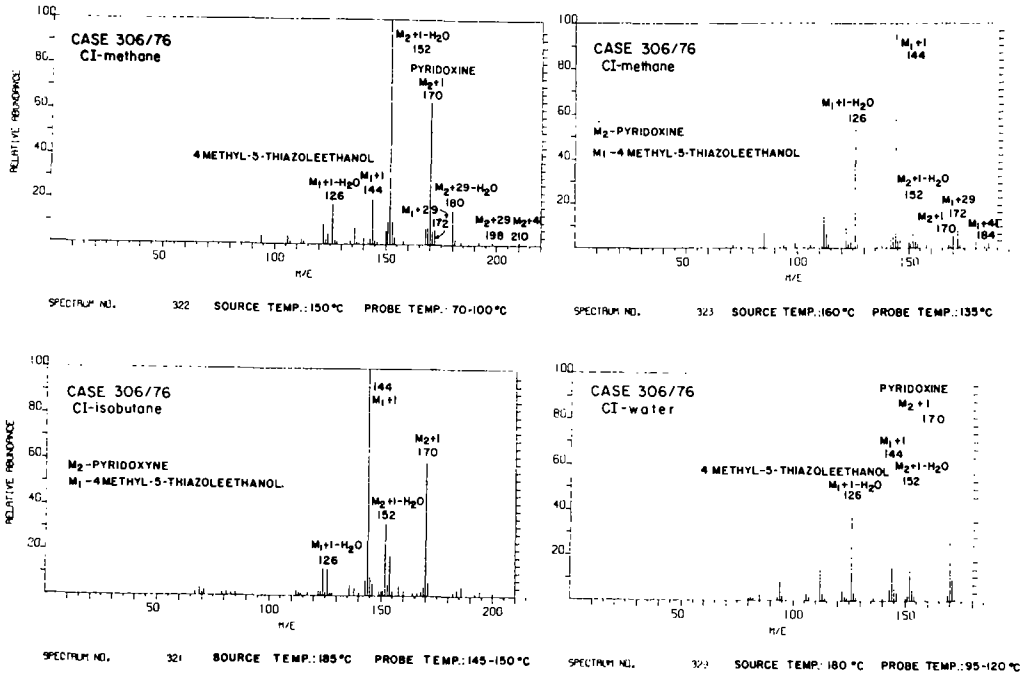

Fig. 6 CI mass spectra of "Case No. 306/76"

RESONANCE ELECTRON CAPTURE NEGATIVE ION CHEMICAL IONIZATION MASS SPECTROMETRY *

Donald F. Hunt, Frank Crow, &
Jamie Lambrecht

Department of Chemistry
University of Virginia
Charlottesville, Virginia 22901

Electron bombardment of isobutane at 1 torr produces the tertiary butyl cation and a population of thermal or near thermal electrons. Many organic sample molecules capture thermal electrons to form collisionally stabilized molecular anions. Experimentally we observe that the negative sample ion currents can be 100 to 1000 times greater than the corresponding positive sample ion current. Derivatizing agents for GC-MS analysis which afford the above sensitivity enhancement will be described. Fragmentation and other reactions of organic radical anions will also be discussed.

* to be published in Analytical Chemistry

MECHANISM OF THE ION-MOLECULE REACTIONS AND PROTON AFFINITY OF PHOSPHIRANE AND PHOSPHIRANE-d_5

Zdenek-Christian Profous, Karl-Peter Wanczek and Hermann Hartmann
Institut für physikalische Chemie der Universität Frankfurt, Frankfurt/Main

The insertion of a phosphorus atom into a three-membered ring leads to an ion chemistry which is entirely different from that of the open-chained phosphines. In this work an ion cyclotron resonance spectrometric investigation of phosphirane, the simplest phosphorus containing three-membered ring, is presented[1].

One of the major common ion-molecule reactions of the methylphosphines[2,3,4] leads to the product ions with the general formula $P_2R_5^+$ (R = H, CH_3):

$$(CH_3)R_2P^{\cdot +} + (CH_3)R_2P \longrightarrow (CH_3)R_4P_2^+ + CH_3^{\cdot} \qquad (1)$$

Similar reactions are not detected in the ion chemistry of phosphirane. In this case all but three of the more abundant product ions are formed by PH transfer reactions:

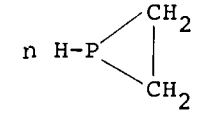

$$R'^+ + n\ H\text{-}P\langle^{CH_2}_{CH_2} \longrightarrow R'(PH)_n^+ + n\ C_2H_4 \qquad (2)$$

R′ = molecular or fragment ion from phosphirane, n = 1,2

The corresponding reaction of the molecular ion of phosphirane yields the product ion $(CH_2)_2PHPH^{\cdot +}$ via a nucleophilic attack of the phosphorus atom of the neutral molecule at the charged phosphorus atom of the ion, followed by a dissociation of ethene. Two structures of this product ion can be discussed: If the phosphirane ring remains intact the product must have the structure (a). However, a ring-expanded structure (b) is more probable, because it is known that phophirane derivatives react as ring-expansion reagents[5].

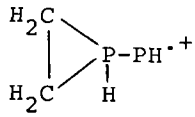

(a)

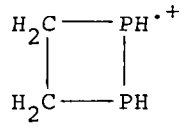

(b)

The C_2H_4 molecule is formed not only from the reacting neutral molecule but also from the molecular ion of phosphirane, if it is cyclic. It can be easily shown by its reaction with trideuteroammonia, that a major proportion of it has a cyclic structure:

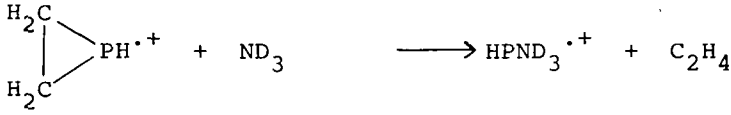

(3)

This reaction proceeds without rearrangement. Reaction (3) is not detected in the case of dimethylphosphine. Therefore in the course of the reaction of the molecular ion of phosphirane with the neutral molecule not only dissociation of one C_2H_4 molecule (reaction 2) is observed, but also dissociation of a second carbon hydride molecule, yielding the abundant product ion m/e = 63, P_2H^+. The composition $H_2P(CH_3)_2^+$, also possible for this ion, is excluded utilising pentadeuterophosphirane. With the perdeuterated phosphirane it has also been shown, that both of the two possible compositions of the product ions m/e = 75 appear. However, the ion $PC_3H_8^+$ is formed by a reaction of the molecular ion, the ion HP_2C^+ by reactions of the fragment ions $HP(CH)_2^{\cdot +}$ and $HPCH^+$.

The molecular ion of phosphirane reacts to four main products, the protonated molecule, the ions $HP(CH_3)_2^{\cdot +}$ and P_2H^+, and the PH transfer ion with almost equal rate constants. Contrary, the molecular ions of the methylphosphines and of tetramethyldiphosphine[6)] undergo only one or two main ion-molecule reactions which form more than 90 % of the total product ion yield. Compared with the methylphosphines, the ring structure of phosphirane causes a further marked difference, the proton affinity of phosphirane of 207 kcal/mole is lowered by 12 kcal/mole compared with dimethylphosphine[1)].

Acknowledgements The authors are pleased to acknowledge the financial support by the Deutsche Forschungsgemeinschaft. One of them (K.-P. W.) is indebted to the Vereinigung von Freunden und Förderern der Johann Wolfgang Goethe Universität for financial support.

References

1. Z.-C. Profous, K.-P. Wanczek, and H. Hartmann, Z. Naturf. 30a, 1470 (1975)
2. R. H. Staley, J. L. Beauchamp, J. Am. Chem. Soc. 96, 6252 (1974)
3. K.-P. Wanczek, Z.-C. Profous, Int. J. Mass Spectrom. Ion Phys. 17, 23 (1975)
4. K.-P. Wanczek, Z. Naturf. 30a, 329 (1975)
5. D. B. Denney, L. S. Shih, J. Am. Chem. Soc. 96, 317 (1974)
6. K.-P. Wanczek, Z. Naturf. 31a, 414 (1976)

Ion-Molecule Reactions in Thiols and Thioethers

Jean E. Kronberg and John A. Stone
Department of Chemistry, Queen's University
Kingston, Ontario K7L 3N6, Canada

The ion-molecule reactions occurring in dimethylsulfide (CH_3SCH_3), dimethyldisulfide (CH_3SSCH_3), methanethiol (CH_3SH) and ethanethiol (CH_3CH_2SH) have been investigated using a field free, high pressure ion source and a quadrupole mass filter. Molecular ions were produced at ambient temperatures by photoionization using interchangeable resonance lamps providing photons of energy 10.0 and 10.6 eV (krypton) and 11.6 and 11.8 eV (argon). For each compound the rate constant for the initial disappearance of the molecular ion (P^+) was determined as were the product yields and pressure dependences of the reactions of P^+ with neutral molecules (P). Only for CH_3SCH_3 was there an effect of photon energy on the observed behaviour.

<u>CH_3SCH_3</u> P^+, formed using the krypton lamp, disappears in an apparently second order reaction ($k = 3.0 \times 10^{-10}$ cm^3 $molecule^{-1}$ sec^{-1}) to yield exclusively the dimeric ion $(2P)^+$, a product that was not observed at a higher temperature in an electron impact study[1]. At higher pressures the trimeric ion $(3P)^+$ is formed in small yield. With higher energy photons (argon lamp) some of the P^+ ions react to yield $(P+1)^+$ ions and at higher pressures $(2P+1)^+$ and $(3P+1)^+$ are observed. These higher energy P^+ ions are generated initially at the second ionization level[2].

<u>CH_3SSCH_3</u> An apparently second order disappearance of P^+ ($k = 2.6 \times 10^{-11}$ cm^3 $molecule^{-1}$ sec^{-1}) leads exclusively to $(2P)^+$ formation. There is no $(P+1)^+$ ion observed with the higher energy photons even though the second ionization level is attained. Small yields of the $(3P)^+$ ion are observed at high pressures together with equally small yields of $C_3H_9S_3^+$ and $C_4H_{11}S_3^+$.

<u>CH_3SH</u> The molecular ion reacts mainly to form $(P+1)^+$ but a very small amount (~ 2%) of $(P-1)^+$ is also formed. The rate constant for the disappearance of P^+ is 3.8×10^{-10}

cc molecule^{-1} sec^{-1}. At higher pressures a major product ion is $(2P+1)^+$ which results from the reaction of $(P+1)^+$ with a neutral molecule. However an ion with comparable yield is the H_2 deficient $(2P-1)^+$. No $(3P+1)^+$ ion is observed, the predominant ions at the highest pressures being $(3P-1)^+$ and $(3P-3)^+$. A $(2P-3)^+$ ion is also significant in the same pressure range.

C_2H_5SH As expected the results for this compound are similar to those for CH_3SH but there are noteworthy differences. No $(P-1)^+$ ion is formed, the $(P+1)^+$ ion being the sole product of the reaction of P^+ with P ($k = 6.1 \times 10^{-10}$ cc molecule^{-1} sec^{-1}). The dimeric ions are $(2P+1)^+$ and $(2P)^+$ which react to yield $(3P-3)^+$, $(3P-1)^+$ and $(3P+1)^+$ at the higher pressures. The latter ion, which is not observed in CH_3SH, has a maximum yield of 7%. The major ion at the highest pressure is $(2P-2)^+$ which appears to have the $(2P+1)^+$ ion as its precursor.

These results show that there are major differences between the reactions of the molecular ions of these alkyl sulfur compounds and those of their oxygen analogues. No $(2P)^+$ ion has been reported for ethers where the competing formation of the $(P+1)^+$ ion is facile[3] in contrast to the endothermic nature of the analogous reaction in thioethers. In alcohols P^+ disappears and the solvated proton series $(nP+1)^+$ predominates, with minor products being formed mainly by loss of H_2O from the series members[4]. The dominant H_2 deficient ions found in the thiols may signify that the formation of S — S bonds leads to more stable structures than the S — H bonded ones associated with proton bound dimers and trimers.

1. B.H. Solka and A.G. Harrison, Int. J. Mass Spec. Ion Phys. 17, 379 (1975).
2. D.C. Frost, F.G. Herring, A. Katrib, C.A. McDowell, R.A.N. McLean, J. Phys. Chem. 76, 1030 (1972).
3. H. Pritchard and A.G. Harrison, J. Chem. Phys. 48, 5623 (1968).
4. L.W. Sieck, F.P. Abramson, J.H. Futrell, J. Chem. Phys. 45, 2859 (1966).

THE ION CHEMISTRY IN ORGANIC RF DISCHARGES: ETHYLENE

by

Michael J. Vasile and Gerald Smolinsky
Bell Laboratories
Murray Hill, New Jersey 07974

This paper reports on a mass spectrometric study of the ionic and neutral species present in a low pressure (0.1 to 1.0 Torr) ethylene discharge. As in the case of methane and ethane, the chemistry observed differs depending on whether the discharge is sampled through the RF sheath in front of the driving electrode or through the plasma-to-wall sheath. The neutral molecules sampled in both regions of the discharge consist of H_2, CH_4, C_2H_2, C_2H_4 and C_2H_6. For any reaction condition, the proportion of H_2 is greater, and that of C_2H_4 less, in the RF than in the plasma-to-wall sheath.

The principal ionic species observed through the RF sheath are $C_2H_2^+$, $C_2H_3^+$ and C_3H^+, $C_3H_2^+$ and $C_3H_3^+$. These ions indicate that the primary ionization mechanism is the formation and ionization of ethyl and vinyl radicals. The distribution of ions sampled from the RF sheath does not vary significantly with changes in pressure or power imput. The condensation products observed in this region are consistent with energetic ion-molecule processes. Ions sampled radially through the wall of the discharge tube represent a fundamentally different situation. Very few C_2-ions are observed, and the principal condensation products observed at high pressures are the $C_4H_8^+$ and $C_5H_9^+$ ions. The ionic products are strongly influenced by the stabilization, or lack thereof, of the two intermediate complexes, $(C_4H_8^+)^*$ and $(C_5H_9^+)^*$ which result from condensation with ethylene of $C_2H_4^+$ and $C_3H_5^+$, respectively. Relatively high pressure and low power input result in collisional stabilization of these complexes.

Publication of a full account of this work is pending in the International Journal of Mass Spectrometry and Ion Physics.

USE OF MOLECULAR SIEVE PELLETS AS A SOURCE OF CI REAGENT GAS OR ADDITIVE WITHIN THE SOLID SAMPLE PROBE

by

S. E. Buttrill, Jr.* and Rad Olson
Department of Chemistry
University of Minnesota
Minneapolis, Minn. 55455

Chemical ionization (CI) mass spectrometry derives its name from the fact that the ions composing the CI spectrum of a compound are formed by chemical reactions; more specifically, they are the products of ion-molecule reactions between reagent ions characteristic of the reagent gas and neutral sample molecules. One of the most appealing aspects of CIMS from an analytical point of view is the prospect of developing schemes of qualitative analysis based on the successive use of different reagent gases with the same unknown compound. While this possibility has been recognized from the very beginning, its realization has been very slow, primarily because of the practical difficulty of rapidly changing reagent gases.

We have developed a method in which reagent gas or additive is generated by heating a substrate within the solid sample probe. The original work used hydrates of inorganic salts as a source of water reagent gas (1). In our more recent work, we have used pieces of Linde 13X Molecular Sieve as substrates. When a piece of sieve saturated with a polar substance to an equilibrium vapor pressure of about 0.1 torr at room temperature is heated in the probe, it releases sufficient gas to operate in the CI mode for 50-100 seconds or to modify a reagent gas such as methane for considerably longer times. The experimental arrangement is shown in Figure 1. The sieve is inserted into the probe first; the sample is placed inside an open length of standard melting point capillary. It is sometimes

Figure 1

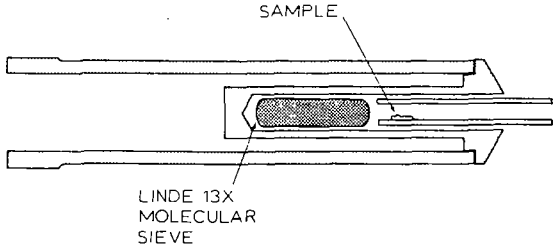

necessary to wrap a small piece of Teflon tape around the outside of the capillary so that it fits firmly into the probe tip. This prevents the capillary being blown out of the probe by the reagent gas evolving from the sieve. The sieve and sample are heated by the standard probe heater (not shown in the Figure) which is coiled about the inner tube of the probe tip.

We have used the molecular sieve substrates to release a num-

ber of different modifiers for the methane reagent gas, including water, formic acid, methanol, ethanol, dimethyl and diethyl ether, acetone, and ammonia. As might be expected, substances such as nitrogen, oxygen, argon and methane cannot be introduced by this technique since they are not strongly absorbed by the sieve.

One valuable piece of information about an unknown compound is its proton affinity, which can be determined rather easily by the bracketing technique (2). Figures 2 and 3 show the CI spectra

Figure 2

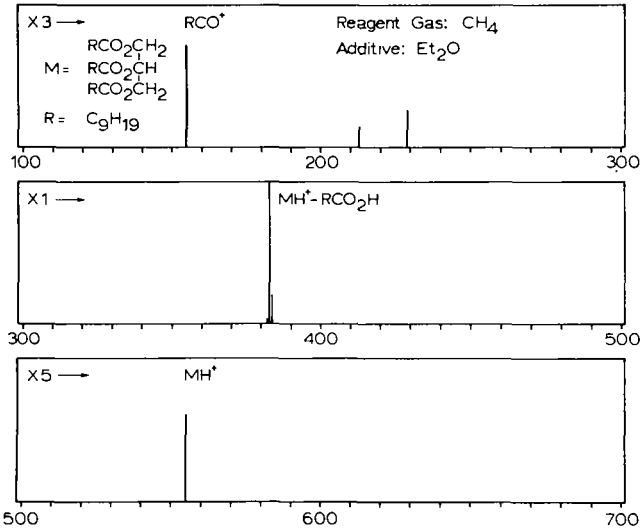

Figure 3

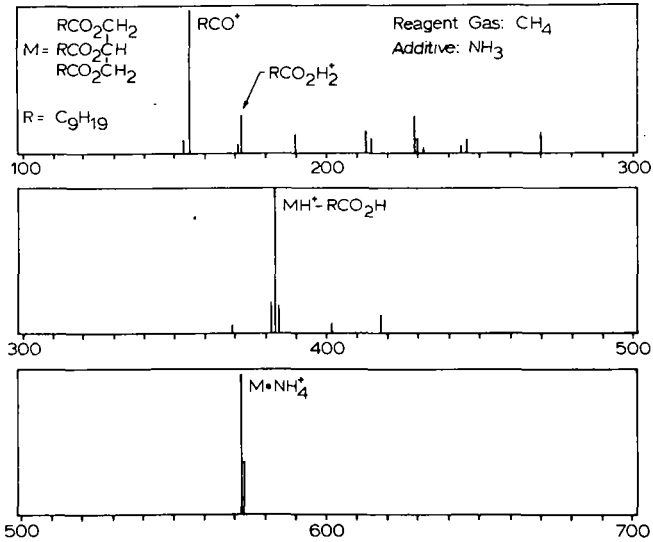

of tridecanoin obtained using ethyl ether and ammonia as modifiers for the methane reagent gas. With the ether, the major reagent ion was Et_2OH^+, but many other ions were present as well. The reagent ion using ammonia was NH_4^+. The ethyl ether CI spectrum of tridecanoin is unusually weak (low sensitivity) but it is normal in that it shows the expected MH^+ ion and the same fragments as in

the water or methane CI. In contrast, the MH^+ ion is totally absent when ammonia is used as the reagent gas modifier. A large $M{\cdot}NH_4^+$ ion is present, presumably due to the formation of a hydrogen-bonded cluster of NH_4^+ with tridecanoin. The absence of proton transfer from ammonia to tridecanoin indicates that its proton affinity is less than 200.7 kcal/mole while proton transfer from diethyl ether to tridecanoin means that PA > 198 kcal/mole. When more information becomes available on the limiting proton affinities (2) of various types of compounds, the determination of proton affinities in this way should have analytical utility.

The variation of the CI spectrum of tridecanoin with reagent gas is interesting because it illustrates the importance of the thermal internal energy of the neutral molecule in determining the fragmentation of the MH^+ ion. The relative amounts of the major sample ions in the CI spectrum of tridecanoin are plotted in Figure 4 as a function of the proton affinity (PA) of the reagent gas additive. When the PA of the additive is very close to the PA of the sample, the formation of the MH^+ is almost thermoneutral. Under these conditions, one might expect to have very little fragmentation of the MH^+, but this is not the case. Even through very little energy is available from the proton transfer reaction, the thermal internal energy of the neutral M is sufficient to cause extensive fragmentation of the MH^+ ion once it is formed. Put another way, at a given temperature, a neutral molecule may be stable while its MH^+ ion is not.

*Present address: Mass Spectrometry Research Center, Stanford Research Institute, Menlo Park, CA 94025.

(1) S. E. Buttrill, Jr. and A. F. Finders, Anal Chem., 48, 626 (1976).

(2) J. Long and B. Munson, J. Amer. Chem. Soc., 95, 2427 (1973).

Figure 4

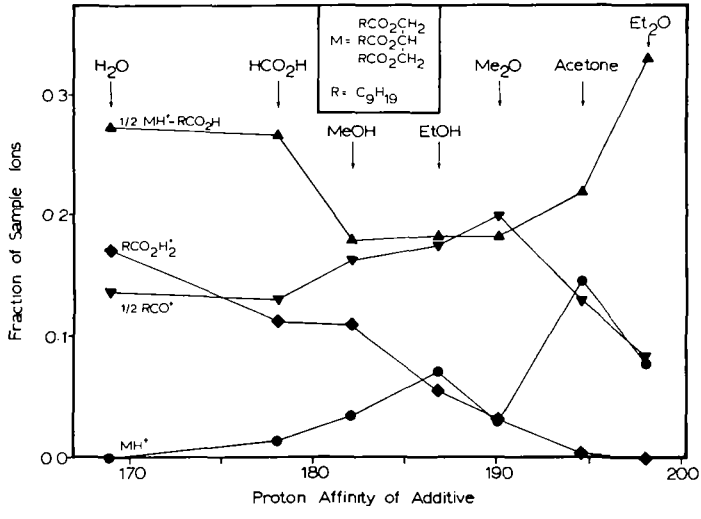

MASS ANALYZER FOR TRACE GAS ANALYSIS

Charles M. Judson
Analog Technology Corporation, Pasadena, CA, 91107
George Wood and Paul Yeager
NASA Langley Research Center, Hampton, Virginia

Analog Technology Corporation has constructed a prototype of the mechanical portion of a miniature mass spectrometer. This spectrometer, using a short quadrupole mass filter, is designed for measuring trace constituents in air. It is a modification of the Astronaut Breath Analyzer which was described by Dr. Brubaker at this meeting in 1972. The present instrument is being constructed under a contract from the Langley Research Center of NASA.

The requirements of the present mass spectrometer differ from those of the previous instrument in that the object is to measure trace rather than major constituents, and that the upper mass range is increased from 44 to 200. The present instrument then requires addition of an electron multiplier, optimization of the design to provide high sensitivity over a wider mass range, and a vacuum system which provides a sufficiently low background level.

The system consists of an analyzer mounted within a vacuum tee and a 30 liter/second ion pump. The vacuum tee is a standard commercial tee, 2.5 inches in diameter, and 8.25 inches long. The mass filter is mounted to the wall of the envelope. The ion source and gas entrance are mounted on one flange, the electron multiplier on the opposite flange, and the ion pump on the third flange at right angles. The ion source, electron multiplier and ion pump can each be independently removed and replaced without removing the mass filter. Alignment of the ion source with respect to the mass filter is maintained by pins which fit into matching holes in the mass filter mounting structure.

The electron multiplier is a high-current, continuous-dynode electron multiplier manufactured by Gallileo Electro Optics. The multiplier is constructed to be operated offset from the mass filter axis.

In the test system, a Granville-Phillips variable-leak valve has been used to control the leak rate and to close the gas entrance line when the system is not in operation. The final instrument will use a leak-valve with a fixed orifice.

The mass filter is two inches long, with hyperbolic electrodes having a radius of 0.150 inches. The electrodes are tungsten. The filter is a single rigid structure of four filter electrodes, with eight insulators connecting the four filter electrodes to four ground plane electrodes. The filter is manufactured by chemical vapor deposition onto a mandrel, with the effect that the dimensions of the electrodes are determined by the dimensions of the mandrel. The process for manufacturing the mass filter was the invention of James Lawrence of Analog Technology Corporation, and was developed prior to the work being reported in this paper.

The ion source is a conventional electron ionization source, with a repeller and an extractor, both insulated from the ion box, and two apertured electrodes between the extractor electrode and the mass filter, both of which are

operated negative with respect to the mass filter axis. The extractor electrode is mounted to an insulator located completely away from the ion source so that fields in the ion source are not affected by charge build-up on this insulator. Two filaments are provided, located opposite eachother. There is a shield located in back of each filament, operated at negative filament potential. There is an electron accelerating slit which is operated positive with respect to the ionization box, and a screen at the wall of the ionization box which shields the box from the electron accelerating voltage. It is expected that the final instrument will have an ion source with a simpler structure than that used in the prototype.

Gas enters the ion source through a tube with a length long compared to its diameter, entering on the axis through the repeller. Calculations indicate that the density of molecules in the ionizing region can be increased over the density present due to the average pressure in the ion source, by use of such a design.

There are entrance electrodes, in quadrupole symmetry, present at the mass filter entrance which are used to obtain delayed-dc entrance fields. These electrodes are constructed in essentially the same way as they were in the Astronaut Breath Analyzer. These entrance electrodes are thin circular electrodes, located nearer to the mass filter axis than the mass filter electrodes, but shielded from the mass filter axis at the entrance by a collar attached to the entrance aperture electrode. This structure was designed to be used with application to each entrance electrode of a dc voltage of polarity opposite to that applied to the adjacent mass filter electrode. These opposite dc voltages reduce the dc field at the entrance, and have an effect similar to that obtained when ac voltage, in phase with the voltage applied to the adjacent mass filter electrodes, is applied to the entrance segments of a segmented-rod mass filter. The present structure can also be operated with ac voltage, attenuated because of the shorter distance from the axis, applied to these entrance electrodes.

The capability for trace detection depends on the sensitivity of the instrument, that is the ion current obtained at a specified pressure in the ion source, and on the background ion current.

The system was designed to operate using an ac frequency of the order of 2 MHz, an ion energy of the order of 2 volts, and a filament emission of the order of 1 milliampere. The ion energy is limited by the requirement that the ions go through a sufficient number of oscillations within the filter in order to be resolved. The system was further designed to operate with a gas flow at the leak-valve of something less than 10^{-4} torr-liters/second in order to allow use of the relatively small 30 liter/second ion pump under conditions of reasonably long pump life. The source presently in use has an exit conductance of about 1 liter/second, so that the pressure in the ion source is something less than 10^{-4} torr.

The specifications called for a resolved ion current of at least 10^{-9} amperes, requiring 10^{-5} amperes/torr at a source pressure of 10^{-4} torr, measured for mass 28 in nitrogen. This is not a particularly high sensitivity, and

a sensitivity greater than this has been easily achieved under the design conditions.

The non spectral background, which provides one possible restriction to the detection limit, involves possible background contributions from the multiplier, from the ion pump, and from the ion source. The ion pump is baffled, and the background from the ion pump is not measurable. The multiplier background is negligible compared to the ion source background. The only significant non-spectral background is the background coming from the ion source. Using an offset multiplier, and a small mass filter entrance aperture, the ion source background can easily be made less than 10^{-16} amperes, so that its intensity is less than 10^{-7} times the intensity of the mass 28 peak in air, and for reasonable measurement times, the noise in the background can be made less than 10^{-9} of the mass 28 peak. The limitation to detection of trace constituents is then the spectral background.

The system is easily baked so that spectral background for most masses is sufficiently low as to permit detection of 0.1 ppm constituents, provided that the system has not been recently subjected to entry of large concentrations of a species having a major mass peak at the mass to be measured. A demonstration of the capability to detect 0.1 ppm can be made by measurement of the isotopes of krypton in air as compared to the background values measured when pure nitrogen is admitted.

One of the advantages of the Astronaut Breath Analyzer was that, over the mass range in which it operated, peaks with steep sides and relatively flat tops were obtained. Peaks with shapes approaching a square or trapezoidal shape provide two advantages: (1) minimum cross-talk at adjacent masses, and (2) precise measurement of peak intensity obtained more easily and less dependent on the stability of the rf-dc voltage. At the upper mass limit of the Astronaut Breath Analyzer in the mass 44 region, the adjacent peak contribution was 0.01% with a width at half-height of 0.6 mass, and a peak top which was rounded but clearly more nearly flat than triangular.

The present instrument was tested for performance at higher mass using the mass 127 peak of SF_6, an easily obtainable gas. Application of dc or ac entrance voltages at this mass provides significant improvement in peak shape. The effect of entrance voltages was considerably greater at higher mass, and at higher mass the use of ac entrance voltage was significantly more effective than the use of dc entrance voltage. A relatively flat top was obtained at mass 127 with a width at half-height of 0.7 mass, a peak shape comparable to that obtained in the Astronaut Breath Analyzer at mass 44. There was, however, a peak tail on the low mass side which has so far prevented obtaining simultaneously flat top peaks and low adjacent peak contributions at mass 127. The cause of this peak tail and the possible methods of its elimination are currently under investigation.

The contract with NASA for development of a trace gas mass spectrometer is now in its second phase in which the electronics, gas sampling system, and computer for control of the system are being developed. Work on optimization of peak shapes is also continuing.

ION OPTICS USING RESISTIVE LENSES

M. W. SIEGEL
Extranuclear Laboratories, Inc.
Pittsburgh, Pennsylvania 15238

The electric fields conventionally used as ion lenses are essentially capacitor fields, generated by fixing the potentials of appropriately shaped isolated metallic conducting surfaces. It is usual to somewhat imprecisely refer to the hardware as if it, rather than the field, were the lens, and we will conform to this usage. These lenses define equipotential contours, and the resulting vacuum electric fields are solutions to $\nabla\cdot\vec{E} = 0$ with boundary conditions requiring the field to be perpendicular to the lens surfaces. Capacitive devices in principle draw no current once charged, and in practice the lens power supplies need to provide only the very small currents required to accommodate the ion beam spray. This absence of a large current demand is historically fortuitous, because while power supplies able to provide a stable voltage at negligible current have been available for many years, only in the last few years have compact and inexpensive stable voltage supplies capable of delivering moderately large currents been available. This new capability, combined with the equally recent commercial development of amorphous materials in a wide range of controlled conductivities makes it possible to seriously consider the routine use of a class of resistive ion optic devices in which the electric field is parallel rather than perpendicular to the lens surfaces, thus simplifying the generation of certain field shapes.

When current flows in a resistive medium, the electric field in the medium is determined by solutions to $\nabla\cdot\varepsilon\vec{E} = \rho$ and $\nabla\times\vec{E} = 0$. While the divergence of this electric field is non-zero, the steady state current density field ($\vec{j}$) does have zero divergence via $\nabla\cdot\vec{j} = -\frac{\partial\rho}{\partial t} = 0$. In a wide variety of amorphous materials the current density field bears a simple scalar relationship to the electric field, $\vec{j} = \sigma\vec{E}$, where σ is the conductivity. This relationship is the microscopic form of Ohm's Law.

The special case relevant to this problem concerns the field relationships at a boundary between a current carrying medium and the vacuum. The perpendicular component of the current density is required by $\nabla\cdot\vec{j} = 0$ to be zero, and thus the perpendicular component of the electric field must be zero. The electric field just inside the boundary surface is parallel to the boundary surface, and of magnitude $E = j/\sigma$. Since $\nabla\times\vec{E} = 0$, the electric field in the vacuum just outside the surface is also parallel to the surface, and also equal to j/σ. The boundary conditions on the vacuum electric field generated by current in a nearby resistive medium are thus simply determined by the solution to the current density problem within the medium. Translated from microscopic (conductivity, field) to macroscopic (resistance, voltage)

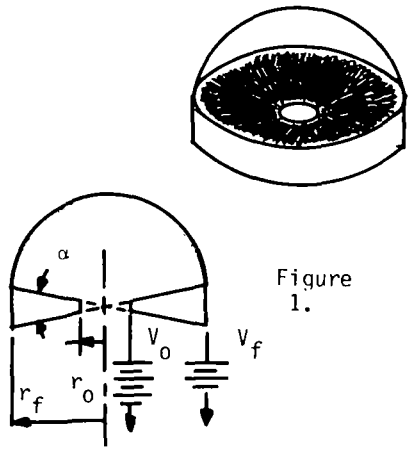

Figure 1.

descriptions, the problem is simply one of finding the current density in a shaped resistor.

Two practical realizations of resistive ion optics are easily visualized: resistors of uniform geometry with locally tailored conductivity, and resistors of uniform conductivity with locally tailored geometry. We first look in general terms at axially symmetric configurations, corresponding to ion optics suitable for accelerating, decelerating, and focusing ion beams.

In the uniform geometry case consider a cylindrical tube of constant inside diameter and wall thickness extending from axial position $z = 0$ to $z = z_0$. If the conductivity is a tailored function of position, $\sigma(z)$, then the axial electric field inside the tube and not too close to either end is

$$E(z) = \frac{V_0}{\sigma(z) \int_0^{z_0} \frac{dz}{\sigma(z)}} \qquad \text{(Eq. 1)}$$

where V_0 is the voltage applied between metallic conducting contacts at the ends.

To determine whether the material employed can dissipate the required ohmic power, it is only necessary to note that the local power dissipation per unit volume is $\vec{j}\cdot\vec{E}$, and $j(z) = \sigma(z)\, E(z)$ so $\vec{j}\cdot\vec{E} = \sigma(z)\, E(z)^2$. This relationship is the microscopic equivalent of the familiar $P = V^2/R$.

In the uniform conductivity case, which is the more practical realization, consider a tube whose geometry is tailored so that it has a uniform inside radius (r_0) and a shaped outside radius ($r(z)$). The lens field is given by

$$E(z) = \frac{V_0}{(r(z)^2 - r_0^2) \int_0^{z_0} \frac{dz}{(r)^2 - r_0^2}} \qquad \text{(Eq. 2)}$$

and the power dissipation is determined as in the previous case.

It is worth pointing out that in neither case does the electric field depend on the absolute magnitude of the conductivity. In the first case any scalar multiple of $\sigma(z)$ gives the same electric field, and in the second case the conductivity does not appear in the expression for the electric field. What the conductivity does determine is the current drawn from the power supply. In order to minimize this current, and thus the power dissipation, it would appear advantageous to minimize the conductivity. On the other hand, in a very low conductivity material (an insulator), very small currents produce very large voltages, and can thus seriously perturb the field. It is of course well known in capacitive ion optics design that ion beam spraying onto insulators is to be avoided. It is equally true that ion beam spraying onto low-conductivity resistive ion lenses is to be avoided. The most desirable compromise is to determine the maximum value of the required electric field in the resistor, and then choose the highest conductivity material compatible with the resulting power dissipation.

As an example of a possible application in an axially symmetric configuration, consider the design of an exponential decelerator. The classical technique is to bias a stack of aperture disks with an exponential resistor ladder.[1] If instead we construct a shaped tubular resistor whose inside radius is constant (r_0) and whose outside radius is given by $r(z) = (D^2e^{\sigma z}-r_0^2)^{\frac{1}{2}}$, where D is a length determined by the wall thickness at z = 0 and

$$\alpha = \frac{1}{z_0} \log_e \frac{V_0}{V_f}$$

where z_0 is the device length, V_0 is the initial (high) ion energy, and V_f is the final (low) energy, then the axial electric field is given, by Eq. 2,as $E(z) = \alpha V_0 e^{-\alpha z}$, and the potential on the axis is given by $U(z) = V_0 e^{-\alpha z}$. It is easily shown that the required dimensions are practical. For example if we choose r_0 = 6.25 mm and D = 1 mm, then a decleration ratio (V_0/V_f) of 1000 is obtained in a 21 cm length. The outside radius at this endpoint, r(21 cm), is 32 mm. If a conductivity of 10^{-8} $(\text{ohm-cm})^{-1}$ is chosen, the required current is about 1mA and the maximum power dissipation (at the thin, high voltage end) is about 600 mW/cm^3.

As a final example, consider a possible design for a very wide acceptance aperture hemispherical energy analyser, as sketched in Figure 1. A biconcave conical disk is imagined machined as shown, its thickness being by $\tau(r) = \alpha r$, where α is the taper angle. The disk may be capped with a hemispherical shell which does not have to be machined to great precision. If the radius of the inside hole is r_0 and the shell radius is r_f, the resistance between the inside and outside contacts is

$$R = \frac{1}{2\pi\sigma\alpha} \left(\frac{1}{r_0} - \frac{1}{r_f}\right)$$

and the electric field is given by

$$E(r) = \frac{V_0 - V_f}{\left(\frac{1}{r_0} - \frac{1}{r_f}\right)} \frac{1}{r^2}$$

which is exactly the form required for a hemispherical analyser. Unlike classical hemispherical analysers, in which fringe fields at the entrance and exit apertures can be minimized only by making the shell spacing (and thus the angular acceptance) small, the angular acceptance of this resistive device should be limited only by small perturbations due to the entrance and exit apertures and by the second order angular focusing failure of the theoretical device.

Reference

1. Vestal, Blakley, Ryan, and Futrell, Rev. Sci. Instr. 47 (1976), p. 19-20. The dimensions chosen for the numerical example correspond to those of the 42 plate exponential decelerator described in this article.

MODIFICATION OF A MATTAUCH-HERZOG MASS SPECTROMETER FOR MEDIUM RESOLUTION ION KINETIC ENERGY SPECTROMETRY[1]

Robert Ryba and Gilbert J. Mains
Department of Chemistry
Oklahoma State University
Stillwater, Oklahoma 74074

INTRODUCTION

Sir, a Mattauch-Herzog Geometry Mass Spectrometer doing Ion Kinetic Energy Spectrometry is like a dog's walking on its hind legs. It is not done well but you are surprised to see it done at all.[2] Of course, the basic geometry problem is the placement of the ion source at the focal point of the electric sector. Hence the ions emerge from the electric sector into the second field-free region in parallel trajectories. The energy resolution is thereby determined by the width of the exit slit from the electric sector and, for the du Pont/CEC 21-110B, corresponds to roughly a 3% energy resolution. Chait[3] first modified his 21-110B to scan I.K.E. spectra and spectra similar to that shown in Figure 1 for n-decane were reported. Because it would be difficult to examine analytical applications of I.K.E.S. with such low resolution data, we addressed ourselves to improving the energy resolution.

EXPERIMENTAL

Since the β slit of the du Pont/CEC 21-110B mass spectrometer is not adjustable on our instrument, we decided to modify the second field-free region. However, any modification had to be removable from the main beam so that the normal analytical functions of the instrument were not impaired. A translatable, adjustable β slit followed by a Bendix Continuous Dynode Multiplier, Model 4700, was designed and retrofitted to the mass spectrometer.[4] The system could be conveniently moved into the ion beam, the β slit adjusted for maximum energy resolution, and the signal from the multiplier plotted on a Keithly Model 317 recorder while the voltage on the electric sector plates was swept from ± 5% of the ion accelerating potential, 7.5 kv, to zero. The improved quality of the I.K.E. spectra can be easily seen by comparing Figures 1 and 2. The C-D peak system is now resolved and this n-decane spectrum is comparable in quality to that reported by Beynon[5] who used a Nier-Johnson geometry instrument. We estimate the energy resolution, $E/\Delta E$, to be roughly 200 depending on one's definitions of resolution. This experimental arrangement was then used to study the I.K.E. spectra of alkyl-substituted thiophenes reported elsewhere in these abstracts in the PSCIa paper.

THEORETICAL

Having developed experience in ion trajectory calculations in designing the adjustable β slit apparatus, we decided to see if we could design an Einzel lens that could be inserted ahead of the adjustable β slit to improve the energy resolution further. While some experimental details were available,[6] designs which approximated our geometry requirements were not available. Techniques for conformally mapping the electric field in the Einzel lens were well known[7] but had not been extended to an eight-element lens system. This was done for an Einzel lens system of the proper gemoetry for the du Pont/CEC 21-110B and ion trajectories were

traced through the system.[4] Figure 3 is the result of these computations for 7300 volt ions focused on the (adjustable) β slit using a "thick electrode" potential of 7440 volts. It was found possible to relate the Einzel lens potential to the energy of the incoming ions so that focus can be maintained while the electric sector voltage is varied. We estimate that the energy resolution ($E/\Delta E$) will be improved to near 10^3 with this modification. Hopefully, we will be able to report at some later A.S.M.S. Meeting that we did indeed teach the canine in question to walk on its hind legs--and walk well.[2]

ACKNOWLEDGEMENTS

One of us (R. R.) wishes to thank Continental Oil Co., Phillips Petroleum Co., and Oklahoma State University for financial support during his doctoral studies. We are especially grateful to Dr. E. Chait, du Pont Instruments, for discussions of the 21-110B mass spectrometer's ion optics and for a second field-free sector which we could modify to improve the energy resolution of our instrument.

REFERENCES

1. A detailed account of this research will be published elsewhere.

2. With apologies to Dr. Samuel Johnson as related by J. Boswell, Random House, N.Y. (1952) p. 126.

3. E. M. Chait and W. B. Askew, Org. Mass Spectrom. 5, 417 (1971).

4. See R. Ryba, Ph.D. Dissertation, Oklahoma State University, May, 1976, for details.

5. J. H. Beynon, J. W. Amy and W. E. Baitinger, Chem. Commun., 713 (1969).

6. Albert Septier, Focusing of Charged Particles, Vol. I, Academic Press, N.Y., 1967, p. 274.

7. M. J. Wallington, J. Phys. E. 4, 1 (1974) and the references to A. J. H. Boerboom therein.

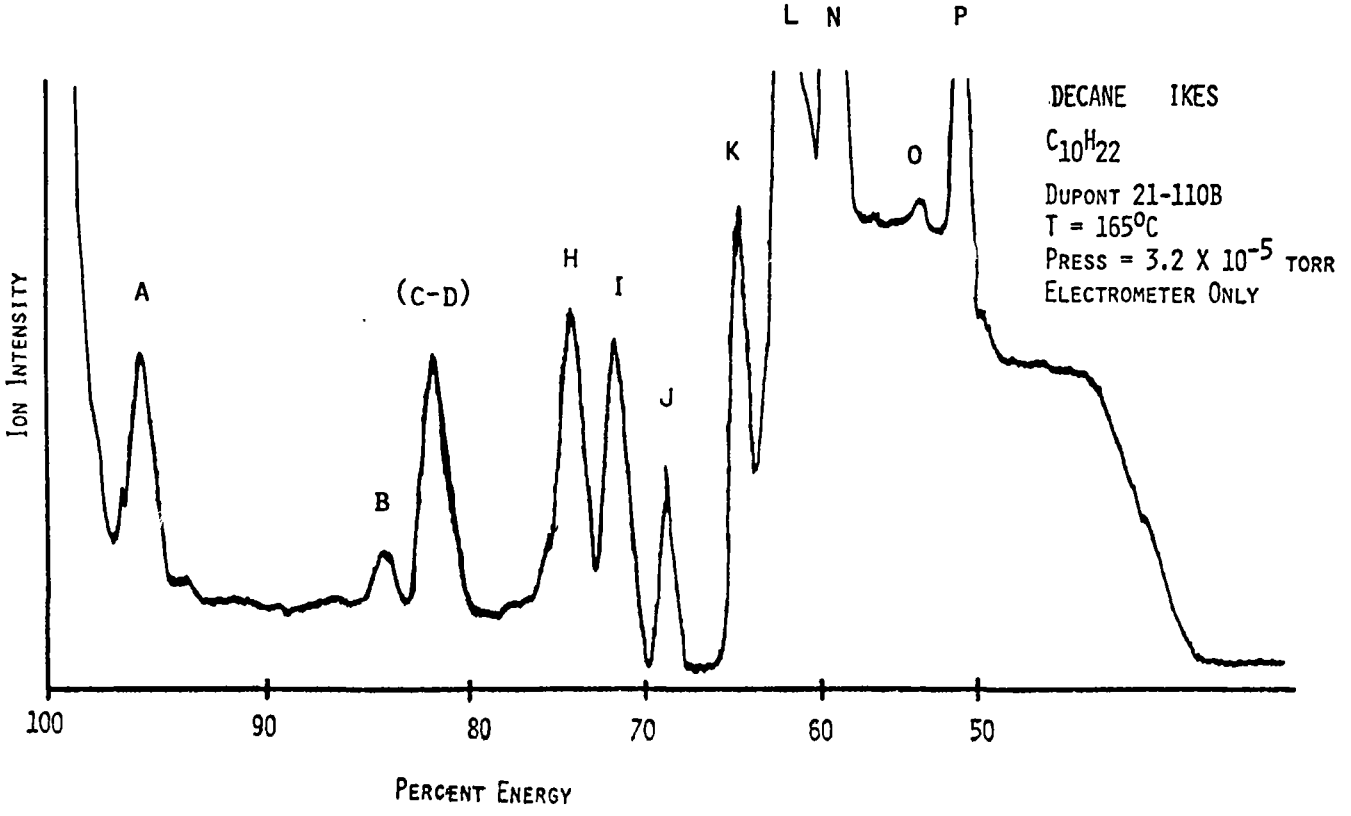
DECANE IKES
$C_{10}H_{22}$
DUPONT 21-110B
T = 165°C
PRESS = 3.2 X 10^{-5} TORR
ELECTROMETER ONLY
A
B
(C-D)
H
I
J
K
L
N
O
P
ION INTENSITY
100
90
80
70
60
50
PERCENT ENERGY

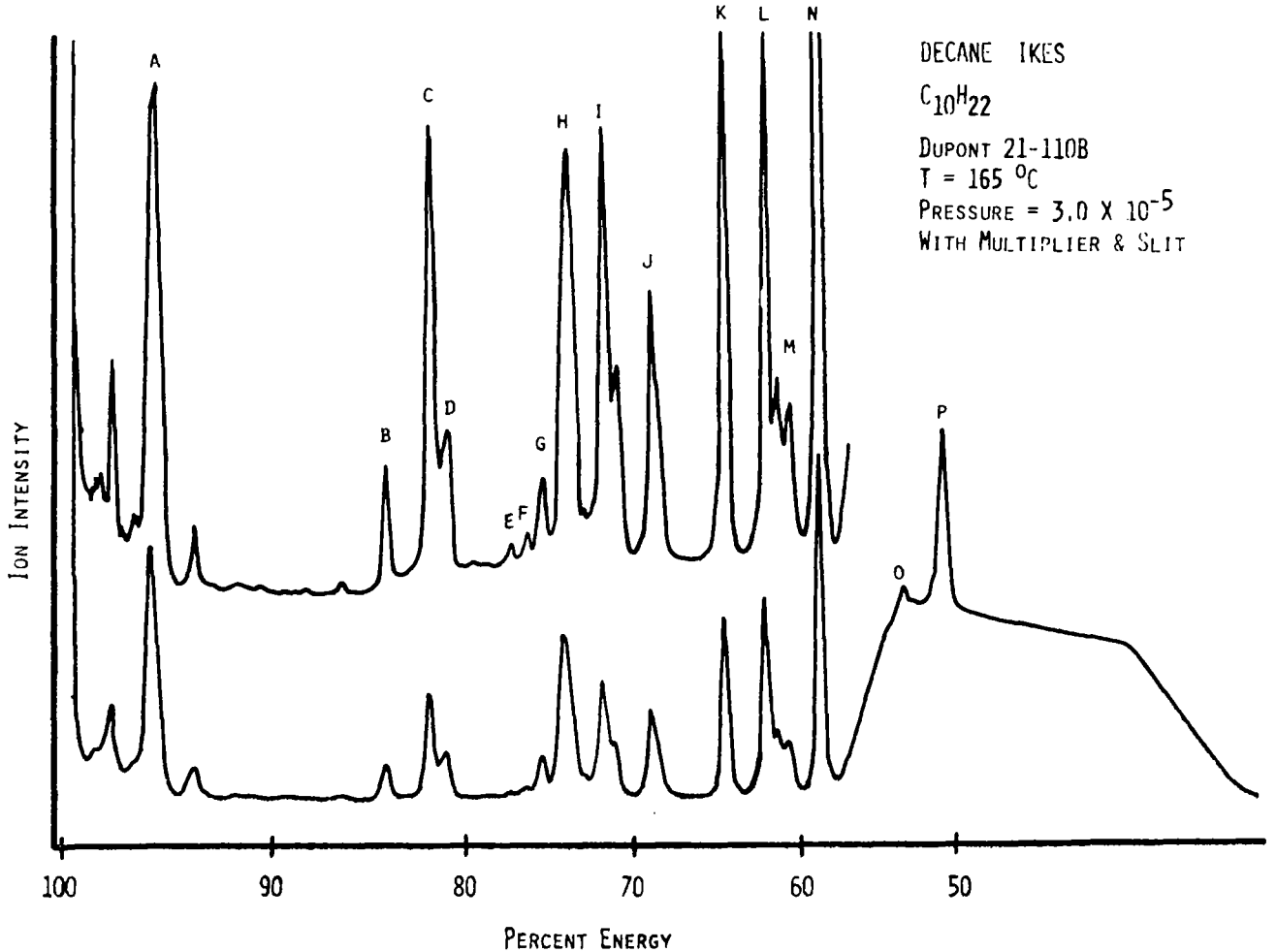
DECANE IKES
$C_{10}H_{22}$
DUPONT 21-110B
T = 165 °C
PRESSURE = 3.0 X 10^{-5}
WITH MULTIPLIER & SLIT
A
B
C
D
E
F
G
H
I
J
K
L
M
N
O
P
ION INTENSITY
100
90
80
70
60
50
PERCENT ENERGY

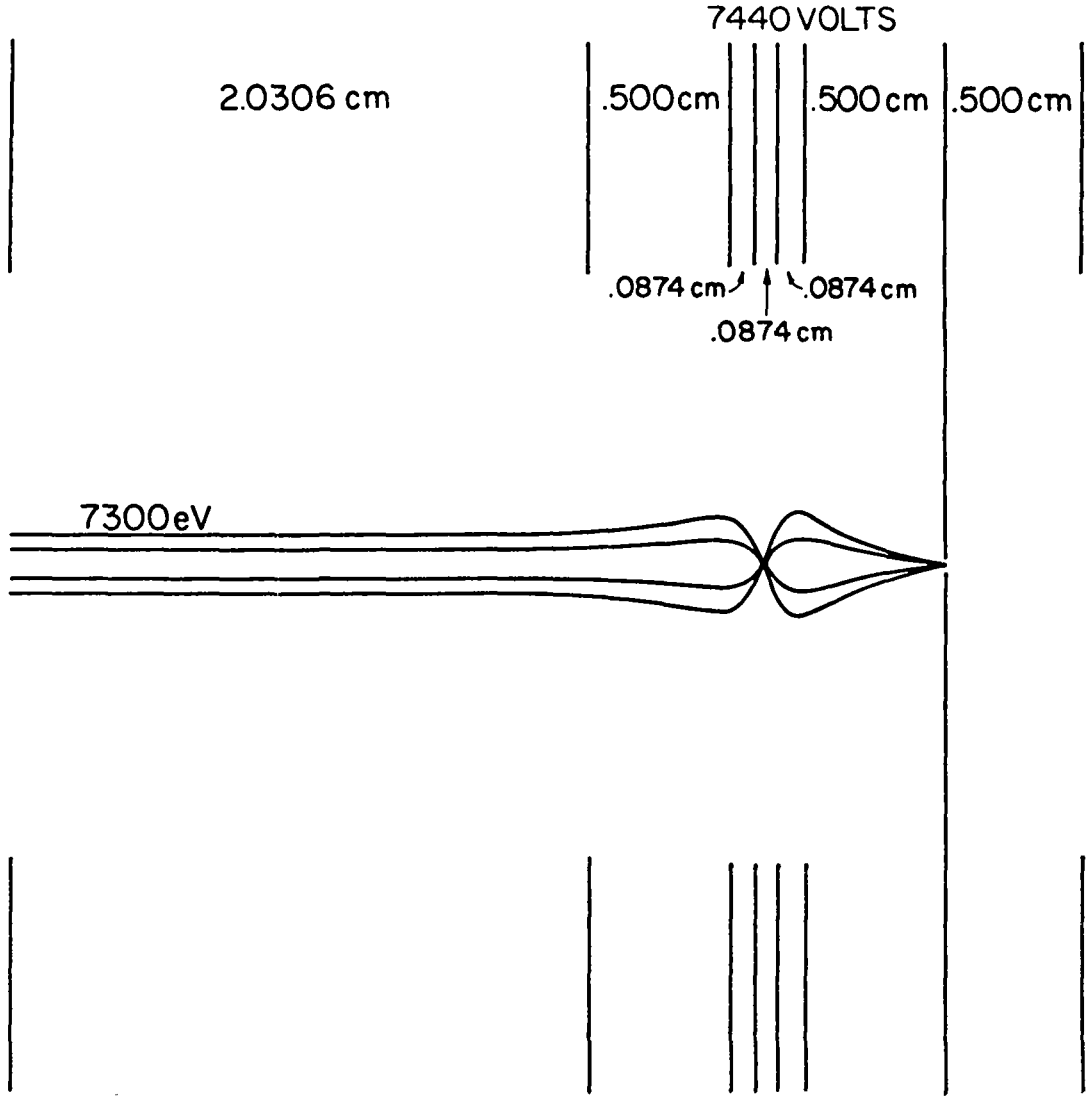
7440 VOLTS
2.0306 cm
.500cm
.500cm
.500cm
.0874 cm
.0874 cm
.0874 cm
7300eV

Voltage Scanning of a Double Focussing Mass Spectrometer Under Computer Control

K.B. Denson, S.P. Taylor, and J.M. Hayes

Departments of Chemistry and Geology
Indiana University
Bloomington, Indiana 47401

A high resolution, Mattauch-Herzog type double focussing mass spectrometer (CEC 21-110B) has been modified so that its ion accelerating voltage (IAV) and electrostatic analyzer (ESA) voltage can be varied over a wide range under computer control. The modified instrument is thus capable of rapid voltage scanning for the performance of GC-MS analyses in the selected ion monitoring mode.

The instrument's original ion accelerator power supply has been replaced with a high speed, digitally programmable 12,000 volt power supply (a prototype version of the Nuclide HV-22 described by Eskew[1]). For the ESA power supply a ±500 volt programmable supply has been constructed and is shown in block diagram form in Fig. 1. Because the IAV and ESA power supplies are controlled by separate 12-bit digital-to-analog converters, these voltages can be independently varied. In this way, it is possible to operate the instrument in the so-called decoupled mode, permitting the direct observation of the parent or daughter ions involved in metastable transitions. The two digital-to-analog converters receive digital information from a Varian 620/i computer via an interface/local control unit built in our laboratory. The portion of the mass range which can be controlled is continuously variable from 0 to 100%, so the 1-part-in-4096 resolution of the 12-bit digital-to-analog converters can be spread over as wide or as narrow a mass range as desired for a given experiment. Thus, it is possible to operate at relatively low mass spectral resolution (~1000) over a wide mass range (60% or greater) or at high resolution over a narrower mass range. A block diagram of the entire instrument is shown in Fig. 2.

The computer controlled ion energy arrangement displays excellent linearity and stability. The system is easily calibrated for any given range setting by locating the centroid of two known peaks at each end of the mass range. It is then possible to calculate very accurately the location of any given ion within the range of the system at the time. The drift of the electronics (ESA, IAV, magnet) is very small, so that mass peaks remain centered on the detector at the calculated IAV values for long periods of time (45 minutes or more). Thus, it doesn't appear that it will be necessary to monitor and correct for drift during a GC run.

The instrument does, of course, display some mass discrimination, as is common with voltage scanning on a conventional magnetic instrument. There is sensitivity loss as the accelerating voltage is decreased due both to ion source effects and to electron multiplier energy response. Table I shows the results of a typical experiment to measure the magnitude of the sensitivity loss. The peak intensities for the magnetic scan were measured with the ion accelerating voltage at about 8 KV. For the voltage scan the accelerating voltage varied from about 8 to 4 KV. It is seen that even over this wide range, the sensitivity loss is quite tolerable, and for narrower ranges of 10 or 20%, there is very little difference be-

tween voltage and magnetic scans.

TABLE I

SENSITIVITY LOSS[1]

MAGNETIC SCAN

MASS	$I/I_{69} \times 100$
69	100.0
93	14.3
100	19.9
131	53.7

VOLTAGE SCAN[2]

MASS	$I/I_{69} \times 100$	DEVIATION FROM MAGNETIC
69	100.0	-----
93	14.4	+0.8%
100	19.2	-3.5%
131	39.1	-27%

[1]Compound - PFK

[2]∿50% Mass Range

Initial performance tests have been satisfactory in all respects, and the way to interesting applications requiring the capabilities of this system is fully open. A detailed report on the design of the ESA power supply and the testing of the dynamic characteristics of both high speed power supplies is in preparation.

We acknowledge with thanks the support of the National Aeronautics and Space Administration, grant NGR 15-003-118.

[1]T.J. Eskew, Proc. of the 23rd Ann. Conf. on Mass Spectrometry and Allied Topics, p. 266 (1975).

Figure 1

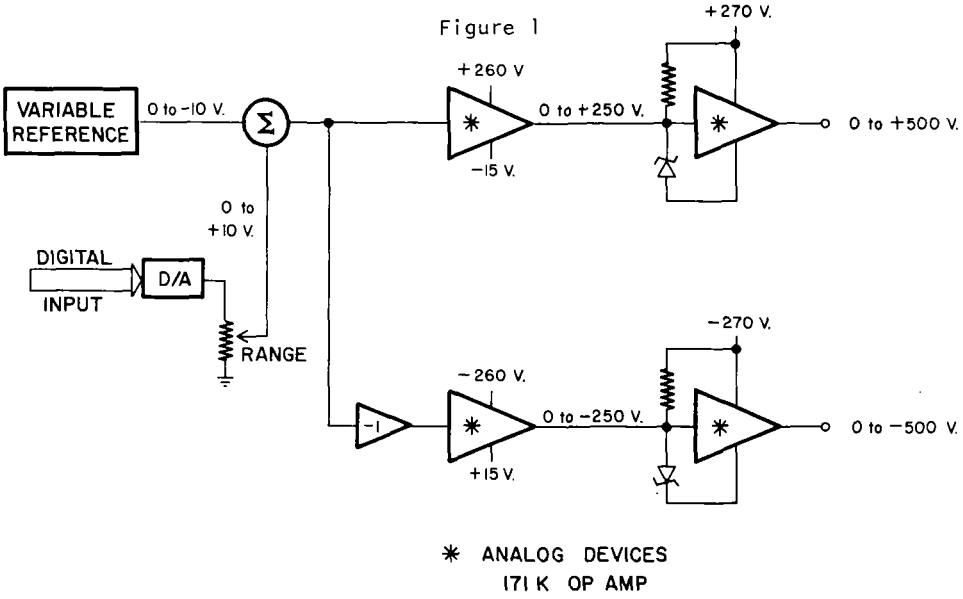

Figure 2

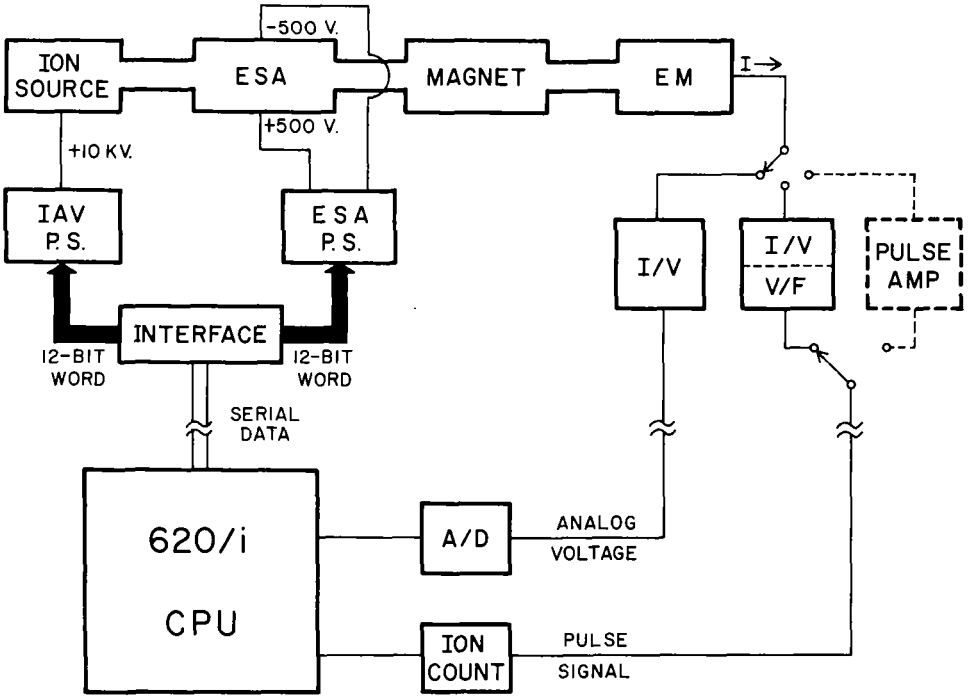

Computerized Routine Mass Fragmentography of Some Transmitter Metabolites. Claes Goeran Fri, Applications Laboratory, LKB-Produkter AB, Stockholm-Bromma, Sweden.

A computerized system for routine Mass Fragmentography or Selected Ion Monitoring in Combined Gas Chromatography Mass Spectrometry using a magnetic sector instrument (LKB 2091) will be described. The system consists of a disk oriented data system capable of measuring up to 16 selected ions with varying measuring times (0.1 sec. to 3200 sec.) and dwell periods (2m sec. to 3.2 sec.). Calculation and adjustment of accelerating voltages for each selected ion is done automatically. System drift can be corrected by using one channel as a reference channel to correct all other channel voltage settings. Each channel can also be voltage modulated so that maximum intensity readings are insured. Accuracy is 14 bits and dynamic range is 17 bits. Routine results using this system will be shown for some transmitter metabolites.

MASS SPECTROMETRY OF NONVOLATILE MATERIALS AND SOLUTIONS BY THE PARTICULATE IMPACT TECHNIQUE

Frank T. Greene
Midwest Research Institute
Kansas City, Missouri 64110

Preliminary results obtained using particulate impact mass spectrometry (PIMS) have been previously reported.[1/] In this technique, a solution of the material to be analyzed is converted into an aerosol, the resulting droplets accelerated to supersonic velocities and directed into a warm plate in the ion source of the mass spectrometer, and mass spectra obtained of the volatilized material. When the PIMS technique was applied to nonvolatile and thermally unstable species, reasonable electron impact mass spectra were obtained, indicating that PIMS may be useful for the analysis of nonvolatile materials.

Additional diagnostic experiments have been carried out, including the determination of combined aerosol velocity distributions and volatilization rates and the determination of the effect of changes in impact plate temperature. Although these data are incomplete, they indicate that the solvent and solute are volatilized together, thereby supporting the hypothesis that the extremely rapid evaporation of the solvent in the droplet into the high vacuum of the ion source carries the solute along.

The useable sensitivity of the PIMS technique with the present system was estimated from the experimental data to be of the order of 1 ppm. Several orders-of-magnitude improvement in sensitivity should be possible with modifications of the system. It therefore appears that PIMS should be useful for LCMS.

1/ Greene, F. T., paper presented at the Twenty-Third Annual Conference on Mass Spectrometry and Allied Topics, Houston, Texas, May 25-30, 1975.

A DIRECT AIR-SAMPLING INLET FOR SURFACE IONIZATION MASS SPECTROMETRY OF AIRBORNE PARTICLES*

J. J. Stoffels

Battelle, Pacific Northwest Laboratory, Richland, Washington 99352

A direct air-sampling inlet for a surface ionization mass spectrometer has been developed. The inlet consists of four elements: 1) a capillary nozzle through which the ambient air is drawn generating a particle beam with small divergence; 2) a "skimmer" which skims off the bulk of the air expanding into a vacuum of 1 Torr while simultaneously transmitting the particle beam; 3) a collimator through which the particle beam also passes and by which another stage of differential pumping is accomplished; and 4) a hot filament to ionize the particles. The air-sampling capacity of the inlet is 6 cm^3/sec and the efficiency of particle transmission to the ionizing filament is approximately 33%. The inlet is incorporated into a transportable instrument for continuous, real-time measurement of airborne particles.

The complete text of this paper will be submitted for publication to the International Journal of Mass Spectrometry and Ion Physics.

---

* This work is supported by the Energy Research and Development Administration.

EXTENDING THE DETECTION LIMITS OF MASS SPECTROMETERS BY ERASING BACKGROUND AND MEMORY PEAKS BY SAMPLE BEAM MODULATION

L. F. Herzog and T. J. Eskew, Nuclide Corporation, 642 East College Avenue, State College, Pennsylvania 16801

Many mass spectrometers that have the sensitivity adequate to detect part-per-billion level constituents in samples cannot be used for this purpose because there are "background" peaks at many mass numbers that have intensities comparable to those given by ppm or even much more abundant species in samples. Ordinarily the major interferences occur at the mass numbers at which abundant atmospheric gases, and gases included in metals, occur, e.g., 2 (H_2), 18 (H_2O), 28 (N_2^+, CO^+, $C_2H_4^+$), 40 (Ar^+) and 44 (CO_2^+). However electron multiplier detectors are so sensitive that there is often a detectable background peak at every mass number.

The traditional approaches to reducing the background interference problem are cleaning and bakeout, using fluidless pumps, and resolving background and sample isobars.

The Cleanup, Bakeout and Fluidless Pump Approaches to Eliminating Interferences

Slide 1 is a background spectrum from one of the 6-60-SGA mass spectrometers Nuclide built for NASA's Lunar Receiving Lab, a mercury-pumped instrument that had had oven bakeout at 300-400 °C. The ion gauge pressure is 1.2×10^{-9} torr; all species above mass 45 are below 10^{-16} A, and above 58, only 79 and 101 (Hg^{++}) are as intense as 10^{-17} A, i.e., less than 10 ppb of a 10^{-9} A total beam. (Sensitivity was set at 10^{-4} A torr.)

Unfortunately, the ultra-clean system approach is of limited usefulness because it is generally too inconvenient, expensive and time-consuming.

Oil diffusion pumps can produce bottoming pressures in the 10^{-9} torr range even when untrapped, but at the sensitivity just stated, 10^{-11} torr = 10^{-15} A = 1 ppm! So a cold trap is mandatory. Using mercury as the fluid does not completely eliminate the problem since the boiler can crack and "recycle" hydrocarbons from samples or backing pump.

Ion pumps do eliminate hydrocarbons, but they have the disadvantage, for applications such as GC-MS with helium carrier gas, of being very inefficient pumps for noble gases. Turbomolecular pumps also use no fluids and pump noble gases as well as other gases of the same mass. However, they also usually have "bottoming" pressures well above 10^{-8} torr unless a cold trap or a backing diffusion pump is used. They do pump heavy species very effectively.

Cryogenic pumping with liquid helium is the most effective "pumping" technique available but its application is limited by cost and the unsuitability of most existing systems to its addition.

But no pumping system can by itself eliminate the background that builds up with time due to the use of the instrument to analyze relatively "dirty" (involatile and/or reactive) samples. Increasing pumping speed will not help much, since the worst contamination site is the instrument's ionization chamber, into which the samples are necessarily dumped, and which has a fixed outflow conductance.

Resolving Sample and Background Isobars

Higher resolution MSs can resolve sample species from isobaric background peaks when they are, in fact, different species, but at a considerable cost in sensitivity — X10 to X100. Slides 4A and 4B show a case where the technique can be used. Unfortunately, in the analysis of organics, background and sample species are usually the same, except at the permanent-gas species masses, such as 28 and 44.

The Pulsed Source/Synchronous Detector Technique

A pulsed ion source and synchronous ion detection system attacks head-on the problem that, immediately after they pass through the ionization process, "samples" become "background," by providing a means of determining where an ion, reaching the detector, originated.

Slide 2 shows such a system. A molecular beam effusing from collimating pinholes or a small-I.D. (e.g., 0.25 mm) tube is chopped by a notched rotating wheel, or a vibrating reed, before it enters the mass spectrometer's ionization chamber, at rates of 10 to over 1000 cps (80 in this case). The chopper also interrupts a light beam to a photocell. The pulsed output is passed through a frequency-to-voltage converter and the output is compared to a reference voltage in a motor control unit, which keeps the chopping frequency constant. The reference square wave signal is also sent to a lock-in amplifier to advise it as to exactly when the rotating shutter is "open". The output of the mass spec's electrometer amplifier is also fed into the lock-in amplifier (LIA). Ideally, ion currents resulting from the presence of background species of constant partial pressure in the source will, as shown on the slide, be relatively steady, essentially, d.c. signals, while ions produced from the sample will arrive only in regular pulses in synchronization with the pulses produced by the light beam.

In the LIA the reference signal reverses an electronic switch so that when the shutter is open, one side of a capacitor is charged, while when it is closed, the current charges the other side. The amplifier outputs the difference in voltage — the sample's signal. (One could in principle obtain the same information by closing a shutter between the crucible and the ionization chamber and recording the background spectrum with the d.c. amplifier — then subtracting — but the sync source/detector does this automatically and at precisely the same point in time for sample and background — both major advantages.)

A sync source/detector system can reduce the relative intensities of background peaks by factors of up to 1000, indexed to the intensities of the sample peaks. Since the signal-to-ion-statistics-noise ratio improves as measurement time increases, the improvement in detection limit afforded by the technique is greatest for trace species that are continuously present (for example, trace constituents in air or tank gases), and least for fast transients. Slides 3A and 3B of Ag 107 and 109 effusing from a crucible illustrate that the sync source/detector technique makes it possible to obtain accurate relative abundance data when isobaric species of different formula are present in the instrument's background, even with instruments of low resolution. Of course if the isobars are in the sample, this will not work — it will be necessary to resolve them.

Slides 4A and 4B show that the technique is applicable to the analysis of organic samples introduced from "solids" probes, reservoirs, or gas chromatographs. These are sections of a two-pen recorder record of an analysis of cholesterol. In each, the upper trace is the conventional DCA spectrum, including background, while the lower trace is the LIA sync source/detector spectrum. Here the resolution has been set sufficiently high that some interfering isobars are resolved — e.g., at m/e 202 and many others in Slide 4B. These, and also identical-formula background species are essentially absent in the LIA spectra. On the other hand a few species such as m/e 400 and 414, that might be assumed to be background, remain, indicating that they are in the sample. The advantage of automatically subtracting-out background before data processing is well illustrated by this example. Note: the complete version of this paper may be obtained from the author (request Nuclide publication no. 1587-1275).

EXHIBIT III: BACKGROUND SPECTRUM — FLOW MODE, M/E 0-70.

Instrument: Nuclide 6-60-SGA; Electron Multiplier Gain: 3×10^{4}; Pressure: 1.2×10^{-9} torr.

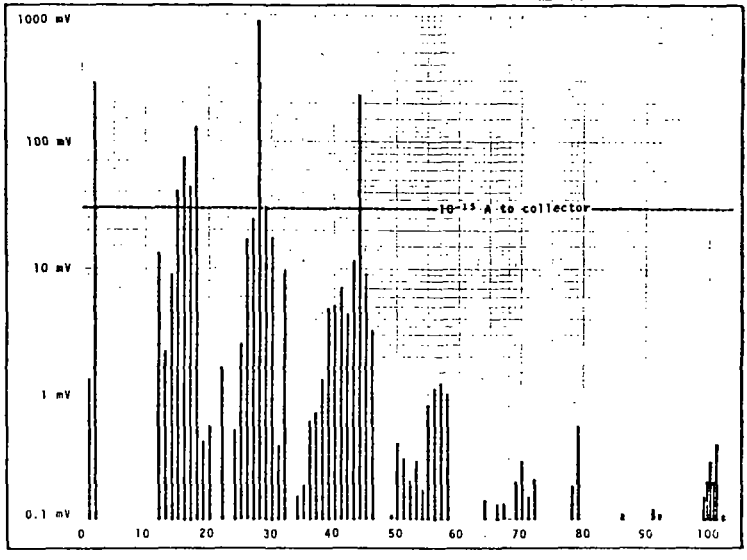

Slide 1

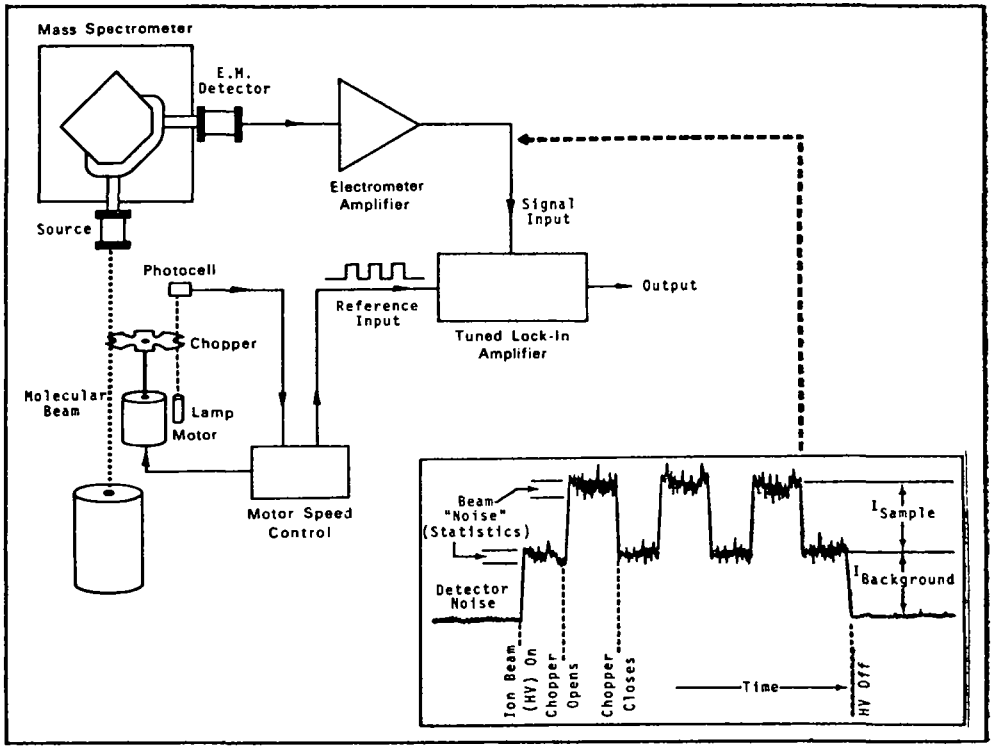

Slide 2

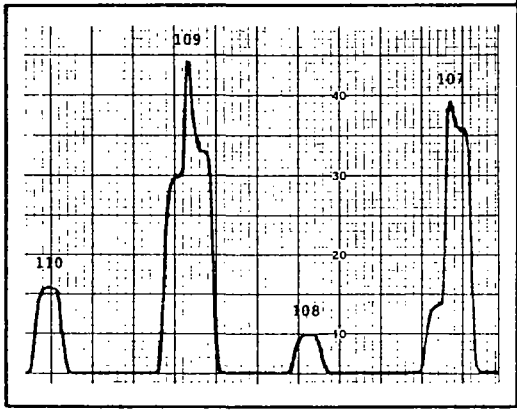

Slide 3A

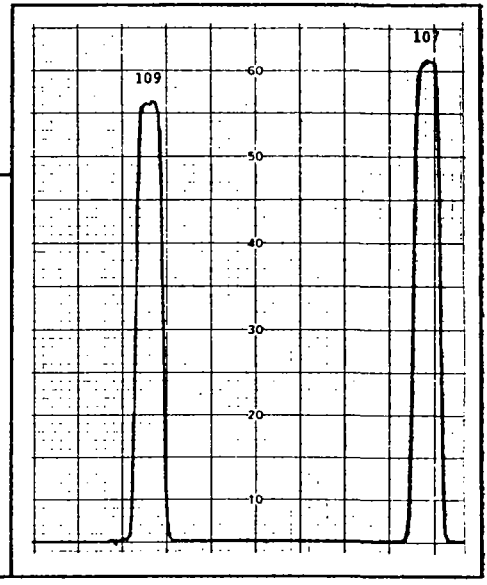

Slide 3B

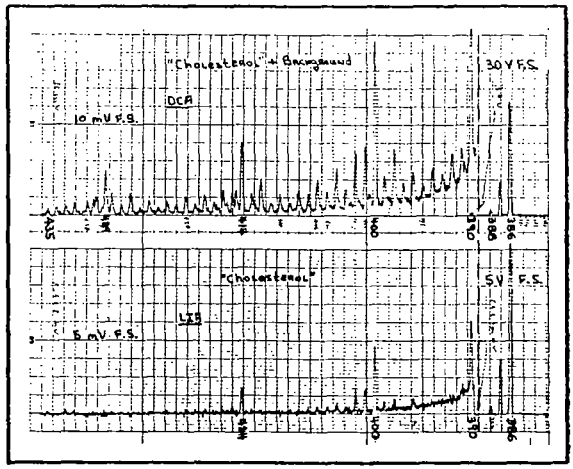

Slide 4A

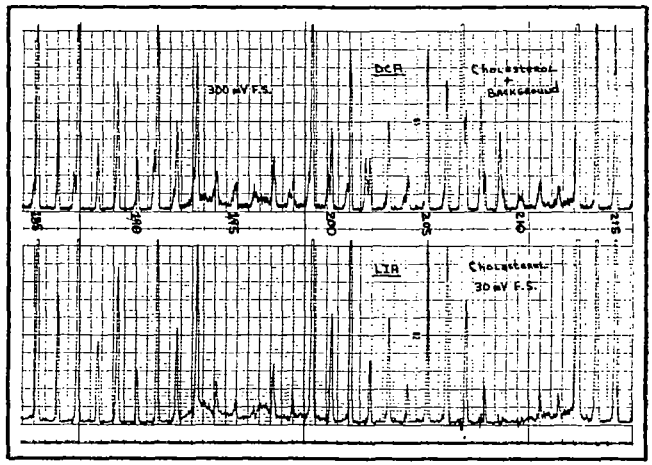

Slide 4B

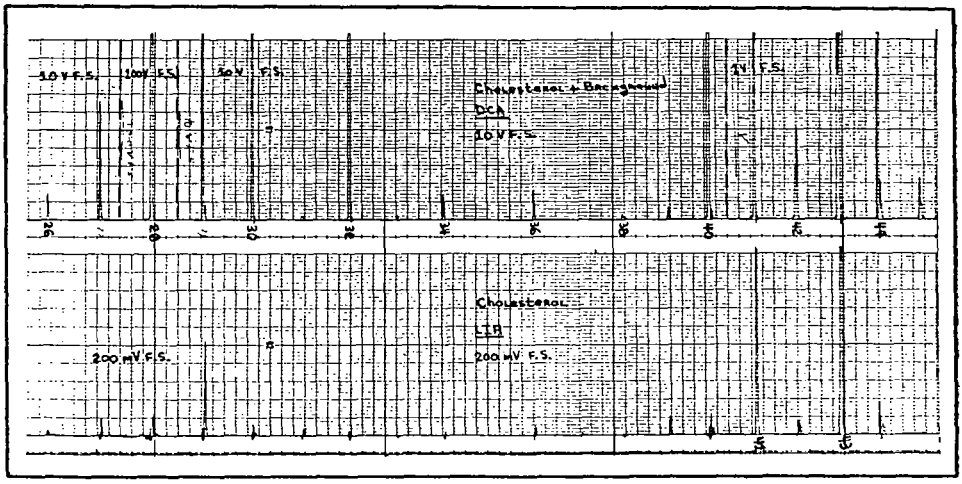

Slide 4C

VELOCITY DISTRIBUTION EFFECTS OBSERVED USING MODULATED MOLECULAR BEAM INLETS

by

Michael J. Vasile and Frederick A. Stevie
Bell Laboratories
Murray Hill, New Jersey 07974

Phase shifts observed as a function of pressure behind the orifice for low frequency (40-100 Hz) modulation of a 76 cm molecular beam inlet are attributed to the transition from effusive flow to supersonic flow with low Mach numbers. Molecular beam velocity distributions ranging from Maxwell-Boltzmann to supersonic at Mach 4 produce a strong dependence of phase on source pressure in the region of 0.1 to 2 Torr with a 0.02 cm dia. orifice. The phase shift becomes constant for velocity distributions of any particular gas with Mach numbers greater than 4. Phase differences between ions originating from molecules of different mass can still be detected, however the mass of the neutral progenitor of a fragment ion cannot be determined from a single phase measurement. Significant changes in focusing of polar molecules also occurs, since the transition to supersonic flow causes rotational cooling.

Flight time distributions of the molecular beam have been measured for modulation at 70 Hz with a 43% duty cycle. The flight time distributions obtained were verified for accuracy by discreet Fourier Transform convolution with the independently measured chopper opening function. The technique has been used to study the vapor phase decomposition of NbF_5 tetramers into dimers and monomers in a double oven. The mass of the dominant neutral species in the molecular beam can be identified with certainty by the flight time distribution method.

A full account of this work is being submitted to the International Journal of Mass Spectrometry and Ion Physics.

Estimation of Ionization Potentials of Heavy Elements Using A Pulse-Counting Mass Spectrometer*.

Ray S. Newbury, Lawrence Livermore Laboratory, Radiochemistry Div. Livermore, California 94550

The ionization potential of an element can be obtained relative to the known ionization potential of a different element by integrating the ion counts of all vaporizing species of both elements in a pulse-counting mass spectrometer. This method involves surface ionization and requires pulse counting to avoid the many errors inherent in current-measuring techniques. To test the method, known amounts of U and Pu were vaporized from the sample filament. From the ratio of their integrated ion efficiencies at constant ionizing filament temperature (assuming the ionization potential of U to be known), a value for the I.P. of Pu was calculated which is in reasonable agreement with the published value. Similar studies on Am with Pu will be discussed.

*Work performed under the auspices of the U.S. Energy Research & Development Administration under contract No. W-7405-Eng-48.

High Temperature Gas-Solid Interaction Studies.

Gary D. Blue, Visiting Scientist; Shen-Yung Tang, NRC Post Doctoral Research Associate, AFML; Edmund J. Rolinski, Air Force Materials Laboratory, (AFML), WPAFB, OH 45433

A Nuclide 12-90-HT mass spectrometer with a calibrated gas inlet source and Knudsen Cell were used to study the mechanism of gas-solid interaction at high temperatures. Initial experiments were performed with oxygen and titanium between 1300°C - 2000°C and oxygen pressure between 10^{-6} to 3×10^{-5} torr. The products of reaction were identified by their isotopic abundance, appearance potential and shutterability. The ion intensity of species were measured as a function of temperature and oxygen pressure. The source temperature was measured independently by Pt/10%Rh thermocouples penned to the bottom of the Knudsen cell and by an automatic recording optical pyrometer.

Stability of Complex Gaseous Cerium and Cerium-Ruthenium Carbides. K. A. GINGERICH, D. L. COCKE and J. E. KINGCADE, Dept. of Chem., Texas A&M Univ., College Station, Texas, 77843.

New types of gaseous transition metal carbides have been observed at temperatures above 2500K over a Ce-Rh-Ru-Os alloy that was contained in a graphite-lined tantalum Knudsen cell. The atomization energies of the molecules CeC_5, CeC_6, Ce_2C_2, Ce_2C_3, Ce_2C_4, Ce_2C_5, RuCeC, $RuCeC_2$ and $RuCeC_3$ have been obtained from measured third law enthalpies of suitable pressure independent reactions. Possible geometries of the new molecules are discussed. The results also permit the prediction of stable not yet known gaseous transition-metal carbides.

Computer Simulation of the Quadrupole Mass Filter.

J. E. CAMPANA, T. H. RISBY, P. C. JURS, Chem. Dept., Penn State Univ., Univ. Park, Pa. 16802.

The quadrupole mass filter has been simulated with a flexible, general, interactive computer program. To generate an ion trajectory, the user inputs the quadrupole settings and an ion's characteristics. The electrostatic forces on the ion are calculated using elementary equations of classical physics. The force field can be defined by any function the user desires to employ. From the forces, the acceleration, the velocity, and the displacement are derived for a time interval. The ion is moved to the new location, and then the cycle is repeated, stepping the ion through the field. The program can display the ion's trajectory visually on a CRT terminal. A comparison has been made with trajectories obtained from direct numerical solution of the Mathieu equation. The simulation can be used to study properties of the quadrupole mass filter that are difficult to observe experimentally.

Theory of Mass-Discrimination Effects in Ion Extraction from a Continuum Plasma

Jen-Shih Chang and J.G. Laframboise

Center for Research in Experimental Space Science and Physics Department, York University, Toronto, Canada

K. Kodera

Groupe de Recherches Ionosphériques, CNET, Issy-Les-Moulineaux, France

Abstract

Mass-discrimination effects in ion extraction have been treated for continuum conditions $\lambda \ll R_p$, $\lambda \ll \lambda_D$, by combining results of the following ion flux calculations: (a) an analytic solution for arbitrarily shaped sampling electrodes in the Laplace limit $\lambda_D \gg R_p$, without flow (b) numerical solutions for the front stagnation point of spheres in flow, for $R_p \ll \lambda_D$ and $R_p \gg \lambda_D$ (c) numerical solutions for spheres at finite R_p/λ_D, without flow. Here λ is ion mean free path, R_p is electrode radius or characteristic size, λ_D is Debye length. The treatment is applicable to: sampling electrode Reynolds numbers Re from 0 to 1000, ion Schmidt numbers Sc from 0 to 10^5, and scaled electrode (extraction) potentials $\varphi_p = eV_p/kT_i$ relative to the plasma, from 0 to $\pm$ 40.

I. Introduction

Ion extraction problems are important in plasma chemistry, plasma chromatography and ion mass spectrometry. An experimental estimation of mass-discrimination effects in ion extraction was first made by Becker et al (1955). Drawin (1968, p. 786) used the charge transport equation to predict mass-discrimination in a nonflowing continuum plasma for $\lambda_D \ll R_p$. Chang (1975) discussed mass-discrimination effects caused by flow tangential to a sampling electrode, in terms of the ion diffusion Reynolds number $Ra_i = 2U_\infty R_p/D_i$, where U_∞ is free-stream flow speed and D_i is ion diffusion coefficient. Here we discuss stagnation-point sampling with and without flow, for various electrode geometries.

II. Theory for stationary (nonflowing) plasma

We assume a constant-property, frozen-chemistry plasma with no magnetic field and only slight ionization, with sampling taking place through a small orifice of radius R_o, in a fully charge-absorbing electrode surface. We assume that ion mean free path $\lambda_i \ll R_p$, $\lambda_i \ll \lambda_D$, and $R_o \ll \lambda_D$. Ion transport is then governed by the nondimensional equation (Lam 1964):

$$\underline{j}_i = Ra_i n_i \underline{u} - n_i \nabla\varphi - \nabla n_i; \qquad \nabla \cdot \underline{j}_i = 0 \tag{2.1}$$

where $\underline{j}_i = \underline{J}_i R_p/D_i N_\infty$, $n_i = N_i/N_\infty$, $\varphi = eV/kT_i$, $\underline{u} = \underline{U}/U_\infty$, and N is number density. An equivalent equation can be written for any negative ion species or for electrons with φ replaced by $-\varphi$. All of the resulting transport equations are coupled together by Poisson's equation, which in nondimensional form (Lam, 1964), contains R_p/λ_D as a parameter. Dimensional analysis of this situation now shows that in the nonflowing limit $Ra_i \to 0$, $\underline{j}_i$ becomes independent of D_i and hence of ion mass. On the electrode surface, we then have:

$$j_i = f(S_p,\ T_i/T_e,\ R_p/\lambda_D,\ \varphi_p) \tag{2.2}$$

where S_p is surface position, and the form of f depends on electrode shape. For spheres, f has been calculated by Chang and Laframboise (1976a, fig.2). If several ionic species are present, the mass-discrimination between two ionic species 1, 2 having equal temperatures is then corrected by the relation:

$$\frac{N_{1\infty}}{N_{2\infty}} = \frac{J_1}{J_2}\ \frac{D_2}{D_1} \tag{2.3}$$

This result is essentially equivalent to Eq.(19) of Drawin (1968), except that it is not restricted to the limit $R_p/\lambda_D \to \infty$.

In the Laplace limit $R_p/\lambda_D \to 0$, Chang and Laframboise (1976a) showed that (2.2) reduces to:

$$j_i = f(S_p)\ \varphi_p/[\exp(\varphi_p) - 1] \tag{2.4}$$

Their work also contained an evaluation of $f(S_p)$ for prolate spheroids, which we now use to estimate effects of electrode shape. We consider a family of prolate spheroids of equatorial radius R_q and half-length R_qL (so that $L \geq 1$, and for $L = 1$, we have a sphere), and for which the relation between R_q and L is chosen so that all spheroids have the same radius of curvature R_p at their end points (poles). This turns out to imply $R_q = LR_p$; $R_qL = L^2R_p$. A straightforward extension of Chang and Laframboise (1976a) then yields:

$$\frac{J_{i,\text{spheroid end}}}{J_{i,\text{ sphere}}} = (1 - 1/L^2)^{\frac{1}{2}} \Big/ \ln\left[\frac{(L+1)^{\frac{1}{2}}+(L-1)^{\frac{1}{2}}}{(L+1)^{\frac{1}{2}}-(L-1)^{\frac{1}{2}}}\right] \to \frac{1}{\ln 2L} \text{ as } L \to \infty \tag{2.5}$$

For the frequently-used blunted-cone-on-cylinder electrode shape, Eq.(2.5) can be used to estimate current reduction due to electrode shape for each ion species, if L is approximated by using cylinder radius for R_q and stagnation-region radius for R_p. Eq.(2.5) can be shown to apply also in the opposite limit $R_p/\lambda_D \to \infty$. In the presence of flow, this shape effect (on stagnation-point J_i values) will change by different amounts for each ion, since Ra_i is different for each. In general, for a given R_p, shape effects on J_i will decrease as Ra_i increases.

III. Theory for flowing plasma

An exact numerical treatment of Eq.(2.1) for spheres in flow, in the Laplace limit $R_p/\lambda_D \to 0$, has been done using $\underline{U}$ values provided by the exact incompressible viscous flow solutions of Dennis and Hudson (1973), for Re values up to 60. This work is to be published separately (Chang and Laframboise, 1976b). For larger Re up to 1000, an approximate treatment of (2.1) has been done (Kodera and Chang, 1976) using the flow solutions of Van Dyke (1964, pp.156-161) together with neglect of transverse in comparison with radial ion diffusion in the stagnation region. The stagnation-point j_i values from both treatments agree within 6% where they overlap. These results can be written in the general form $j_i = j_i(\varphi_p, Re, Sc_i)$, where Sc_i is ion Schmidt number $\nu/D_i = Ra_i/Re$, and ν is neutral gas kinematic viscosity. Mass-discrimination between two ion species is now corrected by using:

$$\frac{N_{1\infty}}{N_{2\infty}} = \frac{J_1\ D_2\ j_2(eV_p/kT_2,\ Re,\ Sc_2)}{J_2\ D_1\ j_1(eV_p/kT_1,\ Re,\ Sc_1)} \tag{3.1}$$

We have fitted these j_i results with various power-law approximations which we present here. For $\varphi_p = 0$, the forms $j_i = 1 + A\,Sc_i^{\alpha}\,Re^{\beta}$ and $j_i = 1 + B\,Ra_i^{\gamma}$ are useful; values of A, B, α, β, γ, together with rangesof applicability, are shown in Fig. 1. These lead, respectively, to the correction formulas:

$$\frac{N_{1\infty}}{N_{2\infty}} = \frac{J_1\ D_2\ (1 + A\ Sc_2^{\alpha}\,Re^{\beta})}{J_2\ D_1\ (1 + A\ Sc_1^{\alpha}\ Re^{\beta})} \to \frac{J_1}{J_2}\left(\frac{D_2}{D_1}\right)^{1-\alpha} \quad \text{for } Ra >> 1 \tag{3.2}$$

$$\frac{N_{1\infty}}{N_{2\infty}} = \frac{J_1\ D_2\ (1 + B\ Ra_2^{\gamma})}{J_2\ D_1\ (1 + B\ Ra_1^{\gamma})} \to \frac{J_1}{J_2}\left(\frac{D_2}{D_1}\right)^{1-\gamma} \quad \text{for } Ra >> 1 \tag{3.3}$$

For $-6 \leq \varphi_p \leq 0$ and $Re \leq 0.2$, the approximation $j_i = j_i(\varphi_p = 0) + Ra^{\gamma}(0.40 + 0.050\varphi_p)$ agrees with the numerical results within 7%. For $\varphi_p < -6$, the asymptotic form $j_i = -\varphi_p$ (Chang and Laframboise, 1976a,b) agrees with

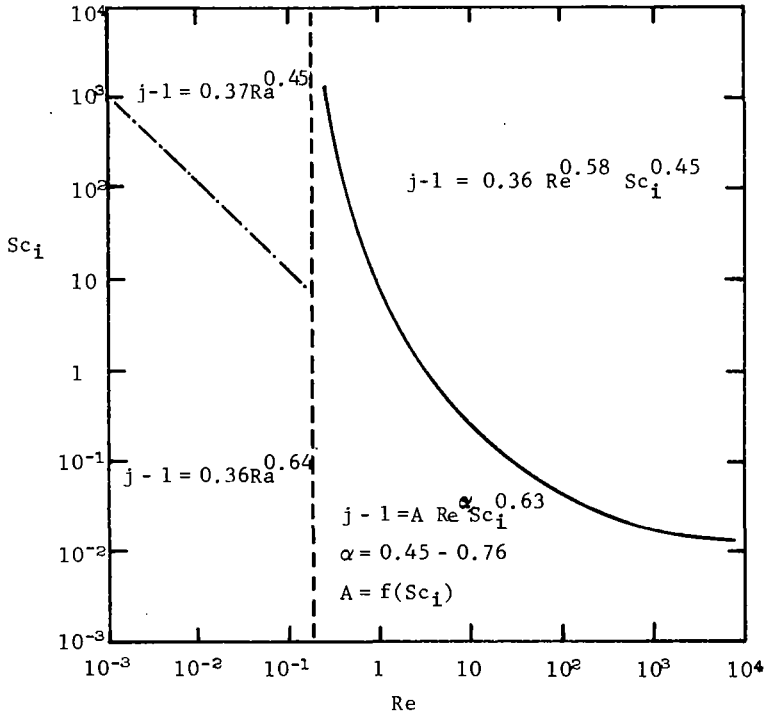

Fig. 1: Ranges of validity of approximations to j_i results for $\varphi_p=0$. These approximations agree with the numerical results of Chang and Laframboise (1976b), and Kodera and Chang (1976) within 6%.

the numerical results within 1%. The results for $\varphi_p = 0$ (Fig. 1) also apply for <u>all</u> φ_p in the opposite limit $R_p/\lambda_D \to \infty$, if D_i is replaced by the ambipolar diffusion coefficient D_a throughout (Chang and Laframboise, 1976b, Appendix A). An approximate interpolation for finite R_p/λ_D is made possible by the results of Chang and Laframboise (1976a, Fig.2). who calculated self-consistently the current collected by stationary spheres for $T_i/T_e = 1$. When $\varphi_p = 0$, our situation is a mathematical analogue of corresponding heat transfer situations (Chang and Laframboise, 1976b, pp.46-47). Kays (1966, p.211) has obtained an approximate solution for axisymmetric stagnation-point heat transfer. Converted to our notation, it is equivalent to the result: $j_i \propto Re^{0.5}\ Sc_i^{0.4}$, and is applicable when $Sc_i \approx 1$. This leads to a result similar to Eq.(3.2).

References

Becker, E.W., K. Bier and H. Burghoff (1955) Z. Naturforsch. 10a, 565

Chang, Jen-Shih (1975) Int. J. Mass Spect. & Ion Phys., 16, 448

Chang, Jen-Shih and J.G. Laframboise (1976a) Phys. Fluids 19, 25

_____(1976b) Centre de Recherche en Physique de l'Environnement, Orleans-La Source, France, Note Technique(In press)

Dennis, S.C.R. and J.D. Hudson (1973) Private communication.

Drawin, H.W. "Plasma Diagnostics" (1968) Chap.13 "Mass Spectrometry of Plasmas" pp.777-841, North Holland.

Kays, W.M. (1966) "Convective Heat and Mass Transfer", McGraw-Hill, New York.

Kodera, K, and Jen-Shih Chang (1976) Centre de Recherche en Physique de l'Environnement, Orleans-La Source, France, Note Technique C.R.P.E./N.T.P./2

Lam, S.H. (1964) AIAA J., 2, 256

Van Dyke, M. (1964) "Perturbation Methods in Fluid Mechanics" Academic Press, New York.

MEASUREMENT OF THE SECONDARY ELECTRON DISTRIBUTIONS FROM POLYATOMIC ION IMPACTS IN THE ENERGY RANGE ≤100 KV: THEORY AND PRACTICE*

Robert J. Beuhler and Lewis Friedman

Department of Chemistry
Brookhaven National Laboratory
Upton, New York 11973

A low noise, high sensitivity, secondary electron detector has been constructed from a modified Dietz[1] design, and at 45 kV has a noise level of ∿5 single electron events per second. In the energy range 21 to ∿100 kV, the average secondary electron yield, $\bar{\gamma}$, from a copper surface is a linear function of ion velocity and is found to be the sum of the yields from the individual constituent atoms in the ion. This information on ion composition derived from $\bar{\gamma}$ allows the determination of charge on an ion which has been selected in a mass spectrometer for m/e. Furthermore the relative electron yield from each constituent atom in the ion at the same velocity is found to be proportional to the electronic stopping power of that atom. This observation suggests a simplified model based on the well known nuclear and electronic stopping power calculations which can be used to predict the average secondary electron yield for an ion of any composition and velocity.

This work has been submitted for publication in the International Journal of Mass Spectrometry and Ion Physics.

*Research carried out at Brookhaven National Laboratory under contract with the U.S. Energy Research and Development Administration.

[1] L. A. Dietz and J. C. Sheffield, Rev. Sci. Instrum. 44, 183-91 (1973)

Preliminary Results with an Electro-Optical Ion Detector (EOID) on a Focal Plane Mass Spectrometer

C. E. Giffin, D. D. Norris, H. G. Boettger
Jet Propulsion Laboratory, Pasadena, CA

INTRODUCTION

Researchers in the field of biomedical mass spectrometry are turning frequently to selected ion monitoring (SIM) in an effort to solve their sensitivity and/or detectability problems. The SIM technique while providing the highest signal-to-noise achievable on a given instrument does so only at the expense of much or all spectral information. Hence the researcher must be meticulous about his chemical protocols and analytical techniques in order to insure against contaminant ions contributing to the m/e peak being monitored.

This paper describes the progress being made by the authors in the development of an electro-optical ion detector (EOID) which is an attempt to preserve the ability to acquire complete mass spectra, over a wide (36:1) mass range, without loosing sensitivity either due to low duty cycle* (as in scanning mass spectrometers) or low inherent sensitivity of photographic emulsions to ions (as in focal plane instruments).

INSTRUMENT DESCRIPTION

The EOID concept has been reported on in the past (1-3) and is illustrated schematically in Figure 1. Ion beams exiting the magnet of a Mattauch-Herzog mass spectrometer are brought to focus at the input of a two-dimensional microchannel electron multiplier array (MCA) where a gain of 10^4 is achieved in the ion to electron conversion process. These electrons are then accelerated to phosphor coated fiber optics where another gain of 20-100 is attained in the electron-to-photon conversion process. The photons are then impinged onto an imaging device where an electrical output proportional to the total integrated ionic charge is generated. While the imaging device depicted in Figure 1 is a photo diode array the imaging system being implemented in this work utilizes a vidicon camera as shown in Figure 2. The fiber optic coupler is a nineteen fold

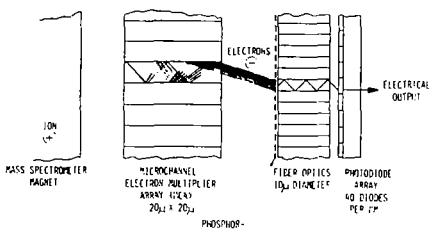

Figure 1

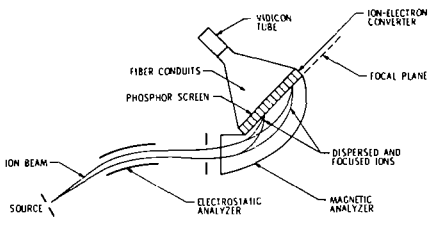

Figure 2

* Duty cycle is defined as the fraction of time spent on any given m/e peak as referenced to the time required to accomplish a complete mass spectral scan.

image dissector which formats the 1 mm high x 361 mm long spectrum of "ion" images produced at its input end into a 19 mm x 19 mm square geometry compatible with the vidicon camera sensitive area (4).

The heart of the detector is shown in crossection in Figure 3. It is comprised of a metal and machinable ceramic structure 390 mm long that supports and references the phosphored fiber optic face plate and fourteen specially constructed MCAs (ITT Corp., Roanoke, VA) with respect to the MS magnet. The MCAs are each 25.4 mm long with an active area height of 1 mm along their full length. The fourteen MCAs are butted end-to-end to form a continuous 356 mm long ion detection surface. Both the MCAs and the phosphored surface of the fiber optics are angled at 20° with respect to the magnet exit face so that the secondary electron accelerating electric field is not orthogonal to the analyzer magnetic fringe field. As detailed in Reference 3 stable electron trajectories to the phosphor are then possible.

The complete EOID layout as retrofitted to a CEC 21-110B mass spectrometer is shown in Figure 4 (with the exception of the vidicon camera which focuses through the window). The magnet shunts were used to linearize the magnetic fringe field in the vertical direction. Three mechanical adjusters were used to align the image dissector with the spectral images on the fiber optic face plate.

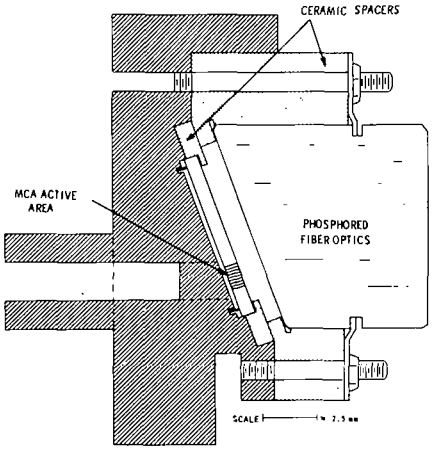

Figure 3

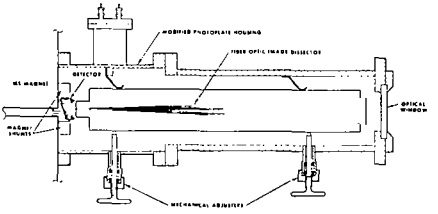

Figure 4

RESULTS

At the time that this paper was presented, the fiber optic image dissector had not been installed and therefore the data presented here will be limited to the spectra observed at the back face of the fiber optic face plate.

Figure 5 is a photograph of the mass spectrometer's magnetic analyzer. The EOID assembly can be seen through a large glass window attached directly to the back of the modified photoplate housing. The EOID is illuminated with a spectrum of perfluorokerosene. The major peaks can

easily be identified over the broad mass range. The most intense image on the left is m/e 31. The last bright image on the right is m/e 455. One can easily note the conspicuous near-absence of m/e 50 and m/e 51 images to the left of the second very bright line representing m/e 69. This is due unfortunately to one of the fourteen MCAs having a low gain. These data were obtained at an ion energy of 2000 volts and magnetic field of 4650 gauss. Figure 6 is a close-up photograph of the last 65 mm of the focal plane at a field setting of 5300 gauss with 4000 volt ions from perfluorokerosene. The major ions are labeled over the mass range from m/e 219 to m/e 293.

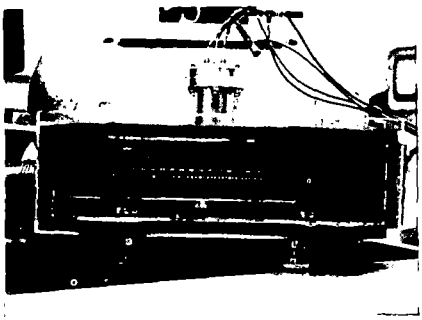

Figure 5

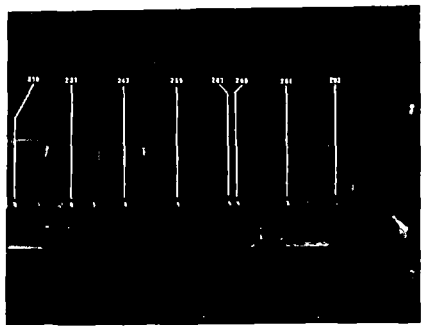

Figure 6

CONCLUSIONS

Implementation of an "electronic photoplate" for a focal plane mass spectrometer is well underway and the first experimental results are very encouraging. The effort is continuing so that the initial design goal of $M/\Delta M=1000$ with a detectability of 10-100 ions can be achieved with the hardware configuration discussed above.

This work was supported by NIH Research Grant No. GM 20850 awarded by the Institute of General Medical Sciences, PHS/DHEW.

REFERENCES

1. Boettger, H. ASMS Transactions (1973) 440.
2. Giffin, et. al. ASMS Transactions (1974) 33.
3. Giffin, et. al. Int. J. Mass Spectrom. Ion Phys., 15 (1974) 437.
4. Norris, D. D. and Giffin, C. E. Proceedings of the SPIE/SPSE Technical Symposium East. Vol. 77., March 1976.

INSTRUMENTATION FOR THE SIMULTANEOUS RECORDING OF POSITIVE AND NEGATIVE ION CHEMICAL IONIZATION MASS SPECTRA*

Donald F. Hunt, George C. Stafford,
Frank Crow, & John W. Russell

Department of Chemistry
University of Virginia
Charlottesville, Virginia 22901

Positive and negative ions of the same mass are transmitted through a quadrupole mass filter under identical conditions. This is because the required rf and dc potentials applied to the rods are independent of the charge polarity of the ion. In this paper we describe a modification to a Finnigan quadrupole mass spectrometer which facilitates simultaneous recording of positive and negative ion CI mass spectra using a conventional oscillographic recorder. Positive and negative ions appear as deflections in opposite directions on this device. Unique analytical applications of the above apparatus will be discussed.

* to be published in Analytical Chemistry

COLLISIONAL ACTIVATION (CA) SPECTRA OF GASEOUS ORGANIC IONS

Claus Köppel, Timothy Wachs, F. M. Bockhoff, B. Van de Graaf, P. P. Dymerski, and F. W. McLafferty

Department of Chemistry, Cornell University, Ithaca, New York 14853

An improved instrumentation system for CA spectra has been developed utilizing a DEC PDP-11/10 computer with the reverse-geometry double-focusing mass spectrometer which has a special collision chamber and high-pressure ion source. Data acquisition and spectral comparison have been automated, with full operator interactive control through a CRT terminal. This instrumentation has been used to investigate a variety of ion structure problems. The formation of the isomeric $C_8H_9^+$ ions ethylenebenzenium, methylphenylcarbenium, methylbenzyl, and methyltropylium has been elucidated with the aid of ^2H and ^{13}C labelling. The isomeric $C_3H_3^+$ and $C_3H_5O^+$ ions have been examined; nine stable forms of the latter have been identified.

The generous support of the National Institutes of Health and the Army Research Office, Durham, is gratefully appreciated.

[1]F. W. McLafferty, P. F. Bente, III, R. Kornfeld, S.-C. Tsai, and I. Howe, J. Am. Chem. Soc., 95, 2120 (1973); F. W. McLafferty, R. Kornfeld, W. F. Haddon, K. Levsen, I. Sakai, P. F. Bente, III, S.-C. Tsai, and H. D. R. Schuddemage, J. Am. Chem. Soc., 95, 3886 (1973).

STATISTICAL ANALYSIS OF ELIMINATION CURVES OBTAINED FROM THE MICRODISTILLATION OF MIXTURES

Ronald D. Grigsby, Eric J. Norman, and
J. Stuart Richardson

Department of Biochemistry and Biophysics
Texas A&M University
College Station, Texas 77843

The microdistillation of mixtures from a mass spectrometer probe has been refined to the point where it can be used routinely in analytical work. Three programs are required to analyze the data. The first of these accepts raw data consisting of intensity of ions vs. probe temperature and calculates intensities corrected for decrease in sensitivity with increasing ion-source pressure. From the corrected data, the second program calculates the least-squares parameters for the curves,the areas under the curves, the maximum heights of the curves, and the temperatures at which the maxima occur--T(IMAX). Limits of error are included. The third program accepts groups of results having common T(IMAX) values and calculates relative intensities including error limits for ions in the groups. The technique is illustrated with results for the microdistillation of mixtures containing oligopeptide derivatives, fungal metabolites, and other low volatility compounds.

MASS SPECTROMETRIC IDENTIFICATION OF THE NON-SAPONIFIABLE LIPIDS OF *EIMERIA TENELLA* OOCYSTS

W.J.A. VandenHeuvel, C.C. Wang and R.M. Weppelman

Merck Sharp & Dohme Research Laboratories
Rahway, New Jersey 07065

The fatty acid and non-saponifiable lipid fractions from oocysts of *E. tenella*, a protozoan parasite which reproduces within the epithelial cells of the caeca of the domestic chicken, have been analyzed by GLC and combined GLC-mass spectrometry. The fatty acids detected were identified as $C_{14:0}$, $C_{16:0}$, $C_{16:1}$, $C_{18:0}$, $C_{18:1}$ and $C_{18:2}$. The non-saponifiable lipids included cholesterol and unbranched primary alcohols of 22, 24, 26, 28, 30, and 32 carbon atoms. Selective ion monitoring demonstrated that saturated and mono-unsaturated members were present for each species of alcohol. Trimethylsilyl derivatives of these fatty alcohols were found to offer several important advantages over the free alcohols for mass spectrometric characterization. Unlike the latter, TMSi ethers yield molecular ions, although these are of low intensity for the saturated alcohols. However, these derivatives yield very intense M-15 ions which are readily identified as they are the only major ions differing by six mass units between the TMSi and TMSi-d_9 ethers. Another advantage of the TMSi ethers is that the m/e 103 ion unique to primary alcohols is significantly more intense than the analogous m/e 31 ion of the free alcohol.

Chemical Ionization Mass Spectrometry of Amino Acid-Fluorescamine Derivatives.

J. J. Shieh, K. Leung and D. M. Desiderio, Institute for Lipid Research and Marrs McLean Department of Biochemistry, Baylor College of Medicine, Houston, Texas 77030

The chemical ionization mass spectra of fluorescamine and fluorophors (fluorescamine-amino acid derivatives) have been studied using methane and ammonia as reagent gas. The major ions in methane CI spectra are $(M+H)^+$, $(M+H-O)^+$, $(M+CH_5)^+$, $(M+CH_5-O)^+$ and $(M+C_2H_5)^+$; while in ammonia CI spectra $(M+H)^+$, $(M+H-O)^+$, $(M+NH_4)^+$ and $(M+NH_4-O)^+$ predominate . Loss of an oxygen atom from the protonated molecule and adduct ions is energetically favorable in this class of compounds. The previous study of the E.I. spectra of this class of compounds has proved that the oxygen atom lost is the phthalan 2' oxygen (1).

For a further mechanistic study of the ammonia CI spectra of these compounds, a series of secondary amines was used as mass marker.

Experimentally, mass spectra were obtained on a CEC 21-110B double-focusing mass spectrometer modified for high pressure work (2). Samples were introduced by direct probe inlet and reagent gas was maintained at ca. 0.4 torr.

REFERENCES

(1) J. J. Shieh, K. Leung and D. M. Desiderio, Org. Mass Spectrom., in press.

(2) I. Dzidic, D. M. Desiderio, M. S. Wilson, P. F. Crain and J. A. McCloskey, Anal. Chem., 43, 1877 (1971).

PSA 10 The GLC/CI/MS Determination of Lithocholic Acid and its Potential Metabolites.* GARY M. MUSCHIK, LYNN H. WRIGHT, JAMES A. SCHROER and WALTER L. ZIELINSKI, JR. NCI Frederick Cancer Research Center, P.O. Box B, Frederick, Maryland 21701

Studies on the anaerobic metabolism of lithocholic acid (3α-hydroxy-5β-cholanic acid) by mixed intestinal fecal bacteria represent part of a research program at the NCI Frederick Cancer Research Center on the evaluation of potential intestinal cancer induction by endogenous carcinogens. Metabolism of specific bile acids leads to a number of bile acid metabolites having chemical structures which are not fully known, and hence requires generation of an analytical data base of sufficient size for structural elucidation.

The data obtained from methane GLC/CI/MS of the isolated metabolites contain a significant amount of information concerning their structure. Methane was used as both GLC carrier gas and CI/MS reagent gas for the determination of GLC separation factors (α), molecular weight data and fragmentation losses. When the functional group types attached to the 5β-cholanic acid moiety versus GLC α values (using a 1% QF-1 liquid phase) are plotted interesting correlations with the monol/diol/triol series, mono-one/di-one/tri-one series, and the [monol, mono-one]/[diol, mono-one] series are seen. Comparisons of GLC α values for 35 bile acid standards presently in our library generate qualitative information useful in the tentative identification of metabolite structural class. The use of methane as the CI/MS reagent gas leads to the formation of quasimolecular ions having $(M + H)^+$, $(M + C_2H_5)^+$, and $(M + C_3H_5)^+$ structures. The appearance of these quasimolecular ions serves to distinguish the molecular weight of the unknown metabolite(s).

Dihydroxy- and trihydroxy cholanic acid methyl esters exhibit weak quasimolecular ions under methane CI/MS conditions. The monols, mono-ones, di-ones, tri-ones, and the saturated and unsaturated 5β-cholanic acid methyl esters, on the other hand, provide appreciable quasimolecular ion intensities. Losses of neutral molecules from substituted methylcholantes help to simplify spectral interpretation. Such losses (water, carbon monoxide, methane, and alcohol) from the quasimolecular ion (and its fragment ions) often determine the number of hydroxyl or keto groups, and frequently their configuration in the unknown metabolite structure. For example, methyl 3β-hydroxy-5β-cholanate has a quasimolecular ion $[(M + H)^+ = 391]$ with an intensity of 28% of the base peak $[(M + H)^+ - H_2O = 373]$, while methyl 3β-hydroxy-5α-cholanate has the same quasimolecular ion $[(M + H)^+ = 391]$ with an intensity of 72% of the base peak $[(M + H)^+ - H_2O = 373]$. This difference in the loss of water from the quasimolecular ion and the difference in GLC α values can be used to clearly distinguish the 5β and 5α isomers of methyl 3β-hydroxycholanate. The 3β-hydroxy and 3α-hydroxy isomers of methyl-5β-cholanate can also be distinguished by their ability to lose water from their respective quasimolecular ion $[(M + H)^+ = 391]$. Furthermore, the 3α-hydroxy epimer of methyl 3β-hydroxy-5β-cholanate does not exhibit an observable quasimolecular ion at m/e 391 and hence readily eliminates a molecule of water. The base peak $[(M + H)^+ - H_2O]$ for this epimer appears at 373. Thus, this difference in the loss of water from the quasimolecular ion, as observed by the intensity of the quasimolecular ion and the respective GLC α values, makes possible the distinction between the methyl 3β- and 3α-hydroxy-5β-cholanates.

We also observed an ion at m/e=357 for methyl 3β-hydroxy-5β-cholanate, possibly resulting from one of two different mechanistic routes. One such route may be represented by the loss of methanol from the quasimolecular ion obtained by hydride abstraction [$(M - H)^+ - CH_3OH$ = 357]. A second potential mechanism could occur by the loss of one molecule each of water and methane from the quasimolecular ion obtained by proton addition [$(M + H)^+ - H_2O - CH_4$ = 357].

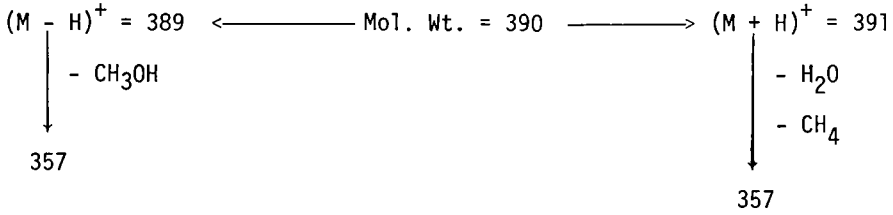

By examining the CI fragmentation pattern of ethyl 3β-hydroxy-5β-cholanate, we determined that the loss of both water and methane from the quasimolecular ion (see above scheme) was probably the mechanism involved in the formation of m/e=357. Bile acid esters having 1-3 keto groups show the loss of water and a larger loss of methanol than was observed for the hydroxylated analogs containing 1-3 hydroxy groups.

The identification of 3β-hydroxy-5β-cholanic, 3α-hydroxy-5β-cholanic and 3-keto-5β-cholanic acids as metabolites of taurolithocholic acid formed in a mixed fecal bacterial culture (following clean-up and methylation) was made tractable by the data base (GLC α values, quasi-molecular ion data and fragmentation patterns) generated in these studies. This substantial data base is expanded by information obtained from the identification of metabolites, allowing enhanced ease of identification for other bile acid metabolites isolated in the continuing endogeneous carcinogen studies at our facility.

* Research sponsored by the National Cancer Institute under Contract No. N01-CO-25423 with Litton Bionetics, Inc.

IDENTIFICATION OF ACIDIC METABOLITES OF CORTICOSTEROID BY MASS SPECTROMETRY

H. J. Lee
School of Pharmacy
Florida A & M University
Tallahassee, Fl. 32307

J. Roboz and C. Monder
Research Institue for Joint Diseases
Mt. Siani School of Medicine
1919 Madison Ave.
New York, N. Y. 10035

Metabolic transformation of corticosteroid 17 beta-ketol side chain to 17 beta-glycollic acids *in vivo* and *in vitro* has been studied. Acidic cortisol metabolites, characterized by having a 21-oic acid group from human urine, constitute 5-25% of the administered cortisol radioactivity (1). Mass spectra of the major esterified metabolites of cortisol were identical with those of authentic epimers of 3α,20β-diacetoxy-17-hydroxy-11-oxo-pregnan-21-oate methyl ester. An enzyme which is responsible for the transformation of corticosteroids to steroidal 20-ol-21-oic acid has been purified 150-fold from cytosol fraction of hamster liver (2). Measurement of enzyme activity was based on the release of tritium as labeled water from (21-^{3}H)-corticosteroids. All 17-ketol steroids were substrates but the detritiation rate varied with ring substituents.

For the positive identification of acidic metabolites of corticosteroids, 100 mg of (4-^{14}C)-11-deoxycorticosterone was incubated with 70 mg of purified enzyme in 200 ml of 0.025 M tris-HCl, pH 8, at 37° for 20 hours. The incubation mixture was adjusted to pH 1 with 2N HCl, and the steroids were extracted from incubation mixture with ethyl acetate. The organic extract was evaporated with a stream of nitrogen, and the resulting residue, dissolved in methanol, was streaked onto silica gel plates. After the plates were developed with chloroform:methanol (98:2), two bands were observed under UV light. One, Rf 0.5, corresponded to the substrate itself; the other remained at the origin. Two radioactive peaks coinciding with the UV opaque components were detected on the plate with a radiochromatogram scanner. The portion containing the nonmobile, polar metabolite was scraped off the plate, eluted with methanol, and further purified by TLC using acidic polar solvent system (upper phase of toluene:acetic acid:water = 50:50:10). A single component was obtained with Rf value in this system of 0.58. The yield of metabolite was 12 mg.

The IR and UV spectra of the 11-deoxycorticosterone metabolite were identical to those of synthesized 20-hydroxy-3-oxo-4-pregnen-21-oic acid.

Conclusive evidence for the structure of the acidic metabolite of 11-deoxycorticosterone was obtained by high and low resolution mass spectrometry. The fragmentation pattern derived from the spectrum revealed a relatively intense molecular ion at M^+ 360, $C_{22}H_{32}O_4$, which corresponds to the molecular weight of 20-hydroxy-3-oxo-4-pregnen-21-oate methyl ester. The formation of ion b., m/e 318, $C_{20}H_{30}O_{31}$, by losing fragment ion CH_2CO from ring A of steroid nuclei with the Δ^4-3-oxo configuration is well established (3). Loss of carbomethoxy group from C-20 of molecular ion a. led to the fragment ion c., m/e 301, $C_{20}H_{29}O_2$. Further loss of CHOH from ion c. yielded ion d., m/e 271, $C_{19}H_{27}O$. The base peak g., m/e 124, $C_8H_{12}O$, is formed by complex hydrogen transfer and cleavage of B ring from ion d., and directly from molecular ion a. (4). The fragmentation pattern was characteristic of a steroid nucleus of Δ^4-3-ketone with a 17 glycollate methyl ester side chain, as shown in Fig. I.

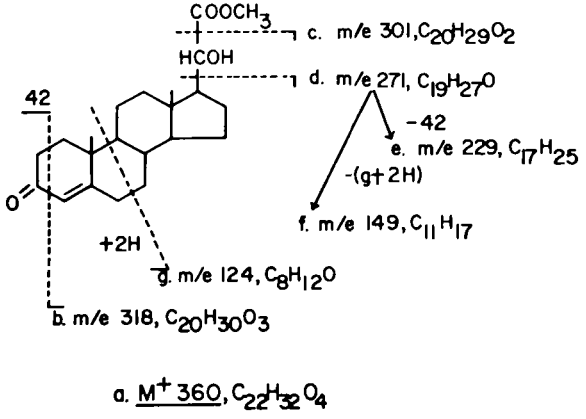

Fig. I. Proposed partial fragmentation of 20-hydroxy-3-oxo-4-pregnen-21-oate methyl ester.

References:

1. Bradlow, H. L., B. Zumoff, C. Monder, H. J. Lee and L. Hellman, J. Clin. Endocrinol. and Meta. 37, 811, 1973.

2. Lee, H. J., K. O. Martin and C. Monder, Fed. Proc. 34, 2516, 1975.

3. Sohubert, K., G. Kaufmann, G. and H. Budzikiewicz, Biochem. Biophys. Acta 176, 170, 1969.

4. Shapiro, R. and C. Djerass, J. Am. Chem. Soc. 86, 2825, 1963.

AROMATIC HYDROXYLATION OF A DEUTERATED ELLIPTICINE IN RATS: LACK OF AN NIH SHIFT

Robert J. Bruni and Vernon N. Reinhold
Arthur D. Little, Inc., Cambridge, Mass. 02140 and Harvard Medical School, Boston, Mass. 02115

Metabolites of the antitumor agent, ellipticine (Fig. 1), are mainly secreted in rat bile as two conjugates of hydroxylated ellipticine.[1] Chromatographic and mass spectral properties of the unconjugated drug have shown identity with an authentic sample of 9-hydroxyellipticine (Figs. 2 and 3).

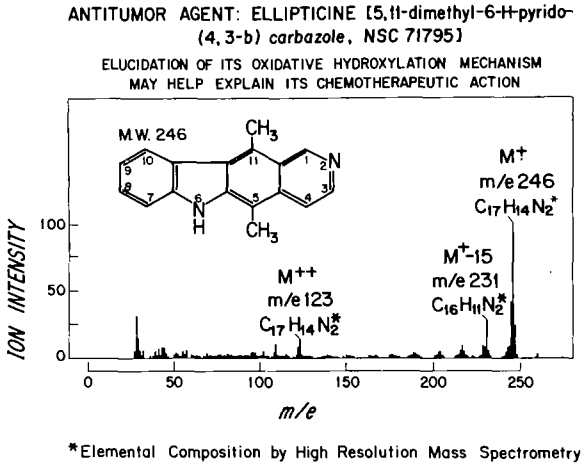

*Elemental Composition by High Resolution Mass Spectrometry

Fig. 1

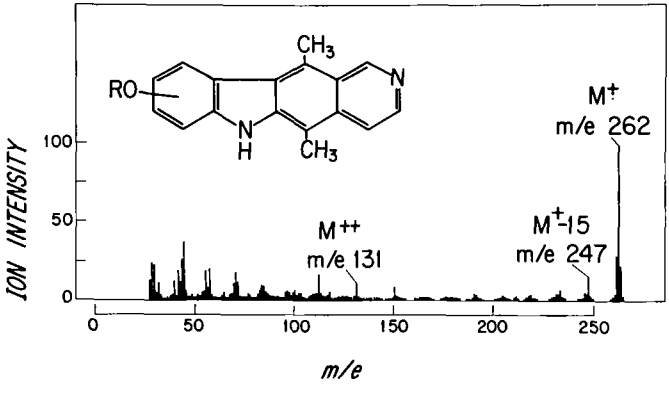

Fig. 2

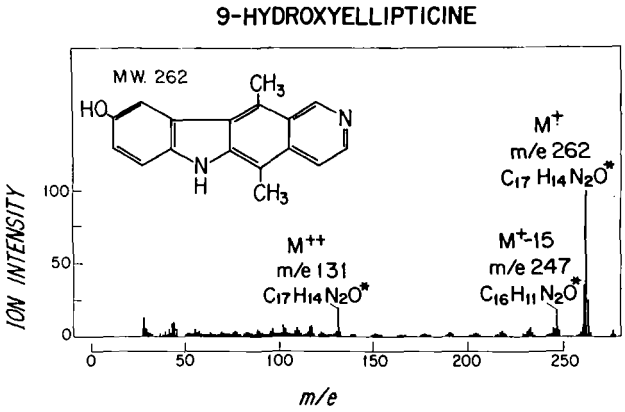

Fig. 3

*Elemental Composition by High Resolution Mass Spectrometry

The possible involvement of an arene oxide intermediate prior to hydroxylation and conjugation has been studied using 7,9-dideutero-ellipticine and by determining the conservation of deuterium in the phenolic products. The deuterated drug was synthesized by acid catalyzed exchange and was characterized by NMR and high and low resolution mass spectrometry (Fig. 4). Mass spectra (Fig. 5) of two conjugated metabolites from rat bile show a mass ion at $m/_e$ 263 (singly deuterated hydroxylated ellipticine).

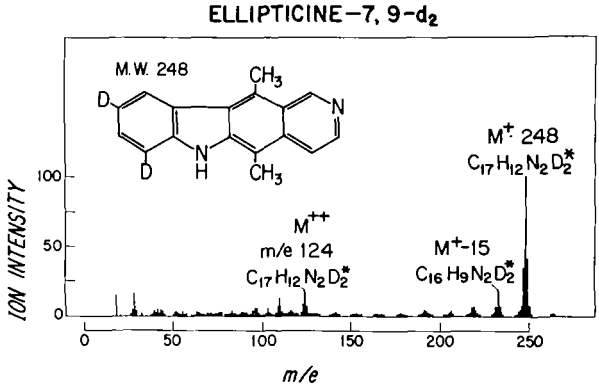

Fig. 4

*Elemental Composition by High-Resolution Mass Spectrometry

TWO MAJOR METABOLITES ISOLATED BY HIGH-PERFORMANCE LIQUID CHROMATOGRAPHY OF AN n-BUTANOL EXTRACT OF BILE FROM ELLIPTICINE-7, 9-d_2-TREATED RATS

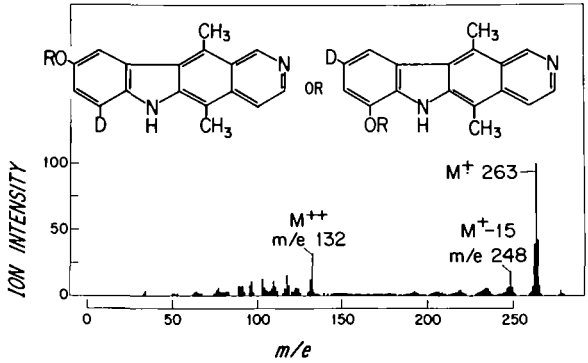

Fig. 5

There was no evidence for conservation at the position of hydroxylation ($m/_e$ 264) according to the following expected NIH shift mechanism.

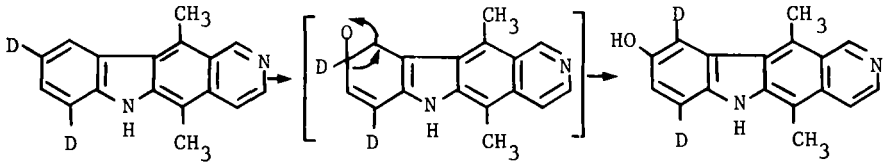

$m/_e$ 248 $m/_e$ 264

These results indicate that the major pathway of metabolism for this cancer chemotherapeutic drug, prior to conjugation and excretion in rat bile, proceeds by aromatic hydroxylation apparently without involving an arene oxide/NIH shift mechanism.[2]

This work was supported by DCT, NCI, NIH Contracts NO1-CM-33727 and NO1-CM-53849.

References

1. V. Reinhold, L. Bittman, R. Bruni, K. Thrun, D. Silveira, Proc. Amer. Assoc. Cancer Res., 16:135 (Abst.538)(1975).

2. J. Daly, in Handbook of Experimental Pharmacology, B.B. Brodie, J.R. Gillette, eds., Springer-Verlag, New York, 1971, Vol. XXVIII/2, Chapter 39.

A paper describing the details of this work has been accepted for publication in Biomedical Mass Spectrometry.

EVALUATION OF ISOTOPIC VARIANTS OF 3-METHOXY-4-HYDROXY-MANDELIC ACID (VMA) FOR SELECTED ION RECORDING. S.P. Markey, M. Claeys, K. Powers, and M. Ebert, Laboratory of Clinical Science, NIMH, NIH, Bethesda, Md. 20014

In the course of studying the kinetics of metabolism of norepinephrine (NE), a strategy similar to that employed for the metabolism of dopamine (1) has been devised. Labeled methionine (trideuteromethyl) is injected into experimental animals, and after some time period, the methylated metabolites of NE are extracted. Measurement of the ratio of deuteromethylated to endogenous VMA, normalized by the deutero/endogenous methionine ratio of each tissue, provides an accurate measure of the rate of synthesis of VMA. Analytically, this assay requires the availability of an internal standard for VMA and CD_3-VMA. In other laboratory studies, quantities of CD_3-VMA were desired to serve as internal standards for the measurement of endogenous VMA. Consequently, the syntheses of 3-trideuteromethoxy-4-hydroxymandelic (CD_3-VMA), 3-hydroxy-4-methoxymandelic (iso-VMA), and 3-hydroxy-4-trideuteromethoxymandelic (iso-CD_3 VMA) were undertaken.

Benzylation or methylation of dihydroxybenzaldehyde at pH 9-10 followed by partitioning of the products was used to selectively block or methylate the 4-position. For iso-VMA, iso-vanillin was used as starting material. iso-, iso-CD_3, and CD_3-vanillin were converted to the corresponding mandelic acids via the nitriles as described by Shaw, et al. (2). An alternate simpler synthesis for CD_3-VMA was also investigated. Catechol was mono-methylated with dimethyl sulfate-d_6 or methyl iodide-d_3 to form CD_3-guaiacol. Condensation with sodium glyoxylate produces CD_3-VMA in a single step (3). Complete details of these syntheses will be published elsewhere.

Standard curves prepared by adding varying amounts of each of the synthetic standards to a fixed amount of VMA in water, extraction at pH 2, and derivatization for gc-ms as the ethyl ester-trifluoroacetates, were examined over a range of 1-1000 ng. CD_3-VMA is linear over the full range, but iso- and iso-CD_3 VMA showed significant deviations from 100-1000 ng. However, in the range of experimental interest (1-100 ng) both iso- and iso-CD_3 VMA are useful internal standards.

References:

1. M. Ebert, W. Havens, K. Powers, S. Markey and I. Kopin, Proc. Soc. Neuroscience, 1976.
2. K.N.F. Shaw, A. McMillan, and M.D. Armstrong, J. Org. Chem. 23, 27 (1958).
3. J. Kamlet, U.S. Patent 2, 640, 083 [Chem. Abstr. 48, 5884 (1954)].

Mass Spectrometric Characterization of 2-Azahypoxanthine: An *in vivo* Diazotization Product of Biogenic 4-Aminoimidazole-5-Carboxamide

Bruce M. Johnson, Gerald M. Lower, Jr., and Steven P. Lanphear

Dept. of Human Oncology, University of Wisconsin Center for Health Sciences, 1300 University Ave., Madison, WI 53706

The biogenic amine, 4-aminoimidazole-5-carboxamide (AIC), is a component of human urine derived from the *de novo* purine biosynthetic pathway. This amine reacts with acidic solutions of inorganic nitrite to give 4-diazoimidazole-5-carboxamide (Diazo-IC) which may then react with suitable nucleophiles or undergo intramolecular cyclization to 2-azahypoxanthine (AH) as shown.

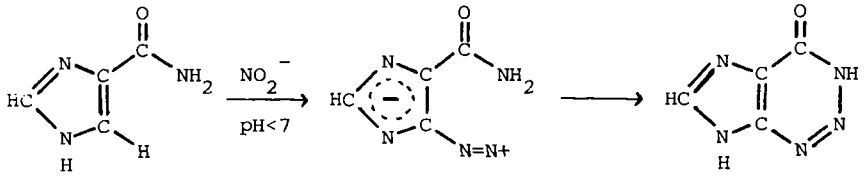

Data presented elsewhere have indicated that concurrent oral administration of AIC and $NaNO_2$ to rats results in the presence of urinary AH [1]. These observations demonstrate the ability of inorganic nitrite and AIC to react under physiological conditions to yield reactive diazonium intermediates.

Urinary AH is isolated by ion exchange chromatography and purified by thin layer chromatography as shown in Figure 1. Since AH crystallizes as a monohydrate, the water must be removed before a mass spectrum is obtained. All attempts to get a spectrum of hydrated material failed. The water was removed by dissolving AH in anhydrous methanol and placing over anhydrous $BaCO_3$. The solution was removed and evaporated using dry N_2 followed by desiccation over P_2O_5.

Mass spectra of authentic and urinary AH were obtained, Figure 2, by heating the direct insertion probe to 200°C. (Hewlett-Packard model 5930A, 70 eV, 0.2 mA, source 200°C). The fragmentation, Figure 3, is characterized by losses of 27, 28, and 43 from the molecular ion. These losses are exhibited by fused ring imidazoles [2] and 1,2,3-triazinones [3]. Successive elimination of these same masses are responsible for the remainder of the spectrum. The ions at m/e 111 and 95 cannot be easily explained from AH, but are resonable if some imidazole-4-carboxamide is present as an impurity. This may result from decomposition of the AH.

[1] G. M. Lower, Jr. and G. T. Bryan, Proc. Am. Assoc. Cancer Res., 16: 42 (1975).

[2] S.-O. Lawesson, G. Schroll, J. H. Bowie, and R. G. Cooks, Tetrahedron, 24: 1875 (1968).

[3] J. C. Tou, L. A. Shadoff, and R. H. Rigterink, Org. Mass Spectrom., 2: 355 (1969).

This investigation was supported by Grant Numbers CA 14524 and CA 14520 awarded by the National Cancer Institute, DHEW.

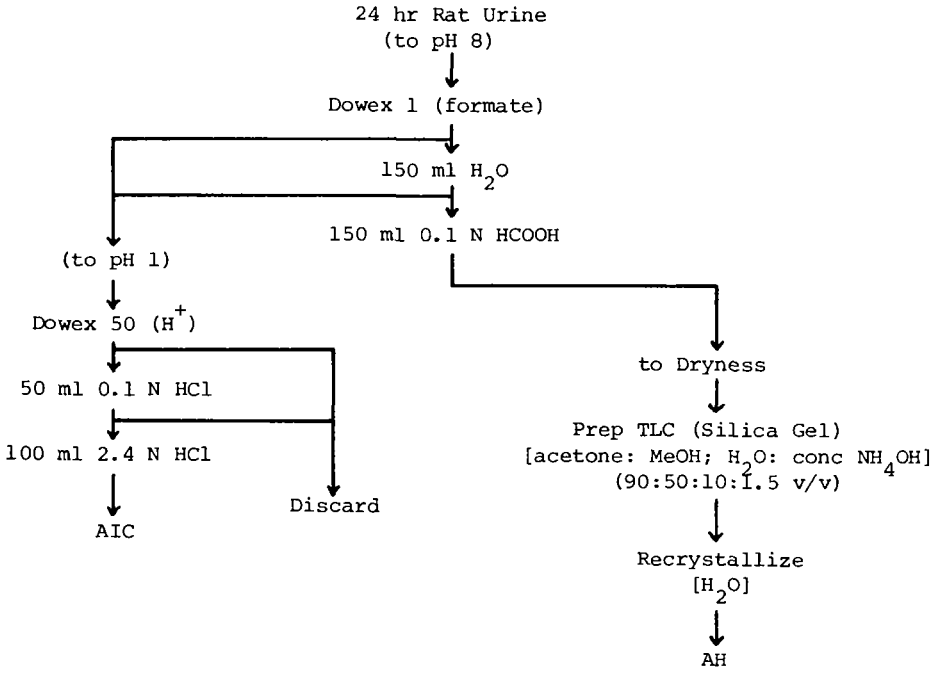

FIGURE 1

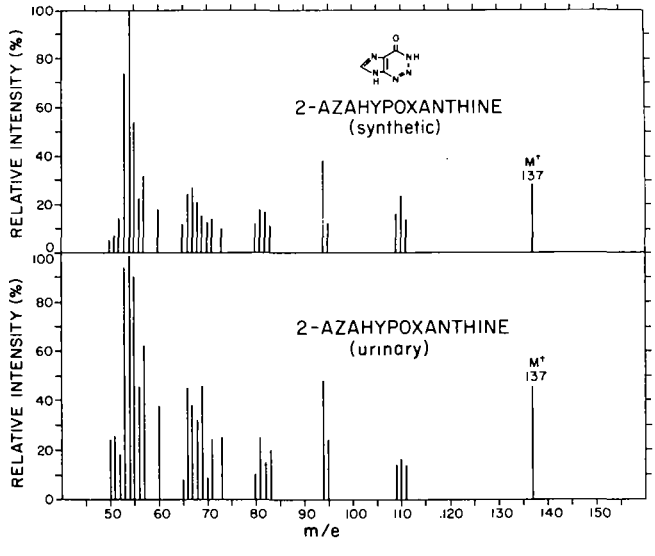

FIGURE 2

m/e

137 $M^{+\cdot}$

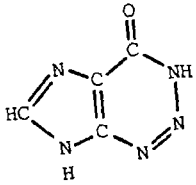

110 -HCN

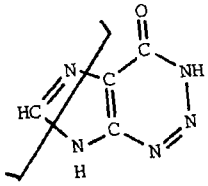

109 -CO

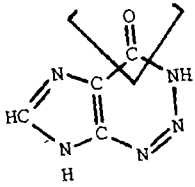

AND $-N_2$

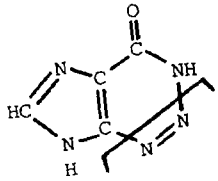

94 -HNCO

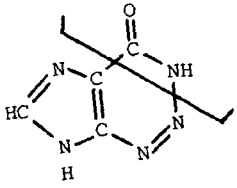

AND $-HN_3$

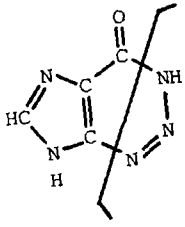

Lower mass ions derived from successive eliminations.

Imidazole-4-carboxamide is a possible decomposition product or contaminant that can give the ions at m/e 111 and 95.

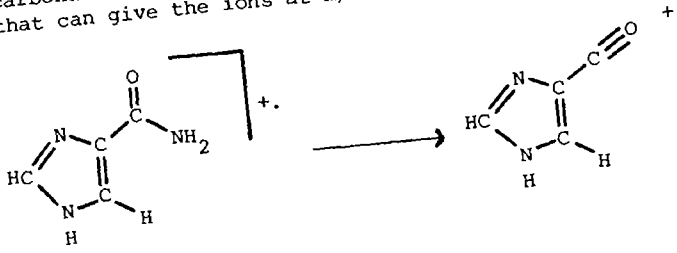

FIGURE 3

Determination of Drug Concentration in Serial Body Fluid Samples from Drug Intoxicated Patients by Mass Spectrometry.

DENIS C. K. LIN and RODGER L. FOLTZ,
Battelle Columbus Laboratories, Columbus, Ohio 43201,
and STEPHEN M. CATTANEO,
Riverside Methodist Hospital, Columbus, Ohio 43214

In cases of drug intoxication, the most often asked questions by physicians are:

1. What is the drug(s) involved?
2. How much is there?
3. Is there anything special that can be done to help the patient?

The first question can be answered accurately and fairly routinely by matching the GC-MS data to the reference spectra using a computer or an index card file. The second question can be answered with confidence by using the selected ion recording technique. The third question can only be answered after studying the pharmacokinetics of the drugs in human at doses much higher than for therapeutic levels.

This study attempts to correlate drug levels with the clinical condition of the patient. The study will also attempt to establish duration of drug activity, toxic metabolites, and adverse reactions of a particular drug in question. These clinical observations will provide information concerning physiological, pathological, and pharmacokinetic effects. The plan is to collect and correlate data concerning the plasma half-life of the parent drug and its metabolites, the potential toxicity of the metabolite(s), and the rate and extent of biotransformation and excretion. Clinical data such as age, sex, weight, and history of metabolic or infectious diseases will also be considered.

Serial body fluid samples were obtained from drug intoxicated patients during their stay at the hospital. Initially, the drug(s) involved was identified by a rapid drug screen using a GC-MS-COMPUTER system. The results were immediately conveyed to the attending physician to help in the diagnosis. The serial samples were analysed by combined gas chromatography and chemical ionization mass spectrometry with selected ion recording technique. The drugs which we can analyse quantitatively by GC-MS are listed in Table 1.

TABLE 1. DRUGS FOR WHICH QUANTITATIVE GC-MS ANALYTICAL METHOD DEVELOPED

Tetrahydrocannabinol	Diazepam
Methadone	N-Demethyldiazepam
Methaqualone	Amitriptyline
Methamphetamine	Phenobarbital
2,5-Dimethoxy-4-Methylamphetamine	Amobarbital
Imipramine	Secobarbital
Phencyclidine	Morphine
Meperidine	Meprobamate
Nortriptyline	Normeperidine

The data we obtained on the several intoxicated patients we have studied thus far are summarized in Table 2.

TABLE 2. DRUG INTOXICATION CASES STUDIED

Case No.	Drugs Present	Peak Level, μg/ml	Plasma Half Life, Hr.	Duration of Study, hr.
3	Phenobarbital	275	-	48
4	Secobarbital	13	12	48
	Amobarbital	10	29	
	Alcohol	2,300	-	
5	Meprobamate	125	9.0	24
7	Meprobamate	152	9.5	50
9	Imipramine	1.2	36	48
	Alcohol	700	-	
13	Secobarbital	31	21	72
14	Methaqualone	13	14	60

In conclusion, we find that the pharmacokinetics of the drugs at overdose level appear to be different from those at therapeutic level. However, a much larger number of cases have to be studied before a definite conclusion can be drawn. We also find that the clinical conditions of the patients appear to correlate with the drug levels; but the symptoms are nonspecific and they can be used only as a rough guide to identify the drug. Perhaps the examination of clinical parameters other than the ones observed in this study will be more useful. We feel that in the limited number of cases studies, quantification of the drugs is of prognostic value if the pharmacokinetics of the drug at overdose level are known.

ACKNOWLEDGEMENT

The work was supported by the National Institute on Drug Abuse, U.S.A. Grant No. DA 00919.

Quantitation of Amino Acids in Physiological Fluids Using ^{13}C Mass Fragmentography.

W. E. PEREIRA, P. J. ANDERSON, E. T. EVERHART, T. C. RINDFLEISCH, and A. M. DUFFIELD, Stanford Univ. Med. Ctr., Dept. of Genetics, Stanford, California 94305.

A rapid computerized method has been developed for the quantitative analysis of 13 amino acids in physiological fluids by the technique of Quadrupole Mass Fragmentography. The procedure involves the addition of a known amount of a mixture of ^{13}C labeled amino acids as internal standards to the biological fluid followed by a quick isolation procedure. The amino acids are then derivatized as the N-TFA-O-n-Butyl derivatives and subjected to computerized Quadrupole Mass Fragmentography. By continuous selected ion monitoring of the unlabeled and labeled species, and measurement of their relative peak height ratios, quantitation could be achieved. The entire procedure including the collection, storage and analysis of data was achieved by mini-computer. The method has been used to study amino acid levels in the urine of a patient with Phenylketonuria and in the urine, plasma and cerebrospinal fluid of a patient with Non-ketotic Hyperglycinemia. The method is ideally suited for the rapid amino acid analysis in physiological fluids of patients with suspected inborn errors of metabolism.

This work was supported by National Institute of Health Grant 1-P01-GM20832 Genetics Research Project.

Mass Spectrometry of 3-Methoxy Fatty Acid Methyl Esters
Origin of the Base Peak at M/e 75

Joseph A. Zirrolli and Robert C. Murphy
University of Colorado Medical Center
Department of Pharmacology
Denver, Colorado 80220

3-Hydroxy fatty acids are widely found in nature. In bacteria these hydroxy acids are often found in the cell membrane esterified to complex lipids such as phospholipids[1] and glycolipids[2]. 3-Hydroxy fatty acids are not commonly found in mammalian cells even though both the biosynthesis and oxidation of all fatty acids involve 3-hydroxy fatty acyl intermediates in these higher organisms[3].

The mass spectra of the 3-hydroxy fatty acid methyl esters show a base peak at m/e 103 due to 3,4 cleavage as well as an ion at m/e 74; the characteristic rearrangement ion of fatty acid methyl esters. When the 3-hydroxy group is methylated, the base peak is surprisingly shifted to m/e 75. Odham and Samuelsen[4] suggested that m/e 75 came from 2,3 cleavage with rearrangement of two hydrogen atoms.

To examine the origin of this ion, m/e 75, several isotopically labelled 3-methoxy fatty acid methyl esters were synthesized (I, II).

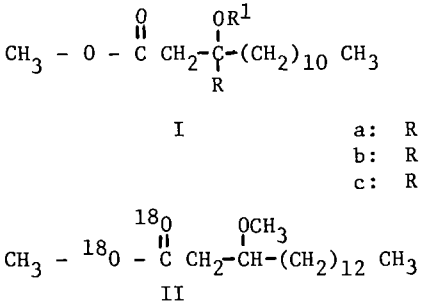

I

a: R = H, R^1 = CH_3
b: R = D, R^1 = CH_3
c: R = H, R^1 = CD_3

II

The results from these labelled analogs indicate that this ion is composed of the:

i) methyl group of the methyl ester[4]
ii) Methyl group of the methyl ether
iii) hydrogen atom from C-3
iv) one of the oxygens from the carboxy group (Table 1)

Also, a very strong metastable was found at m/e 48.1 in the mass spectrum of Ia which would correspond to the transition m/e 117 → m/e 75. The most plausible mechanism for the formation of m/e 75 involves the loss of a neutral ketene molecule from the 3,4 cleavage product of the molecular ion with the simultaneous migration of the carbomethoxy group to C-3 (Fig. 1). A full report of this work will be published shortly[5].

References

1. M. Ikawa, J. Keopfi, S. Mudd, and C. Nieman, J. Am. Chem. Soc., 75, 1035 (1953).

2. S. Bergstrom, H. Theorell, and H. Davide, Arch. Biochem. 10, 165 (1946).

3. A. L. Lehninger, Biochemistry, Worth Publishers, N. Y., 1970, Chap. 19, 23.

4. G. Odham and B. Samuelson, Acta. Chem. Scand., 24, 468 (1970).

5. J. A. Zirrolli and R. C. Murphy, Organic Mass Spect., In press, 1976.

Table I. Selected Ions in the Mass Spectra of 3-Methoxy Fatty Acid Methyl Esters.

Ion	Compound			
	Ia	Ib	Ic	II
Base Peak	75	76	78	77
3,4 Cleavage	117	118	120	121

Figure 1. Fragmentation Scheme.

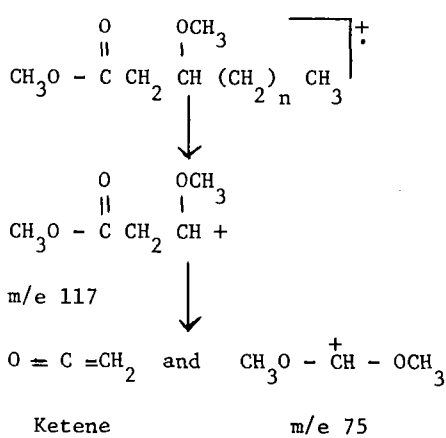

Isotope Dilution Analysis of Drugs and Metabolites Using Field Ionization Mass Spectrometry. M. Anbar, R. Dyer, G. Gonser, H. Heck, K. Maloney, J. McReynolds, and R. Sperry, Stanford Res. Instit., Mass Spec. Res. Center, Menlo Park, Calif. 94025

A number of examples in which isotope dilution analysis and field ionization mass spectrometry are being applied to problems of pharmacological importance will be presented. These will include: (1) the determination of nucleic acid base compositions; (2) investigations of thymidine uptake into DNA *in vitro*; (3) measurements of free thymine and thymidine in plasma; (4) studies of the tissue distributions of parathion and trifluralin in rats; (5) evaluations of the bioavailability of commercial samples of imipramine; and (6) recent results on the pharmacokinetics of methaqualone in man.

APPLICATIONS OF CO_2 CARBON ISOTOPE RATIO MASS SPECTROMETRY IN CLINICAL CHEMISTRY

D. A. Schoeller and P. D. Klein, Argonne National Laboratory, Division of Biological and Medical Research, Argonne, IL 60439, J. F. Schneider and N. W. Solomons, University of Chicago, and J. B. Watkins, Harvard Medical School.

Previously described $^{14}CO_2$ breath tests have been shown to be effective in the diagnosis of fat malabsorption (1), lactose deficiency (2), and bacterial overgrowth in the small intestine (3,4). As a safe alternative to these radiocarbon tests, we have developed several analogous $^{13}CO_2$ breath tests. This development extends the utility of CO_2 breath tests to infants, children, and pregnant women, populations in which the use of radionuclides is severely limited.

The test is performed by measuring the appearance of excess $^{13}CO_2$ in breath following the administration of a ^{13}C-labeled substrate. The substrates are synthesized with the label as part of a low molecular weight group that will be quickly oxidized to CO_2 after cleavage from the substrate. The choice of substrate depends on the enzyme system to be studied.

The amount of excess $^{13}CO_2$ in breath is determined by dual collector, isotope ratio mass spectrometry. The rate and total excretion of label are measures of the oxidative utilization of the substrate and the activity of the enzyme involved in the rate limiting bond cleavage.

METHODS

The patient fasts overnight before the test is administered. A sample of expired CO_2 is collected and used to determine the endogenous $^{13}CO_2/^{12}CO_2$ ratio. The labeled substrate is then administered, and CO_2 samples are collected periodically for 3 to 6 hours. The CO_2 is collected as carbonate in 2 N NaOH solution and later acidified in vacuum to release CO_2. After passage through a dry ice acetone cooled trap to remove water, the CO_2 is collected in a liquid nitrogen cooled trap. The CO_2 is next transferred to the mass spectrometer inlet, and the $^{13}CO_2/^{12}CO_2$ ratio is determined as described by Craig (5).

RESULTS AND APPLICATIONS

The sensitivity and precision of the breath test was limited by the normal variations in the $^{13}C/^{12}C$ ratio of CO_2 in breath. The average standard deviation of the $^{13}C/^{12}C$ ratio for a 6-hour period was 0.72‰. Thus, the minimum detectable change in the ratio is 1.4‰. At a typical CO_2 production, rate of 9 mmoles/(kg-hr), this corresponds to the excretion of 140 nmoles/(kg-hr) of $^{13}CO_2$ derived from the labeled carbon(s).

The $^{13}CO_2$ breath test has been applied to the study of fat malabsorption in infants with cystic fibrosis (6) using carboxyl-labeled trioctanoin. The cystic fibrotics excreted less than 10% the amount of label during the first 6 hours after substrate administration than normal infants. A fivefold increase in excess $^{13}CO_2$ production occurred when pancreatic lipase was added to the meals fed to the infants with cystic fibrosis.

Other applications of the $^{13}CO_2$ breath test have included the monitoring of hepatic microsomal function in a group of patients with primary biliary cirrhosis during treatment with phenobarbital (7) and for the detection of bile acid malabsorption in children due to bacterial overgrowth or intestinal bypass (8). The former study was performed using methyl-labeled aminopyrine and the latter using C-1 and C-1,2 glycine-labeled glycocholate.

The $^{13}CO_2$ breath test is a safe test that can be used in populations in which ^{14}C cannot be used. Since it is a non-invasive test causing no discomfort to the patient, it is ideal for use in pediatrics. The $^{13}CO_2$ breath test has been shown to be clinically useful in assessing fat malabsorption, microsomal function, and bile acid malabsorption.

The authors wish to express their gratitude to the personnel of the respective hospitals who assisted in sample collection and to A. Engelkemeir (ANL) who performed all of the isotopic measurements.

Work supported by the U. S. Energy Research and Development Administration and National Institutes of Health (AM 18741).

---

1. A. D. Schwabe, F. T. Cozzette, L. R. Bennett et al., Gastroenterology 42, 285-291 (1962).
2. Y. Sasaki, M. Iio, H. Kameda et al., J. Lab. Clin. Med. 76, 824-835 (1970).
3. H. Fromm, A. F. Hofmann, Lancet 2, 621-625 (1971).
4. H. P. Sherr, Y. Sasaki, A. Newman et al., New Eng. J. Med. 285, 656-661 (1971).
5. H. Craig, Geochim. Cosmochim. Acta 3, 53-92 (1953).
6. J. B. Watkins, D. A. Schoeller, D. G. Ott et al., Pediatric Res. 9, 310 (1975).
7. J. F. Schneider, D. A. Schoeller, B. Nemchausky et al., Gastroenterology 69, 865 (1975).
8. N. W. Solomons, D. A. Schoeller, J. Wagonfeld et al., Clinical Res. 24, 291A (1976).

DI-ALKANEBORONATES WITH NON-IDENTICAL SIDE CHAINS. APPLICATIONS IN MASS SPECTROMETRY OF CARBOHYDRATE DERIVATIVES.

J. Wiecko and W.R. Sherman

Washington University School of Medicine
Departments of Psychiatry and Biological Chemistry
St. Louis, Missouri 63110

In a previous report at this conference[1] we showed that 1,2:3,5-di-alkaneboronates of α-D-glucose 6-acetate and 6-dimethylphosphate[2], under E.I. conditions, lose an alkyl radical via interaction of the carbonyl (or phosphoryl) group with an alkaneboronate moiety. The ion produced in the case of the butaneboronate is of high abundance.

In this report we present evidence that 1) the interaction of the C=O function is with the adjacent 3,5-alkaneboronate, and 2) that the $[M-alkyl]^+$ ion intensity is enhanced when the departing radical is capable of rearranging to a more stable species.

In the course of this work, n-octaneboronic acid was prepared in a manner analogous to that described in the report of Brown and Gupta[3]. The formation of α-D-glucofuranose cyclic-1,2:3,5-di-1-n-octaneboronate 6-acetate follows the procedure for the formation of other alkaneboronates.

By the reaction of D-glucose with an equimolar mixture of methane- and butaneboronic acids in pyridine followed by treatment with acetic anhydride, both the 1,2-methaneboronate:3,5-butaneboronate and the 1,2-butaneboronate:3,5-methaneboronate of α-D-glucose 6-acetate are formed (the mixed methane-octaneboronates can be prepared in a similar way). The isomeric derivatives can then be separated sufficiently by GC to obtain mass spectra of the individual species.

The spectra show unequivocally that the loss of butyl radical occurs in one isomer and the loss of methyl radical in the other. The earlier eluting species, which loses butyl radical (giving rise to an intense ion at m/e 255) is thus the 1,2-methaneboronate:3,5-butaneboronate; only the butyl radical is lost, no evidence of methyl radical loss is observed. The later GC peak is the 1,2-butaneboronate:3,5-methaneboronate; no loss of butyl radical is observed. Similar behavior is observed in the case of

mixed methane-octaneboronates of 6-acetylglucose: the earlier eluting species again shows an intense ion at m/e 255 (loss of an octyl radical):

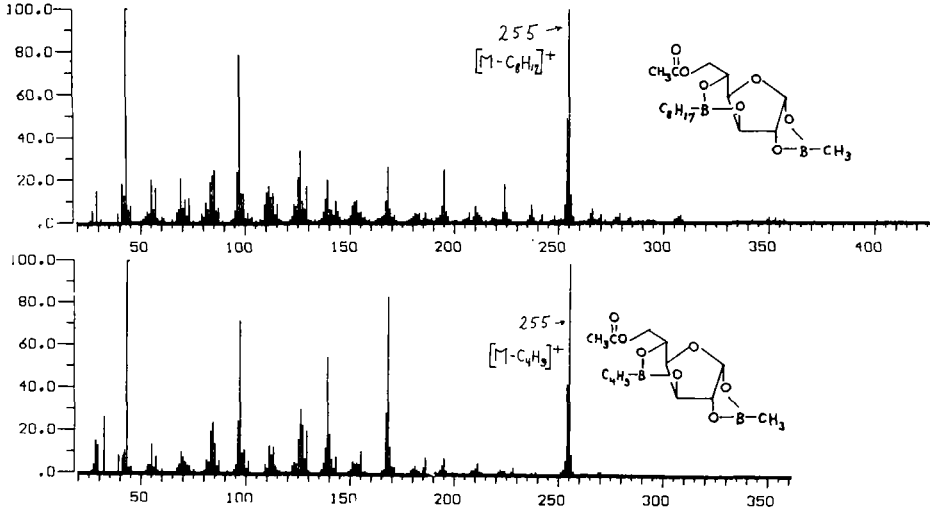

These results clearly show the radical loss to be confined to the cyclic-3,5-boronate moiety.

The loss of a butyl radical from α-D-glucofuranose cyclic 1,2:3,5-di-1-butaneboronate 6-acetate gives rise to a much more abundant ion (Σ_{40} of 6.9%) than the loss of methyl from the di-methaneboronate (Σ_{40} 0.39%). An ion of comparable abundance is obtained by the loss of the n-octyl radical from the di-octaneboronate (Σ_{40} 9.1%).

Two possible reasons for the great difference in abundance of the methyl loss vs the butyl or octyl loss are: 1) reduction of total energy in the molecule by the loss of a large vs small fragment; 2) rearrangement of the radical to a more stable (tertiary) species. The second explanation seems favored in view of similar abundances of ions arising from the butyl and octyl radical loss.

(Supported by RR-00954 and AM-17904)

1. J. Wiecko and W.R. Sherman, 22nd Ann. Conf. on MS and Allied Topics, Philadelphia ,1974, p. 323, paper Q1.
2. J. Wiecko and W.R. Sherman, Org. Mass Spectrom. 10, 1007 (1975).
3. H.C. Brown and S.K. Gupta, J. Amer. Chem. Soc., 93, 1816 (1971).

SIM DETERMINATION OF INOSITOL IN SINGLE CELLS OF THE CENTRAL NERVOUS SYSTEM

W.R. SHERMAN, M.H. LAIRD, R. BOSHANS and P. PACKMAN
Washington University Medical School
St. Louis, Missouri

In this work we want to bring attention to the possibilities of direct analysis of tissue constituents without prior extraction using selected ion monitoring. The procedure reported here is a favorable one in that myo-inositol is present in tissues in high concentrations, however, it should not be considered unique: other substances may be candidates for similar analysis.

myo-Inositol is part of the polar headgroup of a family of phospholipids known to occur widely in nature. One of these, phosphatidyl inositol, is known to undergo hydrolysis, with the release of free myo-inositol, on stimulation with acetylcholine in pancreas[1]. Other evidence suggests this may be a process common to many secretory tissues. We hope that, by studying changes in myo-inositol levels in tissue samples small enough to be representative of a cell type, or in single cells, we can localize the metabolic and secretory events related to this lipid hydrolysis. Furthermore, we may succeed in identifying tissue regions of intense activity not apparent by more macroanalytic methods, which, in requiring large samples, may mask highly localized events.

The method used for this analysis is a combination of standard techniques; SIM with deuterium-labeled myo-inositol (prepared by exchange of myo-inosose-2 in D_2O at pH 10 followed by reductive deuteration) and the techniques of quantitative histochemistry as practiced by Lowry[2]. The latter method entails rapid freezing of tissue following death, preparing 5-10 μm thick slices while frozen and vacuum drying the slices. In this way constituents of the tissue are stabilized both chemically and geographically, reflecting well the original tissue situation. Portions of tissue, as small as 2 ng dry weight, are dissected under a microscope, weighed on a quartz-fiber "fishpole" balance and transferred to 2 mm i.d. borosilicate tubes. Trimethylsilylating agent and d_6-myo-inositol are introduced (10 μl), the tube sealed and after 48 hrs. the entire contents injected into the GC-MS and analyzed by SIM.

The method was validated by comparison with flame ionization detection analysis (Table 1).

Figure 1 shows the relationship between sample weight and myo-

inositol content. The correlation coefficient of the regression line is 0.92, the line intersects the y axis at 0.4 pg.

Figure 2 shows the analysis of a 15.5 ng dry weight sample of the lateral preoptic nucleus of rat hypothalamus. The traces are as follows: m/e 307, TMS d_6-myo-inositol; m/e 305, tissue inositol quantitation peak; m/e 318, tissue inositol reference peak used to calculate the validation index. The m/e 305 trace represents 3.4×10^{-3} mole of inositol.

Some of the samples are small enough so that several sections can be made through a single nerve cell. In this way sections with and without nuclei are obtained and a determination of whether inositol is concentrated in the nucleus can be made (it is not: Table 2).

We believe that one of the advantages of direct analysis is that tissue constituents are protected in the tissue matrix until the moment of derivatization. Thus compounds may not be subjected to, for example, adsorptive losses on glassware prior to being converted to the less polar GC derivatives.

(This work was supported by grants NS-05159, MH-19624, RR-00954 and AM-17904.)

1. M. Hokin-Neaverson, K. Sadeghian, A.L. Majumder and F. Eisenberg Biochem. Biophys. Res. Commun. 67:1537 (1975).
2. D.H. Lowry and J.V. Passonneau A Flexible System of Enzyme Analysis, Academic Press (1972).

TABLE 1

Comparison of SIM and FID Analysis of myo-Inositol in Rat Cerebellar Granular Layer

Method of Analysis	Mean Sample Size	myo-Inositol mmoles/kg dry wt.	C(%)	Validation Index
FID	2.7 μg	21.8 ± 1.4 (8)	18	-------
SIM	16.6 ng	23.9 ± 1.0 (12)	14	1.047

C(%): coefficient of variation. Validation Index: the mean m/e 305/318 ratio of samples divided by the mean ratio obtained from standards.

TABLE 2

myo-Inositol Levels in Rabbit Dorsal Root Ganglion Single Cells

Cells	Mean Sample Size	myo-Inositol mmole/kg dry wt.	C%	Validation Index
With Nucleus	4.1 ng	20.9 ± 1.1 (10)	17	1.096
Without Nucleus	3.7 ng	18.4 ± 1.3 (10)	23	1.122

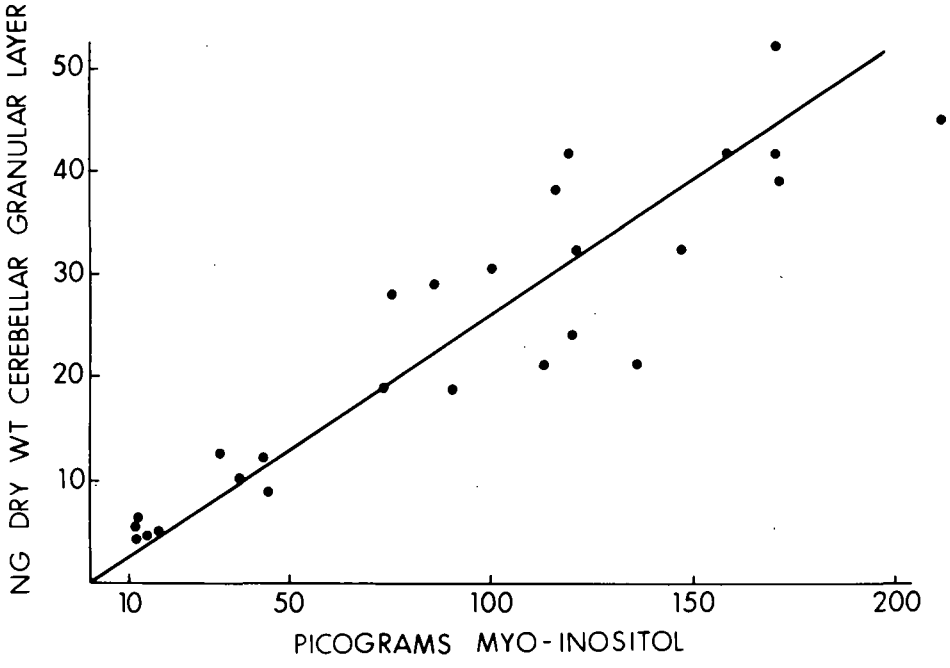

Figure 1

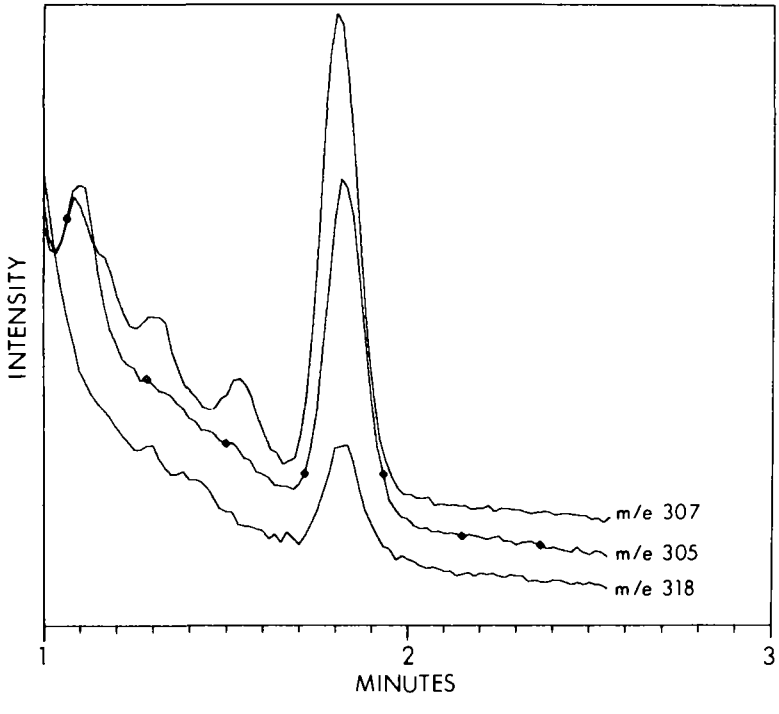

Figure 2

A COMBINED RADIO GAS CHROMATOGRAPH/MASS SPECTROMETER (RGC/MS) DETECTS INTERMEDIATES IN MYCOPHENOLIC ACID BIOSYNTHESIS

C.P. Nulton, J.D. Naworal and I.M. Campbell
Department of Life Sciences
University of Pittsburgh
Pittsburgh, PA 15261

The classical approach to the study of the biosynthesis of some secondary metabolite, P, had several phases. The substance P would first be examined for structural clues regarding possible primary precursors, A, A', A", etc. Each of these would then be tested in isotope incorporation experiments to find the true precursor (A). Next the structure of intermediates between A and P (B, C, D, etc.) would be predicted; they would be synthesized in isotopically-labelled form, and tested for validity by incorporation value analysis. Sometimes mutants that might excrete intermediates prematurely from the cells might be sought.

Apart from the prodigious amount of synthetic and microanalytical work involved, several major problems can occur when the classical approach is used. The most serious is aberrant incorporation. This occurs when an intermediate, B' for instance, which is structurally related to the true intermediate B is accepted by the organism as a precursor of P. A high incorporation value from the process B'→P is therefore recorded but its biological significance is low. A second problem, encountered when excretion products of mutants are examined is that the final excretion product, rather than being a biosynthetic intermediate in the pathway under study, is in fact a detoxification product of such an intermediate. Again the experimental result is misleading.

These problems could be eliminated if a way could be found to locate and identify all the isotopically labelled components in a total extract of a cell. Then if a primary precursor of P was fed to a group of cells, and the cells were examined before all the precursor had been consumed but after isotope had begun to appear in P, intermediates between A and P

could be recognized easily.

Protocols based on combined radio gas chromatograph/mass spectrometry (RGC/MS) fulfill the need. Provided a suitably derivatized total extract of cells that have been exposed to a radioactive tracer, an RGC/MS can locate labelled components, can identify each and can assay mass and isotope levels. A computerized RGC/MS that performs these functions has been constructed in our labs by coupling a Packard 894 gas flow proportional counter to an LKB 9000 GC/MS. A DEC PDP-11/20 computer accepts and processes data from the RGC/MS.

The RGC/MS was used to study mycophenolic acid (I) biosynthesis in *Penicillium brevicompactum*. Three 7-day old surface cultures were fed sodium 2-^{14}C-acetate (3 x 200 μCi, 56 μCi/μM) for 120 minutes. By that time, 19% of the label had been consumed. At the close of the experiment the mycelial mats were homogenized and extracted with ethyl acetate: acetone (2:1). The total extract was methylated with diazomethane and fractionated grossly on a small column of Sephadex LH-20. Each of the ten column cuts was examined by RGC/MS.

In addition to materials such as the methylated forms of malic, 2-ketoglutaric, citric, fumaric, isocitric and homocitric acids, ergosterol, squalene and fatty acid methyl esters, the materials marked (*) in the Figure were identified in radio labelled form. Since these substances were encountered in labelled form in the cells when acetate label was being transferred to mycophenolic acid, they are almost certainly intermediates in the mycophenolic acid biosynthetic pathway. The most likely sequence is as shown in the Figure. The relative specific activities of all the materials marked (*) were 25-fold higher than those of the fatty acids or Krebs Cycle acids and were comparable to that of squalene. Clearly the secondary metabolic pathway leading to mycophenolic acid was at least as active in *P. brevicompactum* at the time of the

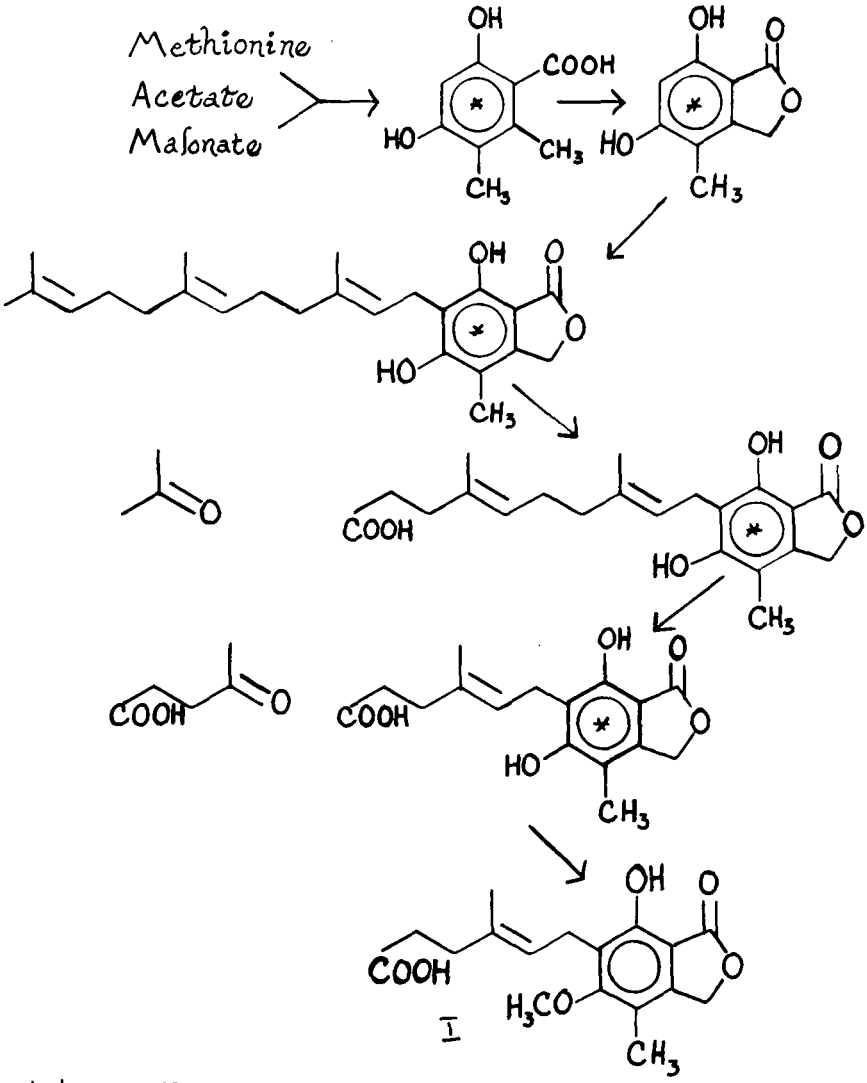

study, as were primary metabolic pathways such as lipid biosynthesis and the Krebs Cycle.

Several other biosynthetic pathways have been examined by similar methods. The procedure can also be applied to the study of catabolic processes, e.g. drug and pesticide metabolism.

The financial assistance of the National Institutes of Health (RR 00273) is gratefully acknowledged.

Simultaneous Quantitation of Glycine, γ-Amino butyrate, Glutamate, and Aspartate in Neural Tissue Using CI-GC-MS-COM.

F. Petty, J. G. Wood, N. Flynn, and J. D. Wander, Depts. Anat. and Biochem., and Neurosci. Lab., U. Tenn. Cent. Hlth. Sci., Mphs. 38163.

Recent evidence suggests a role for the amino acids glycine (GLY), γ-amino butyric acid (GABA), glutamic acid (GLU), and aspartic acid (ASP) in neural transmission in the central nervous system, but elucidation of their precise mechanisms of action requires development of specific and sensitive quantitative technics. For this purpose a procedure has been devised using selective ion monitoring with the GC-MS in the chemical ionization (CI) mode, which offers sub-nanomolar sensitivity, with deuterated internal standards used for each of the compounds. Trifluoroacyl n-butyl derivatives are compared with trimethyl silyl derivatives for ease of sample preparation, stability, chromatography, and sensitivity. Data will be presented comparing sensitivity using methane and isobutane as carrier-reagent gases, and use of short (45 cm) GC columns will be discussed, as will advantages of chemical ionization for these procedures.

The Potential of Ion Traps for Analysis, Robert T. McIver, Jr., E. B. Ledford, Jr., and R. L. Hunter, Dept. of Chem., Univ. of Calif., Irvine, Ca. 92717.

This poster presentation will provide an overview of an exciting new approach to biomedical mass spectrometry--the use of magnetic ion traps for low pressure chemical ionization studies. Our initial experiments in this area have indicated that storing reagent ions for periods on the order of several seconds in specially designed traps is a highly sensitive method of analyzing for compounds with exceedingly low vapor pressures such as diammonium salts of nucleotides and hydrochloride salts of amino acids.[1] A wide variety of positive and negative reagent ions can be generated and trapped at pressures on the order of 10^{-6} Torr for use in chemical ionization studies. In addition, special detection techniques have been recently developed for obtaining high mass resolution and accurate mass measurements for ions stored in the trap.

[1] R. T. McIver, Jr., E. B. Ledford, Jr., and J. S. Miller, Anal. Chem. 47, 692 (1975).

A GC-MS-COM System to Monitor Metabolic Switching of Drug Pathways.

K. R. SOMMER, J-P. THENOT, K. HAEGELE, J. NOWLIN, M. STAFFORD and M.G. HORNING, Baylor College of Medicine, Institute for Lipid Research, Houston, Texas 77030

Gas chromatography-mass spectrometry-computer (GC-MS-COM) systems operated in the chemical ionization (CI) mode have been used to monitor the effect of deuterium substitution on the metabolism of drugs in whole animal and liver homogenate preparations. Metabolic pathway alterations have been observed for drugs such as antipyrine and caffeine, which are metabolized by multiple alternate rather than sequential mechanisms. The major urinary metabolites of antipyrine and N-CD_3-antipyrine (2-trideuteromethyl-3-methyl-1-phenyl-3-pyrazolin-5-one) in rats were 4-hydroxy- and 3-hydroxymethylantipyrine. In contrast, the major metabolites of 3-CD_3-antipyrine (2-methyl-3-trideuteromethyl-1-phenyl-3-pyrazolin-5-one) were 4-hydroxyantipyrine and N-desmethylantipyrine; the metabolism of antipyrine was switched from hydroxylation of the methyl group on carbon-3 to N-desmethylation by isotope substitution. Similar effects were observed in *in vitro* preparations. The magnitudes of metabolic switching as measured by Vmax and apparent Km values were determined where possible.

MASS SPECTRAL ANALYSIS OF GLUTETHIMIDE METABOLITES

W. G. Stillwell and M. G. Horning
Institute for Lipid Research
Baylor College of Medicine
Houston, Texas 77030

and

W. Riess and H. Keberle
Ciba-Geigy Ltd.
Basel, Switzerland

The metabolism of glutethimide (±-2-ethyl-2-phenylglutarimide) has been studied in man, the rat and the guinea pig with the use of gas phase analytical methods (GC and GC-MS). The major metabolites found in the urine of all three species arise from hydroxylation of the glutarimide ring, the ethyl side-chain and the phenyl group. The major components characterized by these methods were three monohydroxy metabolites, a dihydrodiol and three diols. In addition, small amounts of an O-methyl catechol derivative and a hydroxy-O-methyl catechol metabolite were also detected. Structural assignments were based on the ethylated, silylated and perdeuterosilylated derivatives. When the individual (+)- and (-)-enantiomers were administered to rats, GC-MS analysis indicated that the (-)-isomer was metabolized predominantly by hydroxylation of the phenyl ring, while the (+)-isomer was hydroxylated on the ethyl side-chain and the phenyl ring in approximately equal quantities. In guinea pigs, as expected, the dextrorotatory form of glutethimide was hydroxylated in the glutarimide ring, while the levorotatory form was hydroxylated predominantly at the ethyl side-chain. Thus the rat metabolized both the levorotatory and dextrorotatory forms differently from the guinea pig. Full details of this study will be published elsewhere.

QUANTITATION OF CANCER CHEMOTHERAPEUTIC AGENTS: CYCLOPHOSPHAMIDE AND ITS ACTIVE METABOLITES BY GC-CIMS

Ian Jardine, Michael Colvin and Catherine Fenselau
Department of Pharmacology and Experimental Therapeutics
The Johns Hopkins University School of Medicine
Baltimore, Maryland 21205

We have recently identified[1] phosphoramide mustard as a human metabolite of cyclophosphamide, a widely used cancer chemotherapeutic agent. We have also examined[2] the relative alkylating activities of phosphoramide mustard and nornitrogen mustard, both of which are cytotoxic metabolites of cyclophosphamide, and have shown that phosphoramide mustard alkylates as an intact molecule at physiological pH via aziridinium intermediates.

We have now devised methodology[3] to quantitate cyclophosphamide, phosphoramide mustard and nornitrogen mustard in the same patient plasma and urine samples using gas chromatography-chemical ionization mass spectrometry-selected ion recording. N,N-bis(2,2-d_2-2-chloroethyl) amine (D_4 nornitrogen mustard) (A, below).has been synthesized as a general precursor for internal standards for nornitrogen mustard, cyclophosphamide (B, below) and phosphoramide mustard (C, below). Deuterium incorporation is by lithium aluminum deuteride and is consequently very high.

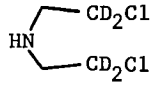

(A)

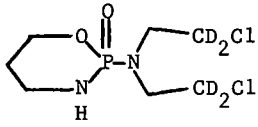

(B)

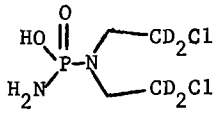

(C)

Cyclophosphamide and nornitrogen mustard are extracted simultaneously from plasma and urine (pH 8.5) with chloroform. Derivatization is by trifluoroacetic anhydride in ethyl acetate (60° for 20 min). Phosphoramide mustard is extracted from plasma and urine (pH 4.5) using an XAD-4 column, washing with water and eluting with methanol. Derivatization is by ethereal diazomethane (ambient). This derivatization produces a mixture of mono-, di- and tri-methylated phosphoramide mustard (~7:2:1) of which the last has the best gc characteristics and is hence monitored for quantitation.

It was determined that during collection, brief frozen storage, extraction and derivatization procedures, neither cyclophosphamide nor its other two major non-cytotoxic metabolites, 4-ketocyclophosphamide and carboxyphosphamide, decomposed to phosphoramide mustard. However, during collection, brief frozen storage and extraction, although not during derivatization, cyclophosphamide, 4-ketocyclophosphamide, carboxyphosphamide and phosphoramide mustard decomposed significantly to nornitrogen mustard. The extent of decomposition was determined by quantitation using internal standards.

The trifluoroacetyl derivatives of cyclophosphamide and nornitrogen mustard and the trimethylated derivative of phosphoramide mustard produce essentially only one ion at MH^+, with corresponding chlorine isotope ions, using isobutane chemical ionization. The MH^+ ions and the $(M + 2)H^+$ chlorine isotope ions for the undeuterated and deuterated materials are monitored for each material. The chlorine isotope ratios provide final confirmation that we are monitoring the correct species. Appropriate calibration experiments were carried out and in general, adequate precision and accuracy is routinely maintained down to 3 ng/ml of urine or plasma for nornitrogen mustard and cyclophosphamide and 30 ng/ml for phosphoramide mustard by keeping the ratio of D_4 standard to unknown within 10:1 or vice versa.

Plasma and urine levels of these three compounds are being routinely measured in patients receiving cyclophosphamide therapy and these results will be discussed fully in Cancer Research.

1. C. Fenselau, M.-N. N. Kan, S. Billets and M. Colvin. Cancer Res. 35, 1453, 1975.
2. M. Colvin, R.B. Brundrett, M.-N. Kan, I. Jardine and C. Fenselau. Cancer Res. 36, 1121, 1976.
3. I.Jardine, R. Brundrett, M. Colvin and C. Fenselau. Cancer Treat. Rep. 60 (4), April 1976.

CHEMICAL IONIZATION AND ELECTRON IMPACT MASS SPECTRA OF 5,6-DIHYDRO-2-METHYL-1,4-OXATHIIN 3-CARBOXANILIDE AND ITS METABOLITES

Francis I. Onuska*, Canada Centre for Inland Waters,
Analytical Methods Research Section
Burlington, Ontario. L7R 4A6.
CANADA
Alex G. Harrison, Dept. of Chemistry, University of Toronto
Toronto, Ontario. CANADA

The electron impact (EI) and the H_2 and CH_4 chemical ionization (CI) mass spectra of 5-6-dihydro-2-methyl-1,4-oxathiin-3-carboxanilide (I), the sulfoxide (II) and sulfone (III) derived therefrom, and 2-(2-hydroxyethylthio) acetoacetanilide enol (IV) have been determined.

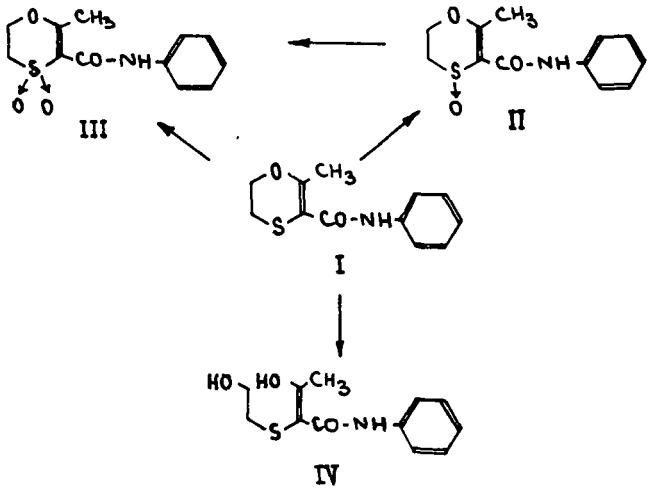

All four compounds show abundant molecular ions in the EI spectra and abundant MH^+ ions in the CH_4CI spectra (along with the expected $M.C_2H_5^+$ and $M.C_3H_5^+$ ions), but relatively low MH^+ ion signals in the H_2CI spectra. From high-resolution mass measurements and metastable transitions determined by metastable ion refocussing, EI fragmentation mechanisms have been established. For I, II, and III the major fragmentation mode involves loss of the anilino radical from

M^+, followed by loss of C_2H_4. Fragmentation to form the aniline molecular ion inecreases in importance with increasing oxidation state of the sulfur. In the CI of I to III, fragmentation of MH^+ proceeds in a similar fashion by loss of neutral aniline and by formation of protonated aniline. The EI mass spectrum of IV is dominated by the molecular ion and the aniline molecular ion. However, in the CI mass spectra characteristic fragment ions involving loss of water and loss of aniline from MH^+, as well as protonated aniline, are observed and serve to characterize the compound.

NOTE: The above paper was accepted for publication by the Journal of Biomedical Mass Spectrometry.

IDENTIFICATION OF TRACE CONTAMINANTS IN ENVIRONMENTAL SAMPLES BY TWO NEW TECHNIQUES: 1. SELECTED ION SUMMATION PROFILE ANALYSIS OF COMPUTERIZED GC/MS DATA 2. DUAL-GC/MS/COM OPERATION FOR THE ANALYSIS OF DIFFERENT SAMPLE TYPES

Douglas W. Kuehl and Gilman D. Veith

Environmental Research Laboratory-Duluth
U.S. Environmental Protection Agency
6201 Congdon Boulevard
Duluth, Minnesota 55804

1. Selected Ion Summation Profile Analysis.

The GC/MS analysis of environmental residues has been a difficult problem because of the complexity of the residues. Analysis of polychlorinated biphenyl isomers, a common environmental contaminant, has been simplified with the use of specific "subset masses" a technique developed on a digital computer controlled quadrapole MS used in a selected ion monitoring mode. Although this technique was very sensitive, ninety-nine percent of the available data is lost by SIM analysis and the technique was not applicable to all GC/MS systems. Selected Ion Summation (SIS) Analysis is a search of a GC/MS data set for a series of selected ions. A result of the search is reported by spectrum number if and only if all specified ions are present in a particular spectrum. The report consists of the spectrum number of the hit, the intensity of the specified ions, and the summation of the intensities of all specified ions. The summation is useful for ultra-trace analysis where an increase in sensitivity is necessary.

2. Dual-GC-MS System.

A Varian MAT CH-5 has been modified to accept GC effluent from two different GC systems without further system modifications or time loss. The double valve system inlet for the CH-5 was modified to accept the batch inlet system and reference inlet system from the back port. A stand was constructed to hold a Varian Areograph Model 1400 GC 16 inches from the front port or the double valve. A 100 foot SCOT column was then interfaced to the MS via a Cangal Model CG-1 membrane separator for capillary GC work. The line-of-sight inlet was maintained as a GC inlet for a packed column system. This system allows for dual capillary/packed column GC/MS analysis which has resulted in a greater use of our GC/MS system.

IDENTIFICATION AND ESTIMATION OF N-NITROSODIMETHYLAMINE IN AMBIENT AIR BY GAS-LIQUID CHROMATOGRAPHY-MASS SPECTROMETRY-COMPUTER

E. D. Pellizzari, J.E. Bunch, R. E. Berkley
and J. Bursey
Research Triangle Institute
Research Triangle Park, N. C. 27709

In view of its broad spectrum of carcinogenic activity in experimental animals, N-nitrosodimethylamine (DMN) must be regarded as potentially carcinogenic for man. The detection and unequivocal identification of DMN in the ambient air of Baltimore, MD., have recently been reported (1,2). In addition to identification of organic vapors present in the ambient atmosphere (3), analysis by techniques developed in this laboratory has provided quantitative information.

Tenax GC (2,6-diphenyl-p-phenylene oxide polymer, Applied Science, State College, PA.) was purified by extracting with methanol for 18 hours in a Soxhlet apparatus. Organic vapors were concentrated on a 1.5 x 6.0 cm bed of Tenax GC (35/60) in a glass cartridge (3-8). All sampling cartridges were preconditioned by heating to 275°C for a period of 20 minutes under a helium purge of 20-30 ml/min. After cooling in precleaned Kimax® culture tubes, the containers were sealed to prevent contamination of the cartridge. Sampling cartridges prepared in this manner were carried by automobile or air freight to the sampling site; 2-3 cartridges were designated as blanks to determine whether any of the cartridges might have been contaminated by the packing and transportation procedure. Cartridges containing some known quantities (100 and 300 ng) of DMN were prepared and carried to and from the field, stored, and analyzed to determine recovery of DMN.

Portable field samplers were designed in conjunction with Dr. L. Ballard of Nutech Corp. [Durham, N.C.] (6), and operating criteria were strictly specified. Replicate samples and blanks were analyzed by capillary gc-ms-computer. Thermal desorption was used to transfer the entire amount of trapped vapors from the cartridge sampler to the analytical system. Design of the injection manifold required careful consideration of properties of sorbent, adsorbed vapors, and requirements of other portions of the analytical system (3-6). A Varian MAT CH-7 glc-ms-computer system was used to perform the analysis. Ambient air samples were analyzed on 55, 80 or 100 m glass SCOT columns coated with either DEGS, OV-101, or OV-225 stationary phase, respectively. Desorption of ambient air pollutants (including nitrosamines) from cartridges was achieved at 265-270°C. A single stage glass jet separator (at 220°C) interfaced SCOT capillary columns to the mass spectrometer. Identification of components was achieved by comparison of mass spectra of unknowns to standard compendia and, in several cases, confirmed by comparison of mass spectra and elution temperatures on two different columns for unknown and authentic compound.

A standard curve for DMN was generated by monitoring mass 74. The standard was constructed from 100 pg to 300 ng, representing the linear concentration range present on a cartridge sampler. The detection limit observed for mass 74 was approximately 0.2 ppt when the ambient air temperature during field sampling is 50°F. Thus, the minimum amount of DMN which can be quantitated under field sampling conditions was approximately 2 ppt. Since Tenax would also concentrate dimethylamine (DMA) if present in ambient air, it was conceivable that in the presence of NO_x

(even though NO_x has a low breakthrough volume) DMA might be nitrosated to form DMN. Laboratory and field experiments were carefully designed to determine whether an in situ reaction could occur on the sampling cartridge. Formation of DMN as an experimental artifact was observed only when levels of DMA sampled exceeded 4000 ppb with NO levels simultaneously 1000 ppb or higher. Additional experiments were conducted during field sampling to determine whether an enhancement in the concentration of DMN above background occurred when a Tenax cartridge was preloaded with DMA. Thus, a blank and DMA-preloaded cartridge were used in parallel sampling and compared. Also, field air was drawn across a permeation tube containing DMA and into the Tenax cartridge. The DMA permeation tube (~2.4×10^{-6} g/min) was placed in front of the glass fiber filter used to remove particulates; DMA was introduced before and after the glass fiber filter. All experiments were conducted in duplicate. A volume of ~120 ℓ of ambient air was sampled in all cases. No artifact formation was detected under field conditions (9).

The fragmentation pattern for DMN (standard vs. unknown) is presented in Figure 1. The base peak of the mass spectrum occurs at mass 74; this ion was chosen for specific ion monitoring to obtain quantitative data (Figure 2). In the Baltimore area, Site 1 was an industrial site, Site 2 was near the Patapsco Sewage Treatment Plant, and Site 3 was near the Chessie Coal Piers (Figure 3). In the case of the Kanawha Valley location (Figure 4) the numbered sites represent locations on the grounds of the plant.

Figure 1 DEGS Glass SCOT column (55 m) was used in both analyses, 70-205° C at 4°C/min

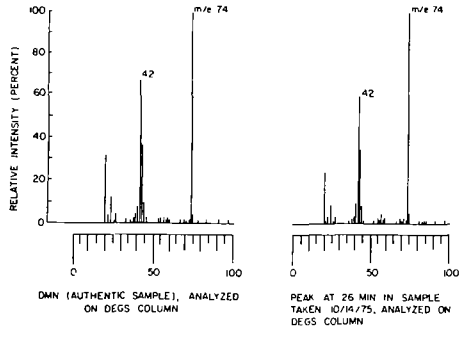

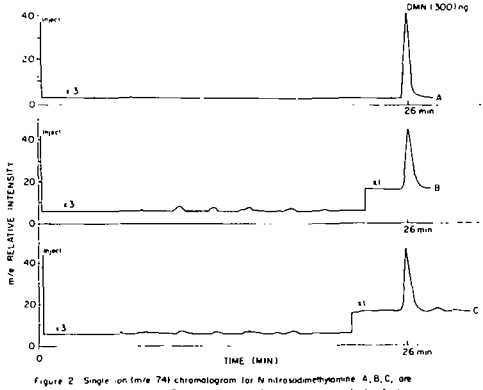

Figure 2 Single ion (m/e 74) chromatogram for N nitrosodimethylamine A, B, C, are traces for standard DMN, and replicate field samples, respectively Analysis on DEGS column, standard conditions

Figure 3. Sampling conditions and concentration of N-nitrosodimethylamine in ambient air*

Date	Time (EDT)	Location	DMN Concentration (ng/m³)
10/14/75	11:00 AM - 2:50 PM	Site 1	2,133†
	3:00 PM - 6:50 PM		10,500 ± 1,167†
	7:00 PM - 10.50 PM		1,375 ± 125†‡
10/15/75	11:00 PM - 2:50 AM		416
	3:00 AM - 6:50 AM		571
10/15/75	11:00 PM - 2:50 AM		3,200†
	3:00 PM - 6:50 PM		13,437 ± 937†‡
10/16/75	10:00 AM - 1:50 PM	Site 2	Trace
	2:00 PM - 5.50 PM		Trace
10/17/75	9:56 AM - 1.46 PM	Site 3	909†
	2:10 AM - 6.00 PM		84†‡
11/19/75	2:00 PM - 4:00 PM	Site 1, 200 yd WNW of dimazine thermal destructor	32,000 ± 1,500†
11/20/75	3:45 PM - 4:45 PM	Town of Fairfield, 200 yd from residential area, Conoco parking lot	1,950†
11/20/75	8:20 PM - 10:20 PM	North of site 1 near Memirac Corporation	1,360 ± 510†
11/24/75	11:50 PM - 1:50 PM	Site 1, SW of dimazine thermal destructor	20,000 ± 4,000†
11/24/75	1:55 PM - 3:55 PM	same	14,000 ± 200†
	6:35 PM - 8:35 PM	same	26,000 ± 500†
11/25/75	1:48 PM - 3:48 PM	Northbridge and Cannery St., downwind of site 1	7,600†

*For detailed information on meteorological conditions, see reference 11.
† = DEGS SCOT column used.
‡ = OV 225 SCOT column used.

Figure 4. Sampling conditions and concentrations of N-nitrosodimethylamine in ambient air in the Kanawha Valley, WV

Site	Location	Date	Time	ng/m³
Belle, WV	Industrial Site* (1)	12/1/75	9:30 PM - 2:17 AM	10.1
Belle, WV	(2)	12/1/75	9:27 PM - 2.19 AM	4.2
Belle, WV	(3)	12/1/75	10:16 PM - 3:09 AM	3.9
Belle, WV	(4)	12/1/75	10.07 PM - 3:07 AM	38.0 ± 6
Belle, WV	(1)	12/2/75	2:29 AM - 6:52 AM	26.0 ± 4
Belle, WV	(2)	12/2/75	2.28 AM - 6.53 AM	12.9 ± 2
Belle, WV	(3)	12/2/75	4:00 AM - 7:11 AM	67.0
Belle, WV	(4)	12/2/75	3:17 AM - 7:12 AM	68.5 ± 5
Belle, WV	(2)	12/2/75	9:00 PM - 3:02 AM	59
Belle, WV	(3)	12/2/75	10:02 PM - 3.18 AM	77.6 ± 6
Belle, WV	(4)	12/2/75	10:05 PM - 3:00 AM	103.0
Belle, WV	(5)	12/4/75	5.10 PM - 7:11 PM	ND‡
Belle, WV	(6)	12/4/75	3:26 PM - 5.24 PM	980
Belle, WV	(7)	12/4/75	4:00 PM - 6:05 PM	500
Belle, WV	(8)	12/4/75	7.06 PM - 9:06 PM	576
Nitro, WV	I-60 & WV25	12/5/75	11:58 AM - 3.48 PM	ND‡
Nitro, WV	I-60 & WV25	12/5/75	11:59 AM - 3:49 PM	ND‡

*The industrial site is near the intersection of Highway 60/21 and Maple Avenue. For more detailed information, see reference 7.
‡Part of Artifact experiment.
‡ND = not detected.

The glc-ms-computer techniques used allow identification of the volatile organic constituents of the ambient air (more than 100 compounds were identified) as well as quantitation of a specific constituent. This characterization of the entire atmosphere is of greatest value when epidemiological correlations are attempted.

ACKNOWLEDGMENTS: This research was supported by EPA Contract Nos. 68-02-1228 and 68-02-2262 of HEW. Assistance by Mr. W. Cooney and Mr. G. Ferreri (State of MD Air Quality), Mr. G. A. DeMerrais, Dr. E. Sawicki, and Mr. K. Krost (EPA) and Dr. M. E. Wall (RTI) was deeply appreciated.

REFERENCES

1. D. Fine, D. Rounbehler, N. Belcher and S. Epstein, Science, in press.
2. E. D. Pellizzari, J. E. Bunch, R. E. Berkley and J. T. Bursey, Biomed. Mass Spectrom., in press.
3. E. D. Pellizzari, J. E. Bunch, R. E. Berkley and J. McCrae, Anal. Chem., 48, 803 (1976).
4. E. D. Pellizzari, J. E. Bunch, B. H. Carpenter and E. Sawicki, Environ. Sci. Techn., 9, 552 (1975).
5. E. D. Pellizzari, B. H. Carpenter, J. E. Bunch and E. Sawicki, Environ. Sci. Techn., 9, 556 (1975).
6. E. D. Pellizzari, "Development of Method for Carcinogenic Vapor Analysis in Ambient Atmospheres", Publication No. EPA-650/2-74-121, Contract No. 68-02-1228, 148 pp., July, 1974.
7. E. D. Pellizzari, "Development of Analytical Techniques for Measuring Ambient Carcinogenic Vapors", Publication No. EPA-600/2-75-076, Contract No. 68-02-1228, 187 pp., November, 1975.
8. E. D. Pellizzari, J. E. Bunch, R. E. Berkley and J. McCrae, Anal. Lett., 9, 45 (1976).
9. E. D. Pellizzari, J. E. Bunch, J. T. Bursey, R. E. Berkley, E. Sawicki and K. Krost, Anal. Lett., in press.

GC/MS Analysis of Products from the Catalyzed Dechlorination of DDT and Heptachlor

WILLIAM J. COOPER and WILLIAM H. DENNIS, Jr.

US Army Medical Bioengineering Research
and Development Laboratory
Ft. Detrick, Frederick, Maryland 21701

Dechlorination represents a potential method for the disposal of organochlorine pesticides and pesticide formulations. DDT (1,1,1,-trichloro-2,2-bis-(p-chlorophenyl)-ethane) and heptachlor (1,4,5,6,7,8,8-heptachloro-1,2,3,9,10-pentahydro-4,7-methanoindene) was dechlorinated by Ni_2B generated in situ in the presence of excess $NaBH_4$. No unreacted pesticide was observed after 30 minutes reaction time. Although totally dechlorinated DDT (1,1-diphenylethane) was found, no totally-dechlorinated heptachlor (4,7-methanoindane) was observed in the reaction product mixture from heptachlor. The probable reaction schemes have been elucidated (1,2) and the products identified using gas chromatography/mass spectrometry.

1. W.H. Dennis and W.J. Cooper, Bull. of Environ. Cont. and Tox., 14:738 (1975).

2. W.H. Dennis and W.J. Cooper, Bull. of Environ. Cont. and Tox., in press.

SAMPLING AND CHARACTERIZATION OF AIR FOR ORGANIC COMPOUNDS. ROBERT D. KLEOPFER, W. W. BUNN, B. HAAS, and E. R. DEANE, Region VII Laboratory, U. S. Environmental Protection Agency, Kansas City, Kansas 66115.

Computerized gas chromatography/low resolution mass spectrometry was applied to the analysis of organic compounds in air at a National Air Surveillance Network station in Kansas City. Sampling approaches used included particulate sampling, adsorption on XAD-2 resin followed by solvent elution, and adsorption on Tenax GC followed by direct desorption onto a gas chromatography column. Eighty-two compounds were identified. Unusually large amounts of phenol and phenol-formaldehyde resin intermediates were found.

LOW- AND HIGH-RESOLUTION GAS-CHROMATOGRAPHY/MASS SPECTROMETRY (GC/MS) METHOD OF ANALYSIS FOR THE PRESENCE OF 2,3,7,8-TETRACHLORODIBENZO-P-DIOXIN (TCDD) IN ENVIRONMENTAL SAMPLES.

R. L. Harless and E. O. Oswald, Environmental Protection Agency, HERL, ETD, ACB, MD-69, Research Triangle Park, NC 27711

INTRODUCTION

An environmental monitoring project is being conducted to determine if TCDD is accumulating in the environment. TCDD is an extremely toxic, chlorocrigenic and teratogenic material[1] and is a possible contaminating by-product in manufacturing processes utilizing tetrachlorbenzene and in the manufacture of herbicides containing esters of 2,4,5-trichlorophenoxy acetic acid. The single oral LD_{50} of this compound in certain species of guinea pigs is six hundred parts per trillion (600 ppt).[2]

The method used for determination of TCDD in environmental samples must be extremely sensitive and specific. The high-resolution GC/MS method of analysis meets these criteria. Ultra high sensitivity and three different degrees of specificity are provided by this technique: 1) GC retention time of TCDD, 2) double ion monitoring response, m/e 320-322, and 3) isotopic ratio of ^{35}Cl and ^{37}Cl. Detection limits below eight parts per trillion (8 ppt) can be obtained from five-gram (5 g) environmental samples that have been subjected to an efficient analytical clean-up procedure prior to GC/MS analysis.

The TCDD analysis procedure is based on a signal averaging technique originally developed by Biros[3] wherein successive scans over a narrow mass range are added together to produce an integrated mass spectrum with a greatly improved signal to noise ratio for single-ion monitoring analysis. Modifications were made to a Varian C-1024 time averaging computer (CAT) and the Varian CH-5 DF mass spectrometer to provide double-ion monitoring capabilities. A block diagram describing this system is shown in Figure 1.

The simultaneous display and accumulation of the masses being monitored is effected as follows: By a switching pulse generator driven by a saw tooth voltage generator of the peak matcher unit, the ion acceleration voltage is switched between the two values, 319.8965 and 321.8936, in such manner that alternate saw tooth voltage scans are made with the two values so that there is an alternate accumulation and display of the low mass and high mass peaks. These signals are introduced into two separate channels of the CAT. The saw tooth voltage waveform sends a trigger signal to the CAT to initiate data acquisition for each channel. The number of beam deflection scans are averaged to produce a composite, integrated narrow range mass spectrum which is then displayed on a strip chart recorder for mathematical analysis.

References:

1. (A) K. D. Courtney and J. A. Moore, Toxicol. Appl. Pharmacol., 20, 396 (1971).
   (B) Schwetz, B. A., Norris, J. M. Sparschu, G. L., Powe, V. K. Gehring, P. J., Emmerson, J. L.Gerbig, C. G., Advances Chem. Ser., 120, 55 (1973).
   (C) Poland, A. P., Smith, D., Matter, G., Possick, P., Arch. Environ. Health, 22, 316 (1971).
   (D) D. Neubert, P. Zens, A. Rothenwaller, and H. J. Merker, Environ. Health Persp. Exper., Issue No. 5, 67 (1973).
   (E) Blair, E. H., Ed., Advances in Chemistry Series No. 120, "Chlorodioxins-Origin and Fate".

2. Executive Office of the President, Office of Science and Technology, "Report on 2,4,5-T," A Report of the Panel on Herbicides of the President's Science Advisory Committee. March 1971.

3. Biros, F. J., Analyt. Chem., 42, 537 (1970).

HIGH-RESOLUTION GC/MS METHOD OF ANALYSIS

A two-stage Biemann-Watson separator is used to interface a Varian model 2700 GC to the MS, thus providing an all glass inlet system. The MS vacuum system consists of a 600 liter/second mercury diffusion pump on the source and two 150 liter/second mercury diffusion pumps on the flight tube and ESA.

Optimum high-resolution (9000) MS conditions were established with PFK, m/e 319, and the magnet current is then turned to m/e 328, ^{37}Cl-TCDD. One hundred picograms (100

pg) of ^{37}Cl-TCDD was injected into the GC, and the signal was monitored on the peak matcher oscilloscope to determine the specific retention time region for TCDD and the appropriate number of peak matcher sweeps necessary for data acquisition by the CAT. All pertinent data are shown in Figures 2 and 3.

Ten percent (10%) of the 60µl environmental sample is used for recovery analysis. Duplicate analyses are performed on the environmental sample (5%) and on a ^{37}Cl-TCDD fortified sample (5%) to determine recovery of a known amount of ^{37}Cl-TCDD that had been added before the sample was subjected to an analytical clean-up procedure. This provides the necessary recovery efficiency value for correcting the ^{35}Cl-TCDD analysis. The accumulated CAT data following each injection is displayed on a strip chart recorder for mathematical analysis.

Ninety percent (90%) of the sample extract remains for ^{35}Cl-TCDD analysis. An aliquot of the sample is fortified with a known amount of ^{35}Cl-TCDD. Duplicate analyses are performed on the environmental sample and on the fortified sample. The accumulated CAT data following each injection are displayed on a strip chart recorder for mathematical analysis. The injection sequence is sample, fortified sample, sample, fortified sample. The ^{35}Cl-TCDD residue level and limit of detection are calculated from these analyses and corrected with the recovery efficiency analysis. A low-resolution mass spectrum of TCDD is shown in Figure 4. The main feature of the spectrum is the molecular ion cluster, m/e 320-322. These are the two masses scanned under high-resolution GC/MS integrating conditions to detect TCDD in ppt levels.

Mass spectrometric data must meet certain criteria before a sample can be reported as containing TCDD, Figure 5. In addition, the TCDD peaks must be clearly defined and must have two sides with a distinct change in slope. The peaks must be clearly separated from base line and must be clearly identifiable. The TCDD content is reported as ND (not detectable) if these conditions are not met.

A tremendous amount of quality control (QC) is employed by separate laboratories, analytical clean-up and MS analysis, to provide valid analytical results. All environmental samples are fortified with ^{37}Cl-TCDD for determination of analytical clean-up efficiency. Also, environmental control samples are fortified with ^{35}Cl-TCDD, 5 to 100 ppt, before being subjected to the clean-up procedure. Additional QC samples containing both ^{37}Cl-TCDD and ^{35}Cl-TCDD in benzene are employed to monitor the MS analysis. These QC sample results must meet certain criteria before analysis results are reported for environmental samples.

IN SUMMARY: The high-resolution GC/MS method of analysis provides the necessary sensitivity, detection limit less than eight parts per trillion (8 ppt), and specificity to monitor the environment for TCDD contamination. The use of internal standards for qualitative and quantitative analysis provides high-quality results and eliminates possible sources of errors. The accuracy routinely attained for 20 to 100 pg quantitation standards and QC samples in benzene is within ±15% of the theoretical value. An efficient analytical clean-up procedure is a prerequisite for meaningful GC/MS analysis. Quality control is very important in these analyses for picogram concentrations of TCDD. Low-resolution GC/MS screening analyses have produced some false positive results; therefore, high-resolution GC/MS analysis must be utilized for more explicit confirmational analyses.

FIGURE 1- BLOCK DIAGRAM OF GC/MS SYSTEM

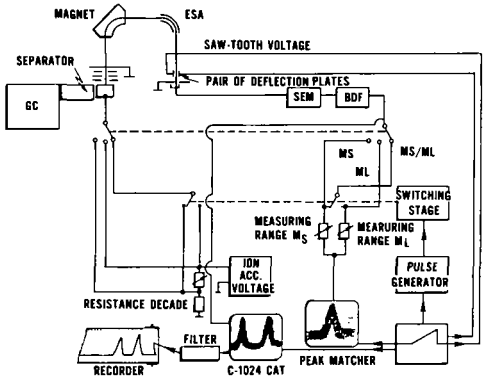

FIGURE 2 - GC CONDITIONS

3' x ¼" OD x 3mm ID	
Glass column	
2% OV3 on chrom W	
Column temperature	208°c
Injection port temperature	245°c
Detector temperature	275°c
Helium flow	20 mls/min
On column injection	
Sample size 4 ul	
Concentration of TCDD standard	5 pg/ul
TCDD elution time	300 - 345 seconds
TMCS treated system at 150°c and again at 250°c as needed to remove active sites	

FIGURE 3 - MS CONDITIONS

Source housing	Heated
Source temperatures	235°c
Source pressure	$5 \times 10^{-6} - 10^{-6}$ Torr
Filament current	1 ma
Ion acc. voltage	3 kv
Frequency, peak matcher	maximum - 5 scans/second
Resistance decade	m/e 320 m/e 322 ratio
BDF filter	3000
ML/MS switch	0.3 V/CM
SEM voltage	3.2 KV - 10^6 to 10^7 gain
Separator temperature	270°c
Separator connecting	250°c
Lines to GC and MS	

FIGURE 4 – LOW RESOLUTION MASS SPECTRUM OF TCDD

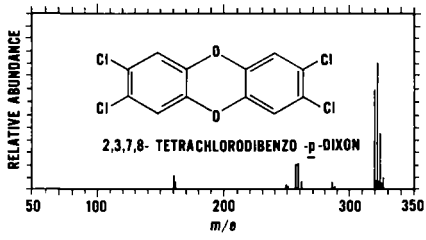

FIGURE 5 - CRITERIA USED TO DEFINE THE PRESENCE OF TCDD IN ENVIRONMENTAL SAMPLES

1. TCDD peak must be greater than 2.5 times the mm of noise.
2. TCDD peak in both m/e 320 and m/e 322.
3. TCDD peak intensity ratio correct, 0.8 to 1.0.
4. TCDD GC retention time correct.

ANALYSIS OF SULFURIC ACID BY MASS SPECTROMETRY

T. Michael Harvey, T. J. Prater and D. Schuetzle
Engineering and Research Staff - Research
Ford Motor Company, P.O. Box 2053, Dearborn, Michigan 48121

During the combustion of fossil fuels, the sulfur present as organic-sulfur compounds is oxidized to SO_2 and SO_3 (or H_2SO_3 and H_2SO_4 in the presence of water), depending upon such factors as combustion temperature, oxygen concentration and the presence of catalytic materials in the exhaust or venting system. After being emitted into the atmosphere, SO_2 and SO_3 are converted to H_2SO_3, H_2SO_4, $(NH_4)_2SO_3$ and $(NH_4)_2SO_4$ in the presence of atmospheric water and ammonia. It is important to distinguish these species for evaluating their environmental impact. The development of an analytical technique for the measurement of sulfuric acid in the atmosphere has been the subject of many papers in the last several years.[1] However, no reliable data on the concentration of this species exists to date.

Electron impact mass spectral analysis of sulfuric acid and sulfate salts (most notably ammonium sulfate from filter samples has not been totally successful.[3,4] Both ammonium and sulfuric acid give only SO_2^+, SO^+ and S^+ fragments under electron impact. Thermal separation of the species using a temperature programmed solids probe in conjunction with monitoring of the SO_2^+ ion (m/e:64) does not provide adequate separation of these two compounds for quantitative work. Other workers have attempted to separate the two species thermally and at atmospheric pressure but may encounter decomposition of the ammonium sulfate at the higher temperatures required for volatilization.[5]

It has been observed that compounds which volatilize from the solid probe under electron impact conditions at a certain temperature will often volatilize at a lower temperature (50°C or more) if the analysis is carried out under chemical ionization conditions with reagent gas sweeping around the probe tip and then into the source. For sulfuric acid a decrease in volatilization temperature of approximately 70°C has been observed between EI and CI analysis. A similar decrease has not been observed for ammonium sulfate, perhaps due to the fact that this species decomposes at about 235°C. The net result is a 70°C thermal separation between the two species when analyzed from the probe in the CI mode. Munson et al[6] have determined the proton affinities for H_2SO_4, SO_2 and SO_3 to be 168 kcal/mole, 155 kcal/mole and 134 kcal/mole, respectively. By proper choice of reagent gas it was possible to selectively ionize some components in the presence of others. Methane was found to be an effective reagent gas for the analysis of these samples.

Aerosol samples were collected on 47 mm fluoropore filters with a 0.2 μ pore size. Both glass and quartz fiber filters were found to be unsuitable for the collection of sulfuric acid due to its reaction with the filter. A small portion of the filter was placed in the MM-16 direct insertion probe. The probe was heated from room temperature to 130°C rapidly when the probe came into contact with the source held at this temperature (Figure 1A). The probe was pulled away from the source and the source heated to 235°C before reinserting the probe (Figure 1B). As shown in these figures the two species, ammonium sulfate and sulfuric acid were easily separated thermally. For both species, a large portion of the total sample ion current for H_2SO_4, $(NH_4)_2SO_4$, SO_2 and SO_3 was concentrated in the HSO_2^+ ion at m/e:64.970 (90%). There was some difference in the abundanc

of the HSO_3 and $H_3SO_4^+$ ions for the two sulfates. Studies with standards show good recovery of the sulfuric acid down to 20 ng. Below 20 ng there is some loss and it is believed that the stainless steel in the source may consume a small quantity of the acid.

Filter samples taken from ambient air presented two problems. If the filter had a heavy accumulation of particulate matter, adsorbed SO_2 could be present. Since SO_2 has been difficult, if not impossible to separate from H_2SO_4 during solid probe volatilization, the alternative was to use H_2O as the reagent gas (Figure 2). This produced a spectrum consisting of $H_3SO_4^+$ (m/e:99) as the most abundant ion. In this manner the sulfuric acid could be selectively ionized (proton affinities of SO_2 and $SO_3 < H_2O < H_2 < H_2SO_4$). No ionization of the $(NH_4)_2SO_4$ took place under these conditions. The second problem resulted from hydrocarbons which have been found in all particulate samples to date. These species produced an interfering ion with H_3SO_4 at m/e:99 (Figure 4). However, by operating the mass spectrometer at an appropriate resolution ($M/\Delta M > 1000$ with 10% valley) the interference was easily overcome.

A limited analysis of aerosols collected in Dearborn, Michigan, have shown that little or no sulfuric acid was present. The dominant sulfate species appears to be ammonium sulfate but it is possible that ammonium hydrogen sulfate is also present. The analysis of aerosol samples collected from other urban areas is now in progress.

REFERENCES

1. J. Forrest and L. Newman, J. Air Pollut. Contr. Assoc., 23, 761, (1973) and references therein.

2. L. W. Richards, Paper No. 47, Division of Water, Air, and Waste Chemistry, 165th ACS National Meeting, Dallas, Texas, April 11, 1973.

3. R. L. Knights, Ph.D. Dissertation, University of Washington, 1973.

4. D. Schuetzle and T. J. Prater, "Proceedings of the 23rd Annual Conference on Mass Spectrometry and Allied Topics," Houston, Texas, May, 1975.

5. J. J. Huntzicker, L. M. Isabelle and J. G. Watson, presented at the 69th Annual Meeting of the Air Pollution Control Association, Portland, Oregon, June, 1976, and references therein.

6. B. Munson, private communication.

Figure 1. The Methane-Chemical Ionization Mass Spectrometric Analysis of One Microgram of Ammonium Sulfate and Sulfuric Acid on a Fluoropore Filter.

(A) High Accuracy Mass Chromatograms Used for the Identification of Sulfuric Acid Volatilized from the Fluoropore Filter.

(B) High Accuracy Mass Chromatograms Used for the Identification of Ammonium Sulfate Volatilized from the Fluoropore Filter.

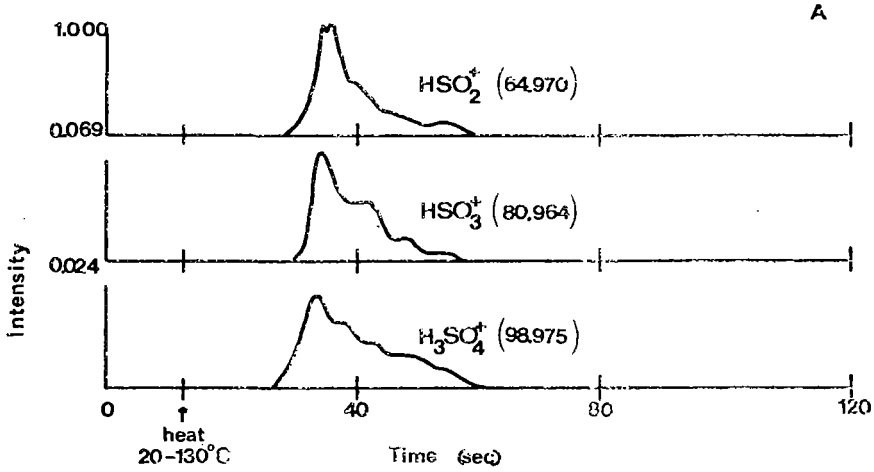

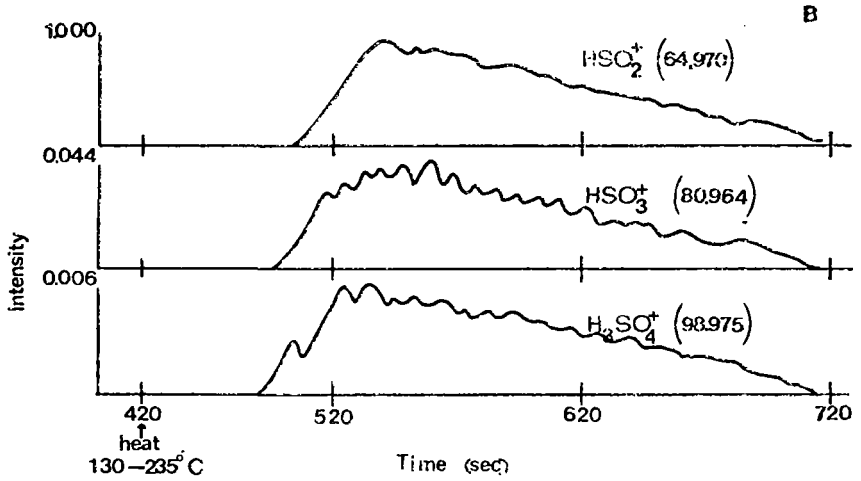

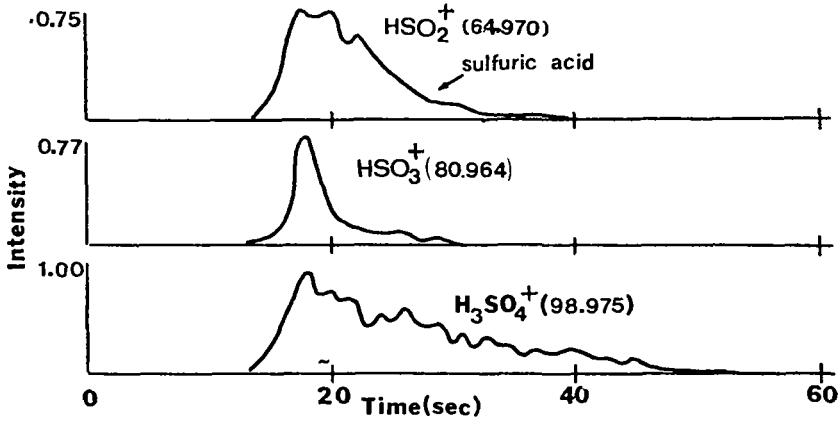

Figure 2. The Water-Chemical Ionization Mass Spectrometric Analysis of One Microgram of Ammonium Sulfate and Sulfuric Acid on A Fluoropore Filter.

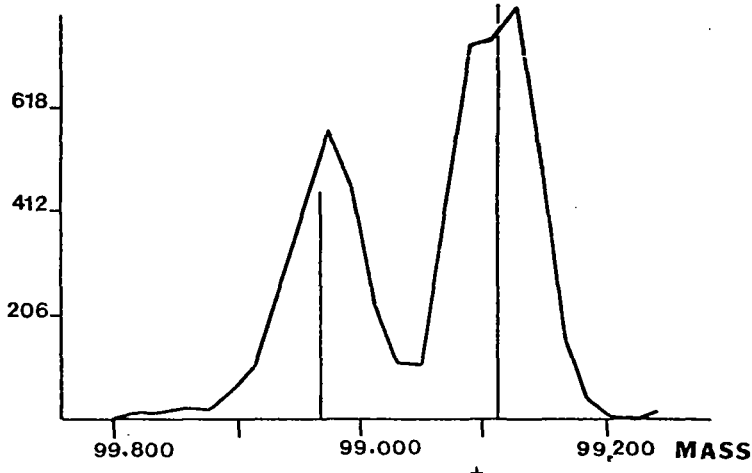

Figure 3. The Ion Profiles for $H_3SO_4^+$(m/e: 98.969) and $C_7H_{15}^+$ (m/e: 99.114) Present at Nominal Mass 99.

CAPILLARY GC/HIGH ACCURACY MASS SPECTROMETRIC ANALYSIS OF EXHAUST EMISSIONS FROM METHANOL FUELED CARS

T. J. Prater, T. Michael Harvey and D. Schuetzle
ENGINEERING AND RESEARCH STAFF - RESEARCH
Ford Motor Company, P. O. Box 2053, Dearborn, Michigan 48121

As the demands on the world's energy reserves increase, alternate fuels for the internal combustion engine are being extensively evaluated. Whenever a new fuel is considered, it is important to know the identity of its emissions in order to assess their environmental impact.

Exhaust emissions from catalyst and non-catalyst vehicles fueled with 100% methanol and 20% methanol-80% gasoline were qualitatively and quantitatively analyzed by computer controlled GC/MS using both stainless steel and glass capillary columns, combined with moderate resolution(1200), high accuracy($<$ 30 ppm) mass chromatograms. The analytical technique was designed to effectively sample and analyze polar organic materials without loss or conversion. The schematic for sampling and analysis is shown in Figure 1. Samples were collected in 70 cc stainless steel containers held at 100°C. A constant volume sample consisting of critical flow orifices was used to proportionately sample from vehicles operating cyclically. The entire 70 cc sample was used for analysis. The large amount of water contained in the exhaust sample was removed with heated(150°C) CaH_2(11 cm x 6 mm ID tube). The sample was pulled by vacuum through the CaH_2 at a rate of 2-4 cc/min and the sample constituents subsequently collected in the N_2 cooled loop of the gas sampling valve. The CaH_2 reacted with water to produce CaOH which acted as a GC column, therefore, it was necessary to pull the sample through the CaH_2 for 15-20 minutes. The effect of CaH_2 on sample components was studied using 100 ng quantities of methanol, acetone and acetaledehyde. It was found that these compounds were not effected by CaH_2 when operated at the above conditions. The effect of CaH_2 on acetic acid was also examined. However, it was found that this species would not elute through the GC with or without CaH_2 and as a result could not be studied.

A 300 meter SF-96 glass capillary column was used for the GC separation and the column conditions were: 1.5 cc/min Helium, 25°C for 20 min., programed from 25°C to 150°C at 2°C/min. The sample was injected into the GC with a gas sampling valve after condensing the sample in a stainless steel loop cooled by liquid N_2 and then heating this loop to 150°C. Helium purge was added (40 cc/min) at the column exit to minimize peak broadening between the GC and MS. The computer controlled MS data was acquired by repetitive scanning at 4.5 second cycle time for 2000 scans using an Incos Corporation data system. Controlling the MS via the computer resulted in very stable and reproducible high accuracy mass measurements without carrying an internal standard, such as PFK, as previously reported by D. Schuetzle, T. J. Prater and D. E. Hagge[1,2]

Approximately two hundred components were measured, most of which were hydrocarbons. These compounds were easily classified and identified using high accuracy mass chromatography. Each mass chromatogram was representative of a particular class of compounds (Table I). High accuracy mass measurements were necessary to separate multiple ion peaks and to facilitate component identifications. Table I lists possible interferring ions for each chemical species that must be separated to enable the positive identification of the identifying ion(s).

The Incos Data System has the capability of deconvoluting multiple ion peak s as they are being acquired. Since an internal standard is not carried along with the sample and moderate resolution is used, each spectra has fewer peaks. In addition, better sensitivity was achieved than with conventional high accuracy mass spectrometry measurements. An example of how this system was used is shown in Figure 1 for C_2 and C_4 alkyl substituted benzenesThese hvdrocarbons were identified by the accurate mass chromatograms at 105.070 ± 10 mmu and 133.102±10mmu, respectively. The various isomers were identified by retention times and/or boiling points. Table 1 lists the compound groups searched for in these studies and indicates if they were found in the exhaust emissions. The sensitivity of measurement was approximately 1 ppm in the original samples.

The compounds were quantitatively measured by comparing the areas of their accurate mass chromatograms to the area of a standard. Methanol response was found linear in the concentration range from 5-500 ppm (gas phase concentration). The concentration of other exhaust components were determined by weighting the response of their identifying accurate masses with appropriate response factors.

REFERENCES

1. D. Schuetzle, T. J. Prater and D. E. Hagge, "Quantitative Analysis of Complex Environmental Samples by Computer Controlled Mass Spectrometry", Proceedings of the 23rd Conference on Mass Spectrometry and Allied Topics, May 25-30, 1975, Houston, Texas.
2. T. J. Prater, D. Schuetzle and D. E. Hagge, "Rapid Survey Analysis of Complex Environmental Samples Using High Accuracy Mass Chromatography", Proceedings of the 23rd Conference on Mass Spectrometry and Allied Topics, May 25-30, 1975, Houston, Texas.

TABLE I

High Accuracy Mass Searches Used for The Preliminary Classification of The Emission Samples

Component Group	Mass Fragments	Mass Nominal	Mass High Accuracy	Most Probable Interfering Fragments	Component Group* Present?
1. Primary Aldehydes	CHO	29	29.003	29.039(C_2H_5) , 29.007($N^{14}N^{15}$)	
	C_2H_3O	43	43.018	43.006(CHNO),43.055(C_3H_7), 43.042(C_2H_5N)	Polymerizes in column
2. Inorganic or Organic Nitrates	NO_2	46	45.993	45.988(CH_2S)	yes
	NO	30	29.998	30.034(CH_4N)	
3. Primary Alchols	CH_3O	31	31.018	30.998(CF), 30.974(P)	yes
	C_2H_5O	45	45.034	44.990($C^{13}O_2$), 44.980(CHS), 45.058(C_2H_7N)	
	C_3H_7O	59	59.050	58.996(C_2H_3S)	
4. Mercaptans	H_2S	34	33.988	-	no
5. Chlorinated Organics, Inorganic Chlorides	Cl^{35}	35	34.969	-	no
	Cl^{37}	37	36.966	-	
	HCl^{35}	36	35.977	-	
	HCl^{37}	38	37.974	-	
6. Alkenes and Substituted Aliphatics	C_4H_7	55	55.055	55.018(C_3H_3O)	yes
	C_5H_9	69	69.070	69.034(C_4H_5O)	
	C_6H_{11}	83	83.086	83.050(C_5H_7O)	
7. Aliphatics					yes
R-C_4H_9	C_4H_9	57	57.070	57.034(C_3H_5O)	
R-C_5H_{11}	C_5H_{11}	71	71.086	71.050 (C_4H_7O)	
R-C_6H_{13}	C_6H_{13}	85	85.012	85.065(C_5H_9O)	
8. Organic Acids	CH_3COOH	60	60.021	60.003(C_2H_6S),60.045(C_2H_6NO)	yes but sample valve holds up acids
	COOH	45	44.998	44.980(CHS), 45.034(C_2H_5O), 44.993($N^{15}O_2$)	
9. Organic Sulfates, Inorganic Sulfates	SO_2	64	63.962	63.944(S_2), 64.003(C_2H_5Cl), 64.031(C_2H_4)	no
	SO	48	47.967	47.977(CHCl), 48.003(CH_4S)	
10. Substituted Phenols	C_6H_5O	93	93.034	92.934(CH_2Br), 93.058(C_6H_7N)	yes
11. Substituted Pyridines	C_5H_3N	77	77.027	77.039(C_6H_5), 77.016(C_3H_6Cl)	yes
12. Substituted Benzenes	C_6H_5	77	77.039	77.027(C_5H_3N),77.016(C_3H_6Cl	yes
	C_7H_7	91	91.055	91.042(C_6H_5N)	
	C_8H_9	105	105.070	105.034(C_7H_5O)	
	C_9H_{11}	119	119.086	119.050(C_8H_7O)	
	$C_{10}H_{13}$	133	133.102	133.066(C_9H_9O)	

*sensitivity is 1 ppm for gc/ms results

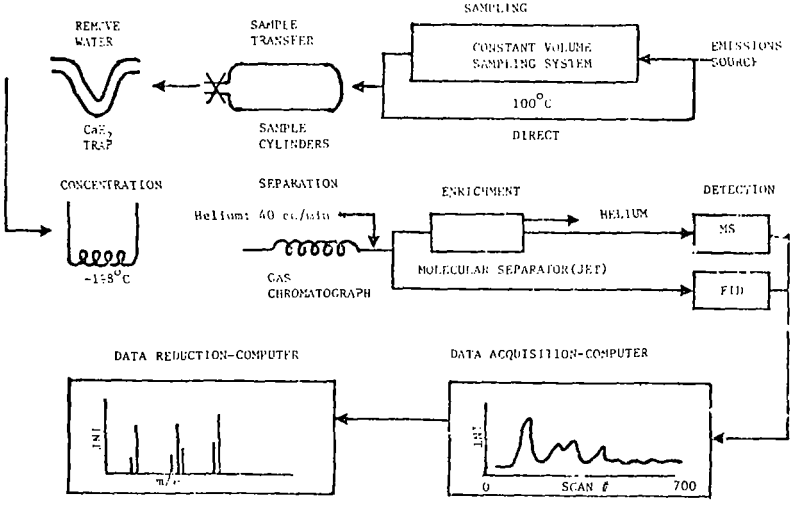

Figure 1. Sampling and Analysis Scheme for Exhaust Emissions from Methanol Fueled Cars.

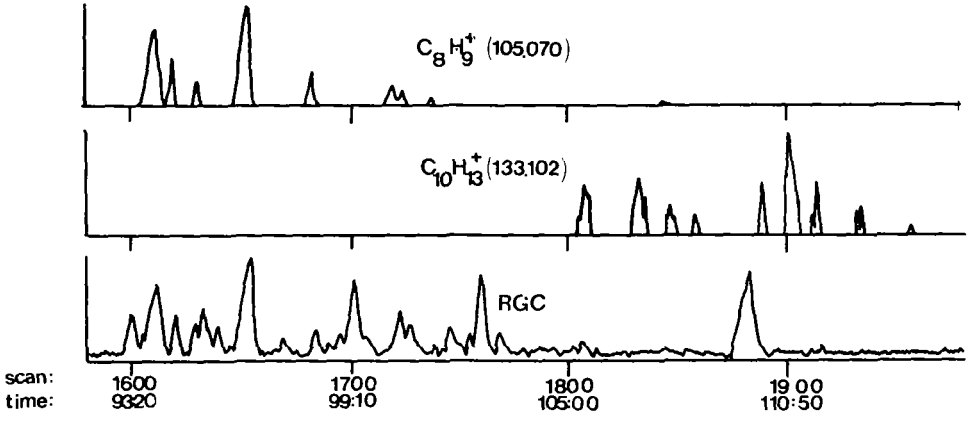

Figure 2. A Portion of The Reconstructed Gas Chromatogram and High Accuracy Mass Searches Used for The Identification of C_2 and C_4 Alkyl Substituted Benzenes in An Automotive Emissions Sample.

Identification of the Origin of Oil Spills by Field Ionization Molecular Weight Profile Analysis, M. E. Scolnick, A. C. Scott, and M. Anbar, Stanford Research Institute, Mass Spectrometry Research Center, Menlo Park, CA 94025

State of the art field ionization mass spectrometry is capable of producing molecular ion profiles of complex mixtures, such as crude and refined oils, that span more than 400 amu. An example of a wide mass range molecular ion spectra are shown in Figure 1.

The computer analysis of 400-dimensional vectors is expensive and unnecessary. The envelope of a spectrum can be digitized by using a technique that imitates analog to digital conversion. The envelope of a 400-peak spectrum can thus be transformed into a histogram whose spectral range (abcissa) is partitioned into, say 10 intervals. In other words, a 400-component spectral representation can be transformed into an arbitrarily smaller dimensionality. Moreover, a unique advantage of field ionization mass spectrometry is that the envelopes of molecular ion distributions of crude oils attain their maximum values at high mass numbers, while those of refined oils peak at relatively low mass numbers. In fact, it is usually possible to identify oils as crudes or refined products by visual inspection of their spectrograms. Therefore, in the case of field ionization spectra, the cumulative spectral distribution appears to be useful as a means of describing the gross characteristics of oil spectra.

The use of the digitized cumulative distribution of a spectrum rather than its constituent peaks precludes many of the problems associated with spectrometer resolution and the deconvolution of fused peaks. To a large extent, it provides a common denominator for sets of spectra whose quality (resolution in particular) is variable. The obvious price that is paid for the advantage of this technique is a loss of spectral information. Notwithstanding this limitation, we were able to classify 154 spectra into 35 different categories with 95% success.

Figure 2 shows the percent cumulative spectral distributions of 34 field ionization mass spectra comprising the molecular weight distributions of 3 different oils. The three distinct families of curves in Figure 2 are evidence of "clustering" or the separation of data into classes.

The cumulative spectral distribution of an oil can be represented by a vector whose jth component is equal to the mass range that is traversed as the distribution passes from the jth percentile point to the $(j + \Delta)$th percentile point, where $\Delta = 10$, for example. The following procedure can be used to define a discriminant function for classifying spectra of oil A:

(1) Obtain a set of spectra of oil A.

(2) Construct a cumulative spectral distribution vector for each of the spectra.

(3) The range for the jth vector components in the training set is $D_j = xmax_j - xmin_j$ and the mid-range is $\tilde{x}_j = xmax_j + xmin_j/2$,

where $xmax_j$ and $xmin_j$ are the largest and the smallest jth components of the set respectively. To test an unknown vector Y with components y_j for membership to class A, we can use the discriminant function defined by

$$|Z_j| \leq t_j \text{ for all } J = 8 \text{ values of } j \text{ simultaneously,}$$

where

$$Z_j = y_j - \tilde{x}_j$$

$$t_j = D_j/2$$

If $|Z_j| \leq t_j$ for J-R values of j, we can say the the oil represented by X^j is an (R+1)th choice for the identity of Y.

This discriminant function insures the correct classification of all members of the "training" set. It does not exclude the possibility of identifying a spectrum from a training set with more than one oil, however. The frequency with which training set spectra are classified ambiguously provides a measure for evaluating the merits of this discriminant function before applying it to spectra of unknowns.

Table 1 summarizes the results of applying the procedure outlined above to 154 field ionization mass spectra comprising 35 different classes ranging in size from 2 to 17. A quadrupole mass separator was used for analyzing specimens prepared by vacuum distillation. Sample sizes are tabulated in the column labeled NS. The number of times an oil (class) was chosen as the first choice for the identification of a spectrum is shown in the column labeled N1. The use of the vector component ranges for defining thresholds implies N1 ≥ NS. The result N1 = NS means that the class discriminant function identified only its own members. The result N1 > NS means that N1 - NS spectra were identified with the class incorrectly, as well as with their own class. Most of the classes are smaller in size than 7, in which cases the estimates of range are unreliable. However, considering that the 8-dimensional vectors represent only the gross characteristics of an oil spectrum it is remarkable that ambiguities resulted in only 5% of the spectra and that all of these were falsely identified with the same oil. (viz. K = 2). Note also the large number of zeros in columns N2 and N3, indicating that these oils never qualified as second or third choices for the identification of any of the 154 spectra - further evidence that the data are separated into isolatable clusters.

Classification of 154 Oil Spectra into 35 Classes. Identifications are unambiguous when N1 = NS. Note: all 8 ambiguities are at K = 2.

K	NS	N1	N2	N3	$\bar{R}$%	IDENTITY
1	17	17	2	5	39.4	SHL-6
2	9	17	18	11	32.5	ZEL-CRU
3	10	10	0	0	60.1	G-6, CIN
4	10	10	0	0	11.8	QQ-CRU
5	13	13	1	1	31.1	G-6, PHIL
6	7	7	1	4	9.4	BOL-CRU
7	3	3	0	0	6.3	G-6, S-FE
8	3	3	0	0	6.8	StS-CRU
9	3	3	0	0	3.6	SAY-6
10	3	3	0	1	15.7	APA-CRU
11	3	3	0	0	3.3	G-6, P.A.
12	3	3	0	0	6.5	IRA-CRU
13	3	3	0	0	3.3	TOB-CRU
14	3	3	0	0	5.2	HAS-CRU
15	3	3	0	0	16.4	SAY-2
16	2	2	0	0	1.4	SAY-LUBE
17	3	3	0	0	4.3	SB-CRU
18	3	3	1	0	5.3	SBD1-CRU
19	3	3	0	0	5.9	SBD4-CRU
20	3	3	1	1	13.0	SH17
21	3	3	0	0	9.5	AMO-4
22	3	3	0	1	6.4	SH17D1
23	3	3	0	1	19.8	SH17D4
24	4	4	14	7	52.7	AMO-4D1
25	3	3	0	0	6.9	AMO-4D4
26	3	3	0	0	9.8	SH33-6
27	3	3	0	0	6.8	SH33-6D1
28	3	3	0	0	4.1	SH33-6D4
29	3	3	0	0	4.5	SHO6
30	3	3	0	0	8.4	SHO6D1
31	3	3	0	2	14.3	SHO6D4
32	3	3	0	0	4.9	EXO-2
33	3	3	0	0	6.2	EXO-2D1
34	3	3	0	1	7.8	EXO-2D4
35	4	4	0	0	8.7	TOBL-CRU

K = class number

NS = class size

N1, N2, N3 = numbers of spectra assigned to Kth class as first, second, and third choices, respectively.

$\bar{R}$ = average spectral acceptance range in percent

Oil Codes: CRU = crude, -N = number N refined oil, D1, D4 = weathered for 1 and 4 days

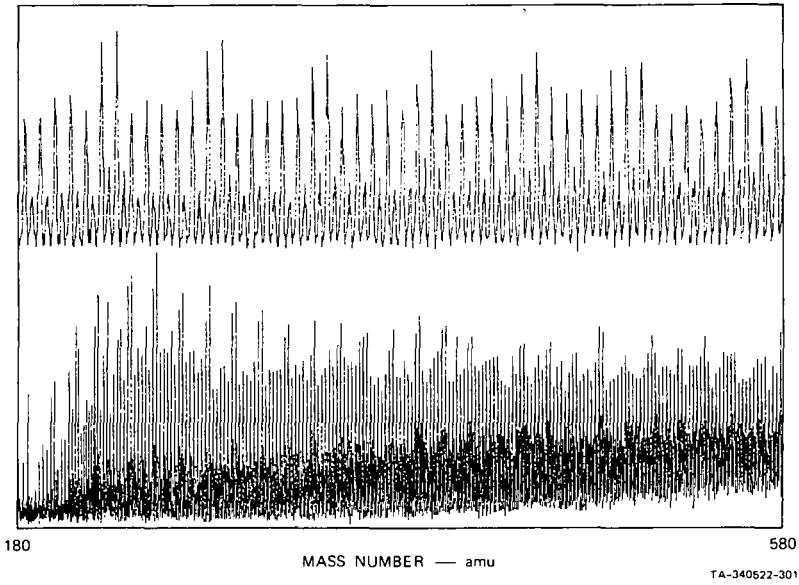

Figure 1

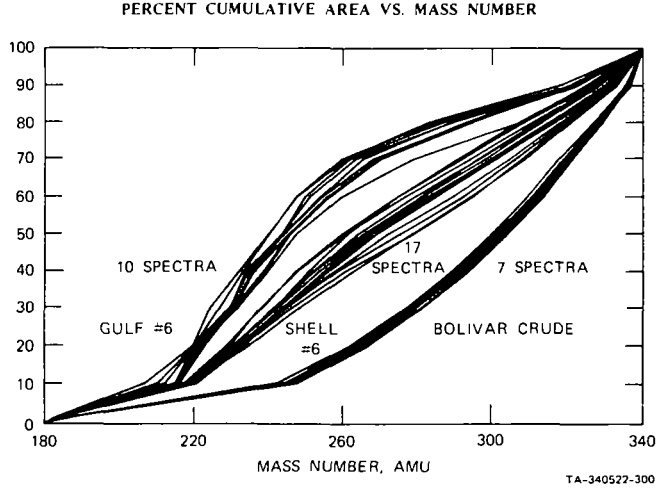

Figure 2

PSBIIb

MASS SPECTROMETRIC ANALYSES PERFORMED ON SAMPLES OF ETHYLENE BIS ISOTHIOCYANATE SULFIDE (EBIS)

R. L. Harless and E. O. Oswald, EPA, MD-69, Research Triangle Park, N. C. 27711

INTRODUCTION:

The degradation products of ethylene bis dithiocarbamates (nabam, maneb, and zineb) fungicides widely used on food crops should be considered in evaluating the hazards of these fungicides. EBIS and ethylene thiourea (ETU) are the major degradation products. EBIS is highly fungitoxic[1,2] and has been postulated to be responsible for the fungitoxicity of these fungicides. It has been shown that ETU is carcinogenic to the thyroid gland of rats.[3] Therefore, tolerance value for food residue determinations of dithiocarbamates should not be related only to the unchanged active substance, but should also include tolerance values and monitoring for the degradation products.

In 1954 Thorn and Ludwig[4] assigned structure 1, Figure 1, to the aeration product of nabam. The structural assignment was reaffirmed by Thorn[5] in 1960. In 1972 Benson, Ross, Chen, and Barron[6] proposed structure 2, Figure 1, based on Mass, Ramen, and NMR spectral data. These data were consistent only with structure 2.

To perform meaningful feeding study experiments it is important that the structure be confirmed and the impurities be identified and removed with an appropriate clean-up procedure. Also a method for detecting low concentrations of EBIS should be available for monitoring activities.

EXPERIMENTAL:

An EBIS sample was subjected to the following mass spectrometric analyses using the direct insertion probe of a Varian CH-5 DF Mass Spectrometer: Low-Resolution Electron Impact (EI), Field Ionization (FI), High-Resolution Mass Measurements (HRMM), Metastable Analyses by the Defocusing Technique, first field free region, and Direct Analysis of Daughter Ions (DADI), second field free region.

Some impurities are evident in the EI spectrum, Figure 2. The FI spectrum, Figure 3, reveals the molecular ion, m/e 176, with only a small amount of fragmentation; also the molecular ions of the other components are evident. The elemental composition of specific ions was determined using the peak matching technique, HRMM, at 10,000 resolution, Figure 4. The metastable analyses, Defocusing and DADI, are shown in Figure 5, from which conclusions as to fragment formation can be drawn and the fragmentation pathways can be easily derived. Figure 6 is the low-resolution EI spectrum of EBIS after it had been subjected to a thin-layer chromatography clean-up procedure which removed the contamination, sulfur, and ethylene thiourea.

EBIS does not chromatograph intact but decomposes, which was noted by Newsome.[7] Therefore a method for detecting low levels of EBIS was developed utilizing the direct insertion probe of the mass spectrometer for sample introduction. High-resolution (9000), double-ion monitoring analysis, m/e 176-178, of the molecular ion region provides a rapid, sensitive, and specific means of detection. Two microliters of EBIS standard solution, 400 pg/µl in benzene, was introduced to a quartz tube, which was then inserted into the direct probe tip. The probe temperature was raised to 70°C to remove the benzene and then cooled to 20°C. The sample was then introduced to the mass spectrometer and the probe temperature was programmed to 150°C in 45 seconds. The output signals were recorded on a strip chart recorder. The reproducibility of the output signal, peak height, on a standard solution of EBIS, was ±5%.

SUMMARY:

The mass spectrometric data are in agreement with the proposed structure 2, Figure 1. The contamination was identified, and the feasibility for removing it by TLC was established. A rapid, sensitive, and specific method of detection was developed. The proton-coupled ^{13}C NMR spectral data, Figure 7, are consistent with the currently accepted structure 2, Figure 1.

ACKNOWLEDGMENTS:

The authorswish to thank Ms. Nancy Wilson, EPA, RTP, NC, for providing the NMR data.

---

1. Pluijgers, C. W., Vonk, J. W., Thorn, G. D., Tetrahedran Letters, (18) 1317-18 (1971).

2. Engst, R., and Schnnak, W., Chemical Abstracts, 67, 116087W (1967).

3. Ulland, B. M., Weisburger, J. H., Weisburger, E. K., Rice, J. M., and Cypher, R., J. Nat. Cancer Inst., 49: 583-584 (1972).

4. Thorn, G. D., Ludwig, R. A., Can. J. Chem., 32, 872 (1954).

5. Thorn, G. D., Can. J. Chem., 38, 2349-2358 (1960).

6. Benson, W. R., Ross, R. D., Chen, Jo-Yum T., Barron, R. P., and Mastbrook, D., J. AOAC, Vol. 55, No. 1 (1972).

7. Newsome, W. H., J. Agr. Food Chem., Vol. 23, No. 2 (1975).

FIGURE 1. PROPOSED STRUCTURES FOR EBIS.

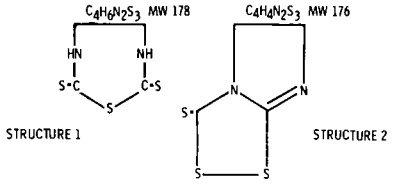

FIGURE 2. ELECTRON IMPACT SPECTRUM OF EBIS AND IMPURITIES

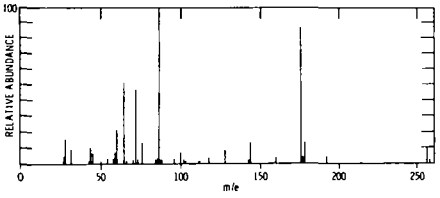

FIGURE 3. FIELD IONIZATION SPECTRUM OF EBIS

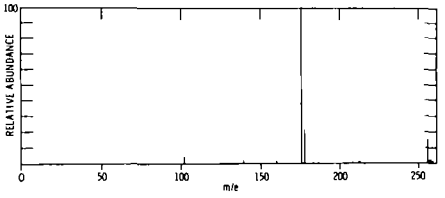

FIGURE 4. ELEMENTAL COMPOSITION OF IONS IN LOW-RESOLUTION EI SPECTRUM OF EBIS.

ELEMENTAL COMPOSITION	EXACT MASS	HRMM MASS
C_2H_5N	43.0422	43.0422
CS	43.9721	43.9723
CHS	44.9799	44.9799
CH_2NS	59.9908	59.9909
S_2	63.9441	63.9443
C_2H_2NS	71.9908	71.9910
CS_2	75.9441	75.9440
C_3H_4NS	86.0064	86.0064
$C_3H_4N_2S$	100.0095	100.0098
$C_3H_6N_2S$	102.0251	102.0254
$C_2H_2NS_2$	103.9629	103.9633
$C_4H_4N_2S_2$	143.9816	143.9815
$C_4H_4N_2S_3$	175.9537	175.9542
$C_4H_4N_2{}^{32}S_2{}^{34}S$	177.9495	177.9498
S_4	127.8883	127.8891
S_6	191.8324	191.8331
S_8	255.7766	255.7764

FIGURE 5. METASTABLE ANALYSES PERFORMED ON AN EBIS SAMPLE.

DEFOCUSING TECHNIQUE	DADI TECHNIQUE
m/e 144 ——→ m/e 176	m/e 176 ——→ m/e 143.4
m/e 100 ——→ m/e 176	" " - - - → m/e 118
m/e 86 ——→ m/e 176	" " - - - → m/e 111
" " - - - → m/e 144	" " ——→ m/e 100
	" " - - - → m/e 86
m/e 76 ——→ m/e 176	m/e 144 ——→ m/e 117
" " - - - → m/e 104.5	" " - - - → m/e 115
m/e 72 ——→ m/e 100	" " ——→ m/e 108
" " ——→ m/e 111.6	" " - - - → m/e 86
" " ——→ m/e 144	" " - - - → m/e 72
" " - - - → m/e 176	m/e 100 - - - → m/e 81
	" " ——→ m/e 73
	" " ——→ m/e 63
	" " ——→ m/e 41
——→ - MAJOR ABUNDANCE	m/e 86 ——→ m/e 60
- - - → - MINOR, LESS THAN 10%	" " ——→ m/e 59
	" " - - - → m/e 44
	" " - - - → m/e 42
	" " - - - → m/e 28
	m/e 72 ——→ m/e 45

FIGURE 6 LOW-RESOLUTION EI SPECTRUM OF EBIS AFTER BEING SUBJECTED TO A TLC CLEAN-UP PROCEDURE

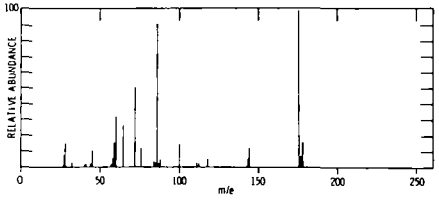

FIGURE 7. NMR SPECTRAL DATA FOR EBIS.

δ, ppm	MULTIPLICITY	ASSIGNMENT	J_{CH} (Hz)
48.1	TRIPLET	$>NCH_2-$	149.1
63.7	TRIPLET	$=NCH_2-$	145.7
138.2	SINGLET	$>C=N-$	---
183.8	SINGLET	$>C=S$	---

VALUES ARE ppm DOWNFIELD FROM TETRAMETHYLSILANE.

SPECTRA WERE OBTAINED ON A SATURATED SOLUTION IN CHLOROFORM - d.

Potential use of GC/MS in regulatory confirmation of sulfonmaide residues in animal tissue. Jacqueline Anderson and J. David King. USDA, APHIS, National Residue Lab., Peoria, Illinois 61604.

Sulfa drugs have wide veterinary applications in the American meat and poultry industry. The potential residues of these sulfonamides in meat reaching the market are monitored by USDA Meat and Poultry Inspection. GC/MS is used as a confirmatory tool for these residues. The mass spectra of these drugs exhibit loss of neutral SO_2 and loss of SO_2 + H from the molecular ion. Mechanisms for observed fragmentations and the potential diagnostic use of these fragmentations in interpreting unknown or metabolized sulfonamides are discussed.

Toxaphene Analysis by Computerized Gas Chromatography-Mass Spectrometry

William L. Budde and James W. Eichelberger

U. S. Environmental Protection Agency
Environmental Monitoring and Support Laboratory
Cincinnati, Ohio 45268

Abstract

Toxaphene, like the polychlorinated biphenyls and several other pesticides, is a complex mixture of a very large number of closely related compounds. The large number of similar components in these materials causes analytical difficulties that are not normally confronted in the analysis of many other pesticides. The routine application of computerized gas chromatography-mass spectrometry (GC/MS) to this difficult analytical problem is an economic approach. One technique of GC/MS is selected ion monitoring (SIM) which is defined as the dedication of a mass spectrometer to the acquisition of ion abundance data at only selected ionic masses in real time. The principal advantage of SIM is that it permits a very substantial improvement in sensitivity, has high selectivity, yet retains much of the qualitative information inherent in a complete mass spectrum. The application of GC/MS and SIM to the qualitative and quantitative analysis of toxaphene will be described.

The full text of this paper will be submitted for publication in the Journal of Food and Agricultural Chemistry.

PSBIIe Spark Source Mass Spectrometric Analysis of Air Pollution Particulates, E. Hunter Daughtrey, Jr., Northrop Services, Inc., Research Triangle Park, North Carolina 27709.

Spark source mass spectrometry (SSMS) has been shown to be a powerful survey tool for trace element analysis. Its application to the analysis of natural and polluted waters has been demonstrated.[1] It is the purpose of this paper to show the utility of SSMS for the analysis of air pollution particulates and related samples.

A wide range of sample types have been submitted to this laboratory for analysis. NBS standard reference materials (coal, fly ash, orchard leaves, and bovine liver) have been used to evaluate the accuracy attainable in this laboratory. Other samples have included oils and other refinery products and residues, coal gasification fluidized bed residues, and source particulate samples from the copper and iron and steel industries.

Compacted graphite electrodes were used for analysis, mixing up to 1:1 sample to graphite ratios (by weight) which are spiked with erbium internal standard. Depending on their organic content, samples may have been previously ashed in a low temperature asher.

An AEI MS702R was used in the photoplate detection mode for this work. The photoplates were reduced using a Joyce-Loebl 3-CS microdensitometer under manual control and calibration was made using the Churchill two-line method. Relative sensitivity coefficients were experimentally determined using commercially prepared mixtures of elements in graphite.

Due to the wide range of results reported in EPA round-robin analysis by various techniques, an investigation into the precision and accuracy of SSMS using NBS SRM's coal and fly ash was performed. Precision on the order of 25% RSD and accuracy of 35% relative difference from the NBS certified value or the NAA results of Ondov, et. al.[2] was obtained. The results of the analyses of the NBS materials are given in Table 1.

An air particulate sample from a copper smelter was analyzed for major and minor constituents. Several elements of environmental

concern were found to be major components: As, 15.7%; Cd, .5%; Sn, .3%; Sb, 6.7%; Pb, 12.7%; Bi, .7%.

The distribution of elemental concentration with particle size for several elements in micron range particulates from a steel-making process was determined. The small weight of sample collected and high blank levels from the aluminum foil collector added greatly to the uncertainty of analysis, but some trends were observable.

Residues from a fluidized bed coal gasification process were also analyzed. Addition of lime (for SO_2 removal) also tended to concentrate some trace elements from the coal, notably Ni and V (at 700 and 6600 ppm in the final residue).

The results presented here are used to demonstrate the utility of SSMS for the analysis of samples of environmental interest. Caution must be taken in attaching any significance to the results themselves, as information was seldom provided with regard to sampling or the processes which generated the samples.

The spark source mass spectrometry laboratory is operated by Northrop Services, Inc. for the Environmental Monitoring and Support Laboratory of EPA at Research Triangle Park, North Carolina, under contract 68-02-1567.

1. C. E. Taylor, 23rd Annual Conference of Mass Spectrometry and Allied Topics, Houston, 1975.

2. J. M. Ondov, et. al., Anal. Chem., 47, 1102 (1975).

TABLE 1.

Comparison of SSMS Results with
NBS Certified and (Non-Certified) Values

	Concentration, μg/g			
	1632 Coal		1633 Coal Fly Ash	
	SSMS	NBS	SSMS	NBS
Ti	730	(800)		
V	43.5	35	250	214
Cr	18.8	20.2	< 450	131
Mn	36	40	471	493
Fe	5300	8700		
Co	4	(6)	50	(38)
Ni	12	15		
Cu	17.7	18	303	128
Zn	35.5	37	< 770	210
As	3.4	5.9	74	61
Se	2.7	2.9	< 110	9.4
Rb			141	(112)
Sr			2060	(1380)
Ag	.056	(≤ .1)		
Cd	.38	.19		
Tl	.98	.59		
Pb	47	30	85	70
Th	4.5	(3)		
U	2.0	1.4		

GC-MS Analysis of Tetrachlorodibenzodioxin

David L. Smith, Fred Hileman and Jean Futrell
Department of Chemistry
University of Utah
Salt Lake City, UT 84112

During the past year we have tried to optimize an AEI MS-30 mass spectrometer for maximum sensitivity and GC resolving power. While our goal of sub-picogram sensitivity under conditions of high mass and GC resolution has not yet been achieved, we will briefly describe our approach to the problem.

The ability to separate dioxin from the complex matrix present in enviromental samples is essential. Since the identity of the matrix is generally unknown, we have depended on high efficiency, general purpose support-coated open-tubular (SCOT) columns which have been fabricated from glass in our laboratory.

In developing the gas chromatographic columns for this project we desired columns which were durable in accepting large injections of solvent, thermally stable, highly inert, with adequate resolving power, and yet able to operate at low flows to allow direct connection of the column to the mass spectrometer. Such columns are now being prepared by a technique whereby we can easily and reproducibly prepare coated glass capillary columns with Silanox as a support and film stabilizer.

Eight m.m. O.D. pyrex glass is pulled into 0.50 mm I.D. capillary tubing using a vertically mounted model 1045A Hupe Busch puller. Immediately after pulling, the capillary is silinized using DMCS followed by methanol. The column is then dried with nitrogen and then filled with a sonicated solution of 12mg/ml of SE-30 and 1mg/ml of Silanox in chloroform. When filling is complete one end of the capillary is sealed using a microtorch and the column is then coiled into a heated drying box as described by Jennings (1). The entrance tube of the drying oven is held at 180°C. while the oven itself is maintained at 150°C. When the column has been completely coiled into the oven it is then placed in a chromatograph and temperature programmed from ambient to 250°C. at 1°/min and left overnight. Columns are usually tested by injecting 1-decanol at 160°C. and checking for the correct retention index and any signs of serious tailing. Plate heights of 0.9 mm at 17 cm/sec flow rate are typically obtained for direct (splitless) injection of straight chain hydrocarbons. A typical separation is shown in Figure 1.

Maximum specificity for dioxin is achieved using combined gas-chromatography-high resolution mass spectrometry. The present method used to effect the high resolution mass analysis is illustrated in Figure 2. Symmetric ramps from a dual output function generator are applied to the electric sector plates and effectively sweep the ion beam across the collector at a frequency of 100 Hz. Individual ions reaching the first dynode of the electron multiplier generate pulses of electrons which are amplified by the preamplifier (Ortec 9301) and are subsequently converted to logical pulses by the amplifier-discriminator (Ortec 9302). These logical pulses are counted simultaneously by two separate sealors.

The timing sequence is illustrated in Figure 3. A pulse from the ramp generator triggers a timing unit (here labelled Gray Box) which sends out a gate pulse to the SSR Dual Channel counter as well as scan initiate and scan terminate pulses to the multi-channel scalor (Tracor Northern TN-1700); all at the appropriate time. The two channel scalor counts ions continuously in the single channel mode during a specified time interval of the

ramp. This is usually chosen as some time (or mass) interval centered about the centroid of the dioxin peak. Displayed as a function of time, this gives a trace that is equivalent to sitting on the centroid of the high resolution mass peak.

The multichannel scaler stores the signal intensity in n channels; each channel being opened during a specified time interval of the ramp. This unit provides a display of signal intensity or counts versus mass.

References

1. W.O. Jennings, et. al., J. Chrom. Sci., Vol. 12, 344 (1974).

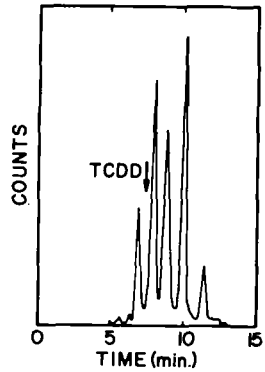

m/e 322 OF AROCLOR 1260

Figure 1.

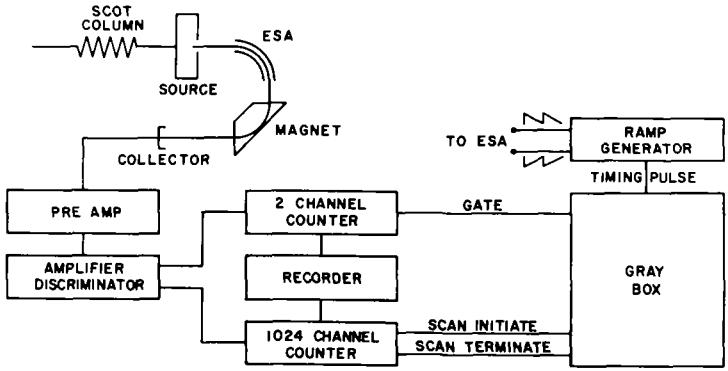

HIGH RESOLUTION DATA ACQUISITION SYSTEM

Figure 2.

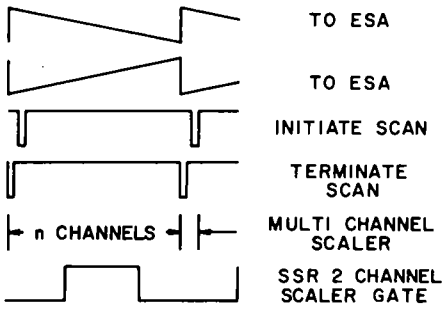

TIMING SEQUENCE FOR HIGH RESOLUTION DATA ACQUISITION

Figure 3.

AFLATOXIN DETECTION USING HIGH RESOLUTION SELECTED ION MONITORING[1]

William F. Haddon
Western Regional Research Center, Agricultural Research Service, U. S. Department of Agriculture, Berkeley, California 94710

The aflatoxins are hepatotoxic-carcinogenic metabolites of *Aspergillus flavus* and are widely distributed in the food chain. Mass spectral detection of the aflatoxins requires special technics owing to their low volatility, unsuitability for derivatization, and reactivity on glass surfaces. The desired specificity for aflatoxin analysis can be realized by employing selected ion monitoring at about 5000 resolution. A corollary advantage of examining aflatoxins in this way is a surprising 1000-fold enhancement in sensitivity relative to highly purified samples; other compounds codeposited from solution either occupy the active cites on the glass introduction capillaries preferentially or shield the aflatoxins from them. This approach to aflatoxin analysis circumvents much of the sample work up normally required with fluorescence-TLC measurements.

[1] A complete account of this work will appear in *J. Assoc. of Official Anal. Chemists*.

Direct Monitoring of Air Pollutants by Field Ionization Mass Spectrometry. G. A. St. John and M. Anbar, Stanford Res. Instit., Mass Spec. Res. Center, Menlo Park, California 94025.

The nonfragmenting nature of field ionization makes it a method of choice for monitoring complex multicomponent mixtures over a wide dynamic range. Field ionization mass spectrometry has been applied, therefore, to monitoring of organic air pollutants. Single, double, and triple GE silicon rubber membranes were compared for their effectiveness of selective transfer of organic air pollutants into a field ionization source. The highest sensitivity for detection of organic pollutants at the ppb (mole/mole) level was attained by a double membrane system. The sensitivity of the mass spectrometric system was limited by the chemical background of air, which contains constituents equivalent to concentrations of the order of ppb practically at every amu in the mass range 100 to 300 amu. Direct monitoring is limited, therefore, to concentrations above this level.

AN IMPROVED SYSTEM FOR SELECTED ION RECORDING

William F. Holmes, Peter D. Norberg, and Robert W. Scheifler

Department of Biological Chemistry
Division of Biology and Biomedical Sciences
Washington University School of Medicine
St. Louis, Missouri 63110

A program which allows the operator considerable flexibility in setting up and running selected ion recording analyses has been written for a display oriented Computer Automation LSI-2/20G computer system (1) linked to a quadrupole mass spectrometer. The parameters for a particular analysis are stored in a file as a set of mass tables, which are used sequentially during a GC run. Each mass table contains the following information - the masses to record, the relative times to spend at each mass, specifications for scanning across the fragment ion peak, the number of data points/second to collect, and the time to switch to the next mass table. From 1 to 12 masses can be monitored at once. Precise mass values are specified so that the fragment ion peaks can be accurately focussed for reproducible data collection. The user can specify mass scanning centered about the precise mass, using any scan range from $\pm$ 0.1 amu to $\pm$ 0.5 amu. The data collected at all points in the scan are summed and averaged. Thus the user can specify either no scanning at all for greatest sensitivity, scanning just over the peak top, or scanning over the entire ion. The relative time spent at each mass (including scanning) can also be specified, so that low intensity ions may be monitored for a longer time relative to more abundant ions. Since as many as twelve masses can be used, certain masses may be selected purely for verification purposes and monitored for brief time periods, with little effect on the precision of the analysis. The entire set of masses can be monitored at either one second or half second intervals, depending on the number of data points needed to accurately define the GC peak under analysis. Data storage can continue indefinitely, limited only by data file capacity or the switching time entered in the mass table. When switching occurs, data collection continues with the next mass table until there are none left. Up to five mass tables can be used. In this way a number of GC peaks can be monitored with optimal recording times for each mass. Similar schemes have been used with magnetically scanned instruments (2,3).

During data collection, the user may monitor the course of the analysis using either a selected ion recording display or a fragment ion intensity vs. mass display. Selected ion recordings of any two masses may be displayed simultaneously at any time and changed at will. Alternatively, the focus conditions for any mass can be monitored, which allows the user to keep track of instrument drift. If minor adjustments are necessary during the course of the analyses, a calibration adjustment table is immediately available. Using a calibration compound and a corresponding mass table, adjustments can be made quickly and with confidence.

After the last mass table has been used, the program automatically enters a data analysis section which is used to generate peak heights, peak areas and their ratios from selected ion recordings or mass chromatograms. Two movable pointers are used to define the outer limits of a GC peak. A background correction line is automatically drawn between the pointers and displayed on the oscilloscope. The background line is used for a point by point correction of the intensities when calculating peak

heights and areas. Up to five masses can be displayed simultaneously, with pointers at identical time points, allowing consistent and optimized peak limits to be established for all of the masses at once. Once the pointers are set, they will not change until they are moved again. If data is collected from another GC run, the pointers will be reset to the same times on the new curves, allowing the user to process his data quickly and reproducibly. A list of masses for output, including ratios, can be specified in a table, so that the data analysis for each GC run can be performed semiautomatically. A key selects each mass in turn for display and possible pointer adjustment before printing the peak height, peak area and averaged background. When all of the data has been printed, the original data acquisition program can be reentered with the same mass tables already set up to use again. These convenience features of the program are intended to maximize both reproducibility and throughput, so that GC parameters become the limiting factors in selected ion recording analyses.

References

1. Berger, P.S., Norberg, P.D., and Holmes, W.F., "Low Cost Computer System for Quadrupole Mass Spectrometers", 23rd Annual Conference on Mass Spectrometry, p. 507 (1975).

2. Pelster, D.R., and Watson, J.T., "A Display-Oriented Data System for Programmable Multiple Ion Detection", 21st Annual Conference on Mass Spectrometry, p. 61 (1973).

3. Young, N.D., Holland, J.F., Gerber, J.N., and Sweeley, C.C., "Selected Ion Monitoring for Multicomponent Analyses by Computer Control of Accelerating Voltage and Magnetic Field", Anal. Chem., 47, 2373 (1975).

Real time GC/MS Data Acquisition and Processing.

Donald E.Hagge and Joel R. Karnofsky, INCOS Corp., 1332 6th St., Berkeley, Ca. 94710 & Emilio J. Gallegos, Chevron Research Co., 576 Standard Ave., Richmond, Ca. 94802.

Long GC/MS sample runs severely restrict the utilization of mass spectrometer data systems. Most manufacturers provide a useful real-time report during data acquisition. However, a true real-time data system allows all data processing, displaying and hard-copying to proceed completely independent of the acquisition status. This means, for example, one can work with the chromatographic peak currently being acquired or on data gathered at an earlier time. Monitoring incoming data with DIMS (Display Isometrically Multiple Scans) allows one to display isometrically spectra or chromatograms of multi scan intervals during either Multiple Ion Detection or continuous scanning acquisition and focus on areas of interest. Any mass chromatograms, spectra or library searches may be conducted. Analyses are sometimes completed during acquisition and long runs can be terminated. Examples of Green River shale GC/MS analyses will be given using a Nuclide 1290G mass spectrometer controlled by an INCOS 2000 data system.

PROGRAMMABLE SELECTED ION MONITORING IN GC-MS

J. Throck Watson and Donald R. Pelster
Department of Pharmacology, Vanderbilt University, Nashville, Tenn.

In programmable selected ion monitoring, the selectivity of detection is changed during the development of the gas chromatogram. This technique permits optimum detection of several sample components that can be separated by gas chromatography. The selectivity of detection is achieved by monitoring only those ions that are characteristic of the compound of interest expected to emerge from the column during a designated time period.

In 1973, we demonstrated the feasibility and utility of monitoring different groups of ions only during the time periods when the corresponding compounds were expected to emerge from a GC column (1). In the interim, other workers extended the mass range of this technique on a magnetic instrument by computer control of both the accelerating voltage and the magnet current (2).

This report describes the use of a dodecapole gas chromatograph-mass spectrometer (Hewlett-Packard 5982A) as controlled by a PDP-12A computer for programmable selected ion monitoring. The mass scale of the dodecapole is controlled via a 16-bit analog to digital converter (ADC). After the chromatographic conditions are established, the duration of specific time periods and the mass values for different groups of ions are entered via a brief, preliminary interaction with the computer. During sample analysis, the time base for data acquisition is initiated by the pressure surge in the ion source due to the solvent front; the computer automatically monitors the ion current for selected ions during the specified time periods. Data acquisition and processing are achieved as described previously (3).

An example of the data record obtained with this technique is illustrated in Figure 1. In the first time period of this selected ion current chromatogram, the ion current at m/e 236, 232, and 260 was acquired. At 1.9 minutes after sample injection (start of second time period), the computer monitored ions of mass 270, 261, and 290 for 1.2 minutes. Finally, during the third time period, the computer-controlled dodecapole monitored the ion current at m/e 269, 237, and 266. The origin of the various ions and the analytical conditions are stated in the legend of Figure 1.

In summary, programmable selected ion monitoring offers an optimum compromise between operating the GC-MS for maximum sensitivity and obtaining high confidence in analytical results. By monitoring more than one ion for each compound of interest, one reduces the probability of reporting false positives. The programmable feature provides the desired selectivity of detection at several points in a gas chromatogram without prohibitive loss in sensitivity resulting from monitoring a large number of ions.

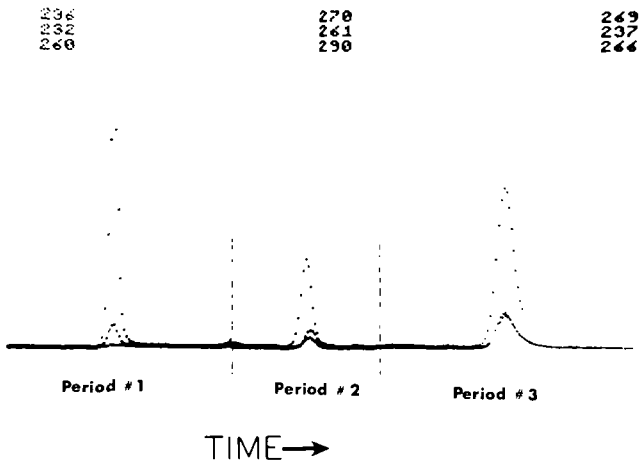

Legend to Figure 1. Selected ion current chromatogram for specified groups of ions acquired during preset time periods. Period #1: dimethyl phenobarbital at m/e 232 and 260; d_4-analog at m/e 236. Period #2: trimethyl-p-hydroxy-phenobarbital at m/e 261 and 290; d_9-analog at m/e 270. Period #3: methyl phentoin at m/e 237 and 266; d_3-analog at m/e 269. Quantities of 5 to 50 ngm of each compound used in this case.

Vertical dashed lines indicate times at which computer changed the selectivity of the GC-MS by monitoring a different group of ions.

GLC conditions were as follows: 2m x 2.5mm of 3% OV-17, programmed at 16°C/min from 200° to 240°C. Membrane separator maintained at same temperature as GLC column.

REFERENCES

1. Pelster, D.R. and Watson, J.T. A display-oriented data system for programmable multiple ion detection. Proc. of the 21st Annal Conference on Mass Spectrom and Allied Topics., San Francisco, May 1973, pp. 61-64.

2. Young, N.D., Holland, J.F., Gerber, J.N., and Sweeley, C.C. Selected ion monitoring for multicomponent analyses by computer control of accelerating voltage and magnetic field. Anal. Chem. 47: 2373-2376, 1975.

3. Watson, J.T., Pelster, D.R., Sweetman, B.J., Frolich, J.C., and Oates, J.A. Display-oriented data system for multiple ion detection with GC-MS in quanitifying biomedically important compounds. Anal. Chem. 45:2071-2078, 1973.

This development work was supported by the Research Center for Clinical Pharmacology and Drug Toxicology (GMS-14531). JTW is the recipient of a PHS Research Career Development Award (GM-50290) for 1973-77.

AN ON-LINE COMPUTER CONTROLLED SYSTEM FOR ION MICROPROBE AUTOMATION

Mitchell C. Gregory, John D. Stein, Howard A. Storms
General Electric Company, Vallecitos Nuclear Center, Pleasanton, CA

We obtained an Applied Research Laboratory Ion Microprobe Mass Analyzer in October of 1971. It became increasingly obvious during its use that automating the ion probe would greatly enhance its usefulness. Two years ago when we began this project no comparable commercial system was available. Choosing the method that offered maximum benefits to the laboratory user within technological and budgetary constraints was a challange. A description of the hardware and examples of the programs developed are given.

Some of the major benefits of computer control are:
1. The data collection capabilities of the system have been extended. The time required to perform an analysis has been reduced by almost an order of magnitude and the data is immediately available in a form that allows on-line manipulation and operator interaction.
2. The computer automation has opened new experimental capabilities, an example of which is multielement depth profiles.
3. The data produced is more reproducible and consistent since the computer carries out procedures in an identical way, time after time. In addition the computer allows diagnostics to be performed on instrument parameters with great ease and frequency.
4. Automation has reduced the requirements on operator time and concentration. This frees the operator from tedious repetitive operations and allows more time to be spent on data interpretation, report preparation and instrument development.

The ion microprobe consists of two major subsystems. The group of components used to provide the ion beam that excites the sample is called the primary ion column, while the system used to analyze ions sputtered from the sample is called the secondary mass spectrometer.

The primary system consists of an ion source (in this case a duoplasmatron) and extraction electrodes, a mass separator to purify the primary ion beam, two electrostatic lenses to focus the beam onto a small area of the sample, and X and Y beam deflector plates to move or raster the beam over the sample surface.

Precise placement of beam and sample can be achieved by moving sample and/or beam while observing the sample through a binocular microscope. The sample can be translated along the X,Y and Z axes and rotated about the Z axis.

Ions sputtered from the sample surface as a result of energetic primary ion bombardment are called secondary ions. These ions are collected and accelerated into the secondary mass analyzer by an electric field between sample and pickup electrode. Direction and energy focusing is accomplished with a combination of electric and magnetic sector fields. By changing the field of the secondary electromagnet the operator can direct the species with the desired mass to the detector. Pulse and integrated current signal output from a "Daly Type" detector are proportional to the secondary ion arrival rate. The outputs are fed into a scaler, a X-Y plotter (e.g., to generate mass spectra), or a cathode ray tube.

The ion microprobe is connected to a Data General Nova 1200 Jumbo Computer by a interface designed and constructed in our laboratory. The central processor has a 1.2 micro second cycle time and is equipped with a 32 K 16 bit core memory, power monitor and auto restart, and a hardware

bootstrap.

The peripheral equipment the computer is interfaced to includes:
1. A dual disk moving head drive with one fixed and one removable disk pack. Total capacity is 2.5 million 16 bit words.
2. A Tektronix Model 2010 video terminal with graphic display capabilities.
3. A Tektronix Model 4610 hard copy unit.
4. A model 33 ASR teletype with a modification to allow the computer to control the reader-punch.
5. A high speed 400 cps paper tape reader.
6. A real time clock.
7. A Systron Donner Model 6151 150 megahertz scaler.
8. A Datel Model 256 analog input-output system.
9. A digital input-output board to the central processor.

The last three items which directly control the ion probe have been interfaced using the Data General general purpose interface board. These are 15 inch square wirewrap boards that fit within the computer mainframe.

The analog portion of the instrument interface is the Datel System 256. This system allows the control of up to 16 digital to analog converters (DACs) and data collection from up to 256 multiplexed analog inputs. Our system is configured to accept 16 differential inputs to a 14 bit analog to digital converter (ADC), and output 4 analog voltages with 14 bit accuracy. The scaler is used to acquire digital input directly from the IMMA counting system.

A number of modifications have been made to the IMMA electronics. In particular; A field stabilization network has been installed in the primary magnet system to reduce interaction between the secondary and primary magnet. A new Hall Probe magnetic field controller has been installed in the secondary magnet system to minimize hysteresis effects. The primary ion beam sweep electronics have been modified for greater stability. None of these modifications have affected the manual operation of the instrument.

The IMMA automation interface consists of two major subsystems, data acquisition and control. For this instrument they involve the following parameters:

Data Acquisition
1. The mass resolved secondary ion current is counted with a 150 megahertz scaler timer with a range of 1 to 10^7 ions per second.
2. The total secondary ion current is monitored at $> 10^{13}$A.
3. The primary ion beam current is monitored at an aperture in the primary column.
4. The magnetic field in the primary and secondary magnet is monitored with 14 bit accuracy.

Control
1. The secondary magnet field can be digitally controlled with 14 bit accuracy.
2. Primary ion beam position on the sample can be controlled in the X and Y axis over a 400 x 400 micrometer area.
3. The sample voltage is directly controllable.
4. The secondary beam exiting the analyzing magnet can be electrostatically deflected over a small range of masses.

5. The sample stage can be controlled in the X and Y axis.

Computer control of the system has been programmed to make use of the NOVA's real time disk operating system (RDOS). For ease in software development, comprehension, and editing the system has been written in Fortran with the drivers for the ADC, DAC and scaler-timer written as Fortran-callable assembly language subroutines.

For programming convenience the drivers for these devices are callable from 2 levels. The first is a subordinate Fortran level which takes the call and does all the conversion necessary to program the specific interface request and translates it into the information (specific bit patterns) needed by the assembly language drivers. The second is the assembly language drivers which transmit the desired signals to the proper interface. This approach has been taken in order to develop a system that is flexible enough to allow for easy expansion of instrument control software and to facilitate data storage and reduction in a disk based system.

To date three principal IMMA control programs have been developed and tested. These three fall into the general categories of mass scanning (all masses), depth profiling (selected masses), and isotopic ratioing.

For the purpose of mass scanning, the magnet is calibrated in terms of mass vs. DAC control voltage. This is done using a polynomial expansions and least squares fitting to known masses.

Because the magnet control current feedback element is a field sensor, hysteresis and non-linearity effects have been minimized. It has been found that using only the first 3 terms gives a mass fit over the range 1-300 amu to better than 0.01 atomic mass unit.

For the depth profiling mode of operation, the software contains a spiral beam control. The beam return path is random to prevent a non-uniform burning of the sample, and data acquisition is computer regulated so as to minimize edge effects.

Data storage on disk is possible for all programs and data reduction is accomplished interactively on a Tektronics 4010 video system.

Ion probe automation has already proven its value in this laboratory. Though it has decreased the time needed to perform a given analysis its major benefits have been that it increases the quality of the data obtained, allows new experimental procedures, and results in reduced operator fatigue.

The work reported in this paper was supported by the United States Air Force (AFTAC/TRE) under contract #F09603-76-C-0061.

AUTOMATED ISOTOPIC ANALYSIS USING A PROGRAMMABLE CALCULATOR

Terry L. Futrell

Union Carbide Corporation - Nuclear Division*
Post Office Box Y
Oak Ridge, Tennessee 37830

Abstract:

A Hewlett-Packard 9821A programmable calculator has been interfaced to an AVCO 901 single focusing mass spectrometer to provide automatic data acquisition and control during isotopic analysis. A specially designed interface is described which provides a 12-bit I/O buss for the calculator. A unique data acquisition method incorporates a least squares smoothing routine for signal enhancement.[1] The program permits the operator to control the number of scans taken and to delete selected scans. The analytical results and a statistical evaluation are printed on a teletype. A comparison of the calculator data system with a commercial system using a minicomputer are presented.

*Operated for the United States Energy Research and Development Administration by Union Carbide Corporation's Nuclear Division.

[1] A. Savistzky and M. J. E. Golay, Anal. Chem. 36: 1627 (1964).

ENDORSEMENT NOTICE

Reference to a company or product name does not imply approval or recommendation of the product by Union Carbide Corporation or the U.S. Atomic Energy Commission to the exclusion of others that may meet specifications.

PSBIIIf. Ion-Counting Interface for LKB-9000 Mass Spectrometer.

R. N. STILLWELL, D. I. CARROLL, S. S. BATES and J. R. JENKINS, Institute for Lipid Research, Baylor College of Medicine, Houston, Texas 77030

Since the signal generated by a mass spectrometer is in the first instance a digital one, consisting of discrete ions, it would seem natural to interface a mass spectrometer to a digital computer by means of a digital interface. Faced with the need to interface a DEC PDP8/I computer to an LKB-9000 mass spectrometer, we elected to use digital circuitry as far as possible. Fig. 1 is a block diagram of the whole interface. The pulses due to the individually detected ions are amplified and counted in hardware; a ratemeter is used for testing only. The digital binary coded decimal output of the LKB mass marker is used for the mass calibration. A digital-to-analog converter can be used to drive the magnet. This feature is at present used only in selective ion monitoring; the normal LKB scan circuit is used for scanned spectra. Figure 2 shows the interface in more detail. A hardware peak detector is provided, although at normal scan rates the computer would have no difficulty in keeping up with the peaks in software. Two programs have been written for the system so far. One is a selective ion monitoring program using the D-A converter to hold the magnet current constant (as measured by the mass marker; some drift still occurs, but it is much less than the LKB circuitry allows). The ion counter is dumped into a buffer and cleared at a user-defined interval. The selection of this interval is tantamount to selection of a combination of gain and time constant with the analog circuit. At the end of the run, the buffer is used to generate a plot. The other program is a data acquisition module for System Industries, Inc., System/150 program. The setup procedure for this program allows the user to divide the total scan into as many as 8 mass ranges and to specify the clock rate for each. This effectively permits the adjustment of the time constant of the system to match the peak width during the scan. The file format and output routines are standard System/150.

The two principal advantages of this interface are (1) that it allows the specification of the time constant for the signal under program control, and (2) that it gives the user a direct measure of the ion count for each peak, and hence an idea of the reliability of his data. A small but structurally significant peak (e.g. M+) in the spectrum of a small sample may contain only 10-20 ions if the scan rate is high; clearly determination of the molecular formula from the ratio of M/M+1/M+2 is impractical in such a case, but this may not be apparent from the usual analog trace. The sensitivity and signal-to-noise ratio of the digital system are about the same as those of the standard analog method, because the noise due to ion statistics is considerably larger than the electronic noise introduced after ion detection in the analog circuitry. The ultimate dynamic range is less than with an analog circuit, since our pulse resolution is in the range 20-50nsec. The overall efficiency of the mass spectrometer (calculated from one experiment as 1 ion/8×10^5 molecules of cholestane injected on the GC column), however, is such that we would have to inject several micrograms before we would lose counts because of pulse coincidence. The practical dynamic range of a digital system with 24-bit counters, on the other hand, is considerably higher than that of a system using a 10- or 12-bit A-D converter, even monitoring 2 or 3 channels at different gains.

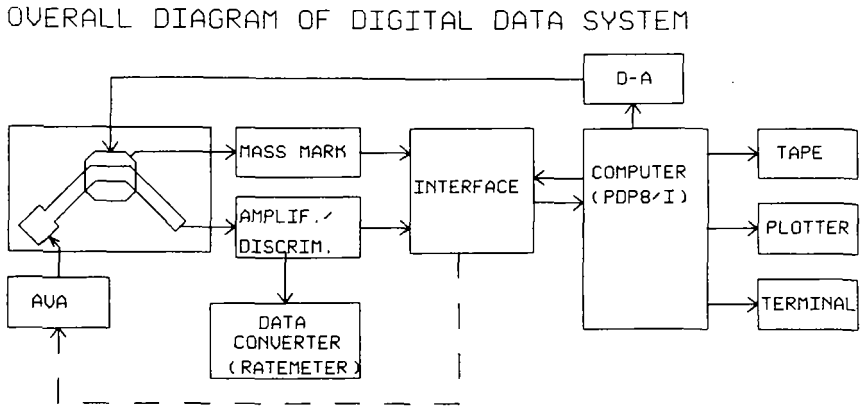

Figure 1

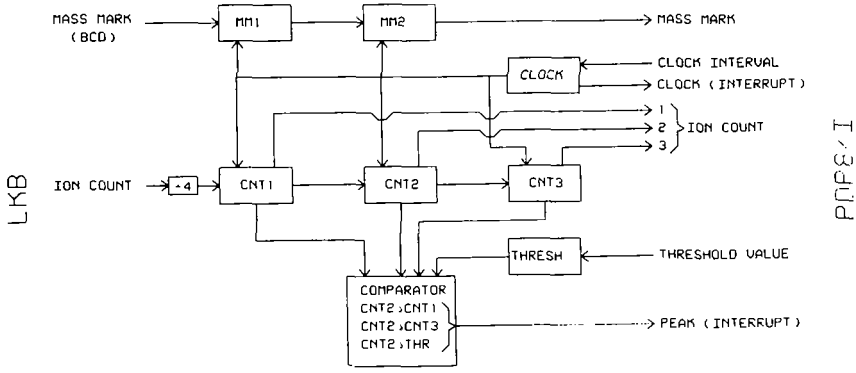

Figure 2

DATA SYSTEM FOR A CHEMICAL IONIZATION MASS SPECTROMETER

by

S. E. Buttrill, Jr.* and Rad Olson
Department of Chemistry
University of Minnesota
Minneapolis, Minn. 55455

Introduction - Chemical ionization (CI) mass spectra characteristically contain only a few peaks, and this fact places special demands on both the data aystem software and the mass spectrometer scan function. Because the CI spectrum is only a small fraction of the total ion current, the system must have high sensitivity, especially at high mass. Since major peaks in a CI spectrum may easily be 50-200 mass units away from neighboring peaks, the spectrometer-data system combination must provide accurate mass identification without using the conventional extrapolation algorithms. Our system uses an independent, digitally driven, magnet scan controller to couple our Du Pont 21-490B mass spectrometer to a PDP-12/30 computer.

Magnet Scan Controller - The magnet scan control unit is outlined in Figure 1. This unit produces a linear mass scan, either up or down, from the output of a crystal clock oscillator. A divide-by-n counter determines the scan time by controlling the rate at which TTL pulses are sent to the 16-bit counter. The contents of the counter are continuously converted to an analog signal by a 16-bit DAC and simultaneously displayed by a five digit decimal readout. A Burr-Brown Square Rooter converts the analog signal from the DAC into a reference voltage for the magnet power supply to produce a linear scan. The starting point of the scan is precisely controlled by loading the contents of a 16-bit latch into the counter. The scan ends when the analog signal equals a set-point voltage as determined by an analog comparator. Each time the counter is incremented, a pulse is sent to the computer to cause the sampling of the mass spectrum. Since the starting point of the scan can be loaded into the computer prior to the scan, the data system knows at all times exactly where it is in the scan.

Data Acquisition Program - This interrupt driven program is the heart of the data system. Data acquisition is initiated by a Start Pulse from the Magnet Scan Controller. Each pulse from the clock to the 16-bit counter also causes the computer to perform an analog-to-digital conversion and if the signal is above an operator specified threshold, it is added to the input buffer. As each peak is acquired, its mass centroid is calculated as well as its intensity. The nominal mass is corrected to actual mass by the addition of a 24-bit correction factor from a 511 entry table. The result is then written

---

*Present address: Mass Spectrometry Research Center, Stanford Research Institute, Menlo Park, CA 94025.

into the output buffer. The output buffer is displayed as a mass spectrum on the CRT in real time as it is acquired, and this feature has proven to be invaluable in helping the operator verify the correct functioning and adjustment of the instrument as data are acquired. Although it is hardly optimized for rapid scanning, a scan from 15 to 500 amu requires less than 20 seconds. In addition to the spectrum itself, the scan number, title, all operator controlled variables and thresholds, and five analog inputs are stored on the disk following each scan.

Calibration Program - This program calculates the table of 511 correction factors by comparing the spectrum of a reference compound or mixture with a table of expected masses and intensities. Although the program can use any reference spectrum, the only system which has proven useful on a routine basis is the argon charge exchange spectrum of perfluorokerosine which normally allows us to calibrate from m/e 18 to above 800.

Report Program - This program can recall spectra from disk or tape, plot them on the CRT or X-Y recorder, subtract background, scale intensities, and generate reports on any system device including the CRT.

Overall Accuracy - The mass calibration stability is limited by drifts in the magnet and its power supply. At present, good stability is obtained only after the magent is left scanning continuously at least overnight. We expect to solve this problem in the near future by regulating magnetic field rather than magnet current. Figure 2 shows the excellent mass measurement precision obtained when scanning a 500 amu mass range (128 samples/amu). The absolute mass measurement accuracy is sufficient to provide information on the elemental composition of CI peaks even though the spectra are run on a 4-inch single-focusing instrument with a resolution (10% valley) of only 750. As shown in Figures 3 and 4, performance scanning a 1000 amu range is somewhat worse since there are now only 64 samples/amu. However, mass measurement accuracy is still considerably better than unit mass and the ability to automatically obtain correct mass assignments for isolated peaks at high mass is invaluable in CI work.

Sensitivity - Two ng of cholestoral in a standard melting point capillary in the solids probe will produce 3 to 7 scans containing a recognizable water CI spectrum (including the M + 1). A 0.5 ng sample usually produced a single scan containing a recognizable spectrum, but a usable spectrum was always detectable using the oscillographic recorder. Thus the instrumental sensitivity is about a factor of four less using the data system than with direct UV chart recording, and we believe that this fact results from the limited resolution of our 10-bit A-D converter.

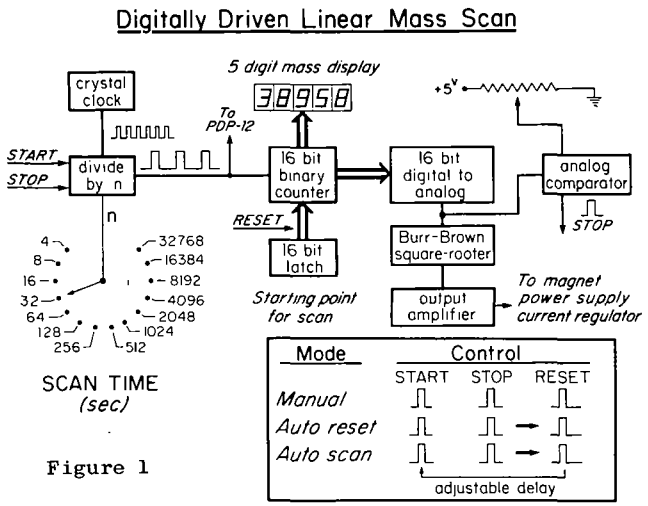

Figure 1

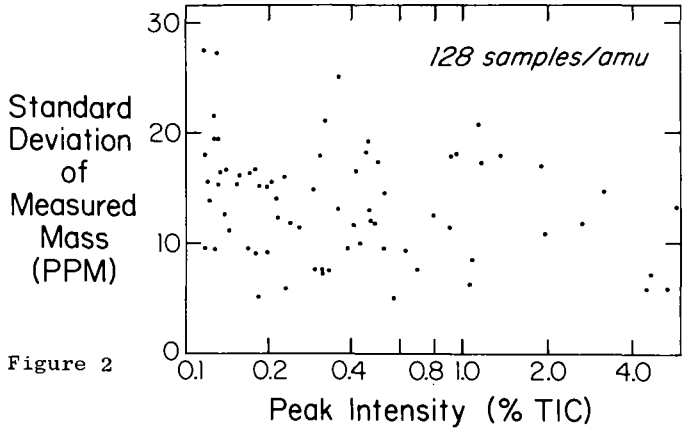

Figure 2

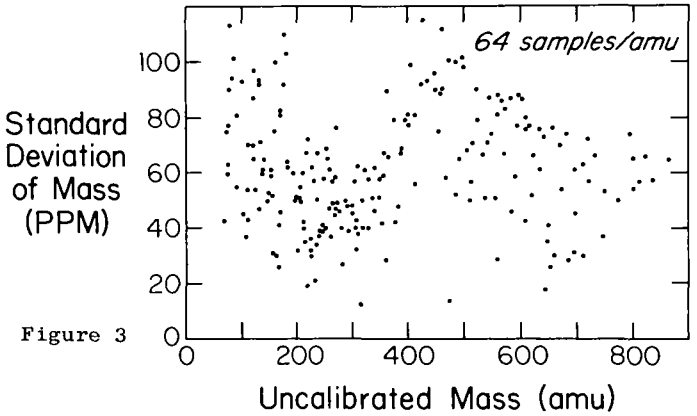

Figure 3

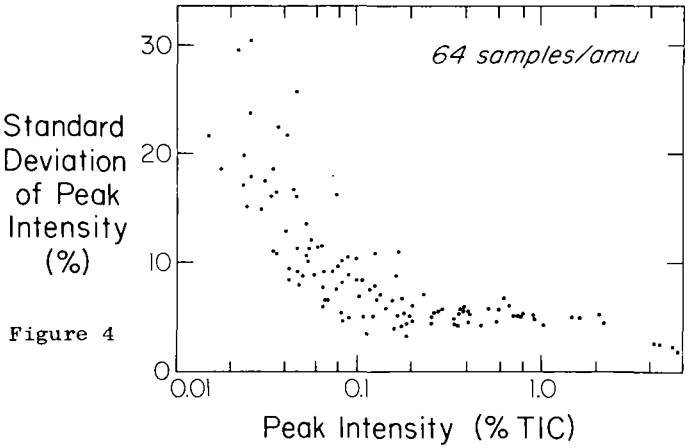

Figure 4

ION KINETIC ENERGY SPECTRA OF ALKYL-SUBSTITUTED THIOPHENES[1]

Robert Ryba and Gilbert J. Mains
Department of Chemistry
Oklahoma State University
Stillwater, Oklahoma 74074

INTRODUCTION

Metastable ions have been understood since Hipple and Condon correctly interpreted them in 1945. However, it was not until the development of double-focusing mass spectrometers that these decompositions, as characteristic of the molecule as the mass spectrum, could be studied conveniently. Beynon and co-workers[2] first described the spectrum of metastable daughter ions as a function of their energy as an ion kinetic energy spectrum (I.K.E.S.) and concentrated interest on this related application of double-focusing mass spectrometers. While all double-focusing mass spectrometers are easily modified to yield I.K.E.S., the Nier-Johnson geometry produces the highest energy resolution with the least modification, $E/\Delta E \approx 4000$. Low resolution I.K.E.S., $E/\Delta E \approx 33$, are easily obtained on the Mattauch-Herzog geometry instruments using techniques developed by Futrell[3] and Chait.[4] We have extended the energy resolution of the du Pont/CEC 21-110B to $E/\Delta E \approx 200$ by techniques which will be described in Paper Z3 and here we present the first I.K.E.S. study using the modified mass spectrometer at Oklahoma State University.

The choice of thiophene-type compounds for the initial I.K.E.S. study resulted from conversations with Mynard Hamming of Continental Oil Co., who pointed out the difficulty in resolving bibenzyl and n-heptylthiophene at m/e = 132 in the high resolution mass spectrum of petroleum fractions. We were fortunate in that many of the thiophene samples used by Eccleston and others at the U.S. Bureau of Mines Laboratory, Bartlesville, Oklahoma, for their detailed mass spectral study (U.S. Bur. Mines Invest. #6433) in 1963 were still available. These were vacuum distilled and found to be 99^+ % pure by gas chromatography and field ionization mass spectrometry. Two compounds, 2-n-butylthiophene and 2-n-heptylthiophene, were synthesized by us and similarly purified and analyzed.

RESULTS AND DISCUSSION

The medium resolution I.K.E.S. of fourteen thiophenes were obtained and discussed at the poster presentation. For brevity, representative examples (thiophene, benzothiophene and n-heptylthiophene) are presented here in Figures 1 through 3 in order of increasing molecular weight. All spectra were obtained using 70 ev ionizing electrons, 100 μampere source current, and 7.5 kv accelerating potential. The other source conditions are noted on the figures. We observe here that ion source pressures were kept below 50 μtorr so that only first-order metastable transitions need be considered. Except for n-heptylthiophene, the transitions assigned to the I.K.E. peaks were based upon precise measurements of the percent energy at the peak maximum. In the case of n-heptylthiophene the I.K.E. peaks were also mass analyzed using the photographic plate system. Although the spectra are only shown to circa 40-50% energy retention, the measurements were extended to zero and for the compounds presented here no light metastable daughters were observed.

The major I.K.E. peaks which arise from thiophene itself, Figure 1, result from the loss of mass 2 (H_2), 26 (C_2H_2), 32 (S), 34 (H_2S), 39 (C_3H_3) and 45 (CHS). This is consistent with the mass spectrum of thiophene. The addition of a conjugated ring as in benzothiophene (Figure 2) results in a shift of these transitions up in energy since the daughter

ion retains a proportionately larger fraction of both the mass and the energy. One also observes the additional complication of transitions from the daughter ion at m/e = 108.

The effects of adding an n-butyl, isobutyl and t-butyl group at the 2-position were also studied and the spectra will be published later.[1] In addition to the expected elimination from the parent ion, m/e = 140, the spectra are rich in daughter ion transitions, including some from the alkyl fragment ions, and the base mass peaks at 97, 97 and 125 respectively. The mass spectra of the n-butylthiophene and isobutylthiophene are very similar and so are their I.K.E. spectra. There is no obvious advantage to analyzing a mixture of these isomeric thiophenes using these or over conventional analytic spectra.

Figure 3 amply illustrates how the addition of a long-chain alkyl group increases the complexity of the I.K.E. spectrum by opening up multiple channels of alkyl ion decomposition, which are superimposed on the anticipated eliminations from the parent ions and base ions. As will be shown, detailed consideration of the assignments is not warranted at this time. In general, the alkylthiophene I.K.E.S. spectra are readily correlated with transitions from the principal peaks in the corresponding mass spectra.

Finally, we discuss n-heptylthiophene (Figure 3) in some detail because we have studied it more completely and because the results suggest directions for future I.K.E. research. The reader will note that the peaks have been labeled alphabetically. Each of these peaks was mass analyzed and the observed metastable masses, m^*, were used to make the assignments shown in Table I.

TABLE I. METASTABLE PEAKS AND TRANSITIONS IN THE IKES OF 2-(n-HEPTYL)THIOPHENE

Metastable Peak	Assigned Transition	Calculated m_2/m_1
A	97 → 45	0.464
B	85 → 43	0.506
C	182 → 97	0.533
	183 → 98	0.536
	84 → 45	0.536
	55 → 29	0.527
D	180 → 98	0.544
	97 → 53	0.546
E	65 → 39	0.600
	111 → 67	0.604
	110 → 66	0.600
	108 → 65	0.602
	97 → 58	0.598
F	67 → 41	0.612
	182 → 111	0.610
	182 → 110	0.604
G	43 → 27	0.628
H	71 → 45	0.634
	153 → 97	0.634
I	97 → 63	0.649
J	84 → 58	0.690
	181 → 125	0.691
	111 → 77	0.694
K	55 → 39	0.709
	97 → 69	0.711

TABLE I (CONTINUED)

Metastable Peak	Assigned Transition	Calculated m_2/m_1
L	153 → 111	0.726
M	182 → 139	0.764
	139 → 105	0.755
	110 → 84	0.764
N	148 → 119	0.804
	149 → 120	0.805
O	182 → 148	0.813
	183 → 149	0.814
P	182 → 153	0.841
	183 → 154	0.842
Q	97 → 84	0.866
R	110 → 96	0.873
S	29 → 26	0.897
T	43 → 39	0.907
U	27 → 25	0.926
	28 → 26	0.929
	29 → 27	0.931
	41 → 38	0.927
	57 → 53	0.930
V	29 → 27	0.931
	30 → 28	0.933
	43 → 41	0.953
	42 → 40	0.952
	47 → 45	0.957
	41 → 39	0.951
	44 → 42	0.955
W	27 → 26	0.963
	28 → 27	0.964
	30 → 29	0.967
	39 → 38	0.974
	40 → 39	0.975
	44 → 43	0.977
	46 → 45	0.978
	55 → 53	0.964
	53 → 51	0.962
	67 → 65	0.970
	68 → 66	0.971
	69 → 67	0.971

Twenty-three I.K.E. peaks are shown to arise from 63 metastable transitions, most of which have not been hitherto reported. It is entirely probable that there are additional metastables between the I.K.E. peaks in Figure 3 but we have not searched in these regions.

CONCLUSIONS

It is clear that there is a wealth of unresolved transitions in all the data presented here. It seems reasonable to conclude that future research should strive toward high resolution I.K.E.S. to complement the advances in high resolution mass spectrometry. Much of the hope for I.K.E.S. as a structural probe may still be fulfilled when we achieve energy resolutions approaching our current mass resolution capabilities. We hope to improve on own energy resolution by techniques described in Paper Z3. However, until these resolutions are achieved, searches for correlations in the lower resolution I.K.E.S. of homologous compounds will

continue to contribute to our ultimate understanding of metastable transitions much as was the case in mass spectrometry. We can foresee analytical applications of "standard" I.K.E. spectra tables similar to those pioneered by the A.P.I. for mass spectra. A.S.M.S. needs to decide on "standard" source conditions so that comparable data accumulation can proceed.

ACKNOWLEDGEMENTS

One of us (R. R.) wishes to thank Continental Oil Co., Phillips Petroleum Co., and Oklahoma State University for financial support during his doctoral studies. Dr. Hamming of Continental Oil Co. is thanked for suggesting the thiophene series to us. We are especially grateful to Dr. E. Chait, du Pont Instruments, for discussions of the 21-110B spectrometer's ion optics and for a second field-free sector which we could modify to improve the energy resolution of our instrument.

REFERENCES

1. A full account of this research including all of the fourteen I.K.E. spectra presented at the poster session will be published elsewhere.

2. J. H. Beynon, R. M. Caprioli, W. E. Baitinger, and J. W. Amy, Int. J. Mass Spectrom. Ion Phys. 3, 313 (1969).

3. L. P. Hills, J. Futrell, and A. Wahrhaftig, J. Chem. Phys. 51, 5255 (1969).

4. E. M. Chait and W. B. Askew, Org. Mass Spectrom. 5, 417 (1971).

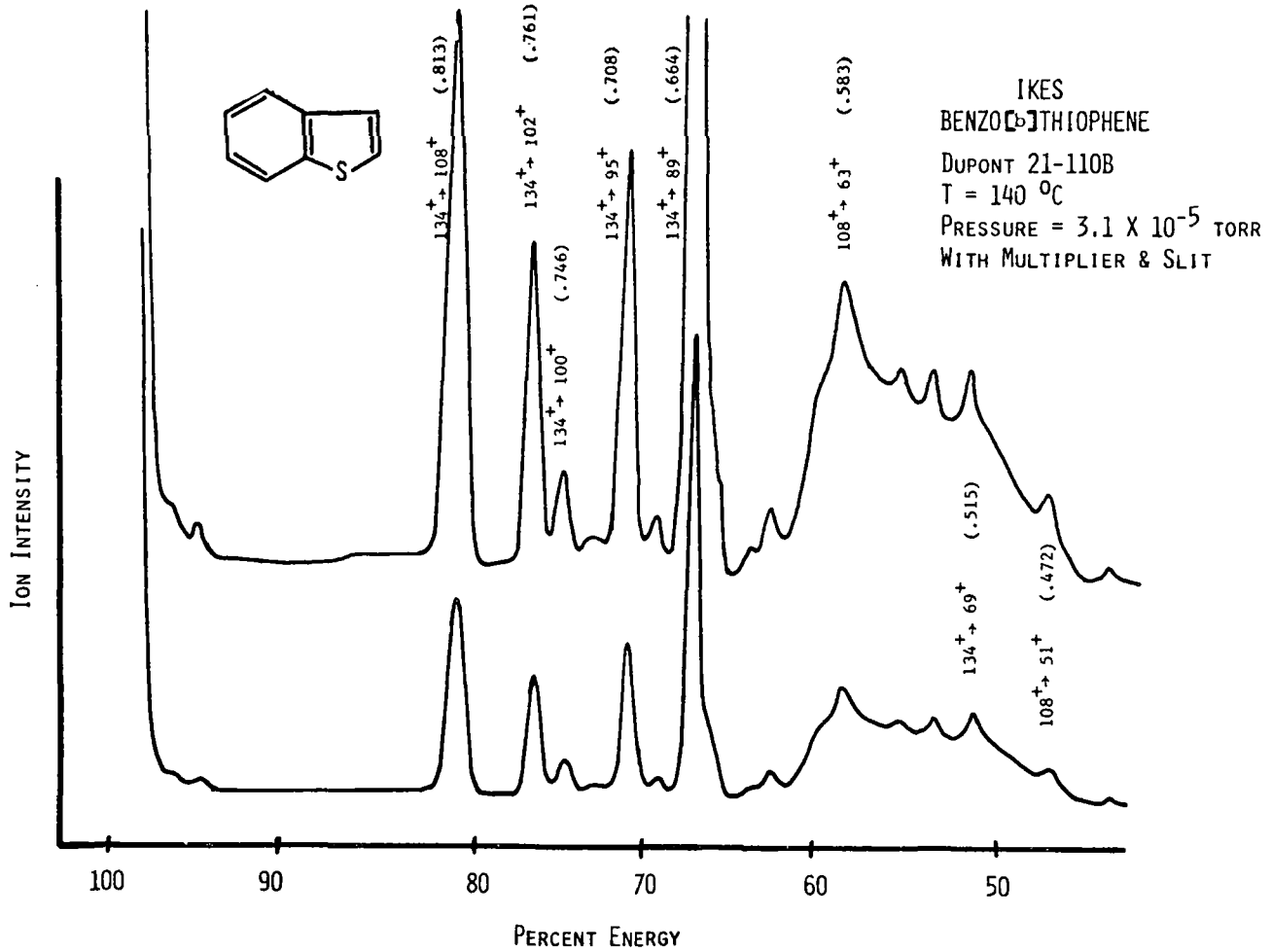
IKES
BENZO[b]THIOPHENE
DUPONT 21-110B
T = 140 °C
PRESSURE = 3.1 X 10^-5 TORR
WITH MULTIPLIER & SLIT
134+ → 108+ (.813)
134+ → 102+ (.761)
134+ → 100+ (.746)
134+ → 95+ (.708)
134+ → 89+ (.664)
108+ → 63+ (.583)
134+ → 69+ (.515)
108+ → 51+ (.472)
ION INTENSITY
100
90
80
70
60
50
PERCENT ENERGY

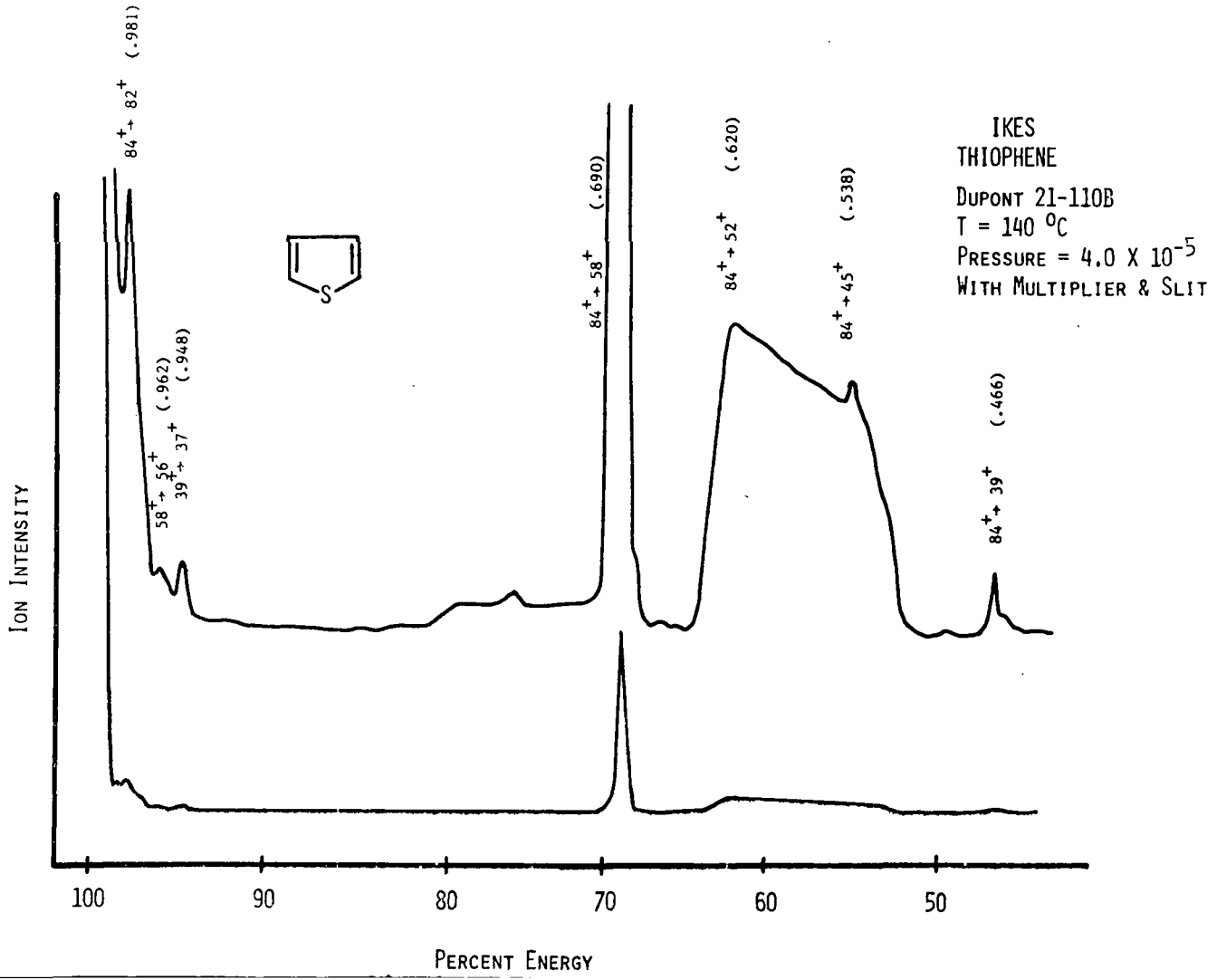
IKES
THIOPHENE
DUPONT 21-110B
T = 140 °C
PRESSURE = 4.0 X 10^-5
WITH MULTIPLIER & SLIT
84+ + 82+ (.981)
58+ + 56+ (.962)
39+ + 37+ (.948)
84+ + 58+ (.690)
84+ + 52+ (.620)
84+ + 45+ (.538)
84+ + 39+ (.466)
S
ION INTENSITY
100
90
80
70
60
50
PERCENT ENERGY

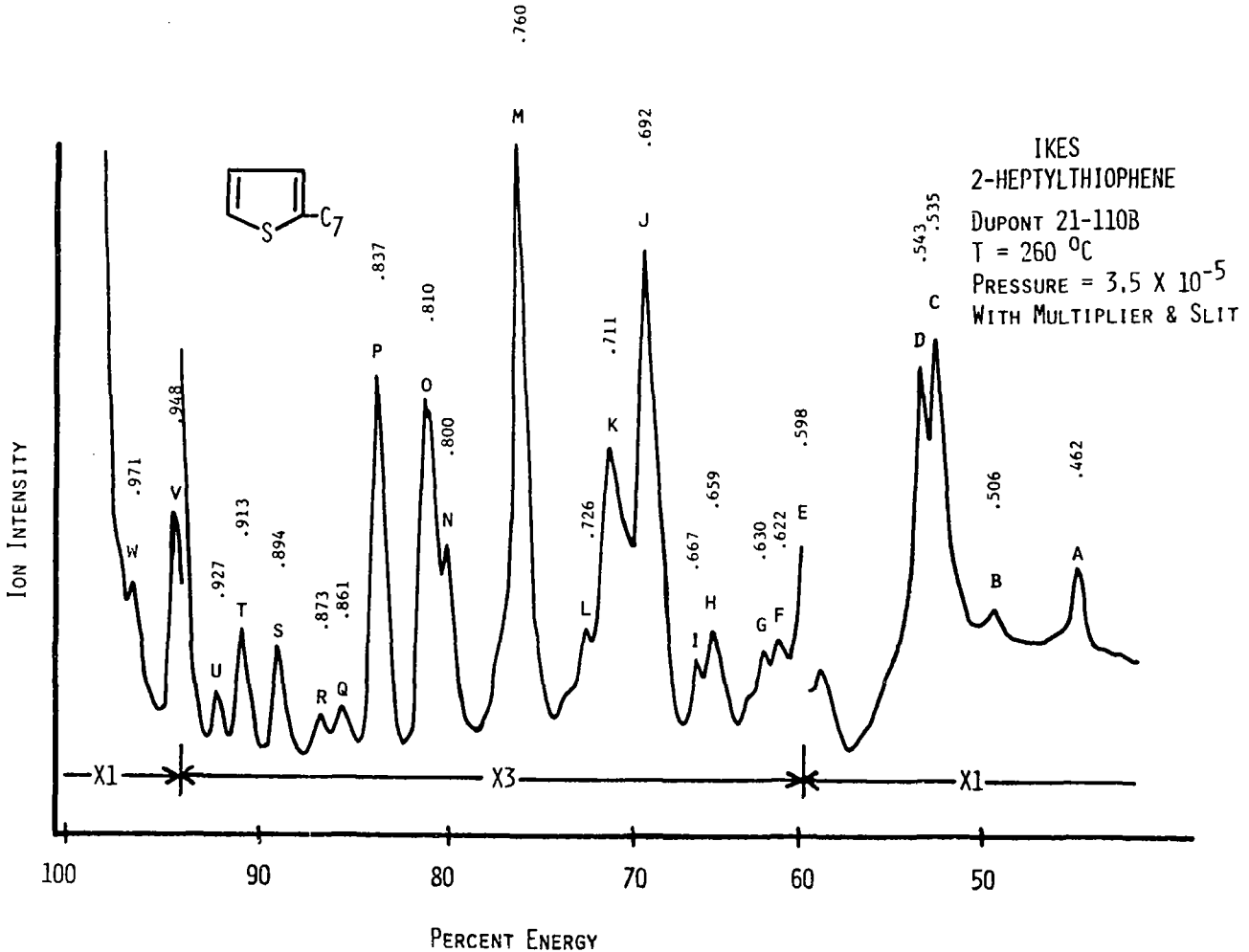
IKES
2-HEPTYLTHIOPHENE
DUPONT 21-110B
T = 260 °C
PRESSURE = 3.5 X 10^-5
WITH MULTIPLIER & SLIT
ION INTENSITY
PERCENT ENERGY
X1
X3
X1
100
90
80
70
60
50
.971
.948
.927
.913
.894
.873
.861
.837
.810
.800
.760
.726
.711
.692
.667
.659
.630
.622
.598
.543
.535
.506
.462
W
V
U
T
S
R
Q
P
O
N
M
L
K
J
I
H
G
F
E
D
C
B
A
C7
S

Kinetic Study of Heterogenuous Reactions by Linear Temperature Programming

Margaret A. Frisch

IBM Watson .RESEARCH Center
Box 218
Yorktown Heights, New York 10598

The thermal stability of a substance is studied by heating the sample in a Knudsen cell at a linear rate while monitoring the gaseous products by beam modulation and mass spectrometric techniques. The cell is a miniature "vacuum system" with the orifice defining the conductance. The reaction rate will be proportional to the effusion rate, if the temperature sweep is long, compared with the characteristic pumping time (volume/conductance). The activation energy and reaction order are derived from the shape of the ion intensity-temperature data by comparison with the theoretical curve, obtained by integrating the rate equation with respect to temperature. The technique has been applied to the pyrolytic decomposition of 1-oxo-2-diazo-napthalene-5-sulfonic acid ester of trihydroxyarylphenone. The rate of nitrogen release, due to the rupture of the diazo linkage, followed accurately the predicted curve for a first order reaction with an activation energy of 41 kcal/mole. The desorption of a small amount of the unesterified trihydroxyarylphenone was also observed with a ΔE of 23 kcal/mole.

Stress Mass Spectrometry of Polymeric Materials*

M.A. Grayson, R.L. Levy, D.L. Fanter, and C.J. Wolf
McDonnell Douglas Research Laboratories
McDonnell Douglas Corporation
St. Louis, Missouri 63166

The failure of a polymeric material subjected to mechanical stress involves a number of complex, partially understood phenomena occurring at the molecular level. An important phenomenon of recent interest (1-3) is stress-induced cleavage of primary bonds in the polymer main chain, and the subsequent formation of volatile degradation products. Stress mass spectrometry, in which polymer samples are subjected to stress and/or fracture directly in the ion source housing of a time-of-flight mass spectrometer (TOFMS), provides a means of studying the volatile products of stress-induced degradation. We report here some details of stress mass spectrometry on two polymeric systems: polystyrene and nylon 66 (poly [hexamethylene adipamide]).

A time-of-flight mass spectrometer (Bendix model 12-107) was used for the analysis and detection of volatile compounds released during mechanical loading of the polymer specimens. The samples were stressed using apparati constructed on the ion source flanges of the TOFMS ion source housing. Samples can be mechanically loaded by bending, by tension of dogbone-shaped specimens, or by tension of monofilaments (Fig. 1).

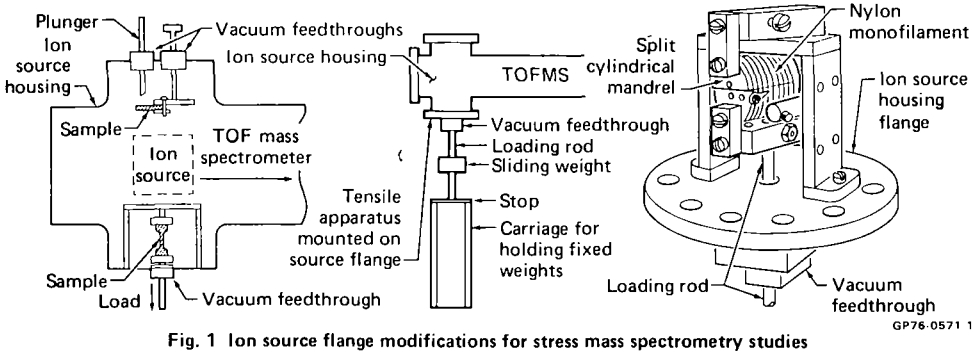

Fig. 1 Ion source flange modifications for stress mass spectrometry studies

Data from these experiments are acquired by either continuous ion monitoring or oscilloscope photography of z-axis modulated mass spectral displays. For the former case, a four-channel monitor (Bendix model MA-006) modified for extended mass range was used. In the latter case, the Rapid Events Mass Spectral Data Acquisition (REMSDA) system was used. The REMSDA system permits acquisition of data during the brief time prior to, during, and immediately following the sample fracture. With this system, z-axis modulated mass spectra (4) can be displayed on the oscilloscope screen for 1.6 ms to 3.2 s with timing intervals from 0.2 ms to 205 ms. A photograph of the REMSDA output is shown in Fig. 2. The mass-to-charge ratio is along the x-axis, elapsed time is along the y-axis, and the intensity of the peak is determined by the brightness of the line (z-axis).

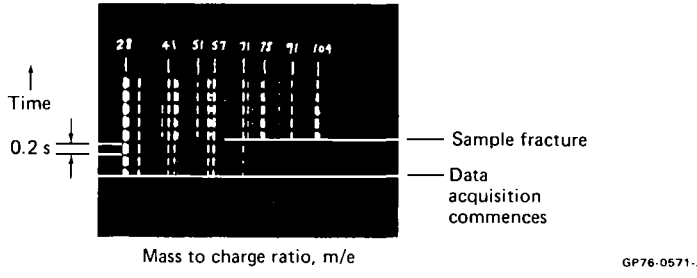

Fig. 2 REMSDA display of volatiles released from as-received polystyrene (70eV)

The volatile organic compounds indigenous to the matrix of the polymer are characterized by Vaporization Gas Chromatography/Mass Spectrometry (VGC/MS) (5). This technique permits efficient sampling of indige-

This research was conducted under the McDonnell Douglas Independent Research and Development Program.

nous volatiles by using the column itself as a trap. After the sampling is complete, conventional GC/MS procedures are used to identify the indigenous volatiles using a mass spectrometer (AEI MS-30 single beam) interfaced to the gas chromatograph with a silver frit molecular effusion separator (6).

An Instem Carrick data acquisition system (7) is used in conjunction with an off-line mass spectral data system (8) to record and analyze the data.

Polystyrene

A detailed discussion of the stress mass spectrometry of polystyrene is available elsewhere (9): only a brief discussion is given here. High-purity, atactic polystyrene (M.P. 140-141°C) was obtained from the Monsanto Company. The results of VGC/MS characterization of the volatile organic compounds trapped in the matrix of the as-received polystyrene indicate the presence of large amounts of styrene monomer. The volatiles evolved from as-received polystyrene when fractured in the TOFMS are shown in the REMSDA display in Fig. 2. It is apparent that indigenous styrene monomer trapped in the matrix of polystyrene is obfuscating attempts to characterize compounds formed during mechanical degradation.

Two methods of sample purification were used to remove the compounds trapped in the polystyrene matrix: vacuum annealing and reprecipitation. The effectiveness of the sample purification methods is shown in Fig. 3. Vacuum annealing does not effectively remove styrene monomer from the polystyrene matrix. During stress mass spectrometry studies of the reprecipitated polystyrene, no mechanical degradation products were detected. The detection limit of the mass spectrometer for styrene monomer in the REMSDA mode was determined to be ~6×10^{11} molecules over a period of 200 ms. Thus the amount of styrene produced by fracture of the reprecipitated polystyrene must be less than 6×10^{11} molecules, indicating that either the number of primary bonds broken in the polymer main chain is small or the subsequent reaction chain length is relatively small.

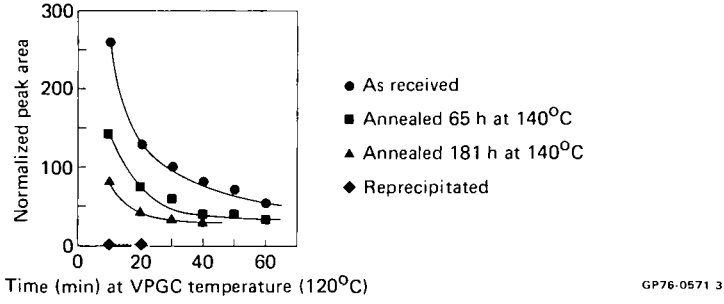

Fig. 3 Relative efficiency of removal of styrene monomer from polystyrene for vacuum annealing and reprecipitation treatments

Nylon 66

This material was investigated because the residual impurities and anticipated degradation products should be quite different, thereby avoiding the major problem encountered in the stress mass spectrometry studies of polystyrene. A nylon 66 (DuPont), free of additives, was studied in the form of a drawn monofilament 0.2 mm in diameter. VGC/MS characterization of the monofilament revealed the indigenous volatiles shown in Fig. 4. In subsequent heats, only a small amount of phenyl phenol was present. These compounds are typical of surface finishes and die lubricants. In addition, cylic hexamethylene adipamide was released when the nylon was heated in the solids probe of the mass spectrometer.

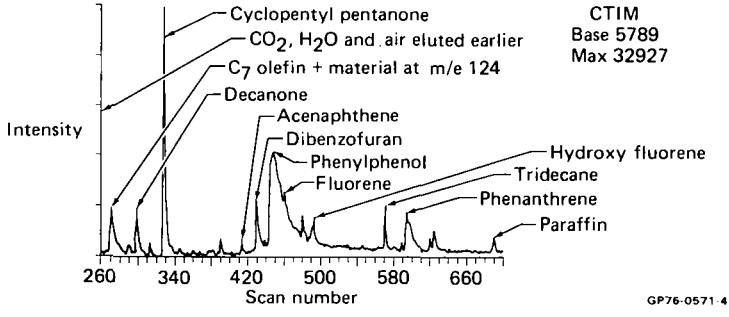

Fig. 4 Identification of volatiles released from nylon 66 (210°C for 15 min)

The samples were loaded in tension to fracture. During loading of the nylon 66 monofilament, no volatile material was detected, even though sample extension was typically 10%. At sample fracture, mechanical degradation products were detected only when one or more of the fracture surfaces was frayed or "fibrillated" (see Fig. 5). No products were detected when the sample fractured cleanly (see Fig. 6).

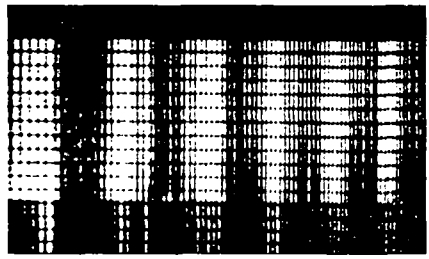

GP76-0571-5

Fig. 5 REMSDA display of volatiles released from nylon 66 upon fracture (70eV)

Clean Fibrillated GP76-0571-6

Fig. 6 Example of fracture surfaces from stressed nylon 66 monofilaments

Low ionization potential mass spectrometry was used to identify many of the products. Ammonia and ethylene were positively identified; ethane, formaldehyde, butenol, and butenal were tentatively identified. These compounds are entirely different from the indigenous volatiles found in the characterization study and hence are assumed to be products of mechanical degradation. The significance of the release of products only upon fibrillation of the fracture surface is not yet certain.

This work indicates that stress mass spectrometry is a useful technique for studying stress-induced chemical reactions in polymeric systems. We have also found that it is imperative to characterize the volatile compounds indigenous to the polymer matrix before meaningful stress mass spectrometry experiments can be conducted.

References

1. *S.N. Zhurkov, V.A. Zakrevskyi, V. Ye Korsukov, and V.S. Kuksendo, J. Polym. Sci. (A-2) 10, 1509 (1972).*
2. *B.A. Lloyd, K.L. DeVries, and M.L. Williams, J. Polym. Sci. (A-2) 10, 1415 (1972).*
3. *V.R. Regel', T.M. Muinov, and O.F. Pozdnyakov, Proceedings of the Physical Basis of Yield and Fracture Conference, Oxford, 1966, pp 194-199.*
4. *K.A. Lincoln, Int. J. Mass Spectrom. and Ion Physics 2, 75 (1969).*
5. *R.L. Levy, C.J. Wolf, and J. Oro', J. Chromatog. Sci. 8, 524 (1970).*
6. *M.A. Grayson, R.L. Levy, J. of Chromatog. Sci. 9, 687 (1971).*
7. *A. Carrick, J. Mass Spectrom. and Ion Physics 2, 333 (1969).*
8. *M.A. Grayson, J.M. Putnam, and F.J. Yaeger, Presented at the 22nd Annual Conference on Mass Spectrometry and Allied Topics, Philadelphia, PA, 19-24 May 1974.*
9. *M.A. Grayson, C.J. Wolf, R.L. Levy, and D.B. Miller, J. Polym. Sci (Phys.) August 1976 (in press).*

A MECHANISTIC STUDY OF THE ELECTRON IMPACT REACTIONS OF SUBSTITUTED BICYCLOPHOSPHATES AND BICYCLOPHOSPHITES by Kent J. Voorhees, Fred D. Hileman, Thomas A. Elwood, and Jean H. Futrell, Flammability Research Center and Department of Chemistry, University of Utah, Salt Lake City, Utah, 84108

A series of 4-alkyl bicyclo(2.2.2)phosphites and 4-alkyl bicyclo-(2.2.2)phosphates have been synthetized using a modification of the Wadsworth method (1).

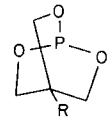

1 R=CH_3

2 R=C_2H_5

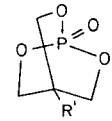

3 R'=CH_3

4 R'=C_2H_5

The major fragment ion for 1 and 2 under electron impact conditions corresponded to the elements of $(R\text{-}C{=}C{=}O)^+$--i.e., for 1 the base peak is m/z55. A loss of 30 amu was also observed (98% for 1 and 90% for 2). This fragment loss has been shown by high resolution mass analysis to result from elimination of CH_2O from the bicyclic system. Figure 1 illustrates the mass spectrum of 2.

The most striking difference between the phosphate and phosphite species was the absence of the $(M\text{-}30)^+$ peak and the appearance of an intense $(M\text{-}28)^+$ peak (69% for 3 and 42% for 4). High resolution mass spectrometry verified the 28-loss as the elimination of C_2H_4. The postulated mechanism is shown in Figure 2. The initial ring-breaking in step 1 has been proposed to explain the fragmentation patterns of phosphoramidic acid esters (2). The final steps in the mechanism involve ring expansion followed by loss of C_2H_4 to give a resonance-stabilized ion.

The question of the direct loss of C_2H_4 from the alkyl substituent for both 3 and 4 will be clarified by deuterium labeling experiments now in progress. The major fragment ion for both 3 and 4 was also the R-C=C=O moiety. The mass spectrum of 4 is represented in Figure 3.

---

1. W. S. Wadsworth, Jr. and W. D. Emmons, J. Amer. Chem. Soc., 84, 610 (1962).

2. P. Jakobsen, S. Treppendahl, and J. Wieczorkowski, Org. Mass. Spectrom., 6, 1303 (1972).

Acknowlegment - This work was partially supported under RANN-NSF GI-33650. The authors wish to thank the late Dr. Ralph Long, project monitor for his constant support during the last three years.

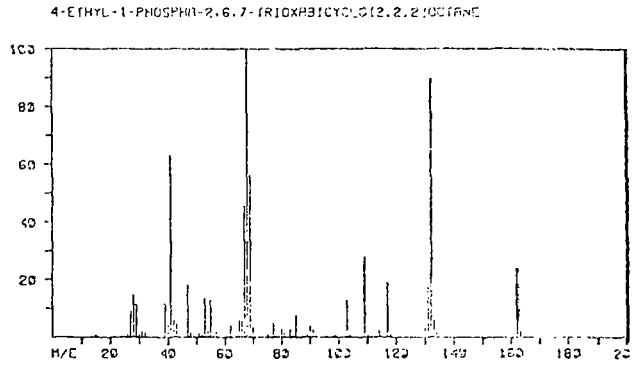

Figure 1. Electron impact mass spectra of ethyl substituted phosphile.

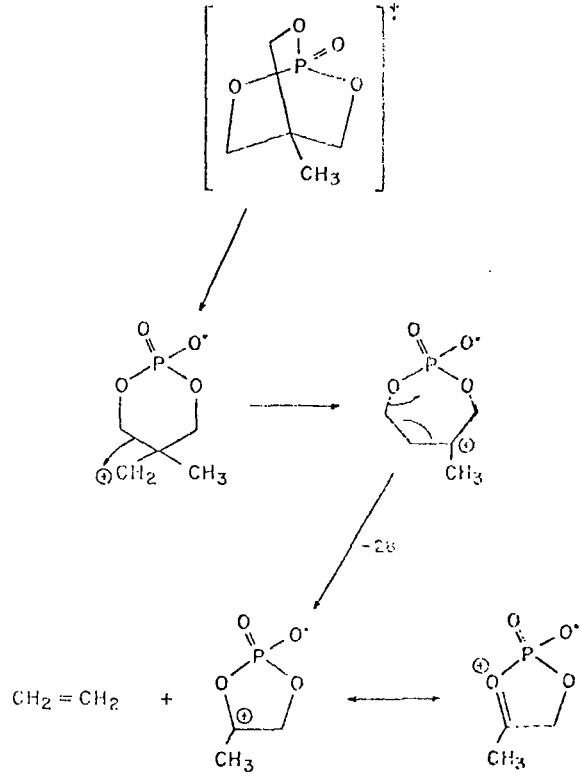

Figure 2. Mechanism for the loss of ethylene from cyclic phosphates.

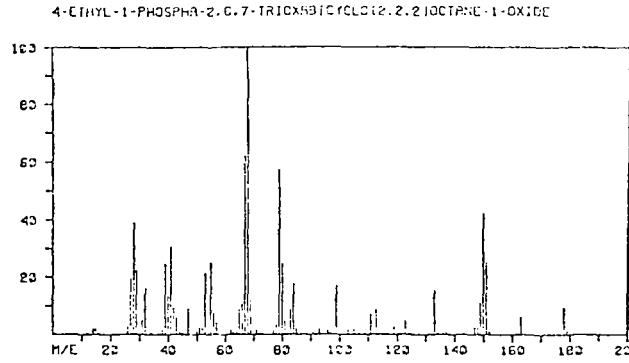

Figure 3. Electron impact mass spectra of ethyl substituted phosphate.

Applications of Pyrolysis GC-MS to the Analysis of Polymers and Other Compounds Adsorbed on Inorganic Substrates.

H. M. CURTIS, JR. and R. B. TWELVES, Halliburton Services, Chemical Research Department, Duncan, Oklahoma 73533

Extensive use of polymers, high molecular weight surfactants, and other compounds of low volatility by the oil field service industry has created the demand for obtaining qualitative and quantitative analyses for these compounds. The analysis becomes difficult when these compounds are adsorbed in small or trace quantities on natural or synthetic oil bearing formation material. Mass spectrometry readily provided the sensitivity required for these analyses, but suffered from limitations. These limitations are related to the maximum temperature capability of the direct probe on the mass spectrometer, and to ion source detuning resulting from sputtering of the inorganic substrate into the source chamber. Furthermore, if direct probe pyrolysis were successful, the mass spectrum would be a complex combination of spectra from all the pyrolysis products, making identification of the individuals components very difficult.

A system was needed which would have none of the disadvantages of the direct introduction probe. This system should allow the use of larger, more representative samples, more control over the pyrolysis temperature, and more precise separation of the pyrolysis products. Pyrolysis gas chromatography mass spectrometry provided the answer.

A pyrolysis apparatus has been constructed which attaches readily to the gas chromatograph-mass spectrometer system consisting of Varian 1440 gas chromatograph and a DuPont 21-491 mass spectrometer. A schematic diagram of the complete system is shown in Figure 1. The pyrolysis unit is shown in Figure 2 and was constructed to meet the following criteria: (1) Low dead volume to eliminate peak broadening, (2) Light weight so that it could be supported by the GC injection block, (3) Quickly removable, to facilitate interconversion between pyrolysis GC-MS and standard GC-MS, (4) Able to accommodate large samples (100 mg) to increase sensitivity.

A pyrolysis unit similar to that reported by E. J. Gallegos[1] was constructed from ¼ inch stainless steel tubing and standard fittings. The heater consists of 26 gauge asbestos covered nichrome wire close-wound on the pyrolysis tube for a length of 2 inches. A Variac is used to control the pyrolysis temperature, which is read on the GC pyrometer from a chromel alumel thermocouple placed on the pyrolysis tube at the center of the heater windings. Two toggle valves allow the carrier gas to be directed to the GC injection port or to the pyrolyzer. The sample container was made from 1/8 inch stainless steel welding rod by drilling a hole in the end and then grinding off one side to form a boat. Quick connect fittings on the carrier gas line and plug-in thermocouple connections permit rapid conversion between pyrolysis GC-MS and standard GC-MS operation. The pyrolysis gases are introduced into the gas chromatograph through an 18 gauge syringe needle which has been punched through two septa. A flared end on the pyrolysis tube and the knurled nut hold the septa and needle against the injection port on the gas chromatograph.

The operating procedure involves heating the pyrolysis zone to 600°C while the sample is held in the cool zone. The sample probe is then pushed into the heated area, causing rapid pyrolysis of the sample. The carrier gas is directed through the pyrolyzer so that the pyrolysis products are swept onto the gas chromatograph column. The chromatograph effluent is monitored both by flame ionization detector (FID) on the gas chromatograph and by the total ion monitor (TIM) on the mass spectrometer. The mass spectrum is scanned as each component elutes from the chromatograph.

The pyrolysis GC-MS system described was used to identify a cationic polymer (PA-1) and to determine the amount of this polymer which had been adsorbed on sandstone and clay core samples. The structure of PA-1 was determined from the pyrolysis GC-MS data. The pyrogram of PA-1 and an outline of the structural deduction are shown in Figures 3 and 4, respectively.

Large amounts of methyl chloride and trimethyl amine were evidence of a quanternary ammonium salt with at least two methyl groups. Dimethylethyl amine, methyldiethyl amine, and ethyl chloride suggested additional groups of at least two carbons attached to the nitrogen. The presence of the pyrazine derivatives indicated a chain length of two carbons between nitrogen atoms. Acetone and propylene suggested groups of three carbon atoms, thus implying branching from the carbons linking the nitrogen atoms. The presence of oxygen in the polymer was shown by acetone, acetaldehyde, and water. The large amount of water indicated an alcohol functional group which was supported by infrared data. The structure deduced from these data is shown in Figure 5.

The amount of PA-1 adsorbed by sandstone and clay core samples was determined. A sensitivity factor for PA-1 was calculated after weighed samples of the pure polymer had been pyrolyzed and the peak area of the methyl chloride peak measured. The methyl chloride peak was selected primarily because of its intensity. In this case the area given by the FID was used, although subsequent investigation has shown that the TIM peak area works equally well. The sensitivity factor was 1.31×10^{-6} g/mm^2.

The samples consisted of sand and clay core specimens which had been treated with PA-1 and washed with large volumes of water. Weighed portions of these samples were pyrolyzed and the peak areas for the methyl chloride peak were measured. The peak area times the sensitivity factor gave the weight of PA-1 adsorbed by the sample. The results shown in Figure 6 are essentially what would be predicted based on the surface chemistry of clays versus quartz.

This technique has been applied to analysis of other polymers including polyacrylamides and cellulose derivatives. The structural correlations obtained for these materials, however, are not as obvious as in the example reported. Further studies of polymeric materials are in progress; also other areas in which the technique should be applicable are under investigation.

---

1. Gallegos, E. J., Proceedings of the 22nd Annual Conference on Mass Spectrometry and Allied Topics (1974) p. 346.

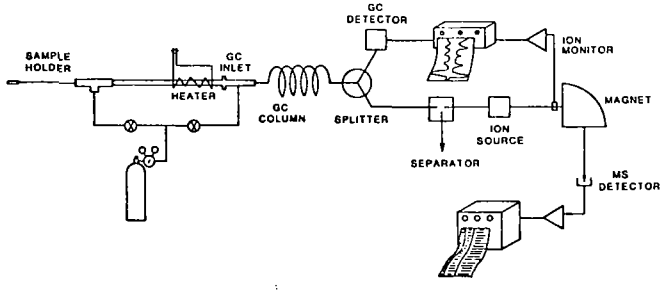

PYROLYSIS GC-MS APPARATUS

Figure 1

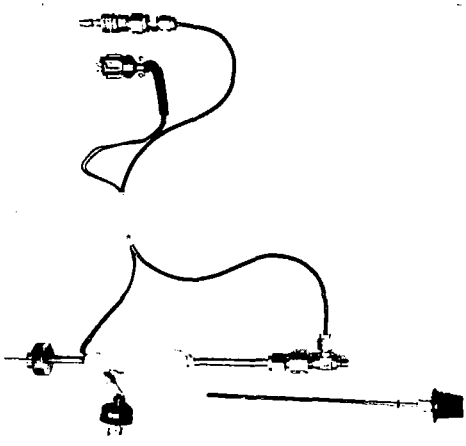

Figure 2

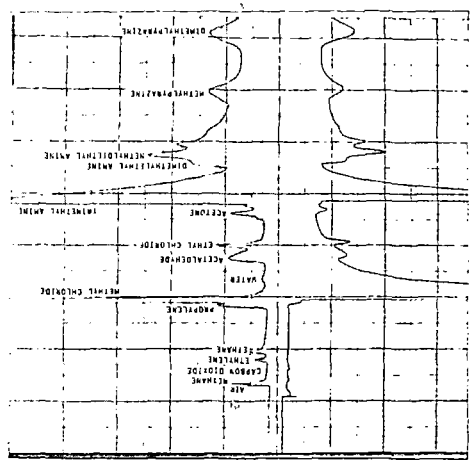

Figure 3

PYROLYSIS PRODUCT	STRUCTURAL FEATURE INDICATED
TRIMETHYL AMINE METHYL CHLORIDE	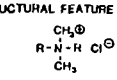
DIMETHYLETHYL AMINE METHYLDIETHYL AMINE ETHYL CHLORIDE	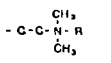
METHYL PYRAZINE *DIMETHYL PYRAZINE*	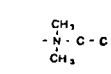
ACETONE PROPYLENE	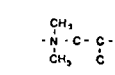
ACETONE ACETALDEHYDE WATER	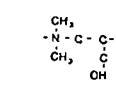

Figure 4

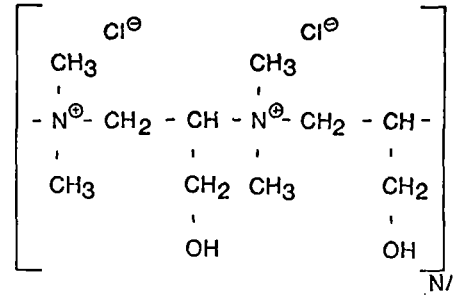

STRUCTURE OF PA-1

Figure 5

QUANTITATIVE RESULTS FOR PA-1
ADSORBED ON INORGANIC SUBSTRATES

PA-1 ADSORBED ON:	WT ON SAMPLE (g)	GC PEAK AREA (mm^2)	PER CENT POLYMER ON SAMPLE
CLAY	.0247	823	4.36
SAND	.0435	12.5	0.04

Figure 6

PSCI 8 EI and CI MASS SPECTRA OF ALKYLDIPHENYL-PHOSPHINE OXIDES

Barbara L. Jelus, Susan D. Goff, and
Edward E. Schweizer
Chemistry Department
University of Delaware
Newark, Delaware 19711

In the 70 eV electron impact mass spectra of a series of alkyldiphenylphosphine oxides, ($R\emptyset_2PO$, R=Me, Et, n - Pr, i - Pr, n - Bu, i - Bu, t - Bu, neopentyl, n - decyl), molecule ions of low abundance are observed and $(M + H)^+$ ions are formed to a small extent at high sample pressures. The major ions include $\emptyset_2PO^+$, $\emptyset_2POH^+$, $O_2CH_2PO^+$, and $\emptyset_2CH_2POH^+$ which are formed by rearrangement and cleavage process.

The chemical ionization mass spectra obtained with methane and isobutane reagents consist of $(M + H)^+$ ions. The proton affinity of $R\emptyset_2PO$ was found to be 219 $\pm$ 2 kcal/mole.

Manuscript submitted to Organic Mass Spectrometry.

Cycloreversion Reactions in the Mass Spectra of Various Tetralins

M.L. Gross and F.R. DeRoos
Department of Chemistry
University of Nebraska
Lincoln, NE 68588

Competitive cycloreversion reactions have been uncovered in the mass spectral fragmentation of 1-tetralol, viz.:

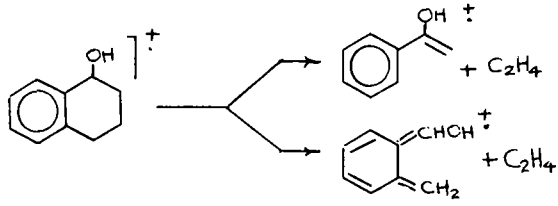

Interestingly, each pathway produces a unique ion structure as proved by isotopic labeling, metastable intensity ratios, and kinetic energy release. However, the primary significance of the study is the clear demonstration of the limitation of metastable characteristics for determining ion structure in the event of competitive pathways to form the ion in question. That is, the metastable decompositions of $C_8H_8O^{+\cdot}$ (the cycloreversion product) are identical with those of isomeric styrene oxide, and without further information (e.g. isotopic labeling) this structure would be assigned to the C_8H_8O fragment.

A detailed exposition of these results is in press in the "Journal of the American Chemical Society" and will appear late 1976 or early 1977.

Hydrogen-bonding Effects in the Mass Spectra of Phenylpyridylketoximes. Theodore L. Folk and Lawson G. Wideman, The Goodyear Tire and Rubber Company, Akron, Ohio 44316

Considerable interest in the electron impact spectra of oximes led us into an investigation of phenylpyridylketoximes. The obvious large difference between the fragmentation of phenyl-2-pyridylketoximes (I) and the other two positional isomers induced us

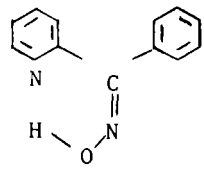

to look further into the hydrogen-bonding causing that difference. Deuterium labeling and mass measurements helped elucidate the fragmentation patterns of (I) and the 3- and 4-position isomers.

Mass Spectrometric Analysis of Polyoxymethylenes.

Rudolf Schubert, Bell Laboratories, Incorporated, Columbus, Ohio 43213.

Evolved gas analysis by mass spectrometry[1] (EGA-MS) of a polyformaldehyde and ethylene oxide as a comonomer was measured from 25°C to 210°C from samples manufactured over a six year span. Objective of the experiment was to determine differences in chemical composition or detect entrained masses and minute impurities which could explain stress cracking of molded samples. The experiments were done using a RF mass spectrometer in ultrahigh vacuum. MS sweep time was 15 sec for 2-200 amu and sample heating rates were typically 10°C/min. Although various differences in evolved gasses such as water vapor, unidentifed trace impurities and polymer decomposition products were seen from sample to sample, they could not be correlated with mechanical stress cracking.

[1]H. L. Friedman, Thermochim. Acta (1970) 199-227.

HYDROGEN-DEUTERIUM EXCHANGE IN WATER VAPOR: THE MASS SPECTROMETRIC SENSITIVITIES AND THE EQUILIBRIUM CONSTANT*

J.W. Pyper, R.J. Dupzyk, R.D. Friesen, S.L. Bernasek,†
C.A. May, A.W. Echeverria, and L.F. Tolman

Lawrence Livermore Laboratory
University of California
Livermore, CA. 94550

ABSTRACT

The equilibrium constant, K_{HDO}, for the reaction $H_2O + D_2O = 2HDO$ can be expressed as an intensity ratio, I, measured mass spectrometrically, times a sensitivity ratio, S, measured in mass spectrometric calibration experiments. The latter is difficult to measure and previously was assumed to be unity. The 2.4% discrepancy between K_{HDO} from theoretical calculations and direct mass spectrometric measurements might be explained by another value of S. We report an indirect measurement of S using a pulsed-molecular beam quadrupole mass filter that has a unique three-chamber, three-leak gas inlet system. The results show the sensitivities are probably equal and therefore $S \cong 1$ and $K_{HDO} = 3.81 \pm 0.09$. Systematic errors were found in the procedure, however, which precluded an unambiguous test of the theory.

---

* Work performed under the auspices of U.S. Energy Research & Development Administration under contract No. W-7405-Eng-48.

This paper has been accepted for publication in the International Journal of Mass Spectrometry and Ion Physics.

† Present address: Department of Chemistry, Princeton University, Princeton, New Jersey 08540

ON THE MEASUREMENT OF TRACE CONCENTRATIONS OF CARBON AND OXYGEN IN SOLIDS BY SSMS,

Donald L. Dugger and Daniel W. Oblas, GTE Laboratories, Waltham, Mass.

INTRODUCTION

A principle shortcoming of the Spark Source Mass Spectrograph (SSMS) is the limitation in the measurement of trace concentrations of carbon, oxygen, hydrogen, and nitrogen at the ppm level and lower. The primary obstacle has been the difficulty in maintaining the partial pressures of the residual gases in the ion source at sufficiently low values to minimize their effect on the analytical results. The problem is particularly severe for reactive metals such as tungsten. The main concern in the measurement of carbon and oxygen is the rise in partial pressure of carbon and oxygen containing compounds particularly during sparking. The major cause for this increase in gas pressure is the bombardment of the walls and components of the ion source chamber by energetic ions or particles coming from the rf spark.

In the design of the ion source of the spark source mass spectrograph, AEI incorporated a tantalum box, called a spark shield which surrounds the sparking electrodes. The spark shield served two functions. It kept the electrode material from depositing on other parts of the source, but more importantly, it reduced the flux of energetic ions striking the walls of the chamber.[1] These particles desorbed gases from the chamber walls which then scattered into the discharge region, became ionized and appeared as trace impurities on the mass spectrogram. In the original design of the AEI ion source, a movable shield or shutter was incorporated to reduce this effect, but it had limited use since it blocked the view of the sample during sparking.

The purpose of this paper is to describe a more convenient modification of the spark shield and show how it can help to improve the detection sensitivity of the SSMS to carbon and oxygen.

EXPERIMENTAL AND RESULTS

In addition to the improved pumping system consisting of a mechanical cryopanel at 14°K and large

diffusion pump, an extended ion source chamber was also constructed. It included a nude ionization gauge, a quadrupole mass spectrometer, a variable leak valve, and a liquid nitrogen cooled zeolite trap for rough pumping. The back of the spark shield, SS, which normally contains a large viewing slit was modified by spot welding a stainless steel grid over this slit (3x3mm) and another grid over the bottom opening (7x12mm) in the SS which is used for illuminating the sparking electrodes.

Several experiments were performed to determine the effectiveness of the SS to reduce gas evolution from the chamber walls due to particle desorption. The source chamber was backfilled with argon to 10^{-6} torr while the cryopanel was at $14^{o}K$. At this temperature argon will condense instantaneously on the panel surface. After several minutes, the argon introduction valve was closed and the remaining argon was pumped by the cryopanel and diffusion pump system. Within 5 minutes the partial pressure of argon in the source was estimated to be less than 10^{-11} torr. The condensed argon could then be desorbed during sparking and be easily identified by a quadrupole mass spectrometer connected to the source chamber.

In order to demonstrate the effectiveness of the spark shield in keeping background gases to a minimum, the sample was sparked without the SS, with the SS in place, and with the SS and grids. The relative partial pressures of Ar desorbed from the cryopanel as a function of the spark shield is listed in Table I along with the observed total pressure readings in the ion source. It was confirmed that by far the largest increase in argon partial pressure occurs when the ion accelerating voltage is present during sparking.

Table I
Comparison of Argon Intensities During Sparking of Ge Sample

Condition	Relative Ar Intensity	Pressure
No shield	705	$8x10^{-7}$ torr
With shield	16.5	$4x10^{-8}$ torr
With shield + grid	1	$5x10^{-9}$ torr
With shield + large grid	21	$2x10^{-7}$ torr

Base pressures of $5x10^{-10}$ torr in the ion source of the experimental system are typical after bakeout at $150^{o}C$. A typical rise in source pressure to 10^{-6} torr

is normally observed when sparking without the spark shield. This has been improved to $3\text{-}5 \times 10^{-9}$ torr as measured by the nude ionization gauge during sparking for duty cycles of 20% (1000 cps, 200 μs) and 40% spark.

CONCLUSIONS

The purpose of these experiments was to demonstrate the extent to which gases desorbed from the walls of the vacuum chamber by energetic particles or ions can be minimized by the use of a modified spark shield in conjunction with an improved vacuum system in the source. An argon covered cryopanel was used to demonstrate this effect. It was confirmed that the largest spectra peaks in the background gas during sparking are due to hydrogen and carbon monoxide. It is therefore concluded that in order to make measurements of C & O at the ppm level and lower, in reactive materials, it is imperative to use the grid covered spark shield to minimize desorption from the chamber walls.

BIBLIOGRAPHY

1. Franzen, J., Trace Analysis by Mass Spectrometry, Ed. Ahearn, A.J., Academic Press, 1972, p. 49.

Mass Spectral Studies of Polymeric Sulfur Nitride

J.R. Wyatt, J.J. DeCorpo, R.D. Smith, and F.E. Saalfeld

Physical Chemistry Branch
Naval Research Laboratory
Washington, D. C. 20375

Polymeric sulfur nitride, $(SN)_x$, is a material having unique characteristics: it has metallic properties; it is a super conductor at 0.3K; it is anisotropic; and it can be sublimated. Because of these recently discovered properties $(SN)_x$ is under intense current investigation. Little information is known about the composition of the vapor of $(SN)_x$, i.e., how can a polymer sublimate? Therefore, we studied the properties of the vapor of $(SN)_x$ using a variety of mass spectrometric techniques. Two methods were used to sample the $(SN)_x$ vapor species: (1) vapors were sampled directly from a Knudsen cell and (2) vapors were sampled after passage through unheated glass tubing constructed to assure wall collisions. Phase-angle molecular-beam mass spectrometry experiments showed that greater than 80% of the ions in the $(SN)_x$ vapor mass spectrum originate from a neutral species having a molecular weight of 190 ± 10, the only reasonable chemical species in this molecular weight range is $(SN)_4$ (MW = 184). The mass spectrum of this molecule is significantly different from that of S_4N_4, which is known to have a "cyclic" structure. Table 1 compares the spectra of S_4N_4 and the starting material S_2N_2 with $(SN)_x$ sampled by both methods. In addition, field ionization (FI) and field desorption (FD) mass spectra were obtained. The FD field emitter was prepared by subliming a sample of $(SN)_x$ crystals, under vacuum at 180-200°C to deposit an $(SN)_x$ film on the field emitter's surface.

Figure 1 compares the 14 eV electron impact (EI), field ionization (FI), and field desorption (FD) mass spectra obtained for $(SN)_x$ and S_4N_4. The FI and FD techniques are characterized by much simpler spectra than those obtained by

conventional electron-impact due to the generation of molecular ions with very small amounts of internal energy. On progression from EI to FI to FD one generally observes less fragmentation, consistent with the spectra reported in Fig. 1. Thus, while the 14 eV EI spectrum of $(SN)_x$ does not show the $(SN)_4^+$ ion [Fig.1(a)'], this species accounts for 10-15 percent of ionization in the FI spectrum of $(SN)_x$ [Fig. 1(b)]. In the FD spectrum, $(SN)_4^+$ is the only ion which may be attributed to $(SN)_x$. The molecular sulfur (S_8^+) evident in the FD spectrum of $(SN)_x$ is the product of a partial decomposition of the $(SN)_x$ at the temperatures (180°C-200°C) used in field emitter preparation. The peaks at m/e 56-58 result from impurities and the gaseous acetone used for tuning by field ionization prior to field desorption.

As noted above, the EI spectrum of $(SN)_x$ vapors and the well known S_4N_4 species are quite different, suggesting that an isomeric $(SN)_4$ species is formed on sublimation of $(SN)_x$. The FI spectrum of S_4N_4 and $(SN)_x$ vapors are in greater contrast; the FI spectrum of S_4N_4 (dashed lines, Fig. 1(b)) contain only the molecular ion, $S_4N_4^+$, whereas approximately 85% of the FI $(SN)_4^+$ ions from $(SN)_x$ vapors (solid lines, Fig. 1(b)), fragment to $S_3N_3^+$. These observations provide support for the existence of a less stable isomer of S_4N_4. Ring opening of a cyclic compound followed by fragmentation requires breaking of at least two bonds, making FI fragmentation unlikely. For example, little or no fragmentation involving the ring structure of cyclic hydrocarbon or heterocyclic compounds under field ionization conditions has been reported. These observations support the electron impact and phase angle mass spectrometry results and lead us to postulate that $(SN)_4$ has a "linear" structure, and not a cyclic structure.

In contrast the FD spectrum of $(SN)_x$ vapors and S_4N_4 are identical (solid and dashed lines respectively in (Fig. 1(c)); both spectra contain only the ion cluster at m/e 184-186. The FD spectrum of $(SN)_x$ is consistent with our conclusions regarding the vapor phase species of $(SN)_x$.

Based upon our data and the chemical behavior of $(SN)_4$ vapor, we believe $(SN)_4$ has a linear bent-chain structure. Comparison of the spectra taken using methods 1 and 2 showed that $(SN)_4$ upon wall collisions can isomerize to "cyclic" S_4N_4, or decompose to form SN, S_2N_2, S_3N_3, and possibly other species including S_4N_2 and S_2N. The presence of these species was inferred from mass spectral intensities and appearance potentials (Table 1) of various ions. Several oxygenated species were observed, but disappeared after the sample was heated for several hours indicating they were due to $(SN)_x$ surface impurities. Hydrogenated S_xN_y species were observed corresponding to one atomic percent hydrogen in the sample. Their intensity was invariant with time implying hydrogen is uniformly distributed throughout the sample of $(SN)_x$. The enthalpy of vaporization was found to be 120 ± 2 kJ/mol over the temperature range 350-420K. No anomaly was observed in the second-law plot which is consistent with a single, reversible vaporization mechanism.

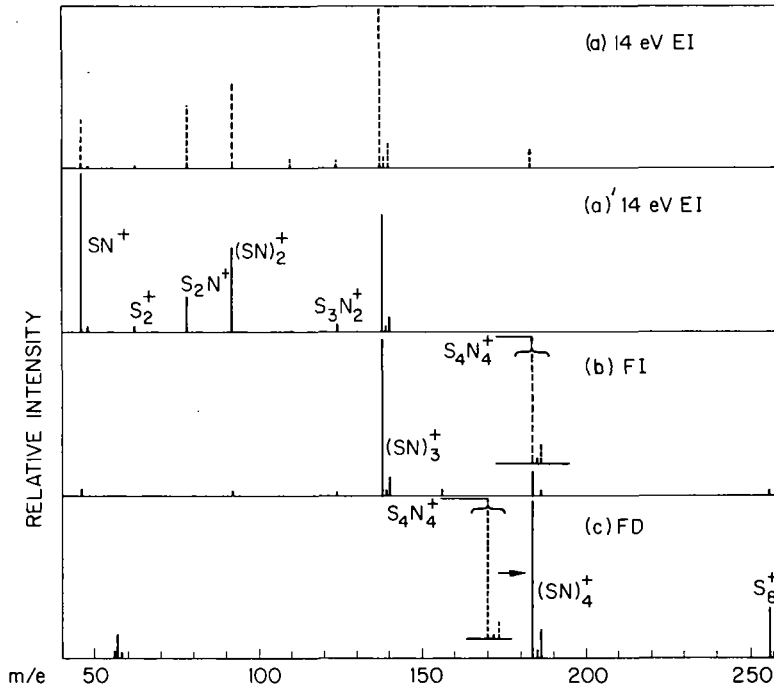

Figure 1 - Comparison of low energy 14 eV electron impact (EI), field ionization (FI), and field desorption (FD) mass spectra of the vapors of $(SN)_x$ (_____) and S_4N_4 (- - -). EI spectra of S_4N_4 and $(SN)_x$ vapors are given in (a) and (a'), respectively. The FI and FD spectra of S_4N_4 and $(SN)_x$ are compared in (b) and (c).

Table 1

Electron Impact Mass Spectra[a] and Appearance Potentials[b] of S_2N_2, S_4N_4, and $(SN)_x$ Vapors

Ion (m/e)	S_2N_2	S_4N_4	$(SN)_x$	
			Direct[c]	Indirect
SN^+ (46)	47 (13.0)	51 (14.1)	100 (13.0)	100 (13.0)
S_2^+ (46)	1.6	0.8	4.3 (12.9)	19 (12.6)
S_2N^+ (78)	3.2 (12.2)	44	19 (10.1)	32 (10.1)
$S_2N_2^+$ (92)	100 (11.5)	70 (13.7)	60 (11.2)	40 (11.5)
S_3N^+ (110)	0.0	6.6	0.6 (11.5)	2.0
$S_3N_2^+$ (124)	0.0	2.1	3.0 (10.5)	3.0 (8.8)
$S_3N_3^+$ (138)	0.0	100 (12.3)	63 (9.5)	20 (9.6)
$S_4N_2^+$ (156)	0.0	0.0	0.2	0.5
$S_4N_4^+$ (184)	0.0	4.2 (10.4)	0.2 (9.8)	0.0

a. Mass spectra represent an average of approximately 20 spectra, using 25 eV electrons, and recorded with identical instrumental settings. Isotopic contributions and those due to impurities are not included.

b. Appearance potentials, given in parentheses, were measured using H_2O (12.6 eV) and N_2 (15.7 eV) as calibrants, and have an estimated accuracy and precision of ±0.6 eV, and ±0.3 eV, respectively.

c. The low A.P. of several of the ions in the "direct" spectra suggest traces of species other than "linear" $(SN)_4$ may be present in the "direct" experiment vapors.

An Evaluation of a Thermal Ionization Mass Spectrometer using a NBS System Calibration Procedure.

V. E. CONNOLLY, E. L. CALLIS, A. W. SUMMERS
New Brunswick Laboratory
U. S. ERDA
New Brunswick, N.J. 08903

A National Bureau of Standards (NBS) type systems calibration[1] was performed on a production analysis mass spectrometer, a 12-inch radius, 60^0 sector instrument equipped with a triple filament source and Faraday cup collector. A series of NBS uranium Standard Reference Materials, U-050 thru U-930, were analyzed in duplicate and the mass discrimination factor calculated for each level from the measured $^{235}U/^{238}U$ ratios. The mass discrimination factor was found to be constant within $\pm 0.05\%$ for ratios in the range 0.05 to 20.

For a complete report of this work see the New Brunswick Laboratory Annual Progress Report for the Period July 1974 through June 1975, (NBL-277 , pp. 38).

1. Garner, E.L., Machlan, L. A., and Shields, W. R., NBS Special Publication 260-27, U. S. Government Printing Office, Washington, D. C. (1971), pp. 20-56.

Pyrolysis-GC-MS Techniques in Organic Geochemistry.

James G. Lawless and Franklin M. Church, Planetary Biology Division, NASA-Ames Research Center, Moffett Field, CA 94035.

Pyrolysis-GC-MS techniques have been used to study the nature of carbon and its compounds in terrestrial and extraterrestrial geological samples. Among the classes of compounds present in these samples are the monocarboxylic acids. In an effort to understand the behavior of these compounds under pyrolytic conditions, the salts of a series of low molecular weight fatty acids were studied to determine mechanism of decompositon and the product distribution. These salts decompose predominatly by decarboxylation and condensation to produce ketones. There appears to be little difference between the pyrolytic products of the sodium and calcium salts.

Mass Spectra of Some Salts of Carboxylic Acids With Group Ia Metals. EDWARD WHITE, V

Smith Kline & French Laboratories
Philadelphia, Pennsylvania 19101

We have examined the behavior under normal electron impact conditions of the salts of the five alkali metals with four simple carboxylic acids chosen to maximize the volatility of the salts and to be representative of acids which may be present after the processing of biological samples.

Table I shows the behavior of the twenty alkali metal carboxylates on heating. Seven of the ten salts of the perfluoroacids decomposed with no metal containing ions observed. The spectra of the volatile decomposition products indicate that the heptafluorobutyrates decompose cleanly to give CO_2 and C_3F_6 and the trifluoroacetates to give CO_2 and material with a spectrum similar to that of mixed perfluoroalkanes. In all cases, a white residue remains which is assumed to be the metal fluoride.

A carboxylate salt must vaporize as an electrically neutral species $(MO_2CR)_n$, most likely with $n \geq 2$. No ions of these masses are observed, but instead as shown in Table II, the metal cation and the even electron ions, $M_n(O_2CR)^+_{n-1}$, are observed which can be formally derived from $(MO_2CR)^+_n$ by loss of a carboxylate radical. These ions are the same as the major ions observed in the field desorption spectra of sodium acetate and in fact, the spectra obtained by these very different ionization processes are quite similar.

A decrease in the number of metal atom containing clusters present and in the intensities of the other metal containing peaks relative to the metal ion occurs as the atomic number of the metal increases.

Table I Temperatures[1] Required for MO_2CR Spectra

M=	R= $-CH_3$	$-C(CH_3)_3$	$-CF_3$	$-CF_2CF_2CF_3$
Li	290	218	230 dec.[2]	212
Na	343	302	dec.[3] 170	240 dec.[2]
K	325 dec.[2]	275	dec.[3] 140	dec.[3] 100
Rb	313	240	dec.[3] 155	dec.[3] 135
Cs	262	221	dec.[3] 145	dec.[3] 130

[1]Probe temperature (°C) on a Finnigan 1015. When metal containing ions were observed, the temperature is that required for an intense spectrum.

[2]Relative intensities changes somewhat during the course of the evaporation of the sample.

[3]Decomposition began at the indicated temperature. No metal containing ions were observed.

Table II Relative Intensities[a] (%) Of Selected Ions In M_2O_2CR Spectra

	$Metal^+$	$M_n(O_2CR)^+_{n-1}$							MO^+	MCO_2^+	$M_2^{\ddot{+}}$	$M_2O^{\ddot{+}}$	$M_2CO_2^{\ddot{+}}$
		n=2	n=3	n=4	n=5	n=6	n=7	n=8					
LiO_2CCH_3	*b*	100.0	1.8	0.6	<0.1	-	-	-	-	5.9	*b*	1.2	*c*
NaO_2CCH_3	2.2	100.0	0.9	0.1	-	-	-	-	3.0	8.0	2.6	2.8	-
KO_2CCH_3	100.0	47.5	0.3	<0.1	-	-	-	-	2.5	10.1	2.2	1.8	-
RbO_2CCH_3	100.0	1.9	-	-	-	-	-	-	1.1	2.6	0.2	0.1	-
CsO_2CCH_3	100.0	0.5	-	-	-	-	-	-	1.0	1.0	-	-	-
$LiO_2CC(CH_3)_3$	*b*	100.0	3.4	4.6	0.5	0.4	0.1	<0.1	-	3.9	*b*	0.7	4.9
$NaO_2CC(CH_3)_3$	18.8	100.0	1.6	1.7	0.2	0.1	-	-	18.1[c]	4.3	4.0	1.8	1.3
$KO_2CC(CH_3)_3$	100.0	19.0	0.5	0.3	-	-	-	-	1.6[c]	1.0	1.4	0.5	-
$RbO_2CC(CH_3)_3$	100.0	6.9	0.2	<0.1	*b*	-	-	-	0.2	0.4	0.6	0.5	-
$CsO_2CC(CH_3)_3$	100.0	2.4	<0.1	*b*	-	-	-	-	0.2	0.1	0.3	0.1	-
LiO_2CCF_3	*b*	80.6	0.8	0.5	-	-	-	-	-	3.8	*b*	-	1.0
$LiO_2CCF_2CF_2CF_3$	*b*	100.0	0.9	2.5	*b*	-	-	-	-	1.2	*b*	-	3.5
$NaO_2CCF_2CF_2CF_3$	-	3.7	-	-	-	-	-	-	-	-	0.5	5.4[c]	-

[a] Intensities are given relative to the base peak.

[b] The expected mass is outside the observable range of 20 to 770.

[c] Alternate composition certain (intensity not given) or likely.

Mass Spectra Obtained by the SRI Field Desorption Source,

G. A. St. John and M. Anbar, Stanford Research Institute, Mass Spectrometry Research Center, Menlo Park, CA 94025

The SRI field ionization source was modified to allow substitution of a broken tungsten rod of 1/16 inch diameter for the deposited multipoint structure used in ionization of gaseous or vaporized solid samples. This configuration allows us to deposit a sample (not volatile enough to be used in a solid sample probe and field ionized) directly on the desorbing surface and introduce this sample and probe into the ionizing region of the source (Figure 1). This sample can be positioned behind the counter electrode slit by rotation and by a linear forward and backward motion with a micrometer thread in the handle of the sample probe. After use, the sample and desorption wire are discarded and a new broken wire positioned in the probe with the aid of a gauge block.

We have used this source to obtain mass spectra of inorganic and organic compounds in both positive ion and negative ion configuration. These spectra show both ionization of neutral molecules in the case of organic molecules and desorption of existing ionic species in the case of inorganic molecules.

The ions formed were accelerated to 7 kV and mass analyzed by a 45° sector magnet. The sample loading was done by immersion of the rod tip in a solution of the tested material or by deposition of a microliter droplet from a micro-syringe onto the active surface. Occasionally a 10% polyvinyl alcohol solution (PVA) was used as matrix for inorganic substrates. The polymer was found to facilitate better control of the rate of field desorption.

Figure 2 shows the positive ion field desorption characteristics of different chlorides. Whereas LiCl field desorbs in the form of Li^{+} plus Cl^{+}, NaCl produces substantial yields of Na_2Cl^{+} and $Na_3Cl_2^{+}$ ions. In the case of NH_4Cl we observe field desorbed predominant clusters as complex as $(NH_4)_5Cl_4^{+}$. It seems that the relative polarizability of the cation and the anion contribute to the probability of cluster formation. This suggestion is borne out in the case of the iodides which shows the existence of $Li_3I_2^{+}$ with no evidence for the analogous sodium, potassium or cesium species. Interestingly enough, in both NaCl and NaI we find the formation of Na_2^{+} with no evidence for the analogous dimers in the case of the other alkalai metals.

Unlike metallic cations, NH_4^{+} does not form anionic complexes and seems to break down to $H^{+} + NH_3$ under negative ion field desorption. Consequently, ammonium salts seem to be ideal carriers for anions formed by field desorption. Figure 3(a) is a mass spectrum of ammonium thiocyanate produced under low temperature and low voltage (1.5 kV). The only species of significance here are SCN^{-} and $H(SCN)_2^{-}$ ions. Under these mild conditions, no ions originating from the polymeric matrix

are observed. Figure 2(b) is a similar spectrum of ammonium fluoroborate exhibiting only the BF_4^- ion. Ammonium nitrate, shown in Figure 2(c), produces only NO_3^- and $HNO_3NO_3^-$ ($HN_2O_6^-$) ions. Ammonium persulfate, Figure 2(d), shows, interestingly enough, $HS_2O_7^-$ and HSO_4^- in addition to $HS_2O_8^-$ ions rather than the double charged anions.

The same broken tungsten ionization tip has been used to field desorb organic molecules. In the latter case we found that using a 1% sucrose solution containing 10^{-6} M NaCl enhances the desorption of organic materials. Fig. 4 shows three spectra produced by this technique--folic acid, glutathione, and maytansine, three highly thermolabile nonvolatile materials. The relatively low temperatures allow field desorption without thermal breakdown. The sucrose containing medium may provide a molten matrix in which the organic solute may migrate to the regions of high field strengths; the sodium ions dispersed in the matrix may allow ionization by charge transfer. This action of sodium ions is different from the "cationization" reported by Shulten, as the folic acid and glutathione molecular ions are produced and not their sodium salts.

An extension of the usefulness of the technique is illustrated in Figures 5 and 6. A polymer of ethylene was ground in toluene to produce a fine emulsion which could be applied to the desorption tip. The spectrum of the polymer appeared at all masses simultaneously in contrast to a field ionization spectrum in which the low masses appear first and only on continued heating and scanning can an approximate mass profile be obtained. This feature is also evident in the butadiene polymer spectrum (Figure 6) showing masses well above the manufacturer's specified molecular weight of 1000.

We feel that the SRI field desorption-field ionization source, with its inexpensive throw-away desorption tip, can aid other laboratories in obtaining mass spectra of materials not easily obtained by conventional methods.

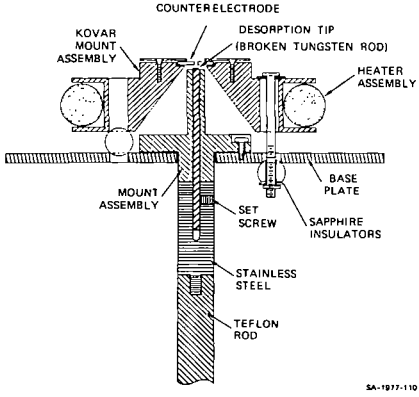

FIGURE 1 FIELD DESORPTION IONIZER WITH SAPPHIRE INSULATORS

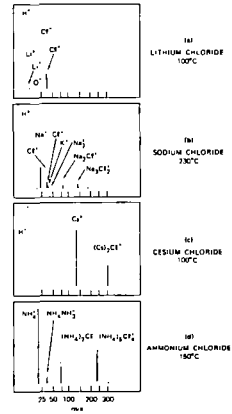

FIGURE 2 FIELD DESORPTION SPECTRA OF MONOVALENT CHLORIDES

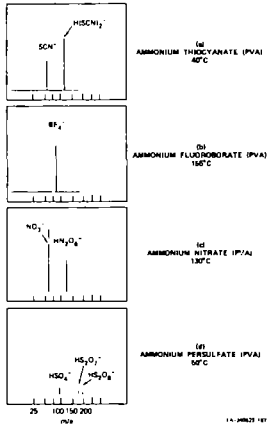

FIGURE 3 NEGATIVE ION FIELD DESORPTION SPECTRA

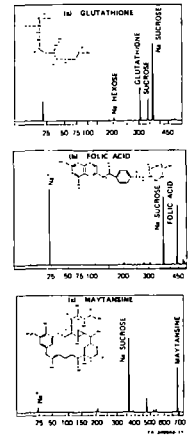

FIGURE 4 FIELD DESORPTION SPECTRA

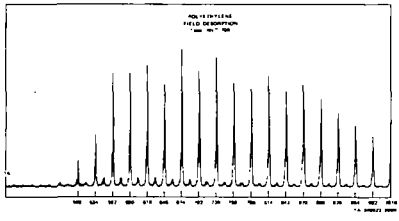

FIGURE 5 FIELD DESORPTION SPECTRUM OF POLYETHYLENE

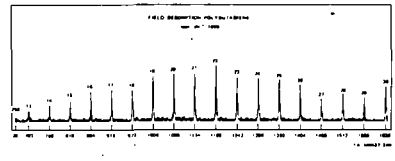

Power Emission: A High Performance Detection System for Ion Cyclotron Resonance Spectroscopy. Richard L. Hunter, Edward B. Ledford, Jr., and R. T. McIver, Jr., Univ. of Calif., Dept. of Chem., Irvine, CA 92717.

A detector circuit has been constructed which allows the detection of power emitted by ions which have been coherently accelerated by an electric field alternating at their resonant cyclotron frequency. By sweeping the frequency of the irradiating RF electric field, ions of different m/e are brought into resonance at constant magnetic field strength. When used with a trapped ion analyzer cell which allows ion trapping times of several seconds, the sensitivity, mass measurement accuracy, and mass resolution of the ICR spectrometer are significantly improved.

A Novel Scanning-Storage System for Magnetic Mass Spectrometers,

G. S. St. John, C. Biltz, and M. Anbar, Stanford Research Institute, Mass Spectrometry Research Center, Menlo Park CA 94025.

We found that we frequently lost transient spectra obtained by field desorption before the automatic scan and data equipment could be properly engaged to record the spectra. To overcome this problem, we devised a data handling system which was "live" all the time during manual search of the spectral range. Our system is used on a manually scanable 7 KV, 45° sector magnetic instrument equipped with the SRI field desorption-field ionization source and operated in the pulse mode of ion detection.

The heart of the new system is an electronic gate and pulse height generator. The inputs to the generator are the outputs of the Hall probe gaussmeter and the pulse train from the detector after amplification and discrimination. A detector pulse triggers a monostable multivibrator which generates a new pulse with an amplitude determined by the Hall probe (magnetic field). The new pulse is applied to the input of an analog-to-digital converter Nuclear Data 560, which converts the pulse height into a channel number of the multichannel analyzer-pulse height analyzer ND100 and adds one to that channel for each incoming pulse. Therefore, all detector pulses are applied to the appropriate channel of the pulse height analyzer and a mass spectrum is accumulated by varying the magnetic field. Under manual scan, the spectrum will not be a quantitative measure of the constituents, but a qualitative spectrum can be obtained, even when searching a mass range for unknown or unsuspected peaks. The input can also be used in any automatic negative scan mode in either increasing or decreasing, linear or nonlinear ramp.

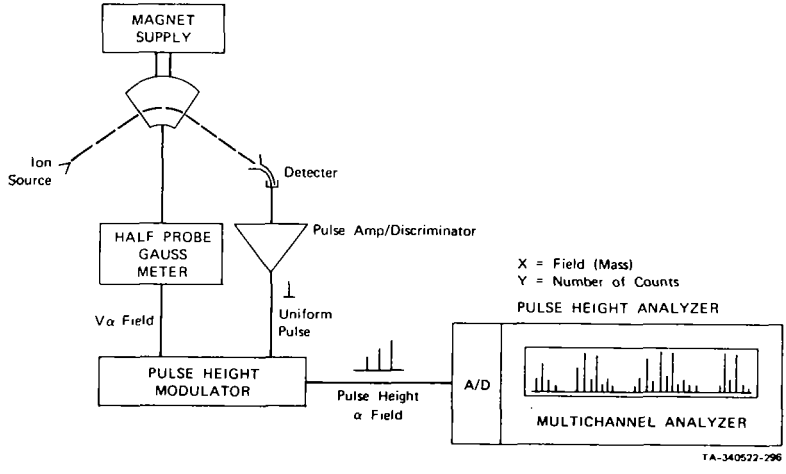

Conversion of Hitachi RMU-6D to GC/MS with Solid State Electronics and Differential Pumping

Roger A. Upham
Department of Chemistry
University of Minnesota
Minneapolis, MN 55455

This poster session described the modifications performed on a single focusing Hitachi RMU-6D to update the electronics and convert it to a GC-MS system. The vacuum system was converted to differential pumping by the addition of a restricter slit between the source and the flight tube. A 790 ℓ/sec. diffusion pump backed by a 300 ℓ/min. rotary pump was used to provide source vacuum by pumping through the variable source slit port. The analyzer vacuum system was simplified by removal of the ASV-50 isolation valve, the N-trap and the inner tube of the D-trap. A single stage glass jet separator (Scientific Glass Equipment) pumped by a 300 ℓ/min. Alcatel rotary pump interfaced the GC to the MS. A dump valve is available to reduce the solvent peak pressure. A completely interlocked circuit provides the instrument with protection from vacuum, water and power failures.

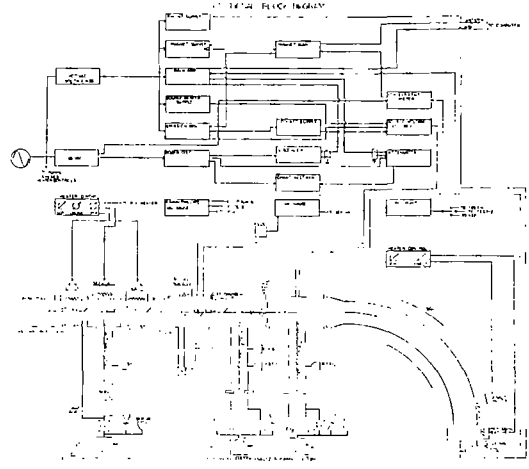

Figure 1: FUNCTIONAL BLOCK DIAGRAM

With the exception of the high voltage supplies, all of the original chasses were replaced with solid state units. The emission regulator was designed to produce the same voltage and current values as the original unit and even utilized most of the original switches and meters. See Figure 2.

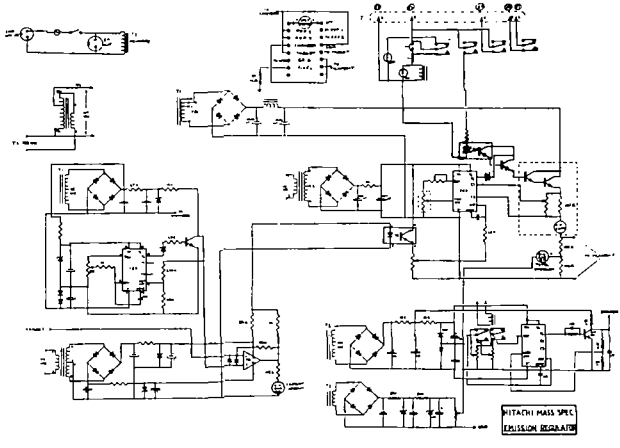

Figure 2: EMISSION REGULATOR

The magnet power supply was based on the design of Holder and Maddux[1]. It operates at 1200 volts and is capable of producing 300 mA of current. See Figure 3.

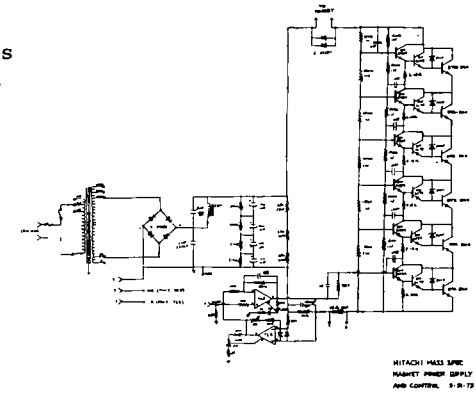

Figure 3: MAGNET POWER SUPPLY

The power supply is controlled by a voltage of 0-10 volts from the magnet scan controller. The controller consists of a 16-bit D/A converter which is fed by an up-down counter. A variable clock provides total count times of from 4 seconds to 8,192 seconds for the 2^{16} counts. The analog voltage from the DAC is fed into an anti-log amplifier which provides the 0-10 volt control signal. The controller can function in either a manual or automatic mode. (See Figures 4 and 5.)

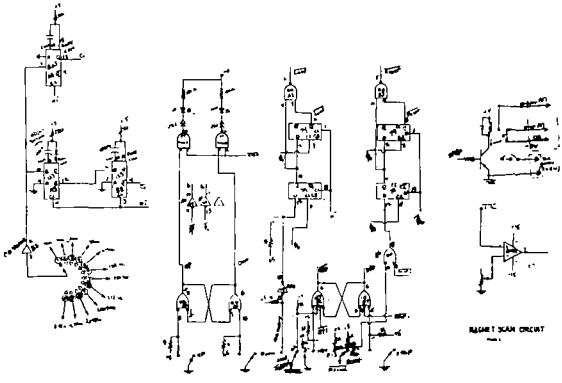

Figures 4 and 5:

MAGNET SCAN CONTROLLER CIRCUITS

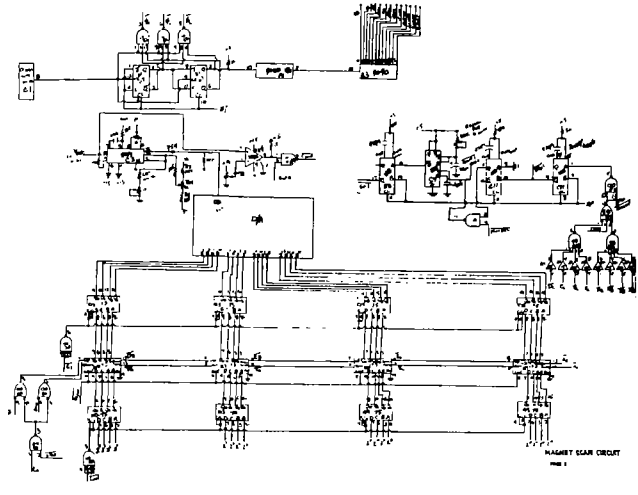

The preamplifier and amplifier circuits are shown in Figure 6. The entire system was designed to operate with a data system.

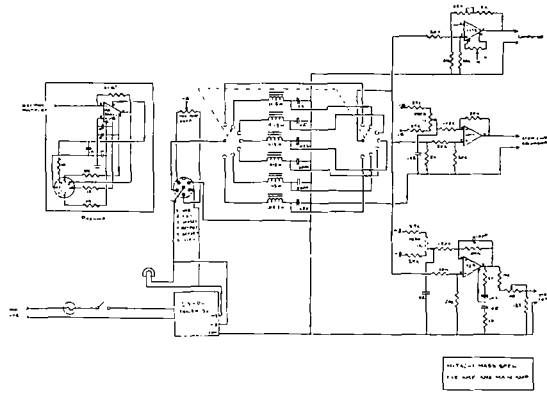

Figure 6: PREAMP AND MAIN MAIN AMPLIFIER CIRCUIT

Acknowledgments. I wish to thank Mr. Peter Kaufmann and Mr. Bruce Runyan for invaluable aid in this modification. I also would like to acknowledge Dr. Gary Gray who provided financial support from his grants from the Graduate School and Grant Number CA 15325, awarded by the National Cancer Institute, DHEW.

Reference

1. Holder, Bert E, and Maddux, Alvin S., Jr., Rev. Sci. Instrum. 45, 1228 (1974).

SOLID STATE MAGNETIC SCANNING UNIT FOR MASS SPECTROMETER

H. Bishop, J. Sharp and P. V. Fennessey

Departments of Bioengineering and Pediatrics

University of Colorado Medical Center
Denver, Colorado

Many laboratories are utilizing a continuous magnetic scanning mass spectrometer for the analysis of complex mixtures and these systems place rather rigid requirements on the stability and repeatability of the magnetic field. If the magnetic field drifts during the course of an analysis, it is impossible to automatically convert the peak centers (usually measured in time) to their corresponding mass/charge values (m/e). Our particular instrument (AEl-MSl2) has a general magnet circuit as shown in Figure 1[1]. The complete details of the circuit are not important for this discussion except to note that the reference sweep rate (lead 62 Figure 1) and the magnetic field voltage (lead 220 Figure 1) are compared by the Magnet Stabilizer Amplifier which in turn adjusts the output of the Magnet Current Regulator to null the two input values.

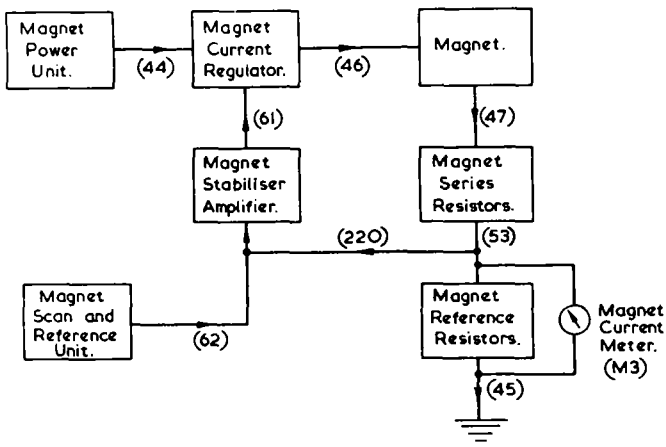

FIGURE 1

Overall magnet control circuit as supplied with AEl MS-12 mass spectrometer. Circuit lead numbers shown in parenthesis.

The current regulator and stabilizer amplifiers supplied with our instrument were of a tube design and were adequate, provided that the tubes were maintained on a regular basis. Recent changes in the cost of the tubes to more than $300 each and the fact that often the most expensive tube (three in series in the current regulator) had to be replaced as a matched set, led us to design and build a solid state unit [2] which would replace the stabilizer amplifier and current regulator. This solid

state unit should also be a direct replacement for the tube units in the AEI MS9 and MS7 series in addition to the MS12.

DESIGN AND PERFORMANCE

The solid state unit shown in the circuit diagram (Figure 2) is a combination of the Magnet Stabilizer Amplifier (surrounded by dashed lines in Figure 2) and the Magnet Current Regulator discussed above. This unit is completely interchangable with the original units and attaches directly to the present leads on our MS12.

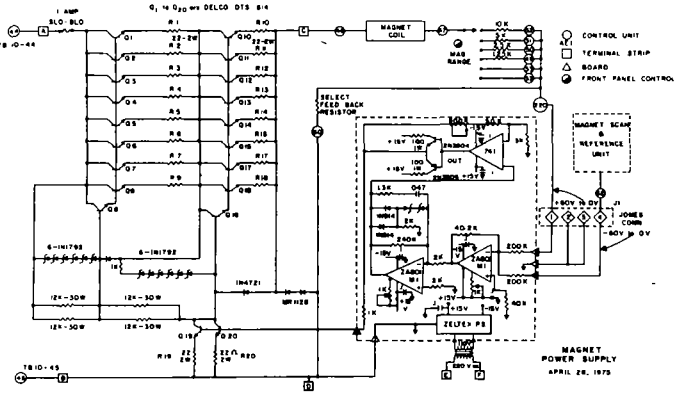

FIGURE 2

Schematic of solid state magnet current regulator and stabilizer amplifier (enclosed in large dotted box).

The solid state unit compares the signal from the magnet scan and reference unit (lead 62) and magnet voltage (lead 220) and drives the power network (16 Delco DTS814) pass transistors to maintain a null voltage from the two input points to less than 100 microvolts difference. The pass transistors are mounted on a water cooled heat sink and were checked on initial installation for more than 3000 volt isolation to prevent any arcing problems.

We have tested this unit in three different ways:

a. Long Term Stability - The magnet was turned to a high setting and m/e 431 of perfluoroalkane (PFA) was focused on the collector. The unit was left overnight and 12 hours later the peak was still in focus.

b. The full magnetic field was continuously swept at the fastest scan speed for one hour and no degradation of the field was noted when converting to m/e for PFA against a PFA standard.

c. The unit was used in a routine manner to collect spectral data from the gas chromatogram of organic acids. The data showed correct mass assignments and repeatability from day to day usage. The unit has been in continuous use for the past year and has shown remarkable stability. We replaced one 2N3904 transistor and one 741 operational amplifier since the original installation.

LITERATURE CITED

1. AEl MSl2 instruction manual, Vol. 1, published by GEC-AEl (Electronic Limited, Manchester, England).

2. Additional details of the circuit can be obtained by contacting H. Bishop, Department of Bioengineering, University of Colorado Medical Center, 4200 East Ninth Avenue, Denver, Colorado 80220.

GC/MS Interfacing Simplified and Quantified

James P. Lehman and Richard A. Day
Department of Chemistry
University of Cincinnati
Cincinnati, Ohio 45221

The salient features of the interface system shown in Fig. 1 are;

1) the solvent peak is vented with minimal interruption of column flow,
2) the 10% split to FID's allows independent use of the GC and an independent check of chromatographic performance,
3) the carrier gas flows in the columns, separator, and MS are directly or readily measured allowing evaluation of separator performance (1),
4) full use of both columns is maintained,
5) the separator is easily changed to accommodate the flow rates of the various GC methods, and,
6) the temperature limit of the system is 300°C.

The effluent of the GC is maintained at atmospheric pressure by the vents at ② and ③. This in conjunction with the ability to measure column flow rates and monitor chromatographic performance with the FID's greatly facilitates the transfer of GC methodology from the GC lab to the GC/MS system.

The carrier gas flow into the separator (He_{SEP}) is controlled by R_{SEP}, .010"I.D. stainless steel capillary having been used here. He_{SEP} is chosen to approximate the column flow rates (He_{COL}) typically used and more than one separator can be prepared to cover the range of column flow rates found in the laboratory. Differences between the He_{COL} and He_{SEP} are taken care of by the vent to atmosphere when $He_{COL} > He_{SEP}$ or by means of ④ when $He_{SEP} > He_{COL}$. The make-up He also allows GC maintenance and column changing without exposing the interface to air.

The heart of the GC/MS interface is the separator which hopefully increases the sample concentration in that portion of the carrier gas that enters the MS ion source. The enrichment seen at the ion source is readily and reliably determined in the following manner if a batch inlet system with a molecular leak is available. The experiment is done once with a simple "T" splitter constructed from a Swagelok "T" and capillary tubing in place of the separator and then with the separator under the experimental conditions of interest.

1) He_{SEP} is determined by closing ⑤ and measuring an excess ($He_{COL} > He_{SEP}$) He flow at ③, switching columns with ① and measuring the total column flow at ②. He_{SEP} is the difference of the measurements.

2) Naphthalene (NAPH) is introduced to the MS via the gas inlet. The temperature of the molecular leak (T_{LEAK}) and the NAPH (T_{NAPH}) are then recorded as is the pressure seen at the source ionization vacuum gauge (BACKGROUND P_{IG}).

3) The GC/MS shutoff valve, ⑦, is opened, taking care that there is a positive flow at ③, and the GC/MS P_{IG} is recorded. The MS is focused on the M^+ of NAPH and adjusted to give a readily measured signal.

4) A NAPH solution is injected on the analytical column, the column effluent being vented at ② until the solvent peak is seen to have passed at the FID. The column is then switched to the separator by ①, the He_{COL} having been previously measured at ② and recorded. The NAPH concentration and injection volume are chosen to give an M^+ peak area approximately equal to the area of the M^+ over a minutes time coming from the gas inlet as shown in Fig. 2.

5) The following value is calculated for each set of experiments.

$$\frac{\text{REDUCED PEAK AREA}}{\text{REDUCED REFERENCE AREA}} \times He_{SEP} =$$

$$\frac{\text{PEAK AREA}}{g_{NAPH}\ \text{Injected} \times P_{IG}} \times \frac{P_{NAPH}\sqrt{T_{LEAK}\ (^{\circ}C) + 273.1}}{\text{REFERENCE AREA}} \times He_{SEP}$$

where P_{IG} = GC/MS P_{IG} - BACKGROUND P_{IG}

If $He_{COL} > He_{SEP}$, then g_{NAPH} Injected is corrected by the factor He_{SEP}/He_{COL}. P_{NAPH} is calculated from

$$\text{Log}_{10}P_{NAPH} = -\frac{3729.2742}{T_{NAPH}\ (^{\circ}C) + 273.1} + 11.450 \qquad (2).$$

The ratio of the calculated values for a given set of separator conditions to the value calculated for the splitter is the enrichment seen at the ion source for that set of experimental conditions. Fig. 3 shows the enrichment data obtained for two glass frit effusion separators. Separator A was supplied by R. H. Allen Co. and separator B by Corning Glass. The seemingly anomalous temperature dependence of enrichment for the two separators is not predicted by theory (3).

Sample yield at the ion source can be determined by calibration of the molecular leak with He by means of a standard volume and a McLead gauge as depicted in Fig. 1 as components of the auxilliary gas manifold. The leak conductance for He (C_{He}) is determined from the relationship

$$C = -\frac{V}{t}\log_e\frac{P}{Po}$$

where V, the inlet system volume is determined using the standard volume and PV = PV. Once C_{He} is known, the source IG is calibrated in terms of He flow from the relationship Q = PC. Then,

$$\%\ \text{YIELD} = \frac{He_{MS}}{He_{SEP}} \times \text{ENRICHMENT} \times 100\%$$

Alternatively the leak conductance for NAPH (C_{NAPH}) can be determined using SF_6, taking care that the T_{LEAK} is close to that used for GC/MS test conditions.

$$C_{NAPH} = C_{SF_6} \frac{\sqrt{SF_6}}{\sqrt{C_{10}H_8}}$$

From Q = PC, the reference area is quantitated in terms of grams of NAPH and

$$\% \text{ YIELD} = \frac{NAPH_{MS}}{NAPH_{SEP}} \times 100\%$$

If both C_{He} and C_{NAPH} are determined, the enrichment can be calculated from

$$\text{ENRICHMENT} = \frac{NAPH_{MS}/He_{MS}}{NAPH_{SEP}/He_{SEP}}$$

using the data collected as above. In this series of experiments the enrichments calculated by both methods were in complete agreement, but it should be noted that this latter method involves considerably more effort and time and is more susceptible to error.

The yield at the ion source and hence the sensitivity is determined by the He_{SEP}, enrichment, and He_{MS}. He_{SEP} and enrichment are determined by the GC methods used and the separator being used. The optimum He_{MS} is determined by introducing NAPH as before and measuring the intensity of the M^+ as the He_{MS} is incremented by adjusting ⑨ and/or by replacing R_{SEP} or R_{MS} with a needle valve. The intensity of the M^+ multiplied by the P_{IG} is plotted versus P_{IG} as in Fig. 4. In region A of Fig. 4 the plot was found to be linear in this and other experiments and no loss of MS resolution was observed. In region B, loss of resolution occurs and sensitivity becomes mean free path limited. In region C sensitivity decreases and the observed mass spectrum changes. Thus the optimal He_{MS} is in the higher pressure portion of region A of Fig. 4.

The interface system is leak-checked by closing ⑤, turning ① halfway, and stoppering ③. The pressure recorded at the thermocouple vacuum gauge at ⑧ is observed while spraying the connections with acetone. The switching valve ① is located in the detector oven where it is essentially under isothermal conditions. Location of ① in the column oven where frequent temperature cycling occurs may lead to leakage problems.

(1) W. H. McFadden, Techniques of combined gas chromatography/mass spectrometry, New York, Wiley (1973).

(2) Handbook of Chemistry and Physics, 47th edition, Chemical Rubber Pub. Co. (1967).

(3) W. Fock, Anal. Chem., 47, 2447 (1975).

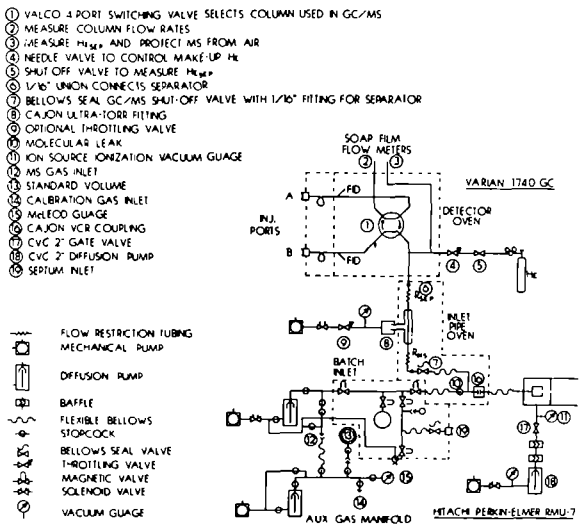

FIG. 1

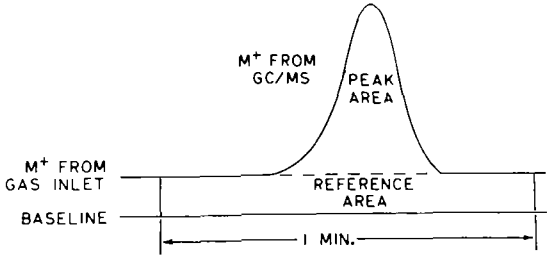

FIG. 2

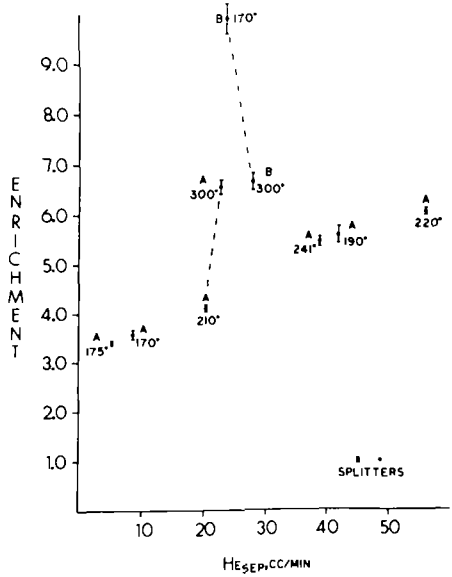

FIG. 3

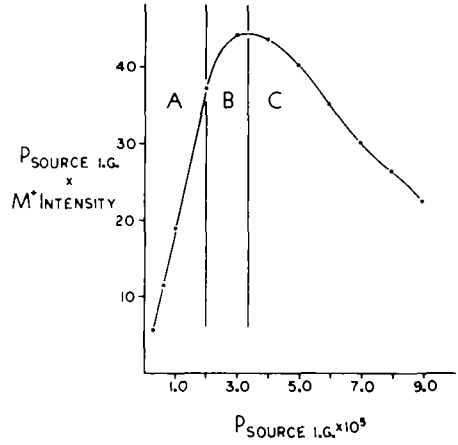

FIG. 4

Studies in GC/CIMS, FRANK HATCH and BURNABY MUNSON, Univ. of Del, Dept. of Chem., Newark, Del 19711.

At an earlier conference a GC/MS interface was described which eliminated the need for a separator and allowed all or part of the effluent from a gas chromatograph to be taken directly into the source of the mass spectrometer.[1] The decrease in ion current of a reactant ion during the course of a gas chromatographic peak can be related simply to the rate constant for reaction of the ion with the added molecules. Relative rate constants can readily be obtained for reactions of an ion with several compounds in a single GC/CIMS experiment. Results for several common CI reactant ions will be reported and compared with available literature data.

[1] F. W. Hatch and B. Munson, Paper C-14 23rd Conference on Mass Spectrometry and Allied Topics, Houston, May 1975.

A Qualitative and Quantitative Comparison of EI Ionization and CI Using Various Reagent Gases.

Rodger L. Foltz and Denis C. K. Lin, Battelle, Columbus Laboratories, Columbus, Ohio 43201

Chemical ionization (CI) is now widely recognized as an extremely useful complement to electron impact (EI) ionization for qualitative analysis. The versatility and sensitivity of CI when used for quantitative analyses are less fully appreciated. In selected ion monitoring the choice of reagent gas can greatly affect the sensitivity and selectivity. In order to provide guidelines for selecting the best mode of ionization for specific analytical tasks we have been comparing both qualitative and quantitative features of CI and EI ionization of a variety of organic compounds. The data presented compare the ion current signals at selected masses generated by injection of the same amount of various drugs into a GC-MS system.

EXPERIMENTAL PROCEDURE

Two quadrupole GC-MS systems were used in the study, one optimized for EI and the other for CI. For each drug we first determined the m/e value most suitable for selected ion monitoring in each of the modes of ionization. We then made repetitive 1 µl-injections of either standard solutions or biological extracts containing known concentrations of the drug and measured the maximum ion current at the selected m/e value. For each series of runs the ion source voltages were adjusted to give the best performance for the particular mode of ionization being used. All other parameters were kept as constant as possible, including the GC conditions, the filament emission, and the electron multiplier gain. The GC-MS interface in the EI system consisted of a Wolen diverter valve and a glass jet separator. The interface in the CI system consisted of a 1/8 inch stainless steel tube and a specially constructed mechanical diverter valve. Comparable relative sensitivities were obtained when the drug samples were introduced via the direct probe inlet, so we are confident that the GC-MS interfaces did not significantly affect the relative sensitivities.

In the CI system the GC carrier gas also served as the CI reagent gas. However, a second reagent gas could be added through a separate inlet into the ion source. Thus, to obtain ammonia-medicated chemical ionization we bled NH_3 into the ion source to give a partial pressure (100 to 300 microns) sufficient to completely suppress the carrier gas ions.

RESULTS

Figure 1 shows spectra obtained for the drug methaqualone. These spectra are fairly typical of most of the drugs we examined. The EI mass spectrum shows a moderately intense molecular ion ($M^{+\cdot}$) and a complex pattern of fragment ions. The methane CI mass spectrum shows an abundant protonated molecule ion (MH^+) as well as alkyl-attachment ions ($M{\cdot}C_2H_5^+$) and a

few fragment ions. Addition of ammonia to the methane reagent gas further simplifies the spectrum so that only a MH^+ peak is seen. Ammonia is a milder reagent gas than methane and causes less fragmentation; that is, transfer of a proton from NH_4^+ to the sample molecule is less exothermic than transfer of a proton from a methane reagent ion to the sample molecule.

Table 1 shows the percent of sample ion current carried by methaqualone ions suitable for selected ion monitoring. Note that the relative response per unit weight of drug follows fairly closely the percent of sample ion current, suggesting that for this drug the efficiency of ionization is nearly the same for all three modes of ionization. However, this is not always the case.

Methadone is a good example of a drug for which CI is clearly preferable to EI. The EI mass spectrum (Figure 2) is dominated by the intense fragment ion at m/e 72, while the $M^{+\cdot}$ is barely detectable. The methane CI mass spectrum shows three major ions: the MH^+ at m/e 310 and fragment ions at m/e 265 and 72. Sometimes it is desirable to monitor two sample ions as an additional check on the occurrence of interfering ions. In these cases the methane CI mass spectrum would be nearly ideal. Addition of ammonia to the methane suppresses fragmentation and increases the response per unit weight of drug by a factor of about 3.

Under EI ionization the $M^{+\cdot}$ is too weak to be useful for selected ion monitoring. On the other hand, the m/e 72 fragment ion gives a very high relative response (Table 2), but is of limited value for selected ion monitoring for two reasons: (1) the chance of interference from other ions at this low mass is very high and (2) if a deuterium-labeled internal standard is used, the deuterium atoms must be attached to carbons retained in the m/e 72 ion structure.

Another drug we have examined is phencyclidine, sometimes called PCP. The internal standard we use has 5 deuterium atoms on the aromatic ring. The EI mass spectrum (Figure 3) shows an abundant ion at m/e 200 resulting from loss of C_3H_7 from the cyclohexyl ring. Consequently, this ion is perfectly satisfactory for selected ion monitoring. Interestingly, in the methane CI mass spectrum the $M^{+\cdot}$ is more intense than the MH^+, suggesting that charge transfer competes effectively with proton transfer when CH_4 is used as the reagent gas. Again, the best sensitivity is achieved with $CH_4 + NH_3$, but the difference in response is less than a factor of 2 over EI (Table 3).

Data for the trimethylsilyl (TMS) ether of Δ^9-THC are shown in Table 4. We normally silylate this drug, primarily to improve its GC characteristics. The $M^{+\cdot}$ at m/e 386 is fairly abundant in the CI mass spectrum (Figure 4). Under methane CI conditions the MH^+ carries a larger percentage of the sample ion current, but the response per unit weight of sample is less than that given by the $M^{+\cdot}$ under EI ionization. Apparently, the Δ^9-THC-TMS is less efficiently ionized under the methane CI conditions than under EI ionization. Once again the best sensitivity is achieved

with CH_4 + NH_3. This was a surprise to us since we did not expect that the Δ^9-THC-TMS would have a sufficiently high proton affinity to be efficiently protonated by NH_4^+.

Table 4 includes data for the reagent gas mixture, N_2 and NH_3. Those who are partial to using N_2 or He as carrier gases can accomplish nearly the same results by simply bleeding a small amount of NH_3 into the ion source along with these gases.

The final example is methamphetamine (Figure 5 and Table 5). Again, we find it advantageous to derivatize the drug. In this case it is converted to the trifluoroacetamide (TFA). Not only does the TFA derivative display better GC behavior, but it also affords ions more suitable for selected ion monitoring. Under EI ionization the highest mass prominent ion occurs at m/e 154. Since we are using a pentadeuterated internal standard with deuterium on carbons retained in this fragment ion, it is a perfectly suitable ion for selected ion monitoring, and in fact, gives a larger response per unit weight of sample than the ions obtained under CI conditions.

Unlike the other examples we have seen, the MH^+ of methamphetamine-TFA is not the largest peak in the methane-ammonia CI mass spectrum. Instead, the most abundant ion corresponds to attachment of NH_4^+ to the drug molecule. This is often the case for compounds which are not basic. Nevertheless, the MNH_4^+ is perfectly satisfactory for selected ion monitoring. In fact, this is an example in which the three methods of ionization each give base peaks at different masses, each of them suitable for selected ion monitoring, thereby providing useful flexibility. If one finds that there is a problem with interfering ions from column bleed or other components of the sample, one can simply change the mode of ionization in order to monitor a different mass.

CONCLUSIONS

Some of the factors which influence sensitivity in selected ion monitoring are: (1) the efficiency with which sample molecules are ionized, (2) the degree to which sample ions are concentrated at a few m/e values, and (3) the degree of interference at the selected ion masses by nonsample ions. If maximum sensitivity is important the mode of ionization should be chosen only after evaluation of each of these factors. For many drugs the highest sensitivity and selectivity is achieved using CI with ammonia as the reagent gas.

ACKNOWLEDGEMENT

This work was supported by the National Institute on Drug Abuse, Contract ADM-45-74-140.

TABLE I RELATIVE RESPONSES FOR PROMINENT IONS IN THE EI AND CI MASS SPECTRA OF METHAQUALONE

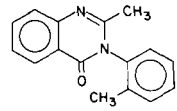

Mol. Wt. = 250

Ionization Method	m/e Monitored	% of Sample Ion Current	Relative Response Per Unit Weight of Drug
EI	250 (M^+)	4	6
	235 (M^+-CH_3)	15	20
CI (CH_4)	251 (MH^+)	57	84
CI (CH_4+NH_3)	251 (MH^+)	74	100

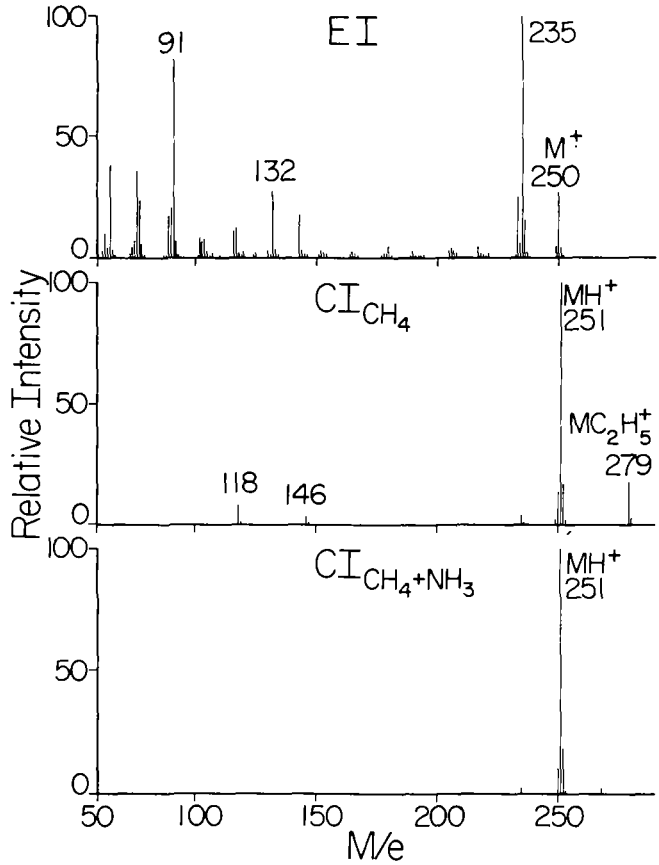

FIGURE 1 MASS SPECTRA OF METHAQUALONE

TABLE 2 RELATIVE RESPONSES FOR PROMINENT IONS IN THE EI AND CI MASS SPECTRA OF METHADONE

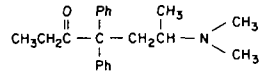

Mol. Wt. = 309

Ionization Method	m/e Monitored	% of Sample Ion Current	Relative Response Per Unit Weight of Drug
EI	309 (M^+)	<0.1	<0.1
	72 ($CH_3CH{=}\overset{+}{N}(CH_3)_2$)	54	750
CI (CH_4)	310 (MH^+)	24	30
CI (CH_4+ NH_3)	310 (MH^+)	76	100

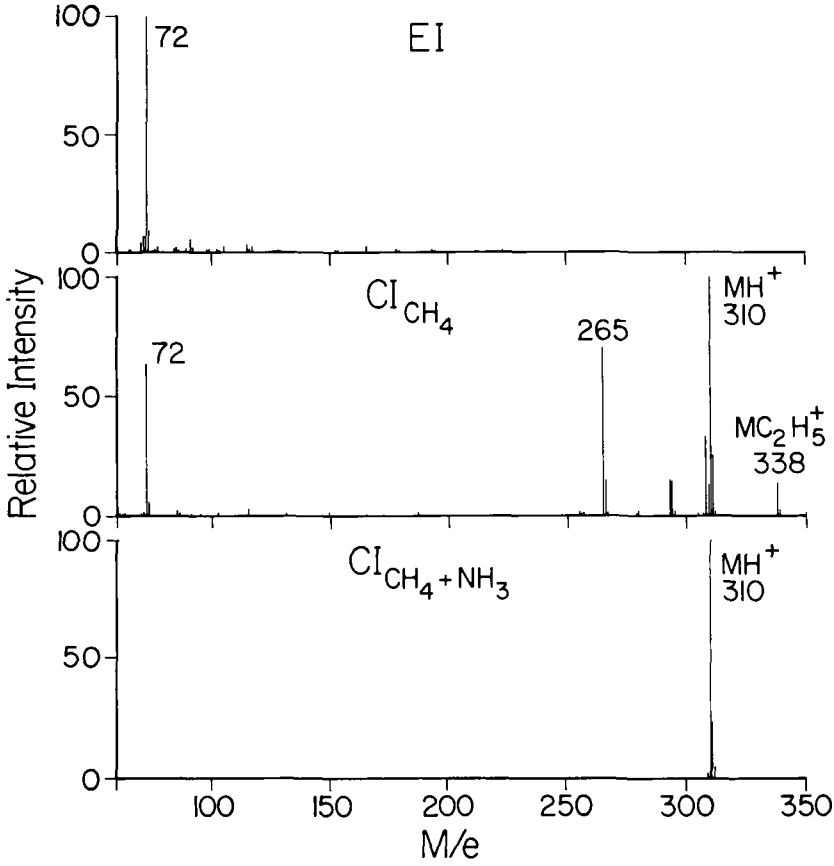

FIGURE 2 MASS SPECTRA OF METHADONE

TABLE 3. RELATIVE RESPONSES FOR PROMINENT IONS IN THE EI AND CI MASS SPECTRA OF PHENCYCLIDINE

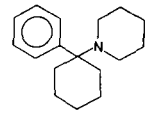

Mol. Wt. = 243

Ionization Method	m/e Monitored	% of Sample Ion Current	Relative Response Per Unit Weight of Drug
EI	200 ($M^+-C_3H_7$)	14	59
CI (CH_4)	243 (M^+)	24	20
CI (CH_4+NH_3)	244 (MH^+)	73	100

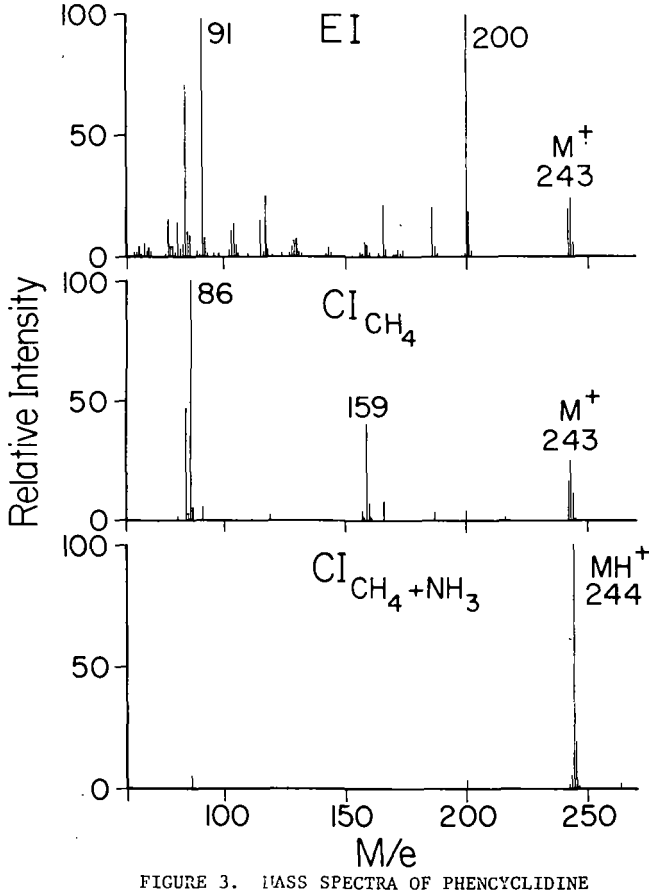

FIGURE 3. MASS SPECTRA OF PHENCYCLIDINE

TABLE 4 RELATIVE RESPONSES FOR PROMINENT IONS IN THE EI AND CI MASS SPECTRA OF THE TRIMETHYLSILYL ETHER OF Δ^9-TETRAHYDROCANNABINOL

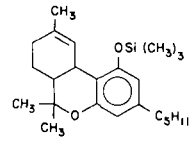

Mol. Wt. = 386

Ionization Method	m/e Monitored	% of Sample Ion Current	Relative Response Per Unit Weight of Δ^9-THC
EI	386 (M^+)	7	50
CI (CH_4)	387 (MH^+)	24	20
CI (CH_4+NH_3)	387 (MH^+)	67	100
CI (N_2+NH_3)	387 (MH^+)	67	80

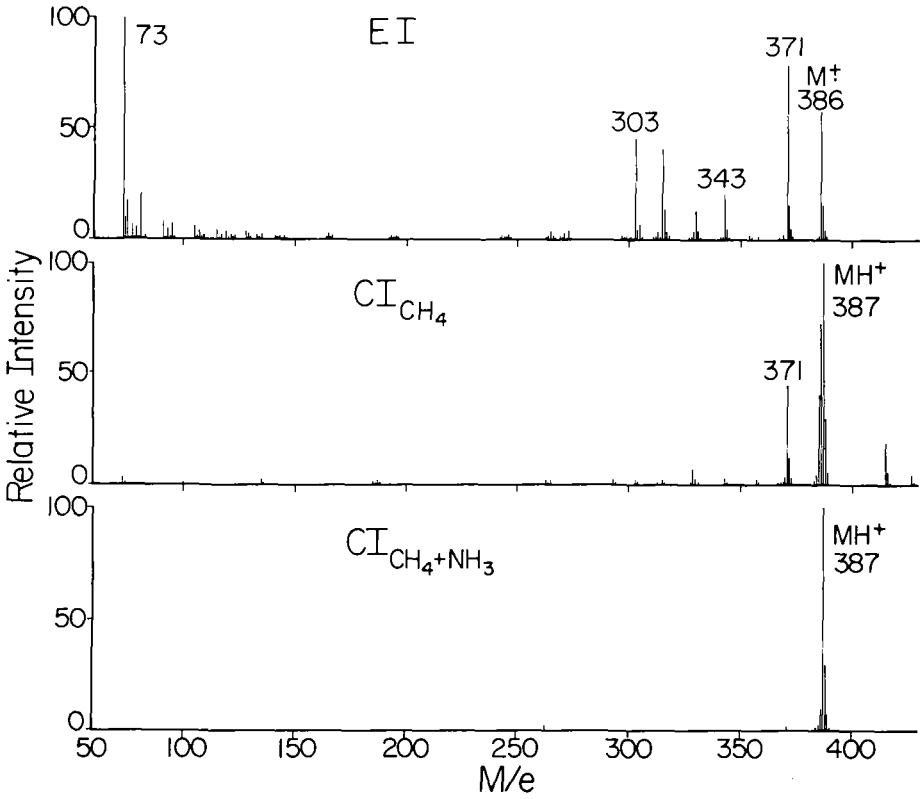

FIGURE 4 MASS SPECTRA OF THE TRIMETHYLSILYL ETHER OF Δ^9-TETRAHYDROCANNABINOL

TABLE 5 RELATIVE RESPONSES FOR PROMINENT IONS IN THE EI AND CI MASS SPECTRA OF THE TRIFLUOROACETAMIDE OF METHAMPHETAMINE

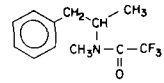

Mol. Wt. = 245

Ionization Method	m/e Monitored	% of Sample Ion Current	Relative Response Per Unit Weight of Drug
EI	154 ($CH_3\overset{+}{N}-\overset{CH-CH_3}{\overset{\|\|}{C}}-\underset{O}{\underset{\|\|}{C}}-CF_3$)	18	100
CI (CH_4)	246 (MH^+)	50	32
CI (CH_4+NH_3)	263 (MNH_4^+)	72	59

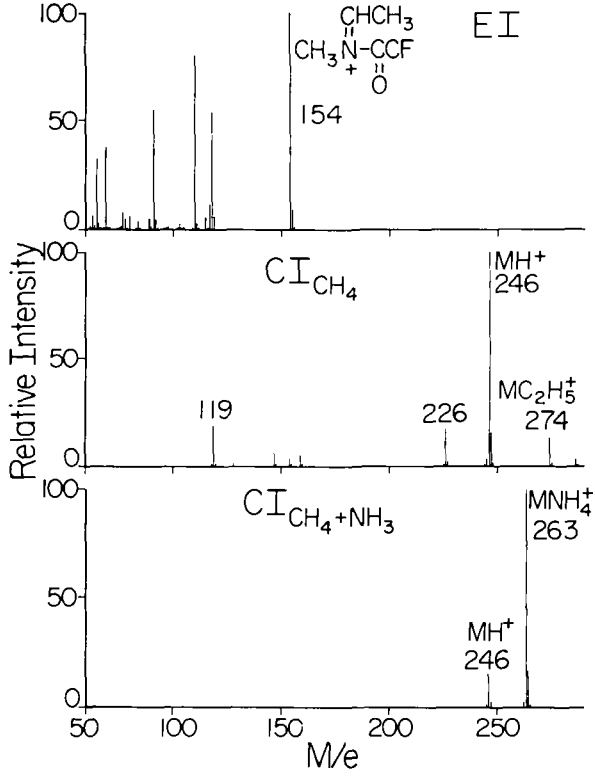

FIGURE 5 MASS SPECTRA OF THE TRIFLUOROACETAMIDE DERIVATIVE OF METHAMPHETAMINE

Alkali Ion Chemical Ionization Mass Spectrometry.

RONALD V. HODGES and J. L. BEAUCHAMP, California Institute of Technology, Dept. of Chem., Pasadena, California 91125.

A major goal in CI mass spectrometry is the production of a molecular or quasi-molecular ion. This can be accomplished by binding a relatively inert reagent ion to the sample molecules. Recent studies in our laboratory suggested that alkali ions would be suitable for this purpose. The binding energies of Li^+ to a variety of compounds have been measured by trapped ion cyclotron resonance techniques and are sufficiently large to permit detection of samples at low concentration. Of the various methodologies explored for obtaining Li^+ CI mass spectra, the most successful involves adding the sample to a large excess of an alkane, such as isobutane. Li^+ initially binds to the alkane and then is transferred to sample molecules in bimolecular reactions.

A Mechanistic Study of the Ammonium Ion in Chemical Ionization Mass Spectrometry. D. JEROLAMON, J. S. SMITH, D. E. SMITH, and E. J. BROZOWSKI, Allied Chemical Corp., CRC, P. O. Box 1021R, Morristown, NJ 07960

While both CH_4 and NH_3 have been used as chemical ionization reagents, a combination of the two producing primarily the NH_4^+ ion has been found to yield significant information in several cases in which the CH_4 or NH_3 alone did not. In an effort to understand the reason for this, an investigation into the mechanisms of proton transfer and ammonium ion addition was undertaken. The nature of the reagent resulting from the combinations: H_2/NH_3, CH_4/NH_3, C_4H_{10}/NH_3, He/NH_3 and N_2/NH_3 was determined as well as the effect of these reagent systems on selected neutral species. Experiments with ND_3 aided in the interpretation of the mechanisms involved.

Quantitative Analysis of Ethylene Glycol Impurities by G.C.-C.I. using Ammonia as the Carrier and Reagent Gas. J. S. SMITH, D. E. SMITH, D. JEROLAMON, and E. J. BROZOWSKI, Allied Chemical Corp., CRC, P. O. Box 1021R, Morristown, NJ 07960

A technique has been developed to detect, identify, and quantify the impurities in virgin and recycled ethylene glycol samples. Utilizing the Finnigan G.C.-C.I.-Computer system we ran ethylene glycol samples with anhydrous ammonia as the G.C. carrier gas as well as the C.I. reagent gas. A two foot Porapak Q G.C. column separated ethylene glycol from propylene, butylene, pentylene glycols and glycerin. Identifications were easily made from the $(M+18)^+$ ion generated from the addition of the ammonium ion to the alcohol. Relative retention time for each impurity was shown by single ion gas chromatogram reconstruction. Quantitative data were obtained by peak area from the reconstructed single ion gas chromatograms and the appropriate use of known compounds. The scope of the method will be discussed. We will include results showing sensitivity and use of single compound monitoring G.C.-C.I.-M.S. for glycerin.

Industrial Applications of Chemical Ionization with the Ammonium Ion. D. E. SMITH, J. S. SMITH, D. JEROLAMON, and E. J. BROZOWSKI, Allied Chemical Corp., CRC, P. O. Box 1021R, Morristown, NJ 07960.

Ammonia has been used as a reagent gas in chemical ionization mass spectrometry for several years. It is not a versatile reagent gas but ammonia has been useful in the analysis of sugar derivatives, amines and some antibiotics. We have found ammonia in methane to be a versatile reagent mixture for probe and G.C. chemical ionization mass spectrometry. Very small amounts of ammonia (ppm level) in methane give predominantly the $NH_4^{\oplus}$ ion with little or no $CH_5^{\oplus}$, $C_2H_5^{\oplus}$ or $C_3H_5^{\oplus}$. This reagent gas system gives $(M+1)^+$ and $(M+18)^+$ ions from compounds that do not give a spectrum in pure ammonia. It also enhances molecular ion identification of compounds that give little or no M+1, M+29 or M+41 in pure methane. We are presently using this reagent gas mixture in combination with pure methane to obtain the maximum amount of information about a sample. We will discuss the scope and uses of this unique methane-ammonia reagent gas for chemical ionization mass spectrometry.

GASEOUS IONIC REACTIONS AND THE PROTON AFFINITY OF NO_2

CHARLES POLLEY and BURNABY MUNSON

Department of Chemistry
University of Delaware
Newark, Delaware 19711

Correlations have been made between ionization potentials and proton affinities of various classes of compounds: as the ionization potentials increase, the proton affinities decrease. NO is anomalous in its behavior when compared with other simple oxygenated compounds: its proton affinity is much lower than the value which is predicted from its low ionization potential. It is possible that this anomalous behavior results from the free radical nature of NO. If so, NO_2 should exhibit a similar anomaly. Consequently, we have determined the proton affinity of NO_2.

Upper and lower limits for $PA(NO_2)$ have been determined by the standard kinetic scheme of observing proton transfer reactions to NO_2 from ionic species with known proton affinities of their conjugate bases and by observing proton transfer from HNO_2^+ to species with known proton affinities. The experiments were done with a Bendix TOF mass spectrometer at pressures of 0.002 to 0.020 torr and at reaction times of 0.5 to 30 usec.

Initial experiments on mixtures of CH_4 and NO_2 showed quite clearly that $PA(CH_4) < PA(NO_2) < PA(C_2H_4)$, since the relative abundance of CH_5^+ passed through a maximum with increasing time and the relative abundance of $C_2H_5^+$ rose to a constant value. Several compounds were compared with NO_2, and the present limits were established by showing that proton transfer occurred from H_2Cl^+ and H_2Br^+ to NO_2 and that HNO_2^+ reacted by proton transfer to CO and C_2H_6. In the course of these experiments, we redetermined the proton affinity of HCl, $PA(CH_4) < PA(HCl) < PA(NO_2)$, and also the proton affinity of HBr, $PA(N_2O) < PA(HBr) < PA(CO)$, as a revision of earlier work (1).

Using the literature values for differences in proton affinities from equilibrium measurements (2), we estimate the following values: PA(HCl) = 133 $\pm$ 2 kcal/mole, PA(HBr) = 137 $\pm$ 2 kcal/mole, and $PA(NO_2)$ = 138 $^{+1}_{-2}$ kcal/mole if $PA(CH_4)$ = 128 kcal/mole (3). However, if the reference value is taken instead to be PA(CO) = 142 kcal/mole (4), then PA(HCl) = 136 $\pm$ 2, PA(HBr) = 140 $\pm$ 2, and $PA(NO_2)$ = 141 $^{+1}_{-2}$ kcal/mole. NO_2, like NO, has a much lower proton affinity than would be expected from a correlation of ionization potentials with proton affinities of other simple oxygenated compounds.

The dominant reaction of most of the protonated species with NO_2 was not simple proton transfer, but rather a more complex reaction which gives NO^+ as the major product ion,

$$H_2X^+ + NO_2 \longrightarrow NO^+ + HX + OH \qquad (1a)$$

$$H_2X^+ + NO_2 \longrightarrow NO^+ + X + H_2O \qquad (1b)$$

The more complex rearrangement reaction, (1b), is more exothermic than the simple dissociative proton transfer reaction, (1a), by 16 - 20 kcal/mole for X = CH_3, Cl, and Br (H_2X^+ = CH_5^+, H_2Cl^+, H_2Br^+). The dissociative proton transfer reaction is endothermic for H_2Br^+ and for H_2Cl^+, and it is only 2 kcal/mole exothermic for CH_5^+. Consequently, we feel that reaction (1b) is the actual pathway.

A formally similar reaction was observed in CH_3F/NO_2 mixtures,

$$CH_2F^+ + NO_2 \longrightarrow NO^+ + HF + CHO. \qquad (2)$$

If the reaction products are assumed to be H_2O and CF, then the reaction is 28 kcal/mole endothermic.

REFERENCES:

(1) M. A. Haney and J. L. Franklin, J. Phys. Chem. 73, 4328 (1969)

(2) D. K. Bohme, "Kinetics and Energetics of Proton Transfer", in Interactions Between Ions and Molecules, Ed. by Pierre Ausloos, Plenum Press, New York, 1974, pp 489-504.

(3) W. A. Chupka and J. Berkowitz, J. Chem. Phys. 54, 4256 (1971)

(4) F. A. Dorman, J. Chem. Phys. 50, 1042 (1969)
A. G. Harrison, J. Chem. Phys. 50, 1043 (1969)
C. S. Matthews and P. Warneck, J. Chem. Phys. 51, 854 (1969)

SIQMS - Secondary Ion Quadrupole Mass Spectrometer

C.W. Magee, W.L. Harrington and R.E. Honig
RCA Laboratories, Princeton, N.J. 08540

The Secondary Ion Quadrupole Mass Spectrometer (SIQMS) described here is the result of an effort to build an instrument for depth profiling by Secondary Ion Mass Spectrometry (SIMS) which would have many of the advantageous features of the small beam ion microprobe machines, but utilizing a somewhat larger primary ion beam in conjunction with a quadrupole mass spectrometer. We have had considerable experience with the CAMECA ion microscope, and we wanted an instrument with comparable sensitivity, depth resolution, mass spectral purity, abundance sensitivity and sputtering rate. We wanted one additional feature not found in the commercially ion microprobes, and that is ultra-high vacuum (1×10^{-8} torr) in the vicinity of the sample during analysis.

The primary ion column of our instrument consists of a colutron ion gun (Colutron Corporation, Boulder, Colo.) capable of producing either argon or cesium ions. The primary ion energy is held down to 5 keV in order to minimize atomic mixing effects in the sample which would degrade depth resolution. The beam is extracted and collimated with an einzel lens and then mass analyzed with a modified Wien filter. The beam is then bent 1° to take out high energy neutrals, and made to pass through a mass defining and differential pumping aperture. The beam is then guided by deflection plates into a second einzel lens which focuses the beam down to a spot from 20 µm @ 100 na to 70 µm at 1200 na. The latter condition results in a current density >25 ma/cm^2 and a sputtering rate in silicon of >1000 Å/sec. The high sputtering rate is in part due to the 60° angle of incidence of the primary ion beam on the sample as can be seen in Figure 1. The static spot is rastered across the sample surface and this reduces the sputtering rate to approximately 20 Å/sec when rastered over a 700 x 700 µm area. This rate allows us to do diffusion profiles in semiconductors to depths of several micrometers in less than one hour.

Alternatively, the two-lens nature of the primary ion column allows us to decrease the current into the objective lens by a factor of 20. This, along with rastering up to our maximum of 1500 x 1500 µm, allows us to sputter at 0.25 Å/sec if very thin films are to be investigated. The ion beam raster unit also includes an independently adjustable electronic aperture to gate out crater edge effects.

The secondary ion optical layout is shown in Figure 2. The secondary ions (either positive or negative) are extracted preferentially from the center 200 micrometers of the rastered crater by a computer designed extraction lens. The ions are then energy analyzed with a 180° spherical electrostatic analyzer. This energy analyzer has a resolution of 4% which allows about a 1.5 eV bandwidth into the quadrupole when working with an extraction potential (V_E) of 35 volts. The spherical geometry also possesses two dimensional directional focusing to maximize transmission. The quadrupole assembly is made by Extranuclear Laboratories, Inc. (Pittsburgh, Pa.) with a rod size of 1.9 cm diameter by 22 cm long, and is driven at 2 MHz with electronics made by UTI (Sunnyvale, CA.) The electron multiplier is a 16-stage focused dynode Cu-Be type with gain greater than 10^7 at 2000 volts applied potential. It is mounted on-axis behind an extraction lens to increase the collection-efficiency for ions transmitted through the quadrupole. This is especially needed for measuring negative ions when the front end of the multiplier is only biased at approximately +900 V. The multiplier is run in a pulse counting mode but an analog output is available simultaneously with the pulse output to measure signals which are too high for the counting electronics to handle. Also associated with the detection electronics is a system for displaying real time ion images on an oscilloscope <u>while</u> depth profiling. The primary use of this system is to get information about the X-Y homogeneity of the profiled species across the sample surface. There have been numerous occasions when, without this capability, grossly erroneous depth profiles would have been recorded.

The entire instrument is made from UHV components. The primary ion gun is differentially pumped with a 1200 ℓ/sec diffusion pump and the target chamber is pumped with a 220 ℓ/sec ion pump and titanium sublimation pump with large ℓN_2 cold wall. The latter two are especially useful when employing an oxygen jet directed at the sample to increase positive secondary ion yields. Cs primary ion bombardment is used to increase negative ion yields. Up to eight samples are mounted on a high precision sample manipulator and are viewed during analysis with a 30X stereo microscope with coaxial illumination normal to the sample surface.

Another very important feature of this instrument is automated instrument control and data collection for multi-element depth profiles. We use a Hewlett-Packard programmable calculator (Model #9830A) to monitor up to six masses with the quadrupole, read the accumulated ion counts from a counter after a preset dwell time on each mass, and process the data at the end of the run and plot the profiles. This is an area where the quadrupole mass spectrometer has an unparalleled advantage over the magnetic sector instrument. Our machine can change 100 amu in less than 10 msec and reproduce peak position to within 0.01 amu with drift of <0.01 amu/hr. The speed and reproducibility of the quadrupole allow data to be taken directly on the peak top (no need to scan over the peak) and, if necessary, all six elements can be measured in less than one second.

Figure 3 shows the importance of sophisticated secondary ion optics. A 150 keV boron implant in silicon was analyzed with 1) static, homogeneous current density primary ion beam, 2) a rastered, focused beam, 3) a rastered beam using only the extraction lens to discriminate against crater edge effects, 4) a rastered beam using the electronic aperture to discriminate against crater edge effects, and 5) using a rastered beam, the electronic aperture and the preferential extraction lens. One can see how high dynamic range in-depth is only possible when using carefully designed ion optics. This preferential extraction is required to discriminate against secondary ions created by processes other than the primary ion bombardment in the rastered crater. In all SIMS instruments there are a large number of reflected primary ions and high energy neutrals which sputter and create secondary ions from lens elements, from the sample holder, and from the sample surface in areas other than the bombarded crater. If the secondary ions created in this manner are not thoroughly discriminated against, they will produce peaks in mass spectrum which can seriously degrade sensitivity and depth resolution.

Figure 4 shows how the UHV sample environment and the secondary ion optics result in a silicon spectrum which is "clean" and does not include large peaks from elements which are not actually in the silicon. Notice the absence of hydrogen, carbon, oxygen, water, sodium, argon and all but the smallest amount of potassium from the spectrum. Also of considerable importance is the absence of silicon oxides from the spectrum.

Figure 5 shows how our SIQMS instrument has sensitivity and depth resolution comparable to those of the commercially available ion microanalyzers. The figure also demonstrates the abundance sensitivity of our instrument, or the ability to measure a very small peak immediately adjacent to a large peak. This profile was taken by monitoring the Al^+ peak at mass 27, 1 amu away from the 92% isotope of silicon at mass 28. The aluminum was followed to a level of 0.2 ppma. Note also the sputtering rate for this analysis of 7.6 Å/sec. This allows us to easily measure diffusion profiles of several micrometers in depth (~20 min/µm) which we are often called upon to do.

Figure 6 is a compilation of depth resolution data from an ASMS Committee VII round-robin series of samples (ANAL. CHEM. <u>45</u>, 398A(1973). The first sample was 1000 Å of Ta_2O_5 on tantalum with a 50 Å thick phosphorus enriched layer buried 500 Å into the oxide. The objects of the analysis were to see how little instrumental broadening of the layer was introduced by the analysis, and to determine the depth of the enriched zone. One can see again that our instrument is comparable to the large ion microanalyzers. The second sample was a 3000 Å thick Ta_2O_5 layer on tantalum with the center 1000 Å of oxide enriched with ^{18}O. The object of this analysis was to measure the concentration of ^{18}O in the enriched layer and to determine the sharpness of the rise of the ^{18}O signal upon reaching the ^{18}O layer and the sharpness of the fall upon sputtering through it into the normal oxide. Again, the interfaces are subject to instrumental broadening effects which result in larger values for the ó rise and ó fall. The data show that our SIQMS instrument introduced less broadening than all of the other instruments. It should also be noted the good vacuum and absence of a water peak at mass 18 allowed us to measure the ^{18}O directly at mass 18 and not indirectly at $Ta^{18}O$ at mass 199 as is necessary on those instruments with poor vacuum in the sample region of the instrument.

As a final note, I would be remiss if I failed to point out that obtaining the performance shown here is not an easy or inexpensive proposition. The mere use of a quadrupole for mass analysis is not an automatic panacea for SIMS instrumentation. It is actually the last ion optical component encountered in the path of primary and secondary ions. If all the necessary measures and precautions are not taken prior to the quadrupole, one cannot expect to obtain performance that is comparable to that of the large ion microanalyzers. We feel that the inexpensive "add-on" quadrupole SIMS systems available today sacrifice too many of the important ion optical considerations needed for high secondary ion collection efficiency (2×10^7 ions/µa sec for $^{30}Si^+$) and for high dynamic range in-depth profiling. For this reason and others of a non-technical nature, we decided to build our own <u>dedicated</u> secondary ion quadrupole mass spectrometer.

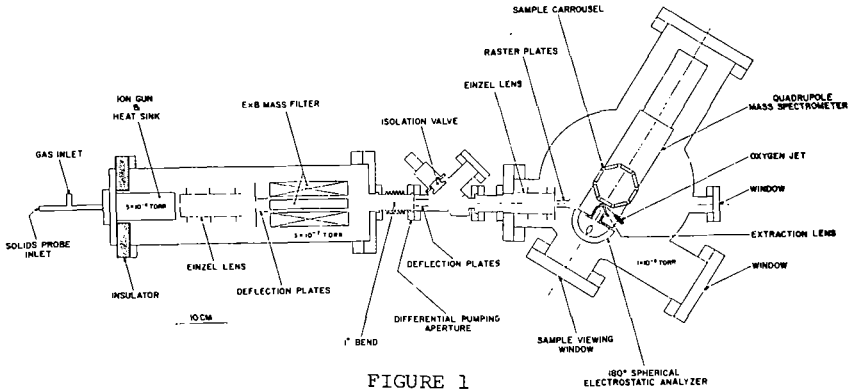

FIGURE 1

LAYOUT OF SECONDARY ION OPTICS

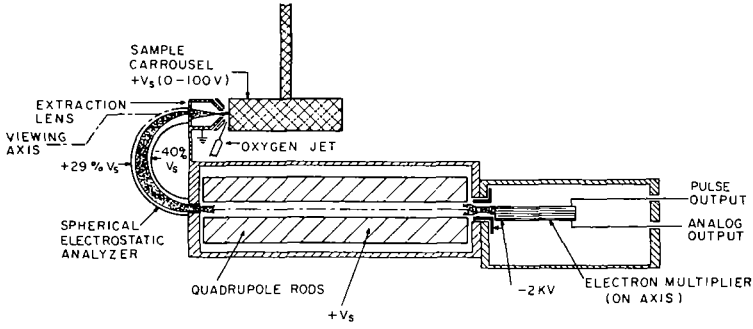

FIGURE 2

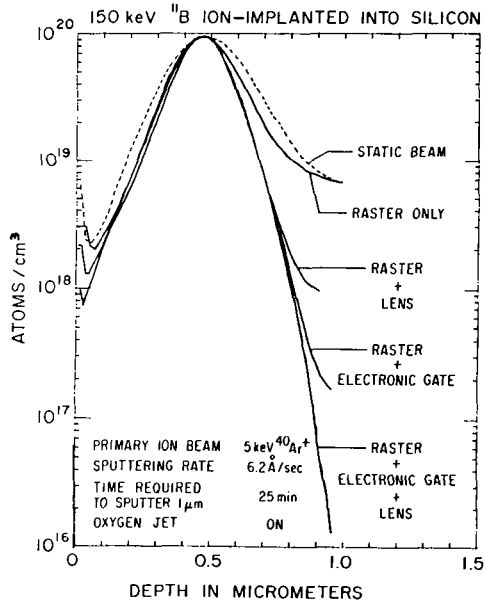

FIGURE 3

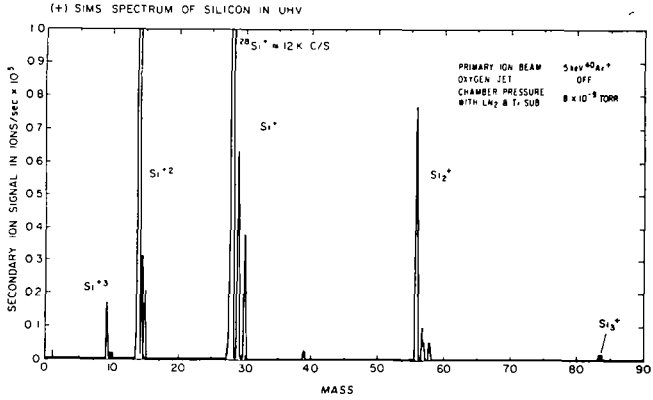

FIGURE 4

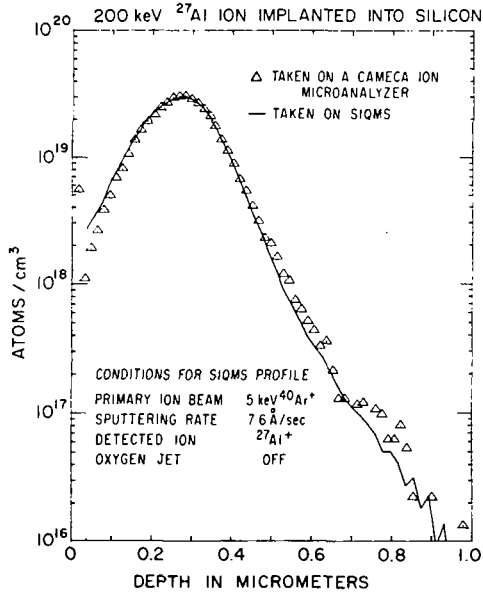

FIGURE 5

ASTM COMMITTEE E41 ROUND ROBIN DEPTH PROFILING RESULTS INCLUDING SIQMS

P IN Ta_2O_5

	SPUTTER RATE Å/min	DEPTH OF P ZONE Å	FWHM	PRIMARY ION	INSTRUMENT
1)	51	500	95.5	5.5 keV $^{16}O_2^+$	CAMECA
2)	210	400	[illegible]	5.5 keV $^{16}O_2^+$	CAMECA
3)	100	490	100	5.5 keV $^{16}O_2^+$	ARL
4)	–	510	100	7.5 keV $^{16}O_2^+$	ARL
5)	75	500	90	5.5 keV $^{16}O_2^+$	CAMECA
6)	264	457	95	5 keV $^{40}Ar^+$	SIQMS

OXYGEN ISOTOPIC GRADIENT

	SPUTTER RATE Å/min	O %	O_{RISE} Å	O_{FALL} Å	PRIMARY ION	INSTRUMENT
1)	282	1.3	185	215	15 keV Ar	
2)	200	2.1	195	255	8.5 keV N_2^+	ARL
3)	–	1.3	210	260	15 keV Ar_2^+	
4)	245	1.5	160	185	5.5 keV Ar^+	CAMECA
5)	268	1.3	170	170	5.0 keV Ar^+	SIQMS

FIGURE 6

Energetics of Formation of $R'CO_2H_2^+$ in the Mass Spectra of $R'CO_2R$. A. G. HARRISON and F. M. BENOIT, Univ. of Toronto, Toronto, Can. and F. P. LOSSING, National Res. Council, Ottawa, Can.

In previous studies of the energetics of (1) in ethyl and propyl esters, to

$$(1)\ R'CO_2R + e \rightarrow R'CO_2H_2^+ + (R\text{-}2H)$$

obtain agreement of $\Delta H_f(R'CO_2H_2^+)$ it was proposed that for propyl esters (R-2H) had the cyclopropyl rather than allyl structure. Using recently established $PA(R'CO_2H)$ it is shown that when $R=C_2H_5$ the threshold for (1) is above $IP(R'CO_2R)$ but when R is propyl the thermochemical threshold, assuming (R-2H)=allyl, is below $IP(R'CO_2R)$. For R=H and CH_3, monoenergetic EI measurements of $AP(R'CO_2H_2^+)$ from propyl esters are in agreement with adiabatic IPs determined by PES, and below the thresholds for cyclopropyl formation. Approximate calculations show that the single H transfer is exothermic and, apparently, occurs without an activation energy, thus providing the excitation energy necessary for the subsequent H transfer and bond cleavage.

Gas Phase Reactions of Metal-Containing Ions in Mixtures of $TiCl_4$ with Alkenes.

John Allison and Douglas P. Ridge
Department of Chemistry
University of Delaware
Newark, Delaware 19711

Titanium has a rich and varied chemistry with organic species. $TiCl_4$, in particular, is important as a catalyst in a number of olefin reactions.

In solution, $TiCl_4$ reacts with virtually any olefin in a unique process:[1]

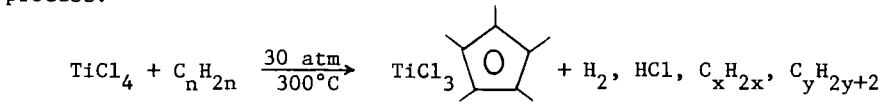

To better understand the interaction of $TiCl_4$ with olefins, we have studied the gas phase ion-molecule reactions of the electron impact fragments of $TiCl_4$ with a series of alkenes. The reaction types observed include (1) elimination of H_2, (2) loss of HCl, (3) elimination of small alkenes, each resulting in the formation of a metal-containing complex.

$$TiCl_n^+ + C_mH_{2m} \rightarrow \begin{cases} TiCl_nC_mH_{2m-2k}^+ + kH_2 & (1) \\ TiCl_{n-1}C_mH_{2m-1}^+ + HCl & (2) \\ TiCl_nC_{m-r}H_{2m-2r}^+ + C_rH_{2r} & (3) \end{cases}$$

Ti^+ and $TiCl^+$ participate almost exclusively in the elimination of H_2, from small olefins such as isobutene and cis-2-butene, giving trimethylene methane and butadiene-metal complexes respectively. We see elimination of two and three H_2's when the reactant alkene contains a five carbon chain. A possible mechanism for loss of two molecules of H_2 from 3-methyl 2-pentene is:

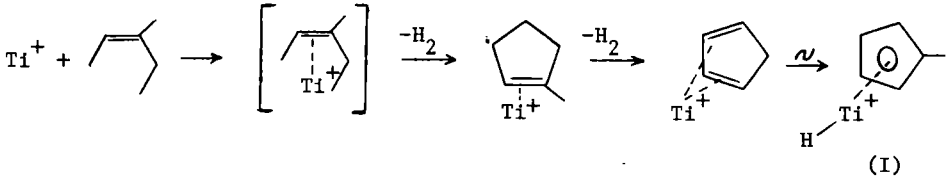

(I)

The ability of metals to form 5-membered rings which can strongly complex with the metal is frequently seen in solution. Evidence for structure (I) is provided by its subsequent reaction:

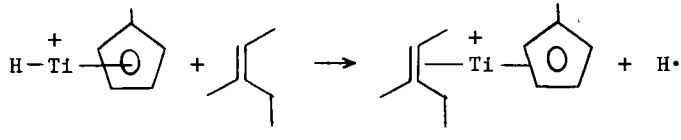

Elimination of three molecules of H_2 from six carbon olefins may result in fulvene or benzene complexes.

The reactions of $TiCl_2^+$ and $TiCl_3^+$ are predominantly HCl and alkene eliminations. HCl elimination probably results in the formation of a 3-electron donor complexed to the metal:

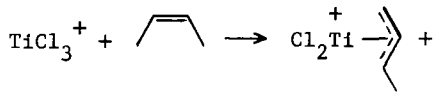

When the reactant alkene is a straight chain, elimination of smaller alkenes are observed with $TiCl_2^+$ and $TiCl_3^+$. Reactions with 1-hexene form propene and ethylene complexes respectively:

$$TiCl_2^+ + 1\text{-}C_6H_{12} \longrightarrow TiCl_2C_3H_6^+ + C_3H_6$$
$$TiCl_3^+ + 1\text{-}C_6H_{12} \longrightarrow TiCl_3C_2H_4^+ + C_4H_8$$

Proposed mechanisms of this C-C cleavage process involve metal-hydrogen bonds, however the final products are metal-olefin complexes. This is indicated by subsequent reactions in which these smaller olefins may be displaced:

$$TiCl_2C_3H_6^+ + 1\text{-}C_6H_{12} \longrightarrow TiCl_2C_6H_{12}^+ + C_3H_6$$
$$TiCl_3C_2H_4^+ + 1\text{-}C_6H_{12} \longrightarrow TiCl_3C_6H_{12}^+ + C_2H_4$$

Butene and pentene eliminations were observed with 2-heptene as the reactant alkene. A mechanism consistent with this involves a 1,3-H shift, through a metal-hydride intermediate.

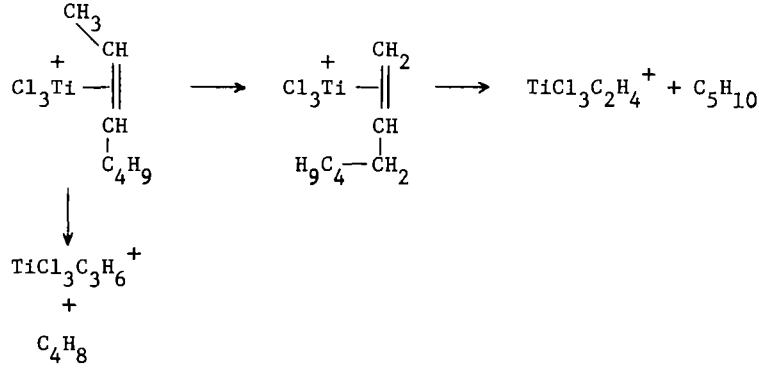

$TiCl_4^+$ was unreactive in all systems studied.

From these results, we see that the $TiCl_n^+$ ions react in specific ways with linear and branched alkenes. These ions may be of use as structural probes for alkenes.

---

[1] H. Roehl, E. Lange, T. Golsal, G. Roth, Angew. Chem., 74, 155 (1962).

The Effects of Methyl Substitution on Negative Ion Stability. JOHN E. BARTMESS and R. T. McIVER, JR., Univ. of Calif., Irvine, Dept. of Chem., Irvine, CA 92717.

The effect of methyl vs. hydrogen substitution on the stability of a variety of negative ions have been investigated by measuring the gas phase acidities of a number of carbon, oxygen, and nitrogen acids using pulsed ion cyclotron resonance spectroscopy. The variation of the methyl effect with the nature of other groups present on the acidic atom will be discussed along with comparisons to solution phase data.

The Gas Phase Acidity Scale. JOHN E. BARTMESS and R. T. McIVER, JR., Univ. of Calif., Irvine, Dept. of Chem., Irvine, Ca., 92717.

Using pulsed ion cyclotron resonance spectroscopy, the relative acidities of a variety of carbon and oxygen acids have been established over a 40 kcal/mole range from H_2O to acetic acid. Structure-reactivity correlations are drawn for several of the series of acids presented, and comparison made to solution phase acidities. Several complete reversals of acidity for given pairs of acids on going from solution to gas phase are discussed.

Relative Stabilities of Carbonium Ions, $(CH_3)_nF_{3-n}C^+$, and Siliconium Ions, $(CH_3)_nF_{3-n}Si^+$, (n = 0-3) in the Gas Phase by Ion Cyclotron Resonance Spectroscopy. M. K. MURPHY and J. L. BEAUCHAMP, California Institute of Technology, Dept. of Chem., Pasadena, California 91125

The fluoride ion transfer reaction

$$(CH_3)_nF_{3-n}Si^+ + (CH_3)_mF_{3-m}CF \rightleftharpoons (CH_3)_mF_{3-m}C^+ + (CH_3)_nF_{3-n}SiF$$

has been examined using trapped ion ICR techniques (where n,m = 0-3) and found to proceed to the right whenever $n \leqslant m+1$. Fluoride affinities ($D\{R^+-F^-\}$, heterolytic bond dissociation energies) of the various siliconium ions are quantified relative to known values for carbonium ion species. In combination with photoionization appearance potential measurements of parent and major fragment ions, these data afford determinations of thermochemical properties (ΔH_f) of the siliconium ions and fluoromethylsilane neutrals. Observed trends are discussed in terms of the effects of methyl- and fluorosubstitution and the silicon-carbon electro-negativity difference.

Li$^+$ Binding Energies by Ion Cyclotron Resonance Spectroscopy.

R. Woodin and J. L. Beauchamp, California Institute of Technology, Dept. of Chem., Pasadena, California 91125

The binding energy of lithium cations to a number of n- and -donor bases has been determined using ion cyclotron resonance spectroscopy. In particular, the Li$^+$ affinities of the series H_2O, CH_3OH, $(CH_3)_2O$ and the methyl substituted amines have been examined in detail. The binding energies are obtained by equilibrium measurements of Li$^+$ transfer between pairs of bases and are in the range 30-40 kcal/mole. The Li$^+$ affinities of the series H_2O, CH_3OH and $(CH_3)_2O$ are found to monotonically increase with methyl substitution. However for the amines an anomoluous ordering is found. These results are interpreted with the aid of ab-initio generalized valence bond calculations for several of the complexes.

Analysis of Ion-Loss Mechanisms in a Magnetic Ion Trap. MICHAEL B. RUGGERA, JR., and R. T. McIVER, JR., Dept. of Chem., Univ. of Calif., Irvine, CA 92717.

Currently, kinetic and equilibrium studies of ion-molecule reactions in pulsed ICR spectrometers are limited to processes in which the ion-loss rate is significantly less than the reaction rate ($k > 10^{-11}$ cm^3 $molecule^{-1}$ sec^{-1}). A random walk model for these ion losses has been constructed. Experiments have been conducted which show the parameters of magnetic field, pressure, etc., to have the predicted effects on ion-loss. Utilization of this theory expands the time range over which equilibrium and rate constant studies can be conducted.

Production of $H_2O^{+\cdot}$ in the Ground Electronic State Using Energy-Resolved Electron Beams.

P. L. Grizzle and S. E. Scheppele, Department of Chemistry, Oklahoma State University, Stillwater, OK 74074.

The ionization of $H_2O(^1A_1)$ leading to $H_2O^{+\cdot}(^2B_1)$ was investigated using energy-resolved electron beams.[1] Figures 1 and 2 present normalized first derivative, $F_T'(IE)$, of the total ionization efficiency, $F_T(IE)$, obtained from a 5-point differentiation[2] of the $F_T(IE)$ curves which were obtained 13 months apart. The first $F_T(IE)$ curve corresponds to 100 sweeps and the second one represents 150 sweeps of F(IE); sector voltages were 15- and 17-V, respectively. The $F_T(IE)$ were not smoothed prior to differentiation. The output of the electrometer for various ionizing energies, the multiplier gain, the measuring time per energy increment, and the number of sweeps of F(IE) were used to calculate the standard deviation at points along each $F_T'(IE)$. These values are represented by error bars in Figures 1 and 2.

Both photoionization[3] and photoelectron spectra[4] show that transitions occur from the (000) vibrational level of $H_2O(^1A_1)$ to the (000), (010), and (100) levels of $H_2O^{+\cdot}(^2B_1)$. The energies of the (010) and (100) states relative to the (000) state are calculated from the experimental vibrational frequencies[4,5] to be 0.175 ± 0.008 and 0.396 ± 0.005 eV. The photoionization efficiency curve also shows structure attributable to autoionization in the regions of the (010) and (100) vibrational states of $H_2O^{+\cdot}(^2B_1)$.[3] Structural details can be observed in Figures 1 and 2 at 0.17 and 0.20-eV, respectively, and at 0.45 ± 0.01-eV above the onset of ionization and are consistent with vibrational excitation of the $H_2O^{+\cdot}$ ion. In addition both Figures indicate the presence of apparent structures in the $F_T'(IE)$ curves between 12.76 and 13.00 eV which may be attributable to autoionization as observed in the photoionization spectrum. However, the total number of ions collected at each value of the electron energy in this region are too few and the electron-energy distribution is insufficiently narrow to provide definitive information. Hence, smooth curves have been drawn through the $F_T'(IE)$ points in this region. Likewise, the limitations imposed by the ion statistics in these experiments preclude drawing conclusions concerning the presence of structure in the $F_T'(IE)$ curves attributable to autoionization above the (100) state. It is important to note that such autoionization could affect the experimental value for the threshold for formation of the (100) state. This conclusion is qualitatively consistent with our ΔE of 0.45- compared to 0.396-eV.

The experimental Franck-Condon factor (FCF) for the (010-000) transition relative to the (000-000) transition is 0.09 by PES[4] and 0.099-0.18 by PI.[3] Figures 1 and 2 yield relative FCF for electron impact of 0.23 and 0.18, respectively. The discrepancy between the relative FCF values obtained from PI, EI, and PES could reflect autoionization in the region of the (010-000) transition. Falloff in the threshold law for formation of the (010) state relative to the (000) state would also produce a lower relative FCF for this state by PES than by either PI or EI because the former technique is measuring the cross sections at energies considerably in excess of their threshold values (8.60 and 8.42 eV for the 000 and 010 states, respectively). The relative FCF for the (100-000) transition is 0.189 by PES[4] and 0.17[3b] and 0.222 ± 0.04[3c] by PI.[6] Figures 1 and 2 yield relative FCF values of 0.26 and 0.19 for electron impact, respectively. The uncertainties in our FCF values are consistent with deviations in the $F_T'(IE)$ curves as calculated from consideration of the ion statistics.

The relative FCF for the (000-000), (010-000), and (100-000) transitions from PES and PI(EI) were multiplied by the function $(V-E_{o,k})$ to generate an F(IE) curve for monoenergetic electrons as a function of the ionizing energy. These F(IE) were then folded into a Gaussian function possessing a FWHM of 80 meV to simulate ionization efficiency curves, $F_S(IE)$, applicable to the experimental apparatus. Figure 3 is the normalized $F_S'(IE)$ curve obtained using the PI relative FCF. The apparent broadening of the electron-energy distribution by differentiation of $F_T(IE)$ or $F_S(IE)$ is ≤ 0.018 eV from the FWHM of $[\partial^2 F_S(IE)/\partial V^2]_{V=12.61}$. Comparison of Figure 3 with Figures 1 and 2 shows that $F_S'(IE)$ generated using relative PI-FCF is in reasonable agreement with the observed $F_T'(IE)$. The shape of the $F_S'(IE)$ curves from *ca.* 12.8 to 13.1 eV does suggest that the occurrence of autoionization in this region would make it difficult to assess the onset of the (100) state of $H_2O^{+\cdot}(^2B_1)$. Normalized $F_T(IE)$ and $F_S(IE)$ curves are reproduced in Figure 4. Correspondence between predicted and experimental IE curves is reasonable. The difference in the curvature near threshold (compare Figures 1 and 2 with Figure 3) is not significantly affected by using a value of 1.1 rather than 1.0 for the value of the exponent in the threshold law for single-direct ionization by electrons. Likewise, increasing the FWHM of the electron-energy distribution did not remove this discrepancy. Such behavior is qualitatively consistent with contributions from transitions occurring from vibrationally-rotationally excited H_2O. The curves in Figures 1 through 4 could be consistent with some contribution of autoionization to the cross section for single direct ionization by electrons possessing energy up to 13.2 eV. These results indicate that the selection rules governing the formation of $H_2O^{+\cdot}(^2B_1)$ are not significantly different for electron impact and photon absorption.

References

1. The authors are indebted to Dr. F. P. Lossing of the National Research Council of Canada, Ottawa, Canada for obtaining the ion efficiency data.
2. A. Savitzky and M. J. E. Golay, *Anal. Chem.*, 36, 1627 (1964).
3. a) V. H. Dibeler, J. A. Walker, and H. M. Rosenstock, *J. Res. Nat. Bur. Stand. (U.S.)*, 70A, 459 (1966); b) B. Brehm, *Z. Naturforsch*, 21A, 196 (1966); c) D. H. Katayama, R. E. Huffman, and C. L. O'Bryan, *J. Chem. Phys.*, 59, 4309 (1973).
4. D. W. Turner, C. Baker, A. D. Baker, and C. R. Brundle, "Molecular Photoelectron Spectroscopy", Wiley-Interscience, New York, N.Y., 1970.
5. R. Botter and H. M. Rosenstock, *J. Res. Nat. Bur. Stand. (U.S.)*, 73A, 313 (1969).
6. Dibeler, Walker, and Rosenstock (Ref. 3a) did not report a value for the relative FCF for the (100-000) transition because of the autoionization structure. The authors in ref. 3c extracted a value of 0.30 ± 0.10 from the data of Dibeler, Walker, and Rosenstock.

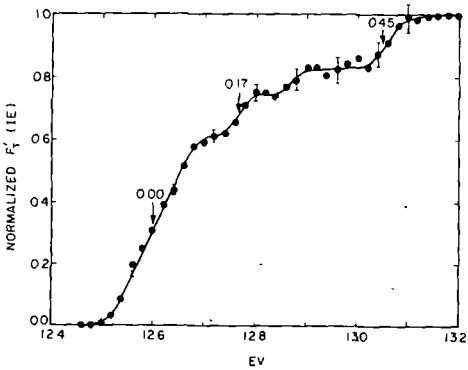

FIGURE 1. FIRST DERIVATIVE OF THE IONIZATION EFFICIENCY FOR FORMATION OF H_2O^+ ($^2B_1$). 15 VOLT ELECTRIC SECTOR.

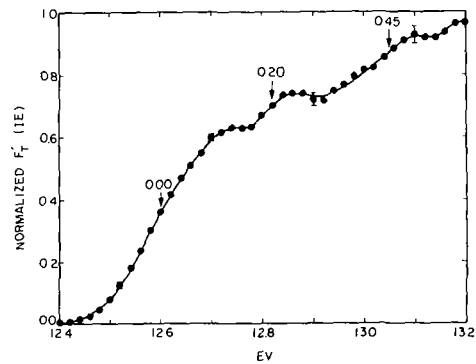

FIGURE 2. FIRST DERIVATIVE OF THE IONIZATION EFFICIENCY FOR FORMATION OF H_2O^+ ($^2B_1$): 17 VOLT ELECTRIC SECTOR.

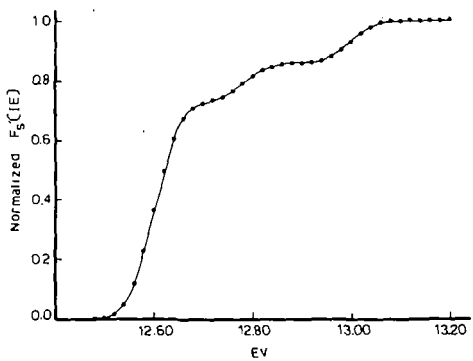

FIGURE 3. SIMULATED FIRST DERIVATIVE OF THE IONIZATION EFFICIENCY CURVE FOR FORMATION OF H_2O^+ ($^2B_1$) USING PI RELATIVE FRANCK-CONDON FACTORS.

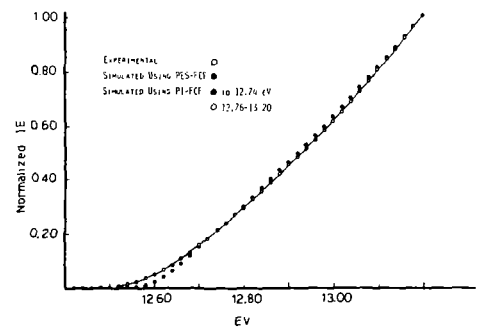

FIGURE 4. EXPERIMENTAL AND SIMULATED ION EFFICIENCY CURVES FOR FORMATION OF H_2O^+ ($^2B_1$).

Photodissociation Study of Parent Ions of Styrene, Cyclooctatetraene and Three C_9H_{10} Hydrocarbons

E. W. Fu and R. C. Dunbar
Department of Chemistry
Case Western Reserve University
Cleveland, Ohio 44106

ABSTRACT

The ICR photodissociation spectroscopy of gas phase ions has been used to approach the difficult problem of differentiating the structures of isomeric ions. The photodissociation study of styrene cations and cyclooctatetraene (COT) cations strongly indicates that these two ions did not rearrange to a common structure on a time scale of seconds. Both styrene cations and COT cations photodissociated according to:

$$C_8H_8^{+\cdot} \xrightarrow{h\nu} C_6H_6^{+\cdot} + C_2H_2$$

The study of three $C_9H_{12}^{+\cdot}$ isomers showed that 1-phenyl-1-propene and 3-phenyl-1-propene molecular ions gave similar spectra while the spectrum of cyclopropyl benzene cations was clearly different. The photodissociation channel for the $C_9H_{10}^{+\cdot}$ isomers was the loss of hydrogen.

CROSSED BEAM TECHNIQUES FOR STUDYING ENERGY TRANSFER PROCESS IN ION-MOLECULE REACTIONS

M.L. Vestal, C.R. Blakley and J.H. Futrell
Department of Chemistry
University of Utah
Salt Lake City, Utah 84112

We have recently developed techniques for applying the crossed beam apparatus[1] to detailed studies of the disposition of available energy in simple ion-molecule reactions. The principal difficulties encountered in attempting to obtain reliable energy distributions in the center-of-mass coordinate frame are due to distortions in the intensity contour maps which are introduced by the apparatus transmission functions and the energy and angular spreads of the reactant beams. By deconvoluting out the contributions that these known distributions make to the observed distributions we can, in principle, obtain more useful results.

The general deconvolution problem consists of measuring some function f(x) which is related to the function h(x) we would like to determine by the integral

$$f(x) = \int_{-\infty}^{\infty} h(x')g(x-x')dx' = h * g \qquad (1)$$

where g(x) is the "apparatus" function which is presumed to be known. The method employed in this work is the Van Cittert solution[2,3] for obtaining an approximate inversion of equation (1). This is accomplished by calculating the functions

$$C_i(x) = f(x) - \int_{-\infty}^{\infty} h_{i-1}(x')\, g\,(x-x')dx' \qquad (2)$$

and the ith estimate of the desired function is given by

$$h_i(x) = h_{i-1}(x) + C_i(x) \qquad (3)$$

The procedure is begun by taking as the zeroth estimate for h(x), the measured function f(x); that is

$$h_o(x) = f(x) \qquad (4)$$

The procedure may be continued until

$$\left|\int_{-\infty}^{\infty} C_i(x)dx\right| \leq \varepsilon \qquad (5)$$

where ε is the maximum acceptable error. As is shown by Wertheim[3] the maximum number of iterations which is useful is limited by noise in the data.

In addition to deconvoluting out the apparatus function this procedure can be extended to removal of distortions introduced by the primary beam distributions. In a crossed beam experiment the total product intensity is

$$I = n_1 n_2 \Delta V v_r \sigma \qquad (6)$$

where I is the product intensity (no./sec), n_1 is the beam 1 density (no./cm^3), n_2 is the beam 2 density (no./cm^3), ΔV in the reaction volume (cm^3), v_r is the relative velocity (cm/sec) and σ is the reaction cross section (cm^2).

For a differential detector accepting products with some laboratory energy, E_L, at an angle, θ, relative to beam one, (in the plane determined by the two beams) the detected intensity is given by

$$I(E_L,\theta) = K \frac{d^3\sigma}{d^2\Omega dE_L} = K\iint v_r \left\{\frac{d^3\sigma}{d^2\omega dE_R}\right\} \left\{\frac{E_L}{E_R}\right\}^{\frac{1}{2}} P_{1,2}(\vec{v}_1,\vec{v}_2) d^3\vec{v}_1 d^3\vec{v}_2 \quad (7)$$

where

$$K = n_1 n_2 \Delta V \quad (8)$$

and E_L,θ are the laboratory energy and angle, respectively, $d^2\Omega$ is the laboratory solid angle element, $d^2\omega$ is the center of mass solid angle element, E_R is the relative energy and $P_{1,2}(\vec{v}_1,\vec{v}_2)$ is the joint density function for $\vec{v}_1$ and $\vec{v}_2$.

If the primary velocities $\vec{v}_1$ and $\vec{v}_2$ were known precisely, then

$$P_{1,2}(\vec{v}_1,\vec{v}_2) = \delta(\vec{v}_1-\vec{v}_1{}^\circ)\,\delta(\vec{v}_2-\vec{v}_2{}^\circ) \quad (9)$$

and

$$\left\{\frac{d^3\sigma}{d^2\omega dE_R}\right\}_\circ = \frac{I}{K}\left\{\frac{E_R}{E_L}\right\}^{\frac{1}{2}} \frac{I^\circ(E_L,\theta)}{v_r^\circ} \quad (10)$$

If we assume $\frac{d^3\sigma}{d^2\omega dE_R}$ is independent of v_r, then

$$I(E_L,\theta)\frac{v_r^\circ}{(E_L)^{\frac{1}{2}}} = \iint I(E_L',\theta')\frac{v_r}{(E_L')^{\frac{1}{2}}} P_{1,2}(\vec{v}_1,\vec{v}_2) d^3\vec{v}_1 d^3\vec{v}_2 \quad (11)$$

where

$$\begin{aligned}\vec{v}_1 &= \vec{v}_1(E_L - E_L', \theta-\theta')\\ \vec{v}_2 &= \vec{v}_2(E_L - E_L', \theta-\theta')\end{aligned} \quad (12)$$

Thus we have a two-dimensional convolution integral of the form

$$f(E_L,\theta) = \iint h(E_L',\theta')\, g(E_L - E_L', \theta-\theta')\, dE_L'\, d\theta' \quad (13)$$

which can be inverted (approximately) by the Van Cittert method.

These deconvolution procedures have recently been applied to the interpretation of crossed-beam data on the endothermic proton transfer retention $H_3^+(Ar,H_2)ArH^+$ and have led to the observation of vibrational structure in the product energy distributions.

References

1. M.L. Vestal, C.R. Blakley, P.W. Ryan and J.H. Futrell, Rev. Sci. Instrum., 47, 15 (1976).
2. P.H. Van Cittert, Z. Phys., 69, 298 (1931).
3. G.K. Wertheim, Rev. Sci. Instrum., 46, 1414 (1975).
4. T.T. Warnock and R.B. Bernstein, J. Chem. Phys., 49, 1878 (1968).

Negative Ions production in CO_2, NO_2 SO_2 and TlCl by electron impact with a high resolution electron beam.

R. ABOUAF, J. P. ZIESEL and F. FIQUET-FAYARD, University of South Paris, Laboratoire de Collisions Electroniques, 91405 ORSAY, France.

The main feature of the present studies is the use of a trochoidal monochromator[1] to produce a quasi-monochromatic electron beam (energy distribution 30 to 60 meV). This good resolution allows us to perform accurate determinations of the appearance potentials, and to identify structures in the ionization efficiency curves. These structures are related to either various electronic or vibrational states of the transitory ions, or to rapid variation of the kinetic energy of the fragments. (to be published in J. Phys. B. Atom. and Molec. Physics)

[1] A. Stamatovic and G. J. Schulz R. S. I. 39 1752 (1968) & 41 423 (1970)

Internal Energy Distribution in the Products of Charge-Transfer Between He^+ and Rare Gases. E. G. JONES, B. M. HUGHES, D. C. FEE and T. O. TIERNAN, Wright State Univ., Dept. of Chem., Dayton, Ohio 45431.

Luminescence arising from impact of 100 eV He^+ ions on rare gases has been analyzed. Cross sections for direct production of individual quantum states have been determined. For the He^+/Xe system identification of the subsequent radiation paths leads to the conclusion that 25% of the observed radiation arises from states populated by cascading rather than direct excitation. The maximum in the internal energy distribution of product Xe^+ states corresponds to the transfer of about 0.5 eV of translational energy to internal energy. The total cross section for exciting radiative states in Xe^+ is 25% of the total charge-transfer cross section. Relative branching ratios of selected states will be compared with their isoelectronic analogues.

EXPERIMENTAL AND THEORETICAL CHARACTERIZATION OF THE $N_2O^-(X^2A')$ POTENTIAL ENERGY SURFACE*

Darrel G. Hopper and Arnold C. Wahl
Argonne National Laboratory, Argonne, Illinois 60439

Richard L. C. Wu and Thomas O. Tiernan
Wright State University, Dayton Ohio 45431

The relationship of the potential energy surface for the X^2A' ground state of the nitrous oxide negative ion N_2O^- to that for the $X^1\Sigma^+(1^1A')$ ground state of the neutral molecule N_2O has been of some concern in recent years(1-13). These molecular systems are interesting in that the possible ionospheric associative detachment reaction

$$O^-(^2P) + N_2(X^1\Sigma_g^+) \rightarrow N_2O(X^1\Sigma^+) + e + 0.21\ eV \qquad (1)$$

is not observable in laboratory experiments conducted at 300°K(2-6, 11,13). The upper bound to the thermal rate coefficient has been placed at about 10^{-12} to 10^{-13} cm^3sec^{-1} by various experimenters(2,3, 5,13). There are conflicting reports of reactivity (11) or a lack of it (13) above 0.3 eV relative collision energy for thermal N_2. The origin of the low thermal rate and an understanding of the possible dynamic hindrance effects of translational excitation (thermal N_2) for this exothermic reaction are determined by the characteristics of the aforementioned potential energy surfaces. The $N_2O^-(X^2A')$ surface connects adiabatically to the reagent asymptote for Reaction (1) and passes in some regions above the $N_2O(X^1\Sigma^+)$ surface (12). Characterization of these potential energy surfaces should also prove useful in predicting the effects of increased vibrational temperature on Reaction (1). Vibrational excitation of nitrogen is common in the ionosphere but has been little investigated in laboratory experiments. Knowledge of the $N_2O^-(X^2A')$ potential energy surface and its relationship to that for $N_2O(X^1\Sigma^+)$ can also contribute to the understanding of other interesting processes, including the recombination reaction

$$O^-(^2P) + N_2(X^1\Sigma_g^+) \xrightarrow{M} N_2O^-(X^2A') \qquad (2)$$

and the dissociative attachment reaction

$$N_2O(X^1\Sigma^+) + e \rightarrow N_2(X^1\Sigma_g^+) + O^-(^2P) - 0.21\ eV\ . \qquad (3)$$

Both experimental and theoretical studies were conducted to characterize the $N_2O^-(X^2A')$ potential energy surface and to relate it to the $N_2O(X^1\Sigma^+)$ surface. The bond dissociation energies and the adiabatic electron affinity were derived from collision-induced dissociation experiments with N_2O^-. Corrections were made for both the dispersion in the ion beam and the translational motion of each target gas. Ab initio multi-configurational self-consistent-field (14) (MCSCF/CI) and other theoretical calculations for $N_2O^-(X^2A')$ yielded the equilibrium geometry, force constants, vibrational frequencies, dipole moment and other properties. The calculations were performed with the BISON-MC computer program system (15). The experiments were made on an in-line tandem mass spectrometer (16,17).

Surface energetic quantities from experiment and surface shape and geometry factors from ab initio calculations were combined in two ways to provide reliable predictions of other quantities of interest. The theoretical potential energy barrier to moving N_2O^- from the ion equilibrium geometry to the neutral equilibrium geometry, ΔE_T^{bend} plus

$\Delta E_T^{contract}$, was combined with the experimental adiabatic electron affinity and the theoretical zero-point energies to predict the value of the vertical electron affinity.

The MCSCF/CI bending potential energy curves for N_2O and N_2O^- over the range 90° to 180° were computed. The latter curves were employed in the combination of the theoretical geometry and surface shape factors with the experimental energy factors. The combination was effected by the use of angular-dependent Morse functions to represent two-dimensional hypersurface cuts $V(R_{AB}, A_{NNO})$. One function $V(R_{AB}, A_{NNO})$ was written for N_2O and one for N_2O^-. The varied bond length was alternatively AB=NN or AB=NO. Then the potential minima were positioned relative to one another according to the vibrationally adjusted adiabatic electron affinity. From this construction the intersection locus of the neutral and negative ion surface representations was obtained. The energy minimum in the intersection locus enables the prediction, after a consideration of zero-point energies, of the activation energies for Reactions (1) and (3).

The results from this study are summarized in Table I. Some of the $N_2O^-(X^2A')$ surface characterizing quantities listed in Table I have been obtained by independent workers; most have not. The best previous value for the adiabatic electron affinity of N_2O was 0.3±0.2 eV (8) compared to the presently reported value of E.A.= 0.22±0.1 eV. The vertical electron affinity of N_2O V.E.A.= -2.23±0.2 eV from the present work is to be compared to the broad feature centered at about 2.2--2.3 eV in the electron scattering spectrum of N_2O (18). The activation energy predicted here for Reaction (3), E_a=0.40±0.1 eV, compares with a value of 0.45±0.02 eV from rate-temperature data (8).

The data from this study have implications for ionospheric chemistry. For instance, Reaction (1) is expected to be thermally very slow due to <u>both</u> the activation energy E_a=0.21±0.1 eV required <u>and</u> the dynamic requirement that the N-N separation at threshold be at least as great as the outter anharmonic turning point of the excited v=1 vibrational state of isolated N_2. Translational excitation of the reagents will remove the first restriction but not the second. Experimental confirmation of this prediction is already at hand: Lindinger et al. (13) report no observable reactivity with thermal nitrogen for collision energies up to 1 eV. Vibrational excitation of reagent N_2 to states with $v \geq 1$ will simultaneously remove both restrictions. Thus, the present work leads also to the prediction of a vibrational enhancement for Reaction (1) at thermal or higher collision energies. Experiments or scattering calculations on the $O^- + N_2(v \geq 1)$ reaction would have to be performed in order to quantitate the predicted enhancement.

A detailed account of the present study will be published elsewhere (19).

REFERENCES

*Research supported in part by the Air Force Office of Scientific Research under Contract F44620-76-C-007 with Wright State University and Contract P7510A with Argonne National Laboratory(USERDA) and supported in part by the Aerospace Research Laboratories, Wright-Patterson AFB, under Contracts F33615-72-M-5015 and MIPR89947400117 with Argonne National Laboratory(USERDA).

1. J. F. Paulson, Adv. Chem. Ser. <u>58</u>, 28(1966).
2. F. C. Fehsenfeld, E. E. Ferguson, and A. L. Schmeltekopf, J. Chem. Phys. <u>45</u>, 1844(1966).
3. F. Kaufman, J. Chem. Phys. <u>46</u>, 2449(1967).
4. E. E. Ferguson, F. C. Fehsenfeld, and A. L. Schmeltekopf, J. Chem. Phys. <u>47</u>, 3085(1967).

5. J. L. Moruzzi, J. W. Ekin, and A. V. Phelps, J. Chem. Phys. 48, 3070(1968).
6. P. J. Chantry, J. Chem. Phys. 51, 3380(1969).
7. J. N. Bardsley, J. Chem. Phys. 51, 3384(1969).
8. W. E. Wentworth, E. Chen, and R. Freeman, J. Chem. Phys. 55, 2075(1971).
9. S. J. Nalley, R. N. Compton, H. C. Schweinler, and V. E. Anderson, J. Chem. Phys. 59, 4125(1973).
10. T. O. Tiernan and R. P. Clow, Adv. Mass. Spect. 6, 295(1974).
11. J. Comer and G. J. Schulz, Phys. Rev. A10, 2100(1974).
12. a. M. Krauss, D. G. Hopper, P. J. Fortune, A. C. Wahl, and T. O. Tiernan, "Potential Energy Surfaces for Air Triatomics. I. Literature Review," ARL(AFSC) TR75-202, Vol.I, June, 1975. Available from NTIS, Springfield VA. 22161.
    b. P. J. Fortune, D. G. Hopper, B. J. Rosenberg, W. B. England, G. Das, A. C. Wahl, and T. O. Tiernan, "Potential Energy Surfaces for Air Triatomics. II. Results of SCF and Preliminary OVC Calculations," ARL(AFSC) TR75-202, Vol.II, June, 1975. Available from NTIS, Springfield VA. 22161.
13. W. Lindinger, D. L. Albritton, F. C. Fehsenfeld, and E. E. Ferguson, J. Chem. Phys. 63, 3238(1975).
14. G. Das and A. C. Wahl, J. Chem. Phys. 56, 1769, 3532(1972).
15. G. Das and A. C. Wahl, "BISON-MC: A FORTRAN Computing System for Multiconfiguration Self-Consistent-Field (MCSCF) Calculations on Atoms, Diatoms, and Polyatoms," Argonne National Laboratory, Technical Report ANL-7955(1972). Available from NTIS, Springfield VA. 22161.
16. T. O. Tiernan and R. E. Marcotte, J. Chem. Phys. 53, 2107(1970).
17. B. M. Hughes and T. O. Tiernan, J. Chem. Phys. 55, 3419(1971).
18. A. Zecca, I. Lazzizzera, M. Krauss, and C. E. Kuyatt, J. Chem. Phys. 61, 4560(1974).
19. D. G. Hopper, A. C. Wahl, R. L. C. Wu, and T. O. Tiernan, "Theoretical and Experimental Studies of the N_2O^- and N_2O Ground State Potential Energy Surfaces. Implications for the $O^- + N_2 \rightarrow N_2O + e$ and Other Processes," manuscript in preparation.

Table I. Summary of the quantities determined in the present study to characterize the $X^2A'(^2//)$ ground state potential energy surface of N_2O^- and to relate it to the $X^1\Sigma^+$ energy surface of N_2O.

X^2A' hypersurface characteristics:

$D(N_2\text{-}O^-)$	0.43±0.1 eV	k_{nn}	11.49±0.4 md/Å
$D(N\text{-}NO^-)$	5.13±0.1 eV	k_{no}	3.83±0.5 md/Å
R^e_{nn}	1.22±0.03 Å	k_{nno}	0.64±0.1 md/Å
R^e_{no}	1.38±0.07 Å	ν_1	912±75 cm^{-1}
A^e_{nno}	132.7±2°	ν_2	555±75 cm^{-1}
μ^{bend}	2.42±0.2 D	ν_3	1666±75 cm^{-1}
ΔE_T	1.10 eV	ε	0.195±0.01 eV
$\Delta E_I^{contract}$	1.40 eV		

Electron affinities: $E.A.(N_2O)=0.22\pm0.1$ eV $V.E.A.(N_2O)=-2.23\pm0.1$ eV

Minimum in the X^2A'--$X^1\Sigma^+(^1A')$ hypersurface intersection:

$V^* - V^e(N_2O^-)$	0.67±0.1 eV	R^*_{nn}	1.18±0.03 Å
A^*_{nno}	154±3°	R^*_{no}	1.28±0.07 Å

Reaction thresholds:

E_a(Rxn.1)	0.21±0.1 eV	E_a(Rxn.3)	0.40±0.1 eV

Author Index

Name	Paper No.
Aberth, W.	G-1, G-4
Abouaf, R.	PSDIII-e
Aczel, T.	V-5
Allison, J.	T-15, PSDII-b
Ampulski, R. S.	K-3
Anbar, M.	G-3, G-4, J-8, P-3, T-1, V-2, PSA-12, PSBII-a, PSBII-h, PSCII-b, PSCIII-b
Andersen, C. A.	M-7
Anderson, J.	PSBII-c
Anderson, P. J.	PSA-10
Anicich, V. G.	Q-11
Appelman, E. H.	O-5
Ast, T.	A-10
Aue, D. H.	T-8, Q-10
Ausloos, P.	T-6, T-7
Baer, T.	O-4
Balle, T.	A-3
Barany, G.	E-8
Baril, M.	M-5
Barker, R. A.	Q-2
Barofsky, D. F.	K-10
Barofsky, E.	K-10
Bates, S. S.	PSBIII-f
Bartmess, J. E.	PSDII-c, PSDII-d,
Bass, L. M.	Q-10
Beauchamp, J. L.	A-13, T-3, T-12, T-14, PSDI-c, PSDII-e, PSDII-f
Beckey, H. D.	K-11, K-12
Beghin, J.	J-12
Beimer, R. G.	H-1
Bekesi, G.	J-5
Bendoraitis, J. C.	V-3
Benoit, F. M.	PSDII-a
Berg, D.	E-1
Bergner, E. A.	F-5
Berkley, R. E.	C-3, PSBI-d
Berkowitz, J.	A-6, O-5
Bernasek, S. L.	PSCII-a
Best, H. T.	V-4
Betowski, L. D.	T-10
Beuhler, R. J.	AA-3
Beynon, J. H.	A-8, A-10
Biemann, K.	P1-1
Bienner, F.	V-3
Bierbaum, V. M.	E-11
Biltz, C.	PSCIII-b
Bishop, H.	PSCIII-d
Blakley, C. R.	Q-4, PSDIII-d
Blaney, P. G.	D-2
Blue, G. D.	Z-11
Bockhoff, F. M.	AA-6
Boettger, H. G.	AA-4
Bohme, D. K.	A-15, T-10, W-5
Bone, L. I.	Q-12
Boshans, R.	PSA-15
Botz, F.	Q-7
Bowen, D. V.	E-8
Bowers, M. T.	Q-1, Q-8, Q-10, T-8
Boyd, R. K.	A-8
Brauman, J. I.	A-12
Brezler, G. L.	D-3
Brooks, C. J.	U-1
Brown, C. L.	W-3, W-4
Brown, F. J.	E-4
Brown, H. L.	G-3
Brown, P.	K-4
Brozowski, E. J.	PSDI-d, PSDI-e,PSDI-f
Bruni, R. J.	PSA-6
Bryant, P. J.	U-5
Buckley, J. A.	S-10
Budde, W. L.	PSBII-d
Bunch, J. E.	C-3, PSBI-d
Bunn, W. W.	PSBI-f
Burke, R. R.	T-9
Burlingame, A. L.	G-1, H-2, S-2
Bursey, J.	C-3, PSBI-d
Bursey, M. M.	A-19
Buttrill, S. E.	Y-1, Y-6, Y-7, Y-15, PSBIII-g
Callis, E. L.	PSCII-e
Campana, J. E.	AA-1
Campbell, I. M.	PSA-16
Carhart, R. E.	D-12
Carlson, G. L.	P-2
Carroll, D. I.	J-6, N-3, PSBIII-f
Cattaneo, S. M.	PSA-9
Cermak, V.	P1-2
Chait, E. M.	H-1
Chan, C. L.	W-4
Chang, J. S.	AA-2
Chang, T.	Y-9
Charles, Jr., H. K.	M-3

Author Index

Name	Paper No.
Charlton, R. C.	R-1, R-3
Chen, A. F. T.	W-3
Chesnavich, W. J.	Q-1
Cho, A. K.	J-3, J-10
Church, F. M.	PSCII-f
Claeys, M.	PSA-7
Cocke, D. L.	Z-12
Cohen, A.	J-9
Colby, B. N.	H-1
Coligan, J. E.	R-8
Colvin, M.	PSA-21
Compson, K. R.	L-2, R-2
Conney, A. H.	J-2
Connolly, V. E.	PSCII-e
Conrad, R. L.	M-7
Conzemius, R. J.	M-10
Cook, Jr., J. C.	C-8, R-4, R-6
Cooks, R. G.	A-10, P-1, R-11
Cooper, W. J.	PSBI-e
Corderman, R. R.	T-12
Corboy, J. F.	M-4
Craig, J. C.	F-10
Cross, R. H.	G-3
Crow, F.	Y-11, AA-5
Cullen, G. W.	M-4
Curtis, Jr., H. M.	PSCI-e
D'Angona, J.	Y-4
Darland, E. J.	O-9
Daughtrey, Jr., E. H.	PSBII-e
Davidson, W. R.	Q-10, T-8
Davis, Jr., G. D.	F-7
Dawkins, B. G.	U-6
Day, R. A.	PSCIII-e
Dayringer, H. E.	D-11
Deane, E. R.	PSBI-f
DeAngelis, M.	T-13
DeCorpo, J. J.	C-1, C-4, PSCII-d
DeJong, A. P.	U-2
Denison, A. B.	O-10
Dennis, Jr., W. H.	PSBI-e
Denson, K. B.	Z-4
DePuy, C. H.	E-11
DeRoos, F. R.	PSCI-g
Desiderio, D. M.	F-2, U-4, PSA-3
Dianico, R. H.	Y-5
Dietrich, M. W.	E-9
Dillard, J. G.	Y-8
Dobberstein, P.	J-1
Dooley, J. E.	V-7
Doty, R. H.	R-10
Dougherty, R. C.	F-5
Downs, J. J.	D-10
Duffield, A. M.	D-5, F-4, PSA-10
Dugger, D. L.	PSCII-b
Dunbar, R. C.	O-6, O-7, PSDIII-c
Dunstan, L. P.	X-2
Dupzyk, R. J.	D-1, PSCII-a
Dyer, R.	J-8, PSA-12
Dymerski, P. P.	O-11, AA-6
Dzidic, I.	J-6, N-3
Eaton, H. G.	C-4
Eaves, G. W.	S-1
Ebert, M.	PSA-7
Echeverria, A. W.	PSCII-a
Eichelberger, J. W.	PSBII-d
Eigendorf, G. K.	G-2
Elwood, T. A.	E-10, PSCI-d
Enke, C. G.	O-9
Eskew, T. J.	Z-8
Evans, S.	L-2, R-2
Everhart, E. T.	F-4, PSA-10
Everhart, W. L.	F-1
Falick, A. M.	G-1, K-5
Fanter, D. L.	PSCI-c
Fassett, J. D.	M-11
Fee, D. C.	PSDIII-f
Fennessey, P. V.	D-8, PSCIII-d
Fenselau, C.	R-9, PSA-21
Ferguson, E. E.	A-18
Ferrer-Correia, A. J.	W-6
Field, F. H.	A-17, E-8, T-2
Fies, W. J.	L-3
Fife, W. K.	J-12
Finkle, B. S.	B-1, R-5
Fiquet-Fayard, F.	PSDIII-e
Flamm, B. L.	J-3
Flynn, N. W.	PSA-17
Folk, T. L.	PSCI-h
Foltz, R. L.	PSA-9, PSDI-b
Fralick, R. D.	M-7
Franchetti, V.	A-10, P-1
Frank, H.	U-4
Franklin, J. L.	T-11, W-1
Freed, C. R.	F-6
Freiser, B. S.	T-14
French, J. B.	S-10
Fri, C. G.	Z-5

Author Index

Name	Paper No.
Friedman, L.	S-7, Y-3, AA-3
Friesen, R. D.	D-1, PSCII-a
Frisch, M. A.	PSCI-b
Fu, E. W.	PSDIII-c
Futrell, J. H.	E-10, Q-4, Q-9, Q-11, PSBII-f, PSCI-d, PSDIII-d
Futrell, T. L.	PSBIII-e
Gaffney, J. S.	Y-3
Gal, J.	J-3, J-10
Gallegos, E. J.	PSBIII-b
Games, D. E.	K-8
Games, L. M.	C-9
Gan, O. H. M.	U-5
Garland, W. A.	J-2
Garner, E. L.	X-2
Gaskell, S. J.	U-1
Gaumann, T.	K-5, R-5
Geiger, D. L.	S-3
Gerber, N.	J-12
Giffin, C. E.	AA-4
Gillies, C. W.	K-2
Gingerich, K. A.	Z-12
Goff, S. D.	PSCI-f
Gonser, G.	PSA-12
Gould, R. K.	S-12
Gower, J. L.	K-8
Graham, R. A.	D-7
Gramlich, J. W.	X-1
Grayson, M. A.	PSCI-c
Green, D. E.	F-9
Green, M. M.	E-4
Greene, F. T.	Z-6
Greenwood, G. J.	V-6
Gregory, M. C.	PSBIII-d
Grigsby, R. D.	PSA-1
Grimm, F. A.	A-1
Grinberg, B. M.	D-2
Grizzle, P. L.	V-6, PSDIII-b
Groos, M. L.	E-12, PSCI-g
Gruber, Jr., C. M.	B-3
Gruenke, L. D.	F-10
Gutshall, P. L.	U-5
Haas, B.	PSBI-f
Haddon, W. F.	PSBII-g
Haegele, K.	E-5, J-11, N-3, U-4, PSA-19
Hagge, D. E.	C-2, D-2, R-1, PSBIII-b
Hagstrum, H. D.	P1-3
Haney, M. A.	B-2
Haraguchi, S.	U-3
Harless, R. L.	PSBI-g
Harrington, W. L.	M-4, PSDI-h
Harrison, A. G.	O-11, W-6, PSBI-a, PSDII-a
Harrison, W. W.	M-6
Hartmann, H.	Y-12
Harvey, T. M.	Y-2, PSBI-h
Hatch, F.	PSDI-a
Hayes, J. M.	N-4, Z-4
Hazelby, D.	L-2, R-2
Heck, H.	PSA-12
Heckel, E. F.	Q-7
Held, R.	K-10
Henchman, M. J.	Q-5
Hendricks, L.	A-10
Henion, J. D.	S-6
Herold, D. A.	E-10
Heron, E. J.	B-4, L-3
Hertz, H. S.	J-9
Herzog, L. F.	Z-8
Hickman, W. M.	P-2
High, J. B.	D-10
Hildenbrand, D. L.	A-5
Hileman, F. D.	PSBII-f, PSCI-d
Hinthorne, J. R.	M-7
Hiraoka, K.	A-16, T-5
Hites, R. A.	C-9
Hodges, R. V.	PSDI-c
Hodshon, B. J.	J-3
Holler, J. S.	K-4
Holme, A. E.	L-2
Holmes, S. A.	V-7
Homes, W. F.	PSBIII-a
Honig, R. E.	PSDI-h
Hopkinson, A. J.	D-9
Hooper, D. G.	PSDIII-g
Horning, E. C.	J-6, N-3, U-7
Horning, M. G.	J-4, J-11, U-7, PSA-19, PSA-20
Horvath, Z.	T-6
Hsiao, K. C.	J-2
Hsu, C. S.	A-10
Huggins, G. R.	R-10
Hughes, B. M.	Q-6, PSDIII-f

Author Index

Name	Paper No.
Hunt, D. F.	Y-2, Y-11, AA-5
Hunter, R. L.	PSA-18, PSCIII-a
Huntress, W. T.	Q-8, Q-11
Ige, J.	Q-5
Inghram, M. G.	O-3
Inoue, Y.	U-3
Issachar, D.	F-3
Jacobs, M. L.	X-4
Jardine, I.	PSA-21
Jeden, D. J.	D-6
Jelus, B. L.	PSCI-f
Jenkins, J. R.	PSBIII-f
Jennings, K. R.	Q-8, W-6
Jennison, T. A.	R-5
Jerolamon, D.	PSDI-d, PSDI-e PSDI-f
Johnson, B. M.	PSA-8
Johnson, W. H.	L-1
Jones, E. G.	Q-6, PSDIII-f
Judson, C. M.	Z-1
Jurs, P. C.	H-3, AA-1
Jungclaus, G.	C-9
Kan, K. L.	R-3
Kane-Maguire, L. A.	K-8
Karasek, F. W.	H-4
Karnofsky, J. R.	PSBIII-b
Katoh, Y.	S-2
Kebarle, P.	A-16, T-4, T-5
Keberle, H.	PSA-20
Kemp, D. L.	A-10
Kempster, E.	V-2
Kenan, Jr., W. R.	A-19, O-4
Keough, T.	A-10
Kerfoot, E. G.	X-4
Kimble, B. J.	H-2
Kinast, O. E.	E-9
King, J. D.	PSBII-c
Kingcade, J. E.	Z-12
Kinser, R. D.	T-13
Kleckner, J. E.	T-3
Klein, P. D.	R-12, PSA-13
Kleineberg, G. A.	S-3
Kleopfer, R. D.	PSBI-f
Klots, C. E.	O-1
Knox, J. M.	O-10
Knudsen, T.	Y-2
Kodera, K.	AA-2
Koenig, T.	A-3
Kondrat, R.	A-10
Koppel, C.	AA-6
Krause, M. O.	A-9
Kronberg, J. E.	Y-13
Kronebusch, P. L.	O-9
Kruger, T. L.	A-10, R-11
Kuczkowski, R. L.	K-2
Kuehl, D. W.	PSBI-c
Kuhara, T.	U-3
Kwolek, W. F.	F-1
Laframboise, J. G.	AA-2
Laird, M. H.	PSA-15
Lambrecht, J.	Y-11
Lanphear, S. P.	PSA-8
Lao, R. C.	C-5
Lattimer, R. P.	U-8
Lau, P. Y.	R-3
Lau, Y. K.	T-4
Laudenslager, J. B.	O-2
Lawless, J. G.	PSCII-f
Layton, S. F.	K-7, K-9
Leclercq, P. A.	U-2
Ledford, Jr., E. B.	L-4, N-1, PSA-18, PSCIII-a
Lee, H. J.	PSA-5
Lee, M. L.	C-9
Lehman, J. P.	PSCIII-e
Leroi, G. E.	O-9
Leung, K.	PSA-3
Levsen, K.	E-6, K-6
Levy, R. L.	PSCI-c
Leys, J. A.	M-2
Lias, S. G.	T-6, T-7
Liebl, H.	M-6
Ligon, Jr., W. V.	C-6, E-7
Lin, D. C. K.	PSA-9. PSDI-b
Lin, P. H.	E-12
Lin, S. N.	U-7
Lineberger, W. C.	A-11
Linnell, L.	R-3
Little, A. D.	PSA-6
Litton, J. F.	A-10, R-11
Lossing, F. P.	A-4, PSDII-a
Lower, Jr., G. M.	PSA-8
Lumpkin, H. E.	V-5
Macfarlane, R. D.	N-2
Mach, M. H.	B-5
Mackay, G. I.	A-15, T-10, W-5

Author Index

Name	Paper No.
Magee, C. W.	M-4, PSDI-h
Mains, G. J.	Z-3, PSCI-a
Maloney, K.	PSA-12
Mandelbaum, A.	E-2
Mangner, T. J.	E-4
Mappes, G. W.	E-9
Marcus, A. B.	V-4
Margrave, J. L.	W-1
Markey, S. P.	PSA-7
Marriott, T. D.	V-6
Marshall, D. J.	K-1
Martinsen, D. P.	Y-6, Y-7
Matsumoto, I.	U-3
Matthews, D. E.	N-4
Maurer, K. H.	J-7
May, C. A.	PSCII-a
McCulloh, K. E.	A-2
McDowell, C. A.	G-2
McDowell, R. A.	R-2
McEwen, C. N.	K-7, K-9
McFadden, W. H.	S-5
McIver, Jr., R. T.	A-14, L-4, N-1, PSA-18, PSCIII-a, PSDII-c, PSDII-d, PSDII-g
McLafferty, F. W.	D-11, U-6, AA-6
McReynolds, J.	G-4, PSA-12
Medved, M.	A-10
Meier, S.	S-9
Meisels, G. G.	Q-7
Meot-Ner, M.	T-2
Merrifield, R. B.	E-8
Merritt, Jr., C.	D-7
Middleditch, B. S.	F-8
Milberg, R. M.	C-8
Miller, C. D.	H-5
Miller, J. S.	A-14
Miller, W. J.	S-12
Mintz, D. M.	O-4
Mitchum, R. K.	W-6
Monder, C.	PSA-5
Moody, J. R.	X-3
Morris, H. R.	R-2
Morrison, G. H.	M-9, M-11
Moskowitz, A. H.	T-13
Munk, M. E.	K-4
Munson, B.	PSDI-a, PSDI-g
Murphy, M. K.	PSDII-e
Murphy, R. C.	F-6, PSA-11
Muschik, G. M.	PSA-4
Narasimhachari, N.	F-9
Naworal, J. D.	PSA-16
Neilson, P.	Q-10
Newbury, R. S.	Z-10
Niu, C. H.	U-5
Noda, T.	S-2
Norberg, P. D.	PSBIII-a
Norman, E. J.	PSA-1
Norris, D. D.	AA-4
Nowlin, J.	J-4, PSA-19
Nulton, C. P.	PSA-16
Oblas, D. W.	PSCII-b
Occolowitz, J. L.	E-1
Olson, K. L.	R-4, R-6
Olson, R.	Y-15, PSBIII-g
Onuska, F. I.	PSBI-a
Orth, R.	O-6
Oswald, E. O.	PSBI-g, PSBII-b
Pabst, M. J. K.	T-11
Pabst, R. E.	W-1
Packman, P.	PSA-15
Pantuck, E. J.	J-2
Patterson, D. G.	K-4
Paulsen, P. J.	X-3
Paulson, J. F.	O-8
Pausch, J. B.	U-8
Payzant, J. D.	W-5
Pellizzari, E. D.	C-3, PSBI-d
Pelster, D. R.	PSBIII-c
Pereira, W. E.	F-4, PSA-10
Perreira, N. B.	V-6
Perry, D. L.	F-2
Petersen, B. A.	K-1
Petterson, D. W.	N-4
Petty, F.	PSA-17
Phillips, J. M.	O-10
Pierce, R. C.	S-7, Y-3
Pintauro, C.	J-3
Polley, C.	PSDI-g
Poon, C. C.	S-10
Powers, K.	PSA-7
Powers, P.	D-9
Prater, T. J.	PSBI-h
Prescott, S. R.	H-3
Preti, G.	R-10

Author Index

Name	Paper No.
Pritchard, D. G.	R-8
Price, P.	Y-1
Profous, Z. C.	Y-12
Pyper, J. W.	PSCII-a
Quilliam, M. A.	E-3
Quinn, C. B.	E-7
Rao, G. N. S.	R-3
Rapp, U.	J-7, S-9
Ray, G. W.	O-9
Reeher, J. R.	S-1, S-8
Refaey, K. M. A.	W-2
Reid, N. M.	S-10
Reinhold, V. N.	PSA-6
Rhyne, T. C.	Y-8
Richardson, J. S.	PSA-1
Ridge, D. P.	O-2, T-13, T-15, Y-5, PSDII-b
Riess, W.	PSA-20
Riggin, M.	O-6
Rindfleisch, T. C.	D-5, F-4, PSA-10
Rinehart, Jr., K. L.	R-4, R-6
Risby, T. H.	H-3, AA-1
Robertson, D. H.	D-7
Robinson, J. D.	D-9
Roboz, J.	J-5, PSA-5
Rohwedder, W. K.	F-1
Rolinski, E. J.	Z-11
Roth, J. R.	M-1
Ruggera, Jr., M. B.	PSDII-g
Russell, D. H.	E-12
Russell, J. W.	AA-5
Ryba, R.	Z-3, PSCI-a
Saalfeld, F. E.	C-1, C-4, PSCII-d
St. John, G. A.	V-2, PSBII-h, PSCII-h, PSCIII-b
Satkiewicz, F. G.	M-3
Schaffer, R.	J-9
Scheifler, R. W.	PSBIII-a
Scheppele, S.	V-6, PSDIII-b
Schiebel, H. M.	R-7
Schneider, J. F.	PSA-13
Schnitzer, R.	P-3, T-1
Schnute, Jr., W. C.	R-8
Schoeller, D. A.	R-12, PSA-13
Schroer, J. A.	PSA-4
Schubert, R.	PSCI-i
Schuetzle, D.	C-2, PSBI-h
Schulten, H. R.	K-11, K-12, R-7
Schwartz, H. L.	S-5
Schweizer, E. E.	PSCI-f
Scilla, G. J.	M-9
Scolnick, M. E.	D-4, J-8, V-2, PSBII-a
Scott, A. C.	PSBII-a
Scott, E.	H-2
Scott, R. B.	K-4
Serrone, M. J.	D-10
Shapiro, R. H.	E-11
Sharkey, Jr., A. G.	V-1
Sharp, J.	PSCIII-d
Sharvit, J.	E-2
Shen, J.	S-4
Sherman, W. R.	L-3, PSA-14, PSA-15
Shieh, J. J.	PSA-3
Shuman, W. R.	PSA-15
Siegel, M. W.	S-11, Z-2
Siegenthaler, K. E.	Q-6
Sivakoff, S.	J-5
Skinner, R. F.	B-4
Smit, A. L. C.	E-8
Smit, A. L. C.	U-2
Smith, D. E.	C-4, PSDI-d, PSDI-e, PSDI-f
Smith, D. H.	D-12
Smith, D. L.	PSBII-f
Smith, J. S.	PSDI-d, PSDI-e, PSDI-f
Smith, R. D.	E-10, Q-9, S-8, PSCII-d
Smith, R. G.	F-7
Smolinsky, G.	Y-4
Snell, W.	A-3
Sofer, Z.	N-4
Solomons, N. W.	PSA-13
Sommer, K. R.	PSA-19
Sparrow, G. R.	M-1, M-2
Sperry, R.	PSA-12
Spigarelli, J. L.	D-10
Stafford, G. C.	AA-5
Stafford, M.	E-5, PSA-19
Staley, R. H.	T-3, T-14
Stefik, M. J.	D-5
Stein, J. D.	PSBIII-d
Steinborn, J. A.	O-6
Stevie, F. A.	Z-9
Stewart, J. H.	E-11
Stewart, J. T.	J-11
Stillwell, R. N.	J-6, N-3, PSBIII-f
Stillwell, W. G.	J-11, PSA-20

Author Index

Name	Paper No.
Stockbauer, R.	O-3
Stoffels, J. J.	Z-7
Stone, J. A.	Y-13
Storms, H. A.	PSBIII-d
Story, M. S.	S-8
Sturm, Jr., G. P.	V-7
Su, L.	Q-12
Su, T.	Q-10
Summers, A. W.	PSCII-e
Sun, T.	J-9
Suzuki, R.	J-5
Svec, H. J.	M-10
Sweeney, G.	M-8
Sweeney, S. L.	X-4
Swofford, Jr., H. S.	Y-1
Taft, R. W.	A-20
Takekoshi, T.	E-7
Tan, H. S.	T-11
Tanaka, K.	T-10, W-5
Tang, S. Y.	Z-11
Taylor, M. L.	H-5
Taylor, S. P.	Z-4
Taylor, T.	S-2
Theard, L. P.	O-2
Thenot, J. P.	E-5, PSA-19
Thomas, R.	T-9
Thomas, R. S.	C-5
Thomas, T. F.	O-8
Thompson, J. A.	D-8
Thompson, R. M.	J-12
Tiernan, T. O.	H-5, Q-6, PSDIII-f PSDIII-g
Tissot, B.	V-3
Todd, C. W.	R-8
Tolman, L. F.	PSCII-a
Torgerson, D. F.	N-2
Tully, F. P.	O-9
Turner, S. P.	E-4
Twelves, R. B.	PSCI-e
Upham, R. A.	PSCIII-c
Urban, W. G.	D-8
Valentine, J. L.	U-5
Vallerand, P.	M-5
Van de Graaf, B.	AA-6
VandenHeuvel, W. J. A.	PSA-2
Vasile, M. J.	Y-14, Z-9
Veith, G. D.	PSBI-c
Venkataraghavan, R.	D-11, U-6
Vestal, M. L.	Q-4, PSDIII-d
Vogh, J. W.	V-7
Vogler, E.	N-4
Voorhees, K. J.	PSCI-d
Vouros, P.	F-9, K-1
Wachs, T.	AA-6
Wahl, A. C.	PSDIII-g
Wahraftig , A. L.	A-7
Wallington, M. J.	D-9
Walls, F. C.	H-2
Wanczek, K. P.	Y-12
Wander, J. D.	PSA-17
Wang, C. C.	PSA-2
Watkins, J. B.	PSA-13
Watson, J. T.	PSBIII-c
Weber, J. H.	O-10, V-8
Weddle, G. H.	Y-8
Weinkam, R. J.	Y-4
Weiss, M. J.	O-5
Weissdorf, M.	E-2
Welch, K. R.	U-8
Weppelman, R. M.	PSA-2
Westmore, J. B.	E-3
Widemann, L. G.	PSCI-h
Wiecko, J.	PSA-14
Wilder, J. T.	G-1
Williams, Jr., C. H.	C-7
Williams, F. W.	C-4
Williamson, A. D.	Q-3
White, V. E.	PSCII-g
Wolen, R. L.	B-3
Wolf, C. J.	PSCI-c
Wolf, D. J.	F-1
Wolstenholme, W. A.	J-1, J-7, S-9
Wood, G.	Z-1
Wood, G. W.	R-1, R-3
Wood, J. G.	PSA-17
Woodin, R.	PSDII-f
Woodward, P. W.	V-7
Wright, J.	J-10
Wright, L. H.	PSA-14
Wu, R. L. C.	H-5, PSDIII-g
Wyatt, J. R.	C-1, C-4, PSCII-d
Yeager, P.	Z-1
Yinon, J.	F-3, Y-10
Zielinski, Jr., W. L.	PSA-4
Ziesel, J. P.	PSDIII- e
Zirrolli, J. A.	PSA-11
Zitrin, S.	Y-10
Zune, A.	J-1, J-7

ASTM COMMITTEE E-14 AND

THE AMERICAN SOCIETY FOR MASS SPECTROMETRY

OFFICERS

Year	President	Vice President Programs	Vice President Arrangements	Vice President Data & Stds.
		ASTM E-14		
1961-2	V. H. Dibeler	R. E. Fox	R. A. Brown	-
1963-4	R. E. Fox	N. D. Coggeshall	A. G. Sharkey	-
1965-6	N. D. Coggeshall	H. M. Rosenstock	M. K. Testerman	-
1967-8	H. M. Rosenstock	J. L. Franklin	D. B. Harrington	-
1968-9	J. L. Franklin	R. E. Honig	C. E. Johannsen	-
		ASMS		
1970	J. L. Franklin	R. E. Honig	C. E. Johannsen	H. R. Harless
1971-2	R. E. Honig	F. H. Field	G. L. Kearns	J. R. Harless
1972-4	F. H. Field	H. J. Svec	A. H. Struck	E. Lumpkin
1974-6	H. J. Svec	J. H. Futrell	W. H. Brubaker	*Position was Deleted in 1973-4.
1976-8	J. H. Futrell	J. A. McCloskey	E. J. Bonelli	

Year	Secretary	Treasurer	Directors At Large	
		ASTM E-14		
1961-2	C. F. Crable	-	J. H. Beynon	C. F. Robinson
1963-4	H. E. Lumpkin	-	S. Meyerson	A. L. Wahrhaftig
1965-6	G. L. Cook	-	H. I. Schiff	W. M. Hickam
1967-8	A. B. King	-	E. E. Muschlitz	R. M. Teeter
1969	J. M. McCrea	-	R. F. Porter	J. T. Herron
		ASMS		
1970	J. M. McCrea	H. D. Cook	R. F. Porter	J. T. Herron
1971-2	F. E. Saalfeld	H. D. Cook	A. G. Sharkey	A. L. Wahrhaftig
1972-4	F. E. Saalfeld	M. T. Laug	J. Berkowitz	E. B. Owens
1974-6	J. A. McCloskey	M. T. Laug	P. Kebarle E. M. Emery	J. L. Margrave
1976-8	K. E. McCulloh	M. T. Laug	H. M. Fales E. G. Carlson	A. G. Harrison

*ASTM E-14 Chairman was dropped as a Vice President and made a Director at Large in 1974.

ASMS COMMITTEES AND ASTM E-14 SUBCOMMITTEES

II (ASMS) Fundamental Aspects. F. E. Saalfeld, Naval Research Laboratory, Code 6110, Washington, D.C. 20375.

III (ASMS) Computers and Data Processing. M. A. Grayson, McDonnell Douglas Research Laboratories, St. Louis, Missouri 63166.

V (ASMS) New Instruments and Techniques. F. W. Karasek, Department of Chemistry, University of Waterloo, Waterloo, Ontario, Canada.

VI (ASMS) Biological Applications. C. C. Fenselau, Department of Pharmacology and Experimental Therapeutics, The Johns Hopkins University School of Medicine, Baltimore Md. 21205.

VII (ASMS) Study of Solids. W. Harrington, RCA Laboratories, Princeton, New Jersey 08540.

VIII (ASMS) High Resolution Studies. H. M. Fales, Laboratory of Chemistry, National Heart and Lung Institute, Bethesda, Maryland 20014.

IX (ASMS) Aids to Education. L. Bone, Department of Chemistry, East Texas State University, Commerce, Texas 75429.

XI (ASMS) Environment and Pollution Studies. J. M. McGuire, Southeast Environmental Research Laboratory, Environmental Protection Agency, Athens, Georgia 30601.

Report on Poster Session Evaluation at San Diego Meeting, May 1976

An evaluation of the poster presentation technique by ASMS members was conducted to obtain; a) the attitude of ASMS members toward use of poster sessions at future meetings, b) feedback from members to be used for author guidelines. Copies of the evaluation forms for attendee and contributor are shown on the following pages. The evaluation was conducted at all four poster sessions.

The response was good; 432 forms were returned, and nearly two-thirds of those had comments. The statistics are summarized below.

	Attendee	Contributor
Total responses	372	60
	(% Yes response is shown)	
Demographics		
Membership in ASMS	76	77
Employment		
University	38	52
Industry	31	23
Government	15	17
Manufacturer	10	3
Other	6	5
General		
Previous participation in poster session	38	12
Suitability of MS work for poster technique	98	97
Estimate of number of persons with whom technical exchange occurred		
Maximum	200	100
Average	10	25
Minimum	0	7
Contributor specific		
Preparation guidelines adequate?	–	77
Employer bias against presenting work in poster session	–	0
Preparation time for poster vs slide presentation was		
Longer	–	18
About the same	–	60
Shorter	–	22
Critique		
Poorly prepared posters?	64	–
Facilities for poster presentations were		
Very good	32	47
Adequate	64	47
Poor	4	6
Comments	60	65
Bottom Line		
Comparison with slide presentation -		
Superior	50	75
About the same	38	22
Inferior	12	3
Should poster sessions be used in future ASMS meetings?	96	–
If so, would you present your work in a poster session	78	88

David Bowen conducted a survey of the conventional oral sessions on Wednesday to ensure sampling of members who might not be attending the poster sessions. The results of this survey (60 responses) were not significantly different from the survey conducted at the poster session with respect to the main question of interest, "Do you endorse poster sessions for next year?" This question received an 82% yes reply from respondents at the conventional oral sessions.

The data gathered in this survey are being studied by the poster session chairmen who will use them to prepare poster presentation guidelines for authors to be approved by the executive board of ASMS.

Poster Session Chairmen at San Diego were:

Milt Levenberg	Abbott Laboratories
Bob Rhodes	Merck Sharp & Dohme
Roger Upham	University of Minnesota
Hank Fales	NIH
Jim Taylor	University of Wisconsin
Mike Grayson	McDonnell Douglas Research Laboratories

Attendee Evaluation Form

1) Are you a member of ASMS? Yes ☐ No ☐

2) Employment

☐ University ☐ Industry ☐ Government ☐ Manufacturer

Other _____

3) Have you ever attended a poster session? Yes ☐ No ☐

4) Do you feel that mass spectrometry lends itself to poster presentations? Yes ☐ No ☐

5) Estimate the number of people you communicated with during the poster session _____

6) How do you compare poster presentations with conventional presentations?

☐ Superior
☐ About the Same
☐ Inferior

7) Did you see any poster presentations which you considered were poorly prepared or presented? Yes ☐ No ☐

If "yes" describe shortcomings in section 12) below

8) Do you endorse poster sessions for next year? Yes ☐ No ☐

9) Will you volunteer to present your work in a poster session if we have them next year? Yes ☐ No ☐

10) Do you feel that the facilities were

☐ Very good
☐ Adequate
☐ Poor

11) Suggestions for improving possible future sessions: _____

_____

_____

_____

12) Comments: _____

_____

_____

_____

Contributor Evaluation Form

1) Are you a member of ASMS? Yes ☐ No ☐

2) Employment

☐ University ☐ Industry ☐ Government ☐ Manufacturer

Other _____

3) Have you ever presented a paper at a poster session? Yes ☐ No ☐

4) Do you feel the guidelines for presentation were adequate for the preparation of your poster? Yes ☐ No ☐

5) Did you have problems justifying to your employer the presentation of a poster which you would not have had if you were giving a 10-15 minute slide presentation? Yes ☐ No ☐

6) In retrospect, do you feel that the material you presented lent itself to a poster presentation? Yes ☐ No ☐

7) Was the time required to prepare your poster presentation

☐ Longer
☐ About the Same
☐ Shorter

as/than time spent in preparation for a 10-15 minute slide presentation.

8) Estimate the number of people with whom you exchanged ideas during your poster presentation _____

9) How would you compare the poster presentation with the 10-15 minute talk?

☐ Favorably
☐ About the Same
☐ Unfavorably

10) Will you prefer to present your work in a poster session if we have them next year? Yes ☐ No ☐

11) Indicate your evaluation of the facilities for the poster presentation session

☐ Very Good
☐ Adequate
☐ Poor

12) Suggestions for improving possible future sessions: _____

13) Comments: _____

The success of this survey is due to the generous contributions of time by numerous ASMS members who helped in the distribution and collection of surveys and collation of the responses throughout the week of the meeting.

Respectfully submitted

M. A. Grayson

M. A. Grayson

McDonnell Douglas Research Laboratories
St. Louis, Missouri 63166

Report of Committee on Computers and Data Processing (III)

Program Exchange

The activities of this Committee in the past year have centered about two central and related goals: 1) establishing a library of computer programs for both dedicated and high-level language machines for exchange and, 2) providing an opportunity for program exchange by dissemmination of the library of programs and mechanisms of exchange to the membership of ASMS. The committee feels that it has successfully achieved these goals with the 18 February 1976 mailing to the membership.

The statistics on program exchange are presented below as of 11 June 1976:

	Dedicated system exchange	QCPE
Programs contributed to Committee III prior to 18 February mailing	11	14
Programs offered in 18 February mailing	11	10
Requests for programs	10 for 43	2 for 2
Request for File search software, courtesy of Steve Heller	25	
Request for data bases, courtesy of Bill Milne	15-20	
Programs contributed to Committee III since 18 February mailing	2	6

The expenses incurred by this Committee during the year are:

Fee for Quantum Chemistry Program Exchange Services	$100.00
Mailing of library and exchange information to ASMS members	150.00
Clerical services	25.00

Business Meeting

The business meeting of the Committee on Computers and Data Processing was held at 5:45 P.M. Tuesday, 11 May 1976 in San Diego. Attendance at the meeting varied from 39 at the beginning to 52 at the maximum. All present had received the Committee III mailing of 18 February. Fred Falkner reported on the status of the dedicated data system program exchange effort (see summary above). The chairman reported on the status of program exchange through QCPE (see summary above).

The ensuing discussion is reported below with sincere thanks to David Bowen for his services as recording secretary.

David Rosenthal commented that the major question is whether the exchange recipients find the program useful. There are no data on this point at the present. He also suggested that the exchange should include small simple programs. Other members commented that we ought to encourage the use of higher level languages in programming dedicated systems and that we should encourage the exchange of algorithms and flow charts in addition to specific programs. Steve Heller stated that NIH and EPA are willing to convert certain analysis programs to PDP 10 form and make them available on the Cyphernetic system. He mentioned that they are adding the MSDC literature search capability at the moment.

It was suggested that the Committee communicate with members more often, but it was pointed out that this costs ~ $150 per mailing. Andrew McCormick said that the MS Bulletin will be willing to publish the list of programs available for exchange and to publish additions to this list from time to time. The task of approaching authors at the ASMS meeting to obtain programs for the exchange was accepted by Paul Fennessey. A vote was taken as to whether the exchange should be continued: about 42 members voted yes, none voted no, and there were about 10 abstentions.

The problem of operating above m/e 1000 was mentioned. About 16 members have requirements in this mass range, but it was agreed to leave this problem to the high-resolution committee, which is dealing with it.

It was suggested that a standard format be developed for mass spectral output from data systems for submission to mass spectral libraries, but after discussion it was agreed that the needs of different data systems and the unforeseen changes which undoubtedly will occur in any "perfect" format make such an effort impractical at the moment.

The possibility of having a symposium on dedicated data systems at the next national meeting was discussed. A number of members seemed enthusiastic about the idea, and David Bowen and Leonard Wojcik were selected as co-chairmen of the proposed symposium. A rough format was outlined including a poster session in which manufacturers will be represented and a workshop discussion in which users will speak and answer questions from the floor.

Activities for 1977

The Committee will act on the following points in the coming year:

1) Continue program exchange efforts through existing mechanisms and search for other effective methods to promote program exchange.
2) Provide Steve Heller with selected programs currently in library of contributed programs for use on Cyphernetics.
3) Make use of MS Bulletin one or more times per year to keep ASMS members up to date on programs for exchange.
4) Proceed with the organization of a symposium on dedicated data systems in conjunction with David Bowen and Leonard Wojcik for the 1977 ASMS meeting in Washington, D.C.
5) Assist Steve Heller in promoting the contribution of reference spectra to the existing data bases.

I should like to thank Fred Falkner, Steve Heller, Bill Milne, and Brian Middleditch for their active participation in the business of this Committee during the past year and also all of those members who were kind enough to volunteer their time and effort to contribute programs for exchange.

As always, the Committee is interested in hearing from ASMS members with ideas, help, programs, mass spectra and constructive criticism.

Respectfully submitted

M.A. Grayson

M.A. Grayson

Chairman, Committee on Computers
and Data Processing (III)

McDonnell Douglas Research Laboratories
St. Louis, Mo. 63166
(314) 232-3877

ASMS COMMITTEE VI. BIOLOGICAL APPLICATIONS

Chairman: C. Fenselau, The Johns Hopkins University School of Medicine, Baltimore, Maryland 21205

Secretary: W. J. A. VandenHeuvel, Merck Sharp & Dohme Research Laboratories, Rahway, New Jersey 07065

Activities for 1975-76

1. A workshop on GLC-MS Systems and Applications, co-sponsored by Committees VI and XI, was held at the 1976 ASMS meeting. Among the topics covered by the speakers were simultaneous pulsed positive and negative ion mass spectrometry, positive and negative features of quadrupole vis-a-vis magnetic sector instruments, and certain aspects of LC-MS. More than 150 people were in attendance.

2. Committee VI also sponsored a symposium on New Perspectives in Biological Mass Spectrometry at the 1976 ASMS meeting. Robert T. McIver, R. D. MacFarlane, E. C. Horning and John Hayes spoke in this well-attended session, co-chaired by C. Fenselau and M. L. Vestal.

Minutes from Business Meeting, May 13, 1976

The meeting was called to order with about 50 persons in attendance. Chairperson C. Fenselau introduced three topics for consideration for special programs to be held at the 1977 ASMS meeting and comments were welcomed: Quantitation of solid samples by direct probe analysis; Analytical applications of negative ion mass spectrometry; Evaluation of dedicated data systems, using a "poster symposium" format. This last possibility, which was conceived in Committee III, was described to Committee VI by D. Bowen. Emphasis would be on demonstrating why commercially available dedicated data systems are truly useful, and what new applications their use allows. Presentations would be by users, with a manufacturer's representative also present. This possibility was well received by those in attendance, and a proposal to approve this event will come before the ASMS Board of Directors in July.

The terminology used for describing the technique employed in following the intensities of pre-selected ions vs time was brought up briefly by C. Fenselau. She summarized the vote in Committee VI in 1975 in favor of selected ion recording, and voting sessions conducted by J. T. Watson and J. Sjovall at recent international mass spectrometry meetings in Sardinia and Chicago. Selected ion monitoring was found to be the term most acceptable to those two international groups. The general concensus of those at the Business Meeting was that selected ion monitoring was suitable and acceptable. C. Fenselau reported that editors of both the International Journal of Spectroscopy and Ion Physics and Biomedical Mass Spectrometry favor Selected Ion Monitoring as acceptable terminology for publications in those journals.

As the last order of business chairperson Fenselau introduced Fred Falkner whom she had invited to prepare a report on the histroy of the development of techniques and terminology for selected ion monitoring as these are documented in the scientific literature. F. Falkner summarized his report, which indicates that the concept was first developed during the 1940's. It is hoped that this report, which is appended, will be used as a source document in any deliberations about the designation of an "official" set of terms for selected ion monitoring.

W. J. A. VandenHeuvel, Secretary

Development of Techniques for Selected Ion Monitoring
as Documented in the Scientific Literature

(A Report Prepared for ASMS Committee VI - Biomedical Applications)

The primary purpose of this document is to trace the historical development up through 1968 of the technique of using a mass spectrometer with a single detector to detect, as a function of time, only the ion current profiles corresponding to a few selected masses. Since this technique involving only a few ions represents an intermediate level between that of focusing continuously at a single m/e value and that of scanning the complete spectrum repeatedly in order to later recreate desired ion profiles, a brief history of the development of these latter two methods will also be presented. However, the development of the latter two techniques will be traced back only as it relates to combined gas chromatography-mass spectrometry (GC-MS) work.

A. Mass Spectrometers, Accelerating Voltage Modulation, and Ion Detection.

The earliest publication of the technique of using a mass spectrometer with a single detector to detect, as a function of time, the ion current at a few selected masses appears to be that of Nier et al. in 1948[1]. Several mass spectrometers designed to analyze continuously the process gas stream in a uranium gaseous diffusion plant were equipped with automatic switching equipment which "varied the ion-accelerating potential through a prearranged sequence of values in order to select the masses desired for making the analysis." The mass spectrometers were magnetic sector instruments, and the ions of interest were m/e 14 (N^+), m/e 19 (F^+), m/e 28 (N_2^+), m/e 32 (O_2^+), and m/e 69 (CF_3^+). Although these authors do not use the term, the early vernacular apparently used to describe this technique was "peak stepping," i.e. switching the accelerating voltage through a series of preset values and sampling at each value without scanning over the peak.

Smith and Damm[2,3] in 1953 used a similar technique to advantage in the mass synchrometer, a novel mass spectrometer which separated ions on the basis of their cyclotron frequencies in a uniform magnetic field. Details of their method of alternately focusing two ions on a detector by modulating the accelerating voltage and the radiofrequency were published at a later date.[4] Accurate mass measurements could be obtained by offsetting the display of the ion profiles on the oscilloscope, a peak matching technique. Although the authors never described this technique as such, the vernacular apparently used to describe it was "jump scanning", i.e. switching the accelerating voltage through a series of preset values and sampling at each value by scanning over the peak.

In 1954 Taylor[5] published a "jump scan" method for measuring ion abundances by modulating the accelerating voltage to focus alternately on the detector the ion beams corresponding to two selected masses. At each mass scanning was conducted electrically over that mass. The scan rate was slow (scan times of 1.5-6 sec.) and conducted only on the flat-topped portion of the peak. Hence, the output could be handled by a single pen recorder and appeared in square wave form.

In the design of a double focusing mass spectrometer for precise determination of atomic masses Quisenberry, Scolman, and Nier[6] (1956) incorporated a method for alternating simultaneously both the accelerating voltage and the deflection voltage in the electrostatic analyzer. The data display of the two ion current profiles was similar to that described by Smith and Damm so that peak matching could be employed to obtain precise mass measurements.

In 1957 Stevens[7] described a modification of the mass spectrometer of Nier[1] which facilitated the measurement of abundance ratios. An automatic attenuator was incorporated into the "peak steppling" circuitry which allowed the abundance ratios between nitrogen, oxygen, and argon to be measured with a precision of one part in one thousand.

A three stage mass spectrometer utilizing two consecutive magnetic analyzers followed by an electrostatic analyzer was equipped with a "four channel modulator" (White, Rourke, and Sheffield, 1958)[8]. This unit "modulated the high voltage in a step-function for pre-set time periods and pre-set mass positions." This mass spectrometer used in the "peak stepping" mode achieved abundance sensitivity measurements of 10^7.

Dietz et al[9] (1960) measured the relative abundances of uranium isotopes "by stepping the accelerating voltage to count the $^{238}U^+$ and $^{235}U^+$ beams for 1 and 10 seconds, respectively." This mass spectrometer had two magnetic sectors in tandem and had a fast pulse counting device for the electron multiplier to improve the precision of the measured ratio.

The first application of such methodology to a problem of biological interest was that reported by Sweeley et al[10] (1966). They used an accelerating voltage alternator which "by switching the accelerating voltage at frequent intervals allowed more or less continuous recording of the change in intensities of two m/e values." The responses for the two ions were recorded as overlapping traces on oscillographic paper. The utility of the technique was further enhanced by the fact that the sample was introduced via a gas chromatograph. Practical application of the technique was demonstrated with a mixture of dehydroepiandrosterone and epiandrosterone (m/e 270 and m/e 272) and a mixture of the trimethylsilyl derivatives of glucose and glucose-d_7 (m/e 217 and m/e 220).

Hammar, Holmstedt, and Ryhage[11] (1968) provided an excellent demonstration of the powerful capabilities of the technique in biomedical work. By use of an accelerating voltage alternator capable of looking at 3 ions, they were able to identify metabolites of chlorpromazine circulating in plasma. Since this report appeared, the technique has been expanded and exploited by many workers and has been reviewed over the period 1968 to early 1975 by a number of review articles (Gordon and Frigerio[12], Holmstedt and Palmer[13], Jenden and Cho[14], Fenselau[15], Falkner, Sweetman and Watson[16], and Palmer and Holmstedt[17]).

B. Single Ion Detection in a GC Effluent.

The pioneer in monitoring the abundance of a single ion generated in the effluent from a GC interfaced to a mass spectrometer appears to be Henneberg[18,19], (1959, 1961, 1966). A splitter at the exit of a GC column diverted part of the effluent into the ion source of a magnetic sector mass spectrometer.

A linear relationship was established between the peak height observed on the GC detector and the appropriate characteristic ion of various isomeric pentanes and hexanes. The dependence of sensitivity on ion source pressure was also noted.

Selke et al[21] (1961) and Gohlke[22] (1962) both used time-of-flight mass spectrometers as detectors for a GC. Selke monitored m/e 15 to mimic the thermal conductivity detector of a GC, while Gohlke took advantage of a gating arrangement in which one collector detected the total ion current while the other detected the ion at m/e 43.

Other workers to use this technique in the mid-sixties included McFadden et al [23,24], Teranishi et al[25], Day and Libbey[26], and Angelini et al[27].

C. Successive Scanning of a GC Effluent for Later Reconstruction of Ion Current Profiles.

The initial use of the technique of acquiring successive scans of a GC effluent and then extracting from this acquired data a profile of abundance vs. scan number (time) for any desired ion or ions can be attributed to Lindeman and Annis[28] (1960). The plotted ion current profiles obtained from scans of hydrocarbon mixtures were done by hand and used for both qualitative identification and quantitative measurement. The early vernacular used to describe the process of elucidating the constituents of a complex GC peak by MS was "peak deconvolution".

Dorsey et al[29] (1963) applied the same methodology to identify components eluting from a capillary GC column into a cycloidal focusing MS. Leemans and McCloskey[30] (1967) scanned repetitively over a single unhomogeneous GC peak and plotted the abundance profiles of selected ions within that peak to elucidate the constituents comprising the peak.

In 1970 Hites and Biemann[31] gave this technique tremendous impetus by acquiring and storing the successive scan data in a computer. The computer could then efficiently generate a total ionization plot or profiles of any desired ion current as a function of scan number.

Respectfully submitted,

Fred C. Falkner
Pfizer Central Research
Groton, Connecticut

References

1. A. O. Nier, T. A. Abbott, J. K. Pickard, W. T. Leland, T. I. Taylor, C. M. Stevens, D. L. Dukey, and G. Goertzel, Anal. Chem., 20, 188 (1948).
2. L. G. Smith and C. C. Damm, Phys. Rev., 90, 324 (1953).
3. L. G. Smith and C. C. Damm, Phys. Rev., 91, 481 (1953).
4. L. G. Smith and C. C. Damm, Rev. Sci. Instr., 27, 638 (1956).
5. C. Taylor, Ark. Fys., 8, 201 (1954).
6. K. S. Quisenberry, T. T. Scolman, and A. O. Nier, Phys. Rev., 102, 1071 (1956).
7. R. H. Stevens, U. S. Atomic Energy Comm., K-1334, 23 (1957).
8. F. A. White, F. M. Rourke, and J. C. Sheffield, Appl. Spectrosc., 12, 46 (1958).
9. L. A. Dietz, C. F. Pachucki, J. C. Sheffield, A. B. Hance, and L. R. Hanrahan, Anal. Chem., 32, 1276 (1960).
10. C. C. Sweeley, W. H. Elliott, J. Fries, and R. Ryhage, Anal. Chem., 38, 1549 (1966).
11. C.-G. Hammar, B. Holmstedt, and R. Ryhage, Anal. Biochem., 25, 532 (1968).
12. A. E. Grodon and A. Frigerio, J. Chromatogr., 73, 401 (1972).
13. B. Holmstedt and L. Palmer, Adv. Biochem. Psychopharmacol., 7, 1 (1973).
14. D. J. Jenden and A. K. Cho, Ann. Rev. Pharmacol., 1973, 371.
15. C. Fenselau, Appl. Spectrosc., 28, 305 (1974).
16. F. C. Falkner, B. J. Sweetman, and J. T. Watson, Appl. Spectrosc. Rev., 10, 51 (1975).
17. L. Palmer and B. Holmstedt, Sci. Tools (The LKB Instrument Journal), 22, 25 (1975).
18. D. Henneberg, Z. Anal. Chem., 170, 365 (1959).
19. D. Henneberg, Z. Anal. Chem., 183, 12 (1961).
20. D. Henneberg and G. Schomberg, Z. Anal. Chem., 215, 424 (1966).
21. E. Selke, C. R. Schofield, C. Evans, and H. J. Dutton, J. Amer. Oil Chem. Soc., 38, 614 (1961).
22. R. S. Gohlke, Anal. Chem., 34, 1332 (1962).
23. W. H. McFadden and R. Teranishi, Nature, 200, 324 (1963).
24. W. A. McFadden, R. Teranishi, J. W. Corse, D. R. Black, and T. R. Mon, J. Chromatogr., 18, 10 (1965).
25. R. Teranishi, J. W. Corse, W. H. McFadden, D. R. Black, and A. I. Morgan, Jr., J. Food Sci., 28, 478 (1963).
26. E. A. Day and L. M. Libbey, J. Food Sci., 29, 583 (1964).
27. P. Angelini, D. A. Forss, M. L. Bazinet, and C. Merritt, Jr., J. Amer. Oil Chem. Soc., 44, 26 (1967).
28. L. P. Lindeman and J. L. Annis, Anal. Chem., 32, 1742 (1960).
29. J. A. Dorsey, R. H. Hunt, and M. J. O'Neal, Anal. Chem., 35, 511 (1963).
30. F. A. J. M. Leemans and J. A. McCloskey, J. Amer. Oil Chem. Soc., 44, 11 (1967).
31. R. A. Hites and K. Biemann, Anal. Chem., 42, 855 (1970).

Appendix

Names which have appeared in the literature to describe the technique of acquiring the ion abundance of only certain chosen ions as a function of time.

1. 1968 Mass Fragmentography
   C.-G. Hammar, B. Holmstedt, and R. Ryhage, Anal. Biochem., 25, 532 (1968).
2. 1970 Selected Ion Peak Recording
   C. Merritt, Jr., Appl. Spectrosc. Rev., 3, 263 (1970).
3. 1971 Multiple Ion Detection
   C.-G. Hammar and R. Hessling, Anal. Chem., 43, 298 (1971).
4. 1971 Ion Specific Detection
   T. E. Gaffney, C.-G. Hammar, B. Holmstedt, and R. E. McMahon, Anal. Chem., 43, 307 (1971).
5. 1972 Tuned Ion Analysis
   R. W. Kelly, in Proceedings of International Symposium on Gas Chromatography-Mass Spectrometry (A. Frigerio, ed.), Isle of Elba, Italy, May 1972, p. 21.
6. 1972 Direct Multiple-Mass Fragmentography
   D. E. Green and I. S. Forrent, in Proceedings of the Fifth International Congress on Pharmacology, Basel, Switzerland, 1972, p. 88.
7. 1973 Selective Ion Detection
   M. G. Horning, J. Nowlin, K. Lertratanangkoon, R. N. Stillwell, W. G. Stillwell, and R. M. Hill, Clin. Chem., 19, 845 (1973).
8. 1973 Multiple Specific Ion Detection
   D. J. Jenden and R. W. Silverman, J. Chromatogr. Sci., 11, 601 (1973).
9. 1973 Multiple Single Ion Detection
   S. Billets and C. Fenselau, in Proceedings of the 21st Annual Conference on Mass Spectrometry and Allied Topics, San Francisco, California, May 1973, American Society of Mass Spectrometry, p. 300.
10. 1973 Multiple Ion Analysis
    M. Hamberg, Anal. Biochem., 55, 368 (1973).
11. 1973 Multiple Ion Monitoring
    W. G. Stillwell, A. Hung, M. Stafford, and M. G. Horning, Anal. Lett., 6, 407 (1973).
12. 1973 Multiple Mass Monitoring
    Nuclide Spectra Bull., 7(1), (1973).
13. 1973 Selective Ion Monitoring
    B. S. Middleditch and D. M. Desiderio, Anal. Chem., 45, 806 (1973).
14. 1974 Selected Ion Monitoring
    R. Hoffenberg, A. M. Lawson, D. B. Ramsden, and F. J. Raw, in Mass Spectrometry in Biochemistry and Medicine (A. Frigerio and N. Castagnoli, eds.), Raven Press, New York, 1974, p. 303.
15. 1975 Selected Ion Recording
    D. K. Lin, A. F. Fentiman, Jr., R. L. Foltz, R. D. Forney, Jr., and I. Sunshine, Biomed. Mass Spectrom., 2, 206 (1975).

MINUTES OF E-14 BUSINESS MEETING

The Business Meeting of ASTM Committee-14 on Mass Spectrometry was held on May 10, 1976 in San Diego, California. The meeting was attended by 11 members and Mr. Dick Sherwood of ASTM Headquarters. A list of attendees is given in Attachment I.

The meeting was opened by E. Emery, the outgoing Chairman, who expressed his thanks to the members for the help received during his term. He also discussed the lack of mention for ASTM-E14 and D-2 functions in the ASMS program. This difficulty was caused by an oversight on the part of the ASMS program committee and the failure of D-2 and E-14 officers to provide ASMS with written information on these functions. The difficulty was resolved by posting notices and frequent announcements at the ASMS sessions. In the future we will rely on written request and on close cooperation between the E-14 Chairman and the ASMS program committee.

Thomas Aczel was appointed to fulfill the unexpired term of Bill Askew (May 10-June 30, 1976), who has retired.

The financial report was presented by Dick Sherwood. On January 1, 1976, not inclusive of 1976 interest, we had $4,544.41. The 1976 expenditures to date amounted to $366.17, leaving a balance of $4,178.24. Funds at hand are residual funds; there is no input or "take" by ASTM, which, however, manages investment of the funds.

The Chairman's report dealt with the election of the officers for the July 1976-July 30 1978 term. He thanked the nominating committee, Rod Page and Ed Howard. The officers are: E. G. Carlson, Chairman; Mynard Hamming, Vice Chairman; Thomas Aczel, Secretary-Treasurer.

Additional reports given at the meeting, or forwarded to the Secretary include a report on E-21 (M. E. Fitzgerald) and D-2 (Thomas Aczel).

Dick Sherwood suggested that E-14 establish liaisons with other ASTM committees, such as E-31 and D-2 which are involved in some aspect of MS or use it. He will furnish a list of potential contacts.

Present membership of the Committee is 61. We received four new applications which have been approved by the Executive Committee.

The meeting was adjourned by the Chairman.

Respectfully submitted,

Thomas Aczel
Secretary-Treasurer

MINUTES OF THE MEETING OF THE EXECUTIVE COMMITTEE ON ASTM COMMITTEE E-14

The Executive Committee met on May 10, 1976, in San Diego, California. Attendees included ASTM officers, E. Emery , E. G. Carlson and Thomas Aczel, and the ASMS Chairman and Chairman-Elect, H. T. Swec, and T. H. Futrell. The latter are ex-officio associate members of the Executive Committee.

Items discussed included ASTM's place on the ASMS program and an informal report on the preceeding E-14 meeting by E. Emory. The difficulties related to the placing of ASTM functions on the ASMS program were resolved with mutual satisfaction.

Respectfully submitted,

Thomas Aczel
Secretary-Treasurer

Attendees-ASTM E-14

Business Meeting

Dick Sherwood, ASTM, 1916 Race St. Phil., Pa. 19103
E. G. Carlson, Shell Dev. Co., Box 1380, Houston, Tx. 77001
R. W. Vander Haar, Std.Oil(Ind), Box 400, Naperville, Ill. 60540
Ahmed Halouma, Ledoux & Co., 359 Alfred Ave. Teaneck, N.J. 07666
D. R. McAdams, Exxon, Box 2226, Baton Rouge, La. 70821
J. T. Hellmann, National Lead Co. Box 39158, Cincinnati, Ohio 45239
J. H. Weber, Lerc-Erda, Box 3395, Laramie, Wyo. 82071
M. E. Fitzgerald, Arco Chem Co., Box 85, Glenolden, Ga. 19036
Thomas Aczel, Exxon Res. & Eng., Box 4255, Baytown, Tex. 77520
H. E. Lumpkin, Exxon Res. & Eng., Box 4255, Baytown, Tex. 77520
Ed Emery, Colgate-Palmolive, 909 River Road, Piscataway, N. J. 08854
A. G. Sharkey, ERDA, 4800 Forbes Ave., Pittsburgh, Pa. 15213

Executive Committee: T. Futrell
H. Swec

ACTIVITIES OF ASTM COMMITTEE D-2

Thomas Aczel, Chairman, Research Division IV, Section M

ASTM Committee D-2, Research Division IV, Section M on mass spectrometric methods coordinates at the present the activities of two task groups.

The first of these, chaired by J. Weber of ERDA, Laramie Research Center, is involved in developing methods for the analysis of shale oil naphthas and middle distillates. The second one, chaired by Janet Schultz of ERDA, Pittsburgh Energy Research Center, is developing methods for the analysis of saturates, aromatics and polars separated from coal liquefaction products.

The two groups met on May 6, 1976, during the ASMS Conference on Mass Spectrometry. This note is a brief summary of the activities of the groups. Inquiries for details should be addressed to the respective Chairpersons. Membership in the groups is open to all interested persons, and inquiries and participation are encouraged.

Task Group on Shale Oil Analysis

Chairperson: Dr. J. A. Weber, LERC/ERDA, Box 3395, Laramie, Wyoming 82071

Meeting of the group was attended by approximately 50-60 people. An attendance list is available from the chairman.

Past activities included the examination of a blend of the aromatic fractions of 12 crudes furnished by Thomas Aczel, in order to assess relative low voltage sensitivities. Data were available from 5 laboratories, including a comparison between low voltage and field ionization sensitivities. Complete evaluation of the data is still in progress. Preliminary results show fair to satisfactory agreement for most labs.

J. Weber of ERDA distributed a set of olefinic fractions, derived from shale oil. Participants will analyze these, using their own methods at first, and will report the data in time for the 1977 ASMS meeting.

Analysis of Coal Liquefaction Products

Chairperson: Dr. J. L. Shultz PERC/ERDA, 4800 Forbes Ave. Pittsburgh, Pa., 15213

The group analyzed a blend of four saturate fractions from Synthoil products, provided by Thomas Aczel. The fractions were separated with a modified clay-gel chromatographic procedure and did not contain but trace amounts of aromatics. Analyses from nine labs were, however, in rather poor agreement. This could be ascribed

to the different instruments used by the participants, and, possibly, to changes in composition during shipment. It was therefore decided to repeat the percolations and to provide a new set of saturate fractions, as well as aromatic and polar ones to the labs interested. This work is in progress--the percolations have been carried out by Exxon Research, and the fractions are now being analyzed prior to blending and shipment.

The Task Group also organized a Symposium on the MS characterization of Synthetic Fuels, co-chaired by A. G. Sharkey of ERDA/PERC and Thomas Aczel. The coal Symposium included eight invited papers. Judging from the attendance (80-100) and the lively discussion following each paper, it was a great success.

Committee IX Aids to Education

Committee IX met on Tuesday May 11, 1976. Two important items of discussion at the meeting resulted in Committee action.

Item 1. Workshop on Training Mass Spectrometry Technicians

It was agreed by the committee and later approved by the ASMS Board of Directors that Committee IX sponsor the workshop. The workshop will be scheduled for the 1977 ASMS meeting in Washington, D.C. It is planned that the workshop will be organized in a panel format. The panel will be made up of representatives from higher educational institutions, industrial laboratories, manufacturing industry, and mass spectrometry technicians. The panel members will discuss the feasibility of establishing formalized training programs for technicians and will enumerate their opinions regarding probable composition and structure of such a program.

Item 2. ASMS - Mass Spectrometer Gift Program

Dr. Mark Green brought to the Committee's attention the fact that many educational institutions teach mass spectrometry without the aid of a mass spectrometer. He further noted that other organizations may have used mass spectrometers available which could be given to the schools. The committee discussed various aspects of the proposed program and after discussion gave the idea its firm support. The general goals and operation of the program would involve the donor, the recepient, and ASMS.

The committee suggests instituting a new ASMS program involving, where appropriate, the gift of used mass spectrometers from the laboratories of our members to schools which could profit educationally from these instruments. It is envisioned that such gifts would take place with considerable fanfare involving publicity to the mass spectrometry laboratory, its parent organization, the school, and the ASMS. It is possible that these gifts would yield tax benefits as well as the considerable good will which such exchanges always involve. The process would necessarily increase interest in mass spectrometry and thereby would benefit us all. In this program the ASMS and Committee IX would simply act to bring the giver and the recipient together, add the ASMS name to exchanges already in contact, and in general act as an agency to facilitate the process.

Questionnaires have been sent to ASMS members requesting information in regard to this program.

The new Chairman, Larry Bone, made a few remarks about the program of Committee IX for the coming year. The Committee adjourned with thanks to the members for their work and support.

A.S.T.M. Publication on Mass Spectrometry

A. Recommended Practices and Methods of Test*

	Title and Citations in 1975 Books of ASTM Standards
D1137-53 (70)	Analysis of Natural Gases and Related Types of Gaseous Mixtures by the Mass Spectrometer, Part 26.
D1658-63 (74)	Carbon Number Distribution of Aromatic Compounds in Naphthas by Mass Spectrometry, Part 23.
D2424-67 (72)	Hydrocarbon Types in Propylene Polymer by Mass Spectrometry, Part 24.
D2425-67 (72)	Hydrocarbon Types in Middle Distillates by Mass Spectrometry, Part 24.
D2498-68 (73)	Isomer Distribution of Straight-Chain Detergent Alkylate by Mass Spectrometry, Part 24.
D2567-68 (73)	Molecular Distribution Analysis of Monoalkylbenzenes by Mass Spectrometry, Part 24.
D2601-68 (73)	Low Voltage Mass Spectrometric Analysis of Propylene Tetramer, Part 24.
D2650-68 (73)	Chemical Composition of Gases by Mass Spectrometry, Part 24.
D2786-71	High Ionizing Voltage Mass Spectrometric Analysis of Gas-Oil Saturate Fractions, Part 24.
D2789-71	Hydrocarbon Types in Low Olefinic Gasoline by Mass Spectrometry, Part 24.
E137-68	Evaluation of Mass Spectrometers for Use in Chemical Analysis, Part 42.
E244-69	Atom Percent Fission in Uranium Fuel, Mass Spectrometric Method, Part 45.
E304-68	Use and Evaluation of Mass Spectrometers for Mass Spectro-chemical Analysis of Solids, Part 42.

B. Other ASTM Mass Spectrometric Information

AMD11	Index of Mass Spectral Data, 1969, (Formerly STP 356).
AMD10a	Mass Spectral Data Structure (Punched Card Index - 3200 cards).
AMD10b	Mass Spectral Data - Name (Punched Card Index - 3500 cards).
AMD10c	Mass Spectral Data - Name (Punched Card Index - 3500 cards).

STP No. 149 Chemical Analysis of Inorganic Solids by Means of Mass Spectrometer, 1951 (out of print, available on microfilm).

STP No. 332a Manual on Hydrocarbon Analysis, 1968 (Revised manual in preparation).

---

*Committee jurisdiction for the mass spectrometric practices and methods is as follows:

Committee D3 - D1137
Committee E10 - E244
Committee E14 - E137 and E304
Committee D2 - all others listed

MASS SPECTROMETRY ORGANIZATIONS

Name	Name and Address for Additional Information
The American Society for Mass Spectrometry	Dr. K. E. McCulloh A 145 Chemistry National Bureau of Standards Washington, D.C. 20234
The Australian and New Zealand Society for Mass Spectrometry	Dr. P. C. Rankin c/o Soil Bureau Private Bag Lower Hutt, New Zealand
Mass Spectroscopy Society of Japan (MSSJ)	Professor Teruo Hayakawa The Mass Spectroscopy Society of Japan Department of Chemistry Faculty of Liberal Arts and Sciences University of Osaka Prefecture Sakai-shi, Osaka, Japan
Mass Spectroscopy Group	Dr. A. Carrick Instem Ltd. Stafford Street Stone, Staffs England
Arbeitegemeinschaft Massenspektroskopie	Dr. H. F. Grutzmacher, Frachbereich Chemie, University Hamburg 2 Hamburg, Germany
Groupement pour l'Avancement des Methodes Physiques d'Analyses (G.A.M.S.)	Madame Frere - GAMS 8, 10 rue de Delta 75 Paris 9 eme, France